

REPORT DOCUMENTATION PAGE Dist: A

Form Approved

OMB No. 0704-0188

Public reporting burden for this collection of information is estimated to average 1 hour per response, including the time for reviewing instructions, searching existing data sources, gathering and maintaining the data needed, and completing and reviewing the collection of information. Send comments regarding this burden estimate or any other aspect of this collection of information, including suggestions for reducing this burden, to Washington Headquarters Services, Directorate for Information Operations and Reports, 1215 Jefferson Davis Highway, Suite 1204, Arlington, VA 22202-4302, and to the Office of Management and Budget, Paperwork Reduction Project (0704-0188), Washington, DC 20503.

1. AGENCY USE ONLY (Leave blank)

2. REPORT DATE

November 15, 1994

3. REPORT TYPE AND DATES COVERED

Final Report 11/1/91 - 10/31/94

4. TITLE AND SUBTITLE

Fundamental Studies of Oxygen Rings and Other High Energy Density Molecular Systems

5. FUNDING NUMBERS

61102F2303B3 FS

6. AUTHOR(S)

Henry F. Schaefer III

7. PERFORMING ORGANIZATION NAME(S) AND ADDRESS(ES)

Georgia Univ Research Foundation Inc
Boyd Grad Studies Res Cntr
Athens, GA 30602PERFORMING ORGANIZATION
REPORT NUMBER

9. SPONSORING/MONITORING AGENCY NAME(S) AND ADDRESS(ES)

Air Force Office of Scientific Research/NL
110 Duncan Avenue
AFOSR/NC; Suite B115
Bolling AFB DC 20332-0001 Dr Berman10. SPONSORING/MONITORING
AGENCY REPORT NUMBER

F49620-92-J-0047

11. SUPPLEMENTARY NOTES

12a. DISTRIBUTION/AVAILABILITY STATEMENT

APPROVED FOR PUBLIC RELEASE; DISTRIBUTION IS UNLIMITED.

12b. DISTRIBUTION CODE

A

13. ABSTRACT (Maximum 200 words)

The *object* of this research is to characterize the energetics, spectroscopic properties, and elementary chemical reactions (including unimolecular reactions) of the oxygen ring molecules O₄ and O₁₂ and related species. The *approach* used will exploit recent developments in *ab initio* molecular quantum mechanics. In a collaborative effort with ongoing experimental research to identify and synthesize high energy density molecules, excited electronic states and positive ions of these species will be studied.

19950201 012

14. SUBJECT TERMS

Ab Initio, computational chemistry, quantum chemistry,
theoretical chemistry, propellants

15. NUMBER OF PAGES

16. PRICE CODE

17. SECURITY CLASSIFICATION
OF REPORT

UNCLASSIFIED

18. SECURITY CLASSIFICATION
OF THIS PAGE

UNCLASSIFIED

19. SECURITY CLASSIFICATION
OF ABSTRACT

UNCLASSIFIED

20. LIMITATION OF ABSTRACT

FINAL TECHNICAL REPORT

Air Force Office of Scientific Research
Grant AFOSR-92-J-0047

"Fundamental Studies of Oxygen Rings and Other High Energy Density Molecular Systems"

Accession For	
NTIS	CRA&I
DTIC	TAB
Unannounced	
Justification	
By	
Distribution /	
Availability Codes	
Dist	Avail and/or Special
A-1	

I. Summary

The development of efficient and safe conventional (i.e., non-nuclear) propellants and/or fuels is a goal of obvious technological significance. A desirable quality of such a propellant is clearly a high ratio of energy release to mass. Much of our research has rested on a simple, but previously (i.e., before our work beginning in 1986) unrecognized, analogy between oxygen and sulfur. Our AFOSR supported research has shown that the proposed oxygen ring systems are sufficiently promising to warrant careful consideration. In fact, several experimental groups have attempted to prepare and characterize oxygen rings in the laboratory. Thus a major emphasis in this phase of the proposed HEDM (high energy density molecules) theoretical research is to work closely with Air Force supported experimental efforts to this end. Our work has also encouraged other theoretical groups to extend our S \rightarrow O analogy to P \rightarrow N, with the work of Lee and Rice on tetrahedral N₄ being a particularly beautiful example.

The potential attractiveness of oxygen rings follows from a number of considerations, including:

- (a) Our theoretical studies to date show that the cyclic O_n systems are definitely high energy density materials. This may be seen in Figure 1, kindly provided to us by Dr. Harvey Michels based on our predicted energetics for O_8 ;
- (b) As cryogenic solid propellants, oxygen rings may plausibly be expected to form a metastable condensed phase by analogy with the valence isoelectronic sulfur rings, which of course are very stable solids under normal conditions;
- (c) The way to use oxygen rings as a rocket fuel is obviously analogous to that for normal molecular oxygen, i.e., O_2 . Furthermore, the complete burning of O_n with molecular hydrogen yields water as the only new molecular product. The absence of hazardous products of combustion is a strong argument in favor of oxygen rings.

The HEDM program has already brought about a remarkably improved stream of communication between chemists and propulsion experts. It has also produced several viable candidates (including cyclic ozone, tetrahedral N_4 , cyclic O_8 and O_{12} , and cubic N_8) for new propellants and/or additives. Furthermore the theoretical component of the HEDM program, and our research in particular, has received favorable attention in a semi-popular review in *Science* of very high visibility.

H_2/O_8 Vacuum Specific Impulse

Chamber Pressure = 1000 psia
Exit pressure = 14.7 psia

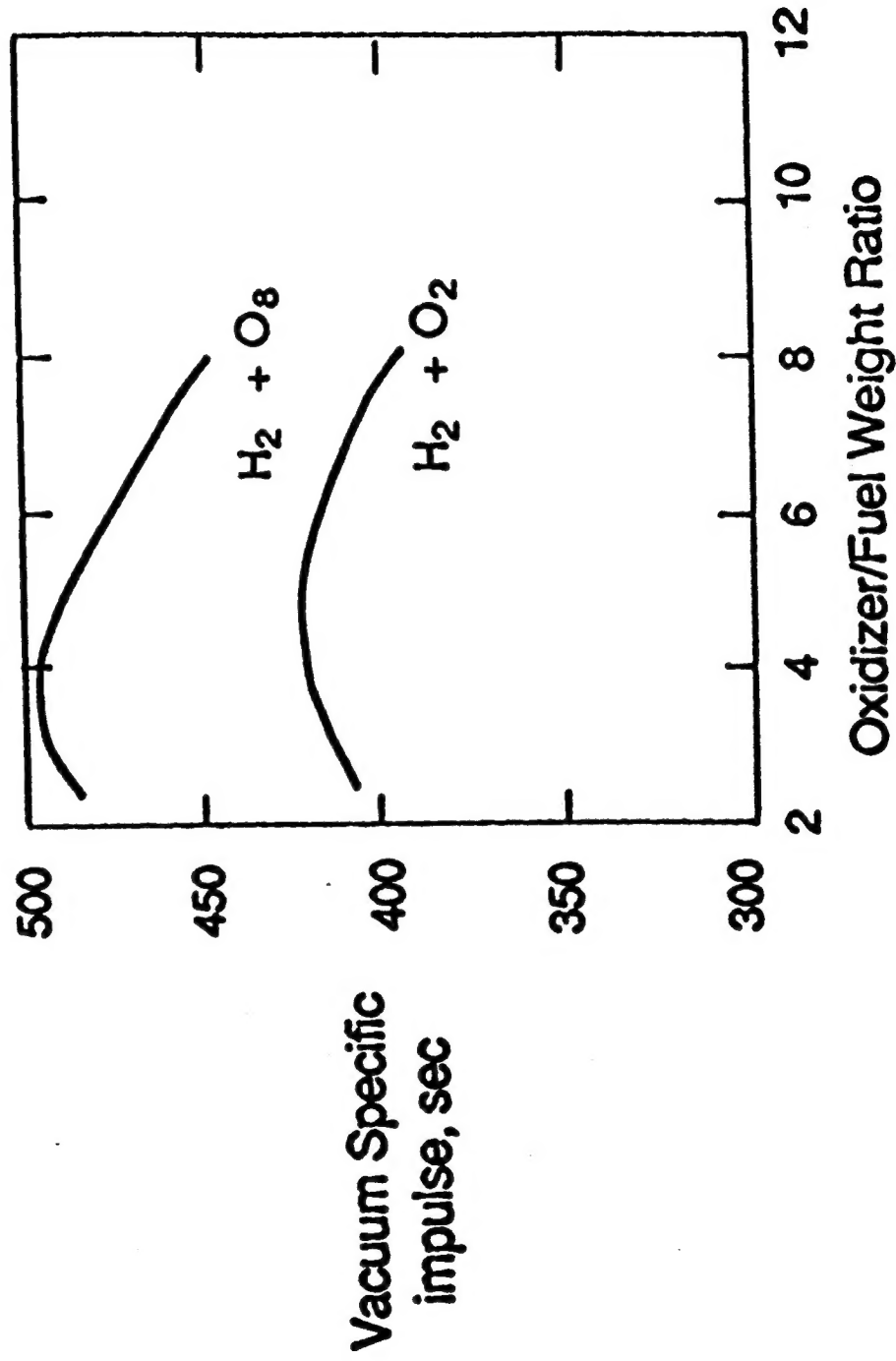


Figure 1. Specific impulse predictions for cyclic O_8 .

II. Progress Report

A. Publications Supported by AFOSR-92-J0047

(January 1, 1992 - October 31, 1994)

1. E. T. Seidl and H. F. Schaefer, "Is There a Transition State for the Unimolecular Dissociation of Cyclotetraoxygen (O_4)?", *J. Chem. Phys.* **96**, 1176 (1992).
2. D. A. Horner, R. S. Grev, and H. F. Schaefer, "Three-Membered Rings of Carbon, Silicon, and Germanium: An Analysis of Thermodynamic Stability to Fragmentation", *J. Amer. Chem. Soc.* **114**, 2093 (1992).
3. M. Shen and H. F. Schaefer, "The Known and Unknown Group 13 Hydride Molecules M_2H_6 : Diborane(6), Dialane(6), and Digallane(6)", *J. Chem. Phys.* **96**, 2868 (1992).
4. C.-H. Hu, M. Shen, and H. F. Schaefer, "Toward the Spectroscopic Observation of SiH_5^+ : The Silanium Ion", *Chem. Phys. Lett.* **190**, 543 (1992).
5. Y. Xie, H. F. Schaefer, J. H. Jang, B. J. Mhin, H. S. Kim, C. W. Yoon, and K. S. Kim, "Sulfur Clusters: Structure, Infrared, and Raman Spectra of Cyclo- S_6 and Comparison with the Hypothetical Cyclo- O_6 Molecule", *Mol. Phys.* **76**, 537 (1992).
6. M. Shen and H. F. Schaefer, "The Fundamental Vibrational Frequencies of the Silyl Anion (SiH_3^-)", *Mol. Phys.* **76**, 467 (1992).
7. I. S. Ignatyev and H. F. Schaefer, "Difluorosulfurane (SF_2H_2): A Molecule Identified in the Laboratory ?", *J. Phys. Chem.* **96**, 6247 (1992).
8. I. S. Ignatyev and H. F. Schaefer, "Diazasilene ($SiNN$). A Comparison of Coupled Cluster Methods with Experiment and Local Density Functional Methods", *J. Phys. Chem.* **96**, 7632 (1992).

9. A. A. Bliznyuk, M. Shen, and H. F. Schaefer, "The Dodecahedral N_{20} Molecule: Some Theoretical Predictions", *Chem. Phys. Lett.* **198**, 249 (1992).
10. B. Ma, Y. Xie, M. Shen, and H. F. Schaefer, " $PO_3^- \cdot (H_2O)_n$ Clusters. Molecular Anion Structures, Energetics and Vibrational Frequencies", *J. Amer. Chem. Soc.* **115**, 1943 (1993).
11. M. Shen, C. Liang, and H. F. Schaefer, "The Tetramer of Borane and Its Heavier Valence-Isoelectronic Analogs: M_4H_{12} with $M = B, Al$, and Ga ", *Chem. Phys.* **171**, 325 (1993).
12. S.-J. Kim, T. P. Hamilton, and H. F. Schaefer, "Methylphosphinidene (CH_3P) and its Rearrangement to Phosphaethylene (CH_2PH): Toward the Observation of Ground State Triplet CH_3P ", *J. Phys. Chem.* **97**, 1872 (1993).
13. Z. Palagyi, H. F. Schaefer, and E. Kapuy, " Ga_2H_2 : Planar Dibridged, Vinylidene-Like, Monobridged, and Trans Equilibrium Geometries", *Chem. Phys. Lett.* **203**, 195 (1993).
14. Z. Palagyi, R. S. Grev, and H. F. Schaefer, "Striking Similarities Between Elementary Silicon and Aluminum Compounds: Monobridged, Dibridged, Trans Bent, and Vinylidene Isomers of Al_2H_2 ", *J. Amer. Chem. Soc.* **115**, 1936 (1993).
15. T. P. Hamilton, Y. Xie, and H. F. Schaefer, " HP_4^- The Monoconjugate Base from Tetraphosphabicyclobutane. Evidence for the *Exo* Ground State Confirmation in the Gas Phase", *Chem. Phys. Lett.* **208**, 106 (1993).
16. J. M. Galbraith, G. Vacek, and H. F. Schaefer, " ClF_2 : Structure and Infrared Spectra of a Weakly Bound Triatomic Molecule", *J. Chem. Phys.* **98**, 8051 (1993).
17. G. Vacek, B. J. DeLeeuw, and H. F. Schaefer, "The \tilde{X} $AlOH$ - \tilde{X} $HAIO$ Isomerization Potential Energy Hypersurface", *J. Chem. Phys.* **98**, 8704 (1993).
18. Z. Palagyi, H. F. Schaefer, and E. Kapuy, " Ge_2H_2 . A Molecule with a Low-Lying Monobridged Equilibrium Geometry", *J. Amer. Chem. Soc.* **115**, 6901 (1993).

19. T. D. Crawford and H. F. Schaefer, "The Equilibrium Geometry of the \tilde{C}^2A_2 State of NO_2 ", *J. Chem. Phys.* **99**, 7926 (1993).
20. R. S. Grev, B. J. DeLeeuw, Y. Yamaguchi, and H. F. Schaefer, "The *Cis* Monobridged Equilibrium Geometries of Si_2H_2 , Ge_2H_2 , Al_2H_2 , Ga_2H_2 : A Fundamentally New Type of Molecular Structure", in *Structures and Conformations of Non-Rigid Molecules*, editors J. Laane, M. Dakkouri, B. van der Veken, and H. Oberhammer, NATO ASI Series C, Volume 410 (Kluwer Academic Publishers, Dordrecht, Holland, 1993). Pages 325-342.
21. B. Ma, Y. Xie, M. Shen, P. R. Schleyer, and H. F. Schaefer, "Isomerization of $PO_3^- \bullet (H_2O)_n$ Clusters to $H_2PO_4^- \bullet (H_2O)_{n-1}$ ", *J. Amer. Chem. Soc.* **115**, 11169 (1993).
22. J. M. Galbraith, G. Vacek, and H. F. Schaefer, "The Vibrational Frequencies of Borane (BH_3): A Comparison of High Level Theoretical Results", Golden Volume, *J. Mol. Struct.* **300**, 281 (1993).
23. C.-H. Hu, M. Shen, and H. F. Schaefer, "Is Dodecahedral P_{20} Special?", Werner Kutzelnigg Issue, *Theoret. Chim. Acta* **88**, 29 (1994).
24. M. Shen and H. F. Schaefer, "Dodecahedral and Smaller Arsenic Clusters: As_n , $n = 2, 4, 12, 20$ ", *J. Phys. Chem.* **101**, 2261 (1994).
25. B. Ma, C. Meredith, and H. F. Schaefer, "Theoretical Studies of Pyrophosphate Structures and Reactions: The Evaluation of Electrostatic Effects on the Pyrophosphates with and without Alkali Cations", *J. Phys. Chem.* **98**, 8216 (1994).
26. C.-H. Hu, P. R. Schreiner, P. R. Schleyer, and H. F. Schaefer, "Structure, Infrared Spectrum and Dissociation Energy of SiH_7^+ ", *J. Phys. Chem.* **98**, 5040 (1994).

27. B. Ma and H. F. Schaefer, "Toward the Observation of Silanone (H_2SiO) and Hydroxysilylene (HSiOH) via Microwave Spectroscopy", *J. Chem. Phys.* **101**, 2734 (1994).
28. E. E. Bolton, H. F. Schaefer, W. D. Laidig, and P.R. Schleyer, "Singlet $\text{C}_2\text{H}_2\text{Li}_2$: Acetylenic and 1,2-Dilithioethene Isomers. A Remarkably Congested Potential Energy Hypersurface for a Simple Organometallic System", *J. Amer. Chem. Soc.* **116**, 9602 (1994).

B. Relationship between Research Completed and that Proposed in November, 1990.

The research completed with AFOSR support during the two and one-half years spans a rather broad range of chemistry. The most obvious task in summarizing this research is to demonstrate that the 1990 goals have been achieved. Therefore we begin with necessarily brief descriptions of completed (or nearly completed) projects proposed in the 1990 document. Interactions with other Air Force-supported efforts in this program are noted.

1. The O_4 and O_6 Rings.

The cyclo- O_4 molecule is isoelectronic with cyclobutane and has been discussed as a potential new high energy density material (HEDM). The important unresolved question has been whether or not cyclo- O_4 is a genuine minimum on the O_4 potential energy hypersurface. During the present grant period the transition state for cyclo- O_4 dissociation to two O_2 molecules has been located at a number of levels of theory using a double zeta plus polarization (DZP) basis set. The theoretical methods with which the transition state

geometry was optimized include two-configuration self-consistent-field (TCSCF), coupled cluster including all single and double excitations (CCSD), and the latter with a perturbative correction for connected triple excitations, CCSD(T). The equilibrium geometry of O_4 has D_{2d} symmetry, while a stationary point of D_2 symmetry is of Hessian index two (i.e., two imaginary vibrational frequencies) at the highest level of theory, DZP CCSD (T). The true transition state lies only slightly lower energetically (classical barrier 7.9 kcal/mole) and is of C_2 symmetry with the DZP CCSD(T) method. The theoretical stationary point geometries are shown in Figures 2 and 3. The activation energy was predicted in a completely consistent manner to be 6.2 kcal/mole. The possibility that this barrier could disappear entirely at higher levels of theory is discussed. It is concluded (reference 1, section IIIA above) that the O_4 barrier is too low for O_4 to be useful as a HEDM.

A primary motivation for our earlier comparative studies of S_{12}/O_{12} and S_8/O_8 was to establish the viability of oxygen rings as high energy density materials (HEDM). A primary conclusion of these studies was that O_8 and O_{12} are somewhat lower-lying energetically than anticipated from back-of-the-envelope calculations. This result may be considered both "good" and "bad" with respect to the design of potential HEDM systems. That is, O_8 and O_{12} are likely to be more stable than originally anticipated, and hence easier to prepare in the laboratory; however, these species will not carry as much excess energy (with respect to $n/2$ separated O_2 molecules) as earlier imagined.

The O_4 system, on the other hand, is quite highly energetic, but appears to have a barrier of less than 6 kcal/mole for dissociation to two O_2 molecules. Perhaps O_6 might provide a happy meeting ground, with substantial energy content and a substantial barrier to dissociation. This was the motivation for the O_6 research carried out during the present grant period (reference 5, section IIIA above).

Except for its dissociation energy and vibrational frequencies, the hypothetical O_6 molecule appears similar to the well-characterized S_6 . As anticipated by back-of-the-envelope calculations O_6 is seen to lie significantly above three separated oxygen

1(a)

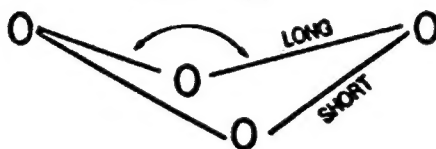
88.2° SCF
87.2° CISD
86.7° CCSD
86.4° CCSD(T)



D_{2d} TORSIONAL ANGLE = 20.4°
24.8°
27.0°
28.0°

1(b)

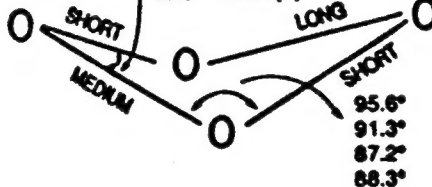
84.9° TCSCF
82.6° CISD
83.7° CCSD
84.2° CCSD(T)



D_2 TORSIONAL ANGLES = 28.9°, 38.4°
32.7°, 47.3°
32.1°, 41.5°
31.8°, 38.8°

1(c)

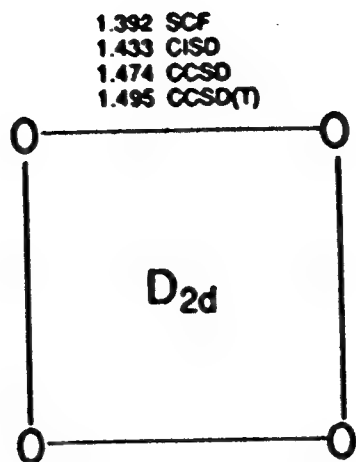
66.6° SCF
73.3° CISD
80.3° CCSD
80.3° CCSD(T)



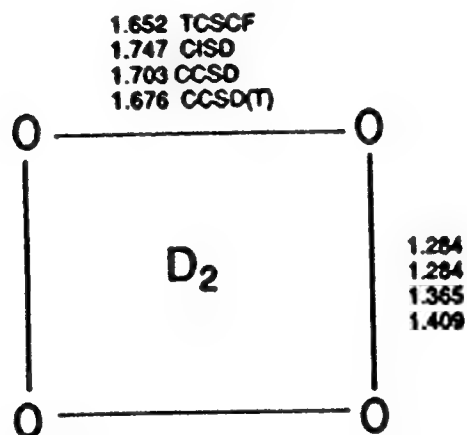
C_2 TORSIONAL ANGLES = 35.7°(2), 43.4°, 62.1°
34.3°(2), 41.9°, 53.0°
32.3°(2), 39.4°, 43.5°
31.9°(2), 36.1°, 40.7°

Figure 2. Predicted angles associated with three stationary points on the O_4 potential energy hypersurface from a side-on perspective: (a) the D_{2d} equilibrium geometry; (b) the D_2 stationary point; (c) the C_2 stationary point. Internuclear distances are shown in Figure 3.

2(a)



2(b)



2(c)

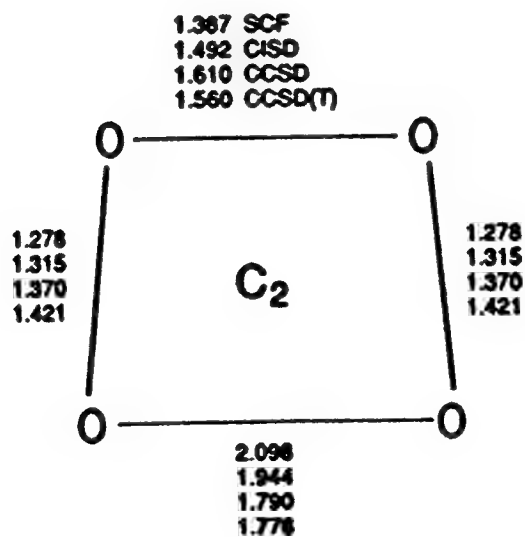


Figure 3. Three stationary points on the O_4 potential energy hypersurface from a top-down perspective (a) the D_{2d} equilibrium geometry, (b) the D_2 stationary point; (c) the C_2 stationary point. Bond angles are shown in Figure 2.

molecules. It is helpful to display the present oxygen ring dissociation energies on a per-atom basis, e.g. for O_6 to divide the quantity

$$E(O_6) - 3E(O_2)$$

by six. When this is done, the following array of dissociation energies may be fashioned:

Level of Theory	O_6	O_8	O_{12}
DZ SCF	22.8	21.3	20.9
DZ+P SCF	22.7	21.6	21.6
DZ+P MP2	16.8	15.4	
TZ+2P SCF	23.3		
TZ+2P MP2	16.5		

At every level of theory O_6 is a more energetic species than O_8 or O_{12} ; however the differences are less than two kcal/mole/O atom. Clearly, the thrust of future theoretical studies of oxygen rings should be directed toward the yet undetermined activation energies of these species for dissociation to separated diatomic oxygen molecules.

Our research on cyclic oxygen molecules has received attention within both the HEDM community and the broader scientific community. An example is Ivan Amato's feature news article "The Ascent of Odorless Chemistry," in the 17 April, 1992 issue of *Science*. Amato's article highlights the AFOSR's theoretical HEDM research in general and our research on O_4 and O_8 in particular.

2. Dodecahedral N_{20}

The intense scientific and popular interest in the C_{60} molecule has naturally raised the question whether other important cluster species have been systematically overlooked.

Our interest in this respect arises from a comparison with the dodecahedrane molecule $C_{20}H_{20}$, the subject of an intense organic synthesis quest that ended in 1982 with the work of Paquette. Isoelectronic with $C_{20}H_{20}$ would be the dodecahedral N_{20} molecule, which presumably would also display I_h symmetry, as seen in Figure 4.

Assuming that dodecahedral N_{20} can be synthesized, it is *not* expected to rival the remarkable stability of C_{60} . Assuming that the thirty equivalent nitrogen-nitrogen single bonds are unstrained, N_{20} would be bound by roughly

$$30 \times (40 \text{ kcal/mole}) = 1200 \text{ kcal/mole}$$

relative to twenty infinitely separated nitrogen atoms. For comparison ten nitrogen molecules (N_2) are bound by

$$10 \times (225 \text{ kcal/mole}) = 2250 \text{ kcal/mole}$$

relative to the same set of twenty nitrogen atoms. Thus our back-of-the-envelope calculation suggests that dodecahedral N_{20} will lie above separated N_2 molecules by roughly 105 kcal per mole of N_2 molecules. One concludes that N_{20} with its weak nitrogen-nitrogen single bonds would be a reasonable candidate for a high energy density material (HEDM).

Ab initio quantum mechanical methods have been applied to the I_h point group isomer of N_{20} and confirm our qualitative estimates. Dodecahedral N_{20} is predicted to be a relative minimum on its potential energy hypersurface, lying above separated nitrogen molecules by about 50 kcal per mole of nitrogen atoms. Vibrational frequencies, infrared intensities, and ionization potentials have also been predicted (reference 9 above).

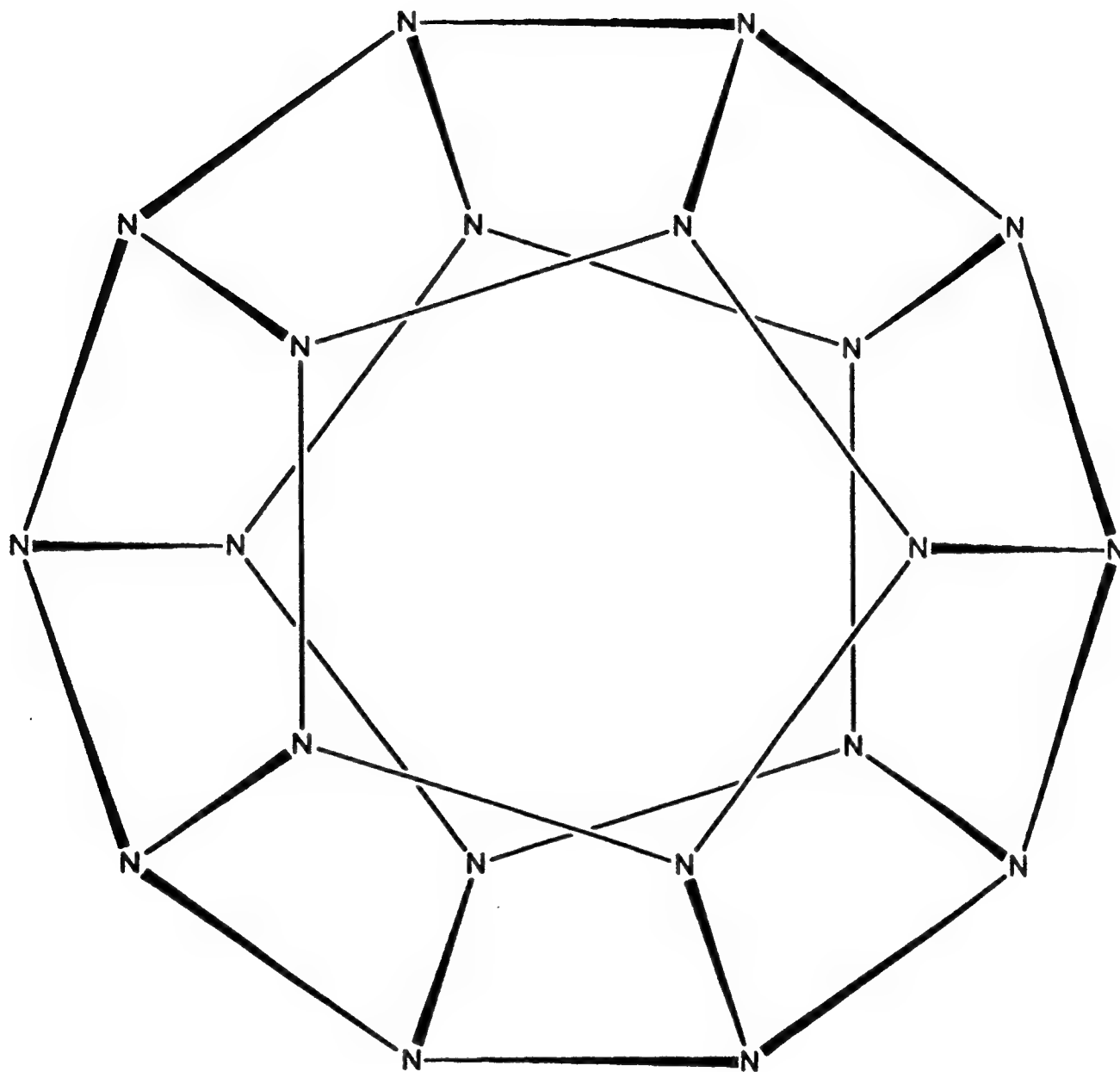


Figure 4. The dodecahedral (I_h symmetry) N_{20} molecule. All atoms are equivalent and all bonds are single nitrogen-nitrogen bonds.

3. The $\text{PO}_3^- (\text{H}_2\text{O})_n$ and $\text{H}_2\text{PO}_4^- (\text{H}_2\text{O})_{n-1}$ Systems and their Interconversions.

Over the past five years, as part of this AFOSR grant's objectives, I have made four scientific visits to the Geophysics Laboratory, Hanscom Air Force Base. As a result we engaged initially in collaborative research with Dr. Carol A. Deakyne, then working with John Paulson's group at Hanscom (now a faculty member at Eastern Illinois University), and more recently in research supportive of the experimental efforts at Hanscom. A significant part of the present grant period has been devoted (references 10 and 21 above) to the $\text{PO}_3^- (\text{H}_2\text{O})_n \rightarrow \text{H}_2\text{PO}_4^- (\text{H}_2\text{O})_{n-1}$ research explicitly proposed three years ago.

The $\text{PO}_3^- (\text{H}_2\text{O})_n$ clusters ($n = 1, 2$, and 3) have been studied using *ab initio* quantum mechanical methods. The most important finding is that the clusters prefer to form high symmetry double-donor double-acceptor hydrogen bonds between the PO_3^- anion and the H_2O molecules. The hydrogen bond lengths increase and the dissociation energies decrease with the addition of successive water molecules. The hydrogen bond in $\text{PO}_3^- \bullet (\text{H}_2\text{O})$ has a dissociation energy ($D_0 = 13.3 \text{ kcal mol}^{-1}$) about $0.5 \text{ kcal mol}^{-1}$ less than that for $\text{NO}_3^- \bullet \text{H}_2\text{O}$. The D_{3h} $\text{PO}_3^- \bullet (\text{H}_2\text{O})_3$ theoretical results do not agree with the experimental thermochemistry concerning the nature of the hydration of $\text{PO}_3^- \bullet (\text{H}_2\text{O})_2$ by the third water molecule.

Several mechanisms for the isomerization reactions of the $\text{PO}_3^- \bullet (\text{H}_2\text{O})_n$ clusters ($n = 1, 2$, and 3) to $\text{H}_2\text{PO}_4^- \bullet (\text{H}_2\text{O})_{n-1}$ have also been studied, resulting in predictions of the transition state structures, isomerization barrier heights, exothermicities and products. Basis sets as large as triple zeta plus double polarization plus f functions have been used with self-consistent-field, second-order perturbation theory, configuration interaction, and coupled cluster methods. The isomerization barrier (ΔG°) for $\text{PO}_3^- \bullet (\text{H}_2\text{O})$ to H_2PO_4^- is 32 kcal mol^{-1} at the DZP+diff SCF level, 25 kcal mol^{-1} at the DZP CISD level, and 22 kcal mol^{-1} at the DZP+diff MP2 level. The isomerization barriers for $\text{PO}_3^- \bullet (\text{H}_2\text{O})_2$ and $\text{PO}_3^- \bullet$

$(\text{H}_2\text{O})_3$ are lower by only a few kcal mol^{-1} than for $\text{PO}_3^- \bullet \text{H}_2\text{O}$ via four-centered transition states and lower by about 5 kcal mol^{-1} by six-center transition states. The PO_3^- anion is thermodynamically stable in the gas phase only when the $\text{PO}_3^- : \text{H}_2\text{O}$ molar ratio is below 1 : 3. However, even with the 1 : 3 molar ratio, the $\text{PO}_3^- \bullet (\text{H}_2\text{O})_3$ cluster is expected to be a product along with $\text{H}_2\text{PO}_4^- \bullet (\text{H}_2\text{O})_2$.

The H_2PO_3^- anion forms double-donor double-acceptor hydrogen bonds with H_2O similar to those predicted for PO_3^- . The C_2 symmetry conformation of H_2PO_4^- is more stable than the C_s form, while the C_{2v} conformation is a stationary point with two imaginary vibrational frequencies. The potential energy surfaces for $\text{H}_2\text{PO}_4^- \bullet \text{H}_2\text{O}$ and $\text{H}_2\text{PO}_4^- \bullet (\text{H}_2\text{O})_2$ are qualitatively similar to that for isolated H_2PO_4^- . The exothermicities ($-\Delta H^\circ$) of the reactions $\text{PO}_3^- \bullet (\text{H}_2\text{O})_n \rightarrow \text{H}_2\text{PO}_4^- \bullet (\text{H}_2\text{O})_{n-1}$ are 18 kcal mol^{-1} ($n=1$), 22 kcal mol^{-1} ($n=2$), and 21 kcal mol^{-1} ($n=3$) at the DZP+diff SCF level of theory. The DZP+diff SCF hydration exothermicity of H_2PO_4^- [i.e. $-\Delta H^\circ$ for $\text{H}_2\text{PO}_4^- + \text{H}_2\text{O} \rightarrow \text{H}_2\text{PO}_4^- \bullet (\text{H}_2\text{O})$] is 14 kcal mol^{-1} , while that for $\text{H}_2\text{PO}_4^- \bullet \text{H}_2\text{O}$ is 8 kcal mol^{-1} . The analogous hydration exothermicities for the isomers $\text{PO}_3^- \bullet \text{H}_2\text{O}$ and $\text{PO}_3^- \bullet (\text{H}_2\text{O})_2$ are 11 and 10 kcal mol^{-1} , respectively. Although much progress has been made, several questions remain concerning the relationships between the present theoretical results and existing experiments.

III. List of Participating Professionals

A. Senior Research Personnel:

Professor Henry F. Schaefer III

Dr. David A. Horner

Dr. Roger S. Grev

Dr. Mingzuo Shen

Dr. Yaoming Xie

Dr. Igor Ignatyev

Dr. Andrey Blizynuk

Dr. Congxin Liang

Dr. Tracy P. Hamilton

B. Junior Research Personnel:

Edward T. Siedl

Ching-Han Hu

Buyong Ma

Seung-Joon Kim

Zoltan Palagyi

John M. Galbraith

George Vacek

Bradley J. DeLeeuw

T. Daniel Crawford

Cynthia Meredith

Peter Schreiner

Evan E. Bolton

IV. Relation to Work at Hanscom Air Force Base

See Section II. B. 3 above.

Is there a transition state for the unimolecular dissociation of cyclotetraoxygen (O_4)?

Edward T. Seidl and Henry F. Schaefer III

Center for Computational Quantum Chemistry, University of Georgia, Athens, Georgia 30602

(Received 8 July 1991; accepted 8 October 1991)

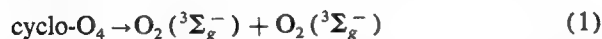
The cyclo- O_4 molecule is isoelectronic with cyclobutane and has been mentioned as a potential new high energy density material (HEDM). The important unresolved question has been whether or not cyclo- O_4 is a genuine minimum on the O_4 potential energy hypersurface. Here the transition state for cyclo- O_4 dissociation to two O_2 molecules has been located at a number of levels of theory using a double zeta plus polarization (DZP) basis set. The theoretical methods with which the transition state geometry was optimized include two-configuration self-consistent-field (TCSCF), configuration interaction including all single and double excitations (CISD), coupled cluster including all single and double excitations (CCSD), and the latter with a noniterative correction for connected triple excitations, CCSD(T). The equilibrium geometry of O_4 has D_{2d} symmetry, while a stationary point of D_2 symmetry is of Hessian index two (i.e., two imaginary vibrational frequencies) at the highest level of theory, DZP CCSD(T). The true transition state lies only slightly lower energetically (classical barrier 7.9 kcal/mole) and is of C_2 symmetry with the DZP CCSD(T) method. The activation energy was predicted in a completely consistent manner to be 6.2 kcal/mole. The possibility that this barrier could disappear entirely at higher levels of theory is discussed. It is concluded that the O_4 barrier is too low for O_4 to be useful as a HEDM.

INTRODUCTION

In recent years one of the more interesting proposals for new high energy density materials has been that of the oxygen rings.¹⁻³ It is now well-established from theory that the cyclic systems O_4 , O_6 , O_8 , and O_{12} all lie significantly higher in energy than the appropriate numbers of separated oxygen molecules O_2 . What is not at all established are the barrier heights for the unimolecular dissociation of these oxygen rings. Among these, the cyclo- O_4 system has the highest energy content per mass and is expected to have the smallest activation energy for dissociation energy.^{1,3}

Previous theoretical studies of cyclo- O_4 have used the self-consistent-field (SCF), single and double excitation configuration interaction (CISD), and single and double excitation coupled cluster (CCSD) methods.^{1,3} The heat of formation of O_4 is predicted to be 83 kcal/mole at the highest level of theory considered to date.³ Thus O_4 is predicted on a per atom basis to lie 21 kcal/mole above two separated O_2 molecules.

From an electronic viewpoint, the dissociation process



is surprisingly complicated, considering that only four atoms are involved. To begin, one starts with a closed-shell singlet state (1A_1 , O_4 , D_{2d} symmetry) involving only single bonds, but ends up with two triplet states involving multiple bonding. Thus, the dissociation reaction involves extensive spin uncoupling and bond rearrangement. Hence, it is impossible for a single configuration wave function that is an exact eigenfunction of S^2 to qualitatively describe both the reactant and product molecules. Therefore, the theoretical prediction of a reliable barrier height for reaction (1) represents a significant challenge.

THEORETICAL APPROACH

The situation described above may not be quite as bleak as pictured in the previous paragraph. This is because we may not need to describe with great exactitude the product triplet oxygen molecules. In principle only the reactant O_4 molecule and the transition state must be treated in a theoretically equivalent manner. For a highly exothermic reaction such as Eq. (1), Hammond's postulate⁴ suggests that the transition state may closely resemble the reactant molecule(s), both structurally and presumably electronically as well. Nevertheless, the history of attempts to reliably predict activation energies from *ab initio* theory⁵ suggests that a method that does poorly for the dissociation limit $O_2(^3\Sigma_g^-) + O_2(^3\Sigma_g^-)$ may yield a barrier height that is too high.

In the present research a double zeta plus polarization (DZP) basis set was used throughout. This is the standard $O(9s5p1d/4s2p1d)$ basis set of Huzinaga⁶ and Dunning.⁷ The d function polarization functions had orbital exponents $\alpha_d(O) = 0.85$. The full set of six Cartesian d -like functions (x^2 , xy , xz , y^2 , yz , and z^2 multiplied by $e^{-\alpha r^2}$) was used.

The simplest level of theory used to attempt to locate the $O_4 \rightarrow 2O_2$ transition state was the DZP self-consistent-field (SCF) method. Stationary points were located using analytic gradient methods⁸ and vibrational frequencies evaluated with analytic second derivative techniques.^{9,10} The two-configuration (TC) SCF method was similarly used in an attempt to describe some of the bond making/breaking and spin recoupling effects that will begin to be visible at the transition state for this highly exothermic unimolecular reaction. Analytic gradients¹¹ were used to locate stationary points and analytic second derivative methods¹² to evaluate

harmonic vibrational frequencies.

The next theoretical method used was configuration interaction including all single and double excitations (CCSD).¹³ In the CI wave functions the four oxygen 1s-like core molecular orbitals are held doubly occupied in all configurations. Similarly the four highest-lying virtual orbitals (core counterparts) are deleted from the CI procedure. The CI wave functions were determined using the shape-driven graphical unitary group approach.¹⁴ Stationary points were located via analytic gradient methods.^{15,16} Harmonic vibrational frequencies were evaluated using finite differences of analytic gradients. For the C₂ stationary point the evaluation of harmonic vibrational frequencies required excursions into C₁ symmetry, in which there are 140,185 configurations in the CCSD wave functions.

The single and double excitation coupled cluster (CCSD) method developed by Purvis and Bartlett¹⁷ was next applied to the O₄ transition state for unimolecular dissociation. The composition of the CCSD wave functions^{18,19} is strictly analogous to the CISC treatment just described; i.e., the four lowest-lying occupied SCF MO's were constrained to be doubly occupied in all configurations and the four highest-lying virtual SCF MO's were deleted from the CCSD procedure. Stationary points were identified using analytic gradients²⁰ and harmonic vibrational frequencies were evaluated via finite differences of analytic gradients.

The explicit treatment of connected triple excitations was accomplished using the CCSD(T) method first suggested by Raghavachari, Trucks, Pople, and Head-Gordon.²¹ The highly efficient implementations of the CCSD(T) total energy and analytic gradient methods were those of Scuseria and Lee²² and Scuseria,²³ respectively.

THE D_{2d} EQUILIBRIUM GEOMETRY AND VIBRATIONAL FREQUENCIES OF O₄

Since this problem has been examined extensively elsewhere,^{1,3} the discussion here is restricted to the CCSD(T) method, which is more advanced than the CISC¹ and CCSD³ methods used in previous studies. Figures 1(a) and 2(a) report the equilibrium geometry of cyclotetraoxygen predicted at several levels of theory. As expected,²⁴ the CCSD(T) bond distance in O₄ is longer (by 0.021 Å) than that predicted at the CCSD level, which does not include connected triple excitations.

With much larger basis sets (e.g., TZ2Pf), the CCSD(T) bond distances will decrease by perhaps 0.01–0.02 Å, bringing the final O–O length close to that observed experimentally for hydrogen peroxide, namely 1.475 Å. In this sense the O–O single bonds in cyclo-O₄ seem relatively normal, given that O–O single bonds are always weak. In addition, the four membered oxygen ring becomes slightly more puckered (the O–O–O bond angle is decreased by 0.3° and the torsional angle increased by 1.0°) in going from DZP CCSD to DZP CCSD(T).

The predicted harmonic vibrational frequencies at the same four levels of theory are given in Table I. There are some significant differences between the CCSD(T) predictions and the CCSD results reported earlier.⁴ As before the totally symmetric ring stretch has the highest vibrational

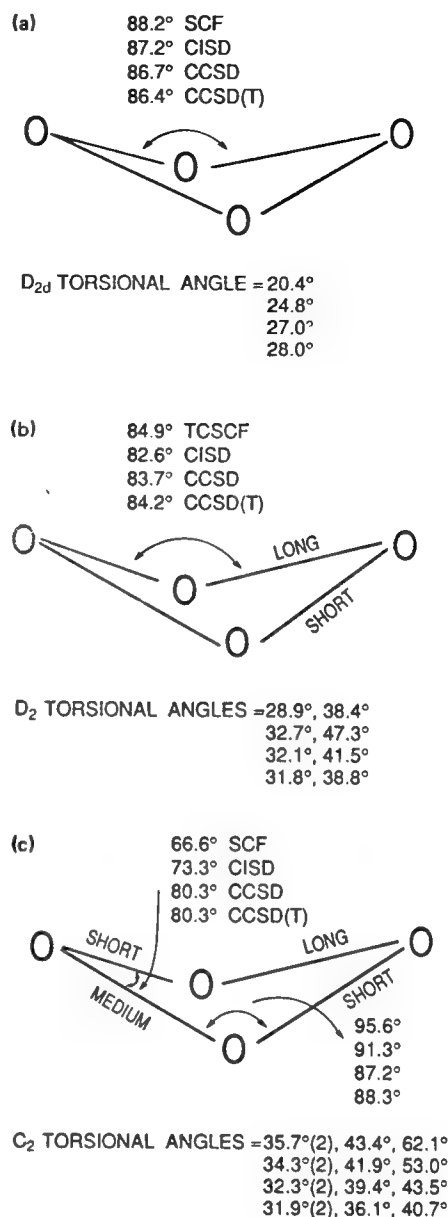


FIG. 1. Side-on perspective. Predicted angles associated with three stationary points on the O₄ potential energy hypersurface: (a) the D_{2d} equilibrium geometry; (b) the D₂ stationary point; (c) the C₂ stationary point. Internuclear distances are shown in Fig. 2.

frequency, and is reduced by 78 cm⁻¹ or 8.2% from CCSD to CCSD(T). With the CCSD(T) method, the second highest harmonic vibrational frequency is the B₂ ring deformation, which decreases by 48 cm⁻¹ or 5.7% from the CCSD value.

The third CCSD(T) harmonic frequency, the B₁ ring deformation, at 783 cm⁻¹, was previously second highest with the CCSD method. It drops sharply, by 110 cm⁻¹ or 12.3%, from CCSD to CCSD(T). A plausible explanation why the B₁ frequency drops more than the B₂ mode with the inclusion of connected triple excitations is the fact that the B₁ is the mode leading primarily to dissociation. This is con-

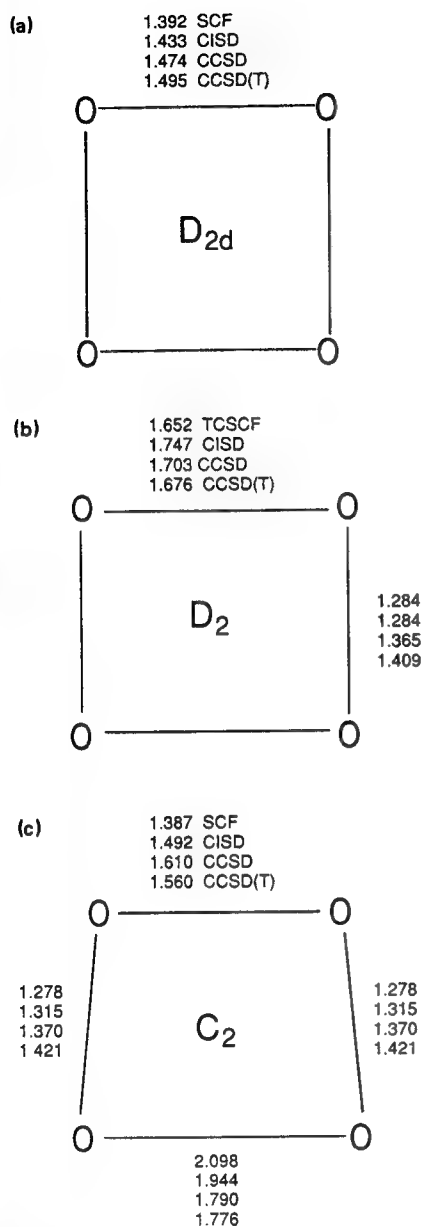


FIG. 2. Top-down perspective. Three stationary points on the O_4 potential energy hypersurface: (a) the D_{2d} equilibrium geometry; (b) the D_2 stationary point; (c) the C_2 stationary point. Bond angles are shown in Fig. 1.

TABLE I. Predicted harmonic vibrational frequencies (in cm^{-1}) for the D_{2d} equilibrium geometry of O_4 .

Assignment		DZP SCF	DZP CISD	DZP CCSD	DZP CCSD(T)
A_1	Ring stretch	1254	1104	955	877
B_1	Ring deformation	1224	1078	893	783
E	Ring deformation	1112	950	784	678
B_2	Ring deformation	1067	942	841	793
A_1	Ring puckering	351	397	397	396

sistent with the fact (see below) that the classical barrier height drops significantly from CCSD to CCSD(T). In this context, a similarly large drop in the E vibrational frequency, 106 cm^{-1} or 13.5%, can be rationalized by the contribution of one of the E components to the dissociation pathway.

The lowest vibrational frequency, the A_1 ring puckering, is virtually unchanged from CISD to CCSD to CCSD(T). A discussion of predicted IR intensities for cyclo- O_4 is given in Ref. 1. To summarize, the two A_1 and the B_1 fundamentals are forbidden, the B_2 frequency (793 cm^{-1} here) has a weak IR intensity (1.2 km/mole), and that of the E mode is very weak.

THE D_2 STATIONARY POINT

Since the $D_{2d}O_4$ structure is a genuine minimum at all four levels of theory utilized in the previous section, there should be a transition state for unimolecular dissociation at each level. We must, however, state candidly that the search for the first of these transition states was not immediately successful. In fact, the present research has been underway for 3 years. Of course, the availability of one transition state greatly simplified the identification of the others. The discussion that follows only became possible after several of the transition states were located.

Going down in symmetry from point group D_{2d} , the D_2 group is a logical next choice. The D_2 stationary point geometries are given in Figs. 1(b) and 2(b). Note that we were unable to find a D_2 stationary point at the single-configuration SCF level of theory. This is probably an indication that no such stationary point exists at this level of theory.

On first glance the D_2 stationary point looks similar to the D_{2d} equilibrium geometry. However, the D_2 structure has two distinct torsional angles within the D_2 structure. The extent of bond alternation in the D_2 stationary point is also significant, the differences in bond distances being 0.314 \AA (CISD), 0.228 \AA (CCSD), and 0.181 \AA , CCSD(T).

At each level of theory, the longer of the two distinct O–O bonds is too long to be a normal single bond. Interestingly, these longer bond distances show exactly the opposite behavior with level of theory as do the equilibrium geometry distances. That is, the longer D_2 oxygen–oxygen distances decrease with level of theory, from 1.747 \AA (CISD) to 1.702 \AA (CCSD) to 1.676 \AA , CCSD(T). The effect of electron correlation is to drive the D_2 stationary point geometry back in the direction of the D_{2d} equilibrium geometry.

The expected behavior with level of theory is seen for the shorter of the D_2 bond distances, which are 1.284 \AA (CISD), 1.365 \AA (CCSD), and 1.409 \AA , CCSD(T). Note also that these D_2 distances are uniformly shorter than the equilibrium (D_{2d} structure) distances, by 0.149 \AA (CISD), 0.109 \AA (CCSD), and 0.086 \AA , CCSD(T). Since the bond distance in ground state diatomic O_2 is much shorter, $r_e = 1.208 \text{ \AA}$, the D_2 structure is truly intermediate between cyclo- O_4 and two separated oxygen molecules.

The predicted harmonic vibrational frequencies for the D_2 stationary point are given in Table II for three levels of theory. The DZP CISD vibrational frequencies exhibited erratic behavior and are considered untrustworthy. Interestingly, the TCSCF method characterizes the D_2 structure as a

TABLE II. Predicted harmonic vibrational frequencies (in cm⁻¹) for the D₂ stationary point geometry of O₄.

	Assignment	DZP TCSCF	DZP CCSD	DZP CCSD(T)
A ₁	Ring stretch	1233	1022	928
B ₁	Ring deformation (bend)	990	833	781
B ₂	Ring deformation (O-O asymmetric stretch)	1009	752	538
A ₁	Ring puckering	577	549	516
B ₃	Ring deformation (O-O asymmetric stretch)	656	124i	194i
A ₁	Ring deformation (stretch)	1780i	997i	1016i

true transition state, with only one imaginary vibrational frequency. However, the more reliable CCSD and CCSD(*T*) methods concur that the D₂ structure has two imaginary vibrational frequencies. The lower of these [194i cm⁻¹ with the CCSD(*T*) method] is the B₃ O-O asymmetric stretch, while the higher (1016i) is the A₁ ring deformation (stretch). To find the true transition state with the CCSD and CCSD(*T*) methods, one must proceed to lower symmetry.

THE C₂ STATIONARY POINT

Since the D₂ structure has two imaginary vibrational frequencies at the highest level of theory, CCSD(*T*), our search for the transition state must continue to lower symmetry. Therefore, several stationary point structures of C₂ symmetry are presented in Figs. 1(c) and 2(c). The C₂ structures have three distinct O-O distances and two distinct O-O-O angles.

The longest of the C₂ structure O-O distances is 1.944 Å (CISD), 1.790 Å (CCSD), and 1.776 Å, CCSD(*T*). These distances exceed those of the longer O-O distance in the D₂ stationary point by 0.197 Å (CISD), 0.088 Å (CCSD), and 0.100 Å, CCSD(*T*). The obvious conclusion is that the O-O bond in the C₂ structure is more nearly broken than that for the D₂ structure.

At the highest level of theory, CCSD(*T*), the two equivalent short O-O distances are 1.420 Å, or 0.075 Å shorter than for the D_{2d}O₄ equilibrium geometry. The single intermediate O-O distance is 1.560 Å or 0.065 Å longer than for the O₄ minimum at the DZP CCSD(*T*) level. Inasmuch as both of the O-O distances are much longer than in diatomic ³Σ_g O₂ (1.208 Å), it is clear that the C₂ structure occurs quite "early" on any proposed reaction pathway. Of course, this confirms the qualitative prediction from Hammond's postulate¹⁴ that for a highly exothermic reaction the transition state should resemble the reactants.

The distinct O-O-O bond angles for the C₂ structure are 80.3° and 88.3° at the DZP CCSD(*T*) level of theory. With the D₂ and D_{2h} structures these two angles are equivalent and have the values 84.2° (D₂) and 86.4° (D_{2d}). It would be of interest to follow these angles and the other O₄ geometrical parameters on the reaction pathway from the transition state to two separated O₂ molecules; however, even the CCSD(*T*) method provides a very poor representation of the wave function as one goes beyond the transition state toward the products.

The predicted harmonic vibrational frequencies at several levels of theory for the C₂ stationary point are reported in Table III. Recall from the previous section that the DZP TCSCF D₂ structure was a true transition state - thus there is no C₂ stationary point expected with the DZP TCSCF method. One of the surprising features of this research was that we did find a C₂ stationary point, which proved to be another transition state. This DZP TCSCF transition state actually lies energetically below the DZP SCF D_{2d} equilibrium geometry. Thus, there is another minimum on the O₄ TCSCF potential energy hypersurface in addition to the expected cyclo-O₄, O₂···-O₂, and infinitely separated O₂ + O₂.

The DZP TCSCF minimum referred to in the previous paragraph is of C₂ symmetry, with one short O-O distance (1.379 Å), two of medium length (1.393 Å), and one long O-O distance (1.535 Å). The first and last of these bond distances are significantly shorter than those for C₂ transition state predicted from the DZP CCSD(*T*) method, the most reliable method used in this research. The energy of this DZP TCSCF minimum is -299.118 81 hartrees, or 30.3 kcal below the SCF energy for the D_{2d} equilibrium ge-

TABLE III. Predicted harmonic vibrational frequencies (in cm⁻¹) for the C₂ stationary point geometry of O₄. Note in Figs. 1 and 2 that the C₂ structure has two short O-O bonds, one medium length O-O bond, and one long O-O bond.

		DZP SCF	DZP TCSCF ^a	DZP CISD	DZP CCSD	DZP CCSD(T)
A	Short O-O symmetric stretch	1334	1157	1184	1017	918
A	Medium O-O stretch	913	1178	525	180	277
B	Ring deformation (bend)	906	834	897	833	779
A	Ring puckering	723	460	663	548	513
A	Long O-O stretch	556i	502i	868i	950i	925i
B	Short O-O asymmetric stretch	1208i	1033	1202	747	515

^a Note that the energy of this second (see Table II for the first) DZP TCSCF transition state is lower than the DZP SCF energy of the expected cyclic equilibrium geometry. See text for discussion.

ometry. This C_2 minimum lies only 2.1 kcal/mole below the C_2 transition state at the DZP TCSCF level of theory. The fact that the DZP TCSCF C_2 minimum is not genuine at higher levels of theory is confirmed by single point energies. This C_2 DZP TCSCF minimum lies above the D_{2d} minimum by 5.3, 8.1, and 10.3 kcal/mole with the CISD, CCSD, and CCSD(T) methods, respectively.

The DZP CISD, CCSD, and CCSD(T) methods concur that the C_2 stationary point is a true transition state. However, several of the changes in predicted vibrational frequencies with level of theory are remarkable. For example, the ordering of the three real oxygen-oxygen stretching vibrational frequencies changes radically from CISD to CCSD. With CISD, the asymmetric stretch of the two short O-O bonds lies highest (1202 cm^{-1}); but this is reduced to 747 cm^{-1} (CCSD) and 515 cm^{-1} with the CCSD(T) method. In contrast the stretching frequency of the symmetric combination of short O-O bonds changes in the anticipated manner, from 1184 cm^{-1} (CISD) to 1017 cm^{-1} (CCSD) to 918 cm^{-1} for the CCSD(T) method. Therefore, while the asymmetric O-O stretch lies 18 cm^{-1} higher with CISD, it lies 403 cm^{-1} below the symmetric stretch with the higher level CCSD(T) method.

The stretching frequency of the O-O bond of medium length [1.560 \AA with the CCSD(T) method] is consistently lowest of the three real O-O vibrations, but it drops precipitously from CISD (525 cm^{-1}) to CCSD (180 cm^{-1}) and then comes part of the way back, to 277 cm^{-1} with the CCSD(T) method. In light of these irregularities, it is surprising that the fourth O-O stretch, the reaction coordinate, is reasonably inert to changes in the level of theory. This A symmetry long O-O stretch is predicted to be $868i\text{ cm}^{-1}$ (CISD), $950i\text{ cm}^{-1}$ (CCSD), and $925i\text{ cm}^{-1}$ with the CCSD(T) method.

There is little doubt in our minds that the CCSD(T) level of theory is the most reliable for the prediction of the structure and vibrational frequencies of the C_2 stationary point. This does not mean that the C_2 stationary point might not disappear at some higher level of theory. But the reaction coordinate corresponding to the stretching of the long O-O bond is consistent with dissociation to two diatomic oxygen molecules.

If we assume the zero-point vibrational energy to be one-half the sum of the harmonic vibrational frequencies, the CCSD(T) ZPVE values are 6.01 kcal/mole for the D_{2d} equilibrium geometry and 4.29 kcal/mole for the C_2 transition state. This means, in simple transition state theory, that the activation energy E_a is predicted to be 1.72 kcal/mole less than the classical barrier height.

DOES THE USE OF ANY METHOD STARTING FROM A HARTREE-FOCK REFERENCE FUNCTION MAKE SENSE?

We noted in the Introduction that the description of the transition state for the $O_4 \rightarrow 2O_2$ reaction will be a severe test for any method that begins with single configuration SCF theory. With the configuration interaction and coupled cluster results in hand, we can now address this question in a

more quantitative manner.

In the CISD wave functions the coefficient of the SCF configuration is 0.923 (D_{2d} minimum), 0.909 (D_2 , Hessian index two), and 0.910 (C_2 transition state). Thus the SCF wave function amounts to 85.2% (D_{2d}), 82.6% (D_2), and 82.8% (C_2) of the total wave function. For a system with only 24 valence electrons, the latter two percentages are sufficiently low to cause concern about the reliability of the CISD approach.

For coupled cluster methods, the T_1 diagnostic^{26,27} has proven to be helpful in assessing the multireference nature of wave functions. For the D_2 and C_2 stationary points, the diagnostic T_1 has the values 0.064 and 0.041, respectively. Both values indicate that the true wave function has significant multireference character, but the situation is much less serious with the C_2 transition state. Comparison with the FOOF molecule is of interest, because O_4 and FOOF differ by only two electrons, and FOOF has been a notoriously difficult molecule to describe theoretically.^{23,26}

In their original discussion of the T_1 diagnostic, Lee and co-workers²⁶ reported a value of 0.033 for FOOF. This suggests that the O_4 transition state may be slightly more difficult to treat theoretically than FOOF. The reader should note, however, that the CCSD(T) method has recently been demonstrated²³ to give reliable results for the problematical molecular structure of FOOF. Thus there is some basis for cautious optimism that the CCSD(T) method might be suitable for the O_4 transition state.

Another way to analyze the multireference character of the C_2 stationary point wave functions is in terms of natural orbitals. For this purpose the DZP CISD wave function was recomputed at its transition state geometry in terms of the CISD natural orbitals. The single configuration reference function ($\dots 9a^2 7b^2$) has a coefficient of 0.912, actually a bit higher than in the CISD wave function built upon the canonical Hartree-Fock molecular orbitals.

There are three other configurations with coefficients greater than 0.05, namely

$$9a^2 \rightarrow 8b^2, \quad C = 0.171,$$

$$8a^2 \rightarrow 9b^2, \quad C = 0.094,$$

$$7a7b \rightarrow 10a10b, \quad C = 0.069.$$

The configuration with coefficient 0.171, corresponding to 2.9% of the wave function, is the one included in the TCSCF treatment. Furthermore, there are another 16 configurations with coefficients between 0.025 and 0.047. Critical (i.e., near the HOMO-LUMO gap) natural orbital occupation numbers are

$$1.967 \quad 7a$$

$$1.966 \quad 7b$$

$$1.953 \quad 8a$$

$$1.911 \quad 9a$$

$$0.097 \quad 8b$$

$$0.048 \quad 9b$$

$$0.031 \quad 10a$$

$$0.030 \quad 10b.$$

TABLE IV. Total energies (in hartrees) and relative energies (in kcal/mole) associated with the O₄ → 2O₂ unimolecular dissociation reaction. All theoretical methods employed the DZP basis set.

Theoretical method	Total energy O ₄ (¹ A ₁ , D _{2d})	Total energy D ₂ stationary point	ΔE(D ₂ - D _{2d})	Total energy C ₂ stationary point	Δ(C ₂ - D _{2d})
SCF	-299.070 57	(...) ^a	(...) ^a	-298.966 97	65.0
TCSCF	(...) ^b	-299.029 60	(25.7) ^c	(...) ^d	(...) ^d
CISD	-299.694 53	-299.632 11	39.2	-299.635 64	36.9
CISD + Davidson	(-299.787 52) ^e	(-299.748 92) ^e	24.2	(-299.749 63) ^e	23.8
CCSD	-299.807 72	-299.783 02	15.5	-299.783 09	15.5
CCSD(T)	-299.838 57	-299.825 81	8.0	-299.826 05	7.9

^aThere appears to be no D₂ stationary point at the DZP SCF level of theory.

^bThe expected two-determinant SCF wave function for the D_{2d} equilibrium geometry of O₄ is not appropriate since the lowest unoccupied molecular orbital (LUMO) is the doubly degenerate 5e MO.

^cIn light of footnote b, this energy difference is E(D₂ TCSCF) - E(D_{2d} SCF).

^dAt the DZP TCSCF level of theory, the D₂ structure is a true transition state (see text). Hence, the C₂ stationary point at this level of theory, refers to a different process; see text.

^eThese energies do not represent optimized stationary point geometries. The geometries used are the DZP CISD optimized stationary point geometries.

Although there is clearly multi-reference character in the C₂ wave function, this second analysis also holds out hope for advanced single reference models such as CCSD(T). This view is supported by recent work on the ozone and FOOF molecules.^{26,28}

THE BARRIER HEIGHT AND ACTIVATION ENERGY FOR O₄ DISSOCIATION

Total and relative energies pertinent to the O₄ unimolecular reaction are presented in Table IV. The decrease in classical barrier heights from 36.9 kcal (CISD) to 23.8 kcal (CISD plus Davidson correction)²⁹ to 15.5 kcal (CCSD) to finally 7.9 kcal with the CCSD(T) method is remarkable. These energetics make it very clear that the C₂ stationary point is poorly described by single-configuration Hartree-Fock theory.

One also notes in Table IV that although the geometries of the D₂ and C₂ stationary points are quite different, the energies are not. The energy lowerings in going from the D₂ stationary point to the C₂ stationary point are 2.3 kcal (CISD), 0.4 kcal (CISD plus Davidson correction), less than 0.1 kcal (CCSD), and 0.1 kcal for the CCSD(T) method. It is clear that the O₄ potential energy hypersurface is rather flat in the region between the D₂ and C₂ stationary points.

As discussed in the section above entitled "The C₂ stationary point" the difference in ZPVE's for the D_{2d} equilibrium geometry and the C₂ transition state is 1.7 kcal/mole. Thus the CCSD(T) activation energy for O₄ → 2O₂ is 6.2 kcal/mole.

CONCLUDING REMARKS

The question of whether or not cyclic O₄ is a genuine minimum on its potential energy hypersurface is a significant challenge to current theoretical methodologies. Among currently available techniques, only the multireference (MR) CISD method seems likely to give a definitive answer. The fact that contemporary MR-CISD methods rarely in-

clude analytic gradient techniques³⁰ may make it particularly difficult to locate the purported C₂ transition state on this extremely flat potential energy hypersurface. Also, the fact that such large drops in the barrier height accompanied the theoretical progression CISD → CISD + Q → CCSD → CCSD(T) suggest that a large MCSCF wave function may be required as a starting point.

Although it would be foolhardy to be insistent on this point, we suspect that some classical barrier (less than 7.9 kcal/mole) will remain on the O₄ → 2O₂ potential surface. A very high level multireference CISD treatment would be required to definitively settle this point. However, even an activation energy of 6.2 kcal/mole [the value predicted here by the CCSD(T) method] will be too small to make O₄ useful as a high energy density material (HEDM). In that sense, the most important scientific question has been answered here. Clearly the focus of future studies should shift to the larger oxygen rings such as the unstrained cyclo-O₈.

ACKNOWLEDGMENTS

This research was supported by the Air Force Office of Scientific Research under Grant No. AFOSR-87-0182. We thank Professor Gustavo Scuseria for the use of his recently developed CCSD(T) analytic gradient methodology.

¹E. T. Seidl and H. F. Schaefer, J. Chem. Phys. **88**, 7043 (1988).

²K. S. Kim, H. S. Kim, S. Kim, J. H. Jang, and H. F. Schaefer, J. Am. Chem. Soc. **111**, 7746 (1989); K. S. Kim, J. H. Jang, S. Kim, B.-J. Min, and H. F. Schaefer, J. Chem. Phys. **92**, 1887 (1990).

³K. M. Dunn, G. E. Scuseria, and H. F. Schaefer, J. Chem. Phys. **92**, 6077 (1990).

⁴G. S. Hammond, J. Am. Chem. Soc. **77**, 334 (1955).

⁵See, for example, H. F. Schaefer, J. Phys. Chem. **89**, 5336 (1985).

⁶S. Huzinaga, J. Chem. Phys. **42**, 1293 (1965).

⁷T. H. Dunning, J. Chem. Phys. **53**, 2823 (1970).

⁸P. Pulay, Mol. Phys. **17**, 197 (1969); **18**, 473 (1970).

⁹J. A. Pople, R. Krishnan, H. B. Schlegel, and J. S. Binkley, Int. J. Quantum Chem. Symp. **13**, 225 (1979).

¹⁰P. Saxe, Y. Yamaguchi, and H. F. Schaefer, J. Chem. Phys. **77**, 5647 (1982).

- ¹¹ J. D. Goddard, N. C. Handy, and H. F. Schaefer, *J. Chem. Phys.* **71**, 1525 (1979).
- ¹² Y. Yamaguchi, Y. Osamura, G. Fitzgerald, and H. F. Schaefer, *J. Chem. Phys.* **78**, 1607 (1983).
- ¹³ I. Shavitt, *Modern Theoretical Chemistry*, edited by H. F. Schaefer (Plenum, New York, 1977), Vol. 3, pp. 189–275.
- ¹⁴ P. Saxe, D. J. Fox, H. F. Schaefer, and N. C. Handy, *J. Chem. Phys.* **77**, 5584 (1982).
- ¹⁵ B. R. Brooks, W. D. Laidig, P. Saxe, J. D. Goddard, Y. Yamaguchi, and H. F. Schaefer, *J. Chem. Phys.* **72**, 4652 (1980).
- ¹⁶ J. E. Rice, R. D. Amos, N. C. Handy, T. J. Lee, and H. F. Schaefer, *J. Chem. Phys.* **85**, 963 (1986).
- ¹⁷ G. D. Purvis and R. J. Bartlett, *J. Chem. Phys.* **76**, 1910 (1982).
- ¹⁸ G. E. Scuseria, A. C. Scheiner, T. J. Lee, J. E. Rice, and H. F. Schaefer, *J. Chem. Phys.* **86**, 2881 (1987).
- ¹⁹ G. E. Scuseria, C. L. Janssen, and H. F. Schaefer, *J. Chem. Phys.* **89**, 7382 (1988).
- ²⁰ A. C. Scheiner, G. E. Scuseria, J. E. Rice, T. J. Lee, and H. F. Schaefer, *J. Chem. Phys.* **87**, 5361 (1987).
- ²¹ K. Raghavachari, G. W. Trucks, J. A. Pople, and M. Head-Gordon, *Chem. Phys. Lett.* **157**, 479 (1989).
- ²² G. E. Scuseria and T. J. Lee, *J. Chem. Phys.* **93**, 5851 (1990).
- ²³ G. E. Scuseria, *J. Chem. Phys.* **94**, 442 (1991).
- ²⁴ G. E. Scuseria, T. P. Hamilton, and H. F. Schaefer, *J. Chem. Phys.* **92**, 568 (1990).
- ²⁵ K. P. Huber and G. Herzberg, *Molecular Spectra and Molecular Structure IV. Constants of Diatomic Molecules* (Van Nostrand Reinhold, New York, 1979).
- ²⁶ T. J. Lee, J. E. Rice, G. E. Scuseria, and H. F. Schaefer, *Theor. Chim. Acta* **75**, 81 (1989).
- ²⁷ T. J. Lee and P. R. Taylor, *Int. J. Quantum Chem. Symp.* **23**, 199 (1989).
- ²⁸ T. J. Lee and G. E. Scuseria, *J. Chem. Phys.* **93**, 489 (1990).
- ²⁹ E. R. Davidson, in *The World of Quantum Chemistry*, edited by R. Daudel and B. Pullman (Reidel, Dordrecht, Holland, 1974), pp. 17–30.
- ³⁰ An exception is the method of M. Page, P. Saxe, G. F. Adams, and B. H. Lengsfeld, *J. Chem. Phys.* **81**, 434 (1984).

Three-Membered Rings of Carbon, Silicon, and Germanium: An Analysis of Thermodynamic Stability to Fragmentation

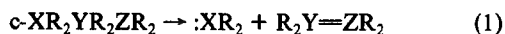
David A. Horner,^{*,†} Roger S. Grev,^{*,†} and Henry F. Schaefer III[†]

Contribution from the Departments of Chemistry and Physics, North Central College, Naperville, Illinois 60566, and Center for Computational Quantum Chemistry, University of Georgia, Athens, Georgia 30602. Received August 26, 1991

Abstract: Ab initio quantum mechanical methods have been used to determine the strain energies of all possible saturated three-membered rings, $c\text{-XH}_2\text{YH}_2\text{ZH}_2$, and the energetics of the decomposition reactions $c\text{-XH}_2\text{YH}_2\text{ZH}_2 \rightarrow \text{:XH}_2 + \text{H}_2\text{Y}=\text{ZH}_2$ for X, Y, Z = C, Si, Ge. The three-membered-ring (3MR) decomposition enthalpy can be semiquantitatively predicted from a simple model using the strain energies along with published single bond dissociation energies, π -bond energies, and divalent state stabilization energies. Of the ten rings studied, germirane ($c\text{-GeH}_2\text{CH}_2\text{CH}_2$) is by far the least stable with respect to dissociation, being only about 20 kcal/mol more stable than $\text{GeH}_2 + \text{H}_2\text{C}=\text{CH}_2$. Thus the lack of success of experimental efforts to form a germirane has a thermochemical origin. This observation also helps account for observed differences in methylene, silylene, and germylene addition reactions to dienes. The estimation of substituent effects on ring decomposition enthalpies is facilitated by this model.

Introduction

In recent years the three-membered rings comprising group 14 elements have received considerable attention.¹⁻⁶ Small-ring compounds seem to be inherently and enduringly interesting to chemists, due in large part to their high strain, novel ring bonding, and, in the case of group 14 cyclotrimetallanes, reactive bonds between heavy atoms (e.g. Si-Ge). The group 14 cyclotrimetallanes are not only interesting, they are also synthetically useful as convenient sources of highly reactive carbene-like species and dimetallenes, because they decompose photolytically via the reaction



where X, Y, Z = group 14 elements.^{2,3} In some cases thermolysis yields the same products.^{3,4,7,8}

Of the ten cyclotrimetallane rings made up of C, Si, and Ge, all have been synthesized to date except the three which contain

a single Ge atom. Among the latter group the germirane (GeC_2) ring is especially notable for its elusiveness. Germiranes have been

- (1) (a) Lambert, R. L.; Seyferth, D. J. *Am. Chem. Soc.* **1972**, *94*, 9246. (b) Ishikawa, M.; Matsuzawa, S.; Sugisawa, H.; Yano, F.; Kamitori, S.; Higuchi, T. *J. Am. Chem. Soc.* **1985**, *107*, 7706. (c) Batcheller, S.; Masamune, S. *Tetrahedron Lett.* **1988**, *29*, 3383. (d) Masamune, S. In *Silicon Chemistry*; Corey, E. R., Corey, J. Y., Gaspar, P. P., Eds.; Ellis Horwood: Chichester, England, 1988; Chapter 25.
- (2) (a) Masamune, S.; Hanzawa, Y.; Murakami, S.; Bally, T.; Blount, J. *J. Am. Chem. Soc.* **1982**, *104*, 1150. (b) Watanabe, H.; Okawa, T.; Kato, M.; Nagai, Y. *J. Chem. Soc., Chem. Commun.* **1983**, 781. (c) Murakami, S.; Collins, S.; Masamune, S. *Tetrahedron Lett.* **1984**, *25*, 2131. (d) Ando, W.; Tsumuraya, T. *Organometallics* **1988**, *7*, 1882. (e) Masamune, S.; Hanzawa, Y.; Williams, D. J. *Am. Chem. Soc.* **1982**, *104*, 6136. (f) Masamune, S.; Murakami, S.; Tobita, H.; Williams, D. J. *Am. Chem. Soc.* **1983**, *105*, 7776. (g) Tsumuraya, T.; Sato, S.; Ando, W. *Organometallics* **1990**, *9*, 2061. (h) Ando, W.; Tsumuraya, T. *Organometallics* **1988**, *7*, 1882.
- (3) (a) Boudjouk, P.; Samaraweera, U.; Sooriyakumaran, R.; Chrusciel, J.; Anderson, K. *Angew. Chem., Int. Ed. Engl.* **1988**, *27*, 1355. (b) Ando, W.; Tsumuraya, T. *J. Chem. Soc., Chem. Commun.* **1989**, 770.
- (4) (a) Baines, K. M.; Cooke, J. A.; Groh, R. J.; Joseph, B., Presented at the 24th Organosilicon Symposium, El Paso, TX, April 1991. (b) Baines, K. M.; Cooke, J. A. *Organometallics*. In press.

[†]North Central College.

[†]University of Georgia.

proposed as intermediates in several reactions but have never been detected,⁹ and an attempt to synthesize a germirane by reacting diazomethane with a germene has been unsuccessful.¹⁰ Other group 14 cyclotrimetallanes have been synthesized via reactions analogous to diazomethane addition to germene, suggesting that the enthalpy change associated with reaction 1 may be significantly lower for germirane than for other three-membered rings.

Qualitative reasons for the differing stabilities of cyclotrimetallane rings with respect to decomposition via reaction 1 may be understood by examining the various contributions to the enthalpy change of this reaction. Consider, for example, the decomposition of silacyclop propane, $c\text{-SiC}_2\text{H}_6$, to silylene, SiH_2 , and ethylene, C_2H_4 . The strengths of the Si-C bonds, the strength of the C-C π -bond, and the ring strain enthalpy are the obvious contributors to $\Delta H(1)$. Thus, because Si-C and C-C single bonds have nearly the same strength (within 2 kcal mol⁻¹),¹¹ the decomposition of silacyclop propane is correctly predicted to be less endothermic than that of cyclopropane due to the higher strain enthalpy of the silacyclop propane ring.⁶ However, this cursory analysis is *quantitatively* flawed. Boatz and Gordon⁶ found that ΔH_0 for the decomposition of $c\text{-SiC}_2\text{H}_6$ to SiH_2 and C_2H_4 is ca. 55 kcal mol⁻¹ less than ΔH_0 for the production of C_2H_4 and singlet CH_2 from cyclopropane, but they also found that the ring strain of silacyclop propane exceeds that of cyclopropane by no more than 14 kcal mol⁻¹. Thus, we are left with a difference of about 40 kcal mol⁻¹ between the reaction enthalpies for which there is no accounting!

Here we present the results of ab initio quantum mechanical determinations of the strain enthalpies¹² of the ten cyclotrimetallanes, $c\text{-XH}_2\text{YH}_2\text{ZH}_2$, composed of C, Si, and Ge atoms and the energetics of decomposition of these compounds via reaction 1. We will show that the decomposition enthalpies can be predicted semiquantitatively from a simple model which expresses the enthalpy of reaction 1 in terms of contributions from single bond dissociation enthalpies (BDE's),¹² strain enthalpy, π -bond enthalpy, and Walsh's so-called divalent state stabilization energy (DSSE).¹¹ It is the DSSE which accounts for most of the 55 kcal mol⁻¹ difference between the cyclopropane and silirane decomposition enthalpies mentioned above. Germirane is, by far, the least stable ring with respect to dissociation via reaction 1. The analysis of the enthalpy of decomposition in terms of the simpler component enthalpies allows for ready estimation of the effects of substituents on this reaction from known substituent effects on the individual components.

Ab Initio Quantum Mechanical Methods

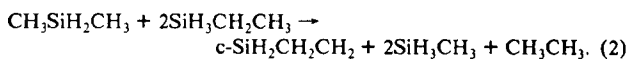
Molecular electronic energies were determined by optimizing structures using restricted Hartree-Fock self-consistent-field (SCF) analytic gradient techniques.¹³ Residual Cartesian and internal coordinate gradients did not exceed 10⁻⁶ au. Analytic second derivative methods¹⁴ were

used to evaluate the quadratic force constants and resulting harmonic vibrational frequencies at the SCF level. For the XH_2 molecules optimizations were carried out on the lowest singlet states.

Our basis set is of double- ζ plus polarization quality for heavy atoms and double- ζ for hydrogen, which is therefore designated DZ+d. Specifically, for carbon and silicon the Huzinaga-Dunning¹⁵ (9s5p/4s2p) and (11s7p/6s4p) sets were augmented with Cartesian polarization functions with exponents $\alpha_d(\text{C}) = 0.75$ and $\alpha_d(\text{Si}) = 0.50$. The hydrogen basis is the Huzinaga-Dunning¹⁵ (4s/2s) set. The germanium basis set is a 7s5p2d segmented contraction¹⁶ of Dunning's 14s11p5d primitive set,¹⁷ to which we have appended an additional polarization d-function [$\alpha_d(\text{Ge}) = 0.25$]. Thus, the germanium basis set is (14s11p6d/7s5p3d). Similarly constructed basis sets^{16,17} for the neighboring atoms gallium and arsenic yield excellent results for geometries and isomeric energy differences when compared to more flexibly contracted basis sets obtained from the same primitive basis set.¹⁸

Reaction enthalpies at 0 K were evaluated by adding to the difference in electronic energies of reactants and products, ΔE_{elec} , the difference in SCF zero-point harmonic vibrational energies ($\Delta ZPVE$) multiplied by a scale factor of 0.91. This scale factor provides an approximate correction for the overestimation of zero-point vibrational energies by the SCF method.¹⁹ To include the effects of electron correlation in estimates of the reaction enthalpies, we employed the size-extensive coupled cluster singles and doubles method (CCSD).²⁰ The CCSD electronic energy of each molecule was evaluated at its SCF-optimized geometry, with all corelike (C 1s; Si 1s, 2s, 2p; Ge 1s, 2s, 2p, 3s, 3p, 3d) orbitals kept frozen.

We determined ab initio strain enthalpies using homodesmotic reactions.²¹ It has been shown that when adequate basis sets and correlated levels of theory are employed, computed heats of homodesmotic reactions agree with experimental values to within a few kcal mol⁻¹.^{6,22} Because there has been some variation in the ways different authors have applied homodesmotic reactions to nonhydrocarbons, we state our approach here. George et al.²¹ defined a homodesmotic reaction of hydrocarbons as one which conserves the number of C-C bonds of each type ($\text{sp}^3\text{-sp}^3$, $\text{sp}^3\text{-sp}^2$, etc.) and the number of groups of each type. Here the word "group" has Benson's meaning: a polyvalent atom together with all of its neighboring atoms.²³ George et al. did not speak explicitly of Benson's groups, but that is the essence of their definition,²¹ and paraphrasing it in terms of groups facilitates its extension to nonhydrocarbons. For example, the strain enthalpy¹² of silacyclop propane is here taken to be the enthalpy change of the reaction



Note that in reaction 2 the numbers of $\text{Si-(C)}_2(\text{H})_2$, $\text{Si-(C)}(\text{H})_3$, $\text{C-(Si)}(\text{H})_3$, $\text{C-(C)}(\text{Si)}(\text{H})_2$, and $\text{C-(C)}(\text{H})_3$ groups (Benson's notation²³) are conserved.

Thermochemical Analysis

A semiquantitative expression for the enthalpy of reaction 1 in terms of the factors (bond enthalpies, strain, etc.) which contribute to it can be deduced by imagining carrying out the reaction in several distinct steps. Consider the decomposition of silacyclop propane, $c\text{-SiH}_2\text{CH}_2\text{CH}_2$, to silylene, SiH_2 , and ethylene. If in the first step a Si-C bond is broken to produce $\text{SiH}_2\text{CH}_2\dot{\text{C}}\text{H}_2$, then a zeroth-order approximation to the corresponding enthalpy

(5) (a) Grev, R. S.; Schaefer, H. F. *J. Am. Chem. Soc.* **1987**, *109*, 6569. (b) Grev, R. S.; Schaefer, H. F. *J. Am. Chem. Soc.* **1987**, *109*, 6577. (c) Schoeller, W. W.; Dabisch, T. *Inorg. Chem.* **1987**, *26*, 1081. (d) Cremer, D.; Gauss, J.; Cremer, E. *J. Mol. Struct. (Theochem)* **1988**, *169*, 531. (e) Nagase, S.; Nakano, M. *J. Chem. Soc., Chem. Commun.* **1988**, 1077.

(6) Boatz, J. A.; Gordon, M. S. *J. Phys. Chem.* **1989**, *93*, 3025.

(7) Gaspar, P. P. In *Reactive Intermediates*; Jones, M., Moss, R. A., Eds.; Wiley: New York, 1981; Vol. 2, p 335.

(8) Birchall, J. M.; Fields, R.; Haszeldine, R. N.; Roberts, D. W. *J. Chem. Soc. C* **1973**, 1071.

(9) (a) Norsoph, E. B.; Coleman, B.; Jones, M. *J. Am. Chem. Soc.* **1978**, *100*, 994. (b) Egorov, M. P.; Kolesnikov, S. P.; Nefedov, O. M.; Krebs, A. *J. Organomet. Chem.* **1989**, *375*, C5. (c) Lazraq, M.; Escudie, J.; Couret, C.; Satgé, J.; Soufiaoui, M. *J. Organomet. Chem.* **1990**, *397*, 1. (d) Bobbitt, K. L.; Maloney, V. M.; Gaspar, P. P. *Organometallics* **1991**, *10*, 2772.

(10) Lazraq, M.; Couret, C.; Declercq, J. P.; Dubourg, A.; Escudie, J.; Riviere-Baudet, M. *Organometallics* **1990**, *9*, 845.

(11) Walsh, R. In *The Chemistry of Organic Silicon Compounds*; Patai, S., Rappoport, Z., Eds.; Wiley: New York, 1989; Chapter 5.

(12) We shall use the terms "strain enthalpy" and "bond dissociation enthalpy" rather than the more colloquial but sometimes imprecise terms "strain energy" and "bond dissociation energy".

(13) (a) Pulay, P. In *Modern Theoretical Chemistry*; Schaefer, H. F., Ed.; Plenum: New York, 1977; Vol. 4, p 53. (b) Dupuis, M.; King, H. F. *J. Chem. Phys.* **1978**, *68*, 3998.

(14) Saxe, P.; Yamaguchi, Y.; Schaefer, H. F. *J. Chem. Phys.* **1982**, *77*, 5647.

(15) (a) Huzinaga, S. *J. Chem. Phys.* **1965**, *42*, 1293. (b) Dunning, T. H. *J. Chem. Phys.* **1970**, *53*, 2823. (c) Dunning, T. H.; Hay, P. J. In *Modern Theoretical Chemistry*; Schaefer, H. F., Ed.; Plenum: New York, 1977; Vol. 3, p 1.

(16) Grev, R. S.; Schaefer, H. F. Unpublished results.

(17) Dunning, T. H. *J. Chem. Phys.* **1977**, *66*, 1382.

(18) (a) Scuseria, G. E. *J. Chem. Phys.* **1990**, *92*, 6722. (b) Duke, B. J.; Liang, C.; Schaefer, H. F. *J. Am. Chem. Soc.* **1991**, *113*, 2884.

(19) Grev, R. S.; Janssen, C. L.; Schaefer, H. F. *J. Chem. Phys.* **1991**, *95*, 5128.

(20) (a) Scuseria, G. E.; Scheiner, A. C.; Lee, T. J.; Rice, J. E.; Schaefer, H. F. *J. Chem. Phys.* **1987**, *86*, 2881. (b) Scuseria, G. E.; Janssen, C. L.; Schaefer, H. F. *J. Chem. Phys.* **1988**, *89*, 7382.

(21) (a) George, P.; Trachtman, M.; Bock, C. W.; Brett, A. M. *Tetrahedron* **1976**, *32*, 317. (b) George, P.; Trachtman, M.; Brett, A. M.; Bock, C. W. *J. Chem. Soc. Perkin Trans. 2* **1977**, 1036.

(22) Disch, R. L.; Schulman, J. M.; Sabio, M. L. *J. Am. Chem. Soc.* **1985**, *107*, 1904.

(23) Benson, S. W. *Thermochemical Kinetics*, 2nd ed.; Wiley: New York, 1976.

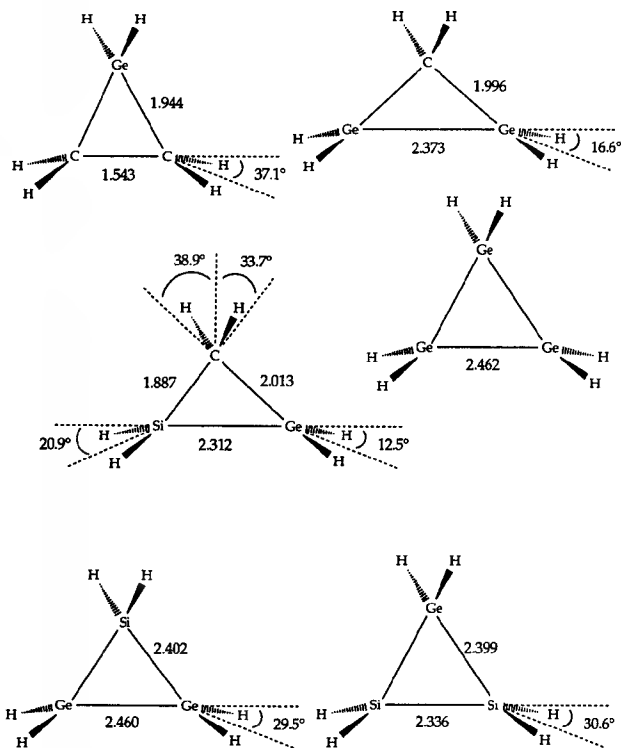


Figure 1. Self-consistent-field (SCF) optimized geometries of the germanium-containing rings investigated in this research. The basis set is of double- ζ plus d (DZ+d) quality. The angles shown are between the H_2M bisector and the extension of the bond between the heavy atoms. Bond distances are in angstroms.

change is the dissociation enthalpy of the SiH_3-CH_3 bond minus the strain enthalpy (because breaking the bond relieves the ring strain). Breaking the second $Si-C$ bond to form SiH_2 and C_2H_4 actually requires less than the SiH_3-CH_3 BDE for two reasons: (1) the dissociation of the second $Si-C$ bond is accompanied by the formation of a $C-C$ π bond, and (2) the breaking bond is more similar to a SiH_2-CH_3 bond than to SiH_3-CH_3 , and in general a bond to a silylene group ($R'-SiR_2$) is weaker than the same type of bond to a silyl group ($R'-SiR_3$).²⁴ Therefore the second $Si-C$ bond in silacyclopentane breaks at an enthalpic cost of approximately $D(SiH_2-CH_3) - D_\pi(H_2C=CH_2)$, where $D_\pi(H_2C=CH_2)$ is the π bond enthalpy in ethylene.²⁵

Quantities such as $D(SiH_3-CH_3)$ are known much better than $D(SiH_2-CH_3)$, so it would be advantageous to recast our expression in terms of the former. We might expect the SiH_3-CH_3 BDE to exceed that of SiH_2-CH_3 by an amount which is roughly equal to the difference between the first and second BDE's of SiH_4 . Walsh¹¹ has defined the latter difference to be the divalent state stabilization energy (DSSE) of SiH_2 , i.e.

$$DSSE(SiH_2) \equiv D(SiH_3-H) - D(SiH_2-H) \quad (3)$$

which allows us to express our approximation in the compact form

$$D(SiH_2-CH_3) \approx D(SiH_3-CH_3) - DSSE(SiH_2) \quad (4)$$

In summary, the foregoing analysis leads to the following expression for the enthalpy change associated with the decomposition of silacyclopentane via reaction 1:

$$\Delta H(1) \approx 2D(SiH_3-CH_3) - \text{strain enthalpy} - D_\pi(H_2C=CH_2) - DSSE(SiH_2) \quad (5)$$

(24) Walsh, R. *Acc. Chem. Res.* **1981**, 246.

(25) This is, effectively, the thermochemical π bond energy of Benson (reference 23), which defines $D_\pi(H_2M=M'H_2)$ as the difference between the BDE's of $MH_3M'H_2-H$ and $MH_2M'H_2-H$ bonds. $D_\pi(H_2M=M'H_2)$ is also commonly defined as the double bond rotation barrier. These two definitions are not identical, but they have been found to yield very similar results where comparison can be made (see refs 30 and 31 for a comparison).

Table I. Divalent State Stabilization Energies (DSSE)^a of Methylene, Silylene, and Germylene

molecule	DSSE, kcal/mol	source(s) of data
CH_2 (triplet)	-5.6	refs 27 and 28
CH_2 (singlet)	-14.6	refs 27 and 28
CF_2 (singlet)	45.4	ref 23
SiH_2 (singlet)	19.3	ref 11
GeH_2 (singlet)	25.8	ref 29

$$^a DSSE(MR_2) \equiv D(MR_3-R) - D(MR_2-R).$$

Table II. π -Bond Enthalpies (D_π) in Group 14 Dimetallenes

bond	D_π , kcal/mol	source(s) of data
$H_2C=CH_2$	65	ref 30
$H_2C=SiH_2$	38	ref 30
$H_2C=GeH_2$	31	ref 31
$H_2Si=SiH_2$	25	refs 30 and 32
$H_2Si=GeH_2$	25	ref 32
$H_2Ge=GeH_2$	25	ref 32

Table III. $H_3M-M'H_3$ Bond Dissociation Enthalpies (kcal/mol) at 298 K

bond	$D(H_3M-M'H_3)$	source of data
H_3C-CH_3	89.9	ref 27
H_3C-SiH_3	88.2	ref 11
$H_3Si-SiH_3$	73.6	ref 11
H_3C-GeH_3	78.2	ref 29
$H_3Si-GeH_3$	70	estimated ^a
$H_3Ge-GeH_3$	65.7	ref 29

^a Estimated to be the geometric mean of SiH_3-SiH_3 and GeH_3-GeH_3 bond dissociation enthalpies. This method of estimation is discussed in ref 26.

For the general case of the decomposition of $c-XH_2YH_2ZH_2$ to XH_2 and $H_2Y=ZH_2$ we obtain

$$\Delta H(1) \approx D(XH_3-YH_3) + D(XH_3-ZH_3) - \text{strain enthalpy} - D_\pi(H_2Y=ZH_2) - DSSE(XH_2). \quad (6)$$

Equations 5 and 6 show that what is missing from the thermochemical analysis discussed in the introduction is the DSSE term, which corrects one of the H_3X-M BDE's for the fact that the second bond being broken is actually a H_2X-M bond.

Results

The optimized geometries of the germanium-containing rings are of special interest and are shown in Figure 1. The rings containing only silicon and carbon have been studied numerous times,^{5,6} and their geometries are not reproduced here. Qualitatively, the germanium rings exhibit the same structural features as silicon rings. Most noteworthy is digermirane, Ge_2CH_6 , which has a very short $Ge-Ge$ bond, 2.373 Å, and nearly planar bonding about the germanium centers, as in a π -complex. At the other extreme is germirane, which exhibits the opposite characteristics in the basal unit: long $C-C$ distances and more highly pyramidalized bonding about the ethylene fragment. These trends are consistent with the notion that the primary determinant of the basal bond lengths in 3MRs is the electronegativity, or π -donating ability, of the apical substituent.^{5b} One curious observation is that cyclotrigermene has bond distances that are longer than those in digermene, Ge_2H_6 , at the same level of theory, 2.462 versus 2.457 Å. This is just the opposite of the case in cyclopropane and cyclotrisilane, where the bond distances in the rings are shorter than those in the straight-chain analogues.

Our thermochemical estimate of $\Delta H(1)$ using eq 6 employs a combination of experimental bond dissociation enthalpies (BDE's) and heats of formation and ab initio quantum mechanical data. DSSE and π -bond enthalpies used in evaluating $\Delta H(1)$ are shown in Tables I and II. The former are derived from experimental data, and the latter are theoretical rotation barriers in dimetallenes. In Table III we list selected values of $H_3M-M'H_3$ BDE's, all of which are experimental results at 298 K except the $H_3Si-GeH_3$ BDE. To our knowledge no reliable experimental or theoretical values of the $H_3Si-GeH_3$ BDE have been published, so we esti-

Table IV. Strain Enthalpies of Group 14 Cyclotrimetallanes

molecule	strain enthalpy, ^a kcal mol ⁻¹			
	this research DZ+d SCF	this research DZ+d CCSD// DZ+d SCF	6-31G(d) SCF ^b	6-31G(d) MP2// 6-31G(d) SCF ^b
C ₃ H ₆	26.1	28.1	25.9	27.3
SiC ₂ H ₆	36.7	35.2	37.6	35.7
GeC ₂ H ₆	38.1	35.8		
CSi ₂ H ₆	39.7	37.0	41.2	38.6
Si ₃ H ₆	36.8	34.5	37.5	35.6
GeSi ₂ H ₆	37.8	35.6		
CGe ₂ H ₆	41.7	39.2		
SiGe ₂ H ₆	38.6	36.3		
Ge ₃ H ₆	39.3	37.3		
CSiGeH ₆	40.8	38.2		

^a ΔH_0 for the homodesmotic reaction $\text{YH}_3\text{XH}_2\text{ZH}_3 + \text{XH}_3\text{YH}_2\text{ZH}_3 + \text{XH}_3\text{ZH}_2\text{YH}_3 \rightarrow \text{c-XH}_2\text{YH}_2\text{ZH}_2 + \text{XH}_3\text{YH}_3 + \text{XH}_3\text{ZH}_3 + \text{YH}_3\text{ZH}_3$.^b Reference 6.**Table V.** Energetics of the Decomposition Reactions $\text{c-XH}_2\text{YH}_2\text{ZH}_2 \rightarrow \text{XH}_2$ (singlet) + $\text{H}_2\text{Y}=\text{ZH}_2$

reaction	ΔE_{elec}^a kcal mol ⁻¹	ΔZPVE^b kcal mol ⁻¹	ΔH , kcal mol ⁻¹	
			ab initio ^{a,c}	estimated ^d
C ₃ H ₆ \rightarrow CH ₂ + C ₂ H ₄	93.2 (106.8)	-9.0	84.9 (98.6)	101
SiC ₂ H ₆ \rightarrow SiH ₂ + C ₂ H ₄	38.1 (47.5)	-4.7	33.9 (43.2)	57
GeC ₂ H ₆ \rightarrow GeH ₂ + C ₂ H ₄	13.1 (22.0)	-4.1	9.3 (18.3)	30
CSi ₂ H ₆ \rightarrow SiH ₂ + CSiH ₄	60.8 (64.7)	-4.9	56.4 (60.3)	67.5
Si ₃ H ₆ \rightarrow SiH ₂ + Si ₂ H ₄	63.0 (66.6)	-4.8	58.7 (62.3)	68
GeSi ₂ H ₆ \rightarrow GeH ₂ + Si ₂ H ₄	55.3 (56.4)	-4.3	51.4 (52.5)	54
CGe ₂ H ₆ \rightarrow GeH ₂ + CGeH ₄	47.2 (48.4)	-4.3	43.3 (44.5)	48
SiGe ₂ H ₆ \rightarrow GeH ₂ + SiGeH ₄	53.4 (53.4)	-4.1	49.7 (49.7)	49
Ge ₃ H ₆ \rightarrow GeH ₂ + Ge ₂ H ₄	51.1 (50.7)	-4.0	47.5 (47.1)	43
CSiGeH ₆ \rightarrow GeH ₂ + CSiH ₄	44.1 (46.9)	-4.4	40.2 (42.9)	46
SiC ₂ H ₆ \rightarrow CH ₂ + CSiH ₄	109.3 (120.5)	-8.4	101.6 (112.8)	119.5
GeC ₂ H ₆ \rightarrow CH ₂ + CGeH ₄	104.5 (114.8)	-8.3	96.9 (107.3)	116
CSi ₂ H ₆ \rightarrow CH ₂ + Si ₂ H ₄	116.5 (127.2)	-7.6	109.5 (120.3)	129
GeSi ₂ H ₆ \rightarrow SiH ₂ + SiGeH ₄	62.9 (63.9)	-4.5	58.8 (59.8)	64
CGe ₂ H ₆ \rightarrow CH ₂ + Ge ₂ H ₄	97.4 (106.5)	-7.1	91.0 (100.1)	107
SiGe ₂ H ₆ \rightarrow SiH ₂ + Ge ₂ H ₄	60.7 (61.4)	-4.4	56.7 (57.3)	59
CSiGeH ₆ \rightarrow SiH ₂ + CGeH ₄	64.3 (66.7)	-4.8	59.9 (62.3)	70
CSiGeH ₆ \rightarrow CH ₂ + SiGeH ₄	107.3 (116.8)	-7.2	110.7 (110.2)	118

^a Values not in parentheses are DZ+d SCF results. DZ+d CCSD//DZ+d SCF data are enclosed in parentheses. ^b Zero-point harmonic vibrational energies determined at the DZ+d SCF level of theory. ^c $\Delta H_0(\text{ab initio}) = \Delta E_{\text{elec}} + (0.91)(\Delta \text{ZPVE})$. ^d Estimated using eq 6, as discussed in the text.

mated this value to be the geometric mean of the H₃Si-SiH₃ and H₃Ge-GeH₃ BDE's.²⁶ Strain enthalpies, assumed to be equal to ΔH of reaction 2, were computed by the ab initio methods discussed earlier. The theoretical thermodynamic data (π -bond and strain enthalpies) are 0 K values.

Our computed ring strain enthalpies are shown in Table IV along with previous theoretical results of Boatz and Gordon.⁶ Electron correlation has only a small (2–3 kcal mol⁻¹) effect upon the strain enthalpies, as is expected for homodesmotic reactions,²² so it is not surprising that the computed strain enthalpy of cyclopropane is close to the value of $\Delta H_{298}(2) = 26.5$ kcal mol⁻¹ obtained from experimental heats of formation.³³ Boatz and Gordon obtained similar results using a 6-31G(d) basis set, which is comparable to our DZ+d set. The strain energy of cyclotri-germane obtained in this study, 37.3 kcal mol⁻¹, is notably smaller than the 44.6 kcal mol⁻¹ value found by Nagase and Nakano^{5c}

using smaller basis sets and SCF energies. In the analysis that follows, only the CCSD strain enthalpies were used to estimate $\Delta H(1)$.

Values of the theoretically obtained enthalpy for the decomposition of each 3-membered ring into a singlet divalent species :XH₂ and a doubly bonded compound H₂Y=ZH₂ (reaction 1) are listed in Table V, along with the predictions obtained using eq 6 and the data in Tables I–IV. The first ten entries in Table V correspond to the most stable products, and these are followed by the remaining eight possible decomposition pathways. Cyclopropane is the only system for which sufficient experimental data are available for comparison, and in that case the CCSD prediction of $\Delta H_0(1) = 98.6$ kcal mol⁻¹ agrees very well with the value of 99.4 kcal mol⁻¹ obtained from 0 K experimental heats of formation.^{28,34} This agreement is not unexpected, because for isogyric³⁵ reactions (of which reaction 1 is an example) correlated ab initio methods usually yield reaction energies which are accurate to within a few kcal mol⁻¹ if polarized basis sets are used.

The estimated cyclotrimetallane decomposition enthalpies (from eq 6) and the CCSD theoretical results differ by fewer than 10 kcal mol⁻¹ in all but two cases, silirane and germirane, for which we observe discrepancies of about 14 and 12 kcal mol⁻¹, respectively. In light of the approximations inherent in eq 6 and the imprecision of the experimental and theoretical data, we judge this to be rather good agreement. On the other hand, the errors

(26) Pauling, L. *The Nature of the Chemical Bond*, 3rd ed.; Cornell University Press: Ithaca, NY, 1960; p 91.(27) Wagman, D. D.; Evans, W. H.; Parker, V. B.; Schumm, R. H.; Halow, I.; Bailey, S. M.; Churney, K. L.; Nuttal, R. L. *The NBS Tables of Chemical Thermodynamic Properties*, *J. Phys. Chem. Ref. Data* **1982**, *11*, Suppl. 2.(28) Leopold, D. G.; Murray, K. K.; Stevens-Miller, A. E.; Lineberger, W. C. *J. Chem. Phys.* **1985**, *83*, 4849.(29) Noble, P. N.; Walsh, R. *Int. J. Chem. Kinet.* **1983**, *15*, 547.(30) Schmidt, M. W.; Truong, P. N.; Gordon, M. S. *J. Am. Chem. Soc.* **1987**, *109*, 5217.(31) Dobbs, K. D.; Hehre, W. J. *Organometallics* **1986**, *5*, 2057.(32) Grev, R. S.; Schaefer, H. F.; Baines, K. M. *J. Am. Chem. Soc.* **1990**, *112*, 9458.(33) Cox, J. D.; Pilcher, G. *Thermochemistry of Organic and Organometallic Compounds*; Academic Press: London, 1970.(34) Lias, S. G.; Bartmess, J. E.; Liebman, J. F.; Holmes, J. L.; Levin, R. D.; Mallard, W. G. *J. Phys. Chem. Ref. Data* **1988**, *17*, Suppl. 1.(35) Hehre, W. J.; Radom, L.; Schleyer, P. v. R.; Pople, J. A. *Ab Initio Molecular Orbital Theory*; Wiley: New York, 1986; p 275.

appear to be systematic; 16 of the 18 estimated values exceed the corresponding CCSD predictions. But even if the theoretical and experimental data were perfectly accurate and eq 6 contained no approximations, each estimated value of $\Delta H(1)$ would exceed the corresponding CCSD prediction by a few kcal mol⁻¹, because the latter are valid for a temperature of 0 K while the former were evaluated using a mixture of 298 and 0 K data. Translational and rotational terms contribute $8RT$, or 4.7 kcal mol⁻¹, to values of $\Delta H(1)$ estimated using 298 K BDE's and 0 K strain enthalpies.

One might begin to refine our thermochemical analysis of cyclotrimetallane decomposition by attempting to include the effect of the third ring atom upon the BDE of the other two. For example, one might replace $2D(\text{SiH}_3\text{--CH}_3)$ in eq 5 by $D(\text{CH}_3\text{--SiH}_2\text{--CH}_2\text{CH}_3) + D(\text{SiH}_3\text{--CH}_2\text{CH}_3)$. It would also be possible to replace eq 4 with a slightly better approximation for $D(\text{SiH}_2\text{--CH}_3)$. However, the cumulative effect of these refinements would probably amount to no more than about 10 kcal mol⁻¹, would not change the trends in $\Delta H(1)$ values, and thus would not give much additional insight into the thermochemistry of cyclotrimetallane decomposition. We believe that more elaborate approximation schemes are not justified at this time given the uncertainties in the experimental BDE's and theoretical data.

Analysis and Discussion

It is interesting that all the 3-membered rings studied here have CCSD strain enthalpies which are clustered within a 5 kcal mol⁻¹ range with the exception of cyclopropane, whose strain enthalpy lies 6 kcal mol⁻¹ below this range (Table IV). Boatz, Gordon, and Hilderbrandt³⁶ have interpreted the strain enthalpies of 3-, 4-, 5-, and 6-membered cycloalkane and monosilacycloalkane rings in terms of a simple group additivity model and found that for any given ring bond angle near 60° a >SiH₂ group is significantly more strained than a >CH₂ group. Our results are not inconsistent with this interpretation and also indicate that >SiH₂ and >GeH₂ groups are about equally strained at 60°.

Because $\Delta S(1)$ should not differ greatly among the 10 cyclotrimetallanes considered here, the relative stabilities of these compounds with respect to dissociation to a carbene-like species and a dimetallene will be determined primarily by $\Delta H(1)$. Therefore, cyclopropane is predicted to be significantly more stable than the other 3-membered rings, consistent with experimental observations, and by far the least endothermic decomposition belongs to the elusive germirane! Silirane and the remaining germanium-containing rings are more susceptible to thermolysis than CSi_2H_6 or Si_3H_6 . Equation 6 readily provides explanations of these trends. Contributing to the instability of GeC_2H_6 relative to C_3H_6 is the former's larger ring strain, the weakness of C–Ge bonds compared to C–C bonds, and a more stable XH_2 decomposition product (manifested in a large positive DSSE for GeH_2 vs a negative DSSE for CH_2). Strong C–C single bonds, low strain, and relatively unstable CH_2 make C_3H_6 the most stable cyclotrimetallane in spite of the extremely strong C–C π -bond. The importance of the DSSE in the thermochemistry of group 14 divalent species is not always appreciated. In fact, the 34 kcal mol⁻¹ difference in the DSSE's of singlet CH_2 and SiH_2 accounts for most of the difference in the enthalpies of the cyclopropane and silirane decomposition reactions!

The disparate behavior of carbenes, silylenes, and germylenes in their addition to 1,3 dienes is conveniently explained by a comparison of the enthalpies of decomposition of the cyclopropane, silirane, and germirane rings. Although the first step in the reaction of singlet carbenes and silylenes with 1,3 dienes is typically 1,2 cycloaddition,^{7,37} germylene reactions yield products consistent with stereospecific, disrotatory 1,4 cycloaddition.³⁸ Thus, the germylene addition is either concerted³⁸ or occurs via an extremely short-lived germirane intermediate,^{3d} consistent with the comparative instability of germirane relative to cyclopropane and

silirane. Like germylenes, stannylenes also react with 1,3 dienes to yield products consistent with stereospecific, disrotatory 1,4 cycloaddition and have never been observed to add to isolated C=C bonds.³⁸ These observations make thermochemical sense; the stannirane ring ($\text{c-SnH}_2\text{CH}_2\text{CH}_2$) might be expected to be even less stable than germirane because Sn–C bonds are weaker than Ge–C bonds.³⁹ Plumbirane is almost certainly thermodynamically unstable with respect to dissociation into ethylene and PbH_2 .

Although the effects of ring substituents upon the enthalpy of ring decomposition have not been studied extensively, these can be estimated from our thermochemical analysis because substituent effects upon BDE's, DSSE's, ring strain, and π -bond enthalpies are known to some extent. This permits us to rationalize the contrasting behaviors of cyclopropane and hexafluorocyclopropane upon heating, for example. Hexafluorocyclopropane is apparently far less stable than cyclopropane with respect to decomposition via reaction 1, because although the former decomposes to difluorocarbene and tetrafluoroethylene at 160 °C,⁸ the latter can be heated to 400 °C before it isomerizes to propene.⁴⁰ The reasons for this are clear: not only is the DSSE of CF_2 roughly 60 kcal mol⁻¹ more positive than that of singlet methylene (see Table I), perfluorination also increases the ring strain of cyclopropane by at least 20 kcal mol⁻¹.⁴¹ These ring-destabilizing effects are only partially moderated by the concomitant weakening of the ethylene π -bond⁴² and strengthening of the C–C single bonds²³ by about 10 kcal mol⁻¹ each upon perfluorination. Therefore, the decomposition of hexafluorocyclopropane is predicted to be less endothermic than that of cyclopropane by a whopping 50–60 kcal mol⁻¹, which is in qualitative agreement with the experimental observations, and a prediction of $\Delta H(1)$ of 36 kcal mol⁻¹ from published heats of formation for $\text{c-C}_3\text{F}_6$, C_2F_4 , and CF_2 .^{34,43} It also makes sense that tetrafluorocyclopropane undergoes thermolysis less readily than hexafluorocyclopropane.⁸

The substituents to the ring can have other interesting effects. For example, the proper choice of substituents can entirely reverse the relative stability of cyclopropane rings relative to disilacyclopropane rings, and even alter the preferred mode of decomposition. Consider the case of cyclopropanone versus disilacyclopropanone, where we have substituted a C=O group for CH_2 in the parent rings. The C=O group is known⁴⁴ to have a huge DSSE of about 73 kcal mol⁻¹. Considering only the relative effects of DSSE on the reaction enthalpy, this suggests that the decomposition of cyclopropanone to carbon monoxide and ethylene is endothermic by about 14 kcal/mol. On the other hand, the disilacyclopropanone decomposition would now take place via extrusion of carbon monoxide, not a silylene as in the parent compound, and would require more energy, about 38 kcal mol⁻¹, than does cyclopropanone, mainly because of the stronger C=C π -bond. Silylene extrusion to form a silaketene would likely require nearly 30 kcal/mol more energy than CO extrusion, because the larger DSSE of CO overwhelms small differences in Si=C versus Si–Si π -bond strengths. Considering an almost certain, probably substantial, increase in strain in these rings due to the presence of an sp^2 -hybridized ring atom, these estimates are all probably too high by 20 kcal mol⁻¹ or more. A similar result is obtained in an analysis of cyclopropanimines relative to disilacyclopropanimines,⁴⁵ because the parent isonitrile $\text{HN}=\text{C}$ also has a large DSSE⁴⁴ of about 78 kcal mol⁻¹. That is, disilacyclopropanimines will preferentially extrude $\text{HN}=\text{C}$ instead of SiH_2 and will be more thermodynamically stable than cyclo-

(39) Carson, A. S.; Laye, P. G.; Spencer, J. A.; Steele, W. V. *J. Chem. Thermodyn.* 1970, 2, 659.

(40) Breslow, R. In *Molecular Rearrangements*; Wiley: New York, 1963; Part 1, Chapter 4.

(41) Smart, B. E. In *Molecular Structure and Energetics*; Liebman, J. F., Greenberg, A., Eds.; VCH: Deerfield Beach, FL, 1986; Vol. 3, p 141.

(42) (a) Wu, E. C.; Rodgers, A. S. *J. Am. Chem. Soc.* 1976, 98, 6112. (b) Wang, S. Y.; Borden, W. T. *J. Am. Chem. Soc.* 1989, 111, 7282.

(43) Paulino, J. A.; Squires, R. R. *J. Am. Chem. Soc.* 1991, 113, 5573.

(44) Grev, R. S. *Adv. Organomet. Chem.* 1991, 33, 125.

(45) Yokelson, H. B.; Millevolte, A. J.; Haller, K. J.; West, R. J. *J. Chem. Soc., Chem. Commun.* 1987, 1605.

(36) Boatz, J. A.; Gordon, M. S.; Hilderbrandt, R. L. *J. Am. Chem. Soc.* 1988, 110, 352.

(37) Tang, Y. In *Reactive Intermediates*; Abramovitch, R. A., Ed.; Plenum: New York, 1982; Vol. 2, p 297.

(38) Neumann, W. P. *Chem. Rev.* 1991, 91, 311.

propanimines with regard to this process.

One can also imagine replacing CH_2 , SiH_2 , and GeH_2 ring atoms by other groups. This would necessitate only minor changes in our working equation, eq 6. One group of possible replacements worth mentioning is the heavier chalcogens, selenium and tellurium. In the last few years, stable M_2Se and M_2Te rings have been synthesized for $\text{M} = \text{Si}$, Ge , and Sn .⁴⁶ On the other hand, C_2Se rings are unstable, and C_2Te rings have apparently never been made. The origin of the relative stability for the Si , Ge , and Sn rings can be traced to the much weaker π -bonds. In the case of C_2Se and C_2Te rings, the strong π -bond in ethylene provides a significant thermochemical driving force for extrusion of a selenium or tellurium atom. In Si , Ge , and Sn rings, this driving force is severely attenuated.

Baines and co-workers^{4b} have just reported a fascinating consequence of what our results suggest is a small enthalpy difference in cyclotrimetallane decomposition enthalpies. With the ultimate goal of obtaining a $\text{Ge}=\text{Si}$ doubly bonded compound, it was decided that the best choice of precursor was a siladigermirane, which it was hoped would decompose according to eq 1 to give the desired germasilene product.³² Unfortunately, and for unknown reasons, the synthetic route also produced some cyclotrigermene, which could not be separated from the desired precursor by traditional means. It was found, however, that the cyclotrigermene was more thermally labile than the siladigermirane, and the minor component Ge_3 ring was eliminated from the mixture by thermolysis at a reduced temperature. According to our results in Table V for the parent hydride compounds, the cyclotrigermene decomposition has an endothermicity of $47.1 \text{ kcal mol}^{-1}$ compared to siladigermirane's $49.7 \text{ kcal mol}^{-1}$. If we assume that the reverse of reaction 1 occurs without barrier so that the

endothermicity can be equated with the activation energy, this corresponds to a factor of 40 in the individual rate constants for decomposition at the temperature employed, 80°C .

Concerning the prospects for synthesizing new cyclotrimetallane rings, we note that the decompositions of GeSi_2H_6 and CSiGeH_6 are no less endothermic than the decompositions of other rings which have already been synthesized (albeit in highly substituted form), suggesting that GeSi_2 and CSiGe rings may be accessible by established synthetic routes. On the other hand, the germirane ring, whose decomposition is ca. 20 kcal mol^{-1} less endothermic than those of any of the other cyclotrimetallanes, clearly presents a greater challenge, and stannirane rings will likely prove even more difficult (*vide ante*). But if the cyclopropane ring can be destabilized by perfluorination then it ought to be possible to stabilize the germirane ring through judicious substitution for the hydrogen atoms. Replacing the H atoms on Ge with electropositive π -acceptor substituents such as SiH_3 may stabilize the germirane ring by reducing both the ring strain⁴⁷ and the DSSE of Ge,⁴⁴ although these effects will probably be mitigated by weakening of the Ge-C bonds.⁴⁸ Reductions in the C-C π -bond enthalpy (assuming it can be equated with the double bond rotation barrier²⁵) of over 20 kcal mol^{-1} can be achieved by placing "push-pull" substituents on the C atoms,⁴⁹ and it may be possible to find a pair of these substituents which produce a low C-C π -bond enthalpy without adversely affecting the other contributions to the enthalpy of reaction 1. Thus, the use of carefully chosen substituents is probably the key to the synthesis of germirane and the stabilization of other cyclotrimetallane rings.

Acknowledgment. This research is supported by the Air Force Office of Scientific Research, Grant AFOSR-87-0182. We thank Kim M. Baines for communicating the results of ref 4 prior to publication.

(46) (a) Batcheller, S. A.; Masamune, S. *Tetrahedron Lett.* **1988**, 29, 3383. (b) Tsumuraya, T.; Sato, S.; Ando, W. *Organometallics* **1988**, 7, 2015. (c) Tsumuraya, T.; Kabe, Y.; Ando, W. *J. Chem. Soc., Chem. Commun.* **1990**, 1159. (d) Tan, R. P.-K.; Gillette, G. R.; Powell, D. R.; West, R. *Organometallics* **1991**, 10, 546. (e) Schafer, A.; Weidenbruch, M.; Saak, W.; Pohl, S.; Marsmann, H. *Angew. Chem., Int. Ed. Engl.* **1991**, 30, 834. (f) Schafer, A.; Weidenbruch, M.; Saak, W.; Pohl, S.; Marsmann, H. *Angew. Chem., Int. Ed. Engl.* **1991**, 30, 962.

(47) Dill, J. D.; Greenberg, A.; Liebman, J. F. *J. Am. Chem. Soc.* **1979**, 101, 6814.

(48) Silyl substituents weaken C-C and Si-Si bonds (see ref 11) and thus are expected to weaken Ge-C bonds also.

(49) Sandstrom, J. In *Topics in Stereochemistry*; Allinger, N. L., Eliel, E. L., Wilen, S. H., Eds.; Wiley: New York, 1983; Vol. 14, p 83.

The known and unknown group 13 hydride molecules M_2H_6 : Diborane(6), dialane(6), and digallane(6)

Mingzuo Shen and Henry F. Schaefer III

Center for Computational Quantum Chemistry, The University of Georgia, Athens, Georgia 30602

(Received 16 September 1991; accepted 4 November 1991)

Molecular structures, harmonic vibrational frequencies, and infrared intensities for diborane B_2H_6 , dialane Al_2H_6 , and digallane Ga_2H_6 have been determined using high level *ab initio* quantum mechanical methods. The highest level of theory employed in this study is the single and double excitation coupled cluster (CCSD) method with double-zeta plus polarization (DZP) basis sets. This study serves to assess the reliabilities of various theoretical methods, laying the foundation for future theoretical studies of larger boron, aluminum, and gallium molecular systems. It appears that the theoretical methods employed here are adequately reliable when compared with existing experiments. Several shortcomings of previous *ab initio* quantum mechanical studies on diborane(6) and its analogs have been addressed.

I. INTRODUCTION

Recently we have carried out several studies on simple hydrides of the group IIIA elements boron, aluminum, and gallium. Liang *et al.*¹ studied the molecular structures and harmonic vibrational frequencies of dialane (Al_2H_6) and digallane (Ga_2H_6), as well as diborane(6). Duke *et al.*² studied several isomers of trialane(9) (Al_3H_9) and trigallane(9) (Ga_3H_9). The present paper considers the heavy atom dimer systems at a level of theory significantly higher than previous studies. This research is also preliminary to a proposed study of tetraborane(12) and its analogs (M_4H_{12} , for $M = B, Al$, and Ga), which may be considered tetramers of MH_3 . Other investigations of digallane and its analogs are reported in Refs. 3 and 4.

Here we report the molecular structures, harmonic vibrational frequencies, and infrared (ir) intensities of diborane and its analogs (M_2H_6 , for $M = B, Al$, and Ga) using all-electron *ab initio* quantum mechanical methods. This study serves two purposes. First, it assesses the reliability of the theoretical methods to be used later for the tetraborane(12) and its aluminum and gallium analogs. This is possible because of the availability of experimental results for diborane and to a limited extent, digallane. Second, diborane and its analogs are important subjects of theoretical and experimental studies in their own right. For the dialane and digallane molecules, the theoretical methods used here are significantly higher in level than those applied previously. Since some of the theoretical methods used here are intended to be used with tetraborane(12) and its analogs as well, our largest basis set in the present paper is moderate for the series M_2H_6 . However, it will be reasonably large for systems such as tetragallane(12). The treatment of electron correlation uses the standard configuration interaction and coupled cluster methods with single and double excitations, i.e., CISD and CCSD.

Diborane(6) (B_2H_6) has achieved a prominent position in borane chemistry,⁵ and has been the subject of many theoretical studies. One of the earliest quantum mechanical stud-

ies was due to Switkes, Stevens, Lipscomb, and Newton.⁶ Diborane(6) was included as a prototypical borane in early systematic *ab initio* quantum chemical studies.⁷⁻⁹ More recent high level *ab initio* quantum chemical studies including substantial basis sets and electron correlation treatments are well worth notice.^{1,2,10-15} More specifically, Stanton, Bartlett, and Lipscomb¹⁰ reported optimized equilibrium geometries and obtained harmonic vibrational frequencies using many-body perturbation theory to second order, designated MBPT(2), with the 6-31G** basis set. Sana, Leroy, and Henriot¹² separately reported an optimized geometry using the CISD method with the 6-31G* basis set.

Experimental studies on diborane(6) are also very rich. A recent review on the molecular structures of boranes and carboranes has been presented by Beaudet.¹⁶ The bridged structure of diborane(6) was experimentally established by the work of Price,¹⁷ and of Hedberg and Schomaker¹⁸ in the late 1940s and early 1950s. Various laboratory techniques have since been applied to the study of diborane(6).¹⁹⁻²⁴ Of particular interest here, Duncan and Harper^{23,24} have reported an experimental equilibrium geometry and (anharmonic) fundamental frequencies for all 18 vibrational modes of diborane, based on infrared, Raman, and microwave techniques using isotopic substitution.

Contrary to the relatively rich literature on diborane(6), the literature on dialane(6) and digallane(6) is very limited. In fact, attempts to isolate dialane have still been unsuccessful to date, and digallane(6) was only isolated in 1989 by Downs, Goode, and Pulham.^{25(a)} Several *ab initio* theoretical studies on dialane(6) and digallane(6) have been published recently.^{1-3,13,14} Liang *et al.*¹ reported all-electron self-consistent field (SCF) computations using basis sets of triple-zeta plus polarization (TZP) quality. Lamertsmma and Leszczyński¹³ reported an optimized equilibrium geometry, harmonic vibrational frequencies, and ir intensities for dialane using the MP2 method with a 6-31G** basis set; the same molecular properties were reported for digallane using the SCF method with a 3-21G* basis set.

II. THEORETICAL DETAILS

In this study we use three basis sets, the DZ, DZd, and DZP, for each of the molecules. The double-zeta (DZ) basis set for hydrogen is the standard Dunning–Huzinaga (4s/2s) contraction,²⁴ with the orbital exponents α multiplied by $(1.2)^2 = 1.44$. The addition of three p functions, with exponent $\alpha_p(H) = 0.75$, to the DZ set completes the double-zeta plus polarization (DZP) basis set for H. The DZ basis set for boron is also a Dunning–Huzinaga contraction,²⁶ (9s5p/4s2p). The addition of six d -type functions, with exponent $\alpha_d(B) = 0.7$, completes the DZP basis set for B. The DZ basis set for aluminum is that of Dunning and Hay,²⁷ designated (11s7p/6s4p). The addition of six d -type functions, with exponent $\alpha_d(Al) = 0.40$, completes the DZP basis set for Al. The DZ basis set for gallium is that of Dunning,²⁸ designated (14s11p5d/7s5p2d). The addition of six d -type functions, with exponent $\alpha_d(Ga) = 0.207$, completes the DZP basis set for gallium. The gallium basis sets designated DZ and DZP are the same as those used previously.^{2,29} In the DZd basis set for a particular molecule, the DZP basis set for boron, aluminum, or gallium and the DZ set for H are used. The DZP basis set includes 62, 78, and 110 basis functions for diborane, dialane, and digallane, respectively.

We use the SCF, CISD, and CCSD methods in this study. Equilibrium geometries for each molecule are optimized under D_{2h} symmetry using analytic gradient methods^{30–32} and four internal coordinates. SCF harmonic vibrational frequencies are obtained using analytic energy second derivatives.³³ CISD and CCSD harmonic vibrational frequencies are obtained by Cartesian finite differences of analytic gradients. Infrared intensities are obtained in the double harmonic approximation from analytic dipole moment first derivatives (with the SCF wave function) or from finite differences of dipole moments (with the CISD and CCSD wave functions). The mass of the most abundant isotope is used for the vibrational frequencies; i.e., ^{11}B , ^{27}Al , or ^{69}Ga . In the finite difference scheme, 13 symmetry-independent Cartesian coordinates are displaced, by 0.001 (for CISD wave functions) or 0.01 (for CCSD wave functions) Å from the equilibrium geometry. In evaluating the CISD and CCSD analytic gradients, the correlation energy must be converged to a higher degree than normal when the geometry alone is optimized. A threshold of 10^{-10} a.u. is used here as recommended. All computer programs are part of the PSI 2.0 package, distributed by PSITECH, Inc., Watkinsville, Georgia. On site DECstation 3100, IBM 3090, and IBM RS6000 computers were used.

We choose a Cartesian coordinate system in which the x axis passes through the heavy nuclei and the xy plane passes through the bridging hydrogen nuclei. In this orientation there are

four	A_g
one	A_u
two	B_{1g}
three	B_{1u}
two	B_{2g}
two	B_{2u}
one	B_{3g}
three	B_{3u}

normal modes. This particular convention was used by Shimanouchi in his well-known tabulation of vibrational frequencies.^{24(b)}

One may readily construct six different right-handed Cartesian coordinate systems for the molecules here. The x , y , or z axis may be chosen to pass through the heavy atom nuclei. With this set, either of the other two axes may pass through the bridge hydrogen nuclei. One may straightforwardly work out the number of modes in each irreducible representation with a chosen Cartesian coordinate system. It turns out that each choice may be distinguished from the set of eight integers denoting the number of vibrational frequencies belonging to each irreducible representation. For example, in Lammertsma and Leszczyński's Cartesian coordinate system, the x axis passes through the heavy nuclei, but it is the xz plane that passes through the bridging hydrogen nuclei.¹³ The same choice is used by Bock *et al.*¹⁴ and Duncan.^{24(a)}

III. RESULTS AND DISCUSSION

A. Diborane (B_2H_6, D_{2h})

Our theoretical results for diborane are collected in Tables I and II—Table I for the equilibrium geometry along with the experimental equilibrium geometry due to Duncan and Harper,²³ and Table II for the harmonic vibrational frequencies, along with the comparable experimental vibrational frequencies due to Duncan.²⁴ In these tables, results from lower levels of theory are included for comparison. The DZP CCSD equilibrium geometry agrees with the experimental structure to within 0.05 Å or 1.5°. The theoretical B–B distance is too long by 0.042 Å. Stanton *et al.*¹⁰ reported various theoretical B–B distances about 0.01 Å too long compared with experiment [using 6–31G* MBPT(2), MBPT(3), CID, and 6–31G** MBPT(2)]. Sana *et al.*¹² reported a B–B distance about 0.03 Å too long (6–31G* CISD), comparable to our DZd CISD value. For diborane it is clear that higher levels of theory (higher correlation level and/or larger basis set) give longer B–B distances. Both higher order correlation effects and (to a larger degree) basis set extension will decrease the DZP CCSD B–B internuclear separation for B_2H_6 , eventually yielding harmony with experiment. Note the close agreement between the DZP CISD and CCSD levels of theory. Comparing SCF and correlated geometries, one sees that the B–B distance is more sensitive to electron correlation than the B–H (both terminal and bridged) distances.

For B_2H_6 we have obtained three sets of correlated harmonic vibrational frequencies—the DZP CISD and CCSD with two frozen core and two deleted virtual orbitals, and the DZP CCSD with no frozen core or deleted virtual orbitals. The DZP CCSD method with/without frozen core orbitals produced very similar harmonic vibrational frequencies, the differences being (fifth minus sixth column in Table II): $-5, -4, 0, -3, -2, -5, -7, -4, +7, 0, -4, +1, -6, -1, +1, -3, -3$, and 0 cm^{-1} . The results from DZP CCSD with two frozen core and two deleted virtual orbitals seem to be slightly preferable. These (fifth column DZP CCSD) vibrational frequencies are higher than the ex-

TABLE I. Total energies and optimized equilibrium geometries predicted at several levels of theory for diborane (B_2H_6 , D_{2h}). Harmonic vibrational frequencies and ir intensities evaluated at their respective optimized equilibrium geometries of various theoretical levels are presented in Table II.

	DZ SCF	DZd SCF	DZd CISD ^a	DZP SCF	DZP CISD ^a	DZP CCSD ^a	DZP CCSD ^b	Expt. ^c
Total energy, a.u.	-52.772 41	-52.808 41	-52.996 94	-52.816 86	-53.050 81	-53.069 32	-53.100 74	...
r_e (BB), Å	1.829	1.794	1.776	1.797	1.787	1.789	1.785	1.743
Terminal r_e (BH), Å	1.183	1.185	1.191	1.188	1.188	1.190	1.189	1.184
Bridge r_e (BH), Å	1.340	1.325	1.322	1.331	1.324	1.326	1.324	1.314
Terminal \angle (HBH)	123.0°	122.7°	122.7°	122.5°	122.9°	123.0°	123.0°	121.5°

^a Two B 1s-type core MOs are frozen and the two corresponding virtual MOs are deleted.

^b No core MOs are frozen and no virtual MOs are deleted.

^c J. L. Duncan and J. Harper, *Mol. Phys.* **51**, 371 (1984). Cited are equilibrium geometrical parameters.

perimental (anharmonic) fundamentals by 6%, 5%, 1%, 3%, -0.5%, 7%, 3%, 6%, 0.5%, 2%, 7%, 1%, 4.5%, 3%, 0.3%, 6%, 9%, 1%, respectively (in the same order as found in Table II). It is clear that the DZP CCSD level of theory is moderately reliable for diborane and we would expect similar reliability when this method is applied to tetraborane (12). The DZP CISD level is quite satisfactory as well. A comparison between the DZP SCF and CCSD levels of theory is interesting. There are five normal modes whose DZP CCSD frequencies are higher than their counterpart DZP SCF values, contrary to normal expectations.³⁴ A simplistic explanation may be that diborane is an electron-deficient system and behaves in somewhat different ways from other molecules. More specifically, B_2H_6 has virtual orbitals which may be bonding in character; the incorporation of these bonding virtual orbitals in a correlated wave function allows some bond distances to decrease and some vibrational frequencies to increase correspondingly.

Previous comparable theoretical results include the harmonic vibrational frequencies using the 6-31G* MBPT(2) method by Stanton *et al.*¹⁰ Bond lengths from Stanton *et al.* are shorter than our DZP CCSD values by as much as 0.03 Å, which is probably the reason that their harmonic vibrational frequencies are generally higher than the DZP CCSD values reported here.

B. Dialane (Al_2H_6 , D_{2h})

Table III shows a comparative study of the effects of frozen core and deleted virtual MOs on the optimized equilibrium geometry of dialane using the CISD and CCSD methods with the DZP basis set. Three types of restrictions are separately applied: (a) freezing the ten Al 1s-, 2s-, and 2p-type core and deleting the ten corresponding virtual MOs; (b) freezing two Al 1s-type core and deleting two cor-

TABLE II. Harmonic vibrational frequencies (in cm^{-1}) predicted at several levels of theory, and infrared intensities (in km/mol) at the DZP CISD and CCSD levels for diborane ($^{11}B_2H_6$, D_{2h}). The optimized equilibrium geometries are presented in Table I.

	DZ SCF	DZd SCF	DZP SCF	DZP CISD ^a	DZP CCSD ^a	DZP CCSD ^b	Expt. ^c
A_g	2735	2752	2719	2699	2671	2676	2526
	2158	2257	2229	2218	2199	2203	2096
	1229	1261	1258	1213	1198	1198	1187
	787	819	818	820	813	816	788
A_u	818	883	872	841	829	831	833
	1801	1893	1864	1891	1878	1883	1756
B_{1g}	883	885	881	896	887	894	860
	2849	2856	2819	2808 (203)	2781 (193)	2785 (191)	2613
B_{1u}	1066	1068	1055	971 (0.1)	956 (0.1)	949 (0.03)	951
	405	396	399	381 (14)	376 (14)	376 (14)	367
	2833	2841	2804	2795	2768	2772	2597
B_{2g}	973	978	971	940	930	929	918
	1905	2032	2002	2024 (33)	2011 (29)	2017 (28)	1924
B_{2u}	1072	1084	1058	1020 (10)	1007 (9)	1008 (9)	974
	1169	1175	1140	1049	1026	1025	1023
B_{3g}	2712	2731	2698	2680 (172)	2653 (166)	2656 (166)	2518
	1717	1804	1754	1764 (680)	1755 (647)	1758 (641)	1615
B_{3u}	1214	1244	1241	1198 (78)	1183 (74)	1183 (72)	1175

^a Infrared intensities (in km/mol) at this level are shown in parentheses. Blanks indicate identically zero values, i.e., fundamentals forbidden in the ir spectrum. Two B 1s-type core MOs are frozen and two corresponding virtual MOs are deleted. 49 141 configurations were included in C_1 symmetry.

^b No core MOs are frozen and no virtual MOs are deleted. 93 961 configurations were included in C_1 symmetry.

^c J. L. Duncan, *J. Mol. Spectrosc.* **113**, 63 (1985). These are anharmonic fundamentals.

TABLE III. Effects of frozen core and deleted virtual MOs in the CISD and CCSD wave functions on the optimized equilibrium geometry for dialane (Al_2H_6 , D_{2h}). In constructing the CISD wave functions, three levels of restriction are used, designated I, II, and III. Two restrictions were used for CCSD, I and III. The DZP basis set was used consistently in the results reported in this table.

	CISD I ^a	CISD II ^b	CISD III ^c	CCSD I ^a	CCSD III ^c
Total energy, a.u.	-487.484 00	-487.683 36	-487.713 17	-487.499 74	-487.754 79
Number of configurations	6 763	47 874	68 356	6 763	493 521 ^d
Equilibrium geometry					
r_e (AlAl), Å	2.5937	2.5899	2.5897	2.5933	2.5892
Terminal r_e (AlH), Å	1.5610	1.5583	1.5581	1.5631	1.5621
Bridge r_e (AlH), Å	1.7184	1.7154	1.7151	1.7190	1.7168
Terminal \angle (HAlH)	127.367°	127.366°	127.362°	127.379°	127.385°
Bridge \angle (AlHAl)	97.998°	98.036°	98.047°	97.924°	97.888°

^aTen occupied (Al 1s-, 2s-, and 2p-type) MOs are frozen and the ten corresponding virtual MOs are deleted. There are 78 basis functions in the DZP basis set for dialane.

^bTwo occupied (Al 1s-type) MOs are frozen and the two corresponding virtual MOs are deleted.

^cAll electrons are explicitly correlated (no frozen core or deleted virtual MOs).

^d493 521 configurations were used in the gradient evaluations (C_1 symmetry), while 68 356 configurations were used in the energy evaluation (D_{2h} symmetry).

responding virtual MOs; and (c) freezing no core and deleting no virtual MOs. It is clear that the latter two levels of restrictions on the CISD wave functions produced nearly identical optimized equilibrium geometries. In order to display the differences, additional digits are required. Also an additional Al-H-Al angle in the bridge is shown. The same two restrictions on the CCSD wave functions did not produce large changes either. Since freezing ten core orbitals and ten virtual orbitals saves considerable processor time and disk space, this approach is the preferred method. With this 10/10 restriction the CISD and CCSD geometries for Al_2H_6 are within 0.002 Å in bond distances and 0.01° in bond angles.

Table IV shows the present predictions for the total energies and equilibrium geometries for dialane, using the various levels of theory. Results from the lower levels of theory are included for comparison. The CISD and CCSD levels are significantly more advanced than the previously used MP2 method for electron correlation.¹³ Comparing SCF and CISD/CCSD bond lengths in Table IV for a given basis set, we see that the DZP CISD/CCSD bond lengths are shorter than the DZP SCF values, which is not expected for normal bonds. Again, this may be qualitatively explained by invoking the general notion (discussed in more detail above) that dialane is an electron-deficient system with bonding virtual orbitals. Missing in this table is an experimental column because dialane has not been observed to date. From the experience with diborane(6) above, we expect that the CISD/CCSD Al-Al length would be too long by a few hundredths of an Ångström. This expectation, of course, requires experimental verification.

Table V shows the theoretical harmonic vibrational frequencies and ir intensities for dialane. Again, the frequencies at the CISD and CCSD levels of theory are of a considerably higher level than from previous computational studies. Of theoretical interest are the vibrational frequencies from CISD with two levels of restriction in the wave function (the

fourth and fifth columns in Table V). The differences between the fourth and fifth column for the rows are: -19, -11, -8, -1, -3, -12, -3, -17, -9, -1, -18, -3, -7, -6, -7, -18, -12, and -7 cm^{-1} . Since including more electrons makes CISD's size inconsistency problem more severe, we expect that the CISD with ten frozen core and ten deleted virtual orbitals (fourth column in Table V) is more reliable than the CISD with two frozen core and two deleted virtual orbitals (fifth column in Table V). That the above differences are all negative is a confirmation of this expectation. The CCSD frequencies are uniformly smaller than the corresponding CISD values, this on top of the observation in Table IV that the CISD and CCSD geometries are almost identical. Comparing frequency values from SCF and CCSD, since the DZP CCSD equilibrium bond lengths are shorter than the DZP SCF values, some of the DZP CCSD harmonic vibrational frequencies are larger than or very close to the corresponding DZP SCF values. Only the DZP CISD and CCSD ir intensities are shown in Table V. The B_{3u} mode at 1598 (SCF), 1610 (CISD), or 1589 (CCSD) cm^{-1} is predicted to be the most intense by all three correlated levels. Furthermore, it is noted that the ir intensities from the three correlated levels of theory follow the same trend and in fact have comparable values.

Liang *et al.*¹ reported harmonic vibrational frequencies at the TZP SCF level of theory. Their results are similar to the DZP SCF predictions reported in Table V. The CCSD frequencies in Table V are smaller than the earlier reported¹ TZP SCF predictions. Their ir intensities are also similar in relative values to the DZP CCSD results in Table V, with the CCSD values generally smaller. Lammertsma and Leszczyński¹³ reported a 6-31G** MP2 optimized equilibrium geometry and harmonic vibrational frequencies for dialane. Their bond lengths are between our DZP SCF and DZP CCSD values, and their harmonic vibrational frequencies are sometimes lower and sometimes higher than the DZP CCSD values, although not by large amounts.

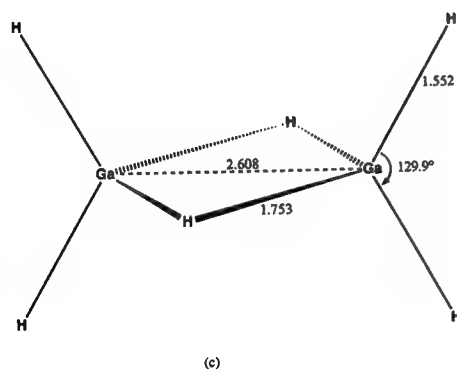
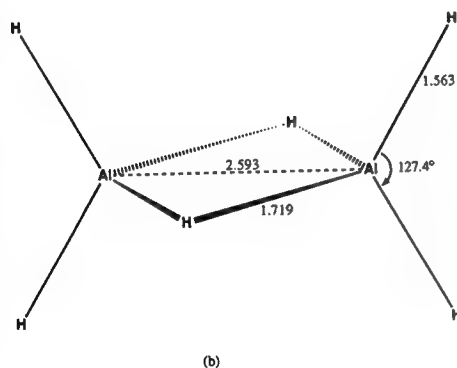
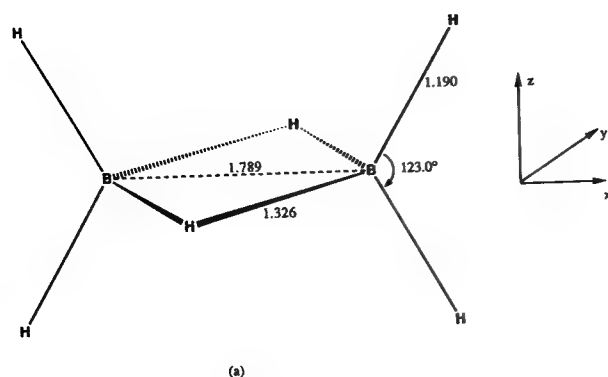


FIG. 1. Optimized equilibrium geometries for diborane, dialane, and digallane using the CCSD method with the DZP basis set. Bond lengths are in Å and bond angles in degrees. The molecular symmetry for all three molecules is D_{2h} . Note that in our Cartesian coordinate system, the x axis passes through the heavy nuclei, and the xy plane passes through the bridging hydrogen nuclei. (a) Diborane: two B $1s$ -type core and corresponding virtual MOs are frozen in constructing the CCSD wave functions. The number of basis functions is 62; 6763 configurations are included in D_{2h} symmetry in the wave function. (When computing harmonic vibrational frequencies using Cartesian displacements, as we did in the present research, C_1 symmetry must be used for some of the points, in which case 49 141 configurations are included in the wave function.) (b) Dialane: ten Al $1s$ -, $2s$ -, and $2p$ -type core and corresponding virtual MOs are frozen. The number of basis functions is 78; 6763 configurations (49 141 for the C_1 symmetry) are included. (c) Digallane: 8 core and 12 virtual MOs are frozen. The number of basis functions is 110; 67 924 configurations are included in the DZP CCSD in D_{2h} symmetry (525 825 configurations in C_1 symmetry in DZP CISD finite difference scheme).

It is worth noting that *ab initio* theoretically predicted bond lengths in dialane are substantially longer than their counterparts in diborane. This confirms the expectation that, in addition to general similarities due to periodicity, there are substantial differences between compounds of second- and third-row elements of a given column in the periodic table. As far as bond lengths are concerned, the valence radius of aluminum is evidently predicted to be substantially larger than that of boron.

C. Digallane (Ga_2H_6 , D_{2h})

For digallane we also make a comparison of the effects of frozen core and deleted virtual MOs on the optimized equilibrium geometry, shown in Table VI. It is interesting to note that the structures in column II (18 frozen core and 12 deleted virtual orbitals) and column IV (2 frozen core and 2 deleted virtual orbitals) are quite similar. Since we expect that the size inconsistency problem is less severe with the wave function in column II, this restriction was used for the computation of DZP CISD harmonic vibrational frequencies.

Table VII presents the total energies and optimized equilibrium geometries for digallane at the various levels of theory, along with the very recent gas-phase electron diffraction structure from Pulham, Downs, Goode, Rankin, and Robertson.^{25(b)} As before, results from lower levels of theory are included for comparison. The DZP CISD and CCSD geometries are very similar, particularly for the Ga-Ga bond lengths. The DZP SCF bond lengths are significantly longer than the corresponding DZP CCSD values, a situation comparable to that for diborane(6) and dialane(6) above and probably arising from a similar origin. Comparing the DZP CCSD bond distances with the r_a structure from Pulham *et al.*^{25(b)} we see that the theoretical Ga-Ga bond length is (as expected) longer than the experimental one by about 0.03 Å. The experimental error bars on the Ga-H bond lengths (terminal and bridged) are larger, but it is probable that the theoretical values are also a bit long. This situation is similar to that found for diborane(6) above. In the comparisons for digallane here, one may keep in mind that the cited experimental structure (r_a , or r_a^0) is not the equilibrium structure. The r_a structure (or the raw structure directly from gas-phase electron diffraction experiments) was not refined to the r_g structure. For discussions of the r_a structure, see Refs. 16(a) and 16(b).

Comparing the bond lengths of dialane and digallane from the DZP CCSD level of theory, we see that the M-M, bridge M-H, and terminal M-H bonds have similar lengths. This similarity indicates that gallium has a similar valence radius as aluminum, expected for a pair of third- and fourth-row elements.⁵ More specifically, however, one may observe that the Al-Al and bridging Al-H bonds are shorter than the Ga-Ga and bridging Ga-H distances. (Also note that the terminal Al-H is longer than terminal Ga-H.) If we assume that shorter bonds indicate greater chemical bonding, we may conclude that dialane is more tightly bound than digallane.

TABLE IV. Total energies and equilibrium geometries predicted at several levels of theory for dialane (Al_2H_6 , D_{2h}). Harmonic vibrational frequencies are presented in Table V. This table shows the effects of basis set and electron correlation.

	DZ SCF	DZd SCF	DZd CISD ^a	DZP SCF	DZP CISD ^a	DZP CISD ^b	DZP CCSD ^a
Total energy, a.u.	-487.223 27	-487.280 01	-487.420 66	-487.291 64	-487.484 00	-487.683 36	-487.499 74
r_e (AlAl), Å	2.705	2.617	2.585	2.616	2.594	2.590	2.593
Terminal r_e (AlH), Å	1.569	1.560	1.568	1.566	1.561	1.558	1.563
Bridge r_e (AlH), Å	1.750	1.721	1.714	1.732	1.718	1.715	1.719
Terminal \angle (HAlH)	128.9°	127.5°	127.6°	127.1°	127.4°	127.4°	127.4

^a Al 1s-, 2s-, and 2p-type MOs are frozen and the ten corresponding virtual MOs are deleted.^b The two Al 1s-type MOs are frozen (i.e., doubly occupied in all configurations) and the two corresponding virtual MOs are deleted.

Harmonic vibrational frequencies for Ga_2H_6 were obtained only from the SCF and CISD wave functions, and these frequencies are seen in Table VIII. It is computation intensive to compute the second energy derivatives using finite differences of energy gradients at the DZP CCSD level. Furthermore, given the results for dialane above, the DZP CCSD harmonic vibrational frequencies for digallane should fall generally between the DZP SCF and DZP CISD values presented in Table VIII. Infrared intensities for Ga_2H_6 are shown in Table VIII at the DZP SCF and CISD levels. The most intense normal mode is again the B_{3u} mode at 1400 (SCF) and 1412 (CISD) cm^{-1} , as is the case for diborane and dialane. Also listed in Table VIII are the experimental fundamentals reported by Pulham *et al.*²⁵ It is to be noted that the authors of Ref. 25(b) accepted the reassignment of several of their experimental vibrational frequencies based on earlier *ab initio* theoretical results of Liang, Davy, and Schaefer.¹ There should be eight ir active modes by symmetry, one of which is very weak, as predicted by the DZP CISD level of theory. The DZP SCF values (harmonic) are larger than the experimental fundamentals

(anharmonic) by 4%, 14%, 5%, 6%, 5%, 10%, and 10%, respectively, for the seven available experimental values. The DZP CISD values are higher by 5%, 10%, 8%, 5%, 6%, 11%, and 8%, respectively; the CISD errors are sometimes larger than the DZP SCF but more uniform. Liang *et al.*¹ have obtained harmonic vibrational frequencies and ir intensities for digallane at the TZP SCF level of theory. Lammertsma and Leszczyński reported 3-21G* SCF harmonic vibrational frequencies and ir intensities, which are (where comparable) similar to our results.

D. Binding energies

The binding energies of diborane and its analogs may be used to assess their thermodynamical stability. While a high level theoretical treatment of the binding energies is beyond the scope of this research, we do have some results of interest. The binding energies of the dimer relative to the monomer within the context of this research are presented in Table IX. To obtain the energy difference between M_2H_6

TABLE V. Harmonic vibrational frequencies (in cm^{-1}) at the DZ, DZd, DZP SCF, DZP CISD, and CCSD levels, and infrared intensities at the DZP CISD and CCSD levels for dialane ($^{27}Al_2H_6$, D_{2h}). The corresponding optimized equilibrium geometries are presented in Table IV.

	DZ SCF	DZd SCF	DZP SCF	DZP CISD ^a	DZP CISD ^b	DZP CCSD ^a
A_g	2038	2099	2059	2050	2069	2030
	1587	1678	1642	1647	1658	1637
	792	823	823	798	806	787
	360	393	393	400	401	399
A_u	459	453	451	448	451	446
	1389	1499	1474	1497	1509	1470
B_{1g}	493	517	519	522	525	518
	2049	2104	2064	2065 (375)	2082 (394)	2047 (344)
	1040	1016	991	964 (332)	973 (341)	954 (317)
	253	248	244	237 (16)	238 (16)	235 (15)
B_{2g}	2042	2098	2058	2059	2077	2041
	468	499	502	495	498	492
B_{2u}	1218	1360	1341	1371 (496)	1378 (514)	1368 (463)
	684	694	692	673 (344)	679 (353)	664 (328)
B_{3g}	879	862	845	832	839	826
B_{3u}	2031	2092	2052	2044 (93)	2062 (96)	2024 (88)
	1535	1625	1588	1598 (1200)	1610 (1224)	1589 (1162)
	736	773	774	753 (721)	760 (742)	744 (684)

^a Al 1s-, 2s-, and 2p-type SCF MOs are frozen and the corresponding virtual MOs are deleted. Infrared intensities (in km/mol) are shown in parentheses. Blanks indicate identically zero intensity values, i.e., ir forbidden fundamentals.^b Al 1s-type and corresponding virtual MOs are frozen/deleted.

TABLE VI. Effects of frozen core and virtual orbitals on the DZP CISD optimized equilibrium geometry for digallane (Ga_2H_6 , D_{2h}).

	I ^a	II ^b	III ^c	IV ^d
Total energy, a.u.	- 3850.072 25	- 3850.201 23	- 3850.234 13	- 3850.441 65
Number of configurations	110 566	134 479	323 346	724 870
Equilibrium geometry				
r_e (GaGa), Å	2.567	2.608	2.587	2.601
Terminal r_e (GaH), Å	1.536	1.547	1.549	1.545
Bridge r_e (GaH), Å	1.710	1.750	1.743	1.747
Terminal \angle (HGaH)	130.0°	129.5°	129.1°	129.3°
Bridge \angle (GaHGa)	97.3°	96.3°	95.8°	96.2°

^a 18 occupied (Ga 1s-, 2s-, 2p-, 3s-, and 3p-type) and 18 corresponding virtual MOs are frozen/deleted. There are 110 basis functions in the DZP basis set used for digallane.

^b 18 occupied (Ga 1s-, 2s-, 2p-, 3s-, and 3p-type) MOs are frozen and 12 virtual orbitals are deleted.

^c Ten occupied (Ga 1s-, 2s-, and 2p-type) MOs are frozen and the ten corresponding virtual MOs are deleted.

^d Two occupied (Ga 1s-type) MOs are frozen and the two corresponding virtual MOs are deleted.

TABLE VII. Total energies and optimized equilibrium geometries predicted at several levels of theory for digallane (Ga_2H_6 , D_{2h}).^a

	DZ SCF	DZd SCF	DZd CISD ^b	DZP SCF	DZP CISD ^c	DZP CCSD ^c	Experiment ^d
Total energy, a.u.	- 3849.669 77	- 3849.705 94	- 3849.993 60	- 3849.717 36	- 3850.201 23	- 3850.212 58	...
Equilibrium geometry							
r_e (GaGa), Å	2.672	2.662	2.616	2.651	2.608	2.608	2.580 ± 0.002
Terminal r_e (GaH), Å	1.561	1.565	1.567	1.561	1.547	1.552	1.519 ± 0.035
Bridge r_e (GaH), Å	1.773	1.780	1.773	1.775	1.750	1.753	1.710 ± 0.038
Terminal \angle (HGaH)	129.8°	129.3°	128.9°	128.9°	129.5°	129.9°	130°

^a The double-zeta (DZ) basis for Ga is the contraction (14s11p5d/7s5p2d), Ref. 28. A set of six d-type basis functions, with orbital exponent 0.207, are added to the DZ set to form the DZP basis for Ga.

^b 18 core (Ga 1s-, 2s-, 2p-, 3s-, and 3p-type) MOs are frozen and 18 virtual MOs are deleted.

^c 18 core (Ga 1s-, 2s-, 2p-, 3s-, and 3p-type) MOs are frozen and 12 virtual MOs are deleted.

^d C. R. Pulham, A. J. Downs, M. J. Goode, D. W. H. Rankin, and H. E. Robertson, J. Am. Chem. Soc. **113**, 5149 (1991). Cited here is the r_e structure obtained by electron diffraction technique at - 15 ~ - 20 °C. D_{2h} symmetry was assumed in the least-squares fitting, and the terminal angle (HGaH) was fixed at 130°.

TABLE VIII. Harmonic vibrational frequencies (in cm^{-1}) at the DZ, DZd, DZP SCF, and DZP CISD, and ir intensities at the DZP SCF and CISD levels of theory for digallane ($^{69}Ga_2H_6$, D_{2h}).

	DZ SCF	DZd SCF	DZP SCF ^a	DZP CISD ^b	Experiment ^c
A_g	2086	2075	2088	2099	
	1576	1542	1560	1577	
	785	787	797	782	
	251	232	236	241	
A_u	470	467	472	473	
B_{1g}	1329	1303	1321	1356	
	369	363	371	406	
B_{1u}	2078	2067	2080 (425)	2101 (353)	1993
	916	866	870 (218)	837 (178)	760
	235	231	234 (7)	225 (7)	
B_{2g}	2078	2067	2075	2096	
	490	491	497	493	
B_{2u}	1240	1245	1258 (377)	1294 (291)	1202
	688	685	692 (189)	682 (165)	~ 652
B_{3g}	836	817	821	808	
B_{3u}	2084	2072	2081 (128)	2093 (120)	1976
	1432	1384	1400 (1366)	1412 (1229)	1273
	721	726	736 (731)	722 (607)	671

^a Infrared intensities (in km/mol) are shown in parentheses; blanks indicate identically zero values, i.e., ir forbidden fundamentals.

^b 18 core (Ga 1s-, 2s-, 2p-, 3s-, and 3p-type) SCF MOs are frozen, and 12 virtual MOs are deleted.

^c C. R. Pulham, A. J. Downs, M. J. Goode, D. W. H. Rankin, and H. E. Robertson, J. Am. Chem. Soc. **113**, 5149 (1991). Cited here are ir spectra (fundamental vibrational frequencies) for digallane in the vapor phase (400–4000 cm^{-1}) at ~270 K, except for the approximate value at 652 cm^{-1} , which is an average of the matrix-split lines in solid argon and nitrogen matrices at 20 K. See also A. J. Downs, M. J. Goode, and C. R. Pulham, J. Am. Chem. Soc. **111**, 1936 (1989).

and MH_3 , the geometry of MH_3 was optimized under the D_{3h} symmetry constraint at the DZ, DZd, DZP SCF, and DZP CCSD levels of theory. The total energies and the equilibrium M–H bond lengths are shown in Table IX. The CISD method is not size-consistent and therefore was not used for the purpose of determining binding energies here. To obtain the zero-point vibrational energy (ZPVE) correction, we obtained the DZP CCSD harmonic vibrational frequencies for BH_3 and AlH_3 via a finite difference scheme, and DZP SCF harmonic vibrational frequencies for GaH_3 using the analytic energy second derivative technique. The DZP CCSD harmonic vibrational frequencies for BH_3 are 2593 (A'_1), 1178 (A'_2), 2743 (E'), and 1198 (E'). The DZP CCSD harmonic vibrational frequencies for AlH_3 are 2010 (A'_1), 742 (A'_2), 2018 (E'), and 841 (E'). The DZP SCF harmonic vibrational frequencies for GaH_3 are 2055 (A'_1), 761 (A'_2), 2028 (E'), and 829 (E').

From Table IX, one sees immediately that the binding energy for dialane (Al_2H_6) relative to alane (AlH_3) is comparable to the binding energies for diborane relative to borane and digallane relative to gallane. Therefore, thermodynamically dialane should have a comparable stability to

digallane. One also notes the well documented behavior that the SCF binding energies are too small compared to those obtained when electron correlation is taken into account, using the CCSD method at present.

IV. CONCLUDING REMARKS

We have used the SCF, CISD, and CCSD methods with DZ, DZd, and DZP basis sets to study the equilibrium geometries, harmonic vibrational frequencies, and ir intensities for diborane, dialane, and digallane. The DZ and DZd results are included for comparison, while the DZP CISD and CCSD results represent significant advances with respect to the existing *ab initio* quantum mechanical literature on these systems. One important purpose has been to compare the various theoretical methods for subsequent studies of tetraborane(12), tetraalane(12), and tetragallane(12). The DZP CCSD bond lengths for diborane are longer than the experimental equilibrium values^{23(a)} by about 0.04 Å, and the bond angles larger by about 1°. DZP CCSD harmonic vibrational frequencies for B_2H_6 are larger than experimental *anharmonic* fundamental values^{24(a)} by an average of less

TABLE IX. Theoretical binding energies of M_2H_6 relative to $2MH_3$ for $M = B, Al$, and Ga , at the DZP CCSD level of theory. Results from the SCF level of theory are included for comparison. The binding energies are defined as $\Delta E_c = 2E(MH_3) - E(M_2H_6)$ and $\Delta E_0 = \Delta E_c + 2ZPVE(MH_3) - ZPVE(M_2H_6)$.

$B_2H_6 \rightarrow 2BH_3$		$E(BH_3)$ (a.u.)	$R_c(B-H)$ (Å)	ΔE_c (kcal/mol)	ΔE_0 (kcal/mol)
DZ SCF		– 26.376 21	1.191	12.5	
DZd SCF		– 26.389 01	1.190	19.1	
DZP SCF		– 26.392 18	1.193	20.4	
DZP CCSD ^a		– 26.505 58	1.195	36.5	30.0
$Al_2H_6 \rightarrow 2AlH_3$		$E(AlH_3)$ (a.u.)	$R_c(Al-H)$ (Å)	ΔE_c (kcal/mol)	ΔE_0 (kcal/mol)
DZ SCF		– 243.595 30	1.580	20.5	
DZd SCF		– 243.618 68	1.568	26.8	
DZP SCF		– 243.623 12	1.573	28.5	
DZP CCSD ^b		– 243.721 53	1.569	35.6	30.8
$Ga_2H_6 \rightarrow 2GaH_3$		$E(GaH_3)$ (a.u.)	$R_c(Ga-H)$ (Å)	ΔE_c (kcal/mol)	ΔE_0 (kcal/mol)
DZ SCF		– 1924.821 95	1.575	16.2	
DZd SCF		– 1924.840 23	1.579	16.0	
DZP SCF		– 1924.845 40	1.574	16.7	
DZP CCSD ^c		– 1925.086 07	1.565	25.4	21.8

^a In the CCSD wave function for BH_3 , one core MO was frozen and one virtual MO deleted, corresponding to the B_2H_6 CCSD wave function in which two core MOs were frozen and two virtual MOs deleted. The zero-point vibrational energies were obtained from DZP CCSD harmonic vibrational frequencies (without scaling). The experimental dissociation enthalpy at ambient temperatures is around 35 kcal/mol—see Ref. 10 for a complete discussion.

^b In the CCSD wave function for AlH_3 , five core MOs were frozen and five virtual MOs deleted, corresponding to the Al_2H_6 CCSD wave function in which ten core MOs were frozen and ten virtual MOs deleted. The zero-point vibrational energies were obtained from DZP CCSD harmonic vibrational frequencies (without scaling).

^c In the CCSD wave function for GaH_3 , nine core MOs were frozen and six virtual MOs deleted, corresponding to the Ga_2H_6 CCSD wave function in which eighteen core MOs were frozen and 12 virtual MOs deleted. The zero-point vibrational energies were obtained from DZP SCF harmonic vibrational frequencies (without scaling).

than 4%. The DZP CCSD equilibrium geometry for digallane is in similar agreement with the experimental r_a structure determined by Pulham *et al.*,^{25(b)} theoretical bond lengths being longer by as much as 0.03 Å. The DZP CISD harmonic vibrational frequencies are larger than the experimental fundamentals from Pulham *et al.* by an average of less than 8%. We expect similar accuracy from these methods when they are applied to B_4H_{12} , Al_4H_{12} , Ga_4H_{12} in the future.

ACKNOWLEDGMENTS

We wish to thank Dr. Yukio Yamaguchi for his help with the finite difference scheme in a Cartesian coordinate system and for other valuable discussions. This research was supported by the U.S. Air Force Office of Scientific Research under Grant No. AFOSR-88-0167.

- ¹C. Liang, R. D. Davy, and H. F. Schaefer, *Chem. Phys. Lett.* **159**, 393 (1989).
- ²B. J. Duke, C. Liang, and H. F. Schaefer, *J. Am. Chem. Soc.* **113**, 2884 (1991).
- ³B. J. Duke, *J. Mol. Struct.* **208**, 197 (1990).
- ⁴M. J. van der Woerd, K. Lammertsma, B. J. Duke, and H. F. Schaefer, *J. Chem. Phys.* **95**, 1160 (1991).
- ⁵N. N. Greenwood and A. Earnshaw, *Chemistry of the Elements* (Pergamon, Oxford, 1985).
- ⁶E. Switkes, R. M. Stevens, W. N. Lipscomb, and M. D. Newton, *J. Chem. Phys.* **51**, 2085 (1969). For the historical perspective, see also (a) H. C. Longuet-Higgins and R. P. Bell, *J. Chem. Soc.* **1943**, 250; (b) K. S. Pitzer, *J. Am. Chem. Soc.* **67**, 1126 (1945); (c) R. P. Bell and H. C. Longuet-Higgins, *Proc. R. Soc. London, Ser. A* **183**, 357 (1945).
- ⁷J. D. Dill, P. von R. Schleyer, and J. A. Pople, *J. Am. Chem. Soc.* **97**, 3402 (1975).
- ⁸R. F. Hout, B. A. Levi, and W. J. Hehre, *J. Comput. Chem.* **3**, 234 (1982).
- ⁹D. J. DeFrees, R. Krishnan, H. B. Schlegel, and J. A. Pople, *J. Am. Chem. Soc.* **104**, 5576 (1982).
- ¹⁰J. F. Stanton, R. J. Bartlett, and W. N. Lipscomb, *Chem. Phys. Lett.* **138**, 525 (1987).
- ¹¹H. Horn, R. Ahlrichs, and C. Kölmel, *Chem. Phys. Lett.* **150**, 263 (1988).
- ¹²M. Sana, G. Leroy, and C. Henriot, *J. Mol. Struct.* **187**, 233 (1989).
- ¹³K. Lammertsma and J. Leszczyński, *J. Phys. Chem.* **94**, 2806 (1990).
- ¹⁴C. W. Bock, M. Trachtman, C. Murphy, B. Muschert, and G. J. Mains, *J. Phys. Chem.* **95**, 2339 (1991).
- ¹⁵A. P. Rendell, T. J. Lee, and A. Komornicki, *Chem. Phys. Lett.* **178**, 462 (1991).

- ¹⁶(a) R. A. Beaudet, in *Advances in Boron and the Boranes*, edited by J. F. Liebman, A. Greenberg, and R. E. Williams (VCH, New York, 1984), pp. 417-490; (b) K. Kuchitsu and S. J. Cyvin, in *Molecular Structures and Vibrations*, edited by S. J. Cyvin (Elsevier, New York, 1972), pp. 183-211.
- ¹⁷W. C. Price, *J. Chem. Phys.* **15**, 614 (1947); **16**, 894 (1948).
- ¹⁸K. Hedberg and V. Schomaker, *J. Am. Chem. Soc.* **73**, 1482 (1951).
- ¹⁹L. S. Bartell and B. L. Carroll, *J. Chem. Phys.* **42**, 1135 (1965).
- ²⁰K. Kuchitsu, *J. Chem. Phys.* **49**, 4456 (1968).
- ²¹D. S. Jones and W. N. Lipscomb, *J. Chem. Phys.* **51**, 3133 (1969).
- ²²D. S. Jones and W. N. Lipscomb, *Acta Crystallogr. A* **26**, 196 (1970).
- ²³(a) J. L. Duncan and J. Harper, *Mol. Phys.* **51**, 371 (1984); (b) see also, M. D. Harmony, V. W. Laurie, R. L. Kuczkowski, R. H. Schwendeman, D. A. Ramsay, F. J. Lovas, W. J. Lafferty, and A. G. Maki, *J. Phys. Chem. Ref. Data* **8**, 619 (1979).
- ²⁴(a) J. L. Duncan, *J. Mol. Spectrosc.* **113**, 63 (1985); (b) see also, T. Shimanouchi, *Tables of Molecular Vibrational Frequencies Consolidated*, Vol. I (National Bureau of Standards, Washington, D.C., 1972), p. 36. Additional references may be found here as well.
- ²⁵(a) A. J. Downs, M. J. Goode, and C. R. Pulham, *J. Am. Chem. Soc.* **111**, 1936 (1989); (b) C. R. Pulham, A. J. Downs, M. J. Goode, D. W. H. Rankin, and H. E. Robertson, *J. Am. Chem. Soc.* **113**, 5149 (1991).
- ²⁶(a) S. Huzinaga, *J. Chem. Phys.* **42**, 1293 (1965); (b) T. H. Dunning, *ibid.* **53**, 2823 (1970).
- ²⁷(a) S. Huzinaga, *Approximate Atomic Wavefunctions. II*, Department of Chemistry Technical Report, University of Alberta (Edmonton, Alberta, 1971); (b) T. H. Dunning and P. J. Hay, in *Methods of Electronic Structure Theory. Modern Theoretical Chemistry*, Vol. 3, edited by H. F. Schaefer (Plenum, New York, 1977), p. 1.
- ²⁸(a) For the primitive basis set $14s11p5d$, see T. H. Dunning, *J. Chem. Phys.* **66**, 1382 (1977). (b) The contraction ($14s11p5d/7s5p2d$) is due to R. S. Grev and H. F. Schaefer.
- ²⁹B. J. Duke, T. P. Hamilton, and H. F. Schaefer, *Inorg. Chem.* **30**, 4225 (1991).
- ³⁰For SCF analytic energy gradient methods, see (a) P. Pulay, *Mol. Phys.* **17**, 197 (1969); **18**, 473 (1970); (b) H. F. Schaefer and Y. Yamaguchi, *J. Mol. Struct.* Robert S. Mulliken Issue **135**, 369 (1986).
- ³¹For CISD analytic energy gradient methods, see (a) B. R. Brooks, W. D. Laidig, P. Saxe, J. D. Goddard, Y. Yamaguchi, and H. F. Schaefer, *J. Chem. Phys.* **72**, 4652 (1980); (b) J. E. Rice, R. D. Amos, N. C. Handy, T. J. Lee, and H. F. Schaefer, *ibid.* **85**, 963 (1986).
- ³²For CCSD analytic energy gradient methods, see (a) A. C. Scheiner, G. E. Scuseria, J. E. Rice, T. J. Lee, and H. F. Schaefer, *J. Chem. Phys.* **87**, 5361 (1987); (b) G. E. Scuseria and H. F. Schaefer, *Chem. Phys. Lett.* **146**, 23 (1988).
- ³³For SCF analytic energy second derivative methods, see (a) J. A. Pople, R. Krishnan, H. B. Schlegel, and J. S. Binkley, *Int. J. Quantum Chem. S* **13**, 225 (1979); (b) P. Saxe, Y. Yamaguchi, and H. F. Schaefer, *J. Chem. Phys.* **77**, 5647 (1982).
- ³⁴For a systematic theoretical study of harmonic vibrational frequencies, see, for example, B. H. Besler, G. E. Scuseria, A. C. Scheiner, and H. F. Schaefer, *J. Chem. Phys.* **89**, 360 (1988).

Toward the infrared spectroscopic observation of SiH_5^+ : the silanium ion

Ching-Han Hu, Mingzuo Shen and Henry F. Schaefer III

Center for Computational Quantum Chemistry, University of Georgia, Athens, GA 30602, USA

Received 12 December 1991; in final form 23 December 1991

Ab initio quantum mechanical methods, including the self-consistent field, single and double excitation configuration interaction, and single and double excitation coupled cluster, have been applied to six stationary points on the SiH_5^+ potential energy hypersurface. Equilibrium geometries were determined using analytic energy first derivative techniques. Relative energies of stationary points have been obtained. Harmonic vibrational frequencies of the global minimum were obtained at all levels of theory. Basis sets used include double-zeta plus polarization and triple-zeta plus double polarization. SiH_5^+ should be regarded as involving weakly bound H_2 and SiH_3^+ subunits, with a dissociation energy of only about 10 kcal/mol. Pseudorotation was found to be unfavorable in the SiH_5^+ ion.

1. Introduction

The silanium ion SiH_5^+ , and its structural analogues BH_5 and CH_5^+ , characterized as eight-electron five-valence species, are of considerable interest in understanding the nature of non-classical bonding. These compounds have been studied theoretically [1–8], and to a lesser degree experimentally [9–13]. The simplest system BH_5 is predicted to be a weakly bonded complex between H_2 and BH_3 subunits. Stanton, Lipscomb and Bartlett [1] reported a hydrogen-molecule dissociation energy D_e for BH_5 of 6 ± 2 kcal/mol. The likelihood of BH_5 pseudorotation (scrambling) was suggested to be small compared to the probability of dissociation. On the other hand, the bonding between carbon and hydrogen atoms within CH_5^+ is much stronger [4–7,10]. In fact the C– H_2 bonding in CH_5^+ may be considered as a three-center two-electron bond [7]. The dissociation energy of CH_5^+ toward CH_3^+ and H_2 is predicted to be about 40 kcal/mol according to Komornicki and Dixon [4]. The proton affinity (PA) of CH_4 is also high, 130.5 kcal/mol from Bohme et al. [13]. Complete hydrogen scrambling was found by Smith and Futrell [11].

The PA of SiH_4 obtained theoretically by Schleyer, Apeloig, Arad, Luke and Pople [8] is 153.1 kcal/mol,

which is in good agreement with experimental values [12]. The dissociation energy of SiH_5^+ , however, is somewhat ambiguous. Schleyer et al. [8] reported 7.2 kcal/mol for the dissociation energy (D_0) from the MP4/6-31G**//6-31G* level of theory and estimated 15 kcal/mol as the best value by comparing their results with the difference between theory and experiment for the CH_5^+ system [13]; but this difference was later reduced by other theoretical workers [4]. Pople and Curtiss [14] reported the heats of formation of SiH_5^+ and SiH_3^+ ; and the dissociation energy (D_0) determined from these values is 10.8 kcal/mol (0 K), which agrees well with the experiment by Rosenstock et al. [15]. However, the dissociation energies reported by other experimental workers varied in a range of about 10 kcal/mol [8,16–18].

Silanes are widely used as catalysts in organic reactions, due to their polar Si–H bonds [19,20]. Recently Olah, Heiliger, Aniszfeld and Prakash [19] have successfully showed for the first time that silicon undergoes pure electrophilic hydrogen–deuterium exchange reactions in a system incapable of stabilizing the transition state by electron lone-pair donation. Penta-coordinated silanium cation appears to play an important role in hydrogen exchange for such systems. More stringent require-

ments for knowledge concerning silanium species prompted us to study the structure and energetics of SiH_3^+ . In this work the harmonic vibrational frequencies and infrared (IR) intensities of SiH_3^+ are presented in an attempt to assist experimentalists in the spectroscopic observation of this important species. There is no previous report of the infrared intensities of SiH_3^+ , and the only theoretical prediction of the vibrational frequencies was at the single configuration self-consistent-field level of theory with a modest basis set [14].

2. Theoretical approach

In this study we applied three distinct theoretical methods, self-consistent field (SCF), configuration interaction with single and double excitations (CISD), and coupled cluster with single and double excitations (CCSD). Three different basis sets have been used: the STO-3G^{#1}, double-zeta plus polarization (DZP^{#2}), and triple-zeta plus double polarizations (TZ2P^{#3}). The DZP basis set is designated as Si(11s7p1d/6s4p1d), H(4s1p2s1p). Orbital exponents for the polarization functions are $\alpha_d(\text{Si})=0.50$, $\alpha_p(\text{H})=0.75$. The TZ2P basis set is designated as Si(12s9p2d/6s5p2d), H(5s2p/3s2p), with polarization function orbital exponents $\alpha_d(\text{Si})=1.00$, 0.25 , $\alpha_p(\text{H})=1.50$, 0.375 .

The geometries of the various structures have been optimized within the given symmetries using single configuration SCF, single reference configuration interaction (CISD), and coupled cluster (CCSD) analytic first energy derivative methods [28–33]. Harmonic vibrational frequencies were determined via analytic second derivative techniques [34] at the SCF level of theory, from which we can also determine whether each stationary point within the stated point group is a local minimum. For the CISD and CCSD treatments, harmonic vibrational frequencies were obtained from finite differences of analytic first energy derivatives. The displacements in bond length

are 0.001 \AA and the displacements in bond angles are 0.05 rad . At the CISD level of theory we have applied the frozen core and deleted virtual orbital restriction. Specifically, the five lowest occupied molecular orbitals (Si 1s, 2s, 2p like orbitals) were held doubly occupied (cores) and the five highest lying virtual orbitals (Si core counterparts) were deleted (virtuals) in all configurations. All molecular orbitals were explicitly included at the CCSD level of theory.

Total energies of the H_2 , SiH_3^+ and SiH_4 fragments have been computed at the SCF and CCSD levels of theory. The hydrogen molecule dissociation energy and the proton affinity were obtained by the energy difference for the following reactions:



The total energy of the proton was taken as zero. At the CISD level of theory, the former reaction enthalpy was obtained by separating the $\text{H}_2\text{--SiH}_3^+$ species to 100 \AA to avoid the size-consistency problem.

All codes employed in this study belong to the suite known as PSI. (PSI is distributed by PSITECH Inc., Watkinsville, GA.) The University of Georgia IBM 3090 machine was used for all computations.

3. Results and discussion

We considered six geometries in this study (see fig. 1). Total energies (au) are summarized in table 1. Two C_s structures, connected by a very floppy internal rotation, were found to be the lowest in energy among the six structures. However, the potential energy surface between structures $C_s(1)$ and $C_s(2)$ is very flat. At most of the levels of theory, the $C_s(1)$ structure is lower in energy than $C_s(2)$ at the sixth decimal place. The detailed geometry of the $C_s(1)$ structure is shown in fig. 2, where it is clearly shown that two hydrogen atoms are separated from silicon atom at a distance (1.910 \AA , TZ2P CCSD) much longer than those in the SiH_3^+ fragment (1.460 \AA , TZ2P CCSD). The H–Si–H angles in SiH_3^+ are very close to 120° , so that it can be considered to be a trigonal planar fragment. For comparison purposes, comparable structural optimizations of SiH_3^+ , H_2 and

^{#1} See for hydrogen ref. [21] and for silicon ref. [22].

^{#2} For primitive basis sets see ref. [23], for hydrogen see ref. [24], and for silicon see ref. [25].

^{#3} For the primitive basis set for silicon, see ref. [26], and for the contracted basis set for silicon, see ref. [27].

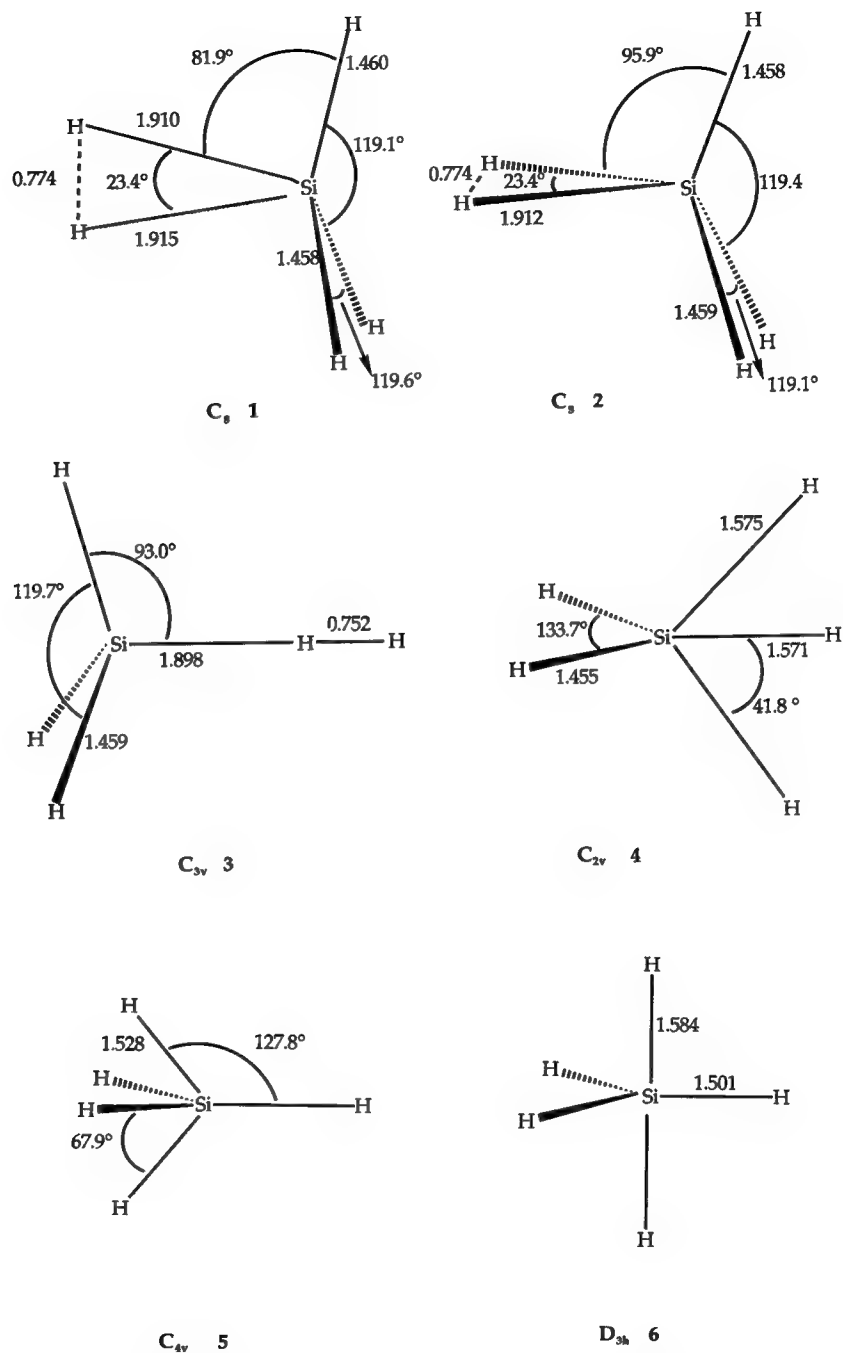
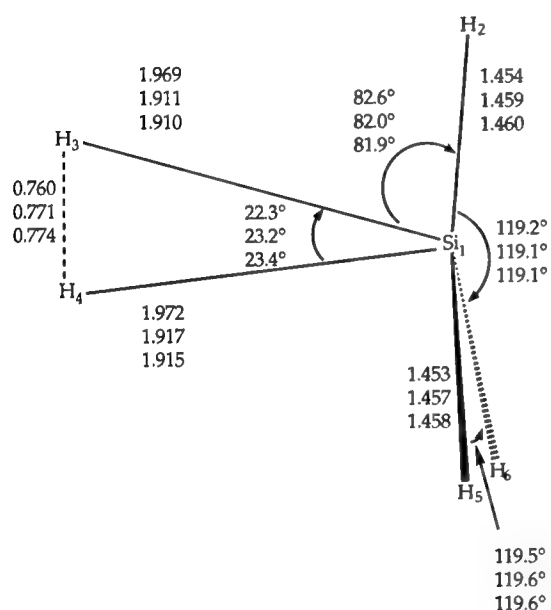


Fig. 1. Geometries examined in this study, including structural parameters obtained at the TZ2P CCSD level of theory.

Table 1

Total energies (in hartree) of six SiH_5^+ stationary point structures from seven distinct levels of theory. Each energy reported corresponds to a stationary point at that particular level of theory

	$C_s(1)$	$C_s(2)$	C_{3v}	C_{2v}	C_{4v}	D_{3h}
MBS/SCF	-288.268169	-288.268169	-288.262436	-288.197913	-288.128623	-288.078354
DZP/SCF	-291.481310	-291.481306	-291.469440	-291.427861	-291.354598	-291.303084
TZ2P/SCF	-291.508278	-291.508275	-291.494231	-291.453736	-291.382258	-291.329634
DZP/CISD	-291.622872	-291.622865	-291.610069	-291.580117	-291.519483	-291.480800
TZ2P/CISD	-291.658874	-291.658873	-291.644522	-291.614748	-291.558337	-291.519443
DZP/CCSD	-291.694135	-291.694122	-291.681535	-291.652391	-291.593848	-291.558903
TZ2P/CCSD	-291.804194	-291.804192	-291.790167	-291.761299	-291.707617	-291.672532



first entry TZ2P SCF
second entry TZ2P CISD
third entry TZ2P CCSD

Fig. 2. Molecular structure of the global minimum SiH_5^+ (C_s structure 1). Bond distances are in Å, and bond angles in deg.

SiH_4 were carried out. The three equivalent Si-H bond distances in the $C_s(1)$ structure (1.460 Å) are slightly shorter than those for gas phase SiH_3^+ (1.461 Å, TZ2P CCSD). The bond distance within the weakly bonded H_2 fragment (0.774 Å, TZ2P CCSD) is slightly longer than for isolated H_2 (0.742 Å) at the same level of theory. Similar arguments hold for the $C_s(2)$ structure.

Harmonic vibrational frequencies and intensities

Table 2

Symmetrized internal coordinates for the global minimum structure of SiH_5^+ (C_s structure 1)^{a)}

		Symmetrized internal coordinates ^{b)}
A'	S_1	$(1/\sqrt{3})(r_{12} + r_{15} + r_{16})$
	S_2	$(1/\sqrt{6})(2r_{12} - r_{15} - r_{16})$
	S_3	$(1/\sqrt{2})(r_{13} + r_{14})$
	S_4	$(1/\sqrt{2})(r_{13} - r_{14})$
	S_5	r_{34}
	S_6	$(1/\sqrt{3})(\alpha_{516} + \alpha_{215} + \alpha_{216})$
	S_7	$(1/\sqrt{6})(2\alpha_{516} - \alpha_{215} - \alpha_{216})$
	S_8	$(1/\sqrt{12})(2\alpha_{213} + 2\alpha_{214} - \alpha_{316} - \alpha_{416} - \alpha_{315} - \alpha_{415})$
A''	S_9	$(1/\sqrt{2})(r_{16} - r_{15})$
	S_{10}	$(1/\sqrt{2})(\alpha_{216} - \alpha_{215})$
	S_{11}	$\frac{1}{2}(\alpha_{316} + \alpha_{416} - \alpha_{315} - \alpha_{415})$
	S_{12}	$(1/\sqrt{6})(2\delta_{2314} - \delta_{5314} - \delta_{6314})$

^{a)} Refer to fig. 2 for the numbering of atoms.

^{b)} Symmetry definitions used in this table are: r_{ij} = distance between atoms i and j . α_{ijk} = angle between atoms i , j and k . δ_{ijkl} = angle of atom i out of the plane defined by atoms j , k , and l plane.

of $C_s(1)$ were computed at all levels of theory. The symmetrized internal coordinates used in our analysis are presented in table 2. The vibrational frequencies and intensities are summarized in table 3. Descriptions in terms of the symmetrized internal coordinates for the twelve normal modes are also included.

An interesting feature of the vibrational frequencies and infrared intensities (see table 3) is that the frequencies for ω_7 and the intensities for ω_8 are not consistent between the SCF method and the correlated levels of theories (CISD and CCSD). The de-

Table 3
Harmonic vibrational frequencies (cm^{-1}), IR intensities (km/mol), and potential energy distributions ^{a)} (PEDs) for the global minimum structure of the SiH_3^+ cation (C_s structure 1)

Mode	DZP SCF	TZ2P SCF	DZP CISD	TZ2P CISD	DZP CCSD	TZ2P CCSD	PED ^{b)}	Description
ω_1 (A')	4247 (168.9)	4218 (207.0)	4059 (136.0)	4038 (173.9)	4059 (131.7)	3991 (169.2)	S_5 (100%)	H_2 stretch
ω_2	2493 (4.8)	2459 (3.4)	2453 (1.8)	2392 (0.4)	2437 (1.4)	2370 (0.2)	S_2 (99%)	SiH_3 deg. stretch
ω_3	2442 (0.5)	2407 (0.1)	2398 (0.4)	2340 (0.0)	2381 (0.4)	2316 (0.0)	S_1 (99%)	SiH_3 sym. stretch
ω_4	1090 (41.4)	1045 (8.8)	1111 (42.0)	1029 (19.2)	1104 (41.5)	1012 (18.3)	S_4 (98%)	H_2 rock
ω_5	1019 (95.7)	1007 (91.0)	979 (75.1)	954 (70.3)	970 (72.2)	944 (68.2)	S_7 (98%)	SiH_3 deg. bend
ω_6	959 (145.4)	944 (139.4)	926 (79.4)	897 (92.7)	919 (69.0)	888 (83.7)	S_8 (91%), S_7 (-9%)	stretch of H_2 , SiH_3 units
ω_7	686 (95.5)	654 (46.1)	778 (167.5)	718 (100.8)	781 (168.0)	719 (99.0)	S_3 (76%), S_6 (20%), S_8 (-3%)	H_2 , SiH_3 rock
ω_8	651 (65.5)	621 (65.8)	666 (4.1)	638 (2.9)	664 (3.7)	635 (2.5)	S_8 (90%), S_3 (6%)	H_2 , SiH_3 rock
ω_9 (A'')	2497 (7.0)	2465 (3.4)	2460 (3.3)	2400 (0.9)	2445 (2.7)	2378 (0.5)	S_9 (100%)	SiH_3 asym. stretch
ω_{10}	1018 (96.8)	1007 (74.9)	976 (79.3)	947 (63.1)	967 (76.5)	937 (60.3)	S_{10} (100%)	SiH_3 asym. bend
ω_{11}	673 (2.5)	646 (0.4)	682 (2.9)	656 (0.7)	680 (2.8)	653 (0.7)	S_{11} (99%)	asym. H_2 , SiH_3 rock
ω_{12}	42 (0.0)	34 (0.1)	60 (0.0)	26 (0.1)	61 (0.0)	25 (0.1)	S_{12} (52%), S_{11} (44%)	torsional twist

^{a)} The PEDs reported here are defined following ref. [35].

^{b)} See table 2 for the definitions of the symmetrized internal coordinates. Contributions of the symmetrized internal coordinates at the TZ2P CCSD level are given in parentheses; sign indicates phase of displacement relative to the defined symmetrized internal coordinates.

pendence of ω_8 on electron correlation can be understood from the contributions of the symmetrized internal coordinates (table 2) to the potential energy distribution. With the DZP basis set, the percentage contributions (in parentheses) of the important internal coordinates to ω_8 are

SCF S_3 (43%) S_6 (10%) S_8 (45%) ,

CISD S_3 (6%) S_6 (1%) S_8 (91%) ,

CCSD S_3 (5%) S_6 (1%) S_8 (91%) .

(Note that the sign of the PED indicates the phase of displacement relative to the defined symmetrized internal coordinate.) We can see that the potential energy distributions at the CISD and CCSD levels are dominated by S_8 , which corresponds to the SiH_3^+ rocking (see table 2). The infrared intensities for ω_8 at the CISD and CCSD levels are much smaller as a result of the importance of S_8 , with which the molecule has much smaller dipole moment derivative than the other two internal coordinates (about 10% of S_3 and 1% of S_6). For ω_7 , the contributions of the symmetrized internal coordinates to the potential energy distribution (DZP basis set) are

SCF S_3 (47%) S_6 (11%) S_8 (-41%) ,

CISD S_3 (68%) S_6 (28%) S_8 (-3%) ,

CCSD S_3 (67%) S_6 (30%) S_8 (-3%) .

Here the potential energy distributions at the CISD and CCSD levels do not involve comparable S_8 input, but contain larger contributions from S_6 . The S_6 internal coordinate, which corresponds to the symmetric bending of the SiH_3^+ counterpart (see table 2), has a much greater force constant than S_3 and S_8 (about 30 times that of S_3 and 60 times that of S_8). Thus larger IR intensities for ω_7 are obtained at the CISD and CCSD levels.

From the vibrational frequency analyses at the SCF level of theory, there is no imaginary vibrational frequency for the $C_s(1)$ structure, while one imaginary vibrational frequency was found for the $C_s(2)$ structure (see table 4). The comparable eleven real harmonic vibrations of both structures have virtually identical frequencies and intensities, and the imaginary vibrational mode ω_{12} (torsional twist) for structure $C_s(2)$ also has the same absolute value and

Table 4
Hessian index, or number of imaginary vibrational modes, for each SCF stationary point geometry

	DZP SCF	TZ2P SCF
$C_s(1)$	0	0
$C_s(2)$	1	1
C_{3v}	2	2
C_{2v}	1	1
C_{4v}	2	2
D_{3h}	3	3

intensity as the real ω_{12} for $C_s(1)$ at both the DZP SCF and TZ2P SCF levels of theory. We thus conclude that the $C_s(1)$ structure is the genuine minimum on the SiH_3^+ potential energy hypersurface. The $C_s(1)$ structure may be considered as a weakly bound $H_2-SiH_3^+$ complex, while the $C_s(2)$ structure is a saddle point with respect to the H_2 fragment rotation. The rotational energy barrier is extraordinarily small (less than 10^{-3} kcal/mol), so it may be considered as an essentially free rotation.

The theoretical predictions for the hydrogen molecule dissociation energy of SiH_3^+ and the proton affinity of SiH_4 are summarized in table 5. Zero-point vibrational energy (ZPVE) corrections were included at the DZP SCF, TZ2P SCF, DZP CCSD and TZ2P CCSD levels of theory. The proton affinity is in good agreement with the 153 ± 3 kcal/mol experimental value of Cheng and Lampe [12] and with the earlier theoretical study of Schleyer et al. [8]. These values are all much greater than the experi-

mental proton affinity [13] for CH_4 . We have mentioned earlier that the experimental values for the SiH_3^+ dissociation energy are somewhat ambiguous. The reason for the discrepancies between different experimental studies comes from the variance in the heat of formation of the SiH_3^+ ion [15,16,18]. Taking the heat of formation of SiH_3^+ as 219.0 kcal/mol [36], the experimental dissociation energy obtained via the heats of formation of SiH_3^+ from refs. [15,16,18] will be 10.0, 15.2 and 20.0 kcal/mol, respectively. Our theoretical result at the TZ2P CCSD level predicts $D_e = 14.1$ kcal/mol. If we approximate the zero-point vibrational energy (ZPVE) correction by using one half the sum of the TZ2P CCSD harmonic vibrational frequencies (3.8 kcal/mol), this D_0 value is 10.3 kcal/mol.

As stated above, the SiH_3^+ cation is best considered as involving weakly bound SiH_3^+ and H_2 subunits. We are therefore interested in the energetics and mechanism for pseudorotation. Schleyer et al. [8] have proposed a C_{2v} structure for the transition state for pseudorotation. We have analyzed this problem using the vibrational frequencies arising from each stationary point. From the number of imaginary vibrational frequencies, one can tell whether an energy stationary point is a local minimum (all real frequencies), a saddle point (one imaginary frequency), or a higher order saddle point (more than one imaginary frequency). The numbers of imaginary frequencies (also called Hessian indices) for each structure at the DZP SCF and TZ2P SCF levels are listed in table 4. We see that the $C_s(2)$ and C_{2v}

Table 5
Proton affinity (kcal/mol) of silane ^{a)} and dissociation energy of SiH_3^+ ^{b)}

	Proton affinity	Dissociation energy (D_e)	Dissociation energy ^{c)} (D_0)
DZP/SCF	154.8 (150.2) ^{c)}	9.4	5.4
DZP/CISD ^{d)}	157.0	6.9	
DZP/CCSD	157.4	12.5	
TZ2P/SCF	157.6 (153.2) ^{c)}	10.4	6.6
TZ2P/CISD ^{d)}	157.5	7.4	
TZ2P/CCSD	157.6	14.1	
experiment	153 \pm 3 [12]		10.0 [15], 15.2 [18], 20.0 [16]

^{a)} Energy difference for $SiH_3^+ \rightarrow SiH_4 + H^+$.

^{b)} Energy difference for $SiH_3^+ \rightarrow SiH_4^+ + H_2$.

^{c)} Zero-point vibrational correction included.

^{d)} SiH_3^+ and H_2 separated by 100 Å.

structures are genuine transition states with respect to certain internal motions. We have noted above that $C_s(2)$ is a transition state for the near-free rotation of the H_2 moiety within SiH_5^+ . Next we turn to the C_{2v} structures, which appear to be pertinent to pseudorotation. To convince ourselves that this is the true transition stationary point for pseudorotation, we followed the imaginary internal motion (which is the motion across the saddle) from the C_{2v} stationary point, and optimized the structure within C_1 symmetry at the TZ2P SCF level. Happily, the $C_s(1)$ structure was obtained. The energy barrier for pseudorotation may be taken as the energy difference between the $C_s(1)$ and C_{2v} structures. From the TZ2P CCSD method, this value is 26.9 kcal/mol, indicating that SiH_5^+ will not undergo pseudorotation readily, i.e. dissociation is preferred. This appears to agree with current experimental understandings [37].

4. Concluding remarks

Analytic derivative methods and finite difference treatments were applied to obtain harmonic vibrational frequencies and infrared intensities for the global minimum stationary point, structure $C_s(1)$. The vibrational frequencies ω_7 and ω_8 are found to be more sensitive to electron correlation than the others. The $C_s(2)$ structure is a transition state for the twisting or torsion of the H_2 fragment, and the energy barrier for this internal rotation is so low that it may effectively be considered a free rotor. The C_{2v} structure was proven to be the transition state for pseudorotation (scrambling). However, the energy barrier (26.9 kcal/mol) is higher than the dissociation energy, and thus it may be concluded that SiH_5^+ will not undergo hydrogen scrambling readily. Also presented is a discussion of the dissociation energy of SiH_5^+ and the proton affinity of SiH_4 . The proton affinities from all levels of theories are in good agreement with experimental measurements. The hydrogen molecule dissociation energy, however, deviates from the experimental value. The result from the highest level of theory (TZ2P CCSD) is $D_e(SiH_5^+ - H_2) = 14.1$ kcal/mol ($D_0 = 10.3$ kcal/mol with zero-point energy correction).

Acknowledgement

This research was supported by the US Air Force Office of Scientific Research, Grant AFOSR-88-0167. We wish to thank Dr. Roger S. Grev, Dr. Yaoming Xie, and Dr. Yukio Yamaguchi for valuable discussions on the subject matter.

References

- [1] J.F. Stanton, W.N. Lipscomb and R.J. Bartlett, *J. Am. Chem. Soc.* 111 (1989) 5173.
- [2] J.B. Collins, P. von R. Schleyer, J.S. Binkley, J.A. Pople and L. Radom, *J. Am. Chem. Soc.* 98 (1976) 3436.
- [3] C. Hoheisel and W. Kutzelnigg, *J. Am. Chem. Soc.* 97 (1975) 6970.
- [4] A. Komornicki and D.A. Dixon, *J. Chem. Phys.* 86 (1987) 5625.
- [5] D.J. DeFrees and A.D. McLean, *J. Comp. Chem.* 7 (1986) 321.
- [6] V. Dyczmons and W. Kutzelnigg, *Theoret. Chim. Acta* 33 (1974) 239.
- [7] V. Dyczmons, V. Staemmler and W. Kutzelnigg, *Chem. Phys. Letters* 5 (1970) 361.
- [8] P. von R. Schleyer, Y. Apeloig, D. Arad, B.T. Luke and J.A. Pople, *Chem. Phys. Letters* 95 (1983) 477.
- [9] F.A. Olah, P.W. Westermann, Y.K. Mo and G. Klopman, *J. Am. Chem. Soc.* 94 (1972) 7859.
- [10] M.D. Sefcik, J.M.S. Henis and P.P. Gasper, *J. Chem. Phys.* 61 (1974) 4321.
- [11] R.D. Smith and J.H. Futrell, *Chem. Phys. Letters* 36 (1975) 5451.
- [12] T.M.H. Cheng and F.W. Lampe, *Chem. Phys. Letters* 19 (1973) 532.
- [13] D.K. Bohme, G.I. Mackay and H.I. Schiff, *J. Chem. Phys.* 73 (1980) 4978.
- [14] J.A. Pople and L.A. Curtiss, *J. Phys. Chem.* 91 (1987) 155.
- [15] H.M. Rosenstock, K. Draxl, B.W. Steiner and J.T. Herron, *J. Phys. Chem. Ref. Data* 6, Suppl. 1 (1977).
- [16] P. Potzinger, A. Ritter and J. Krause, *Z. Naturforsch.* 30A (1975) 347.
- [17] J.D. Morrison and J.T. Traeger, *Intern. J. Mass Spectrom. Ion Phys.* 11 (1973) 289.
- [18] J.M. Dyke, N. Jonathan, A. Morris, A. Ridha and M.J. Winter, *Chem. Phys.* 81 (1983) 481.
- [19] G.A. Olah, L. Heiliger, R. Aniszfeld and G.K.S. Prakash, *New J. Chem.* 14 (1990) 877.
- [20] L.H. Sommer, *Stereochemistry, mechanism and silicon* (McGraw-Hill, New York, 1967).
- [21] W.J. Hehre, R.F. Stewart and J.A. Pople, *J. Chem. Phys.* 56 (1969) 2657.
- [22] W.J. Hehre, R. Ditchfield, R.F. Stewart and J.A. Pople, *J. Chem. Phys.* 52 (1970) 2769.
- [23] S. Huzinaga, *J. Chem. Phys.* 42 (1965) 1293.

- [24] T.H. Dunning, J. Chem. Phys. 53 (1970) 2823.
- [25] T.H. Dunning and P.J. Hay, in: Modern theoretical chemistry, Vol. 3. Methods of electronic structure theory, ed. H.F. Schaefer III (Plenum Press, New York, 1977) pp. 1-27.
- [26] S. Huzinaga, Department of Chemistry Report II, University of Alberta, Edmonton, Alberta, Canada (1971).
- [27] A.D. McLean and G.S. Chandler, J. Chem. Phys. 72 (1980) 5639.
- [28] P. Pulay, in: Modern theoretical chemistry, Vol. 4. Applications of electronic structure theory, ed. H.F. Schaefer III (Plenum Press, New York, 1977) pp. 153-185.
- [29] H.F. Schaefer III and Y. Yamaguchi, J. Mol. Struct. 135 (1986) 369.
- [30] J.D. Goddard, N.C. Handy and H.F. Schaefer III, J. Chem. Phys. 71 (1979) 1525.
- [31] B.R. Brooks, W.D. Laidig, P. Saxe, J.D. Goddard, Y. Yamaguchi and H.F. Schaefer III, J. Chem. Phys. 72 (1980) 465.
- [32] P. Saxe, D.J. Fox, H.F. Schaefer III and N.C. Handy, J. Chem. Phys. 77 (1982) 5584.
- [33] A.C. Scheiner, G.E. Scuseria, J.E. Rice, T.J. Lee and H.F. Schaefer III, J. Chem. Phys. 87 (1987) 5361.
- [34] P. Saxe, Y. Yamaguchi and H.F. Schaefer III, J. Chem. Phys. 77 (1982) 5674.
- [35] Y. Morino and K. Kuchitsu, J. Chem. Phys. 20 (1952) 1809; J.H. Schachtschneider and R.G. Snyder, Spectrochim. Acta 19 (1963) 117.
- [36] S.G. Lias, J.F. Liebman and R.D. Levin, J. Phys. Chem. Ref. Data 13 (1984) 695.
- [37] M.D. Sefcik, J.M.S. Henis and P.P. Gasper, J. Chem. Phys. 61 (1974) 4329.

Sulfur clusters: structure, infrared, and Raman spectra of cyclo-S₆ and comparison with the hypothetical cyclo-O₆ molecule

By YAOMING XIE and HENRY F. SCHAEFER III

Center for Computational Quantum Chemistry, University of Georgia, Athens,
Georgia 30602, USA

JEE HWAN JANG, BYUNG JIN MHIN, HO SOON KIM,
CHANG WOO YOON and KWANG S. KIM

Department of Chemistry, Pohang Institute of Science and Technology,
P.O. Box 125, Pohang 790-600, Korea

(Received 25 September 1991; accepted 14 November 1991)

Ab initio quantum mechanical methods have been applied to the S₆ and O₆ molecules at their respective D_{3d} hexagonal chair equilibrium geometries. Double zeta plus polarization (DZ + P) and triple zeta plus double polarization (TZ + 2P) basis sets have been used in conjunction with the self-consistent field (SCF) method and second-order perturbation theory. Equilibrium geometries, harmonic vibrational frequencies, infrared intensities, and Raman intensities have been predicted for the two cyclic molecules. Two previous vibrational difficulties between theory and experiment for S₆ have been resolved. The O₆ molecule appears to be similar to the well-characterized S₆ in several respects. However, its dissociation energy and vibrational frequencies reveal a much flatter potential energy surface for O₆ in the region of the equilibrium geometry. While still predicted to correspond to a genuine potential minimum, O₆ nevertheless lies about 100 kcal mol⁻¹ above three separated O₂ molecules. From a methodological viewpoint, the single configuration Hartree-Fock approach is found to be qualitatively satisfactory for S₆ but very poor for O₆.

1. Introduction

In 1891 Engel [1] prepared a rhombohedral form of elemental sulfur, named ϵ -sulfur. By 1961, ϵ -sulfur was clearly established [2] to be the six-membered ring compound cyclo-S₆. Although the monocyclic S₈ dominates elemental sulfur, the S₆ molecule is now fairly well characterized, including its crystal structure [3], with bond distances 2.068 Å and bond angles 102.6° arranged in D_{3d} hexagonal chair form. As noted in the text by Greenwood and Earnshaw [4], the six equivalent bond angles, as well as the dihedral angles (73.8°), in cyclo-S₆ are the smallest of any poly-sulfur species for which laboratory data exist. There also exist infrared and Raman spectroscopic data [5-8] as well as optical absorption spectra [9] for cyclo-S₆.

Important theoretical studies of cyclo-S₆ include the density function work of Hohl, Jones, Car, and Parrinello [10] and the very recent *ab initio* studies of Dixon and Wassermann [11] and of Raghavachari, Rohlfing, and Binkley [12]. Both the density functional [10] and Raghavachari [12] studies consider a variety of sulfur clusters from S₂ to S₁₂. In the Raghavachari, Rohlfing, and Binkley paper [12], structural optimization and vibrational frequency evaluations were carried out with 3-21 G* basis set self-consistent field (SCF) method. For the S₁₂ system, such theoretical studies represent

a major accomplishment at the present time. The Dixon and Wasserman study [11] was limited to S_4 through S_8 but used a larger basis set, designated valence double zeta plus polarization (DZ + P). Specifically, Dixon and Wasserman predicted molecular structures and harmonic vibrational frequencies at the SCF level with the S(12s8p1d/5s3p1d) contracted Gaussian basis of McLean and Chandler [13].

In previous studies [14–16], we have considered theoretically the properties of S_4 , S_8 , and S_{12} . The levels of theory employed ranged from configuration interaction including all single and double excitations (CISD) with a triple zeta plus double polarization (TZ + 2P) basis set for S_4 to DZ SCF for the larger S_{12} molecule. In the present research on S_6 , we report the first molecular structure and set of vibrational frequencies obtained using post-Hartree–Fock methods. In addition, we report SCF predictions using basis sets significantly larger than those employed in references [11] and [12]. It is hoped that the resulting theoretical predictions will stimulate new experiments on the gas-phase S_6 molecule.

2. Theoretical approach

The double zeta plus polarization (DZ + P) basis used here is the S(11s7p1d, 6s4p1d) Dunning–Hay contraction [17] of Huzinaga's primitive Gaussian set [18], augmented by a set of five d functions ($\alpha = 0.532$) on each sulfur atom. The larger basis used in this work approaches triple zeta plus double polarization (near TZ + 2P) quality. The 'near TZ' part of this basis set is obtained from the McLean–Chandler S(12s9p/7s5p) basis [13] by simply releasing one primitive Gaussian function of s symmetry. Thus the contractions are s(6 2 1 1 1 1) and p(5 2 1 1 1). We must emphasize that this 'near TZ' basis is not true of valence triple zeta quality. Only two of the s and two (or perhaps three) of the p type primitive Gaussians lie squarely in the region of the 3s and 3p atomic orbitals, respectively. However, our (7s5p) near TZ basis is much more flexibly contracted than the (5s3p) set of Dixon and Wasserman [11]. An indication of this difference in basis sets is given by the comparison between our near TZ + 2P SCF energy for S_6 (–2385.23542) and the SCF energy reported in reference [11], namely –2385.03624 hartrees. The sulfur d function orbital exponents in the near TZ + 2P basis are $\alpha_d(S) = 1.0, 0.25$.

Although the sulfur basis set labeled 'near TZ + 2P' here represents a significant improvement over earlier theoretical studies of S_6 , it is by no means complete. The referee has reasonably stated that a true 'DZ' basis set for sulfur should already include one set of d functions; that a true 'DZ + P' basis should have two sets of d functions; and that a 'TZ + 2P' basis should include three sets of d functions and a set of f functions.

For the comparable studies of cyclo- O_6 , the DZ + P basis is the standard O(9s5p1d/4s2p1d) set of Dunning [19] and Huzinaga [20], with oxygen atom d function exponents $\alpha_d(O) = 0.85$. The TZ + 2P basis for oxygen incorporates Dunning's (5s3p) contraction [21] of Huzinaga's (10s6p) primitive Gaussian basis [20]. Oxygen atoms polarization functions in the TZ + 2P set had Gaussian orbital exponents $\alpha_d(O) = 1.5, 0.35$.

Equilibrium geometries were located for the D_{3d} hexagonal chair structures of S_6 and O_6 using both the DZ + P SCF and TZ + 2P SCF theoretical methods. Furthermore, the Gaussian 90 programs [22, 23] developed by Pople and coworkers and the Turbomole programs developed by Ahlrichs and coworkers [24] were used to determine MP2 (Møller–Plesset second-order perturbation theory) equilibrium

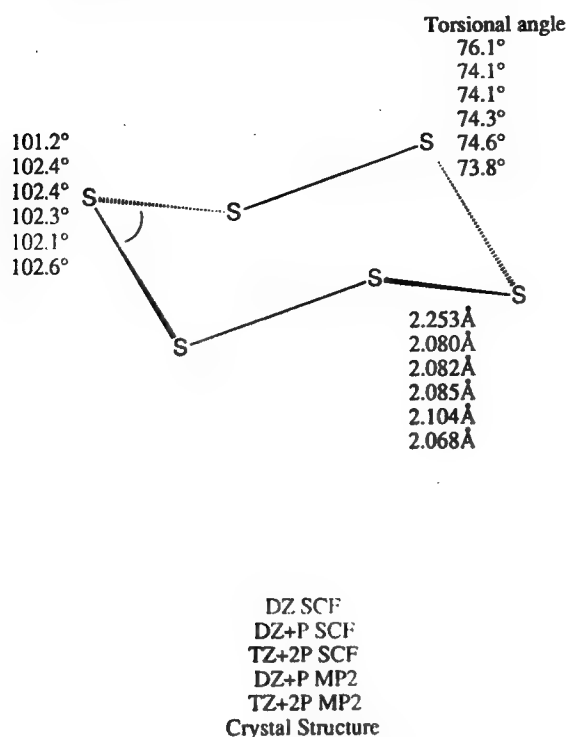


Figure 1. Predicted D_{3d} equilibrium geometries for S_6 .

geometries. In the MP2 treatment the core SCF molecular orbitals (corresponding to oxygen 1s and sulfur 1s, 2s, and 2p atomic orbitals) were frozen (i.e., fully occupied), but all virtual orbitals were explicitly included. The above geometry optimizations were carried out using total energies only, i.e., without analytical gradients.

For both the O_6 and S_6 molecules, harmonic vibrational frequencies were evaluated analytically using the DZ + P SCF and TZ + 2P SCF methods. Going beyond the Hartree-Fock approximation, harmonic vibrational frequencies were also evaluated (via finite differences of analytical gradients) at the DZP MP2 level of theory, with all orbitals (occupied and virtual) explicitly included.

3. Equilibrium geometries for S_6 and O_6

The theoretical predictions for the D_{3d} hexagonal chair equilibrium geometry of S_6 are compared with the experimental crystal structure [3] in figure 1. However, there will be inherent differences [25] between the crystal structure and the gas phase r_e structure, even if the latter were known from laboratory studies. Plausible estimates of the solid state-gas phase r_e structural differences might be $\Delta r = 0.01 \text{ \AA}$ in bond distances and $\Delta\theta = 0.5^\circ$ in bond angles.

As noted earlier [15] for S_8 and presumed [16] for S_{12} , at the DZ SCF level of theory S—S bond distances are too long by nearly 0.2 \AA . With the DZ + P basis set, this difference between theory and experiment is reduced to 0.012 \AA . With the largest basis set, TZ + 2P, the SCF bond distance is only 0.014 \AA longer than that found experimentally in the S_6 crystal structure [3]. The effect of the second-order perturbation theory with the DZ + P basis set is to slightly (by 0.005 \AA) increase the S—S

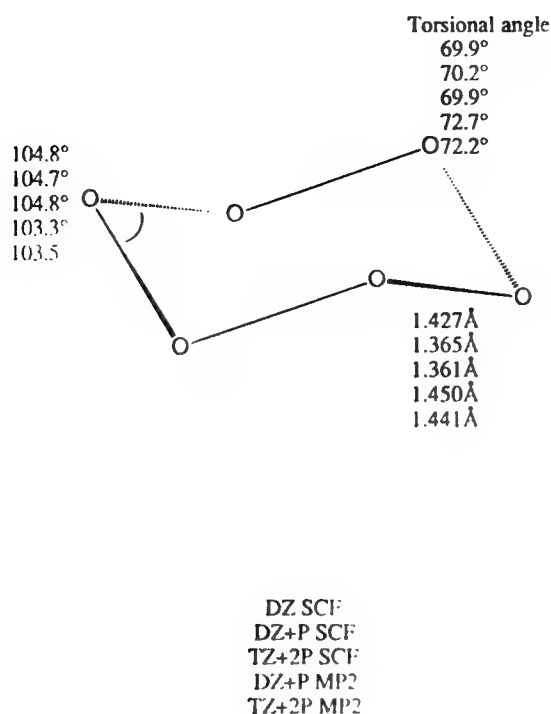


Figure 2. Predicted D_{3d} equilibrium geometries for O_6 .

distances. With the larger TZ + 2P basis set the MP2 S—S equilibrium distance is 0.022 Å longer than the SCF result. Except for the DZ SCF method, all theoretical bond angles and torsional angles for S_6 agree well with experiment [3].

Figure 2 shows the analogous theoretical predictions for the yet-unknown cyclo- O_6 molecule. For O_6 the effects of basis set extension from the DZ SCF point of reference are less severe. The differences between DZ SCF and DZ + P SCF O—O bond distances is 0.062 Å, while further extension to TZ + 2P SCF reduces the DZ + P SCF O—O distance by only 0.004 Å. However, the effects of electron correlation on molecular structure are much greater for O_6 than for S_6 . Specifically, MP2 with the DZ + P basis set increases the O—O distance by 0.085 Å, decreases the OOO bond angle by 1.3°, and increases the torsional angle by 2.5°. This is, of course, consistent with the view that O_6 sits in a much more shallow potential well than does the strongly bound S_6 molecule. Similarly, with the larger TZ + 2P basis set, second-order perturbation theory increases the O—O distances by 0.080 Å, decreases the OOO bond angles by 1.4° and increases the torsional angles by 2.3°.

4. Energetics

Total energies for S_6 and O_6 at various levels of theory are given in table 1. The comparable restricted Hartree-Fock (RHF) energies for diatomic S_2 are -794.93007 (DZ basis, $r_e = 2.013$ Å), -795.00181 (DZ + P basis, $r_e = 1.881$ Å), and -795.06294 hartrees (TZ + 2P basis, $r_e = 1.880$ Å). The experimental equilibrium bond distance [26] for the $^3\Sigma_g^-$ ground state of S_2 is 1.889 Å. For diatomic O_2 the comparable RHF total energies are -149.57130 (DZ basis, $r_e = 1.199$ Å),

Table 1 Total energies (in hartrees) for the cyclo-S₆ and cyclo-O₆ molecules. Relative energies (ΔE) are given in kcal mol⁻¹. The signs of the energetic quantities indicate that S₆ lies below three S₂ molecules, while O₆ lies above three O₂ molecules.

	S ₆	ΔE (S ₆ - 3S ₂)	O ₆	ΔE (O ₆ - 3O ₂)
DZ SCF	-2384.80231	-7.6	-448.49598	+136.7
DZ + P SCF	-2385.03895	-21.0	-448.69111	+136.2
DZ + P MP2	-2385.82819	-36.7	-449.77655	+100.8
TZ + 2P SCF	-2385.23542	-29.2	-448.74848	+139.5
TZ + 2P MP2	-2386.09797	-51.1	-450.02987	+99.0
Experiment		-67.8 ± 2		

-149.63605 (DZ + P basis, $r_e = 1.166$ Å), and -149.65694 hartrees (TZ + 2P basis, $r_e = 1.154$ Å). The experimental bond distance [25] for O₂ is $r_e = 1.208$ Å.

Also reported in table 1 are the energies of S₆ and O₆ relative to the dissociation limits 3S₂ and 3O₂. Since some experimental data [27] are available for gas phase S₆, these results will be discussed first. At the SCF level of theory, S₆ is predicted to lie 7.6 (DZ basis), 21.0 (DZ + P basis), and 29.2 kcal mol⁻¹ (TZ + 2P basis) below three isolated S₂ molecules. The experimental heat of formation of S₆ at 298.15 K has been estimated to be 101.9 ± 8 kJ mol⁻¹, or 24.4 ± 2 kcal mol⁻¹. The comparable heat of formation of gaseous ³Σ_g⁻ S₂ is 128.60 ± 0.30 kJ mol⁻¹, which is readily translated for three separated S₂ molecules to 92.2 ± 0.2 kcal. Thus one finds, to the degree that the experimentally deduced heat of formation of S₆(g) is correct, the result

$$\Delta H[S_6(g) \rightarrow 3S_2(g)] = 67.8 \pm 2 \text{ kcal mol}^{-1}$$

It is clear from table 1 that single-configuration SCF theory does a poor job of predicting the dissociation energy of S₆. The same result was found earlier [15] for the better experimentally characterized S₈ system. In reference [15], the use of DZ + P MP2 theory significantly improved the DZP SCF dissociation energy for S₈. For an open-shell system like the ³Σ_g⁻ ground state of S₂ the Gaussian codes mandate the use of unrestricted Møller-Plesset second-order perturbation theory (UMP2). The TZ + 2P UMP2 equilibrium geometry for S₂ has $r_e = 1.939$ Å and total energy -795.33886 hartrees; the expectation value of S² is 2.052. The comparable results for O₂ are $r_e = 1.233$ Å, $E(\text{TZ} + 2\text{P UMP2}) = -150.06255$ hartrees; the expectation value of S² is 2.049. As an aside, it is interesting that the TZ + 2P UMP2 method predicts the S₂ and O₂ r_e values to be too long by 0.050 Å and 0.025 Å, respectively.

In the above described manner, the quantity

$$\Delta E(S_6 - 3S_2) = E(S_6, \text{TZ} + 2\text{P MP2}) - 3E(S_2, \text{TZ} + 2\text{P UMP2})$$

is predicted to be -51.1 kcal mol⁻¹. (The zero-point vibrational energy correction at the TZ + 2P SCF level of theory is +3.0 kcal mol⁻¹. Although this result still falls significantly short of the experimental estimate of -68 ± 2 kcal mol⁻¹, it represents a major improvement over the SCF prediction.

5. O₆: a high energy density molecule

A primary motivation for our previous comparative studies [15, 16] of S₁₂/O₁₂ and S₈/O₈ was to establish the viability of oxygen rings as high energy density materials (HEDM). A primary conclusion of these studies was that O₈ and O₁₂ are somewhat

lower-lying energetically than anticipated from back-of-the-envelope calculations [28]. This result may be considered both 'good' and 'bad' with respect to the design of potential HEDM systems. That is, O_8 and O_{12} are likely to be more stable than originally anticipated, and hence easier to prepare in the laboratory; however, these species will not carry as much excess energy (with respect to $n/2$ separated O_2 molecules) as earlier imagined.

The O_4 system, on the other hand, is quite highly energetic, but appears to have a barrier of less than 10 kcal mol^{-1} for dissociation to two O_2 molecules [29]. Perhaps O_6 might provide a happy meeting ground, with substantial energy content and a substantial barrier to dissociation.

It is helpful to display the oxygen ring dissociation energies on a per-atom basis, e.g., for O_6 to divide the quantity

$$E(O_6) - 3E(O_2)$$

given in table 1 by six. When this is done, the following array of dissociation energies may be fashioned:

	O_6	O_8	O_{12}
DZ SCF	22.8	21.3	20.9
DZ + P SCF	22.7	21.6	21.6
DZ + P MP2	16.8	15.4	
TZ + 2P SCF	23.3		
TZ + 2P MP2	16.5		

At every level of theory, O_6 is a more energetic species than O_8 or O_{12} ; however, the differences are less than 2 kcal/mol^{-1} per O atom. Clearly, the thrust of future theoretical studies of oxygen rings should be directed toward the yet undetermined activation energies of these species for dissociation to separated diatomic oxygen molecules.

6. Infrared and Raman spectra

Table 2 reports the present theoretical predictions for the harmonic vibrational frequencies and infrared and Raman intensities for S_6 . Our DZ + P SCF and TZ + 2P SCF predictions are only somewhat different from the smaller basis theoretical results reported earlier by Dixon and Wasserman [11]. Furthermore, from the SCF studies alone, we might concur with their conclusion that the feature inferred by Nimon, Deff, Cantley, and Buttlar [6] at 390 cm^{-1} appears too low in frequency to be assigned to the a_{1g} fundamental vibration. For this IR forbidden a_{1g} fundamental, our TZ + 2P SCF frequency (500 cm^{-1}) is only 18 cm^{-1} below that of Dixon and Wasserman. A less serious point is the e_g stretching fundamental assigned at 448 or 450 cm^{-1} , for which our $\omega(\text{TZ} + 2\text{P SCF})$ lies 18 cm^{-1} below that of Dixon and Wasserman. This small difference, however, nicely accounts for most of the difference of $\sim 30 \text{ cm}^{-1}$ between experiment and Dixon and Wasserman's scaled theoretical value. Note, of course, that our harmonic vibrational frequencies should also be scaled. The true fundamentals are expected to lie about 10% lower than the present TZ + 2P SCF harmonic vibrational frequencies.

Table 2 *Ab initio* theoretical predictions for the infrared and Raman spectra of S₆

Symmetry	DZ + P SCF			TZ + 2P SCF			DZ + P MP2		Experiment	
	ω cm ⁻¹	IR intensity kmol ⁻¹	Raman intensity A ⁴ amu	ω cm ⁻¹	IR intensity kmol ⁻¹	Raman intensity A ⁴ amu	ω cm ⁻¹		Berkowitz [5]	Nimon [6]
e _g	528	0	25	518	0	15	462		450	448
a _{1g}	523	0	60	512	0	56	493		478	471
e _u	515	1.2	0	504	0.9	0	472		462	463
a _{1u}	509	0	0	500	0	0	399		—	390
a _{2u}	353	3.5	0	344	1.6	0	323		312	313
a _{1g}	282	0	13	278	0	10	270		264	262
e _g	233	0	12	227	0	9	209		201	202
e _u	174	1.0	0	173	0.9	0	166		—	180

A much more satisfactory rendering of the experimental S_6 fundamentals is provided by going beyond Hartree-Fock theory. Most significantly in table 2, the a_{1u} harmonic vibrational frequency is reduced from 509 cm^{-1} (DZ + P SCF) to 399 cm^{-1} (DZ + P MP2). Thus the conflict with Nimon's assigned a_{1u} fundamental [6] at 390 cm^{-1} disappears. Similarly the e_g harmonic vibrational frequency (528 cm^{-1} , DZ + P SCF; 518 cm^{-1} , TZ + 2P SCF) is reduced to 462 cm^{-1} (DZ + P MP2), in much closer agreement with the experimental values [5, 6] of 448 and 450 cm^{-1} .

The Raman intensities, predicted here for the first time for S_6 , agree well with the experimental observations [5, 6]. Specifically, Berkowitz, Chupka, Bromels, and Belford [5] observe Raman peaks in the following order of magnitude: a_{1g} (478) > a_{1g} (264) > e_g (201) > e_g (450). In table 2, both the DZ + P SCF and TZ + 2P SCF methods predict the higher a_{1g} Raman intensity to be the largest. Nimon [6] independently identifies his 471 cm^{-1} Raman feature as 'very strong'. The other three fundamentals observed in the Raman also have substantial theoretical intensities.

For O_6 , theoretical vibrational frequencies and IR and Raman intensities are reported in table 3. The DZ + P SCF and TZ + 2P SCF predictions are qualitatively similar. The larger basis set decreases the four highest harmonic vibrational frequencies (from 5 cm^{-1} to 20 cm^{-1}) and increases the five lowest frequencies (from 4 cm^{-1} to 9 cm^{-1}). Likewise, there are no qualitative changes in IR or Raman intensities in going from DZ + P SCF to TZ + 2P SCF. However, the most striking feature of table 3 is that second-order perturbation theory (i.e., MP2) radically changes the predicted vibrational frequencies for O_6 . This is not a surprise, given the change in the geometrical structure of O_6 from SCF to MP2 and the fact that the O_6 potential energy surface is much flatter than that for S_6 . Even so, the change in the a_{1u} harmonic vibrational frequency from 1088 cm^{-1} (DZ + P SCF) to 361 (DZ + P MP2) is remarkable. All the vibrational frequencies are significantly reduced as electron correlation is incorporated into the theoretical treatment. Although MP2 may exaggerate the importance of double excitations, it is clear that single configuration Hartree-Fock theory is fundamentally flawed for O_6 .

The lowest O—O stretch (a_{2u}) is the best candidate ($\omega = 805\text{ cm}^{-1}$, DZ + P MP2) for observation in the IR, while the second highest O—O stretch (a_{1g} ; $\omega = 886\text{ cm}^{-1}$, DZ + P MP2) should be most readily observable in the Raman spectrum of O_6 . The same fundamentals have the highest intensities for the valence isoelectronic S_6 molecule.

7. Conclusions

The S_6 molecule has been studied at higher levels of theory than previously considered, along with parallel studies of the hypothetical O_6 molecule. This work resolves one major and one minor discrepancy between theory and experiment concerning the fundamental frequencies of S_6 . Specifically, second-order perturbation theory does very well in describing the very weak IR band observed at 390 cm^{-1} by Nimon and coworkers [6] and assigned by them to the a_{1u} fundamental.

Except for its dissociation energy and vibrational frequencies, the hypothetical O_6 molecule appears similar to the well-characterized S_6 . As anticipated by the back-of-the-envelope calculations [28], O_6 is seen to lie significantly above three separated oxygen molecules. Its barrier to exothermic dissociation will prove critical in evaluating its potential usefulness as a high energy density material [29].

This research was supported by the United States Air Force Office of Scientific

Table 3 *Ab initio* theoretical predictions for the infrared and Raman spectra of O₆.

Symmetry	DZ + P SCF			TZ + 2P SCF			DZ + P MP2		
	ω cm ⁻¹	IR intensity km mol ⁻¹	Raman intensity Å ⁴ amu	ω cm ⁻¹	IR intensity km mol ⁻¹	Raman intensity Å ⁴ amu	ω cm ⁻¹	IR intensity km mol ⁻¹	IR intensity km mol ⁻¹
e _g	1137	0	17	1121	0	13	667	0	0
a _{1g}	1124	0	39	1119	0	36	886	0	0
e _u	1093	5.5	0	1084	3.8	0	782	5.6	5.6
a _{1u}	1088	0	0	1068	0	0	361	0	0
a _{2u}	1014	16	0	1023	13	0	805	4.5	4.5
a _{1g}	710	0	7	716	0	6	591	0	0
e _g	655	0	4	659	0	3	530	0	0
e _u	447	2.9	0	453	2.7	0	387	1.4	1.4

Research under Grant No. AFOSR-92-J-0047 and by the Pohang Institute of Science and Technology.

References

- [1] ENGEL, M.R., 1891, *C.R. Acad. Sci. Paris*, **112**, 866.
- [2] DONOUE, J., 1974, *The Structures of the Elements* (Wiley).
- [3] STEIDEL, J., PICKARDT, J. and STEIDEL, R., 1978, *Z. Naturf. B*, **33**, 1554.
- [4] GREENWOOD, N. N., and EARNSHAW, A., 1984, *Chemistry of the Elements*, pp. 757-881 (Pergamon).
- [5] BERKOWITZ, J., CHUPKA, W. A., BROMELS, E., and BELFORD, R. L., 1967, *J. Chem. Phys.*, **47**, 4320.
- [6] NIMON, L. A., NEFF, V. D., CANTLEY, R. E., and BUTTLAR, R. O., 1967, *J. Molec. Spectrosc.*, **22**, 105.
- [7] NIMON, L. A., and NEFF, V. D., 1968, *J. Molec. Spectrosc.*, **26**, 175.
- [8] STEUDEL, R., 1975, *Spectrochim. Acta. A*, **31**, 1065.
- [9] STEUDEL, R., JENSEN, D., GÖBEL, P., and HUGO, P., 1988, *Ber. Bunsenges. Phys. Chem.*, **92**, 118.
- [10] HOHL, D., JONES, R. O., CAR, R., and PARRINELLO, M., 1988, *J. chem. Phys.*, **89**, 6823.
- [11] DIXON, D. A., and WASSERMAN, E., 1990, *J. phys. Chem.*, **94**, 5772.
- [12] RAGHAVACHARI, K., ROHLFING, C. M., and BINKLEY, J. S., 1990, *J. chem. Phys.*, **93**, 5862.
- [13] MCLEAN, A. D., and CHANDLER, G. S., 1980, *J. chem. Phys.*, **72**, 5639.
- [14] QUELCH, G. E., SCHAEFER, H. F., and MARSDEN, C. J., 1990, *J. Am. chem. Soc.*, **112**, 8719.
- [15] KIM, K. S., JANG, J. H., KIM, S., MHIN, B.-J., and SCHAEFER, H. F., 1990, *J. chem. Phys.*, **92**, 1887.
- [16] KIM, K. S., KIM, H. S., KIM, S., JANG, J. H., and SCHAEFER, H. F., 1989, *J. Am. chem. Soc.*, **111**, 7746.
- [17] DUNNING, T. H., and HAY, P. J., 1977, *Modern Theoretical Chemistry*, Vol. 3 (Plenum Press) pp. 1-27.
- [18] HUZINAGA, S., 1971, *Approximate Atomic Wavefunctions. II*, Department of Chemistry Report (University of Alberta, Edmonton, Canada).
- [19] DUNNING, T. H., 1970, *J. chem. Phys.*, **53**, 2823.
- [20] HUZINAGA, S., 1965, *J. chem. Phys.*, **42**, 1293.
- [21] DUNNING, T. H., 1971, *J. chem. Phys.*, **55**, 716.
- [22] HEHRE, W. J., RADOM, L., SCHLEYER, P. R., and POPLE, J. A., 1986, *Ab Initio Molecular Orbital Theory* (Wiley).
- [23] FRISCH, M. J., HEAD-GORDON, M., TRUCKS, G. W., FORESMAN, J. B., SCHLEGEL, H. B., RAGHAVACHARI, K., ROBB, M., BINKLEY, J. S., GONZALEZ, C., DEFREES, D. J., FOX, D. J., WHITESIDE, R. A., SEEGER, R., MELIUS, C. F., BAKER, J., MARTIN, R. L., KAHN, L. R., STEWART, J. P. J., TOPIOL, S., and POPLE, J. A., Gaussian 90, Release F (Gaussian Inc., Pittsburgh, PA).
- [24] AHLRICHS, R., BÄR, M., HÄSER, M., and HORN, H., 1989, *Chem. Phys. Lett.*, **162**, 165.
- [25] See, for example, LAURIE, V. W., 1974, Definitions and general theory of interatomic distances, *Critical Evaluation of Chemical and Physical Structural Information*, edited by, LIDE, D. R., and PAUL, M. A., p. 67. (National Academy of Sciences, Washington, D.C.)
- [26] HUBER, K. P., and HERZBERG, G., 1979, *Molecular Spectra and Molecular Structure Volume IV, Constants of Diatomic Molecules* (Van Nostrand Reinhold).
- [27] CHASE, M. W., DAVIES, C. A., DOWNEY, J. R., FRURIP, D. J., McDONALD, R. A. and SYVERUD, A. N., 1986, *JANAF Thermochemical Tables 3rd Edn* (American Institute of Physics, New York).
- [28] SEIDL, E. T. and SCHAEFER, H. F., 1988, *J. chem. Phys.*, **88**, 7043.
- [29] SEIDL, E. T., and SCHAEFER, H. F., 1992, *J. chem. Phys.*, **96**, 1176.

The fundamental vibrational frequencies of the silyl anion (SiH_3^-)

By MINGZUO SHEN and HENRY F. SCHAEFER III

Center for Computational Quantum Chemistry, The University of Georgia,
Athens, Georgia 30602, USA

(Received 5 November 1991; accepted 28 November 1991)

Ab initio quantum mechanical methods have been used to predict the vibrational frequencies for the silyl anion (SiH_3^- , C_{3v}). In the present study, the self-consistent field, the configuration interaction with single and double excitations, and the coupled cluster with single and double excitations wavefunctions were used in conjunction with the triple zeta plus double polarization plus diffuse function basis set. Anharmonicity has been explicitly considered using vibrational perturbation theory. The effects of diffuse s functions on the hydrogen atoms are found to be surprisingly large.

1. Introduction

Recently, we have carried out systematic theoretical studies on the silyl anion, SiH_3^- [1, 2]. Molecular geometries and harmonic vibrational frequencies for the pyramidal (C_{3v}) and planar (D_{3h}) structures of the silyl anion were considered in the first paper [1]. Subsequently, the anharmonic corrections to the harmonic vibrational frequencies were investigated using *ab initio* potential energy surfaces [2]. In particular, cubic and quartic force constants with respect to symmetrized curvilinear internal coordinates were obtained with the self-consistent field (SCF) and configuration interaction with single and double excitations (CISD) wavefunctions spanned by the triple zeta plus double polarization plus diffuse function (TZ2P + diff(Si)) basis set (which has three p diffuse basis functions on the silicon atom). Finite difference schemes were used in the cases where analytical derivative techniques have not yet been implemented. In determining the anharmonic corrections from the cubic and quartic force constants, both second order perturbation theory [3] and vibrational theory [4] were used.

In the study of the fundamental vibrational frequencies [2], it was found that the anharmonic corrections ($\Delta\nu_i = \nu_i - \omega_i$) for all the vibrational modes are relatively stable (in terms of changes in the absolute value) with respect to the improvement of wavefunctions (namely, from SCF to CISD) and to the improvement of basis set [i.e., from DZP to TZ2P to TZ2P + diff(Si)]. One potential problem with the largest basis set TZ2P + diff(Si) was that, while it has diffuse p basis functions on Si, it does not have diffuse basis functions on the hydrogen atoms. This could cause the basis set to be biased, because normally the hydrogen atom is more electronegative than the silicon atom, and thus the negative charge is shared by the hydrogen atoms in the silyl anion. We therefore carried out another complete set of computations using a single s diffuse basis function on each H. This paper reports the additional results, which are somewhat surprising.

2. Theoretical details

The TZ2P + diff(Si) basis set is the same as used before [1, 2]. That is, the TZ basis for Si is the contraction (12s9p/6s5p) given by McLean and Chandler [5]. The TZ basis for H is the (4s/3s) contraction given by Dunning [6]. The two sets of polarization functions have orbital exponents $\alpha_d(\text{Si}) = 1.00, 0.25$, $\alpha_p(\text{H}) = 1.50, 0.375$. The diffuse p functions on Si have orbital exponent $\alpha_p(\text{Si}) = 0.02$. The TZ2P + diff(Si, H) basis set incorporates three more basis functions than TZ2P + diff(Si), namely one s functions on each H, with orbital exponent $\alpha_s(\text{H}) = 0.04$.

The wavefunctions used in the present study include SCF, CISD, and coupled cluster with single and double excitations (CCSD). We optimized the molecular geometry using the analytical gradient techniques for each respective wavefunction. With the SCF wavefunction, quadratic and cubic force constants were computed analytically. Quartic force constants were evaluated using finite differences of analytical cubic force constants. We also determined quadratic force constants using the CISD and CCSD wavefunctions via finite differences of analytical gradients. Since analytical higher derivatives are not yet available for the CISD and CCSD wavefunctions, we did not determine CISD and CCSD higher derivatives in the present study. Previously, we obtained approximate CISD cubic and quartic force constants using the TZ2P + diff(Si) basis sets via a multiple finite difference scheme involving analytical gradients [2].

These computations were performed using the PSI suite of computer programs, distributed by the Psitech, Inc., Watkinsville, GA, USA. The University of Georgia IBM 3090 computer was used for all except C_1 symmetry CCSD analytical gradients. The IBM RS6000 530 workstation on site was used for the CCSD analytical gradients of the C_1 displacements (necessary in the finite difference scheme for quadratic force constants). A total of 132,355 singly and doubly excited configurations were included for the C_1 symmetry CCSD analytic gradient computations. Note that since in CCSD wavefunctions all electrons were explicitly correlated, and in CISD wavefunctions five core MOs (silicon 1s, 2s, and 2p-like) were frozen and one virtual MO was deleted, and since the CCSD method treats electron correlation more completely than the CISD method, the CCSD correlation energies are larger (roughly twice in the present case) than the CISD correlation energies.

Standard definitions of the symmetrized internal coordinates were used in the present study (identical to those defined previously in reference [2]). For convenient reference, these coordinates are defined in equation (1), where r_i is one of the SiH bond distances, and α , one of the HSiH bond angles opposite to r_i .

$$S_1 = \frac{1}{\sqrt{3}} (\Delta r_1 + \Delta r_2 + \Delta r_3), \quad (1a)$$

$$S_2 = \frac{1}{\sqrt{3}} (\Delta \alpha_1 + \Delta \alpha_2 + \Delta \alpha_3), \quad (1b)$$

$$S_{3a} = \frac{1}{\sqrt{6}} (2\Delta r_1 - \Delta r_2 - \Delta r_3), \quad (1c)$$

$$S_{3b} = \frac{1}{\sqrt{2}} (\Delta r_2 - \Delta r_3), \quad (1d)$$

$$S_{4a} = \frac{1}{\sqrt{6}} (2\Delta \alpha_1 - \Delta \alpha_2 - \Delta \alpha_3), \quad (1e)$$

Table 1. Theoretical molecular geometries and total energies for the silyl anion (SiH_3^- , C_{3v}). Geometries with TZ2P and TZ2P + diff(Si) basis sets are taken from our previous study for comparison [1, 2]. There are two reasons that the CCSD correlation energies are larger than the CISD correlation energies: (i) in the CCSD wavefunctions all electrons were explicitly correlated, while in the CISD wavefunctions five (silicon 1s-, 2s-, and 2p-like) MOs were frozen and one virtual MO was deleted; and (ii) the CCSD method treats electron correlation more completely than the CISD method.

Level of theory	$r_e(\text{SiH})/\text{\AA}$	$\angle(\text{HSiH})$	Total energy/ E_h^a
		SCF	
TZ2P	1.530	96.4°	-290.63559
TZ2P + diff(Si)	1.528	97.3°	-290.63902
TZ2P + diff(Si, H)	1.532	96.8°	-290.64137
		CISD	
TZ2P	1.532	95.0°	-290.78955
TZ2P + diff(Si)	1.531	95.9°	-290.79278
TZ2P + diff(Si, H)	1.535	95.4°	-290.79540
		CCSD	
TZ2P	1.534	94.7°	-290.93643
TZ2P + diff(Si)	1.534	95.6°	-290.93978
TZ2P + diff(Si, H)	1.537	95.1°	-290.94259

^a $E_h \approx 4.35975 \times 10^{-18} \text{ J}$.

$$S_{4b} = \frac{1}{\sqrt{2}} (\Delta\alpha_2 - \Delta\alpha_3), \quad (1f)$$

3. Results and discussion

Theoretical molecular geometries predicted for the silyl anion (SiH_3^- , C_{3v}) at the various levels of theory are presented in table 1, where some theoretical geometries determined previously are also included for comparison. With the addition of one diffuse s function on each H, the theoretical bond length $r_e(\text{SiH})$ increased slightly (0.004 Å) and bond angle $\angle(\text{HSiH})$ decreased slightly (-0.5°) with the SCF, CISD, and CCSD wavefunctions, compared with the values without diffuse basis functions on the hydrogen atoms. Although these changes are not large in absolute terms, they are substantial when one considers the completeness of the TZ2P + diff(Si) basis set.

Harmonic vibrational frequencies are presented in table 2. Also, some previous results [1, 2] are listed for comparison. The most striking observation is that, with the addition of diffuse s basis functions on the hydrogens, the predicted harmonic vibrational frequencies for the totally symmetric stretch and the degenerate modes drop significantly, while that for the totally symmetric bend (or umbrella) mode remains virtually unchanged, regardless of the wavefunction used. More specifically, the drop for the totally symmetric stretch is about 30 cm^{-1} , that for the degenerate stretch is about 40 cm^{-1} , and that for the degenerate bend is about 10 cm^{-1} . If we take a closer look at the behaviour of the geometry with respect to basis set change, we see that the TZ2P + diff(Si, H) is more balanced than the TZ2P + diff(Si), so that the harmonic vibrational frequencies at the TZ2P + diff(Si, H) CCSD level is currently our best theoretical results. Also shown in table 2 are the available experimental results of Bürger and Eujen [7], and Nimlos and Ellison [8]. In particular, the value from Nimlos and Ellison is reported to be a harmonic vibrational frequency [1]. The

Table 2. Theoretical harmonic vibrational frequencies (in cm^{-1}) for the SiH_3^- anion (C_{3v}). Predictions made with the TZ2P and TZ2P + diff(Si) basis sets are taken from our previous work [1, 2] for comparison. Note the substantial decrease in vibrational frequencies with the addition of diffuse s functions on hydrogen.

Level of theory	Symm. stretch A_1	Stretch E	Bend E	Umbrella A_1
SCF				
TZ2P	2032	1992	1054	966
TZ2P + diff(Si)	2027	1993	1048	934
TZ2P + diff(Si, H)	1990	1953	1037	935
CISD				
TZ2P	1984	1956	1002	916
TZ2P + diff(Si)	1976	1954	994	890
TZ2P + diff(Si, H)	1943	1917	984	888
CCSD				
TZ2P	1959	1933	991	907
TZ2P + diff(Si)	1949	1928	983	880
TZ2P + diff(Si, H)	1918	1892	972	879
Experiment	1888 ^a	1891 ^a	899 ^a	870 ^a , 880 ^b

^aBürger, H., and Eujen, R., 1974, *Z. Naturf. B*, **29**, 647. These are fundamental vibrational frequencies for the silyl anion in hexamethylphosphoric triamide solution with K^+ as the counter ion.

^bNimlos, M. R., and Ellison, G. B., 1986, *J. Am. chem. Soc.*, **108**, 6522. This is a harmonic vibrational frequency for the umbrella mode of the silyl anion in the gas phase.

changes due to diffuse s functions on hydrogen significantly improve the agreement with experiment.

The quadratic force constants with respect to the symmetrized internal coordinates defined in equation (1) have also been determined and presented in table 3. Only results from the present research are shown in table 3, and these should be compared with our previous theoretical results. There are six such nonzero and symmetry independent quadratic force constants [9].

Cubic and quartic force constants at the TZ2P + diff(Si, H) SCF level of theory have also been determined. Since we found previously that these higher force constants are relatively stable with respect to improvement in wavefunction (from SCF to CISD) [1, 2], and since analytical higher derivatives techniques for CISD and CCSD are not yet available, we did not determine higher derivatives using the CISD and CCSD wavefunctions in this study. The units of the force constants are as before.

Table 3. Theoretical quadratic force constants with respect to the symmetrized curvilinear internal coordinates defined in equation (1), for the silyl anion. All results in this table are from the present research. The units of the force constants are consistent with the energy in aJ or mdyne Å, distance in Å, and angle in radians.

Constant	TZ2P + diff(Si, H) SCF	TZ2P + diff(Si, H) CISD	TZ2P + diff(Si, H) CCSD
F_{11}	2.29	2.18	2.12
F_{12}	0.21	0.19	0.18
F_{22}	0.67	0.59	0.57
F_{3a3a}	2.18	2.10	2.05
F_{3a4a}	-0.05	-0.04	-0.04
F_{4a4a}	0.69	0.63	0.62

Table 4. Theoretical anharmonic corrections (in cm^{-1}) Δv_i obtained from the full quartic force field. The TZ2P + diff(Si, H) SCF values have not been reported previously. Note that $\Delta v_i \equiv v_i(\text{anharmonic}) - v_i(\text{harmonic})$.

Level of theory	Symm. stretch A_1	Stretch E	Bend E'	Umbrella A_1
Perturbation				
DZP SCF	-83	-78	-16	-9
TZ2P SCF	-87	-85	-17	-10
TZ2P + diff(Si) SCF	-81	-88	-17	-10
TZ2P + diff(Si, H) SCF	-84	-96	-19	-11
TZ2P + diff(Si) CISD	-88	-93	-15	-13
Variation				
DZP SCF	-60 ^a	-64	-21	-16
TZ2P SCF	-55	-69	-22	-18
TZ2P + diff(Si) SCF	-61	-74	-22	-18
TZ2P + diff(Si, H) SCF	-60	-78	-24	-19
TZ2P + diff(Si) CISD	-69	-73	-20	-20

^aThe anharmonic constant for this mode cannot be unambiguously defined with the DZP SCF method, due to an artificial Fermi resonance brought about by the relatively low theoretical level. We used the arithmetic average of the two interacting frequencies to obtain this anharmonic correction.

namely consistent with the energy in aJ or mdyne Å (or 10^{-18} J), distance in Å, and angle in radians. There are 14 independent cubic and 28 independent quartic force constants [9] with respect to the symmetrized internal coordinates in equation (1). The cubic force constants with respect to the symmetrized internal coordinates determined at the TZ2P + diff(Si, H) SCF level of theory are: $F_{111} = -6.24$, $F_{112} = -0.22$, $F_{122} = 0.17$, $F_{13a3a} = -6.11$, $F_{13a4a} = 0.15$, $F_{14a4a} = -0.28$, $F_{222} = 0.34$, $F_{23a3a} = 0.11$, $F_{23a4a} = 0.11$, $F_{24a4a} = -0.50$, $F_{3a3a3a} = -4.32$, $F_{3a3a4a} = -0.16$, $F_{3a4a4a} = 0.09$, $F_{4a4a4a} = 0.09$. The quartic force constants at the same level of theory are: $F_{1111} = 14.82$, $F_{1112} = -0.53$, $F_{1122} = 0.02$, $F_{113a3a} = 14.62$, $F_{113a4a} = 0.01$, $F_{114a4a} = 0.06$, $F_{1222} = 1.03$, $F_{123a3a} = -0.17$, $F_{123a4a} = -0.02$, $F_{124a4a} = 0.10$, $F_{13a3a3a} = 10.20$, $F_{13a3a4a} = 0.08$, $F_{13a4a4a} = 0.04$, $F_{14a4a4a} = 0.07$, $F_{2222} = 0.82$, $F_{223a3a} = -0.04$, $F_{223a4a} = -0.22$, $F_{224a4a} = 0.14$, $F_{23a3a3a} = -0.13$, $F_{23a3a4a} = 0.21$, $F_{23a4a4a} = -0.01$, $F_{24a4a4a} = -0.47$, $F_{3a3a3a3a} = 22.35$, $F_{3a3a3a4a} = 0.10$, $F_{3a3a4a4a} = -0.25$, $F_{3a4a4a4a} = -0.50$, $F_{4a4a4a4a} = -0.12$, $F_{4a4a4a4a} = 1.14$.

Anharmonic corrections for the vibrational modes have been determined using the standard vibrational second order perturbation theory [3] and vibrational variation theory [4] from the higher force constants determined at the TZ2P + diff(Si, H) SCF level of theory. For detailed discussion of the methods, see references [3] and [4] and references cited in reference [2]. In table 4 we present the new anharmonic corrections, along with our previous results for comparison. The observation from table 4 is still the same as discussed previously [2], namely that the variation of anharmonic corrections with respect to the basis set and wavefunctions (among SCF and CISD) is relatively small in terms of absolute values. Also, the systematic difference between the perturbation and variation theories for vibration still remains. In particular, we see that the diffuse s basis function on the hydrogens have a much smaller effect on the anharmonic corrections than on the harmonic vibrational frequencies (except for the umbrella mode, of course).

To better visualize the behaviour of the anharmonic corrections one may plot the

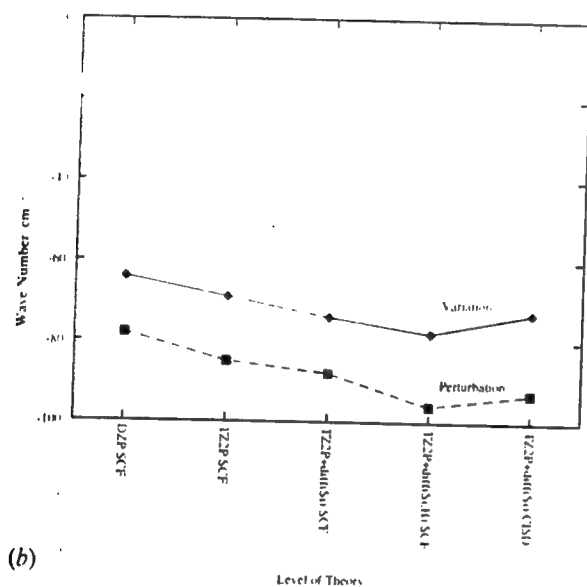
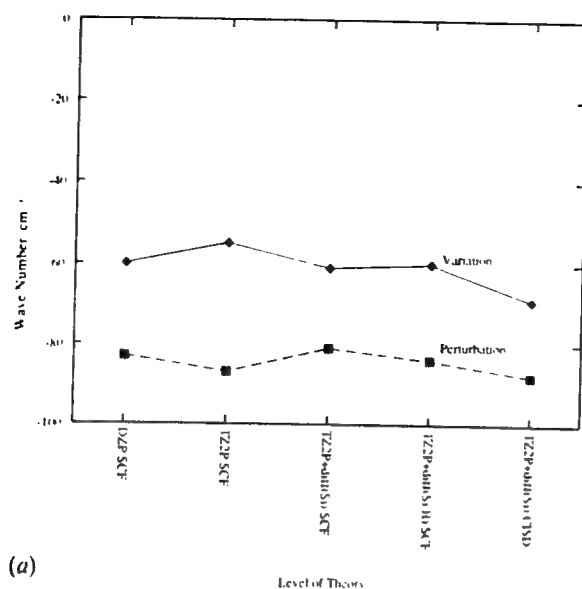
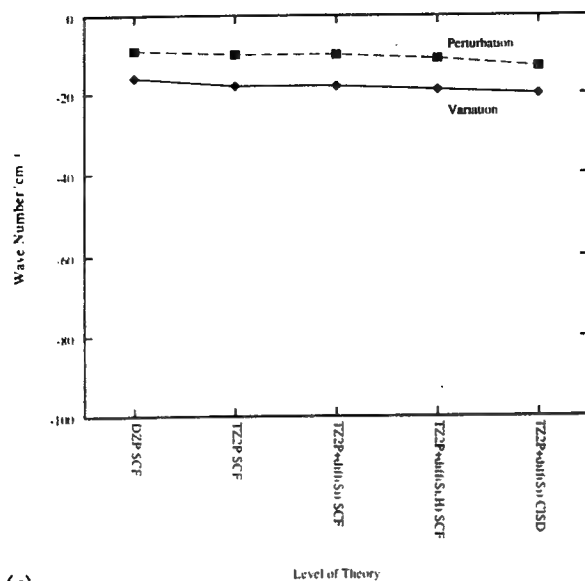
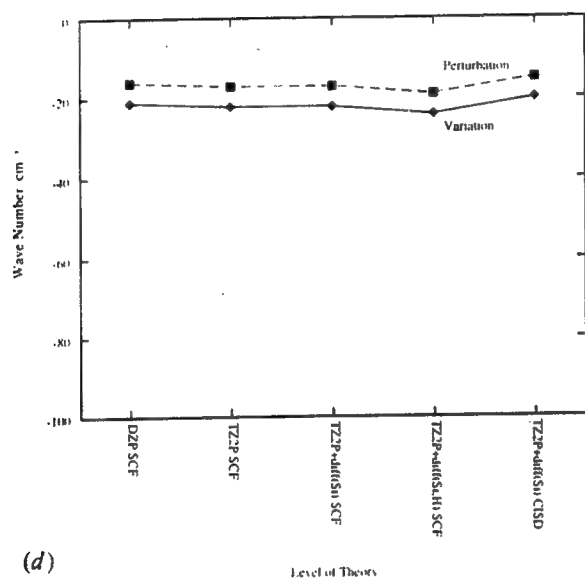


Figure 1. Anharmonic corrections plotted against the various levels of theory. This is a visualization of the data presented in table 4. All four parts are drawn using the same scale and format. (a) Totally symmetric stretch mode A_1 ; (b) degenerate stretch mode E ; (c) degenerate bend mode E ; (d) umbrella mode (totally symmetric bend) A_1 . Values from vibrational perturbation theory [3] are connected by dashed lines, while values from the variation theory [4] are connected by solid lines.

anharmonic corrections from the various levels of theory in graphs, as in figure 1. Figure 1 has four parts, where (a) shows the anharmonic corrections for the totally symmetric stretch mode, (b) the degenerate stretch mode, (c) the degenerate bend mode and, finally, (d) the umbrella mode. This figure is similar to figure 3 in reference [2], except for the newly added TZ2P + diff(Si, H) SCF set of values. As noted



(c)



(d)

Figure 1. (continued).

previously [2], the fact that the lines are nearly flat indicates the relative stability of the anharmonic corrections with respect to the basis sets and electron correlation. The fact that the lines are nearly parallel indicates that the difference between the perturbation and variation theories for vibration is quite systematic for the silyl anion.

4. Conclusion

The present study shows that the addition of diffuse s functions on hydrogen (to an otherwise rather complete basis set) significantly changes the quantitative predictions of the fundamental vibrational frequencies of the SiH_3^- anion. The indirectly

formulated assumption that the diffuse functions support a charge transfer from the lone pair at the silicon atom to the hydrogens is, however, not entirely obvious. A simple analysis shows that the a_1 projection of the additional s functions has a factor of 1.24 higher density at the silicon nucleus than at the hydrogens. The density maximum of this symmetry adapted orbital lies on the symmetry axis, closer to the silicon (0.805 Å) than to the hydrogens (1.310 Å). What is clear is that the molecular electron distribution for SiH_4 is generally more diffuse than one might have anticipated.

This research was supported by the U.S. Air Force Office of Scientific Research under Grant AFOSR-88-0167. The authors wish to thank Drs. Yukio Yamaguchi and Yaoming Xie for their help with the vibrational perturbation and variation theories and for many valuable discussions. The referee who commented on the possible inadequacy of the TZ2P + diff(Si) basis set used in reference 2 is acknowledged for motivating the present work.

References

- [1] SHEN, M., XIE, Y., and SCHAEFER, H. F., 1990, *J. chem. Phys.*, **93**, 8098.
- [2] SHEN, M., XIE, Y., YAMAGUCHI, Y., and SCHAEFER, H. F., 1991, *J. chem. Phys.*, **94**, 8112.
- [3] MILLS, I. M., 1972, *Molecular Spectroscopy: Modern Research*, edited by K. N. Rao and C. W. Mathews (Academic Press), p. 115.
- [4] PULAY, P., 1981, *Abstracts of Texas Conference on Theoretical Approaches to Chemical Dynamics* (The Institute of Theoretical Chemistry of the University of Texas, Austin, Texas), p. 47.
- [5] MCLEAN, A. D., and CHANDLER, G. S., 1980, *J. chem. Phys.*, **72**, 5639.
- [6] (a) HUZINAGA, S., 1965, *J. chem. Phys.*, **42**, 1293; (b) DUNNING, T. H., 1970, *J. chem. Phys.*, **53**, 2823.
- [7] BÜRGER, H., and EUJEN, R., 1974, *Z. Naturf. B*, **29**, 647.
- [8] NIMLOS, M. R., and ELLISON, G. B., 1986, *J. Am. Chem. Soc.*, **108**, 6522.
- [9] WATSON, J. K. G., 1972, *J. molec. Structure*, **41**, 229.

measurements; fundamental = 1.064 μm). This value is consistent with the result in ref 48. In ref 48, $\chi^{(3)}$ of a solution of C_{60} (mole fraction = 0.001) is given as $\sim 9 \times 10^{-14}$ esu. $\chi^{(3)}$ for solid C_{60} can be estimated as 9×10^{-11} esu, a value similar to the result obtained by Hoshi et al. A much larger value than this was obtained by: Blau, W. J.; Byrne, H. J.; Cardin, D. J.; Dennis, T. J.; Hare, J. P.; Kroto, H. W.; Taylor, R.; Walton, D. R. M. *Phys. Rev. Lett.* 1991, 67, 1423. Their values ($\gamma = 1.1 \times 10^{-28}$ esu, and $\chi^{(3)}$ of solid $\text{C}_{60} = 6 \times 10^{-8}$ esu,

obtained from degenerate four-wave mixing measurements using a wavelength of 1.064 μm) is 10^{2-3} times larger than those obtained by Wang and Cheng or Hoshi et al.

(50) Matsuzawa, N.; Dixon, D. A. *J. Phys. Chem.*, preceding paper in this issue.

(51) Calculations on C_{60} derivatives with a forced zwitterionic structure lead to enhanced values of γ by factors of 150.

Diffluorosulfurane (SF_2H_2): A Molecule Identified in the Laboratory?

Igor S. Ignatyev[†] and Henry F. Schaefer III*

Center for Computational Quantum Chemistry, University of Georgia, Athens, Georgia 30602

(Received: January 14, 1992)

The structure of the SF_2H_2 molecule was optimized and the vibrational spectrum was evaluated at the SCF level with DZP and TZ2P+f basis sets and at the CISD and CCSD levels of theory with the DZP basis set. Only one minimum on the potential energy surface was found, corresponding to the structure with the two fluorine atoms in axial positions. The structure and the vibrational spectrum of the well characterized SF_2 molecule were also predicted to assess the quality of the theoretical vibrational frequencies for the SF_2 moiety within the SF_2H_2 molecule. Neither of the two sets of vibrational frequencies considered for SF_2H_2 in experimental studies is in keeping with the theoretical predictions. The main feature of the predicted IR spectrum is the presence in the 600–650 cm^{-1} frequency range of the asymmetric S–F stretching fundamental with very high intensity.

Introduction

Sulfuranes, e.g. SF_4 and the thus-far hypothetical SH_4 , have attracted the attention of theoretical chemists since the 1960s and 1970s as "hypervalent" molecules, in which the octet rule is broken.^{1,2} The main topics of discussion in such studies were the qualitative description of the bonding in these molecules and the participation of the vacant atomic sulfur d-orbitals therein.

It was early shown by microwave spectroscopy³ that the SF_4 molecule has a C_{2v} trigonal bipyramid structure in which the axial bonds are significantly longer than equatorial and the axial FSF angle is about 187°. However, for the related hypothetical SH_4 molecule high levels of theory find only one energy minimum (C_{4v}), corresponding to a square pyramidal structure.⁴

The structure of the SF_2H_2 molecule was previously optimized at the 4-31G* SCF level by Eggers, Livant, and McKee.⁵ Variation of the equatorial HSH angle in the 80°–120° range showed negligible changes in the other geometry parameters in contrast to the earlier qualitative predictions of Chen and Hoffmann.² The search for a local energy minimum at values of the axial FSF angle (θ_s) less than 180° was also undertaken by starting the geometry optimization from (θ_s) = 168°; however no minima were found in going from the latter angle to the equilibrium value of 193°. Although experimental evidence⁶ and the qualitative predictions of Chen and Hoffmann² consider the axial position for the more electronegative substituents preferable for sulfuranes, there exists a possibility of finding a local minimum for FSF angles lying in the 80–120° range, i.e. for the isomer with the hydrogens in axial positions.

Our interest in this molecule was inspired by the recent studies of the IR matrix isolation spectra of the products of the reactions between molecular fluorine and various sulfides.^{7,8} In both of these works several bands were found which may be tentatively assigned to the SF_2H_2 molecule. However these two sets of experimental IR bands differ significantly. In the work of Machara and Ault⁷ the peaks lie at 380, 727, 760, and 2596 cm^{-1} , while McInnis and Andrews⁸ assigned to SF_2H_2 IR features at 280, 386, and 533 cm^{-1} .

In the light of these differences it is a challenge for theoretical methods to predict the vibrational spectrum of this molecule and to compare it to the two sets of experimental results in order to confirm or to deny the tentative experimental identification of the SF_2H_2 molecule.

Theoretical Approach

Theoretical methods employed here included the restricted self-consistent field (SCF) approximation, the configuration interaction method including all single and double excitations (CISD),⁹ and the coupled cluster method including all single and double excitations (CCSD).¹⁰ For the SCF studies the following basis sets were used: a minimal basis set STO-3G* with d-functions on sulfur;¹¹ a double ζ plus polarization (DZP) basis set constructed as S(11s7p1d/6s4p1d) with $\alpha_d(\text{S}) = 0.50$, F(9s5p1d/4s2p1d) with $\alpha_d(\text{F}) = 1.00$, and H(4s1p/2s1p) with $\alpha_p(\text{H}) = 0.75$; a triple ζ plus double polarization plus f function on S (abbreviated as TZ2P+f) basis set constructed as S-(12s9p2d1f/6s5p2d1f) with orbital exponents $\alpha_d(\text{S}) = 1.40, 0.35$ and $\alpha_f(\text{S}) = 0.55$, F(10s6p2d/5s3p2d) with orbital exponents $\alpha_d(\text{F}) = 2.00, 0.50$, and H(5s2p/3s2p) with $\alpha_p(\text{H}) = 1.50, 0.375$.

Only the DZP basis set was used for the correlated studies. In the CISD method the corelike orbitals ($1s^2 2s^2 2p^6$ for S and $1s^2$ for F) were kept fully occupied and the four highest virtual orbitals were deleted. This resulted in 31 867 configurations for the SF_2H_2 molecule in C_{1v} symmetry, and 123 256 in C_1 symmetry. Vibrational frequencies were evaluated analytically at the SCF level and at correlated levels by finite differences of analytic gradients obtained through two-sided distortions of the equilibrium geometry.

Results and Discussion

In order to find minima on the potential energy surface corresponding to different conformers of the SF_2H_2 molecule, the geometry optimization at the STO-3G* level was started from three structures. Structure 1 (supposed to be the most favorable according to qualitative theoretical considerations² and experimental evidence⁶ indicating that in SX_2Y_2 molecules the more electronegative substituents should take axial positions) contains fluorine atoms in the axial positions. In the second structure (2)

[†] Permanent address: The Institute for Silicate Chemistry, Academy of Sciences, 199034, Makarov Quay 2, St. Petersburg, Russia.

TABLE I: Theoretical Equilibrium Geometrical Parameters (Bond Lengths in Å) and Total Energies (in hartrees) for the SF₂H₂ Molecule and the SH₂ and F₂ Molecules Separated by 100 au

	STO-3G SCF	DZP SCF	TZ2P+f SCF	DZP CISD	DZP CCSD
SF ₂ H ₂					
<i>r</i> (SH)	1.364	1.325	1.316	1.331	1.340
<i>r</i> (SF)	1.605	1.710	1.691	1.731	1.744
θ _s HSH, deg	105.3	101.6	101.7	100.4	99.6
θ _s FSF, deg	191.1	191.8	191.9	191.7	191.6
- <i>E</i> _{tot}	589.38036	597.51823	597.60119	597.99579	598.15295
SH ₂ + F ₂					
<i>r</i> (SH)	1.341	1.335	1.328	1.336	1.343
<i>r</i> (FF)	1.315	1.335	1.336	1.385	1.419
θ HSH, deg	91.9	94.0	94.1	92.9	92.4
- <i>E</i> _{tot}	589.34517	597.41104	597.47296	597.88513	598.04599
Δ <i>E</i> (SF ₂ H ₂ → SH ₂ + F ₂), kcal mol ⁻¹	22.1	67.3	80.5	69.4	67.1

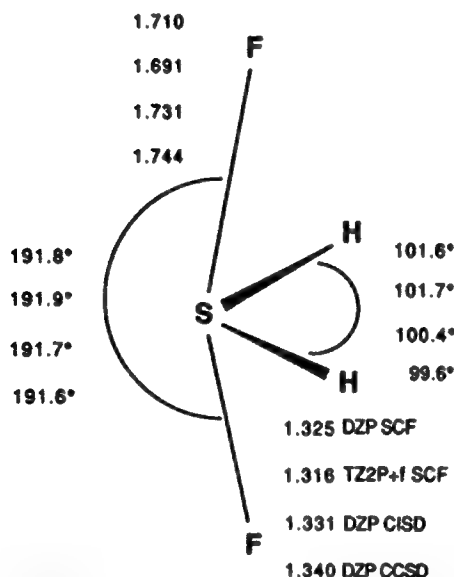
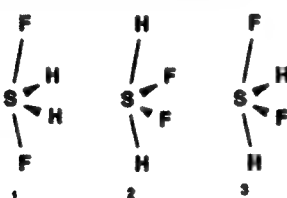


Figure 1. Predicted equilibrium geometries for difluorosulfurane. Bond distances are in Å.

axial positions are occupied by hydrogens. In the third (asymmetric) structure (3) one hydrogen and one fluorine atom were placed in each of two positions.



No minima were found for two last conformers with the STO-3G* SCF method. Motion on the PES from both structures 2 and 3 is possible without any barrier in the direction of structure 1. At the DZP SCF level the optimization of the second structure brought the same results. Thus it seems likely that for the SF₂H₂ molecule there exists only one minimum on the PES, namely that which refers to the structure with the two fluorine atoms in axial positions.

The equilibrium geometry of the SF₂H₂ molecule is represented in the Table I and Figure 1. There is considerable variation of the equilibrium bond lengths obtained at different levels of theory; however the bond angles, especially the FSF angle, do not vary significantly. The total energy of the SF₂H₂ molecule is 60–80 kcal mol⁻¹ lower than those for separated fragments (SH₂ + F₂) at all levels of theory excluding the unreliable STO-3G* results. Note, however, that according to the DZP SCF calculations of McInnis and Andrews¹ the most stable product of the SH₂ + F₂ reaction is a HSF–HF complex which is about 30 kcal mol⁻¹ lower than the SF₂H₂ molecule.

TABLE II: Theoretical Harmonic Vibrational Frequencies (cm⁻¹) and IR Intensities (km mol⁻¹) for the SF₂H₂ Molecule

description of vibrations and symmetry	DZP SCF	TZ2P+f SCF	DZP CISD	DZP CCSD
<i>ν</i> _{as} SH ₂ (B ₂)	2943 (3.3)	2936 (3.7)	2875 (1.3)	2790 (3.2)
<i>ν</i> _s SH ₂ (A ₁)	2914 (5.2)	2912 (4.1)	2847 (2.5)	2761 (1.1)
δ HSF (B ₁)	1348 (4.3)	1389 (6.0)	1257 (1.9)	1208 (1.8)
δ HSF (A ₂)	1306 (0)	1349 (0)	1211 (0)	1162 (0)
δ SH ₂ (A ₁)	1212 (0.0)	1216 (0.4)	1166 (0.1)	1136 (0.1)
<i>ν</i> _{as} SF ₂ (B ₁)	674 (668.2)	655 (658.9)	689 (575.8)	682 (523.4)
<i>ν</i> _s SF ₂ (A ₁)	604 (0.9)	601 (1.4)	580 (0.6)	559 (0.5)
δ HSF (B ₂)	404 (59.6)	410 (51.4)	377 (52.4)	361 (15.4)
δ SF ₂ (A ₁)	391 (50.9)	394 (41.2)	367 (44.4)	354 (41.7)

TABLE III: Theoretical Equilibrium Geometries, Harmonic Vibrational Frequencies (in cm⁻¹) and IR Intensities (in km/mol) for the SF₂ Molecule Compared to Experiment (IR Intensities Shown in Parentheses)

	experimental	DZP SCF	DZP CISD	DZP CCSD
<i>r</i> _s (SF), Å	1.587 ^a	1.592	1.620	1.634
θ(FSF), deg	98.05	97.4	97.7	97.9
<i>ν</i> _s SF ₂ (A ₁)	836, ^b 832, ^c 825 ^d	924 (105.0)	866 (80.4)	832 (69.5)
<i>ν</i> _{as} SF ₂ (B ₁)	810, 804, 799	896 (175.0)	842 (146.2)	812 (132.3)
δ FSF (A ₁)	357, 358, 358	384 (8.6)	350 (7.2)	336 (6.6)

^aEquilibrium structure obtained from the microwave spectrum.¹²

^bObtained with the harmonic force constants deduced from the observed centrifugal distortion constants.¹² ^cIR spectrum of the molecule trapped in an Ar matrix.¹³ ^dIR spectrum of the molecule trapped in a N₂ matrix.¹³

Vibrational frequencies evaluated theoretically at the equilibrium geometry are reported in Table II. As one might expect the theoretical frequencies decrease in going from the SCF to the CISD and CCSD methods (with one exception that will be discussed later). The increase in the number of basis functions from 66 (DZP) to 113 (TZ2P+f) does not bring any prominent change in the vibrational frequencies, indicating that the DZP basis set should probably be adequate to describe the vibrational frequencies at the SCF level. The further lowering of the frequencies was achieved only at correlated levels of theory and the CCSD values may be expected to be close to the experimental fundamentals with the exception of the SH₂ stretching frequencies, for which the difference between experimental and theoretical harmonic frequencies may be of the order of 200 cm⁻¹. The general tendency toward vibrational frequency lowering in going from DZP to DZP CCSD has one exception. The frequency of the *ν*_{as} SF₂ (B₁) vibration does not decrease but rather slightly increases while going from SCF to correlated levels. The frequency of the corresponding symmetric S–F vibration exhibits a slight but constant tendency to decrease with increase in the level of theory.

There is another feature which distinguishes *ν*_{as} SF₂ (B₁) from other vibrations, i.e. the huge theoretical IR intensity. Moreover, its value does not depend significantly upon the level of theory. The high intensity of the *ν*_{as} SF₂ mode in SF₂H₂, and its insensitivity with respect to variation of the theoretical method at which it is evaluated, may be rationalized by taking into account the nearly linear configuration of the SF₂ moiety in the SF₂H₂ molecule, the long SiF bond lengths, and the large charges on the

TABLE IV: Theoretical Harmonic Vibrational Frequencies (cm^{-1}) for the SF_2H_2 and SF_2D_2 Compared to Experimental IR Frequencies Tentatively Considered for These Molecules

		B_2	A_1	B_1	A_1	B_1	A_1	B_2	A_1
DZP CCSD	SF_2H_2	2790	2761	1208	1136	682	559	361	354
expt ^a	SF_2H_2	2596				760	727	380	
expt ^b	SF_2H_2					533		386	280
DZP CCSD	SF_2D_2	2010	1978	882	829	673	559	345	344
expt ^b	SF_2D_2					519		387	282

^aReference 7. ^bReference 8.

S and F atoms (Mulliken net charges evaluated at the CCSD level are +0.77 and -0.53, respectively). The presence in the theoretical IR spectrum of only one strong band in the SF_2 stretching region minimizes the likelihood of the assignment by Machara and Ault⁷ of the species with two bands of comparable intensity (they are both designated as medium in ref 7) in the 700–800 cm^{-1} range to the SF_2H_2 molecule (Table IV). However, in the spectrum considered by McInnis and Andrews⁸ for the SF_2H_2 molecule, there is only one IR band in this region, namely at 533 cm^{-1} . Can the usually reliable CCSD method give an error of about 150 cm^{-1} ? To check the quality of our theoretical methods for predictions of the SF_2 group vibrational frequencies we have evaluated the vibrational frequencies of the isolated SF_2 molecule, for which a reliable assignment of the experimental IR bands exists.

The vibrational spectrum of this simpler molecule predicted at different levels of theory is reported in Table III. The CCSD method gives an excellent reproduction of the SF_2 stretching frequencies, while the frequency of a bending mode is about 20 cm^{-1} lower than the experimental. It should be noted, however, that in contrast to the SF_2H_2 molecule and due to the small FSF angle, the intensities of the ν_{as} SF_2 (B_1) and ν_s SF_2 (A_1) vibrations are comparable, from both theory and experiment. All this makes it quite improbable that the ν_{as} SF_2 (B_1) fundamental in the SF_2H_2 molecule lies at 533 cm^{-1} . It should be noted also that two other bands considered by McInnis and Andrews⁸ to be disulfur hexafluoride, i.e., 386 and 280 cm^{-1} , exhibit no frequency shifts in the deuterated molecule while our theoretical evaluation predicts a 16 and 12 cm^{-1} shift of these bands upon deuteration (Table IV).

Concluding Remarks

Thus, both sets of experimental vibrational frequencies^{7,8} proposed for the SF_2H_2 molecule are inconsistent with our theoretical predictions. The IR spectrum of this molecule should contain a very intense band in the 620–690 cm^{-1} range, two rather intense bands centered near 340–390 cm^{-1} , and five bands with very low intensity near 550, 1130, 1200, 2620, and 2650 cm^{-1} . The latter two harmonic vibrational frequencies were multiplied by 0.95 to take into account the difference between DZP CCSD harmonic and fundamental vibrational frequencies. This set of frequencies may be useful in further attempts to identify the SF_2H_2 molecule.

Acknowledgment. We thank Professor Lester Andrews for suggesting this work. I.S.I. thanks Dr. Mingzuo Shen and Dr. Yaoming Xie for their help in computations. This research was supported by the U.S. Air Force Office of Scientific Research under Grant Number AFOSR-92-J-0047.

References and Notes

- (1) Willett, R. D. *Theor. Chim. Acta* 1964, 2, 393. Santry, D. P.; Segal, G. A. *J. Chem. Phys.* 1967, 47, 158. Santry, D. P. *J. Am. Chem. Soc.* 1968, 90, 3309. Brown, R. D.; Peel, J. B. *Aust. J. Chem.* 1968, 21, 2605, 2617. Musher, J. I. *Angew. Chem., Int. Ed. Engl.* 1969, 8, 54. Musher, J. E. *J. Am. Chem. Soc.* 1972, 94, 1370. Schwenzer, G. M.; Schaefer, H. F. *J. Am. Chem. Soc.* 1975, 97, 1391. Radom, L.; Schaefer, H. F. *Aust. J. Chem.* 1975, 28, 2069.
- (2) Chen, M. L.; Hoffmann, R. *J. Am. Chem. Soc.* 1976, 98, 1647.
- (3) Tolles, W. H.; Gwinn, W. D. *J. Chem. Phys.* 1962, 36, 1119. Kimura, K.; Bauer, S. U. *J. Chem. Phys.* 1963, 39, 3172. Ewing, V. C.; Sutton, L. E. *Trans. Faraday Soc.* 1963, 59, 1241.
- (4) Yoshioka, Y.; Goddard, J. D.; Schaefer, H. F. *J. Chem. Phys.* 1981, 74, 1855.
- (5) Eggers, M. D.; Livant, P. D.; McKee, M. L. *J. Mol. Struct. THEO-CHEM* 1989, 186, 69.
- (6) Muetterties, E. L.; Mahler, W.; Packer, K. J.; Schmutzler, R. *Inorg. Chem.* 1964, 3, 1298.
- (7) Machara, N. P.; Ault, B. S. *J. Mol. Struct.* 1988, 172, 129.
- (8) Andrews, L.; McInnis, T. C.; Hannichi, Y. *J. Phys. Chem.* 1992, 96, 4248.
- (9) Saxe, P.; Fox, D. J.; Schaefer, H. F.; Handy, N. C. *J. Chem. Phys.* 1982, 77, 5584.
- (10) Scuseria, G. E.; Janssen, C. L.; Schaefer, H. F. *J. Chem. Phys.* 1988, 89, 7382.
- (11) Hehre, W. J.; Stewart, R. F.; Pople, J. A. *J. Chem. Phys.* 1969, 51, 2657.
- (12) Endo, Y.; Saito, S.; Hirota, E. *J. Mol. Spectrosc.* 1979, 77, 222.
- (13) Haas, A.; Willner, H. *Spectrochim. Acta* 1978, 34A, 541.

Diazasilene (SiNN). A Comparison of Coupled Cluster Methods with Experiment and Local Density Functional Methods

Igor S. Ignatyev[†] and Henry F. Schaefer III*

Center for Computational Quantum Chemistry, University of Georgia, Athens, Georgia 30602
(Received: May 15, 1992)

Ab initio quantum mechanical methods have been applied to the $^3\Sigma^-$ electronic ground state of the diazasilene molecule SiNN. Higher level electron correlation methods are found to significantly effect the predicted equilibrium geometry. The self-consistent-field (SCF) and single and double excitation configuration interaction (CISD) methods predict a loosely bound Si \cdots N \equiv N structure. The single and double excitation coupled cluster method (CCSD) predicts both the loose structure and a tightly bound Si-N₂ structure, with the latter lying 2.3 kcal/mol lower in energy. The highest level theoretical method, CCSD(T), includes all connected triple excitations and predicts only the tight Si-N₂ structure. The CCSD(T) vibrational frequencies are in close agreement with experiment and in qualitative agreement with local density functional methods.

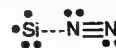
Introduction

In 1977 Lembke et al.¹ prepared the diazasilene molecule SiNN by the reaction of a beam of silicon atoms with N₂ and trapped the product in various matrices at 4 K. Due to the extraordinary strength of the nitrogen-nitrogen triple bond in N₂, the Si-N₂ bond is expected to be relatively weak. Lembke's ESR studies¹ suggest a linear $^3\Sigma^-$ ground electronic state for SiNN in a neon matrix; in the argon matrix a small fraction of the SiNN molecules are slightly bent in their sites. In the pure N₂ matrix it appeared that most of the SiNN molecules are bent. Presumably the neon matrix results most reliably simulate the gas phase. The Weltner group also recorded the infrared spectrum of SiNN and assigned the N-N stretching fundamental to 1731 cm⁻¹ and the Si-N stretching fundamental to 485 cm⁻¹. The former result is a bit surprising, as it corresponds to a downward shift in N-N stretching

frequency of about 600 cm⁻¹ compared to the free N₂ molecule. The Si-N stretch at 485 cm⁻¹ also evidences the existence of significant bonding between silicon and nitrogen.

Theoretical Background

The first ab initio theoretical studies² of SiNN were completely unsuccessful in reproducing the experimental infrared spectrum. Five different theoretical methods produced only a weakly bound complex in which the nitrogen-nitrogen triple bond is retained (1).



1

Both double- ζ plus polarization (DZP)³⁻⁵ and triple- ζ plus double polarization (TZ2P)⁶ basis sets were used in ref 2 in conjunction with self-consistent-field (SCF), single and double excitation configuration interaction (CISD),⁷ and complete active space (CAS)⁸ SCF methods. Although it was shown that an

[†] Permanent address: The Institute for Silicate Chemistry, Academy of Sciences, 199034, Makarov Quay 2, St. Petersburg, Russia.

TABLE I: Theoretical Equilibrium Geometrical Parameters (Bond Lengths in Å), Vibrational Frequencies (cm⁻¹), Force Constants (mdyn/Å, mdyn/rad), and Total Energies (hartrees) for the SiNN Molecule, in Its ³Σ⁻ Electronic Ground State

	LDF ^a	LDFG ^a	DZP SCF ^b	DZP CISD ^b	DZP CCSD	DZP CCSD(T)	expt ^c
Loose Structure							
<i>r</i> _e (SiN)			3.190	2.782	2.660		
<i>r</i> _e (NN)			1.082	1.109	1.120		
- <i>E</i> _{tot}			397.790 12	398.119 77	398.157 66		
Tight Structure							
<i>r</i> _e (SiN)	1.749	1.737			1.788	1.770	
<i>r</i> _e (NN)	1.164	1.167			1.153	1.168	
- <i>E</i> _{tot}					398.161 37	398.179 49	
ω ₁	1821	1823			1825	1726	1731
ω ₂	569	605			393	467	485
ω ₃	321	338			375	325	
<i>f</i> ₁₁	14.60				15.68	13.96	
<i>f</i> ₁₂	1.59				2.41	2.22	
<i>f</i> ₂₂	2.68				1.49	1.94	
<i>f</i> ₃₃	0.28 ^d				0.40	0.30	

^aReference 3. LDF results from the DMol program; LDFG results from DGAUSS. ^bReference 2. ^cReference 1. ^dThe value reported in ref 3 is 0.14 mdyn/Å. However, it seems obvious (although not mentioned) that this value should be multiplied by the SiN and NN bond lengths to be compared with our results.

increase of 0.07 Å in the N-N distance yields the observed 600-cm⁻¹ downshift in the nitrogen-nitrogen stretching frequency, DeKock et al.² found no minimum on the SiNN potential energy hypersurface for such stretched N-N distances. In concluding, the authors stated "we cannot provide a satisfactory interpretation of the experimental infrared spectra" for SiNN.

A much more successful theoretical study of SiNN has recently been completed by Dixon and DeKock.⁹ Their work was carried out within the local density functional (LDF) approximation¹⁰ using two independent systems of computer programs, DMol¹¹ and DGAUSS.¹² DMol employs numerical basis sets, whereas DGAUSS employs Gaussian basis sets. Both LDF methods yield a tight structure with a normal Si-N single bond. More importantly, the predicted vibrational frequencies are in qualitative agreement with experiment.¹ With DMol the nitrogen-nitrogen stretching frequency is 5.2% above experiment and the Si-N stretch is similarly 17.3% high. With DGAUSS the comparable differences between theory and experiment are 5.3% and 24.7%. Although one may argue the success of the LDF methods is due in part to the unnaturally large dissociation energies produced by these methods,¹³ the fact is that the two LDF methods are clearly superior to ab initio SCF, CISD, and CASSCF methods for the vibrational frequencies of the SiNN molecule.

The Present Theoretical Approach

Since the appearance of the 1988 ab initio study of SiNN, far more powerful methods for the systematic study of open-shell molecules have become available. Specifically, we refer to the open-shell single and double excitation coupled cluster (CCSD) method and the extension of that method to include all connected triple excitations, namely, CCSD(T).¹⁴ Although there is yet no analytic gradient method¹⁵ available for these advanced techniques, the triatomic SiNN molecule is simple enough to allow optimization of structures and evaluation of vibrational frequencies based on total energies alone. It is of considerable interest to apply these new open-shell coupled cluster methods to the SiNN molecule. A number of previously intractable theoretical problems, for example, the structure of the FOOF molecule,¹⁶ have been solved recently using the CCSD(T) method.¹⁷

The DZP basis set used in this research was the same as that employed in ref 2. The technical designation is

$$\text{Si}(11s7p1d/6s4p1d) \alpha_d(\text{Si}) = 0.50$$

$$\text{N}(9s5p1d/4s2p1d) \alpha_d(\text{N}) = 0.80$$

The nitrogen basis set is that of Huzinaga³ and Dunning,⁴ while the silicon set is from Dunning and Hay.⁵ All six d-like functions were used on each atom, yielding a total of 56 contracted Gaussian functions. In the CCSD and CCSD(T) procedures, the seven core SCF molecular orbitals (effectively Si 1s, 2s, 2p_x, 2p_y, 2p_z, and N 1s) were held doubly occupied in all configurations, while the

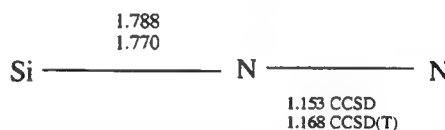


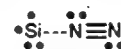
Figure 1. Equilibrium geometries of the diazasilene molecule in its ³Σ⁻ ground electronic state, with bond distances in angstroms. A double ζ plus polarization (DZP) basis set was used with both theoretical methods.

four highest virtual orbitals were not used in the treatment of electron correlation. In this manner 57 932 single and double excitations are included in C_s symmetry, required for the evaluation of the bending vibrational frequency.

Since analytic gradients are not currently available for the open-shell CCSD and CCSD(T) methods,¹⁴ a sequential univariate search was used for the equilibrium geometries. The search process was terminated when the variations in the two bond distances became less than 0.0005 Å. Vibrational frequencies were evaluated as numerical second derivatives (of the total energy) with respect to internal coordinates.

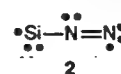
CCSD Results

The present theoretical results are summarized in Figure 1 and Table I, which also includes the earlier DZP SCF and DZP CISD results² and the local density functional results of Dixon and DeKock.⁹ As discussed above the SCF and CISD results show only the loosely bound

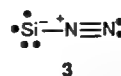


structure, while the LDF methods⁹ yielded a tightly-bound, singly bonded Si-N species with vibrational frequencies in qualitative agreement with experiment.

Remarkably, the DZP CCSD method predicts the existence of both loose and tight minima. A simple valence structure for the latter is



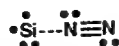
while an ionic structure



is also plausible. In stating, based on their ESR observations, that the unpaired "electron spins are largely in the p_x orbitals of Si", Lembke, et al.¹ would appear to favor the ionic valence structure 3 over the neutral structure 2.

The loose DZP CCSD structure is significantly tightened with respect to the earlier reported² CISD structure. Specifically, the Si-N bond distance is 0.122 Å shorter with CCSD than CISD.

Similarly the nitrogen–nitrogen distance in the



structure is 0.011 Å longer with CCSD than CISD. Thus the loose structure 1 is migrating very slowly in the direction of the tight structure (2 and/or 3) as the level of theory is raised. However, the global minimum of SiNN at the DZP CCSD level of theory is the tightly bound structure, which is predicted to lie 2.3 kcal/mol below the loose structure 1.

The CCSD vibrational frequencies for the tight structure of SiNN are in reasonable agreement with experiment. The N–N stretching frequency (1825 cm⁻¹) is virtually indistinguishable from the LDF results (1821 and 1823 cm⁻¹). And the Si–N stretching frequency is 81% of experiment, while the two LDF predictions are 117% and 125% of experiment. Thus the DZP CCSD description of SiNN is of about the same accuracy as the LDF methods.

CCSD(T) Results

The loose structure disappears entirely when connected triple excitations are incorporated in the theoretical method via the CCSD(T) method.^{14,17} Only a single minimum remains, the tight structure, qualitatively described as 2 and/or 3. The DZP CCSD(T) equilibrium geometry is qualitatively similar to the two LDF structures. The CCSD(T) Si–N single bond distance (1.770 Å) is significantly shorter (by 0.018 Å) than our CCSD result (i.e., for the tight CCSD structure), but still 0.039 and 0.051 Å, respectively, longer than the LDF distances. Taking into account an expected decrease in the CCSD(T) Si–N distance with progression to a much larger basis set, the comparison with the standard Si–N single-bond distance (1.72 Å) in disilylamine¹⁸ seems reasonable.

The three theoretical N–N bond distances are nearly the same: 1.168 DZP CCSD(T), 1.164 DMol, and 1.167 DGauss. On the basis of these bond distances, how should the nitrogen–nitrogen bond in SiNN be characterized? The benchmark N–N distances in such a comparison are those for N₂ (triple bond, 1.098 Å)¹⁹ and HN=NH (double bond, 1.252 Å).²⁰ In this light, the theoretical nitrogen–nitrogen bond distances for SiNN are slightly closer to the triple bond value than to the double bond. From this perspective the electronic structure of SiNN is modeled as a nearly equal superposition of structures 2 and 3.

The DZP CCSD(T) vibrational frequencies provide the best agreement to date with experiment of any theoretical method. The N–N stretching frequency is 0.3% below experiment, while the Si–N stretch is 3.7% lower than experiment.¹ In comparison the LDF differences⁹ with experiment are +5.2 and +5.3% for N–N and +17.3% and +24.7% for Si–N.

The DZP CCSD(T) nitrogen–nitrogen harmonic vibrational frequency (1726 cm⁻¹) is far below the experimental triple-bond value (2359 cm⁻¹)¹⁹ in isolated N₂. In fact, the 1726-cm⁻¹ result from theory is closer to the 1333-cm⁻¹ experimental N=N double bond stretching fundamental of diimide.² From this perspective, then, the nitrogen–nitrogen bond in ground-state SiNN is closer to double than triple bond in character.

Also included in Table I are force constants for the ³Σ⁻ ground state of SiNN. As expected, along with the decrease of the equilibrium SiN bond length in going from CCSD to CCSD(T), the diagonal force constant for SiN stretching (*f*₂₂) increases. The analogous effect in the opposite direction (increasing bond distance, decreasing force constant) is observed for the theoretical NN bond length and force constant (*f*₁₁). The off-diagonal force constant (*f*₁₂) with both CCSD and CCSD(T) methods is significantly larger than with the LDF method. In fact, *f*₁₂ becomes even larger than the SiN stretching diagonal force constant. The LDF and CCSD(T) methods give almost the same value of the bending force constant, while the CCSD estimation is 0.1 mdyn/rad higher. Although the bending fundamental was not observed in the experimental work, theoretical predictions of its frequency being in the general vicinity of about 300 cm⁻¹ seem to be reasonable,

taking into account the experimental evidence that indicates the presence of the bent SiNN molecules in a nitrogen matrix.¹

Concluding Remarks

Much of our discussion of the SiNN molecule has been directed toward the comparison between different theoretical methods. Thus we have seen that the two standard local density functional (LDF) methods DMol and DGauss are superior to the SCF and CISD methods and comparable to the CCSD method. The CCSD(T) method, a coupled cluster approach including all triple excitations, is superior to the LDF methods, even when a double ζ plus polarization (DZ) basis set is used. Experience suggests that the CCSD(T) results will improve further when a larger basis set (for example, triple ζ plus double polarization plus *f* functions) is used.

The above methodological discussion notwithstanding, there are some insights concerning the nature of the diazasilene molecule that arise from this research. First, the unknown harmonic bending frequency of SiNN should be close to the value 325 cm⁻¹ predicted by the DZP CCSD(T) method. Second, the best simple picture of the electronic structure of diazasilene is a superposition of the valence structures.



The theoretical equilibrium geometry slightly favors the triply bond N≡N structure (right side), while the vibrational frequencies suggest that the contribution of the double bond N=N structure (left side) is more important.

At the DZP CCSD(T) equilibrium geometry, a population analysis was carried out using the DZP CISD wave function. The results were +0.16 (Si), -0.11 (central N), and -0.05 (terminal N). These populations together with the small predicted dipole moment (*μ* = 0.275 D) tend to favor the N=N double-bonded structure. However, the Mulliken and Löwdin nitrogen–nitrogen bond orders are 2.17 and 2.58, respectively, again supporting a degree of resonance between the two valence structures.

Acknowledgment. We thank Roger DeKock, David Dixon, Roger Grev, and Yaoming Xie for helpful discussions. This research was supported by the U.S. Air Force Office of Scientific Research under Grant Number AFOSR 92-J-0047.

References and Notes

- (1) Lembke, R. R.; Ferrante, R. F.; Weltner, W. *J. Am. Chem. Soc.* **1977**, *99*, 416.
- (2) DeKock, R. L.; Grev, R. S.; Schaefer, H. F. *J. Chem. Phys.* **1988**, *89*, 3016.
- (3) Huzinaga, S. *J. Chem. Phys.* **1965**, *42*, 1293.
- (4) Dunning, T. H. *J. Chem. Phys.* **1970**, *53*, 2823.
- (5) Dunning, T. H.; Hay, P. J. *Modern Theoretical Chemistry*; Schaefer, H. F., Ed.; Plenum: New York, 1977; Vol. 3, pp 1–27.
- (6) McLean, A. D.; Chandler, G. S. *J. Chem. Phys.* **1980**, *72*, 5639.
- (7) Shavitt, I. *Modern Theoretical Chemistry*; Schaefer, H. F., Ed.; Plenum: New York, 1977; Vol. 3, pp 189–275.
- (8) Werner, H. J.; Knowles, P. J. *J. Chem. Phys.* **1985**, *82*, 5053.
- (9) Dixon, D. A.; DeKock, R. L. *J. Chem. Phys.* **1992**, *97*, 1157.
- (10) Parr, R. G.; Yang, W. *Density Functional Theory of Atoms and Molecules*; Oxford: New York, 1989.
- (11) Delley, B. *J. Chem. Phys.* **1990**, *92*, 508.
- (12) Andzelm, J. W.; Wimmer, E. *J. Chem. Phys.* **1992**, *96*, 1280.
- (13) Fitzgerald, G.; Andzelm, J. *J. Phys. Chem.* **1991**, *95*, 10531.
- (14) Scuseria, G. E. *Chem. Phys. Lett.* **1991**, *176*, 27.
- (15) For the closed-shell CCSD gradient, see: Scheiner, A. C.; Scuseria, G. E.; Rice, J. E.; Lee, T. J.; Schaefer, H. F. *J. Chem. Phys.* **1987**, *87*, 5361.
- (16) Scuseria, G. E. *J. Chem. Phys.* **1991**, *94*, 442.
- (17) The CCSD(T) method was initially proposed by: Raghavachari, K.; Trucks, G. W.; Pople, J. A.; Head-Gordon, M. *Chem. Phys. Lett.* **1989**, *157*, 479.
- (18) Rankin, D. W.; Robiette, A. G.; Sheldrick, G. M.; Sheldrick, W. S.; Aylett, B. J.; Ellis, I. A.; Monaghan, J. J. *J. Chem. Soc. (London) A* **1990**, 1224.
- (19) Huber, K. P.; Herzberg, G. *Constants of Diatomic Molecules*; Van Nostrand Reinhold: New York, 1979.
- (20) Carloti, M.; Johns, J. W. C.; Trombetti, A. *Can. J. Phys.* **1974**, *52*, 340.
- (21) Wiberg, N.; Fisher, G.; Bachuber, H. *Angew. Chem., Int. Ed. Engl.* **1977**, *16*, 780.

The dodecahedral N_{20} molecule. Some theoretical predictions

Andrey A. Bliznyuk¹, Mingzuo Shen and Henry F. Schaefer III

Center for Computational Quantum Chemistry, University of Georgia, Athens, GA 30602, USA

Received 23 July 1992; in final form 4 August 1992

Ab initio quantum mechanical methods have been applied to the I_h point group isomer of N_{20} . Dodecahedral N_{20} is predicted to be a relative minimum on its potential energy hypersurface, lying above separated nitrogen molecules by about 50 kcal per mol of nitrogen atoms. Vibrational frequencies, infrared intensities, and ionization potentials are also predicted.

The intense scientific and popular interest in the C_{60} molecule [1] has naturally raised the question whether other important cluster species have been systematically overlooked. Our interest in this respect arises from a comparison with the dodecahedrane molecule $C_{20}H_{20}$, the subject of an intense organic synthesis quest that ended in 1982 with the work of Paquette [2]. Isoelectronic with $C_{20}H_{20}$ would be the dodecahedral N_{20} molecule, which presumably would also display I_h symmetry, as seen in fig. 1.

Assuming that dodecahedral N_{20} can be synthesized, it is *not* expected to rival the remarkable stability of C_{60} . Assuming that the thirty equivalent nitrogen–nitrogen single bonds are unstrained, N_{20} would be bound by roughly^{#1}

$$30 \times (40 \text{ kcal/mol}) = 1200 \text{ kcal/mol},$$

relative to twenty infinitely separated nitrogen atoms. For comparison ten nitrogen molecules (N_2) are bound by^{#2}

$$10 \times (225 \text{ kcal/mol}) = 2250 \text{ kcal/mol},$$

Correspondence to: H.F. Schaefer III, Center for Computational Quantum Chemistry, University of Georgia, Athens, GA 30602, USA.

¹ Permanent address: Institute of Bioorganic Chemistry, Lavrentjev Avenue 8, Novosibirsk, 630090, Russian Federation.

^{#1} The standard N–N single bond energy is about 40 kcal/mol. See, for example, Appendix III of ref. [3]

^{#2} The dissociation energy D_0 of N_2 is 225 kcal/mol. See ref. [4].

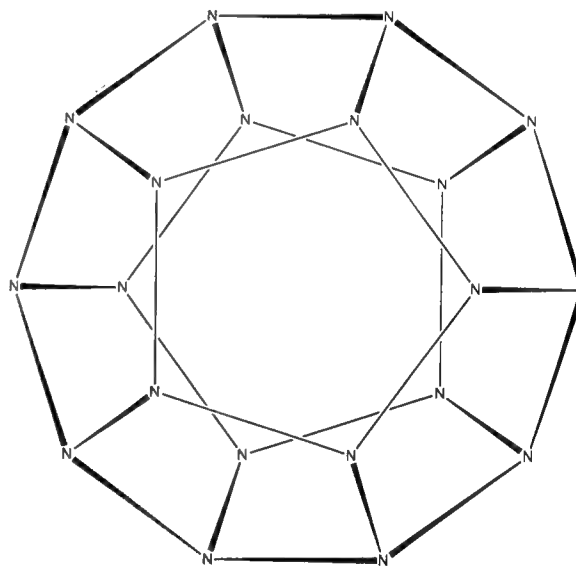


Fig. 1. The dodecahedral (I_h symmetry) N_{20} molecule. All atoms are equivalent and all bonds are single nitrogen–nitrogen bonds.

relative to the same set of twenty nitrogen atoms. Thus our back-of-the-envelope calculation suggests that dodecahedral N_{20} will lie above separated N_2 molecules by roughly 105 kcal per mol of N_2 molecules. One concludes that N_{20} with its weak nitrogen–nitrogen single bonds would be a reasonable candidate for a high energy density material (HEDM) [5].

The first mention of N_{20} in the chemical literature appears in footnote 11 of the 1978 paper by Schulman and Disch [6]. They reported MINDO/3 valence orbital energies for dodecahedral N_{20} with geometry $r(N-N)=1.36$ Å. The second theoretical consideration of N_{20} appears in the 1991 paper of Alkorta et al. [7]. For dodecahedral N_{20} they report MINDO and AM1 heats of formation of 485.8 and 1095.4 kcal/mol, respectively. The most comprehensive study of dodecahedral N_{20} is the 1992 work of Chen et al. [8]. These authors note that the N-N-N bond angles in dodecahedral N_{20} are exactly 108° , very close to the tetrahedral bond angle 109.47° , suggesting that N_{20} may be relatively unstrained. Chen et al. have applied the semi-empirical MINDO/3, MNDO, and AM1 methods [9] to dodecahedral N_{20} and some of their results are included in table 1. Unfortunately, the semi-empirical results are inconsonant, even with respect to the question of whether dodecahedral N_{20} lies energetically above $10N_{20}$ (it obviously does; see discussion above). Moreover, for such a novel species as dodecahedral N_{20} , it is not a priori obvious which of these three semi-empirical methods will be the most reliable.

In this research, the structure of dodecahedral N_{20} has been predicted using ab initio quantum-mechanical methods. The minimum basis STO-3G set of Hehre et al. [10] was used in preliminary studies. This was followed by the N(9s5p/4s2p) double-zeta (DZ) basis of Huzinaga and Dunning [11,12]. The double-zeta plus polarization (DZP) basis added a set of d functions on each nitrogen atom, with orbital exponent $\alpha_d(N)=0.8$. Finally, the Huzinaga-Dun-

ning triple-zeta plus double polarization (TZ2P) basis set [11,13], designated N(10s6p2d/5s3p2d), was used. In the TZ2P basis set of 480 contracted Gaussian functions the polarization function orbital exponents were $\alpha_d(N)=1.6, 0.4$. In addition to the self-consistent field (SCF) method, used here with all basis sets, second-order perturbation theory (designated [14] MP2 here) was used in conjunction with the DZP basis set. All computations were carried out using the TURBOMOLE programs of Ahlrichs and co-workers [15].

Table 1 shows the ab initio bond distances and dissociation energies for N_{20} and compares these with the semi-empirical results of Chen et al. [8]. At the SCF level of theory, the N-N bond distance appears to be reasonably converged with the DZP basis set. Extension from DZP to TZ2P decreases the SCF bond distance by only 0.001 Å.

The treatment of electron correlation effects using second-order perturbation theory is seen to significantly increase the N-N single bond distances – by 0.065 to 1.503 Å. Given the tendency of the MP2 method to somewhat exaggerate correlation effects and the expected shortening of bonds with larger basis sets^{#3}, we suggest a final N-N bond distance of about 1.48 Å. Thus the MINDO/3 method is seen to be severely deficient, the MNDO method fair, and the AM1 method exemplary in their predictions of the N_{20} bond distances. This 1.48 Å bond distance

^{#3} For example, for O_6 (another plausible HEDM species) the predicted O-O distances decrease by 0.009 Å in going from DZP MP2 to TZ2P MP2. See ref. [16].

Table 1
Total and relative energies and bond distances for dodecahedral N_{20}

	E (hartree)	$\Delta E_e(N_{20}-10N_2)$ (kcal/mol)	$r_e(N-N)$
MINDO/3 ^{a)}	–	–406	1.347
MNDO ^{a)}	–	486	1.426
AM1 ^{a)}	–	1095	1.484
minimum basis			
STO-3G SCF	–1074.28955	450	1.506
DZ SCF	–1087.18536	1002	1.486
DZP SCF	–1087.94298	1031	1.438
TZ2P SCF	–1088.08644	1107	1.437
DZP MP2	–1091.42677	924	1.503

^{a)} Ref. [6].

is somewhat longer than the "normal" nitrogen-nitrogen single bond distance [17] of 1.447 Å in hydrazine, H₂N-NH₂.

The ab initio binding energies of N₂₀ relative to ten separated N₂ molecules are consistent with the back-of-the-envelope arguments given in the introduction to this paper. Expansion of the basis set favors 10N₂ relative to N₂₀, due no doubt to the importance of polarization functions in describing the N₂ triple bond. However, second-order perturbation theory is more important for N₂₀ than for 10N₂. A reasonable final ab initio estimate for $\Delta E(N_{20} - 10N_2)$ is about 1000 kcal/mol, or 50 kcal per mol of nitrogen atoms. Thus N₂₀ would be a very effective high energy density material [5] if it could be readily synthesized. The highly constrained dodecahedral structure of this N₂₀ isomer suggests that a substantial barrier to fragmentation may exist. As with the structural results, the ab initio energetic predictions confirm the reasonableness of the AM1 predictions [7,8] but discredit the MINDO/3 and MNDO methods.

Predicted DZ SCF and DZP SCF vibrational frequencies for dodecahedral N₂₀ are reported in table 2. All of the N₂₀ vibrational frequencies are remotely distant from the isolated N₂ harmonic vibrational frequency, 2359 cm⁻¹. Unfortunately only the T_{1u} vibrational frequency among the fundamentals is al-

lowed in the infrared^{#4}. The IR intensity of the T_{1u} fundamental decreases drastically from the DZ SCF (13 km/mol) to the DZP SCF (0.4 km/mol) level of theory. Experience suggests that the DZ SCF results should not be taken very seriously, as polarization functions are mandatory for reliable IR intensity predictions [19]. Although the theoretical magnitude (0.4 km/mol) of the T_{1u} intensity is weak, the unusual simplicity of the expected IR spectrum may make detection of this feature near 770 cm⁻¹ possible. The one A_g and three H_g fundamentals are Raman allowed, but this is unlikely to be the first experimental technique applied to dodecahedral N₂₀. To estimate the true fundamentals, the DZP SCF harmonic vibrational frequencies (table 2) should be multiplied by a factor [20] close to 0.9, as was done above to obtain the T_{1u} estimate of 770 cm⁻¹.

Finally, in table 3 are reported DZP SCF and TZ2P SCF ionization potentials (IPs) for dodecahedral N₂₀ from Koopmans' theorem. The highest-occupied molecular orbital (HOMO) IP is substantial, 11.5 eV (TZ2P SCF). The comparable theoretical HOMO IP for dodecahedrane [21] C₂₀H₂₀ is lower, 10.2 eV. For the expected N₂₀ fragmentation product N₂, the observed ionization potential is 15.6 eV, in no danger whatever of being confused with the N₂₀ IP.

In summary, several properties of the hypothetical dodecahedral N₂₀ molecule have been predicted. The most plausible experimental means for the initial detection of this remarkable species would appear to be mass spectrometry. This work also suggests the possibility of dodecahedral P₂₀, which will be thermodynamically far more stable relative to 10P₂ (than N₂₀ is to 10N₂) due to the greater strength (≈ 55

Table 2
Vibrational frequencies (cm⁻¹) and infrared intensities (km/mol, in parentheses) for dodecahedral N₂₀

Symmetry	DZ SCF	DZP SCF
H _g	1231	1350
H _u	1185	1318
G _u	1052	1160
G _g	975	1138
T _{2u}	958	1121
H _g	850	974
T _{2u}	802	946
G _g	768	922
T _{1u}	746(13)	854(0.4)
A _g	677	755
T _{2g}	724	753
G _u	637	733
H _g	535	586
H _u	510	543

^{#4} This was pointed out for the isoelectronic C₂₀H₂₀ molecule some time ago, see ref. [18].

Table 3
Valence electron orbital energies smaller in magnitude than 20 eV for the dodecahedral N₂₀ molecule

Symmetry	E(DZP SCF)	E(TZ2P SCF)
1h _u	-20.05	-19.63
4h _g	-17.31	-16.93
3g _u	-14.24	-13.83
3t _{2u}	-14.05	-13.78
HOMO 3g _g	-11.88	-11.54
LUMO 4t _{1u}	+2.35	+2.61

kcal/mol) of P–P single bonds and smaller dissociation energy ($D=116$ kcal/mol) of P_2 .

This research was supported by the US Air Force Office of Scientific Research under Grant No. AFOSR-92-J-0047. We are grateful to Ching-Han Hu for his preliminary theoretical study of N_{20} .

References

- [1] R.F. Curl and R.E. Smalley, *Science* 242 (1988) 1017; R.E. Smalley, *The Sciences*, March/April 1991 (New York Academy of Sciences, New York) pp. 22–28.
- [2] L.A. Paquette, *Chem. Rev.* 89 (1989) 1051.
- [3] A. Streitwieser and C.H. Heathcock, *Introduction to organic chemistry*, 3rd Ed. (Macmillan, New York, 1985) p. 1153.
- [4] K.P. Huber and G. Herzberg, *Constants of diatomic molecules* (Van Nostrand Reinhold, New York, 1979).
- [5] E.T. Seidl and H.F. Schaefer III, *J. Chem. Phys.* 88 (1988) 7043.
- [6] J.M. Schulman and R.J. Disch, *J. Am. Chem. Soc.* 100 (1978) 5677.
- [7] I. Alkorta, J. Elguero, I. Rozas and A.T. Balaban, *J. Mol. Struct.* 228 (1991) 47.
- [8] C. Chen, L.-H. Lu and Y.-W. Yang, *J. Mol. Struct.* 253 (1992) 1.
- [9] M.J.S. Dewar and W. Thiel, *J. Am. Chem. Soc.* 99 (1977) 4499; M.J.S. Dewar, E.G. Zoebisch, E.F. Healy and J.J.P. Stewart, *J. Am. Chem. Soc.* 107 (1985) 3902.
- [10] W.J. Hehre, R.F. Stewart and J.A. Pople, *J. Chem. Phys.* 51 (1969) 2657.
- [11] S. Huzinaga, *J. Chem. Phys.* 42 (1965) 1293.
- [12] T.H. Dunning, *J. Chem. Phys.* 53 (1970) 2823.
- [13] T.H. Dunning, *J. Chem. Phys.* 55 (1971) 716.
- [14] W.J. Hehre, L. Radom, P.R. von Schleyer and J.A. Pople, *Ab initio molecular orbital theory* (Wiley, New York, 1986).
- [15] R. Ahlrichs, M. Bär, M. Häser, H. Horn and C. Kölmer, *Chem. Phys. Letters* 162 (1989) 165.
- [16] Y. Xie, H.F. Schaefer III, J.H. Jang, B.J. Mhin, H.S. Kim, C.W. Yoon and K.S. Kim, *Mol. Phys.* 76 (1992) 537.
- [17] K. Kohata, T. Fukuyama and K. Kuchitsu, *J. Phys. Chem.* 86 (1982) 602.
- [18] O. Ermer, *Angew. Chem. Intern. Ed. Engl.* 16 (1977) 411.
- [19] Y. Yamaguchi, M.J. Frisch, J.F. Gaw, H.F. Schaefer III and J.S. Binkley, *J. Chem. Phys.* 84 (1986) 2262.
- [20] B.H. Besler, G.E. Scuseria, A.C. Scheiner and H.F. Schaefer III, *J. Chem. Phys.* 89 (1988) 360.
- [21] C.A. Scamehorn, S.M. Hermiller and R.M. Pitzer, *J. Chem. Phys.* 84 (1986) 833.

Reprinted from the Journal of the American Chemical Society, 1993, 115.
Copyright © 1993 by the American Chemical Society and reprinted by permission of the copyright owner.

$\text{PO}_3^{--}(\text{H}_2\text{O})_n$ Clusters. Molecular Anion Structures, Energetics, and Vibrational Frequencies

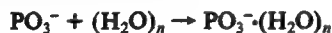
Buyong Ma, Yaoming Xie, Mingzuo Shen, and Henry F. Schaefer, III*

Contribution from the Center for Computational Quantum Chemistry, The University of Georgia, Athens, Georgia 30602. Received July 20, 1992

Abstract: The $\text{PO}_3^{--}(\text{H}_2\text{O})_n$ clusters ($n = 1, 2$, and 3) have been studied using ab initio quantum mechanical methods. Self-consistent field (SCF), configuration interaction with single and double excitations (CISD), and coupled cluster single and double excitation (CCSD) levels of theory were employed in conjunction with basis sets of quality double-zeta (DZ), double-zeta plus polarization (DZP), and DZP plus diffuse functions. The most important finding is that the clusters prefer to form high-symmetry double donor–double acceptor hydrogen bonds between the PO_3^{--} anion and the H_2O molecules. The hydrogen bond lengths increase and the dissociation energies decrease with the addition of successive water molecules. The hydrogen bond in $\text{PO}_3^{--}\text{H}_2\text{O}$ has a dissociation energy ($D_0 = 13.3 \text{ kcal mol}^{-1}$) about $0.5 \text{ kcal mol}^{-1}$ less than that for $\text{NO}_3^{--}\text{H}_2\text{O}$. The $D_{3h} \text{ PO}_3^{--}(\text{H}_2\text{O})_3$ theoretical results do not agree with the experimental thermochemistry concerning the nature of the hydration of $\text{PO}_3^{--}(\text{H}_2\text{O})_2$ by the third water molecule. The latter finding is consistent with the conclusions of Keesee and Castleman.

1. Introduction

Beginning with the experiments of Henschman, Viggiano, Paulson, Freedman, and Wormhoadt,¹ the metaphosphate anion, PO_3^{--} , has been shown to be relatively stable and unreactive in the gas phase.² However, there is strong laboratory evidence that the PO_3^{--} anion does not exist as a free entity in aqueous solution,³ unlike its nitrogen congener NO_3^{--} . This fact, together with the well-known role of PO_3^{--} in biological systems⁴ and interesting features associated with its bonding and electronic structure,⁵ has given impetus to several theoretical and experimental studies. Very recently, experiments have established that PO_3^{--} is a weaker base than I^- and that PO_3^{--} is one of the least reactive bases to have been characterized thermodynamically.⁶ Therefore, it is important to understand the unusual behavior of PO_3^{--} in the gaseous phase. The key reactions with water are²



The intermediate clusters $\text{PO}_3^{--}(\text{H}_2\text{O})_n$ are very important to the understanding of the properties of PO_3^{--} in both the gaseous and solution phases. Experimentally it has been shown¹ that the $\text{PO}_3^{--}(\text{H}_2\text{O})_n$ clusters are stable in the gaseous phase and that the isomerization barrier varies with the number of water molecules, n . Unfortunately, there is no theoretical research concerning the $\text{PO}_3^{--}(\text{H}_2\text{O})_n$ clusters. Although there is considerable laboratory thermochemical data from the important work of Keesee and Castleman,² there is very little experimental structural information concerning PO_3^{--} and its clusters. In fact, since $\text{PO}_3^{--}(\text{H}_2\text{O})_{n+1}$ and $\text{H}_2\text{PO}_4^{--}(\text{H}_2\text{O})_n$ are indistinguishable by mass spectrometry, there may be some uncertainty about the nature of the observed clustering as well as the isomerization behavior of PO_3^{--} .

Since the hydrogen bonding in the $\text{NO}_3^{--}\text{H}_2\text{O}$ system has been investigated previously,^{7,8} the current study attempts to make meaningful comparisons between the hydration behaviors of PO_3^{--} and NO_3^{--} . This paper will consider the structures and properties of the $\text{PO}_3^{--}(\text{H}_2\text{O})_n$ clusters, for $n = 0, 1, 2$, and 3 . Such a theoretical investigation was explicitly called for in the 1989 laboratory study of Keesee and Castleman.²

2. Theoretical Methods

The basis sets adopted here include STO-3G (minimum basis set),⁹ double-zeta (DZ),^{10,11} double-zeta plus polarization (DZP),¹² and DZP plus diffuse functions (DZP+diff) for the P and O atoms. The basis set denoted DZP for hydrogen is the (4s/2s) set⁸ with the set of p functions having orbital exponents $\alpha_p(\text{H}) = 0.75$; for the oxygen and phosphorus atoms we chose the Huzinaga–Dunning–Hay bases^{10–12} O(9s5p/4s2p),

(1) Henschman, M.; Viggiano, A. A.; Paulson, J. F.; Freedman, A.; Wormhoadt, J. J. *Am. Chem. Soc.* **1985**, *107*, 1453.

(2) Keesee, R. G.; Castleman, A. W., Jr. *J. Am. Chem. Soc.* **1989**, *111*, 9015.

(3) (a) Jencks, W. P. *Acc. Chem. Res.* **1980**, *13*, 161. (b) Ramirez, F.; Marecek, J.; Minor, J.; Srivastava, S.; leNoble, W. J. *Am. Chem. Soc.* **1986**, *108*, 348. (c) Burgess, J.; Blundell, N.; Cullis, P. M.; Hubbard, C. D.; Misra, R. J. *Am. Chem. Soc.* **1988**, *110*, 7900. (d) Freeman, S.; Friedman, J. M.; Knowles, D. J. *Am. Chem. Soc.* **1987**, *109*, 3166. (e) Cullis, P. M.; Nicholls, D. J. *Chem. Soc., Chem. Commun.* **1987**, 783.

(4) Westheimer, F. H. *Chem. Rev.* **1981**, *81*, 313. Westheimer, F. H. *Science* **1987**, *235*, 1173. Related systems of biological significance have been the subject of many theoretical studies, for example: Pullman, A.; Berthod, H.; Gresh, N. *Chem. Phys. Lett.* **1975**, *33*, 11.

(5) Rajca, A.; Rice, J. E.; Streitwieser, A., Jr.; Schaefer, H. F. *J. Am. Chem. Soc.* **1987**, *109*, 4189.

(6) Viggiano, A. A.; Henschman, M. J.; Dale, F.; Deakne, C. A.; Paulson, J. F. *J. Am. Chem. Soc.* **1992**, *114*, 4299.

(7) Shen, M.; Xie, Y.; Schaefer, H. F.; Deakne, C. A. *J. Chem. Phys.* **1990**, *93*, 3379.

(8) Shen, M.; Xie, Y.; Schaefer, H. F.; Deakne, C. A. *Chem. Phys.* **1991**, *151*, 187.

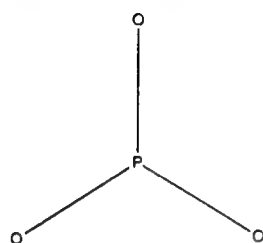
(9) Hehre, W. J.; Stewart, R. F.; Pople, J. A. *J. Chem. Phys.* **1969**, *51*, 2659.

(10) Huzinaga, S. *J. Chem. Phys.* **1965**, *42*, 1293.

(11) Dunning, T. H. *J. Chem. Phys.* **1970**, *53*, 2823.

Table I. Theoretical Total Energies, Equilibrium Geometries, and Vibrational Frequencies for PO_3^- (Figure 1)

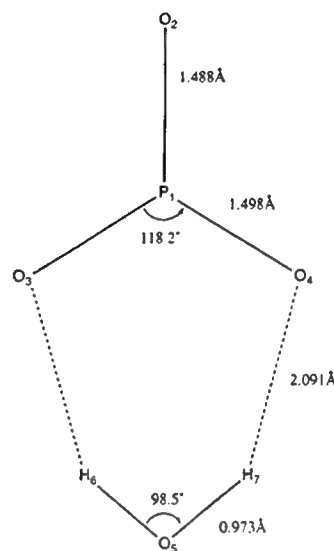
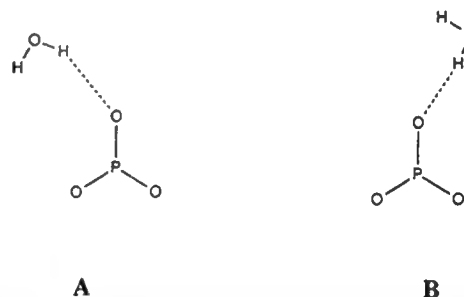
	DZ SCF	DZP SCF	DZP+diff SCF	DZP CISD	DZP+diff CISD	DZP CCSD	DZP+diff CCSD
total energy, au	-565.224 36	-565.483 64	-565.494 19	-566.037 56	-566.058 22	-566.124 74	-566.149 93
$R_e(\text{P-O})$, Å	1.561	1.464	1.465	1.482	1.484	1.495	1.498
harmonic vib freq, cm^{-1}							
A_1' (P-O stre)		1136	1129				
E' (P-O stre)		1426	1407				
E' (bend)		544	537				
A_2'' (umbrella)		556	549				

 D_h **Figure 1.** Theoretical equilibrium geometries for the metaphosphate anion, PO_3^- .

$\text{P}(11s7p/6s4p)$ with five pure spherical d functions used as polarization functions, the orbital exponents being $\alpha_d(\text{O}) = 0.85$, and $\alpha_d(\text{P}) = 0.6$. The diffuse functions include both s and p functions on the heavy atoms and have orbital exponents^{13,14} $\alpha_s(\text{O}) = 0.0845$, $\alpha_p(\text{O}) = 0.0845$, $\alpha_s(\text{P}) = 0.0348$, and $\alpha_p(\text{P}) = 0.0348$.

The Hartree-Fock or self-consistent field (SCF) approach has been used to locate stationary points for several conformations via analytic first derivative techniques. Subsequently, analytic energy second derivative techniques are used to determine whether each stationary point is a local minimum. Finally, the configuration interaction method with single and double excitations (CISD)^{15,16} and the coupled cluster method including single and double excitations (CCSD)^{17,18} are used to independently optimize the geometries. For the CISD and CCSD methods, only the valence electrons were explicitly correlated. Thus the core-like (phosphorus 1s, 2s, and 2p; oxygen 1s) SCF molecular orbitals were constrained to be doubly occupied in all configurations. Also the corresponding virtual orbitals were excluded from the CISD and CCSD procedures. With the DZP basis set, the numbers of basis functions for PO_3^- , $\text{PO}_3^-\cdot\text{H}_2\text{O}$, $\text{PO}_3^-(\text{H}_2\text{O})_2$, and $\text{PO}_3^-(\text{H}_2\text{O})_3$ are 68, 93, 118, and 143, respectively. The CISD wave functions for PO_3^- , $\text{PO}_3^-\cdot\text{H}_2\text{O}$, $\text{PO}_3^-(\text{H}_2\text{O})_2$, and $\text{PO}_3^-(\text{H}_2\text{O})_3$ included 30 100, 116 632, 318 287, and 709 829 configurations, respectively. With the DZP+diff basis set, the CISD wave functions for PO_3^- and $\text{PO}_3^-\cdot\text{H}_2\text{O}$ include 59 242 and 210 034 configurations, respectively. The computations were carried out using the program PSI developed in this research group.

Basis set superposition errors (BSSE) were not applied in this research. With the DZP SCF method, the BSSE corrections to the $\text{PO}_3^-(\text{H}_2\text{O})_n$ dissociation energies are substantial, yielding a significant reduction in the predicted D_e and D_0 values. However, it is known¹⁹ that DZP SCF dissociation energies agree well with experiment for the water dimer and other hydrogen-bonded systems. The reason for this is a consistent approximate cancellation between the effects of basis set incompleteness and electron correlation. Thus the application of BSSE corrections to DZP SCF energetic results is a priori expected to give poor agreement with experiment. Since correlation effects are not too important for the dissociation energies predicted here, the same remarks apply to the CISD

**Figure 2.** The C_{2v} global minimum equilibrium geometry for $\text{PO}_3^-\cdot\text{H}_2\text{O}$ at the DZP CCSD level of theory.**Figure 3.** Two closely related conformations of the $\text{PO}_3^-\cdot\text{H}_2\text{O}$ system. Both are minima with the STO-3G SCF method but collapse to the global minimum (Figure 2) when more complete basis sets are used at the SCF level.

and CCSD energetics. Ultimately, of course (for example, the DZP full CI method), the use of the DZP basis set will fail, yielding hydrogen-bonding dissociation energies that are too large when a sufficiently complete description of electron correlation effects is achieved.

3. Results and Discussion

A. Metaphosphate Anion PO_3^- . Our results for the isolated PO_3^- anion are presented in Table I and Figure 1. The introduction of diffuse basis functions lengthens the P-O bond slightly, but electron correlation effects increase the bond length more significantly, i.e., by 0.02 Å with the CISD method, and by 0.03 Å with the CCSD method. As expected, the harmonic vibrational frequencies with the SCF method generally become smaller when the larger DZP+diff basis set is used.

There have been several previous theoretical studies of the metaphosphate anion. For comparison, our most reliable P-O bond length is probably the DZP+diff CISD result, 1.484 Å, which is somewhat longer than previous values of 1.468 Å²⁰ or

(12) Dunning, T. H.; Hay, P. J. In *Theoretical Chemistry*; Schaefer, H. F., Ed.; Plenum Press: New York, 1977; Vol. 3, p 1.

(13) Clark, T.; Chandrasekhar, J.; Spitznagel, G. W.; Schleyer, P. v. R. *J. Comput. Chem.* **1983**, *4*, 294.

(14) Spitznagel, G. W.; Clark, T.; Schleyer, P. v. R. *J. Comput. Chem.* **1987**, *8*, 1109.

(15) Brooks, B. R.; Laidig, W. D.; Saxe, P.; Goddard, J. D.; Yamaguchi, Y.; Schaefer, H. F. *J. Chem. Phys.* **1980**, *72*, 4652.

(16) Rice, J. E.; Amos, R. D.; Handy, N. C.; Lee, T. J.; Schaefer, H. F. *J. Chem. Phys.* **1986**, *85*, 963.

(17) Purvis, G. D.; Bartlett, R. J. *J. Chem. Phys.* **1982**, *76*, 1910.

(18) Scuseria, G. E.; Janssen, C. L.; Schaefer, H. F. *J. Chem. Phys.* **1989**, *89*, 7382.

(19) See, for example: Feller, D. *J. Chem. Phys.* **1992**, *96*, 6104 and references therein.

(20) Lohr, L. L.; Boehm, R. C. *J. Phys. Chem.* **1987**, *91*, 3203.

Table II. Equilibrium Geometries for the Global Minimum Structure of PO₃⁻·H₂O (Figure 2)^a

theoretical level	r _e (P ₁ -O ₂)	r _e (P ₁ -O ₃)	r _e (O ₃ -H ₆)	r _e (O ₅ -H ₆)	θ _e (O ₃ -P ₁ -O ₄)	θ _e (H ₆ -O ₅ -H ₇)
DZ SCF	1.555	1.562	2.188	0.957	117.2	107.8
DZ CISD	1.580	1.588	2.154	0.974	117.2	106.3
DZ CCSD	1.601	1.610	2.157	0.958	117.3	105.3
DZP SCF	1.458	1.466	2.197	0.952	118.4	101.1
DZP CISD	1.473	1.482	2.107	0.963	118.2	99.5
DZP CCSD	1.488	1.498	2.091	0.973	118.2	98.5
DZP+diff SCF	1.460	1.467	2.216	0.952	118.4	101.5
DZP+diff CISD	1.476	1.484	2.121	0.963	118.2	99.9

^a All bond distances are in Å and angles in deg.

Table III. Harmonic Vibrational Frequencies (cm⁻¹) for the Global Minimum Structure of PO₃⁻·H₂O (Figure 2)

no.	symmetry	mode	DZP SCF	DZP+diff SCF
1	B ₁	O-H stretch	4141 (3031) ^a	4138 (3030) ^a
2	A ₁	O-H stretch	4084 (2948)	4080 (2945)
3	A ₁	H-O-H bend	1846 (1347)	1824 (1332)
4	A ₁	P-O stretch	1443 (1446)	1426 (1428)
5	B ₁	P-O stretch	1405 (1405)	1392 (1392)
6	A ₁	P-O stretch	1136 (1136)	1130 (1130)
7	B ₂	puckering	716 (503)	694 (491)
8	A ₁	sym def	553 (553)	548 (548)
9	B ₂	O-P out-of-plane	545 (568)	539 (557)
10	B ₁	O-P-O bend	543 (543)	537 (537)
11	A ₂	asym torsion	408 (291)	404 (289)
12	A ₁	O-H stretch	378 (271)	365 (262)
13	A ₁	O-H stretch	165 (158)	158 (151)
14	B ₁	O-H stretch	82 (80)	77 (75)
15	B ₂	asym torsion	47 (47)	43 (43)

^a The values in parentheses refer to PO₃⁻·D₂O.

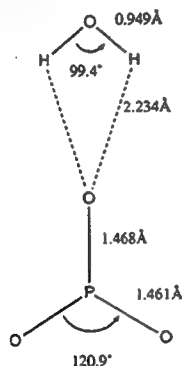


Figure 4. A transition state for PO₃⁻·H₂O obtained at the DZP SCF level of theory.

1.475 Å.²¹ Although the DZP+diff CCSD wave functions are more complete than the DZP+diff CISD, the CCSD method generally requires a larger basis set than DZP+diff for truly quantitative structural predictions. The DZP+diff CCSD total energy is -566.149 93 hartrees (versus -566.087 56 hartrees, the lowest energy reported in earlier theoretical work²⁰). Because the main goals of the present study involve the complexes of the metaphosphate anion with water molecule(s), the above results for isolated PO₃⁻ are presented for comparison and completeness.

B. Metaphosphate Anion-Water Complexes PO₃⁻·H₂O. We have investigated six arrangements of the metaphosphate anion complex with one water molecule. Two of the arrangements (those sketched in Figure 3) exist only at the minimum basis set (STO-3G) SCF level of theory and collapsed when larger basis sets were used. There are four stationary points on the SCF DZP potential energy surface (Figures 2, 4, 5, and 6). The global minimum is illustrated in Figure 2, and it is the *only* PO₃⁻·H₂O minimum located in this research. The structure illustrated in Figure 4 is a transition state, and those illustrated in Figures 5

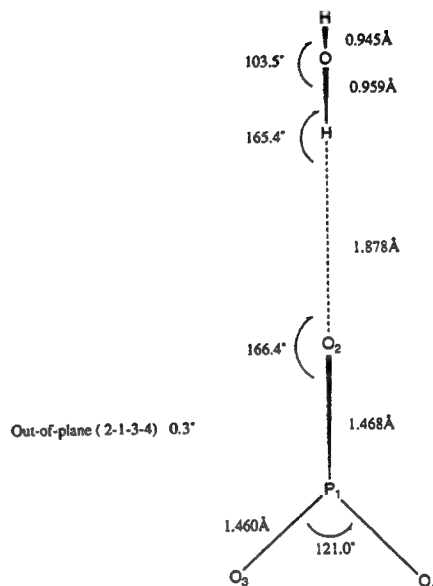


Figure 5. A C_{2v} stationary point (with two imaginary vibrational frequencies) of PO₃⁻·H₂O with a single hydrogen bond at the DZP SCF level of theory. The symmetry plane contains the water molecule and the out-of-plane P-O bond.

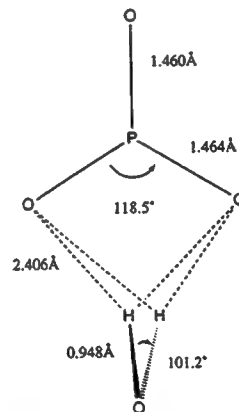


Figure 6. A C_{2v} stationary point (with two imaginary vibrational frequencies) for PO₃⁻·H₂O optimized at the DZP SCF level of theory.

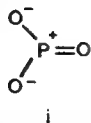
and 6 both have two imaginary vibrational frequencies.

The optimized theoretical geometries for the global minimum are presented in Table II, and the harmonic vibrational frequencies and their assignments in Table III. The global minimum of PO₃⁻·H₂O incorporates two distinct hydrogen bonds. In Figure 2 we note that, compared with the free anion in Figure 1, the formation of the two hydrogen bonds decreases both the O₃P₁O₄ angle in PO₃⁻ and the H₆O₅H₇ angle in H₂O. The bond angle in the isolated water molecule is 106° at the DZP SCF level of theory, while the H₆O₅H₇ angle in the complex is 101° at same theoretical level. The O₃P₁O₄ bond angle in PO₃⁻·H₂O is 2° smaller than the ideal 120° found for the isolated PO₃⁻ anion. The P₁-O₃ and P₁-O₄ bonds increase by 0.002-0.003 Å with both

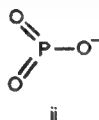
(21) O'Keeffe, M.; Domenges, B.; Gibbs, G. V. *J. Phys. Chem.* **1985**, *89*, 2304.

the SCF and CCSD methods, and a change of less than 0.001 Å was found with the CISD method.

Meanwhile, the P–O₂ bond, which does not participate in the hydrogen bonding, is about 0.006–0.009 Å shorter than the P–O bond in the free metaphosphate anion at the same theoretical level. Therefore, the PO₃[−] moiety in the global minimum of PO₃[−]·H₂O exhibits some contribution from the Lewis-type structure⁵ i. Note



that when two hydrogen bonds are required to be connected to only one of the oxygen atoms in PO₃[−], as in Figure 4 (a transition state), then this P–O bond lengthens slightly while the other two become a bit shorter. By the same line of reasoning, the PO₃[−] moiety thus incorporated has a greater contribution from the Lewis structure⁵ ii. This kind of behavior corroborates the classic Lewis



structure of PO₃[−] as a resonance hybrid of the two Lewis structures i and ii.

Harmonic vibrational frequencies for the PO₃[−]·H₂O complex are reported in Table III. There are some common features concerning the change of vibrational frequencies in PO₃[−]·H₂O and NO₃[−]·H₂O relative to the isolated PO₃[−] and NO₃[−] anions. For example, the degeneracy of the E' (A–O stretch, A = P or N) mode vibrational frequencies of the anions is removed. But in PO₃[−]·H₂O the previously degenerate lower E' (bend) mode frequencies now differ by about 10 cm^{−1}, whereas in the NO₃[−]·H₂O system this mode remains essentially degenerate.⁷ Also the hydrogen bond in PO₃[−]·H₂O is comparable to that in NO₃[−]·H₂O; this is demonstrated by the three highest "new" vibrational modes: 716 cm^{−1}, 408 cm^{−1}, and 378 cm^{−1} in PO₃[−]·H₂O versus 729 cm^{−1}, 316 cm^{−1}, and 210 cm^{−1} in NO₃[−]·H₂O. However, since frequencies are mass-weighted, a force constant comparison would be more meaningful. The corresponding normal coordinate force constants (mdyn/Å) associated with the "new" modes are 0.345 (716 cm^{−1}), 0.016 (408 cm^{−1}), and 0.013 (378 cm^{−1}) in PO₃[−]·H₂O, and 0.438 (729 cm^{−1}), 0.014 (316 cm^{−1}), and 0.011 (210 cm^{−1}) in NO₃[−]·H₂O.

Consistent with the vibrational analysis, there are some differences between the two anions with respect to their potential surfaces.^{7,8} Two of the starting arrangements we have used, shown in Figure 3, are analogous to the structures found to be minima at the STO-3G SCF level for NO₃[−]·H₂O. Both structures A and B (in Figure 3) of PO₃[−]·H₂O are also minima at the STO-3G SCF level. However, for NO₃[−]·H₂O, only structure B remains a minimum at higher levels of theory. In contrast, for PO₃[−]·H₂O, neither A nor B remains a minimum at higher levels of theory.

For coplanar configurations, the second PO₃[−]·H₂O stationary point is a transition state illustrated in Figure 4, which is about 3.2 kcal mol^{−1} higher in energy than the global minimum of Figure 2. There is one imaginary vibrational frequency, corresponding to the movement of the water molecule toward the global minimum. In this structure (Figure 4), the bond angle of H₂O is significantly smaller (99.4°) than that for the isolated water molecule. Since this structure is a transition state, we did not pursue it further with correlated wave functions.

We found only one stationary point that incorporates one conventional monodonor–monoacceptor hydrogen bond, namely, that shown in Figure 5. This structure lies 2.3 kcal mol^{−1} above the global minimum and has two imaginary vibrational frequencies with the DZP SCF method. It is interesting to note that the water H–O–H angle in this structure is still smaller (103.5°) than that of free H₂O (106.3°) at this level of theory, indicating that there is some weak interaction between the second hydrogen atom in water and the oxygen atom in PO₃[−].

From its position in the global minimum (Figure 2), if the H₂O molecule is rotated 90° about the C₂ axis such that the two molecular planes are perpendicular to each other, we find another stationary point with two imaginary vibrational frequencies; this structure is shown in Figure 6. This configuration is about 5.6 kcal mol^{−1} higher in energy than the PO₃[−]·H₂O global minimum (Figure 2).

It should be mentioned that, for all the structures discussed above, their total energies are lower than the sum of the separated PO₃[−] and H₂O, even though they have energies above that of the global minimum and have one or more imaginary vibrational frequencies on their SCF potential energy surfaces.

The total energies and dissociation energies for the PO₃[−]·(H₂O)_n clusters are reported in Table VII, in which the energy differences upon the formation of the clusters are defined as follows:

$$\text{PO}_3^{\cdot-} \cdot (\text{H}_2\text{O})_n:$$

$$n = 1 \quad D_e = E(\text{PO}_3^{\cdot-}) + E(\text{H}_2\text{O}) - E(\text{PO}_3^{\cdot-} \cdot \text{H}_2\text{O})$$

$$n = 2 \quad D_e = E(\text{PO}_3^{\cdot-}) + 2E(\text{H}_2\text{O}) - E(\text{PO}_3^{\cdot-} \cdot (\text{H}_2\text{O})_2)$$

$$n = 3 \quad D_e = E(\text{PO}_3^{\cdot-}) + 3E(\text{H}_2\text{O}) - E(\text{PO}_3^{\cdot-} \cdot (\text{H}_2\text{O})_3)$$

For the SCF and CCSD methods, *E* is the total energy as indicated above. However, for the CISD method, the total energies of the asymptotic system PO₃[−]·(H₂O)_n are used instead of the sum of the separated energies, owing to the lack of size consistency in the CISD method. For the asymptote, the intermolecular distances between the PO₃[−] anion and the H₂O molecules are 500 bohrs, and the geometries of the PO₃[−] anion and the H₂O molecules are separately optimized with the DZP CISD or DZP+diff CISD methods. The zero-point corrected energy differences (*D*₀) are based on the zero-point vibrational energies evaluated using the DZP SCF and DZP+diff SCF methods, and are reported in Table VIII.

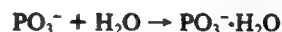
For the energetic comparisons with experimental data, the enthalpies changes are evaluated as follows:²²

$$\Delta H^\circ = D_e + \Delta E_v^\circ + \Delta(\Delta E_v)^{298} + \Delta E_i^{298} + \Delta E_t^{298} + \Delta PV$$

where ΔE_v° is the difference between the zero-point vibrational energies of reactants and product at 0 K; $\Delta(\Delta E_v)^{298}$ is the change in the vibrational energy difference in going from 0 to 298 K. The final terms are for changes in the number of rotational and translation degrees of freedom and the work term.

Entropy changes (ΔS°) have been evaluated from standard statistical mechanical relationships,²³ and finally free energy changes (ΔG°) are calculated. The theoretical values of ΔH° , ΔS° , and ΔG° are reported in Table IX. In all calculations the vibrational frequencies evaluated at the DZP SCF and DZP+diff SCF levels are used. The standard state is 1 atm at 298 K.

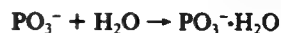
Usually, theoretical and spectroscopic absolute entropies agree very well.²³ For example, our theoretical entropy value of water molecule at the DZP+diff SCF level is 45.1 cal/K·mol, exactly the same as experimental value.²³ For the reaction



the agreement between the theoretical ΔS° and the experimental ΔS° is satisfactory. The experimental $-\Delta S^\circ$ reported in ref 2 is 93 ± 4 J/K·mol, with a 10-J/K·mol uncertainty. Thus the experimental upper bound of $-\Delta S^\circ$ is about 25.6 cal/K·mol, while our theoretical $-\Delta S^\circ$ is 25.8 cal/K·mol at the DZP+diff SCF level of theory.

Compared with the experimental enthalpy change² ΔH° for the formation of the PO₃[−]·H₂O cluster, the theoretical value of $-\Delta H^\circ$ with the DZP SCF method (12.6 kcal mol^{−1}) is slightly lower, while the DZP CISD (14.8 kcal mol^{−1}) and DZP CCSD (15.1 kcal mol^{−1}) methods give values higher than the experimental $-\Delta H^\circ$ (12.9 kcal mol^{−1}).

Closer agreement with the experimental enthalpy change for



(22) Del Bene, J. E.; Mettee, H. D.; Frisch, M. J.; Luke, B. T.; Pople, J. A. *J. Phys. Chem.* 1983, 87, 3279.

(23) Hout, R. F. Jr.; Levi, B. A.; Hehre, W. J. *J. Comput. Chem.* 1982, 3, 234.

Table IV. Equilibrium Geometries for the Global Minimum Structure of PO₃⁻·(H₂O)₂ (Figure 7)^a

theoretical level	r_e (P ₁ -O ₂)	r_e (P ₁ -O ₃)	r_e (O ₃ -H ₇)	r_e (O ₃ -H ₉)	r_e (O ₂ -H ₇)	r_e (O ₂ -H ₉)	θ_e O ₃ -P ₁ -O ₄	θ_e H ₇ -O ₂ -H ₉	θ_e P ₁ -O ₃ -H ₇
DZ SCF	1.564	1.557	0.956	0.957	2.271	2.166	122.9	108.5	105.1
DZ CISD	1.588	1.579	0.972	0.973	2.229	2.140	122.9	107.1	104.8
DZP SCF	1.468	1.461	0.951	0.951	2.224	2.236	121.6	101.7	107.0
DZP CISD	1.483	1.474	0.960	0.961	2.151	2.132	121.8	100.3	105.9
DZP+diff SCF	1.469	1.462	0.951	0.951	2.240	2.252	121.6	102.0	107.1

^a All bond distances are in Å and angles in deg.Table V. Harmonic Vibrational Frequencies (cm⁻¹) for the Global Minimum Structure of PO₃⁻·(H₂O)₂ at the SCF Level of Theory (Figure 7)

mode	symmetry	DZP	DZP+diff	mode	symmetry	DZP	DZP+diff
sym O-H	A ₁	4160 (3046) ^a	4155 (3043) ^a	sym def	A ₁	546 (546)	541 (541)
asym O-H	B ₁	4157 (3044)	4152 (3041)	O-P out-of-plane	B ₂	533 (570)	528 (559)
sym O-H	A ₁	4095 (2956)	4091 (2952)	asym torsion	B ₂	395 (283)	391 (281)
asym O-H	B ₁	4093 (2954)	4089 (2951)	asym torsion	A ₂	386 (274)	382 (272)
trigonal def	A ₁	1846 (1348)	1825 (1332)	asym def	A ₁	366 (265)	352 (256)
trigonal def	B ₁	1834 (1336)	1814 (1323)	asym def	B ₁	365 (260)	352 (251)
asym P-O	B ₁	1440 (1445)	1427 (1431)	O-H stretch	B ₁	161 (155)	155 (149)
sym P-O	A ₁	1405 (1407)	1399 (1397)	O-H stretch	A ₁	150 (143)	145 (138)
sym P-O	A ₁	1137 (1136)	1132 (1132)	O-H stretch	B ₁	95 (93)	90 (88)
puckering	B ₂	639 (474)	674 (467)	asym torsion	A ₂	51 (51)	47 (47)
puckering	A ₂	667 (488)	651 (476)	O-H stretch	A ₁	49 (48)	46 (45)
asym def	B ₁	555 (555)	551 (551)	asym torsion	B ₂	38 (38)	34 (34)

^a The values in parentheses refer to PO₃⁻·(D₂O)₂.

is found when diffuse functions are added to the basis set. Specifically, the diffuse functions decrease the CISD $-\Delta H^\circ$ from 14.8 (DZP) to 13.8 kcal mol⁻¹ (DZP+diffuse). With the DZP+diffuse CCSD method, $-\Delta H^\circ$ (PO₃⁻·H₂O) is also predicted to be 13.8 kcal mol⁻¹, indicating that theoretical value may be almost converged.

It is interesting that theory and experiment agree very well for the ΔG° value for the reaction above. The theoretical ΔG° at the DZP CCSD, DZP+diff CISD, and DZP+diff CCSD levels are within the stated error bars of Keesee and Castleman's experiment.²

Generally, the main error in the theoretical ΔH and ΔS values arises from the harmonic approximation. However, this shortcoming may be partly cancelled in evaluating theoretical ΔG values from the relationship

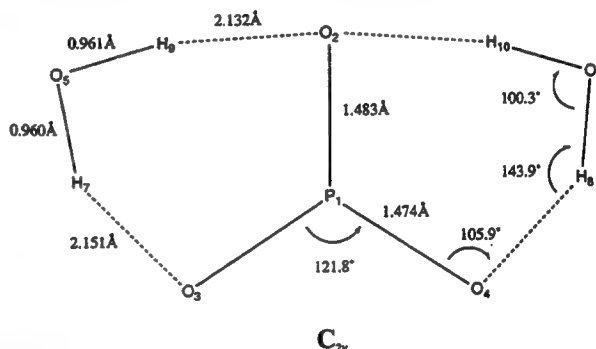
$$\Delta G = \Delta H - T\Delta S$$

In the case of the reaction above, the change of zero-point vibrational energies ΔE_v° is 2.3 kcal mol⁻¹, and $\Delta(\Delta E_v)_{298}^\circ$ is 1.9 kcal mol⁻¹. The vibrational term contribution to ΔS° is 14.0 cal/K·mol. Thus the total vibrational contribution to ΔG° is 0.0 kcal mol⁻¹ at 298 K.

This agreement means that the correlated levels of theory describe the reaction very well with respect to ΔG° , providing that vibrational term contributions cancel each other at a particular temperature. However, it is fortuitous that this temperature happened to be 298 K for the reaction above.

There is one apparent discrepancy between theory and experiment in Table IX. Namely, the experimental PO₃⁻·H₂O enthalpy change (12.9 kcal mol⁻¹) is greater than the analogous PO₃⁻·D₂O value (12.6 kcal mol⁻¹). Theory shows the opposite trend, with the PO₃⁻·H₂O enthalpy change being smaller by 0.4 kcal mol⁻¹ using the DZP SCF zero-point vibrational energies (ZPVE's) and smaller by 0.2 kcal mol⁻¹ with the DZP+diffuse SCF ZPVE's. With the latter basis set the individual ZPVE's are 24.8 kcal mol⁻¹ (PO₃⁻·H₂O), 8.0 kcal mol⁻¹ (PO₃⁻), 14.5 kcal mol⁻¹ (H₂O), 20.3 kcal mol⁻¹ (PO₃⁻·D₂O), and 10.6 kcal mol⁻¹ (D₂O). The theoretical results would appear to be more reasonable than the experiments in this regard. The D₂O complex sits lower in the potential minima, and therefore ZPVE effects should be smaller for PO₃⁻·D₂O than for PO₃⁻·H₂O. That is, the theoretical D_0 values for PO₃⁻·D₂O are closer to the D_e values than are the PO₃⁻·H₂O results.

The overall effect of ZPVE is to make $D_0 < D_e$ since the PO₃⁻·H₂O and PO₃⁻·D₂O complexes have six more vibrational

Figure 7. The global minimum of PO₃⁻·(H₂O)₂ at the DZP CISD level of theory.

degrees of freedom than do separated PO₃⁻ + H₂O or PO₃⁻ + D₂O. However, the difference between D_0 and D_e should be less for the D₂O complex than for the H₂O complex. Thus the experimental ordering² of PO₃⁻·H₂O and PO₃⁻·D₂O dissociation energies appears to be incorrect.

C. Metaphosphate Anion-Two Water Clusters, PO₃⁻·(H₂O)₂

It is important to understand the structure and properties of this cluster. The experiments of Keesee and Castleman² have suggested that for the PO₃⁻·(H₂O)_n family, PO₃⁻·(H₂O)₂ is the most reactive cluster in the gas phase. Our results show that PO₃⁻ and H₂O still have a strong tendency to form double donor-double acceptor hydrogen bonds in this cluster. The theoretical optimized geometries for the global minimum of PO₃⁻·(H₂O)₂ are given in Figure 7 and Table IV, and the harmonic vibrational frequencies and normal mode assignments in Table V. This global minimum may be thought of as a descendant of Figure 2, the global minimum for PO₃⁻·H₂O. The hydrogen-bonding structure, the binding energy, and the vibrational frequencies follow the same pattern as predicted for PO₃⁻·H₂O. In PO₃⁻·(H₂O)₂, the binding energy for the second water molecule is smaller than that of the first. The frequencies of the new vibrational modes due to the formation of additional hydrogen bonds are generally smaller than those of PO₃⁻·H₂O (Table V). The frequency of the A₂'(umbrella) vibrational mode in PO₃⁻, which is the O-P out-of-plane mode in PO₃⁻·H₂O and PO₃⁻·(H₂O)₂, decreases as successive water molecules are added.

For the cluster formation step (1, 2), the experiments of Keesee and Castleman² were only possible with D₂O. This was not

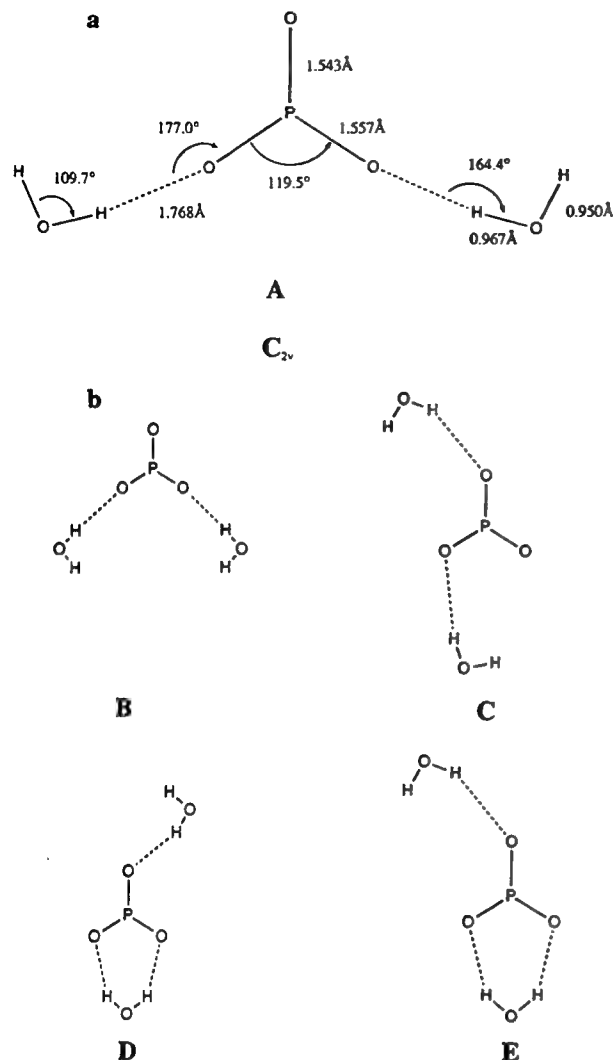


Figure 8. (a) A conformer of $\text{PO}_3^-(\text{H}_2\text{O})_2$ with two conventional hydrogen bonds. This structure was obtained at the DZ SCF level of theory. It collapses to Figure 7 at DZP SCF level of theory. (b) Several additional conformations of $\text{PO}_3^-(\text{H}_2\text{O})_2$.

expected to be a problem since the experimental dissociation energies of $\text{PO}_3^-\text{H}_2\text{O}$ and $\text{PO}_3^-\text{D}_2\text{O}$ differ by only 0.3 kcal mol⁻¹, as discussed above. For the reaction



the experimental ΔH° value is -11.4 kcal mol⁻¹. Our comparable DZP+diff SCF ΔH° (-10.8 kcal mol⁻¹) for $\text{PO}_3^-(\text{D}_2\text{O})_2$ formation agrees with this deuterated ΔH° value to within 0.6 kcal mol⁻¹. As was true of the $\text{PO}_3^-\text{D}_2\text{O}$ complex, the SCF $-\Delta H^\circ$ values are lower than the experimental $-\Delta H^\circ$ for the $\text{PO}_3^-(\text{D}_2\text{O})_2$ complex. However, as was also seen for $\text{PO}_3^-\text{D}_2\text{O}$, the DZP CISC method increases $-\Delta H^\circ$ (1, 2) significantly, to 13.0 kcal mol⁻¹. When the latter prediction is lowered slightly to reflect the effect of diffuse basis functions, the agreement with experiment is quantitative.

Figure 8 gives some structures that appear only at the STO-3G or DZ SCF levels. With the DZP SCF method these structures collapse to Figure 7, the global minimum, and Figure 9, another $\text{PO}_3^-(\text{H}_2\text{O})_2$ minimum. This general sort of behavior was also observed in the case of $\text{PO}_3^-\text{H}_2\text{O}$ discussed above. But unlike $\text{PO}_3^-\text{H}_2\text{O}$, which has only one structure that is a true minimum, for $\text{PO}_3^-(\text{H}_2\text{O})_2$ we find two distinct minima. Note that Figure 9 is a minimum very close to a planar transition state. Because the transition state has a structure almost identical with the minimum, no separate structure is shown for the planar transition state. The particular structure shown in Figure 9 is a minimum because the first H_2O molecule forms double donor-double acceptor hydrogen bonds, thus blocking the site for the second H_2O

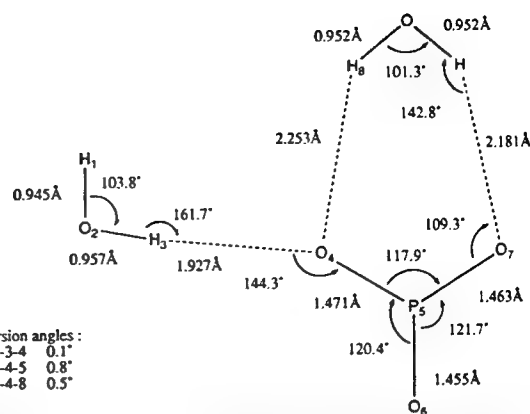
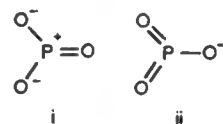


Figure 9. A C_1 minimum of $\text{PO}_3^-(\text{H}_2\text{O})_2$ at the DZP SCF level of theory. The structure of the C_1 transition state is almost identical except that all atoms are in the same plane.

molecule to form such bonds. The corresponding planar transition state has one imaginary vibrational frequency (15i cm⁻¹), which corresponds to the torsional movements (torsion 1-2-3-4 and torsion 2-3-4-5) of the H_2O molecule distorting from the constrained coplanar symmetry. This imaginary vibrational frequency is so small that removal of the C_1 symmetry decreases this torsional angle to a mere 0.8° and the energy difference to 0.000 006 kcal mol⁻¹! Thus there is essentially no structural difference between this local minimum and the planar transition state. This secondary minimum lies 2.1 kcal mol⁻¹ higher above the global minimum. Even though the second H_2O forms only one hydrogen bond, there may be a very slight interaction with the oxygen atom O_6 . The bond angle $\text{O}_4\text{-P}_5\text{-O}_6$ is slightly smaller than $\text{O}_6\text{-P}_5\text{-O}_7$. The P-O bonds behave in the same manner as for $\text{PO}_3^-\text{H}_2\text{O}$; the two complexed P-O bonds become longer, while the uncomplexed bond ($\text{P}_5\text{-O}_6$) becomes shorter. This configuration has some character of the valence structure i, but the global minimum (Figure 7) has more of the hypervalent character of ii.



For $\text{PO}_3^-(\text{H}_2\text{O})_2$, there is a "true" transition state (Figure 10) similar to the transition state for $\text{PO}_3^-\text{H}_2\text{O}$ (Figure 4). This structure has one imaginary vibrational frequency, corresponding to the movement of the water molecule toward the global minimum. In the $\text{PO}_3^-(\text{H}_2\text{O})_2$ transition state, the three P-O bond lengths are almost equal, suggesting that all three oxygen atoms in the PO_3^- anion experience comparable interactions with the H_2O molecule.

Figure 11 depicts some additional stationary points for $\text{PO}_3^-(\text{H}_2\text{O})_2$. It is interesting to note that there can be hydrogen bonding between H_2O molecules within the cluster. One of those structures, C in Figure 11b, has a lower energy than structures D and E in the same figure due to the weak secondary hydrogen bond formed between the two water molecules. Among these $\text{H}_2\text{O}\cdots\text{H}_2\text{O}$ stationary points, the most interesting are structures A and B of Figure 11a. The starting points for optimization of the structures reported in Figure 11a were derived from Figure 2, the global minimum for $\text{PO}_3^-\text{H}_2\text{O}$, plus a second H_2O in the plane perpendicular to the $\text{PO}_3^-\text{H}_2\text{O}$ plane. When the arrangement of the second H_2O is such that the two hydrogen atoms point toward $\text{PO}_3^-\text{H}_2\text{O}$, the potential surface leads this water molecule in the direction of structure A in Figure 11a. When the orientation of the second H_2O molecule is such that the oxygen atom in H_2O points toward $\text{PO}_3^-\text{H}_2\text{O}$ (i.e., the arrangement opposite to that described above), then the potential surface leads this H_2O in the direction of structure B in Figure 11a. In the latter case the second water molecule hydrogen bonds with the water molecule in $\text{PO}_3^-\text{H}_2\text{O}$ rather than with the PO_3^- moiety. As might be expected, this hydrogen bonding is weaker than that

Table VI. Harmonic Vibrational Frequencies (cm⁻¹) for the D_{3h} Symmetry Global Minimum Structure of PO₃⁻·(H₂O)₃ at the SCF Level of Theory (Figure 12)

mode	symmetry	DZP	DZP+diff	mode	symmetry	DZP	DZP+diff
sym H-O	E'	4174 (3057) ^a	4169 (3053) ^a	O-P out-of-plane	A ₂ ''	520 (570)	515 (559)
asym H-O	A ₂ '	4170 (3054)	4166 (3051)	asym torsion	E''	378 (272)	374 (269)
sym H-O	A ₁ '	4104 (2962)	4100 (2958)	asym def	A ₁ ''	366 (259)	361 (255)
asym H-O	E'	4102 (2960)	4098 (2957)	asym def	E'	354 (253)	339 (242)
trigonal def	A ₁ '	1845 (1349)	1824 (1334)	asym def	A ₂ '	354 (259)	339 (249)
trigonal def	E'	1827 (1332)	1808 (1319)	O...H stretch	E'	154 (148)	148 (142)
P-O	E'	1422 (1427)	1412 (1417)	O...H stretch	A ₁ '	135 (129)	131 (124)
sym P-O	A ₁ '	1138 (1137)	1134 (1133)	O...H stretch	A ₂ '	103 (99)	97 (93)
puckering	A ₂ ''	674 (450)	656 (443)	asym torsion	E''	50 (49)	45 (44)
puckering	E''	633 (464)	618 (453)	O...H stretch	E'	45 (44)	42 (41)
asym def	E'	553 (553)	549 (549)	asym torsion	A ₂ ''	27 (26)	23 (23)

^a The values in parentheses refer to PO₃⁻·(D₂O)₃.**Table VII.** Total Energies and Dissociation Energies for the Global Minimum Structures for PO₃⁻·(H₂O)_n Clusters

theoretical level	total energies (hartrees)			D _e (kcal mol ⁻¹)			D ₀ (kcal mol ⁻¹)		
	n = 1	n = 2	n = 3	n = 1	n = 2	n = 3	n = 1	n = 2	n = 3
DZP SCF	-641.553 29	-717.620 51	-793.685 60	14.5	27.5	39.1	12.1	22.9	32.4
DZP CISD	-642.260 42	-718.471 99	-794.672 41 ^a	16.7	31.2	43.5 ^a	14.3	26.6	36.8 ^a
DZP CCSD	-642.402 06			17.0			14.6		
DZP+diff SCF	-641.565 76	-717.635 17	-793.702 60	13.7	26.1	37.3	11.4	21.6	30.8
DZP+diff CISD	-642.284 20			15.6			13.3		
DZP+diff CCSD ^b	-642.430 91			15.6 ^b			13.3 ^b		

^a Single-point evaluations at the DZP SCF optimized geometries. ^b Single-point evaluations at the DZP+diff CISD optimized geometries.

of the former case, but it is still significant.

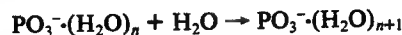
The DZP SCF total energy of the structure B in Figure 11a is -717.616 24 hartrees. Since the total energy of H₂O is -76.046 55 hartrees and the total energy of the structure for the global minimum of PO₃⁻·H₂O in Figure 2 is -641.553 29 hartrees at the same theoretical level, the binding energy for the second H₂O attaching to the first H₂O is 10.3 kcal mol⁻¹. Thus the PO₃⁻·H₂O·H₂O binding energy is almost twice as large as that of the water dimer. It is interesting to note the geometry change within PO₃⁻·H₂O after it binds with the second water molecule to form PO₃⁻·H₂O·H₂O. For PO₃⁻·H₂O, the hydrogen bond length is 2.197 Å and the O₃-P₁-O₄ bond angle is 118.4° at the DZP SCF level (Table II), but the corresponding values for PO₃⁻·H₂O·H₂O are 2.116 Å and 117.8°. This suggests that the formation of the second hydration product increases the interaction between the anion and the first water molecule.

Figure 11c shows the energies of these five stationary points relative to the global minimum for PO₃⁻·(H₂O)₂. Structure A in Figure 11a has a lower energy than the structure in Figure 9, a minimum of PO₃⁻·(H₂O)₂. Clearly this is a result of the different orientations of the second water molecule. In Figure 9, the oxygen atom O₆ is free, whereas for the structure A in Figure 11a, all three oxygen atoms in the PO₃⁻ anion directly participate in hydrogen bonding.

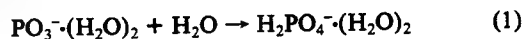
D. Metaphosphate Anion-Three Water Clusters, PO₃⁻·(H₂O)₃. It is found that for the family of reactions



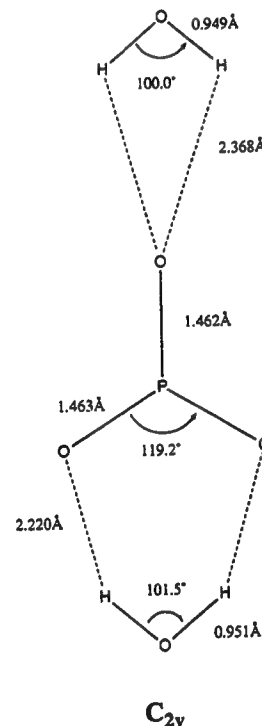
mass spectrometry² confirms the presence of the six hydrogen atoms expected for PO₃⁻·(H₂O)₃. For the cluster formation step (n, n + 1)



some experimental peculiarities² are exhibited in step (2, 3). The enthalpy change -ΔH is significantly higher in this step than in steps (0, 1) and (1, 2), and the reaction rate is slower. The experimentalists (who used D₂O instead of H₂O for their observations) explain the abnormality in ΔH as being due to the isomerization



The present theoretical investigation confirms that PO₃⁻·(H₂O)₃ is a stable species, as indicated in Figure 12. The theoretical structure of D_{3h} symmetry appears consistent in structure, vi-

**Figure 10.** A transition state for PO₃⁻·(H₂O)₂ optimized at the DZP SCF level of theory.**Table VIII.** Zero-Point Vibrational Energy Corrected Energy Changes for the Formation of the PO₃⁻·(H₂O)_n Clusters (kcal mol⁻¹)^a

(n, n + 1) ^b	theoretical ΔE ₀				
	DZP SCF	DZP CISD	DZP CCSD	DZP+diff SCF	DZP+diff CISD
(0, 1), H ₂ O	12.1	14.3	14.6	11.4	13.3, (13.3) ^c
(0, 1), D ₂ O	12.7	14.9	15.2	11.9	13.8, (13.8) ^c
(1, 2), H ₂ O	10.7	12.1		10.2	
(1, 2), D ₂ O	11.3	12.6		10.7	
(2, 3), H ₂ O	9.6	10.2		9.2	
(2, 3), D ₂ O	10.1	10.8		9.7	

^a Based on the geometries for the global minima of the clusters.^b Refers to the reactions: PO₃⁻·(H₂O)_n + H₂O = PO₃⁻·(H₂O)_{n+1}.^c DZP+diff CCSD level of theory, assuming DZP+diff CISD stationary point geometries.

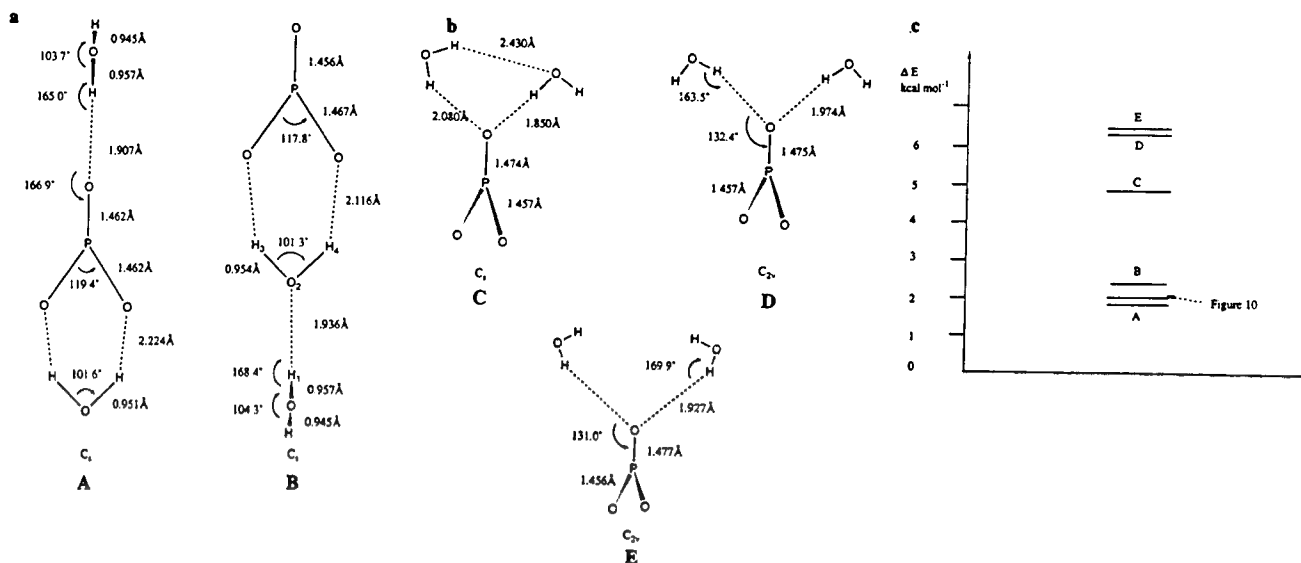


Figure 11. (a) Two stationary points of $\text{PO}_3^{--}(\text{H}_2\text{O})_2$ obtained at the DZP SCF level of theory. In both cases the C_s symmetry plane contains the P-O bond and the out-of-plane H_2O molecule. (b) Additional stationary points for $\text{PO}_3^{--}(\text{H}_2\text{O})_2$ optimized at the DZP SCF level of theory. The symmetry planes contain two H_2O molecules and the P-O bond. (c) The energies of the stationary points shown in (a) and (b) relative to the global minimum of $\text{PO}_3^{--}(\text{H}_2\text{O})_2$ (Figure 7).

Table IX. Thermochemical Data for the Formation of the $\text{PO}_3^{--}(\text{H}_2\text{O})_n$ Clusters^a

(n, n + 1) ^b	DZP SCF			DZP+diff SCF			DZP CISD		DZP CCSD		DZP+diff CISD ^c		experimental data ^d		
	$-\Delta H^\circ$	$-\Delta S^\circ$	$-\Delta G^\circ$	$-\Delta H^\circ$	$-\Delta S^\circ$	$-\Delta G^\circ$	$-\Delta H^\circ$	$-\Delta G^\circ$	$-\Delta H^\circ$	$-\Delta G^\circ$	$-\Delta H^\circ$	$-\Delta G^\circ$	$-\Delta H^\circ$	$-\Delta S^\circ$	$-\Delta G^\circ$
(0, 1), H_2O	12.6	26.2	4.8	11.9	25.8	4.2	14.8	7.0	15.1	6.2	13.8	6.1	12.9	22.3	6.3
(0, 1), D_2O	13.0	26.7	5.0	12.1	26.3	4.3	15.2	7.2	15.5	6.4	14.0	6.2	12.6	20.8	6.4
(1, 2), H_2O	11.1	27.5	2.9	10.6	27.0	2.5	12.7	4.5							
(1, 2), D_2O	11.5	27.9	3.1	10.8	27.6	2.6	13.0	4.6					11.4	22.0	4.9
(2, 3), H_2O	9.9	28.8	1.3	9.5	28.1	1.1	10.5	1.9							
(2, 3), D_2O	10.2	29.1	1.5	9.7	28.6	1.2	11.1	2.4					16.3	36.4	5.5

^a Based on the geometries for the global minima of the clusters. The values of ΔH and ΔG are in kcal mol⁻¹, and ΔS in cal/K-mol. The standard state is 1 atm at 298 K. ^b Refers to the reactions: $\text{PO}_3^{--}(\text{H}_2\text{O})_n + \text{H}_2\text{O} = \text{PO}_3^{--}(\text{H}_2\text{O})_{n+1}$. ^c The values are the same as the DZP+diff CCSD level of theory, assuming DZP+diff CISD stationary-point geometries. ^d Keesee and Castleman, ref 2.

brational frequencies (Table VI), and characteristics of hydrogen bonding with the smaller complexes $n = 1$ or 2.

We must be careful to state that Keesee and Castleman² in no way exclude the possibility of a D_{3h} minimum for $\text{PO}_3^{--}(\text{H}_2\text{O})_3$. They do say (as confirmed here by theory) that the third dissociation energy (2, 3) for D_{3h} $\text{PO}_3^{--}(\text{H}_2\text{O})_3$ should be less than that for (0, 1) and (1, 2). On this basis Keesee and Castleman conclude that their data are best explained by an isomerization from the D_{3h} $\text{PO}_3^{--}(\text{H}_2\text{O})_3$ minimum to a lower energy structure, plausibly $(\text{HO})_2\text{PO}_2^{--}(\text{H}_2\text{O})_2$.

The D_{3h} equilibrium geometry of Figure 12 confirms that all of the $\text{PO}_3^{--}(\text{H}_2\text{O})_n$, $n = 1, 2$, and 3, structures are of the double donor-double acceptor type. This is not an intuitively required result. For example, in their thoughtful and excellent analysis, Keesee and Castleman² assume linear hydrogen bonds of length 1.5 Å. New experiments to confirm or deny these fresh theoretical structures would certainly be welcome.

Figure 13 shows two configurations that exist only on the STO-3G and DZ SCF potential energy hypersurfaces. Both of these stationary points collapse to the global minimum D_{3h} structure at the DZP SCF level. We find that polarization basis functions are important in determining the nature of the hydrogen bonding in the clusters. For example, even when electron correlation effects are considered at the DZ CISD level, the C_{2v} symmetry $\text{PO}_3^{--}(\text{H}_2\text{O})_3$ in Figure 13, A, does not collapse to the D_{3h} structure.

In a manner similar to $\text{PO}_3^{--}(\text{H}_2\text{O})_2$, the lowest vibrational frequencies due to hydrogen bonding continue to decrease for $\text{PO}_3^{--}(\text{H}_2\text{O})_3$. The smallest DZP SCF harmonic vibrational frequency is 27 cm⁻¹, and the addition of diffuse basis functions reduces this result to 23 cm⁻¹.

In one of the earliest ab initio studies of PO_3^{--} , Loew suggested that PO_3^{--} may be both an electrophile and an anion,²⁴ because

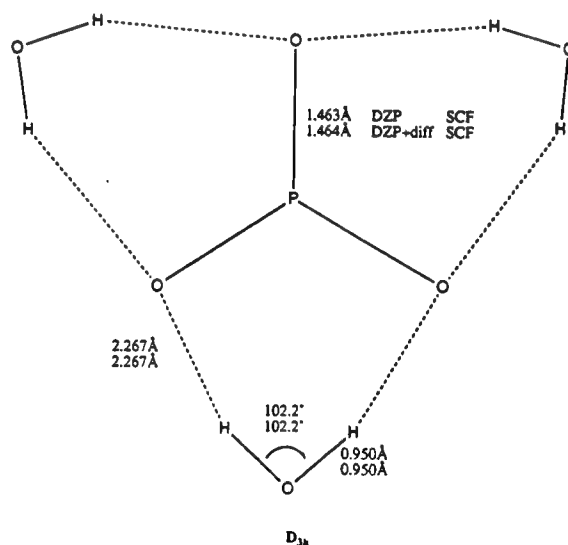


Figure 12. The global minimum equilibrium geometry for $\text{PO}_3^{--}(\text{H}_2\text{O})_3$.

there is a positive charge "hole" in phosphorus. Of course, the preferred approach for a nucleophile is along a path perpendicular to the molecular plane. But Henchman refuted this possibility based on his experiments.¹ In our research, for $n = 1, 2$, and 3, we have tried to locate some stationary points for which the oxygen atom in a water molecule can approach the phosphorus atom along the axial path perpendicular to the PO_3^{--} plane. However, our results do not support such a possibility. In the C_{2v} coplanar

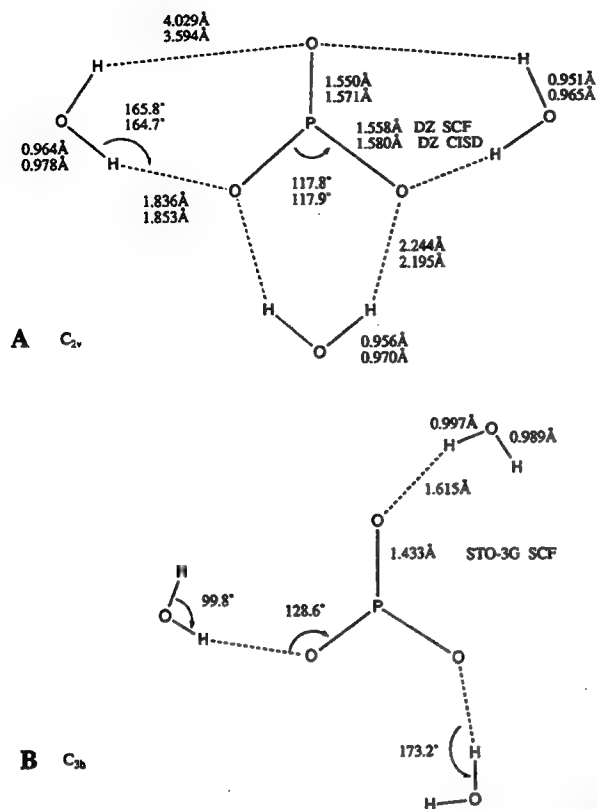


Figure 13. Two structures of PO₃⁻·(H₂O)₃ predicted at the STO-3G SCF and DZ SCF levels of theory. Both structures collapse to the higher symmetry structure of Figure 12 at the DZP SCF level of theory.

approach, as the lone pair of the water oxygen atom moves toward PO₃⁻, the H₂O remains far away; i.e., there is no stationary point for such orientation at the DZP SCF level. This situation is no better in the axial direction, and even for $n = 2$, where the third water molecule may have a greater chance to approach in this manner, the result is still negative. As previously mentioned (Figure 11a) in forming PO₃⁻·(H₂O)₃, we may suppose that the PO₃⁻·(H₂O)₂ collides with the third H₂O molecule in different orientations. The different orientations lead to the "products" in Figures 14 and 15, respectively. In both Figure 14 and 15, it may be seen that the oxygen atom in PO₃⁻ cannot afford to form hydrogen bonds with three hydrogen atoms as a triple acceptor. The approach of the third H₂O "breaks" some of the previously formed hydrogen bonds, and monodonor hydrogen bonding is preferred for these two stationary points. There is little difference between these two structures (Figures 14 and 15). Except for the orientation of the H₂O moieties, the PO₃⁻ anion is unchanged under the influence of these two different H₂O approaches. These two stationary points lie about 4.6 and 4.4 kcal mol⁻¹ higher than the global minimum, respectively.

4. Conclusions

In this paper we have presented detailed theoretical studies of the PO₃⁻·(H₂O)_n clusters. The highest theoretical level used is the DZP+diff CCSD method. For $n = 0, 1, 2$, and 3 , the global minima are shown in Figures 1, 2, 7, and 12, respectively. The theoretical results confirm the presence of PO₃⁻·(H₂O)_n clusters found experimentally. Our most important result is that the clusters tend to form high-symmetry double donor hydrogen bonds between the PO₃⁻ anion and the H₂O molecules. The hydrogen-bond lengths are 2.1–2.2 Å. The hydrogen bond in PO₃⁻·H₂O is very comparable to that for NO₃⁻·H₂O. It is also interesting that the hydrogen bonds can be formed between the H₂O moieties in the cluster; these have larger binding energies than that for the isolated water dimer. The theoretical results agree quantitatively with the experimental thermochemistry² for the reaction steps (0, 1) and (1, 2). However the third water molecule in the D_{3h} PO₃⁻·(H₂O)₃ equilibrium structure is significantly less strongly

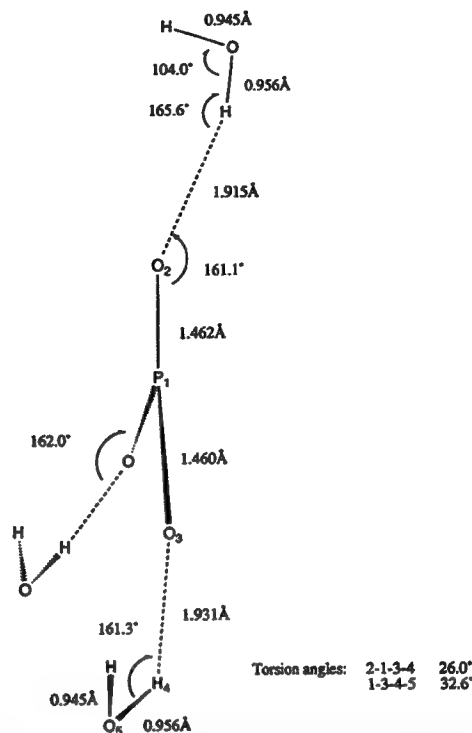


Figure 14. Another stationary point for PO₃⁻·(H₂O)₃ optimized at the DZP SCF level of theory. The C_s symmetry plane contains the upper H₂O molecule and the in-plane P–O bond.

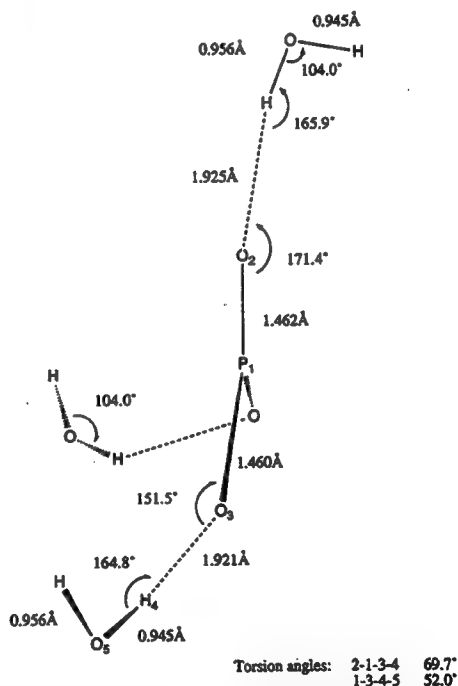


Figure 15. A final stationary point for PO₃⁻·(H₂O)₃ obtained at the DZP SCF level of theory. The C_s symmetry plane contains the upper H₂O molecule and the in-plane P–O bond.

bound than observed. This prediction is consistent with the intuitive analysis of Keesee and Castleman.² Whether there is a lower energy PO₆H₆⁻ isomer such as (HO)₂PO₂⁻·(H₂O)₂ remains an important unresolved question.

Acknowledgment. Helpful discussions with Dr. Y. Yamaguchi, Mr. Ching-han Hu, Mr. C. A. Richards, Jr., and Ms. Cynthia Meredith are greatly appreciated. This research was suggested by Drs. Michael Henchman, John Paulson, and Albert Viggiano. The work was supported by the U. S. Air Force Office of Scientific Research under Grant No. AFOSR-92-J-0047.

The tetramer of borane and its heavier valence-isoelectronic analogs: M_4H_{12} with $M = B, Al,$ and Ga

Mingzuo Shen, Congxin Liang¹ and Henry F. Schaefer III

Center for Computational Quantum Chemistry, The University of Georgia, Athens, GA 30602, USA

Received 25 November 1992

Ab initio all-electron quantum mechanical methods were applied to the tetramers of borane (BH_3) and its analogs in the periodic table, namely the molecules B_4H_{12} (tetraborane(12) or $(BH_3)_4$), Al_4H_{12} (tetraalane(12) or $(AlH_3)_4$), Ga_4H_{12} (tetragallane(12) or $(GaH_3)_4$). Four closed-shell stationary points were found for each tetramer. In addition, the butterfly tetraborane(10) (B_4H_{10}) and its analogs tetraalane(10) (Al_4H_{10}) and tetragallane(10) (Ga_4H_{10}) were investigated at comparable levels of theory. Geometry optimizations were performed at correlated levels whenever practical, and at the Hartree-Fock level otherwise, using sizeable basis sets. In most cases, energetic information was obtained from correlated methods. It is confirmed that the most recent (1981) experimental structures for tetraborane(10) have an error for one of the bridging B–H bond distances, as noted recently by Bühl and Schleyer. However, the other three experimental structures for B_4H_{10} also have serious problems. Our results suggest that the molecular structures of butterfly M_4H_{10} , $M = B, Al, Ga$, are very similar. The structures of M_4H_{12} , $M = B, Al, Ga$, although still quite similar, show more variations. We found that the butterfly (12) structures, belonging to the point group C_{2v} , are local minima at the SCF potential energy surfaces. The butterfly tetraborane(12) is energetically less stable than the butterfly tetraborane(10) plus molecular hydrogen. The butterfly tetraalane(12) is, in contrast, energetically more stable than the butterfly tetraalane(10) plus molecular hydrogen. The butterfly tetragallane(12) displays a third behavior – energetically comparably stable with the butterfly tetragallane(10) plus molecular hydrogen. In all cases electron correlation effects were found to stabilize the butterfly(10) structures more than the butterfly(12) structures.

1. Introduction

Recently we have carried out some systematic ab initio quantum mechanical studies of the group IIIA hydrides. Shen and Schaefer [1] studied diborane(6) and its analogs in the periodic table using correlated methods with quite large basis sets. The agreement with available experimental molecular geometries and vibrational frequencies was found to be satisfactory. Duke, Liang and Schaefer [2] studied the properties of triborane(9), triallane(9), and trigallane(9) at comparable levels of theory. A cyclic, and an acyclic structure with one pentacoordinated heavy atom were studied. The present paper reports our study of the borane tetramer, $(BH_3)_4$ or B_4H_{12} , and its analogs in the periodic table, $(AlH_3)_4$ or Al_4H_{12} , and $(GaH_3)_4$ or Ga_4H_{12} . The present re-

search may be viewed as a continuation of the trimer study [2]. While the structures of the tetramers (M_4H_{12}) are of interest in their own right, they may also be related to those of the dimers (M_2H_6 , $M = B, Al, Ga$).

It is experimentally well known that tetraborane(10) B_4H_{10} is stable and has a “butterfly” (belonging to the point group C_{2v}) structure. For purpose of comparison the butterfly tetraborane(10) and its analogs tetraalane(10) Al_4H_{10} and tetragallane(10) Ga_4H_{10} were included in the present study.

Previous theoretical studies of the tetraborane(12) molecule include those of Pepperberg, Halgren and Lipscomb [3] who studied only one structure (belonging to the D_{4h} point group) using the partial retention of differential diatomic overlap (PRDDO) method with geometry optimization and the ab initio SCF method with moderate basis sets without geometry optimization. Four years later McKee and Lipscomb [4] used higher-level ab initio

¹ Permanent address: Biosym Technologies Inc., 9685 Scranton Road, San Diego, CA 92121, USA.

methods. For tetraborane(12) still only one structure was investigated. In 1985 McKee and Lipscomb [5] reported further theoretical studies on tetraborane(12). While the level of theory employed remained largely unchanged, the potential energy surface was searched more thoroughly. Three stationary points belonging to the D_{2d} , C_{4v} , and C_{2v} point groups, respectively, were found at the 3-21G SCF level. Harmonic vibrational frequencies were used to characterize the stationary points. The C_{2v} structure was found to be a local minimum with a lower energy than the other two stationary points. The total energies were also estimated using the 6-31G SCF, 6-31G* SCF, and 6-31G MP2 methods. Bock, Roberts, O'Malley, Trachtman and Mains [6] have very recently reported theoretical results for B_4H_{12} and Al_4H_{12} . Experimentally, tetragallane(12) was invoked as a molecule produced in matrix study of digallane(6), by Pulham, Downs, Goode, Rankin and Robertson [7].

Tetraborane(10) appears to have been well characterized experimentally. Jones, Hedberg and Schomaker [8] determined the molecular geometry using the gas phase electron diffraction technique. Nordman and Lipscomb [9,10] determined the molecular structure of tetraborane(10) using X-ray crystallography. Existing structural data were refined by Moore, Dickerson and Lipscomb later [11]. More recently Simmons, Burg and Beaudet [12] reported microwave spectra and a new structure for tetraborane(10), while Dain, Downs, Laurenson and Rankin [13] reported a new electron diffraction structure. There are quite a number of previous theoretical studies on tetraborane(10) as well. The question of the relative stability of the butterfly (C_{2v}) and the chain-like tetraborane(10) structures has been addressed theoretically [14]. Bühl and Schleyer [15] optimized the geometry for the butterfly tetraborane(10) at the 6-31G* and 6-31G** MP2 levels, while concentrating on the ^{11}B chemical shifts. McKee [16] seems to have reported the first theoretical study on tetraalane(10). Duke and Schaefer [17] reported a theoretical study of 1-gallatetraborane(10). Apparently no previous theoretical studies have been reported for tetragallane(12) and tetragallane(10).

In the present research *ab initio* methods of considerably higher level than used before were applied to tetraborane(12) and tetraborane(10) and their

analogs. Since there are virtually no experimental data concerning the molecular geometries of the tetramers, only four stationary points on the closed-shell SCF potential surfaces were located for each tetramer ($M=B, Al, Ga$). The emphasis was on the comparisons within group IIIA in the periodic table. Since tetraborane(10) is known to have the butterfly structure, the chain-like structures for the aluminum and gallium analogs were not investigated.

2. Theoretical details

Three basis sets [18–20] ^{#1} were used in this study, identically to those used in ref. [1]. In increasing size, these are labeled “DZ”, “DZd(5d)”, “DZd”, “DZP(5d)” and “DZP”. There are two variations in the “DZP basis set”; in the following “DZP” will denote the basis in which sets of six d-like basis functions were used, while “DZP(5d)” will denote the basis set in which five pure d basis functions were used. Similarly there are two variations in the “DZd basis set”, labeled “DZd(5d)” and “DZd”. In the DZP basis set for tetraborane(12) there are 124 basis functions. In the DZP basis set for tetraalane(12) there are 156 basis functions. In the DZP basis set for tetragallane(12) there are 220 basis functions, while in the DZP(5d) basis set there are 208 functions.

We used four different methods including the self-consistent field (SCF) method, configuration interaction with single and double excitations (CISD) method, coupled cluster with single and double excitations (CCSD) method, and second-order Møller-Plesset perturbation theory (MP2). For the tetraborane(12) and tetraborane(10) structures, geometry was optimized using analytic SCF, CISD, and CCSD energy gradient techniques ^{#2}. Harmonic vibrational frequencies and infrared (IR) intensities were obtained using analytic SCF energy second-derivative techniques ^{#3}. In the CISD and CCSD wavefunctions

^{#1} For the primitive basis set 14s11p5d, see ref. [20]. The contraction (14s11p5d/7s5p2d) is due to R.S. Grev and H.F. Schaefer, unpublished.

^{#2} For SCF analytic energy gradient techniques, see ref. [21]. For CISD analytic energy gradient techniques, see ref. [22]. For CCSD analytic energy gradient techniques, see ref. [23].

^{#3} For SCF analytic energy second-derivative techniques see ref. [24].

the boron 1s-like core MOs were frozen and the corresponding highest lying virtual MOs were deleted. For the tetraalane(12) and tetraalane(10) structures, the geometry was optimized using analytic SCF energy gradients only [21]. CISD and CCSD total energies were evaluated at the SCF optimized geometries. Harmonic vibrational frequencies and IR in-

tensities were obtained using analytic SCF energy second-derivative techniques [24]. In the CISD and CCSD wavefunctions, the aluminum 1s-, 2s-, and 2p-like core MOs were frozen and the corresponding highest lying virtual MOs deleted. For the tetragallane(12) and tetragallane(10) structures, the geometry was optimized using analytic SCF energy gra-

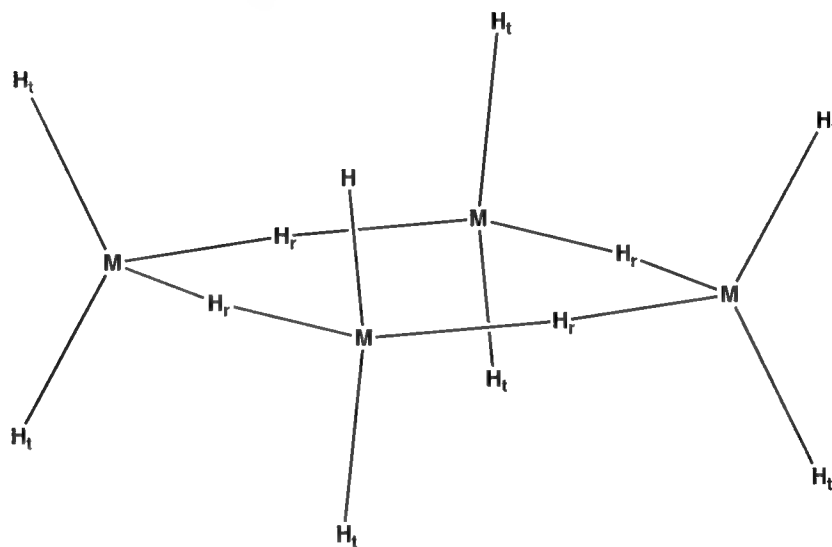


Fig. 1. Qualitative sketch of D_{4h} tetraborane(12) B_4H_{12} and the analogous aluminum and gallium structures.

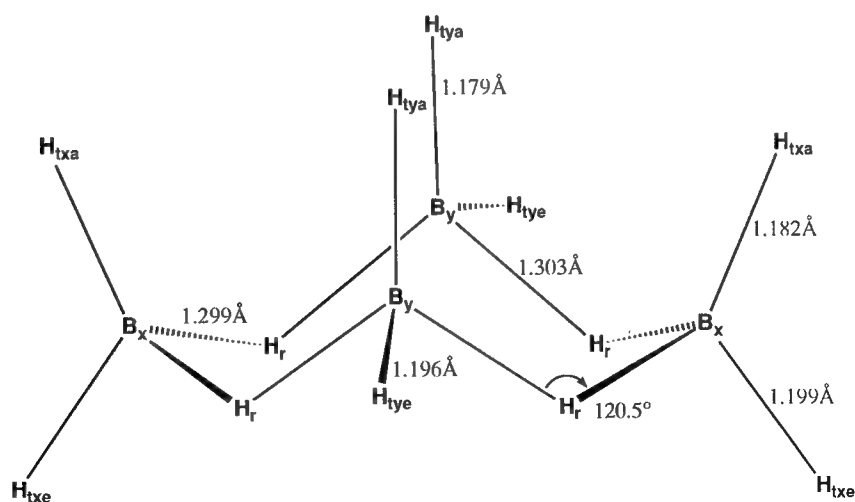


Fig. 2. C_{2v} deformed ring (or "butterfly") structure for tetraborane(12) B_4H_{12} . This structure is energetically lowest lying and a local minimum on the SCF potential energy surface. The B–H–B bridge bonds are pronouncedly bent. The indicated geometrical parameters were obtained at the DZP CCSD level of theory.

dients techniques [21], and in the case of DZP(5d) the direct SCF technique was used [25]. Harmonic vibrational frequencies and IR intensities were obtained for the DZP(5d) basis set. MP2 total energies were evaluated at the SCF optimized geometries. In the MP2 treatment of electron correlation, all MOs were included.

Three different *ab initio* quantum mechanical computer program systems were used. The PSI program system^{‡‡} was used for the SCF geometry optimization, harmonic vibrational frequencies and IR

^{‡‡} The PSI system is distributed by PSITECH Inc., Watkinsville, GA, USA.

Table 1

D_{4h} tetraborane(12) B₄H₁₂: theoretical total energies, equilibrium geometries, and imaginary harmonic vibrational frequencies at various levels of theory. The molecular structure of tetraborane(12) D_{4h} is shown in fig. 1

	DZ SCF	DZd SCF	DZd CISD	DZP SCF	DZP CISD
total energy (au)	−104.49491	−105.54863	−105.89506	−105.55855	−105.99852
equilibrium geometry					
ring r_e (BH _r) (Å)	1.305	1.299	1.287	1.297	1.282
terminal r_e (BH _t) (Å)	1.183	1.182	1.187	1.185	1.185
terminal \angle (H _t BH _t) (deg)	125.6	125.6	125.9	125.4	125.9
ring \angle (H _r BH _r) (deg)	99.7	100.3	102.2	102.0	101.2
ring \angle (BH _r B) (deg)	170.3	169.7	167.8	168.0	168.8
Symmetry	ω (cm ^{−1})				
b _{2g}	183i	256i		330i	
c _g	281i	323i		405i	
a _{2u}	262i	304i		393i	
b _{1u}	275i	323i		403i	
b _{2u}	54i	59i		68i	

Table 2

C_{2v} tetraborane(12) B₄H₁₂: theoretical total energies and equilibrium geometries obtained at various levels of theory. The molecular structure of tetraborane(12) C_{2v} is shown in fig. 2^{a)}

	DZ SCF	DZd SCF	DZd CISD	DZP SCF	DZP CISD	DZP CCSD
total energy (au)	−105.50226	−105.56018	−105.91709	−105.57714	−106.02048	−106.09677
equilibrium geometry ^{b)}						
ring r_e (B _x H _r) (Å)	1.315	1.307	1.295	1.310	1.296	1.299
ring r_e (B _y H _r) (Å)	1.316	1.310	1.299	1.314	1.300	1.303
terminal r_e (B _x H _{txe}) (Å)	1.187	1.189	1.197	1.194	1.194	1.199
terminal r_e (B _y H _{tya}) (Å)	1.178	1.177	1.180	1.179	1.178	1.182
terminal r_e (B _y H _{tye}) (Å)	1.186	1.187	1.193	1.191	1.191	1.196
terminal r_e (B _y H _{tya}) (Å)	1.176	1.174	1.176	1.175	1.174	1.179
terminal \angle (H _{txe} B _x H _{tya}) (deg)	123.0	122.2	120.0	121.2	120.6	120.6
terminal \angle (H _{tye} B _y H _{tya}) (deg)	123.0	122.3	120.1	121.5	120.8	120.7
ring \angle (H _r B _x H _r) (deg)	102.6	103.5	105.8	104.0	104.7	104.9
ring \angle (H _r B _y H _r) (deg)	96.0	95.7	95.5	95.1	94.6	94.5
\angle (H _{tya} B _x H _r) (deg)	113.6	115.0	117.8	116.6	117.9	118.2
τ (BBBB) (deg)	23.0	22.3	21.1	21.2	21.1	21.1
τ (H _{txe} B _x H _r B _y) (deg)	176.9	178.6	179.2	179.9	179.9	179.6
τ (H _{tye} B _y H _r B _x) (deg)	156.1	155.0	155.1	154.6	154.6	154.6

^{a)} There are seven symmetry independent atoms, as labeled in fig. 2. The following abbreviations have been used for the labels: (x) on the x axis (in the present choice of molecular orientation); (y) on the y axis (the B_xB_x distance is longer than B_yB_y); (r) on the bridge (in the ring); (t) on the terminal; (e) equatorial; (a) axial (roughly parallel to the C₂ symmetry axis).

^{b)} r_e (XY) = bond distance in Å, \angle (XYZ) = bond angle in degrees, τ (WXYZ) = absolute value of torsional angle in degrees.

intensities, CISD and CCSD geometry optimization and total energies for the tetraborane(12) and tetraborane(10) structures. The PSI and CADPAC [26] systems were used for tetraalane(12) and tetraalane(10), and for tetragallane(12) and tetragallane(10). CADPAC was used for SCF geometry optimization, harmonic vibrational frequencies and IR intensities. The CADPAC and TURBOMOLE [27] systems were used for the tetragallane(12) and tetragallane(10) structures. TURBOMOLE was used for the DZd(5d) and DZP(5d) SCF harmonic vibrational frequencies and IR intensities, and MP2 energies at the SCF optimized geometries. The choice of different computer program systems was due to considerations of available CPU time, software capabilities (e.g. only PSI provides CCSD energy gradients and only TURBOMOLE handles the tetragallane(12) DZd(5d) and DZP(5d) SCF harmonic vibrational frequency computations) and hardware capabilities. These program systems ran on the University of Georgia IBM 3090 (PSI and CADPAC), the group DECstation 3100 (TURBOMOLE), and the group IBM RS/6000 (PSI and TURBOMOLE) computers. For all cases, the geometry was optimized using symmetrized internal coordinates [28] under appropriate symmetry constraints. Irreducible representations (symmetry species) for the normal modes were obtained using TURBOMOLE for the full point group of a molecule. Standard conventions for the irreducible representations were followed [29]. The harmonic vibrational frequencies reported were for the masses of major isotopes; namely, for hydrogen atoms 1.007825, for boron atoms 11.00931, for aluminum atoms 26.98154, and for gallium atoms 68.92558.

3. Results and discussion

The results will be presented in three subsections, one each for tetraborane(12) and tetraborane(10); tetraalane(12) and tetraalane(10); and tetragallane(12) and tetragallane(10). Finally we will compare the behavior of these molecules as predicted by the theoretical methods employed.

3.1. Tetraborane(12) and tetraborane(10)

We have found four stationary points for tetraborane(12), B_4H_{12} , belonging to the D_{3h} , D_3 , D_{4h} , and

Table 3
 C_{2v} tetraborane(12) B_4H_{12} : harmonic vibrational frequencies (in cm^{-1}) and IR intensities (in km/mol) determined at the SCF level of theory

Symmetry	DZ SCF	DZd SCF	DZP SCF
a_1	2882	2911	2879(198)
	2853	2875	2839(56)
	2737	2760	2717(4)
	2714	2737	2694(35)
	2437	2448	2373(87)
	1425	1541	1603(9)
	1216	1246	1250(0)
	1163	1198	1202(14)
	1142	1142	1110(15)
	827	830	823(4)
	611	628	632(0)
	393	398	403(0)
	271	302	342(7)
	117	139	149(0)
	2130	2184	2171
	1466	1575	1628
a_2	1188	1204	1193
	970	982	981
	686	733	758
	642	704	724
	287	296	333
	229	233	251
	2856	2878	2841(42)
	2716	2739	2695(86)
	2388	2397	2332(2318)
	1440	1545	1599(5)
b_1	1193	1222	1226(19)
	1122	1144	1139(560)
	947	950	929(92)
	819	832	839(30)
	609	631	641(2)
	282	304	343(1)
	2867	2895	2863(9)
	2729	2754	2713(135)
	2432	2448	2390(1637)
	1456	1572	1632(11)
	1206	1230	1230(6)
	1108	1129	1121(381)
	955	965	957(63)
	792	798	789(75)
b_2	617	633	635(2)
	208	222	266(1)

C_{2v} point groups, the latter two shown in figs. 1 ($M=B$) and 2. The D_{3h} structure incorporates a boron atom that is the bridgehead of six B–H–B bridges

and has two imaginary vibrational frequencies. The D_3 structure results from distortion of the D_{3h} structure, and was found to be a local minimum at the DZP

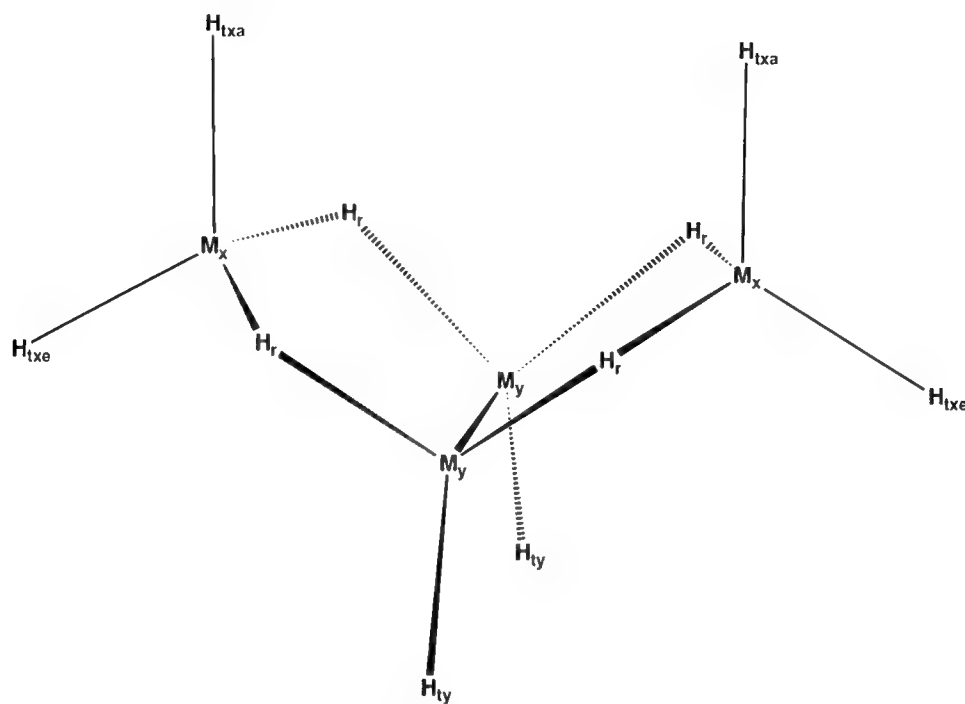


Fig. 3. Qualitative sketch of C_{2v} tetraborane(10) B_4H_{10} and the analogous aluminum and gallium structures.

Table 4

C_{2v} tetraborane(10) B_4H_{10} : theoretical total energies and equilibrium geometries at various levels of theory. The molecular structure of tetraborane(10) is shown in fig. 3

	DZ SCF	DZd SCF	DZd CISD	DZP SCF	DZP CISD	DZP CCSD
total energy (au)	−104.38926	−104.45486	−104.81395	−104.46998	−104.89644	−104.96475
equilibrium geometry ^{a)}						
ring $r_e(B_xH_r)$ (Å)	1.455	1.429	1.416	1.429	1.414	1.416
ring $r_e(B_yH_r)$ (Å)	1.260	1.252	1.254	1.257	1.254	1.259
terminal $r_e(B_xH_{txe})$ (Å)	1.181	1.183	1.188	1.186	1.186	1.190
terminal $r_e(B_yH_{txa})$ (Å)	1.185	1.186	1.192	1.190	1.190	1.195
terminal $r_e(B_xH_{ty})$ (Å)	1.175	1.179	1.181	1.181	1.179	1.183
$r_e(B_yB_y)$ (Å)	1.752	1.747	1.731	1.744	1.730	1.733
terminal $\angle(H_{txe}B_xH_{txa})$ (deg)	121.0	120.5	119.7	120.4	120.1	120.1
ring $\angle(H_rB_xH_r)$ (deg)	134.8	135.9	138.0	135.8	137.2	137.5
$\angle(H_{txe}B_xH_r)$ (deg)	103.6	103.8	103.9	104.1	104.4	104.5
$\tau(BBBB)$ (deg)	53.9	53.6	53.3	53.6	53.3	53.3
$\tau(H_{txa}B_xH_rB_y)$ (deg)	123.5	125.0	125.8	125.6	126.4	126.5
$\tau(H_{ty}B_yH_rB_x)$ (deg)	123.7	123.6	123.2	123.6	123.2	123.0

^{a)} There are six symmetry independent atoms in the present molecule, as labeled in fig. 3. The B_x atoms are directly bonded to two terminal hydrogens, while the B_y atoms are each directly bonded to one hydrogen atom.

SCF level, similar to the one reported by Bock et al. [6]. The D_{4h} ring structure (fig. 1) contains four B–H–B bridges in one plane. The C_{2v} deformed ring structure (fig. 2) is a distortion from the D_{4h} geometry, and was found to be a local minimum on the SCF potential energy surface with the DZ, DZd, and DZP basis sets. One interesting feature to note about the C_{2v} structure is the bent B–H–B bridges. Also this structure is more or less closely related to the tetraborane(10) butterfly, and therefore may be called the “butterfly” tetraborane(12).

At the DZP SCF level of theory (with optimized geometry in each case), the D_{3h} , D_3 , D_{4h} , and C_{2v} structures have the following relative energy: 27.5, 19.0, 11.7, 0.0 kcal/mol. At the DZd CISD level of theory (with optimized geometries), the relative energies in the same order are: 19.6, 11.0, 13.8, 0.0 kcal/mol. At the DZP CISD level of theory (with optimized geometries) the relative energies for the D_{3h} , D_{4h} , and C_{2v} structures are: 18.4, 13.8, 0.0 kcal/mol. With these relative energies we tend to conclude that the six-coordinated tetraborane(12) (D_3) is not the global minimum.

The optimized stationary point geometries and total energies for the D_{4h} ring structure are shown in table 1, along with its five imaginary harmonic vibrational frequencies (one of which doubly degenerate). Since there is more than one imaginary vibrational frequency, it is obviously not a transition state on the SCF potential energy surface. The lowest imaginary vibrational frequency, of irreducible representation b_{2u} , is only $68i\text{ cm}^{-1}$ at the DZP SCF level. Previously McKee and Lipscomb [5] reported 3-21G SCF harmonic vibrational frequencies for this structure. McKee and Lipscomb found only four imaginary vibrational frequencies (one of which doubly degenerate), and the lowest was $44i\text{ cm}^{-1}$.

The optimized equilibrium geometries and total energies for the C_{2v} deformed ring tetraborane(12) structure are shown in table 2. The harmonic vibrational frequencies using the SCF method are shown in table 3, with the DZP SCF IR intensities in parentheses in the last column. As seen from the SCF vibrational frequencies this structure is a local minimum and therefore the geometry was optimized at the DZP CCSD level in addition to the DZP CISD level. We note that the difference between DZP CISD and CCSD optimized equilibrium bond lengths are

not greater than 0.005 \AA for the valence internal coordinates used in table 2. For the benefit of later discussions, the DZP SCF and CCSD optimized geometries may be compared. It is seen that the DZP SCF BH_r (boron to ring hydrogen atom) bond lengths are too long by about 0.010 \AA , while the BH_t (boron to terminal hydrogen) bond lengths are too short by about 0.005 \AA . The opposite behavior in the theoretical bond lengths is not entirely surprising if we note that a boron–ring hydrogen bond is part of an elec-

Table 5

C_{2v} tetraborane(10) B_4H_{10} : theoretical harmonic vibrational frequencies (in cm^{-1}) and IR intensities (in km/mol) in parentheses determined with the SCF method

Symmetry	DZ SCF	DZd SCF	DZP SCF
a_1	2841	2842	2807(225)
	2826	2828	2793(10)
	2719	2735	2700(70)
	2300	2374	2333(73)
	1554	1644	1641(25)
	1210	1241	1237(16)
	1123	1126	1096(2)
	898	914	912(2)
	816	832	832(0)
	722	715	704(0)
	506	534	528(0)
	238	241	233(4)
	2299	2371	2334
a_2	1470	1544	1548
	1166	1180	1158
	1106	1113	1100
	884	930	932
	601	651	660
	418	427	427
	2829	2832	2795(92)
	2714	2729	2695(122)
b_1	2314	2383	2345(352)
	1350	1397	1390(0)
	1194	1223	1220(56)
	1008	1025	1010(10)
	826	880	884(122)
	433	420	418(12)
	64	229	263(0)
	2821	2823	2792(53)
	2270	2345	2307(18)
	1542	1634	1639(120)
b_2	1208	1213	1185(9)
	1101	1114	1094(76)
	961	964	955(25)
	819	835	828(0)
	554	579	579(55)

iron-deficient two-electron three-center bond, while a boron-terminal hydrogen bond is a "normal" two-electron two-center linkage. "Normal" chemical bonds are generally predicted to become shorter as the basis set size increases and longer as electron correlation effects are taken into account. However, boron hydrides (and closely related compounds with

unoccupied bonding MOs) sometimes display shorter bridging bond distances when correlation effects are included. The overall molecular shape of C_{2v} tetraborane(12) is that of a rectangular solid, with the $B_x B_x$ distance longer than the $B_x B_y$. The lowest few harmonic vibrational frequencies in table 3 are quite small, but increase as the basis set size increases. The

Table 6

A comparison of the theoretical and experimental geometries for the butterfly tetraborane(10) (C_{2v}). Bond distances are in Å, and "BBB-BBB" denotes the dihedral angle in degrees between the two BBB planes (alternatively, the torsional angle $B_x B_y B_x$)^{a)}

	$B_y B_x$	$B_y B_y$	$B_x B_x$	$B_y H_r$	$B_y H_t$	$B_x H_r$	BBB-BBB
JHS	1.85	1.76	2.88	1.43	1.19	1.33	124.5
NL	1.845(2)	1.750	2.786	1.21(3)	1.11(4)	1.37(10)	118.1
MDL	1.842	1.712	2.800	1.16	1.10	1.37	—
SBB	1.854(2)	1.718(2)	2.806(1)	1.428(20)	—	1.425(20)	117.4
DDLRL	1.856(4)	1.705(12)	—	1.315(9)	1.221(14)	1.484(9)	—
DZ SCF	1.928	1.752	2.916	1.260	1.175	1.455	116.2
DZd SCF	1.900	1.747	2.864	1.252	1.179	1.429	116.1
6-31* MP2 ^{b)}	1.835	1.714	—	1.252	—	1.410	—
DZd CISD	1.866	1.731	2.807	1.254	1.181	1.416	116.2
DZP SCF	1.903	1.744	2.874	1.257	1.181	1.429	116.3
6-31* MP2 ^{b)}	1.838	1.715	—	1.245	—	1.405	—
DZP CISD	1.872	1.730	2.821	1.254	1.179	1.414	116.3
DZP CCSD	1.872	1.733	2.820	1.259	1.183	1.416	116.4

^{a)} Key for the first column: JHS stands for Jones, Hedberg and Schomaker (1953) gas-phase electron-diffraction structure, ref. [8]. NL stands for Nordman and Lipscomb (1953) X-ray crystallographic structure, refs. [9,10]. MDL stands for Moore, Dickerson and Lipscomb (1957) least square refinement of existing data, ref. [11]. SBB stands for Simmons, Burg and Beaudet (1981) microwave spectroscopic structure, ref. [12]. DDLRL stands for Dain, Downs, Laurenson and Rankin (1981) gas-phase electron-diffraction structure, ref. [13].

^{b)} Ref. [15].

Table 7

Energies pertinent to the reaction $B_4H_{12}(C_{2v}) \rightarrow B_4H_{10} + H_2$. ΔE_c is defined by $E(B_4H_{10}) + E(H_2) - E(B_4H_{12})$, as predicted in this research^{a)}

Method	$E(B_4H_{12})$ (au)	$E(B_4H_{10}) + E(H_2)$ (au)	ΔE_c (kcal/mol)
DZ SCF	-105.50226	-104.38926 - 1.12666	-8.6
DZd SCF	-105.56018	-104.45486 - 1.12666	-13.4
DZd CISD	-105.91709	-105.95855 ^{b)}	-26.0
DZd CISD(Q)	-105.96465	-106.00959 ^{b)}	-28.2
DZP SCF	-105.57714	-104.46998 - 1.13109	-15.0
DZP CISD	-106.02048	-106.05338 ^{c)}	-20.6
DZP CISD(Q)	-106.08412	-106.11853 ^{c)}	-21.6
DZP CCSD	-106.09677	-104.96475 - 1.16671	-21.8

^{a)} The zero-point vibrational energy (ZPVE) correction to the reaction energy (which changes ΔE_c to ΔE_0), using the unscaled harmonic vibrational frequencies obtained at the DZP SCF level, is $\Delta ZPVE \equiv ZPVE(B_4H_{10}) + ZPVE(H_2) - ZPVE(B_4H_{12}) \equiv 72.0 + 6.6 - 83.3 = -4.7$ kcal/mol.

^{b)} Total energy of the supermolecule $B_4H_{10} \cdots H_2$ whose components have their respective DZd CISD optimized geometries (for the H_2 molecule, the DZ basis set is equivalent to the DZd basis set).

^{c)} Total energy of the supermolecule $B_4H_{10} \cdots H_2$, the individual molecules having their respective DZP CISD optimized geometries.

Table 8

D_{4h} tetraalane(12) Al_4H_{12} : theoretical total energies and equilibrium geometries. The molecular structure of tetraalane(12) D_{4h} is shown in fig. 1. The DZP CISD and DZP CCSD total energies at the DZP SCF equilibrium geometry are -974.95111 and -975.01133 hartree

	DZ SCF	DZd SCF	DZP SCF
total energy (au)	-974.49678	-974.58182	-974.59516
equilibrium geometry			
ring $r_e(AlH_r)$ (Å)	1.705	1.696	1.694
terminal $r_e(AlH_t)$ (Å)	1.573	1.561	1.566
terminal $\angle(H_tAlH_t)$ (deg)	127.1	127.0	126.9
ring $\angle(H_rAlH_r)$ (deg)	93.2	93.4	93.9
ring $\angle(AlH_rAl)$ (deg)	176.8	176.6	176.1

a_2 normal modes are IR forbidden by symmetry and their IR intensities are identically zero. The other modes are IR allowed by symmetry, but a number of them have theoretical IR intensities smaller than 1 km/mol.

For the tetraborane(10) molecule only the known butterfly structure is investigated (fig. 3). The optimized equilibrium geometries and total energies are shown in table 4, and the SCF harmonic vibrational frequencies are shown in table 5. Similar to the tetraborane(12) C_{2v} structure above, the geometry was optimized at the DZP CCSD as well as DZP CISD level, and the resulting difference in bond lengths are not greater than 0.005 Å for the valence internal coordinates used. Butterfly tetraborane(10) is the only molecule in the present study for which there are existing experimental data pertaining to the molecular geometry. A comparison with these experimental data is presented in table 6. The particular internal coordinates in table 6 are those deduced from the four different experiments, and do not form a complete set of totally symmetric internal coordinates; the twelve internal coordinates shown in table 4, when properly symmetrized, do form a complete set of totally symmetric internal coordinates used in the actual geometry optimization [28]. The highest level of theory for tetraborane(10) is DZP CCSD, which should be compared with the experiments. However results from the lower levels of theory are included for comparison, as the CISD and CCSD methods are inaccessible at the present time for the aluminum and gallium counterparts. As seen from table 6 the theoretical values for the geometrical parameters are often quite close to the experimental values, with the CISD and CCSD values agreeing more closely than the SCF

Table 9

D_{4h} tetraalane(12) Al_4H_{12} : harmonic vibrational frequencies (in cm^{-1}) predicted at the SCF level of theory

Symmetry	DZ SCF	DZd SCF	DZP SCF
a_{1g}	2030	2102	2062
	1109	1050	969
	797	814	809
	274	273	273
a_{2g}	1910	1905	1915
	553	555	552
	2165	2192	2187
b_{1g}	1988	2047	2021
	744	766	765
	138	139	139
	907	893	867
b_{2g}	338	290	279
	264	230	146
	2028	2099	2061
	1001	956	892
e_g	491	490	491
	174	130	43
	491	486	488
a_{1u}	2035	2105	2067
a_{2u}	1085	1033	955
	182	141	81
	943	904	852
b_{1u}	196	153	77
	2024	2095	2058
b_{2u}	482	485	486
	17i	17i	19i
e_u	2115	2147	2135
	1988	2035	2018
	919	881	841
	764	785	779
	624	612	585
	274	273	273

values. Bühl and Schleyer have optimized the geometry of tetraborane(10) at the MP2 level using the 6-31G* and 6-31G** basis sets, which are of similar quality as the DZd and DZP basis sets, respectively, used in this work. Their internuclear boron–boron distances are somewhat smaller than those in the current work, compared to the DZP CISD and CCSD values.

The theoretical results point rather unambiguously to an error in the electron diffraction analysis of Jones, Hedberg and Schomaker [8] and the microwave structure of Simmons, Burg and Beaudet [12]. Their B_y-H_r distances of 1.43 and 1.428 Å, respectively, are much longer than the CISD and CCSD predictions, 1.254 and 1.259 Å. Moreover, the long experimental B_y-H_r distances are inconsistent with the crystal structure results of Nordman and Lipscomb [9,10] (1.21 Å) and Moore, Dickerson and Lipscomb [11] (1.16 Å). The likelihood that all of the theoretical methods are wrong for this bridging B–H distance would appear to be virtually nil. The 1981 Dain et al. [13] gas-phase electron diffraction B_y-H_r distance is closer to the theoretical result. Unfortunately, there also appear to be serious problems with the experimental crystal structures [9–11]. Specifically, the

terminal B_y-H_i distance appears to be 0.06–0.08 Å too short in the crystal structures [9–11]. In addition, the bridging B_x-H_r distance appears to be about 0.04 Å too short. Although the results of Dain et al. [13] are closer overall to the theoretical results, the discrepancies are still substantial. These problems send out an urgent call for new experimental studies of the molecular structure of the butterfly tetraborane(10).

We have compared the total energies of tetraborane(12) and tetraborane(10), in table 7. Here the total energies are evaluated at the optimized equilibrium geometries for each level of theory. Since the CISD method is not size consistent, a supermolecule is used for tetraborane(10) plus hydrogen at an intermolecular separation of 500 au. As might be expected, tetraborane(12) (C_{2v}) is energetically less stable than tetraborane(10) plus hydrogen, as a set of possible dissociation products. The dissociation energy ΔE_c (ΔE_0) is about 22 (26) kcal/mol. As has been noted earlier (ref. [1] and references cited therein), the dissociation energy predicted by the SCF method for such species may be off by as much as a factor of two. In other words, the effects of correla-

Table 10

C_{2v} tetraalene (12) Al_4H_{12} : theoretical total energies and equilibrium geometries. The molecular structure of tetraalene (12) C_{2v} is shown in fig. 4^{a)}. The DZP CISD and DZP CCSD total energies at the DZP SCF equilibrium geometry are –974.95188 and –975.01224 hartree

	DZ SCF	DZd SCF	DZP SCF
total energy (au)	–974.49694	–974.58203	–974.59560
equilibrium geometry			
ring $r_e(Al_xH_r)$ (Å)	1.704	1.695	1.694
ring $r_e(Al_yH_r)$ (Å)	1.704	1.695	1.694
terminal $r_e(Al_xH_{lre})$ (Å)	1.573	1.561	1.566
terminal $r_e(Al_xH_{lra})$ (Å)	1.573	1.560	1.566
terminal $r_e(Al_yH_{lye})$ (Å)	1.573	1.560	1.566
terminal $r_e(Al_yH_{lya})$ (Å)	1.573	1.561	1.566
terminal $\angle(H_{lre}Al_xH_{lra})$ (deg)	127.2	127.2	127.1
terminal $\angle(H_{lye}Al_yH_{lya})$ (deg)	127.2	127.2	127.1
ring $\angle(H_rAl_xH_r)$ (deg)	92.6	93.3	94.2
ring $\angle(H_rAl_yH_r)$ (deg)	92.6	93.3	94.2
$\angle(H_{lra}Al_xH_r)$ (deg)	108.2	108.1	108.0
$\tau(AlAlAlAl)$ (deg)	22.1	26.0	32.1
$\tau(H_{lre}Al_xH_rAl_y)$ (deg)	97.8	95.7	92.2
$\tau(H_{lye}Al_yH_rAl_x)$ (deg)	121.8	124.0	127.8

^{a)} There are seven symmetry independent atoms, as labeled in fig. 4. The abbreviations have a similar meaning in B_4H_{12} (fig. 2) although the molecular structure has changed significantly.

tion stabilize tetraborane(10) plus molecular hydrogen more than tetraborane(12).

3.2. Tetraalane(12) and tetraalane(10)

We located four stationary points for tetraalane(12) similar to those described for tetraborane(12) above. The D_{3h} structure now has only one imaginary vibrational frequency (DZP SCF), so it is a true transition state. The D_3 structure was found to be a local minimum at the DZP SCF levels of theory. At the DZP SCF level of theory (optimized geometries), the relative energies for the D_{3h} , D_3 , D_{4h} , and C_{2v} are: 19.5, 5.9, 0.3, and 0.0 kcal/mol. At the DZP CISD level (still DZP SCF geometries) the relative energies for D_{3h} , D_{4h} , and C_{2v} are: 13.6, 0.5, and 0.0 kcal/mol. At the DZP CCSD level (also DZP SCF geometries) the relative energies for D_3 , D_{4h} , and C_{2v} are: -2.2, 0.6 and 0.0 kcal/mol. Bock et al. [6] have earlier reported a D_3 structure (closely related to the D_{3h}), which was found to be a local minimum. Their optimized geometry and harmonic vibrational frequencies (6-31G* RHF) are consistent with ours; DZP is a more complete basis set than 6-31G*, with DZP containing polarization functions on all the hydrogen atoms.

Under D_3 symmetry, using the DZP(5d) basis set, the total SCF energy for the D_3 Al_4H_{12} (or, $Al(AlH_4)_3$ in the notation of Bock et al. [6]) was found to be -974.58533 au. The optimized geometrical parameters are (parameters from Bock et al. in parentheses): $Al_c-Al=2.621$ (2.639) Å, $Al_c-H_b=1.743$ (1.756) Å, $Al-H=1.566$ (1.575) Å, $Al-H_b=1.718$ (1.733) Å, and $\angle(H-Al-H)=127.7^\circ$ (128.3°). The harmonic vibrational frequencies in cm^{-1} at the DZP(5d) SCF level (under D_3 symmetry and with atomic masses 26.98154 for Al and 1.007825 for H) are as follows. Bock et al.'s values for the degenerate normal modes are in parentheses. They did not distinguish between the a_1 and a_2 irreducible representations. a_1 : 283, 337, 811, 870, 1648, 1750, 2056; a_2 : 127, 354, 598, 869, 1339, 1600, 2059; e: 80 (78), 260 (252), 392 (380), 458 (445), 568 (544), 776 (754), 783 (767), 999 (964), 1291 (1274), 1444 (1406), 1518 (1477), 1671 (1633), 2054 (2054), 2061 (2065). The a_1 normal modes are infrared (IR) inactive by symmetry. By the double harmonic approximation, the theoretically strongest IR normal modes

are found to be: fifth highest a_2 , $\omega=1339$ cm^{-1} , $I=963$ km/mol; seventh, eighth, tenth and eleventh highest e normal modes, $\omega=783, 999, 1444, 1518$ cm^{-1} , and $I=692, 386, 400, 1646$ km/mol, respectively. With the DZP(6d) SCF optimization, the geometrical parameters did not change to within the

Table 11

C_{2v} tetraalane(12) Al_4H_{12} : harmonic vibrational frequencies (in cm^{-1}) and IR intensities (in km/mol) in parentheses predicted at the SCF level of theory

Symmetry	DZ SCF	DZd SCF	DZP SCF
a_1	2166	2192	2183(342)
	2034	2105	2066(715)
	2029	2102	2062(0)
	2025	2096	2058(0)
	1988	2048	2020(215)
	1114	1055	982(0)
	1087	1034	956(633)
	796	813	810(0)
	746	768	767(332)
	478	478	472(0)
	279	280	283(0)
	219	207	208(0)
	115	91	50(1)
	24	23	27(0)
a_2	1911	1908	1920
	935	892	867
	906	891	835
	553	553	550
	520	519	531
	324	295	292
	247	189	86
	191	144	52
	2115	2146	2130(1290)
	2028	2098	2060(133)
b_1	1987	2033	2014(1336)
	1001	956	895(117)
	924	887	850(968)
	764	783	777(1267)
	633	627	618(141)
	474	462	445(0)
	277	277	281(2)
	176	129	32(0)
	2115	2146	2130(1290)
	2028	2098	2060(133)
b_2	1987	2033	2014(1336)
	1001	956	895(117)
	924	887	850(968)
	764	783	777(1267)
	633	627	618(141)
	474	462	445(0)
	277	277	281(2)
	176	129	32(0)

significant digits shown above. The total SCF energy changed to -974.58624 au, 5.9 kcal/mol higher than the deformed ring C_{2v} structure. At the DZP(6d) SCF

optimized geometry, the DZP(6d) CCSD total energy was determined to be -975.01573 au, which is lower than the deformed ring C_{2v} (see below) struc-

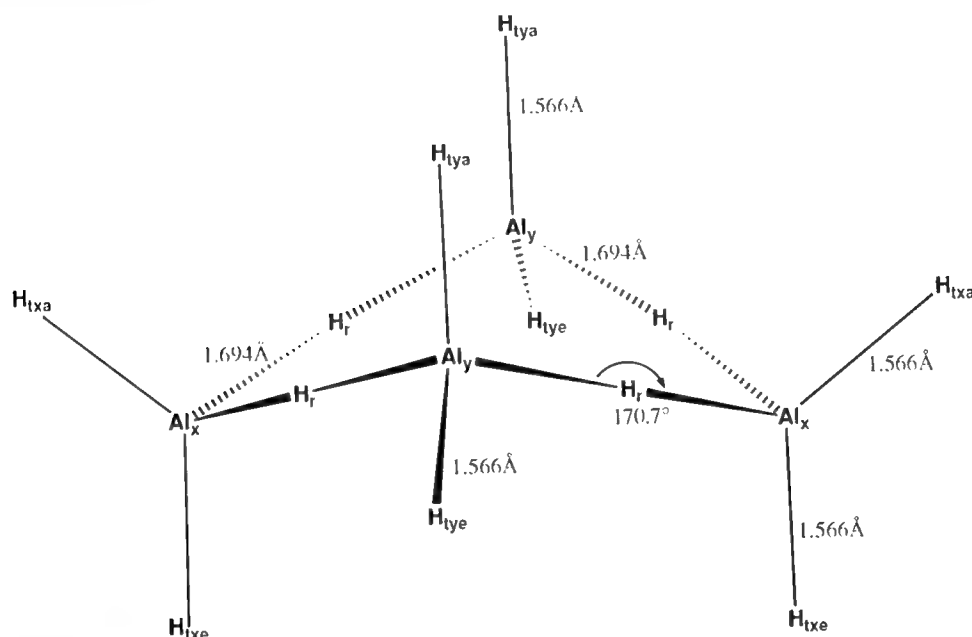


Fig. 4. C_{2v} deformed ring (or "butterfly") structure for tetraalane(12), Al_4H_{12} . This structure is energetically comparable to the D_3 structure found by Bock et al. [6] and a local minimum on the SCF potential energy surface. The Al-H-Al bridge bonds are nearly linear, and the ring is virtually rhombic when projected on a plane perpendicular to the C_2 rotation axis. It may be noted that the C_{2v} tetragalane (12) Ga_4H_{12} stationary points also have this geometrical feature at the DZ and DZd SCF levels of theory. This equilibrium geometry should be compared with the B_4H_{12} structure shown in fig. 2. The indicated geometrical parameters were obtained at the DZP SCF level of theory.

Table 12

C_{2v} tetraalane (10) Al_4H_{10} : theoretical total energies and equilibrium geometries. The molecular structure of tetraalane (10) is shown in fig. 3. The DZP CISD and DZP CCSD total energies at the DZP SCF equilibrium geometry are -973.76019 and -973.81489 hartree

	DZ SCF	DZd SCF	DZP SCF
total energy (au)	-973.32169	-973.40941	-973.42682
equilibrium geometry			
ring $r_e(Al_xH_r)$ (Å)	1.734	1.714	1.718
ring $r_e(Al_yH_r)$ (Å)	1.751	1.731	1.733
terminal $r_e(Al_xH_{txe})$ (Å)	1.575	1.565	1.571
terminal $r_e(Al_xH_{txa})$ (Å)	1.572	1.561	1.567
terminal $r_e(Al_yH_{tye})$ (Å)	1.573	1.561	1.566
$r_e(Al_xAl_y)$ (Å)	2.622	2.552	2.546
terminal $\angle(H_{txe}Al_xH_{txa})$ (deg)	128.2	127.9	127.6
ring $\angle(H_rAl_xH_r)$ (deg)	89.3	95.8	98.7
$\angle(H_{txe}Al_xH_r)$ (deg)	106.6	105.7	105.7
$\tau(AlAlAlAl)$ (deg)	65.5	63.2	61.2
$\tau(H_{txa}Al_xH_rAl_y)$ (deg)	120.2	130.1	136.9
$\tau(H_{tye}Al_yH_rAl_x)$ (deg)	153.4	146.8	142.8

ture by 2.2 kcal/mol. After the zero-point vibrational energies (ZPVEs) from SCF are scaled [30] by 0.91 and taken into account, the D_3 structure is *higher* by 1.9 kcal/mol as the more compact D_3 structure has a higher ZPVE. Bock et al. [6] did not consider the alternative ring structures (D_{4h} and C_{2v}).

The D_{4h} ring structure (fig. 1, for $M=Al$) also has only one imaginary vibrational frequency and thus is a transition state. The theoretical stationary point geometries and total energies are presented in table 8, and harmonic vibrational frequencies in table 9. The normal mode of the imaginary vibrational frequency, of irreducible representation b_{2u} , is ring puckering in nature and leads to the C_{2v} deformed ring structure discussed below. The imaginary frequency is very small in magnitude, but remains virtually constant with respect to the three basis sets used. In other words, the energy barrier for the ring puckering is very small, and the ring structure as a whole is floppy with respect to ring pucker. The theoretical equilibrium geometries and total energies for the C_{2v} deformed ring structure are shown in table 10, and the harmonic vibrational frequencies in table 11, along with the IR intensities (in parentheses) in the last column. As seen from the harmonic vibrational frequencies this structure is a local minimum, with some very small vibrational frequencies in keeping with the above-noted floppy nature of the ring with respect to puckering. While the boron and aluminum tetramer D_{3h} and D_{4h} structures look very much the same, the tetraalane(12) C_{2v} deformed ring structure looks a little different from its tetraborane(12) counterpart. The tetraalane(12) C_{2v} structure is shown in fig. 4, where one notes immediately that the Al–H–Al bridges are much more nearly linear. Another feature of the optimized geometry is that the ring is virtually rhombic (all four sides of equal lengths) if projected on a plane perpendicular to the C_2 rotation axis, although the overall symmetry is still C_{2v} . The geometrical parameters reported in table 10 are all independently optimized, although some of them have identical values to the number of significant digits shown. The DZP CISD geometry optimization was impractical; but we may speculate that the DZP SCF Al–H bond lengths in the ring are slightly too long and the Al–H bond lengths at the terminal are slightly too short, as discussed above for the C_{2v}

tetraborane(12) structure. The DZP SCF Al–Al distances may also be slightly too long, similar to the behavior of the theoretical B–B distances shown in table 6.

For the butterfly tetraalane(10) structure, the theoretical equilibrium geometry and total energy are shown in table 12, and the harmonic vibrational frequencies in table 13, along with the IR intensities in parentheses in the last column. From the low vibrational frequency of irreducible representation a_1 , we

Table 13

C_{2v} tetraalane(10) Al_4H_{10} : theoretical harmonic vibrational frequencies (in cm^{-1}) and IR intensities (in km/mol) in parentheses determined at the SCF level of theory

Symmetry	DZ SCF	DZd SCF	DZP SCF
a_1	2035	2099	2057(24)
	2027	2096	2056(215)
	2020	2083	2043(199)
	1844	1866	1839(1074)
	1119	1187	1206(478)
	1028	976	932(128)
	765	790	790(178)
	560	563	557(126)
	379	391	395(5)
	343	368	368(0)
	245	205	202(0)
	74	57	55(2)
	1613	1659	1654
	956	1081	1116
a_2	822	826	820
	577	590	585
	473	494	501
	276	260	255
	137	147	151
	2032	2097	2055(7)
	2017	2080	2040(68)
b_1	1766	1785	1765(2592)
	1027	1109	1124(255)
	872	845	827(141)
	741	767	767(1049)
	534	533	534(201)
	286	263	274(1)
	156	99	100(2)
	2013	2084	2046(302)
	1712	1770	1760(356)
b_2	1031	1129	1159(843)
	909	891	863(266)
	621	652	648(234)
	447	481	489(1)
	361	380	380(6)
	263	254	252(3)

also conclude that the ring is quite floppy.

The comparison between the total energies of tetraalane(12) (C_{2v}), and tetraalane(10) and hydrogen is shown in table 14. In contrast to the boron counterpart shown in table 7, the relative energy is

positive. In other words, tetraalane(12) (C_{2v}) is energetically more stable than tetraalane(10) and hydrogen. The CISD and CCSD relative energies were evaluated at the DZP SCF optimized geometries. As seen in table 14, correlation effects decrease this en-

Table 14

Energy quantities for the reaction $Al_4H_{12}(C_{2v}) \rightarrow Al_4H_{10} + H_2$. Here ΔE_c is defined by $E(Al_4H_{10}) + E(H_2) - E(Al_4H_{12})$, as predicted using the various methods in this research ^{a)}

Method	$E(Al_4H_{12})$ (au)	$E(Al_4H_{10}) + E(H_2)$ (au)	ΔE_c (kcal/mol)
DZ SCF	-974.49694	-973.32169 - 1.12666	+30.5
DZd SCF	-974.58203	-973.40941 - 1.12666	+28.8
DZP SCF	-974.59560	-973.42628 - 1.13109	+23.7
DZP CISD	-974.95188	-974.91755 ^{b)}	+21.5
DZP CISD(Q)	-975.00147	-974.96916 ^{c)}	+20.3
DZP CCSD	-975.01224	-973.81489 - 1.16666	+19.3

^{a)} The zero-point vibrational energy (ZPVE) correction to the reaction energy (which changes ΔE_c to ΔE_0), using the unscaled harmonic vibrational frequencies obtained at the DZP SCF level, is $\Delta ZPVE \equiv ZPVE(Al_4H_{10}) + ZPVE(H_2) - ZPVE(Al_4H_{12}) = 49.6 + 6.6 - 57.6 = -1.4$ kcal/mol.

^{b)} Total CISD energy of the supermolecule $Al_4H_{10} \dots H_2$, the components of which have their respective DZP SCF optimized geometries. The supermolecule was chosen to have a separation of 200 au.

^{c)} Total CISD plus Davidson corrected energy of the supermolecule $Al_4H_{10} \dots H_2$, the components of which have their respective DZP SCF optimized geometries.

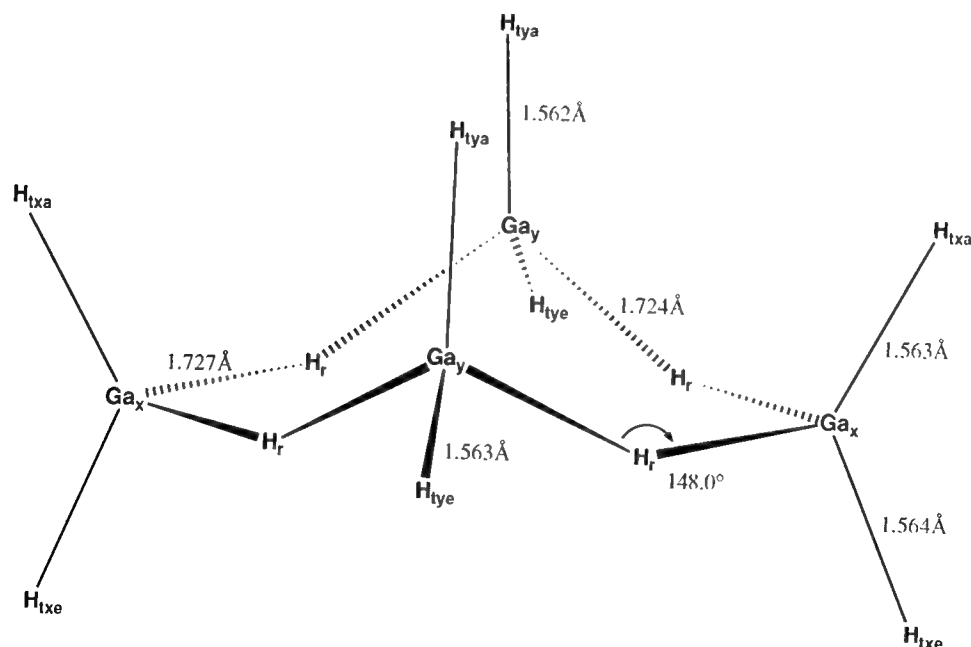


Fig. 5. C_{2v} deformed ring (or "butterfly") structure for tetragallane(12), Ga_4H_{12} . This structure is energetically lowest among the four stationary points found for tetragallane(12) in this research. The Ga-H-Ga bridge bonds are bent. According to the SCF method with the DZP basis set, C_{2v} tetragallane(12) is very floppy with respect to ring puckering. This structure should be compared with those shown in figs. 2 and 4 for B_4H_{12} and Al_4H_{12} , respectively. The indicated geometrical parameters were obtained at the DZP SCF level of theory.

ergy difference. In other words the correlation effects stabilize tetraalane(10) more than tetraalane(12), which is similar to the boron counterpart above. With the available theoretical data the energy difference ΔE_e (ΔE_0) may be estimated at about 19 (18) kcal/mol.

3.3. Tetragallane(12) and tetragallane(10)

As with the aluminum tetramers discussed in the previous subsection, we have located four stationary points for tetragallane(12) on the SCF potential energy surface. Perhaps surprisingly, the D_{3h} structure is no longer a transition state, but rather has two imaginary vibrational frequencies (one doubly degenerate) similar to the D_{3h} tetraborane(12). The D_3 structure for tetragallane(12), of the form $\text{Ga}(\text{GaH}_4)_3$ is a local minimum. At the DZP(5d) SCF level of theory, the total energy is -7699.29325 au. The optimized geometrical parameters are: $\text{Ga}_c\text{--Ga}=2.663$ Å, $\text{Ga}_c\text{--H}_b=1.806$ Å, $\text{Ga}\text{--H}=1.560$ Å, $\text{Ga}\text{--H}_b=1.752$ Å, and $\angle(\text{H}\text{--Ga}\text{--H})=130.5^\circ$. The harmonic vibrational frequencies in cm^{-1} and using atomic masses 68.92558 for Ga and 1.007825 for H

are as follows. a_1 : 171, 325, 777, 831, 1533, 1621, 2091; a_2 : 49, 301, 534, 792, 1174, 1478, 2082; e: 46, 220, 254, 353, 435, 731, 772, 881, 1108, 1292, 1333, 1581, 2083, 2088. According to the double harmonic approximation, the strongest IR normal modes are the fifth a_2 ($\omega=1174$ cm^{-1} , $I=570$ km/mol), and the sixth and tenth e normal modes ($\omega=731$, 1292 cm^{-1} , $I=1000$, 2183 km/mol, respectively).

The D_{4h} ring structure (fig. 1, for $M=\text{Ga}$) is a stationary point, but the number of imaginary harmonic vibrational frequencies changes between the DZd and the DZP basis sets. There is only one imaginary vibrational frequency when the DZ and DZd basis sets are used, similar to the aluminum case. However there are five imaginary vibrational frequencies (one doubly degenerate) at the DZP SCF level, similar to the boron case. This change of theoretical behavior was also observed for the C_{2v} deformed ring structure. With the DZ and DZd basis sets, the C_{2v} tetragallane(12) structure resembles fig. 4, with nearly linear Ga–H–Ga bridges. However with the DZP and DZP(5d) basis sets the stationary point is more closely related to the C_{2v} tetraborane(12) and is shown in fig. 5. From the results obtained for the

Table 15

C_{2v} tetragallane(12) Ga_4H_{12} : theoretical total energies and equilibrium geometries. The theoretical molecular structure of C_{2v} tetragallane(12) at the DZP SCF level is shown in fig. 5 ^{a)}

	DZ SCF	DZd SCF	DZd(5d) SCF	DZP SCF	DZP(5d) SCF
total energy (au)	–7699.36092	–7699.42493	–7699.31420	–7699.44344	–7699.33427
equilibrium geometry ^{b)}					
ring $r_e(\text{Ga}_x\text{H}_r)$ (Å)	1.722	1.722	1.717	1.727	1.723
ring $r_e(\text{Ga}_y\text{H}_r)$ (Å)	1.722	1.722	1.717	1.728	1.724
terminal $r_e(\text{Ga}_x\text{H}_{\text{tce}})$ (Å)	1.566	1.568	1.567	1.564	1.563
terminal $r_e(\text{Ga}_x\text{H}_{\text{tca}})$ (Å)	1.565	1.568	1.567	1.563	1.563
terminal $r_e(\text{Ga}_y\text{H}_{\text{tce}})$ (Å)	1.565	1.568	1.567	1.563	1.562
terminal $r_e(\text{Ga}_y\text{H}_{\text{tca}})$ (Å)	1.566	1.568	1.567	1.562	1.562
terminal $\angle(\text{H}_{\text{tce}}\text{Ga}_x\text{H}_{\text{tca}})$ (deg)	128.9	129.2	129.0	128.6	128.7
terminal $\angle(\text{H}_{\text{tce}}\text{Ga}_y\text{H}_{\text{tca}})$ (deg)	128.9	129.2	129.0	128.8	128.9
ring $\angle(\text{H}_r\text{Ga}_x\text{H}_r)$ (deg)	94.0	95.6	95.2	96.4	96.5
ring $\angle(\text{H}_r\text{Ga}_y\text{H}_r)$ (deg)	94.0	95.6	95.3	93.4	93.7
$\angle(\text{H}_{\text{tca}}\text{Ga}_x\text{H}_r)$ (deg)	107.3	106.6	106.8	108.8	108.6
$\tau(\text{GaGaGaGa})$ (deg)	27.5	40.8	36.1	28.0	28.4
$\tau(\text{H}_{\text{tce}}\text{Ga}_x\text{H}_r\text{Ga}_y)$ (deg)	94.3	86.5	86.2	173.4	171.0
$\tau(\text{H}_{\text{tce}}\text{Ga}_y\text{H}_r\text{Ga}_x)$ (deg)	124.2	132.3	126.2	155.2	157.3

^{a)} There are seven symmetry independent atoms, as labeled in fig. 5. The following abbreviations have been used for the labels: (x) on the x axis (in the present choice of molecular orientation); (y) on the y axis; (r) on the bridge (in the ring); (t) on the terminal (in contrast to being in the ring); (e) equatorial; (a) axial (roughly pointing up in fig. 5).

^{b)} $r_e(\text{XY})$ = bond distance in Å, $\angle(\text{XYZ})$ = bond angle in degrees, $\tau(\text{WXYZ})$ = absolute value of torsional angle in degrees.

D_{4h} and C_{2v} structures, one may conclude that the DZ and DZd basis sets have certain significant deficiencies in describing tetragallane(12), due to the lack of hydrogen p functions. The theoretical results for the D_{3h} and D_{4h} are omitted, and the theoretical results for the C_{2v} tetragallane(12) are shown in tables 15 and 16. At the DZP SCF level of theory, the relative energies for the D_{3h} , D_3 , D_{4h} , and C_{2v} structures are: 36.0, 26.3, 0.9, 0.0 kcal/mol. At the DZP(5d) MP2 level (SCF geometries) the relative energies are: 26.5, 17.5, 1.6, and 0.0 kcal/mol.

The theoretical equilibrium geometry and total energy for the butterfly tetragallane(10) are shown in table 17, and harmonic vibrational frequencies in table 18, with the IR intensities in parentheses in the last column. The optimized structure is similar to the boron and aluminum counterparts in fig. 3. Interestingly, for tetragallane(10) the basis sets DZ and DZd produced close results to DZP and DZP(5d). In other words one does not see any deficiency in the DZ and DZd basis sets for tetragallane(10).

A comparison of the total energies for the C_{2v} tetragallane(12), and tetragallane(10) and hydrogen is shown in table 19. As the gallium molecules are substantially larger than the previous boron and aluminum counterparts, only the MP2 energies were available as an estimation of the electron correlation effects. Using the SCF method, Ga_4H_{12} again lies below $Ga_4H_{10} + H_2$, but to a much smaller degree than predicted for the aluminum counterpart. One also notes that there does not seem to be an abrupt discontinuity in the energy difference from DZ, DZd basis sets, to the DZP basis set. Electron correlation effects, to the extent covered by MP2, make the energy difference smaller. The magnitude of the decrease may be an artifact of the MP2 over-correction. We nevertheless see the trend that electron correlation effects stabilize tetragallane(10) more than tetragallane(12), similar to the boron and aluminum cases above.

4. A comparison across the group IIIA: concluding remarks

In the above subsections the theoretical results for tetraborane(12) and tetraborane(10), and its aluminum and gallium counterparts have been pre-

sented. We are now in a position to make a comparison across the group IIIA in the periodic table.

First, the D_{3h} structures for the tetramers are very similar, with the expected proximity of the aluminum structure to the gallium structure rather than to

Table 16
 C_{2v} tetragallane(12) Ga_4H_{12} : harmonic vibrational frequencies (in cm^{-1}) and IR intensities (in km/mol) in parentheses predicted at the SCF level of theory

Symmetry	DZ SCF	DZd(5d) SCF	DZP(5d) SCF
a_1	2115	2112	2102(2)
	2074	2073	2089(179)
	2072	2071	2081(347)
	2063	2064	2072(109)
	1990	1991	1932(318)
	954	890	943(301)
	942	856	839(114)
	778	783	790(23)
	717	725	733(164)
	448	444	447(0)
	178	188	295(3)
	175	178	118(0)
	54	27	65(0)
	15	16	24(0)
a_2	1785	1799	1716
	837	800	886
	826	794	798
	522	547	546
	460	452	434
	236	234	311
	125	64	69
	111	43	11
b_1	2092	2091	2091(1)
	2066	2065	2073(11)
	1957	1959	1881(3443)
	883	830	918(3)
	816	795	791(40)
	729	723	712(1936)
	597	597	585(21)
	447	435	452(4)
	179	182	272(0)
	97	29	92(0)
b_2	2092	2091	2094(8)
	2066	2065	2075(178)
	1957	1959	1893(2586)
	883	831	906(112)
	816	795	789(88)
	729	722	718(1347)
	597	597	579(108)
	447	436	430(24)
	179	180	279(2)
	97	33	34(0)

the boron structure (e.g. see ref. [1]). We have considered the six-coordinated molecules of the form $M(MH_4)_3$, distorted from the D_{3h} by the rotation of the two sets of bridging hydrogen atoms, recently studied in considerable detail by Bock et al. [6]. The six-coordinated boron molecule is considerably higher in energy than the deformed ring structure. At the highest level of theory practical at the present (DZP(6d) CCSD energy at the DZP(6d) CISD or SCF optimized geometries), we are unable to reach a definite conclusion as to whether the six-coordinated aluminum ($Al(AlH_4)_3$, D_3 , Bock et al. [6]) or the deformed ring form (Al_4H_{12} , C_{2v} , this work) is the global minimum. At the Hartree–Fock level, the six-coordinated gallium (D_3) is energetically considerably higher (26.3 kcal/mol) than the deformed ring (C_{2v}) form. Although the electron correlation effects are expected to decrease this gap (as in the case of the aluminum structures; 17.5 kcal/mol at the MP2 level), we are uncertain if they will bring the six-coordinated form lower than the deformed ring form. This seems to deviate from an expected smooth trend among the B, Al, and Ga analogs.

Second, the D_{4h} ring structures for the B, Al, and Ga tetramers are also very similar, again probably due to symmetry constraints. The aluminum D_{4h} structure is unique with respect to the other two in that it is a genuine transition state for ring puckering. At the most reliable level of theory used in this research for harmonic vibrational frequencies (namely, DZP(5d)

or DZP SCF) the tetraborane(12) and tetragallane(12) structures have five imaginary vibrational frequencies (one doubly degenerate).

Third, the C_{2v} deformed ring structures for the tetramers are all local minima. At the DZP SCF level, the tetraalane(12) structure is again unique with its nearly linear M–H–M ($M=Al$) bridges, while for the tetraborane(12) and tetragallane(12) structures, the M–H–M bridges are considerably more bent. As an index of comparison, the M–H–M bond angles are: 124.8° for B_4H_{12} at DZP SCF, 170.7° for Al_4H_{12} at DZP SCF, 165.4° and 148.0° for Ga_4H_{12} , at DZd SCF and DZP SCF, respectively. On the other hand the tetraalane(12) and tetragallane(12) rings are significantly more floppy with respect to ring puckering than tetraborane(12). As another index of comparison, the energy differences between the C_{2v} and D_{4h} structure are 11.7 (for $M=B$), 0.3 ($M=Al$), and 1.1 ($M=Ga$) kcal/mol at the DZP SCF level. Although the magnitude of this energy difference increases as the electron correlation effects are included via CISD and CCSD (for the B and Al systems), the trend is clearly seen from the results from the DZP SCF level. More explicitly, the energy difference is 13.8 kcal/mol for B_4H_{12} at the DZP CISD level with the DZP CISD optimized geometries; and 0.5 and 0.6 kcal/mol for Al_4H_{12} at the DZP CISD and CCSD levels, respectively, with the DZP SCF optimized geometries.

Fourth, the comparison between the tetramers and

Table 17

C_{2v} tetragallane (10) Ga_4H_{10} : theoretical total energies and equilibrium geometries. The molecular structure of tetragallane (10) is shown in fig. 3

	DZ SCF	DZd SCF	DZd(5d) SCF	DZP SCF	DZP(5d) SCF
total energy (au)	–7698.20967	–7698.28224	–7698.16779	–7698.29904	–7698.18794
equilibrium geometry					
ring $r_e(Ga_xH_r)$ (Å)	1.754	1.755	1.754	1.755	1.753
ring $r_e(Ga_yH_r)$ (Å)	1.777	1.780	1.779	1.777	1.775
terminal $r_e(Ga_xH_{ter})$ (Å)	1.568	1.572	1.570	1.568	1.566
terminal $r_e(Ga_xH_{tra})$ (Å)	1.563	1.567	1.567	1.564	1.563
terminal $r_e(Ga_yH_{tr})$ (Å)	1.561	1.566	1.564	1.560	1.558
$r_e(Ga_yGa_y)$ (Å)	2.475	2.469	2.469	2.469	2.468
terminal $\angle(H_{ter}Ga_xH_{tra})$ (deg)	129.9	129.1	129.1	128.8	129.0
ring $\angle(H_rGa_xH_r)$ (deg)	96.2	100.0	99.4	101.2	100.9
$\angle(H_{ter}Ga_xH_r)$ (deg)	105.2	105.7	105.8	105.8	105.8
$\tau(GaGaGaGa)$ (deg)	64.4	63.8	64.4	62.8	63.3
$\tau(H_{tra}Ga_xH_rGa_y)$ (deg)	126.1	128.7	126.3	131.8	129.7
$\tau(H_{tr}Ga_yH_rGa_x)$ (deg)	147.6	147.1	148.7	145.1	146.4

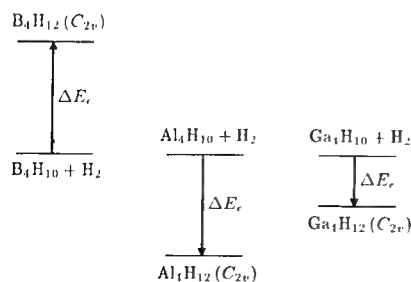
the butterfly(10) structures is of interest. The C_{2v} tetraborane(12) is energetically less stable than tetraborane(10). Although the C_{2v} tetraalane(12) and tetragallane(12) are energetically more stable than tetraalane(10) and tetragallane(10), respectively, the tetramers were found to be floppy. Since this work emphasizes comparison across the periodic table and the tetramers, we have only studied the butterfly(10) structures. McKee [16] has reported theoretical predictions that the butterfly tetraalane(10) was actually energetically less stable than the chain-like Al_4H_{10} structure. Further work along this line seems warranted. A schematic diagram showing the relative energetic stabilities of the butterfly(12), and butterfly(10) and hydrogen may be useful (scheme 1; drawn roughly to scale, DZP CCSD for boron, DZP CCSD for aluminum, DZP SCF for gallium). Although the D_3 tetraalane(12) may be a lower lying isomer than the C_{2v} , its hypervalent structure is qualitatively different from that of the C_{2v} tetraalane(10) considered in this work.

Fifth, one may certainly argue that a more interesting comparison of total energies may be that between the tetramers and the dimers. Such a comparison may also shed light on the stability of the dimers. We present such a comparison in table 20. The comparison between the C_{2v} tetraborane(12) and diborane(6) is the most complete, while the aluminum and gallium counterparts are limited by a lack of the highest quality theoretical results (due to the size of the tetramers). As seen from table 20, the C_{2v} tetraborane(12) is energetically less stable than diborane(6), by about 26 (28 if the zero point vibrational energy (ZPVE) correction is taken into account) kcal/mol. For the boron comparison (first part of table 20), if we ignore the probably fortuitous DZ SCF result, we

Table 18

C_{2v} tetragallane(10) Ga_4H_{10} : theoretical harmonic vibrational frequencies (in cm^{-1}) and IR intensities (in km/mol) in parentheses determined at the SCF level of theory

Symmetry	DZ SCF	DZd(5d) SCF	DZP(5d) SCF
a_1	2075	2067	2087(65)
	2075	2066	2078(171)
	2059	2053	2062(172)
	1706	1670	1661(1275)
	1119	1124	1154(224)
	903	858	845(123)
	748	757	763(179)
	554	547	548(137)
	332	338	339(3)
	263	268	270(0)
	136	137	135(0)
	28	38	37(0)
	1486	1477	1478
	1025	1057	1090
a_2	793	773	776
	580	583	586
	403	405	407
	201	197	191
	130	132	136
b_1	2072	2063	2075(9)
	2057	2051	2060(159)
	1625	1592	1585(2735)
	1059	1077	1103(219)
	794	762	763(12)
	719	722	723(956)
	526	530	535(265)
	192	189	195(2)
b_2	114	111	108(1)
	2065	2061	2078(323)
	1594	1581	1583(368)
	1054	1073	1108(570)
	849	830	822(118)
	642	639	644(190)
	436	444	453(7)
	300	304	306(26)
	162	164	163(0)



Scheme 1.

see that electron correlation effects (DZP CCSD) make the energy difference smaller. In other words, tetraborane(12) is stabilized more than diborane(6). For the aluminum comparison (second part of table 20), there is a considerable difference in ΔE_c between DZd and DZP SCF. The C_{2v} tetraalane(12) is energetically more stable than dialane(6), by about 8 (9 including ZPVE correction) kcal/mol. Note that the ZPVE correction is positive. Correlation effects make ΔE_c larger; i.e. C_{2v} tetraalane(12) is stabilized more than dialane(6) by electron correlation. For the

Table 19

Energies pertinent to the reaction $\text{Ga}_4\text{H}_{12}(\text{C}_{2v}) \rightarrow \text{Ga}_4\text{H}_{10} + \text{H}_2$. Here ΔE_e is defined by $E(\text{Ga}_4\text{H}_{10}) + E(\text{H}_2) - E(\text{Ga}_4\text{H}_{12})$, as predicted using the various methods in this research ^{a)}

Method	$E(\text{Ga}_4\text{H}_{12})$ (au)	$E(\text{Ga}_4\text{H}_{10}) + E(\text{H}_2)$ (au)	ΔE_e (kcal/mol)
DZ SCF	-7699.36092	-7698.20967 - 1.12666	+15.4
DZd SCF	-7699.42493	-7698.28224 - 1.12666	+10.1
DZd(5d) SCF	-7699.31420	-7698.16779 - 1.12666	+12.4
DZd(5d) MP2 ^{b)}	-7700.87152	-7699.72898 - 1.14387	-0.8
DZP SCF	-7699.44344	-7698.29904 - 1.13109	+8.4
DZP(5d) SCF	-7699.33427	-7698.18794 - 1.13109	+9.6
DZP(5d) MP2 ^{b)}	-7701.00378	-7699.84104 - 1.15850	+2.7

^{a)} The zero-point vibrational energy (ZPVE) correction to the reaction energy (which changes ΔE_e to ΔE_0), using the unscaled harmonic vibrational frequencies obtained at the DZP(5d) SCF level, is $\Delta\text{ZPVE} \equiv \text{ZPVE}(\text{Ga}_4\text{H}_{10}) + \text{ZPVE}(\text{H}_2) - \text{ZPVE}(\text{Ga}_4\text{H}_{12}) = 47.1 + 6.6 - 55.7 = -2.0$ kcal/mol.

^{b)} The MP2 energies were obtained at the DZP(5d) SCF optimized geometries.

gallium comparison (last part of table 20), the SCF predictions are similar to the aluminum case except for the smaller magnitudes. In this case the effects of

electron correlation have not been explicitly evaluated, but from the boron and aluminum comparisons we may speculate that ΔE_e will be more positive when

Table 20

A comparison of the tetramer-dimer energy differences. The reaction energy for $\text{M}_4\text{H}_{12}(\text{C}_{2v}) \rightarrow 2\text{M}_2\text{H}_6$ is defined as $\Delta E_e = 2E(\text{M}_2\text{H}_6) - E(\text{M}_4\text{H}_{12})$, for M=B, Al, or Ga

	$E(\text{M}_2\text{H}_6)$ (au)	$E(\text{M}_4\text{H}_{12})(\text{C}_{2v})$ (au)	ΔE_e (kcal/mol)
boron ^{a)}			
DZ SCF	-52.77241	-105.50226	-26.7
DZd SCF	-52.80841	-105.56018	-35.5
DZP SCF	-52.81686	-105.57714	-35.5
DZP CCSD ^{b)}	-53.06932	-106.09677	-26.3
aluminum ^{c)}			
DZ SCF	-487.22327	-974.49694	+31.6
DZd SCF	-487.28001	-974.58203	+13.8
DZP SCF	-487.29164	-974.59560	+7.7
DZP CCSD ^{d)}	-487.49974	-975.01224	+8.0
gallium ^{e)}			
DZ SCF	-3849.66977	-7699.36092	+13.4
DZd SCF	-3849.70594	-7699.42493	+8.2
DZP SCF	-3849.71736	-7699.44344	+5.5

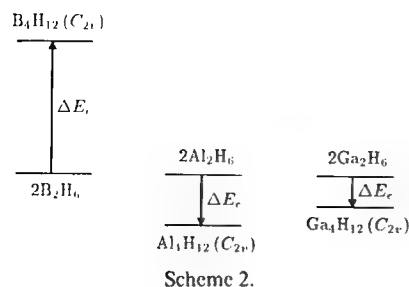
^{a)} The ZPVE correction to ΔE_e is defined as $\Delta\text{ZPVE} \equiv 2\text{ZPVE}(\text{M}_2\text{H}_6) - \text{ZPVE}(\text{M}_4\text{H}_{12})$. For the boron reaction, $\Delta\text{ZPVE} = 2 \times 40.8 - 83.3 = -1.7$ kcal/mol, as evaluated using the unscaled harmonic vibrational frequencies at the DZP SCF level (the harmonic vibrational frequencies for B_2H_6 are taken from ref. [1]).

^{b)} Boron 1s-type core MOs were frozen and the corresponding four highest lying virtual MOs deleted from the CCSD wavefunctions. Total energies were determined at the respective DZP CCSD optimized geometries for the tetramer and dimer.

^{c)} The ZPVE correction (DZP SCF) for the aluminum reaction is $\Delta\text{ZPVE} = 2 \times 29.3 - 57.6 = +1.0$ kcal/mol.

^{d)} Aluminum 1s-, 2s-, and 2p-type core MOs were frozen and the corresponding twenty highest lying virtual MOs deleted from the CCSD wavefunctions. The dimer total energy (ref. [1]) was determined at the DZP CCSD optimized geometry, while the tetramer total energy at the DZP SCF optimized geometry. Therefore the actual DZP CCSD ΔE_e , when the tetramer DZP CCSD optimized geometry is used, should be more positive than 8.0 kcal/mol.

^{e)} The ZPVE correction (DZP SCF for the dimer and DZP(5d) SCF for the tetramer) for the gallium reaction is $\Delta\text{ZPVE} = 2 \times 28.0 - 55.7 = +0.3$ kcal/mol.



electron correlation is considered. The ZPVE correction (also positive in sign) is smaller than was the case for boron and aluminum. A schematic diagram illustrating the theoretical relative stabilities of the tetramers and dimers may be useful (scheme 2; drawn roughly to scale, DZP CCSD for B, DZP CCSD for Al, and DZP SCF for Ga).

Acknowledgement

This work was supported by the Air Force Office of Scientific Research under Grant AFOSR-92-J-0047. The authors have benefitted from discussions with Professor Brian J. Duke, and Dr. Roger S. Grev, Dr. Yaoming Xie, and Dr. Yukio Yamaguchi.

Note added in proof

Additional computations at the DZP CISD and CCSD levels of theory have been performed on the D_3 tetraborane(12) structure. The geometry has been fully optimized at these two levels. At the DZP CISD level (optimized geometries), the relative energies for the D_{3h} , D_3 , D_{4h} and C_{2v} tetraborane(12) structures are: 18.4, 11.0, 13.8, 0.0 kcal/mol. At the DZP CCSD level of the theory (optimized geometries), the D_3 structure is higher than C_{2v} by 9.1 kcal/mol. These results add support for our conclusion that the D_3 structure is not likely to be the global minimum of tetraborane(12).

For completeness, the total energies for the D_3 tetraborane(12) are: -106.00298 (DZP CISD), -106.06909 (DZP CISD(Q)), and -106.08223 (DZP CCSD). The CISD wavefunction has a leading term with coefficient $C_0=0.925$ and includes 390625 configuration state functions (under C_2). The optimized geometrical parameters are compared with

Table 21
Selected optimized geometrical parameters for the D_3 tetraborane(12)

	6-31G*		DZP(6d)		
	HF	MP2	HF	CISD	CCSD
B _c -B (Å)	1.850	1.819	1.859	1.841	1.845
B _c -H _b (Å)	1.437	1.441	1.447	1.439	1.444
B-H _b (Å)	1.265	1.257	1.275	1.267	1.270
B-H (Å)	1.187	1.191	1.188	1.186	1.191
HBH (deg)	124.2	124.1	124.5	125.0	125.3

those of Bock et al. [6] in table 21, where Bock's results are found in the first two columns.

References

- [1] M. Shen and H.F. Schaefer, J. Chem. Phys. 96 (1992) 2868.
- [2] B.J. Duke, C. Liang and H.F. Schaefer, J. Am. Chem. Soc. 113 (1991) 2884.
- [3] I.M. Pepperberg, T.A. Halgren and W.N. Lipscomb, Inorg. Chem. 16 (1977) 363.
- [4] M.L. McKee and W.N. Lipscomb, Inorg. Chem. 21 (1982) 2846.
- [5] M.L. McKee and W.N. Lipscomb, Inorg. Chem. 24 (1985) 2317.
- [6] C.W. Bock, C. Roberts, K. O'Malley, M. Trachtman and G.J. Mains, J. Phys. Chem. 96 (1992) 4859.
- [7] C.R. Pulham, A.J. Downs, M.J. Goode, D.W.H. Rankin and H.E. Robertson, J. Am. Chem. Soc. 113 (1991) 5149.
- [8] M.E. Jones, K. Hedberg and V. Schomaker, J. Am. Chem. Soc. 75 (1953) 4116.
- [9] C.E. Nordman and W.N. Lipscomb, J. Am. Chem. Soc. 75 (1953) 4116.
- [10] C.E. Nordman and W.N. Lipscomb, J. Chem. Phys. 21 (1953) 1856.
- [11] E.B. Moore, R.E. Dickerson and W.N. Lipscomb, J. Chem. Phys. 27 (1957) 209.
- [12] N.P.C. Simmons, A.B. Burg and R.A. Beaudet, Inorg. Chem. 20 (1981) 533.
- [13] C.J. Dain, A.J. Downs, G.S. Laurensen and D.W.H. Rankin, J. Chem. Soc. Dalton Trans. (1981) 472.
- [14] M.L. McKee and W.N. Lipscomb, Inorg. Chem. 20 (1981) 4452;
B.J. Morris-Sherwood and M.B. Hall, Chem. Phys. Letters 84 (1981) 194;
M.L. McKee, Inorg. Chem. 25 (1986) 3545.
- [15] M. Bühl and P.R. Schleyer, J. Am. Chem. Soc. 114 (1992) 477.
- [16] M.L. McKee, J. Phys. Chem. 95 (1991) 6519.

- [17] B.J. Duke and H.F. Schaefer, *J. Chem. Soc. Chem. Commun.* (1991) 123.
- [18] S. Huzinaga, *J. Chem. Phys.* 42 (1965) 1293;
T. Dunning, *J. Chem. Phys.* 53 (1970) 2823.
- [19] S. Huzinaga, Approximate atomic wavefunctions. II, Department of Chemistry Technical Report, University of Alberta, Edmonton, Alta. (1971);
T.H. Dunning and P.J. Hay, in: *Methods of electronic structure theory, modern theoretical chemistry*, vol. 3, ed. H.F. Schaefer (Plenum Press, New York, 1977) p. 1.
- [20] T.H. Dunning, *J. Chem. Phys.* 66 (1977) 1382.
- [21] P. Pulay, *Mol. Phys.* 17 (1969) 197; 18 (1970) 473;
H.F. Schaefer and Y. Yamaguchi, *J. Mol. Struct. Robert S. Mulliken Issue* 135 (1986) 369.
- [22] B.R. Brooks, W.D. Laidig, P. Saxe, J.D. Goddard, Y. Yamaguchi and H.F. Schaefer, *J. Chem. Phys.* 72 (1980) 4652;
J.E. Rice, R.D. Amos, N.C. Handy, T.J. Lee and H.F. Schaefer, *J. Chem. Phys.* 85 (1986) 963.
- [23] A.C. Scheiner, G.E. Scuseria, J.E. Rice, T.J. Lee and H.F. Schaefer, *J. Chem. Phys.* 87 (1987) 5361.
- [24] J.A. Pople, R. Krishnan, H.B. Schlegel and J.S. Binkley, *Intern. J. Quantum Chem. S* 13 (1979) 225;
P. Saxe, Y. Yamaguchi and H.F. Schaefer, *J. Chem. Phys.* 77 (1982) 5647.
- [25] J. Almlöf, K. Faegri and K.J. Korsell, *J. Comput. Chem.* 3 (1982) 385.
- [26] R.D. Amos and J.E. Rice, CADPAC: The Cambridge analytic derivatives package, Issue 4.0, Cambridge, England (1987).
- [27] R. Ahlrichs, M. Bär, M. Häser, H. Horn and C. Kölmel, *Chem. Phys. Lett.* 162 (1989) 165.
- [28] P. Pulay, G. Fogarasi, F. Pang and J.E. Boggs, *J. Am. Chem. Soc.* 101 (1979) 2550.
- [29] F.A. Cotton, *Chemical applications of group theory*, 4rd Ed. (Wiley, New York, 1990).
- [30] R.S. Grev, C.L. Janssen and H.F. Schaefer, *J. Chem. Phys.* 95 (1991) 5128.

Methylphosphinidene (CH_3P) and Its Rearrangement to Phosphaethylene (CH_2PH): Toward the Observation of Ground-State Triplet CH_3P

Seung-Joon Kim, Tracy P. Hamilton,[†] and Henry F. Schaefer, III*

Center for Computational Quantum Chemistry, University of Georgia, Athens, Georgia 30602

Received: November 18, 1992

The CH_3P radical, which may be produced in the pyrolysis of $(\text{CH}_3)_3\text{P}$, has not been observed experimentally. Starting from the potential energy surfaces for the $\text{CH}_3\text{P} \rightarrow \text{CH}_2\text{PH}$ rearrangement, we examine the properties of the lowest singlet ($^1\text{A}'$) and triplet ($^3\text{A}_2$) states of CH_3P . The geometry optimizations are performed at the CISD level of theory with the TZ2P+f basis set. For the closed-shell singlet state of $\text{CH}_2=\text{PH}$, the highest level and basis set is the CCSD level with the TZ2P basis. The lowest singlet state of CH_3P is described starting from the two-configuration (TC) SCF method. As expected, the lowest excited singlet and triplet states of CH_3P are subject to Jahn-Teller distortion and thus exhibit C_2 symmetry. The singlet-triplet energy separations for CH_3P and CH_2PH are predicted to be -22.6 and 41.7 kcal/mol, respectively. The triplet-triplet excitation energy for CH_3P is also predicted and compared with the experimental value for the parent molecule, PH. The theoretical geometry for the ground state ($^1\text{A}'$) of CH_2PH agrees well with the experimental structure.

Introduction

The pyrolysis of $(\text{CH}_3)_2\text{PH}$ or CH_3PH_2 produces phosphoethylene ($\text{CH}_2=\text{PH}$), the simplest unstable phosphoalkene. Since phosphoethylene was first detected by Kroto and co-workers¹ in 1976, subsequent microwave studies²⁻⁴ have confirmed this tentative identification, and determined the molecular structure and dipole moment. However, because of phosphoethylene's instability, relatively little data for the vibrational frequencies are available experimentally. The C=P and P-H stretching vibrations were assigned from the low temperature (77 K) infrared (IR) spectrum of CH_2PH by Pellerin, Guenot, and Denis⁵ in 1987. In the same year, Ohno and co-workers⁶ observed the C=P stretching vibrations from the gas-phase IR spectra of several unstable phosphoalkenes. In the following year, the electronic structure for this molecule was deduced from its photoelectron spectrum (PES).⁷ Recently, many experimental and theoretical investigations⁸⁻¹¹ of the C=P double bond and the ionization potentials of $\text{CH}_2=\text{PH}$ have been published. These studies focused on the C=P bond strength, reactivity, and thermodynamic properties of this species.

In 1986, the first theoretical study of methylphosphinidene (CH_3P) was published by Nguyen, McGinn, and Hegarty,¹² who investigated the singlet and triplet energy surfaces for this isomer at the MP4SDQ/6-31++G**/HF/3-21G* level of theory. Their research shows that the ground state ($^3\text{A}_2$) of CH_3P could be stable at low pressures, with a predicted energy barrier of 53.8 kcal/mol for the rearrangement to triplet CH_2PH . However, there has been no experimental observation or measurement of the spectroscopic properties of CH_3P .

In this paper, we describe the triplet ground state and the lowest-lying singlet state ($^1\text{A}'$) of CH_3P and the rearrangement to CH_2PH on their respective potential energy surfaces. The geometric parameters, harmonic vibrational frequencies, ultraviolet (UV) spectra, and the energy separation between the singlet and triplet states for CH_3P and CH_2PH are obtained using large basis sets and an extensive treatment of electron correlation. For the lowest singlet state of CH_3P , two-configuration (TC) SCF wave functions are used. The energy barriers for the rearrangement of singlet and triplet CH_3P to CH_2PH are also predicted.

Theoretical Methods

Three basis sets—designated DZP, TZ2P, and TZ2P+f—were used in this research. The DZP basis set is the standard Huzinaga-Dunning^{13,14} double zeta P(11s7p/6s4p), C(9s5p/4s2p), and H(4s/2s) contracted basis augmented with a single set of polarization functions (d functions on carbon and phosphorus, and p functions on hydrogen) with orbital exponents of $\alpha_d(\text{C}) = 0.75$, $\alpha_d(\text{P}) = 0.6$, and $\alpha_p(\text{H}) = 0.75$. The second basis, TZ2P, is of triple zeta (TZ) quality with two sets of polarization functions with exponents $\alpha_d(\text{C}) = 1.5$, 0.375, $\alpha_d(\text{P}) = 1.2$, 0.3, and $\alpha_p(\text{H}) = 1.5$, 0.375. The TZ basis consists of the McLean-Chandler¹⁵ (12s9p/6s5p) contracted basis set for P, the Huzinaga-Dunning (10s6p/5s3p) set for C, and the (5s/3s) set for H. The TZ2P+f basis set consists of the TZ2P basis described above with sets of f functions on C and P with exponents $\alpha_f(\text{C}) = 0.8$, $\alpha_f(\text{P}) = 0.45$, and d functions on H with $\alpha_d(\text{H}) = 1.0$.

The structures of the lowest singlet and triplet states for methylphosphinidene (CH_3P), methylenephosphine (CH_2PH), and the transition state were fully optimized using analytic gradient techniques at the self-consistent field (SCF)¹⁶ level of theory for each basis set. For the lowest singlet state of CH_3P , the two-configuration (TC) SCF method was employed to describe the lower state arising from two nearly degenerate closed-shell configurations. At the optimized geometry the CI coefficients of the two configurations are 0.7072 ($3a''^2$) and -0.7070 ($10a''^2$) at the TZ2P+f TCSCF level of theory.

For all three molecules, the geometries of minima and the triplet transition state were optimized at the single and double excited configuration interaction (CISD) level of theory with the DZP, TZ2P, and TZ2P+f basis sets; and that of the singlet transition state with DZP and TZ2P bases by employing analytic CISD gradient methods.¹⁷ Note in particular that the geometry of singlet CH_3P was optimized using two reference TC-CISD wave functions. For the singlet transition state, the TZ2P+f CISD single-point energy was obtained using the TZ2P CISD optimized geometry. In the CISD optimization, six frozen core and two deleted virtual molecular orbitals were used. The CISD energies were corrected for unlinked quadruple excitations by using Davidson's method,¹⁸ and the corrected energies are denoted by CISD+Q.

Optimized DZP and TZ2P geometries also were obtained for the singlet ground state of $\text{CH}_2=\text{PH}$ at the single and double excitation coupled cluster (CCSD) level of theory by using analytic first derivative methods.¹⁹ For all triplet states, the single-point

[†] Present address: Department of Chemistry, University of Alabama, Birmingham, Alabama 35294.

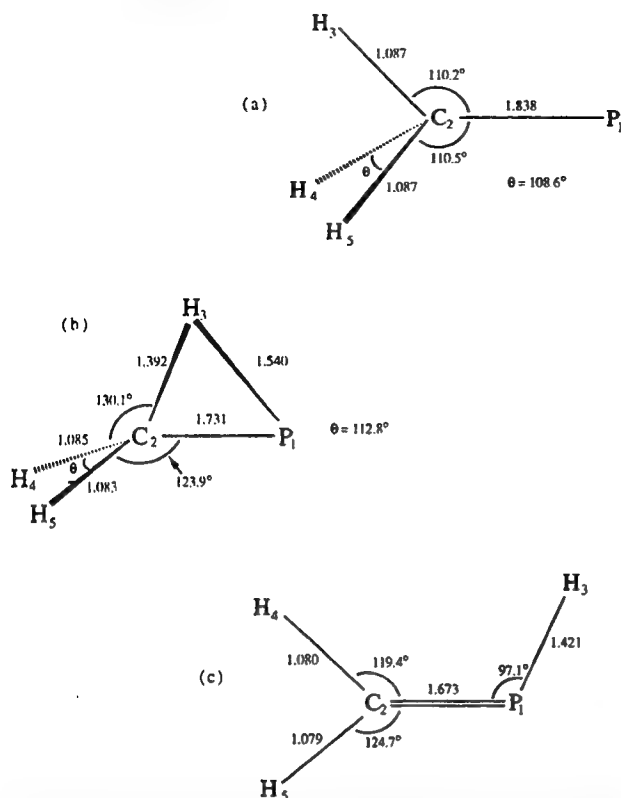


Figure 1. Predicted geometries for the singlet-state stationary points of (a) CH₃P, (b) the transition state, and (c) CH₂=PH, based on the highest level of theory employed. Bond lengths are in Å. In the transition state, with respect to the plane defined by P₁, C₂, and the H₄C₂H₅ bisector, the hydrogen atom H₃ is out-of-plane by 30.0°.

energies were located at the DZP and TZ2P CCSD levels of theory using their respective CISD-optimized structures.

Harmonic vibrational frequencies and infrared intensities were evaluated via analytic second energy derivatives²⁰ at the SCF level for all of the above states and by finite displacements of analytic gradients at the CISD level for the ³A₂ state of CH₃P and the ¹A' state of CH₂=PH.

Results and Discussion

Singlet-State Stationary Points. The optimized geometries at the highest level of theory and the nuclear arrangements for the singlet states of CH₃P, CH₂=PH and the transition state connecting them appear in Figure 1, and the geometrical parameters at other levels of theory are listed in Table I. The highest levels of theory with which geometrical optimizations were performed are TZ2P CISD for the transition state, TZ2P+f CISD for CH₃P, and TZ2P CCSD for CH₂=PH. The C=P bond distance for CH₂=PH decreases with increasing basis set size from the DZP to the TZ2P basis for both the SCF and CISD levels. More complete treatments of electron correlation increase this bond length from 1.647 Å (SCF) to 1.662 Å (CISD) and to 1.673 Å (CCSD) in conjunction with the TZ2P basis set. The C=P bond length of 1.673 Å at the TZ2P CCSD level agrees essentially perfectly with the experimental values of 1.671³ and 1.673 Å.⁴ Moreover, other predicted geometrical parameters for CH₂=PH are in very good agreement with experiment, as shown in Table I. We suggest for the angle θ (CPH) that Kroto's experimental value is superior to that of ref 4. However, Brown's experimental value for θ (HCP) = 119.1° appears preferable to that of ref 3.

The ¹E state of CH₃P is subject to a Jahn-Teller distortion that results in the ¹A' and ¹A'' electronic states of C_s symmetry. In describing the lowest closed-shell singlet state (¹A') for CH₃P, we employed the two-configuration (TC) SCF method. The two

closed-shell electronic configurations include a doubly-occupied in-plane 3p orbital and a doubly-occupied out-of-plane 3p orbital on the phosphorus atom. The ¹A' structure distorted from C_{3v} symmetry shows one short (1.0870 Å) and two long (1.0874 Å) C-H bonds at the TZ2P+f TC-CISD level of theory, while the geometry for the ¹A'' (open-shell singlet) state has one long (1.0875 Å) and two short (1.0871 Å) C-H bonds at the TZ2P+f CISD level of theory. This pattern of one long and two short bonds for one state and vice versa for the other is common in Jahn-Teller distorted C_{3v} molecules. The predicted C-P bond distance of 1.838 Å for ¹A' CH₃P is 0.01 Å shorter than that of the triplet ground state of CH₃P.

Both CH₃P and CH₂=PH have C_s symmetry, but their symmetry planes are perpendicular to each other; hence, by following an out-of-plane mode of hydrogen migration we found a transition state of C_i symmetry. The twist angle from C_s symmetry for the C_i structure of the transition state is about 30° at the TZ2P CISD level of theory. Electron correlation decreases the P-H₃ bond and increases the C-H₃ bond distance. The best predicted P-H₃ and C-H₃ bond lengths at the transition state are 1.392 and 1.540 Å, respectively. The C-P bond length predicted here (1.731 Å) is appropriately intermediate between those of CH₃P (1.838 Å) and CH₂=PH (1.673 Å).

Table II gives the harmonic vibrational frequencies for the singlet ground state of CH₂=PH at its equilibrium geometry. Since these frequencies do not take into account anharmonicity, the predicted SCF frequencies are expected to be approximately 10% higher than the experimental fundamentals. Employing configuration interaction in conjunction with the TZ2P basis set can reduce this error to about 5%.²¹ The experimental vibrational frequencies in Table II were obtained in a low-temperature IR spectrum by Pellerin et al.⁵ They assigned a strong band at 2260 cm⁻¹ to the P-H stretch and tentatively assigned a large band at 850 cm⁻¹ to the C=P stretching frequency. Our TZ2P CISD frequency of 2402 cm⁻¹ for the P-H stretch agrees quite well with the above experimental value and can be compared with the experimental values of 2287.5 cm⁻¹ in (CH₃)₃PH²² and of 2305 cm⁻¹ in CH₃PH.²³ after reducing the TZ2P CISD frequencies by 5%. The predicted C=P stretching frequency of 1027 cm⁻¹ is somewhat larger (17%) than the above tentatively assigned value of 850 cm⁻¹, but is consistent with the intrinsic C=P stretching frequency of 980 cm⁻¹ which was determined by Ohno et al.⁶ for a variety of related phosphalkenes. Our IR intensity analysis shows that the peak at 850 cm⁻¹ could be reassigned to the CH₂ wagging frequency which has strong intensity (64 km/mol) as shown in Table II.

The vibrational analysis for the singlet transition state structure of Figure 1b confirms that this is a true transition state with a single imaginary vibrational frequency of absolute value 1548 cm⁻¹. This reaction coordinate is composed of C-H and P-H stretches and a CHP out-of-plane bend. At the TZ2P+f SCF level of theory the vibrational frequencies for the carbon-phosphorus stretches increase from 725 cm⁻¹ for the single bond in CH₃P to 951 cm⁻¹ for the transition state and to 1086 cm⁻¹ for the double bond in CH₂=PH. This result is consistent with the decreasing CP bond lengths from CH₃P to CH₂=PH (see Figure 1). The vibrational frequencies for the first excited singlet state (¹A') of CH₃P will not be reported here, since symmetry breaking makes it difficult to obtain reliable a'' frequencies for this Jahn-Teller distorted state.

Absolute and relative energies for the singlet CH₃P, CH₂=PH, and transition state are shown in Table III. For the CISD and CISD+Q zero-point vibrational energy correction (ZPVE), the SCF frequencies are used and scaled by a factor of 0.91.²⁴ Note also that electron correlation and Davidson's correction increase the CH₂=PH→CH₃P isomerization energy. The TZ2P+f CISD+Q isomerization energy of 35.3 cm⁻¹ and ZPVE-corrected value of 34.1 cm⁻¹ are about 7 and 9 kcal/mol lower, respectively, than those predicted by the previous theoretical study (MP4SDQ/

TABLE I: Theoretical Geometrical Parameters for the Lowest Singlet States of CH₃P, CH₂PH, and the Transition State (Bond Lengths in Å, Angles in deg)

	SCF			CISD			CCSD		experiment	
	DZP	TZ2P	TZ2P+f	DZP	TZ2P	TZ2P+f	DZP	TZ2P	Brown ^a	Kroto ^b
CH₃P										
<i>r</i> ₁₂	1.845	1.848	1.845	1.839	1.846	1.838				
<i>r</i> ₂₃	1.088	1.083	1.084	1.096	1.086	1.087				
<i>r</i> ₂₄	1.088	1.083	1.084	1.096	1.086	1.087				
θ ₁₂₃	110.9	110.4	110.5	111.3	110.2	110.5				
θ ₁₂₄	111.0	110.3	110.5	111.4	110.5	110.8				
θ ₄₂₅	108.0	108.6	108.4	107.6	108.6	108.3				
T.S.										
<i>r</i> ₁₂	1.720	1.719	1.716	1.729	1.731					
<i>r</i> ₁₃	1.522	1.527	1.523	1.537	1.540					
<i>r</i> ₂₃	1.469	1.470	1.468	1.382	1.392					
<i>r</i> ₂₄	1.087	1.081	1.082	1.096	1.085					
<i>r</i> ₂₅	1.084	1.078	1.079	1.094	1.083					
θ ₄₂₅	112.5	113.1	112.8	112.1	112.8					
CH₂PH										
<i>r</i> ₁₂	1.651	1.647	1.645	1.666	1.662	1.657	1.676	1.673	1.671	1.673
<i>r</i> ₁₃	1.413	1.411	1.412	1.414	1.415	1.415	1.418	1.421	1.425	1.420
<i>r</i> ₂₄	1.079	1.074	1.075	1.087	1.077	1.078	1.091	1.081	1.082	1.09
<i>r</i> ₂₅	1.078	1.072	1.073	1.086	1.075	1.076	1.090	1.079	1.082	1.09
θ ₃₁₂	98.9	99.0	99.1	97.5	97.6	97.9	97.0	97.1	95.5	97.4
θ ₁₂₄	119.6	119.4	119.5	119.7	119.3	119.3	119.7	119.4	119.1	118.4
θ ₁₂₅	125.0	124.7	124.9	125.1	124.7	124.9	125.1	124.7	124.5	124.4

^a Reference 3. ^b Reference 4.**TABLE II: Vibrational Frequencies (in cm⁻¹) for the Ground State (¹A') of CH₂=PH**

	SCF/ DZP	SCF/ TZ2P	SCF/ TZ2P+f	CISD/ DZP	CISD/ TZ2P	exp ^a
CH str (a')	3405	3387	3372 (0)	3329	3317	
CH str (a')	3310	3297	3283 (6)	3232	3224	
PH str (a')	2504	2463	2481 (125)	2471	2402	2260
HCH bend (a')	1588	1582	1577 (3)	1526	1505	
CPH bend (a')	1133	1121	1119 (34)	1096	1070	
C=P str. (a')	1092	1079	1086 (0)	1044	1027	850
CH ₂ wag (a'')	1023	1023	1026 (64)	950	938	
H ₃ oop (a'')	944	939	940 (14)	889	883	
CH ₂ rock (a')	812	799	796 (2)	788	761	

^a Reference 5. The values in parentheses are IR intensities in km/mol.

6-31++G**//HF/3-21G).¹² This is because of the appropriate use here of TCSCF wave functions, which lower the energy of the ¹A' state of CH₃P.

The DZP relative energies for the transition state with respect to CH₂=PH are not significantly affected by electron correlation. However, for the larger basis sets, correlation lowers the transition state's energy relative to CH₂=PH. The TZ2P+f CISD single-point energy of this state was obtained using the TZ2P CISD optimized geometry. The classical energy barrier for the rearrangement of singlet CH₃P to CH₂=PH is 20.2 kcal/mol and the ZPVE correction reduces this value to 19.8 kcal/mol at the TZ2P+f CISD+Q level of theory. This barrier is 6.3 kcal/mol higher than the previous theoretical prediction of 13.5 kcal/mol.

Triplet-State Stationary Points. The predicted geometries and the nuclear arrangements for the triplet states of all three structures at the TZ2P+f CISD level of theory are shown in Figure 2 and the geometrical parameters at other levels of theory are listed in Table IV. These results are qualitatively similar to those of Nguyen et al. on CH₃P. By analogy with CH₃N,²⁵ the ground state of CH₃P is the ³A₂ state of C_{3v} symmetry. CH₂PH and the transition state have C_s symmetry, which implies that, like the triplet CH₃N, this isomerization maintains a plane of symmetry. The first excited triplet state (T₁) of CH₃P is also subject to Jahn-Teller distortion to yield in C_s symmetry a ³A' state, which is distorted from the ³E state of C_{3v} symmetry.

For ³A₂ CH₃P, there is very little change in the predicted geometries from the SCF to the CISD level, which indicates that the geometrical parameters for this state are not affected significantly by electron correlation. Including f functions on the heavy atoms and d functions on the hydrogens decreases the C-P bond length by 0.010 Å at the CISD level. The predicted C-P bond distance of 1.848 Å at the highest level of theory may be compared with the related experimental values of 1.863 Å in CH₃PH₂,²⁶ 1.853 Å in (CH₃)₂PH,²⁷ and 1.843 Å in (CH₃)₃P.²⁸ The shorter C-P bond length in CH₃P than in CH₃PH₂ is qualitatively consistent with the trend of the shorter C-N bond distance in CH₃N with respect to CH₃NH₂.²⁵ This could result from the greater p character in the C-P bond of CH₃PH₂ than in that of CH₃P. The T₁ state of CH₃P has a relatively long C-P bond distance of 2.082 Å at the TZ2P+f CISD level of theory due to the one-electron transfer from the C-P bonding molecular orbital to the p_y nonbonding orbital on the phosphorus atom. Other geometrical parameters for this state are the following: *r*₂₃ = 1.079 Å, *r*₂₄ = 1.076 Å, θ₁₂₃ = 98.5°, θ₁₂₄ = 103.2°, and θ₄₂₅ = 116.8°.

The structure of the lowest triplet state of CH₂PH—like that of triplet CH₂NH—is twisted and pyramidalized. However, the angle of 5.4° for the pyramidalization of the carbon atom in CH₂PH is much smaller than the value of 24.5° in triplet CH₂NH.²⁹ The C-P bond distance of 1.790 Å for triplet CH₂PH at the TZ2P+f CISD level of theory is rather short relative to the CP single-bond lengths mentioned above, which indicates that this CP bond is structurally unusual. As expected by Hammond's postulate,³⁰ the transition state for this endothermic rearrangement from CH₃P to CH₂PH more closely resembles that of the product, CH₂PH, than of the reactant, CH₃P. However, the C-P bond distance (1.822 Å) predicted for the transition state is intermediate between those of triplet CH₃P (1.848 Å) and CH₂PH (1.790 Å).

For all three triplet structures, harmonic vibrational frequencies evaluated at the TZ2P+f SCF level of theory are shown in Table V. From the single imaginary frequency for the structure of Figure 2b, we can confirm that this is a true transition state. The reaction coordinate is composed of C-H and P-H stretching contributions, consistent with the fact that the absolute value of this imaginary frequency (2640i cm⁻¹) falls between the C-H stretch in CH₃P and the P-H stretch in CH₂PH. At

TABLE III: Absolute and Relative Energies for the Singlet CH₃P → CH₂PH Rearrangement at Various Levels of Theory

	absolute energies, hartrees			rel energies, kcal/mol		
	CH ₂ =PH	T.S.	CH ₃ P	CH ₂ =PH	T.S.	CH ₃ P
DZP SCF	-380.29970	-380.20587	-380.26266	0.0	58.9 (57.3)	23.2 (22.1)
TZ2P SCF	-380.33247	-380.23907	-380.29373	0.0	58.6 (57.0)	24.3 (23.8)
TZ2P+f SCF	-380.33626	-380.24317	-380.29846	0.0	58.4 (56.8)	23.7 (22.5)
DZP CISD	-380.56020	-380.46747	-380.50409	0.0	58.2 (56.6)	35.2 (34.1)
TZ2P CISD	-380.61698	-380.52631	-380.56424	0.0	56.9 (55.3)	33.1 (32.6)
TZ2P+f CISD	-380.64847	-380.55905 ^a	-380.59683	0.0	56.1 (54.5)	32.4 (31.2)
DZP CISD(+Q)	-380.58855	-380.49555	-380.52614	0.0	58.4 (56.8)	39.2 (38.1)
TZ2P CISD(+Q)	-380.64986	-380.55986	-380.59249	0.0	56.5 (54.9)	36.0 (35.5)
TZ2P+f CISD(+Q)	-380.68477	-380.59629 ^a	-380.62857	0.0	55.5 (53.9)	35.3 (34.1)
MP4SDQ/6-31++G* ^b	-380.55382	-380.46064	-380.48674	0.0	58.5 (56.5)	42.1 (43.0)

^a Indicates the single-point energy at the TZ2P/CISD optimized geometry. ^b Reference 12, at HF/3-21G* geometry. The values in parentheses include the zero-point vibrational energy (ZPVE) correction.

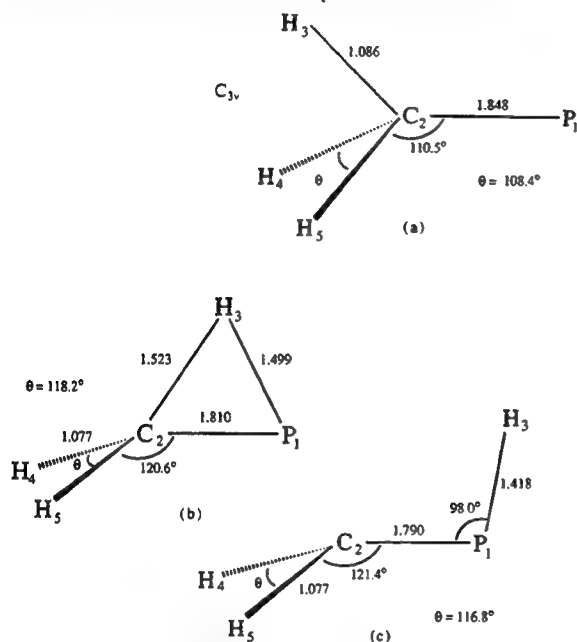


Figure 2. Predicted geometries for the triplet state stationary points of (a) CH₃P, (b) the transition state, and (c) CH₂PH, at the TZ2P+f CISD level of theory. Bond lengths are in Å.

the TZ2P+f SCF level of theory, the vibrational frequency for the C–P stretch increases from 720 cm⁻¹ in CH₃P to 784 cm⁻¹ in CH₂PH. This is consistent with the shorter C–P bond in CH₂PH compared to CH₃P.

Table VI gives the harmonic vibrational frequencies for the triplet ground state of CH₃P at the various levels of theory with the experimental vibrational frequencies (except for the P–H motions) for the related molecule, CH₃PH₂.²³ A comparison of our CH₃P frequencies with those of CH₃PH₂ shows strong similarities when the TZ2P CISD frequencies are reduced by 5%. The exception occurs for the CH₃ rocking vibrations, which are extensively mixed with the PH₂ wagging and twisting motions in CH₃PH₂. Our CISD frequency of 694 cm⁻¹ for the C–P stretch in CH₃P compares favorably with the experimental value of 675.7 cm⁻¹ for the related molecule CH₃PH₂.

The absolute and relative energies for the rearrangement from triplet CH₃P to CH₂PH at the various levels of theory appear in Table VII. The triplet ground state of CH₃P lies lower than the global minimum closed-shell singlet state of CH₂=PH at the SCF level. However, correlation effects reverse this order, and finally the ³A₂ state of CH₃P is predicted to lie 12.7 kcal/mol above the ground state of CH₂=PH at the highest level of theory. The triplet isomerization of CH₃P to CH₂PH is endothermic with energy differences of 25.5 and 26.9 kcal/mol at the TZ2P+f CISD+Q and TZ2P CCSD levels of theory, respectively, including the ZPVE correction. The polarization functions, Davidson correction, and correlation effects do not appreciably change the

TABLE IV: Theoretical Geometrical Parameters for the Lowest Triplet States of CH₃P, CH₂PH, and the Transition State (Bond Lengths in Å, Angles in deg)

	SCF			CISD		
	DZP	TZ2P	TZ2P+f	DZP	TZ2P	TZ2P+f
CH ₃ P						
r ₁₂	1.852	1.857	1.853	1.850	1.858	1.848
r ₂₃	1.087	1.082	1.083	1.095	1.085	1.086
θ ₁₂₃	110.8	110.3	110.4	111.1	110.2	110.5
θ ₄₂₅	108.1	108.6	108.5	107.7	108.7	108.4
T.S.						
r ₁₂	1.812	1.812	1.807	1.819	1.822	1.810
r ₁₃	1.509	1.512	1.509	1.500	1.504	1.499
r ₂₃	1.484	1.487	1.487	1.520	1.526	1.523
r ₂₄	1.077	1.072	1.073	1.086	1.075	1.077
θ ₁₂₄	120.9	120.7	120.8	121.2	120.7	120.6
θ ₄₂₅	117.9	118.6	118.3	117.7	118.6	118.2
CH ₂ PH						
r ₁₂	1.804	1.804	1.800	1.797	1.797	1.790
r ₁₃	1.414	1.413	1.414	1.417	1.418	1.418
r ₂₄	1.078	1.072	1.073	1.087	1.076	1.077
θ ₃₁₂	98.3	98.5	98.6	97.5	97.8	98.0
θ ₁₂₄	121.6	121.4	121.5	121.7	121.4	121.4
θ ₄₂₅	116.7	117.3	117.0	116.3	116.9	116.8

magnitude of this endothermicity. The predicted isomerization energy of 26.9 kcal/mol is consistent with the previous theoretical value of 28.9 kcal/mol.

At the TZ2P CCSD level of theory, the energy barrier for the triplet rearrangement of CH₃P to CH₂PH is predicted to be 50.6 kcal/mol, which implies that this rearrangement will be difficult to achieve; therefore, the lowest triplet CH₃P could be stable in the absence of molecular collisions. The barrier predicted here is 3.2 kcal/mol lower than the previous theoretical result¹² of 53.8 kcal/mol and can be compared with the barrier of 48.9 kcal/mol for triplet CH₃N.³¹

Table VIII focuses on the energetics for the excited singlet and triplet states of CH₃P. The energy separation between the lowest singlet and triplet states varies depending upon the size of the basis set; specifically, increasing the basis set size decreases this energy difference. The Davidson correction and correlation effects also decrease the energy separation. The final singlet-triplet energy splitting is 22.6 kcal/mol, which is about 10 kcal/mol lower than the previously obtained theoretical value¹² of 33 kcal/mol. As mentioned above, the two-configuration (TC) SCF wave functions reduce this energy separation by lowering the first excited singlet state of CH₃P. The energy difference between the two lowest triplet states of CH₃P increases from SCF to CISD but decreases significantly with increasing basis set size and has converged to within 1 kcal/mol in going from the TZ2P to the TZ2P+f basis set. The UV spectrum for the T₀–T₁ transition of CH₃P is predicted to appear near 81.7 kcal/mol including the ZPVE correction at the TZ2P+f CISD+Q level of theory. This value is similar to the experimental value of 29321.9 cm⁻¹ (83.8

TABLE V: Vibrational Frequencies (in cm^{-1}) for the Lowest Triplet States of CH_3P , CH_2PH , and the Transition State Connecting Them at the TZ2P+f SCF Level of Theory

CH_3P		transition state		CH_2PH	
CH_3 deg str (e)	3229	CH_2 asym str (a'')	3389	CH_2 asym str (a'')	3371
	3229	CH_2 sym str (a')	3273	CH_2 sym str (a')	3268
CH_3 sym str (a_1)	3154	$\text{CH}+\text{PH}$ str (a')	2120	PH str (a')	2458
CH_3 deg bend (e)	1574	CH_2 scissor (a'')	1489	CH_2 scissor (a')	1515
	1574	CH_2 twist (a'')	909	CPH bend (a')	912
CH_3 sym bend (a_1)	1430	CP str (a')	801	CH_2 rock (a'')	814
CH_3 rock (e)	874	CH_2 rock (a'')	791	CP str (a')	784
	874	CH_2 wag (a')	571	H_3 oop (a'')	523
C-P str (a_1)	720	reaction coord (a')	2640i	CH_2 wag (a')	352

TABLE VI: Vibrational Frequencies (in cm^{-1}) for Triplet CH_3P

	SCF/DZP	SCF/TZ2P	SCF/TZ2P+f	CISD/DZP	CISD/TZ2P	expt ^a CH_3PH_2
CH_3 deg str. (e)	3260	3242	3229	3198	3184	3003
	3260	3242	3229	3198	3184	2990
CH_3 sym str (a_1)	3175	3167	3154	3105	3100	2936
CH_3 deg def (e)	1573	1583	1574	1493	1504	1435
	1573	1583	1574	1493	1504	1429
CH_3 sym def (a_1)	1446	1438	1430	1382	1347	1296
CH_3 rock (e)	887	879	874	839	831	1017
	887	879	874	839	831	978
C-P str (a_1)	739	714	720	724	694	676

^a Reference 23.**TABLE VII: Absolute and Relative Energies for the Triplet $\text{CH}_3\text{P} \rightarrow \text{CH}_2\text{PH}$ Rearrangement**

	absolute energies, hartrees			relative energies, kcal/mol		
	CH_3P	T.S.	CH_2PH	CH_3P	T.S.	CH_2PH
DZP SCF	-380.30845	-380.20246	-380.26271	0.0	66.5 (62.2)	28.7 (25.2)
TZ2P SCF	-380.33859	-380.23440	-380.29350	0.0	65.4 (61.0)	28.3 (24.7)
TZ2P+f SCF	-380.34058	-380.23797	-380.29687	0.0	64.4 (60.1)	27.4 (23.9)
DZP CISD	-380.54815	-380.45633	-380.50043	0.0	57.6 (53.3)	29.9 (26.4)
TZ2P CISD	-380.60586	-380.51340	-380.55723	0.0	58.0 (53.7)	30.5 (26.9)
TZ2P+f CISD	-380.63405	-380.54465	-380.58743	0.0	56.1 (51.7)	29.3 (25.8)
DZP CISD(+Q)	-380.57012	-380.48284	-380.52326	0.0	54.8 (50.5)	29.4 (25.9)
TZ2P CISD(+Q)	-380.63349	-380.54466	-380.58533	0.0	55.7 (51.3)	30.2 (26.6)
TZ2P+f CISD(+Q)	-380.66460	-380.57930	-380.61836	0.0	53.5 (49.2)	29.0 (25.5)
DZP CCSD	-380.56706	-380.47902	-380.51993	0.0	55.2 (50.9)	29.6 (26.1)
TZ2P CCSD	-380.62997	-380.54240	-380.58156	0.0	55.0 (50.6)	30.4 (26.9)
MP4SDQ/6-31++G* ^a	-380.54036	-380.44605	-380.48815	0.0	59.2 (53.8)	32.8 (28.9)

^a Reference 12, at HF/3-21G* geometry. The values in parentheses include the zero-point vibrational energy (ZPVE) correction.**TABLE VIII: Absolute and Relative Energies for CH_3P at Various Levels of Theory^a**

	absolute energies, hartrees			excitation energies, kcal/mol	
	P-CH_3 (T_0)	P-CH_3 (S_0)	P-CH_3 (T_1)	$\Delta E(T_0-S_0)$	$\Delta E(T_0-T_1)$
DZP SCF	-380.30845	-380.26266	-380.17560	28.7	83.4 (81.7)
TZ2P SCF	-380.33859	-380.29373	-380.21048	28.2	80.4 (78.9)
TZ2P+f SCF	-380.34058	-380.29846	-380.21273	26.4	80.2 (78.8)
DZP CISD	-380.54815	-380.50409	-380.40612	27.6	89.1 (87.4)
TZ2P CISD	-380.60586	-380.56424	-380.47060	26.1	84.9 (83.4)
TZ2P+f CISD	-380.63405	-380.59683	-380.50025	23.4	84.0 (82.6)
DZP CISD(+Q)	-380.57012	-380.52614	-380.42841	27.6	88.9 (87.2)
TZ2P CISD(+Q)	-380.63349	-380.59249	-380.49900	25.7	84.4 (82.9)
TZ2P+f CISD(+Q)	-380.66460	-380.62857	-380.53214	22.6	83.1 (81.7)

^a The values in parentheses include the zero-point vibrational energy (ZPVE) correction.

kcal/mol) for the parent molecule, PH ,³² which implies that the triplet-triplet excitation energy is minimally affected by the substitution of methyl group.

Conclusions

The lowest singlet state of CH_3P , having arisen from a Jahn-Teller distortion, is of $^1A'$ symmetry. This state is predicted to lie 22 kcal/mol above the ground state (3A_2) of CH_3P . This singlet-triplet energy separation is much smaller than that of CH_3N (44 kcal/mol).²⁹ The first excited triplet state (T_1) of CH_3P (also of C_s symmetry) is a $^3A'$ state. The triplet-triplet excitation energy should be observed in the UV spectrum near 82 kcal/mol. The energy barrier for the rearrangement of singlet

CH_3P to CH_2PH is predicted to be 20 kcal/mol, as shown in Figure 3. This energy barrier is large enough to be allow experimental observation, if singlet CH_3P can be made by the photolysis or pyrolysis of $(\text{CH}_3)_3\text{P}$. It is interesting to note by comparison that previous theoretical studies^{31,33} of singlet CH_3N show that there is little or no energy barrier for the rearrangement to singlet CH_2NH . The triplet barrier is predicted to be 49 kcal/mol, and the 3A_2 state would thus be expected to be stable at low pressures. The best way to observe the triplet ground state of CH_3P might be via the matrix isolation IR spectrum.

The structure of the ground state of $\text{CH}_2=\text{PH}$ was precisely optimized using high levels of theory. The TZ2P CCSD equilibrium geometry is in excellent agreement with the exper-

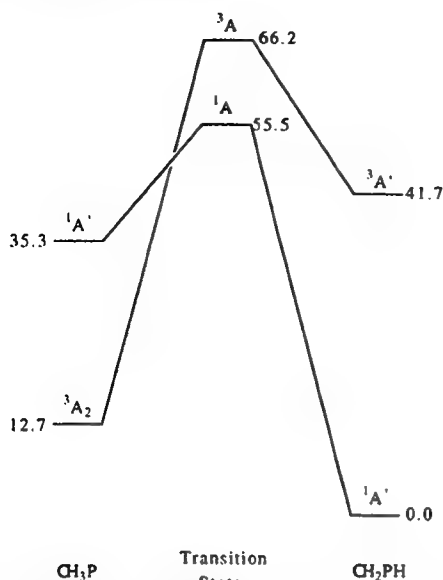


Figure 3. Relative energies (in kcal/mol) predicted for the singlet and triplet CH₃P → CH₂PH rearrangements.

imental structures. Our vibrational frequency for the P–H stretch agrees very well with the experimental assignment of Pellerin et al.,⁵ but their tentative assignment for the C=P stretching vibration is inconsistent with our predicted value. From our IR intensity analysis and the intrinsic C=P stretching frequency obtained by Ohno et al., which agrees quite well with our theoretical prediction, the peak at 850 cm⁻¹ assigned to the C=P stretching vibration could be reassigned to the CH₂ wagging vibration. The singlet–triplet energy separation for CH₂PH is predicted to be 42 kcal/mol.

Acknowledgment. This research was supported by the U.S. Air Force Office of Scientific Research under Grant No. AFOSR-92-J-0047. We thank Professor Herbert S. Gutowsky for suggesting a theoretical study of CH₃P and (CH₃)₂P. We would like to thank Dr. Yukio Yamaguchi, Dr. Yaoming Xie, and Cynthia Meredith for their thoughtful advice and help. We also appreciate very helpful discussions with Dr. Roger S. Grev.

References and Notes

- (1) Hopkinson, M. J.; Kroto, H. W.; Nixon, J. F.; Simmons, N. P. C. *J. Chem. Soc., Chem. Commun.* 1976, 513.
- (2) Kroto, H. W.; Nixon, J. F.; Ohno, K.; Simmons, N. P. C. *J. Chem. Soc., Chem. Commun.* 1980, 709.
- (3) Brown, R. D.; Godfrey, P. D.; McNaughton, D. *Aust. J. Chem.* 1981, 465.
- (4) Kroto, H. W.; Nixon, J. F.; Ohno, K. *J. Mol. Spectrosc.* 1981, 90, 367.
- (5) Pellerin, B.; Guenot, P.; Denis, J. M. *Tetrahedron Lett.* 1987, 28, 5811.
- (6) Ohno, K.; Kurita, E.; Kawamura, M.; Matsuura, H. *J. Am. Chem. Soc.* 1987, 109, 5614.
- (7) Lacombe, S.; Gonbeau, D.; Cabioch, J.-L.; Pellerin, B.; Denis, J.-M.; Pfister-Guillouzo, G. *J. Am. Chem. Soc.* 1988, 110, 6964.
- (8) Schmidt, M. W.; Truong, P. N.; Gordon, M. S. *J. Am. Chem. Soc.* 1987, 109, 5217.
- (9) Schleyer, P. v. R.; Kost, D. *J. Am. Chem. Soc.* 1988, 110, 2105.
- (10) Chow, J. R.; Beaudet, R. A.; Goldwhite, H. *J. Phys. Chem.* 1989, 93, 421.
- (11) Watts, J. D.; Rittby, M.; Bartlett, R. J. *J. Am. Chem. Soc.* 1989, 111, 4155.
- (12) Nguyen, M. T.; McGinn, M. A.; Hegarty, A. F.; *Inorg. Chem.* 1986, 25, 2185.
- (13) Huzinaga, S. *J. Chem. Phys.* 1965, 42, 1293.
- (14) Dunning, T. H. *J. Chem. Phys.* 1970, 53, 2823.
- (15) McLean, A. D.; Chandler, G. S. *J. Chem. Phys.* 1980, 72, 5639.
- (16) Pulay, P. In *Modern Theoretical Chemistry*; Schaefer, H. F., Ed.; Plenum: New York, 1977; Vol. 4, p 153. Goddard, J. D.; Handy, N. C.; Schaefer, H. F. *J. Chem. Phys.* 1979, 71, 1525.
- (17) Brooks, B. R.; Laidig, W. D.; Saxe, P.; Goddard, J. D.; Yamaguchi, Y.; Schaefer, H. F. *J. Chem. Phys.* 1980, 72, 4652.
- (18) Langhoff, S. R.; Davidson, E. R. *Int. J. Quantum Chem.* 1974, 8, 61.
- (19) Scheiner, A. C.; Scuseria, G. E.; Rice, J. E.; Lee, T. J.; Schaefer, H. F. *J. Chem. Phys.* 1987, 87, 5361.
- (20) Saxe, P.; Yamaguchi, Y.; Schaefer, H. F. *J. Chem. Phys.* 1982, 77, 5647.
- (21) Thomas, J. R.; DeLeeuw, B. J.; Vacek, G.; Crawford, T. D.; Yamaguchi, Y.; Schaefer, H. F. to be published.
- (22) McKean, D. C.; McQuillan, G. P. *J. Mol. Struct.* 1978, 49, 275.
- (23) Lannon, J. A.; Nixon, E. R. *Spectrochim. Acta.* 1967, 23A, 2713.
- (24) Grev, R. S.; Janssen, C. L.; Schaefer, H. F. *J. Chem. Phys.* 1991, 95, 5128.
- (25) Xie, Y.; Scuseria, G. E.; Yates, B. F.; Yamaguchi, Y.; Schaefer, H. F. *J. Am. Chem. Soc.* 1989, 111, 5181.
- (26) Kojima, T.; Breig, E. L.; Lin, C. C. *J. Chem. Phys.* 1961, 35, 2139.
- (27) Durig, J. R.; Hudson, S. D.; Jalilian, M. R.; Li, Y. S. *J. Chem. Phys.* 1981, 74, 772.
- (28) Bryan, P. S.; Kuczkowski, R. L. *J. Chem. Phys.* 1971, 55, 3049.
- (29) Richards, C.; Meredith, C.; Kim, S.-J.; Quelch, G. E.; Schaefer, H. F. to be published.
- (30) Hammond, G. S. *J. Am. Chem. Soc.* 1955, 77, 334.
- (31) Pople, J. A.; Raghavachari, K.; Frisch, M. J.; Binkley, J. S.; Schleyer, P. v. R. *J. Am. Chem. Soc.* 1983, 105, 6389.
- (32) Pearse, R. W. B. *Proc. Roy. Soc. London* 1930, 129, 328.
- (33) Demuynck, J.; Fox, D. J.; Yamaguchi, Y.; Schaefer, H. F. *J. Am. Chem. Soc.* 1980, 102, 6204.

Ga₂H₂: planar dibridged, vinylidene-like, monobridged, and trans equilibrium geometries

Zoltán Palágyi¹, Henry F. Schaefer III

Center for Computational Quantum Chemistry, University of Georgia, Athens, GA 30602, USA

and

Ede Kapuy

Department of Theoretical Physics, József Attila University, 6720, Szeged, Hungary

Received 13 November 1992

The singlet potential energy surface of Ga₂H₂ has been studied using the self-consistent-field (SCF), single and double excitation configuration interaction (CISD), and single and double excitation coupled cluster (CCSD) methods. Optimized geometries and harmonic vibrational frequencies were obtained for four geometrical isomers with a double-zeta plus polarization basis set (DZP). Relative energies of the above structures were also predicted using a triple-zeta plus polarization basis set augmented with a set of *f* functions on the gallium atoms (TZP+*f*). For final energetic predictions with this basis set we included the effects of triple excitations perturbatively using the CCSD(T) method. The planar dibridged structure is the global minimum – two additional low-lying minima were found, corresponding to trans-bent and vinylidene-like structures. Our analysis also predicts the existence of a remarkable low-lying monobridged minimum, which has recently been observed experimentally for Si₂H₂, and predicted by *ab initio* methods for the valence-isoelectronic Al₂H₂.

1. Introduction

The hydrides of gallium have received increasing attention in recent years, especially since the synthesis and characterization of digallane Ga₂H₆ by Downs et al. [1]. Several theoretical studies have appeared for Ga_xH_y systems [2–6] as well as related systems including boron [7–10], aluminum [11,12], aluminum–boron [13], silicon [14–17], and germanium [16–18] hydrides. A common feature of these systems is the presence of electron-deficient hydrogen bridges, which have been studied extensively by Trinquier [16,17,19].

The remarkable recent experimental discovery [20] of the nonclassical monobridged structure of Si₂H₂ has focused increasing interest on these unconventional structures, which have been found to

be low-lying stable minima in theoretical studies of B₂H₄ [7], Al₂H₂ [21], Al₂H₄ [12], and Ga₂H₄ [2], as well as in the heavier group 14 compounds Sn₂H₄ and Pb₂H₄ [17].

In the present Letter, *ab initio* methods explicitly including electron correlation effects are applied to study various isomers of Ga₂H₂ – including the monobridged structure – a system on which no theoretical or experimental data have been available until now. By comparing the results for Ga₂H₂ with the previously studied Al₂H₂ [21] system, we see a remarkable similarity in the behavior of gallium and aluminum in their hydrides. Thus the absence of a successful synthesis of dialane Al₂H₆ becomes more puzzling.

2. Theoretical methods

Several stationary points on the Ga₂H₂ potential

¹ Permanent address: Quantum Theory Group, Physical Institute, Technical University, 1521, Budapest, Hungary.

energy surface were initially located by using SCF gradient techniques [22,23] in conjunction with a basis set designated double-zeta plus polarization (DZP). The DZP basis for gallium consists of Dunning's [24] 14s11p5d primitive set of Gaussian functions contracted to 7s5p2d^{#1} augmented by a set of six Cartesian d-like functions ($\alpha_d(\text{Ga})=0.207$). For hydrogen we used the standard Huzinaga–Dunning–Hay [26–28] double-zeta basis set augmented by a set of p-like functions ($\alpha_p(\text{H})=0.75$). The contraction scheme for this DZP basis is

Ga[6112211/61211/411], H[31/1].

For the evaluation of the relative energies of various structures we employed a basis set designated triple-zeta plus polarization plus f functions (TZP+f). For gallium, it consists of the above primitive set more loosely contracted to 10s8p2d [4] augmented with a set of d- and f-like polarization functions, [$\alpha_d(\text{Ga})=0.16$], [$\alpha_f(\text{Ga})=0.33$] [5]. For hydrogen it is the standard Huzinaga–Dunning triple-zeta basis set augmented by a set of p-like functions ($\alpha_p(\text{H})=0.75$). Thus the contraction scheme for this basis set is

Ga[511111111/41111111/411/1], H[311/1].

We determined DZP SCF quadratic force constants and harmonic vibrational frequencies using analytic energy second derivative methods [29]. Starting with the DZP SCF geometries and force constants, we then reoptimized the structures using the configuration interaction (CI) method [30], and then the coupled cluster (CC) method [31] in conjunction with the DZP basis set. Only the valence electrons have been correlated explicitly; the core-like SCF molecular orbitals (Ga 1s, 2s, 2p, 3s, 3p, 3d) and the virtual orbital counterparts (Ga 1s, 2s) were not included in the CI and CC procedures. Otherwise, all single and double excitations from the SCF reference wavefunction have been included (CISD, CCSD). For final energy predictions the effects of triple excitations were also included perturbatively using CCSD(T) wavefunctions. The CISD energies have been corrected to approximately include the effects of unlinked quadruple excitations using Dav-

idson's formula [32]. These corrected energies are denoted CISD+Q. We obtained CISD and CCSD harmonic vibrational frequencies by taking finite differences of analytic energy gradients [33,34].

3. Results and discussion

In this section results are presented for the stationary point geometries depicted in figs. 1–4. Three levels of theory (SCF, CISD, CCSD) have been used to obtain these structures, each with the basis sets designated DZP. The relative energies as well as the total energies for the global minimum dibridged structure are given in table 1. Table 2 summarizes the predicted harmonic vibrational frequencies and

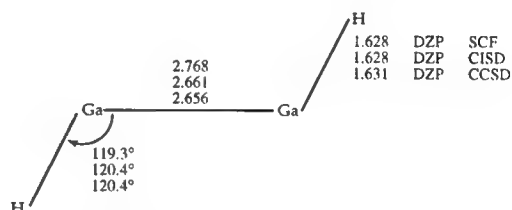


Fig. 1. Theoretical geometries for the trans closed-shell singlet of Ga_2H_2 . Bond distances are in Å.

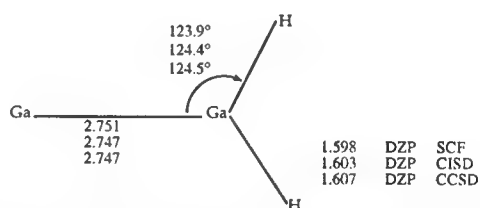


Fig. 2. Theoretical geometries for the vinylidene-like closed-shell singlet state of Ga_2H_2 . Bond distances are in Å.

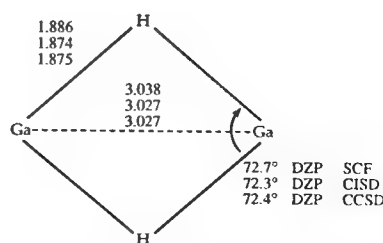


Fig. 3. Theoretical equilibrium geometries for the closed-shell singlet, planar dibridged electronic ground state of Ga_2H_2 . Bond distances are in Å.

^{#1} The contraction (14s11p5d/7s5p2d) is due to R.S. Grev and H.F. Schaefer III [25].

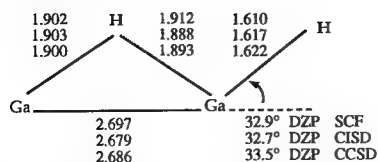


Fig. 4. Theoretical geometries for the monobridged closed-shell singlet state of Ga_2H_2 . Bond distances are in Å.

infrared (IR) intensities. Table 3 contains a list of the largest CI coefficients for each wavefunction and the corresponding electron configurations.

Unless otherwise indicated, data reported explicitly in this discussion were obtained with the DZP CCSD method, except relative energies, which are TZP+f CCSD(T) results including DZP CCSD harmonic zero-point vibrational energy corrections (see the final column of table 1). Standard Cotton coordinate systems have been used, and whenever there is a choice of coordinate systems the Ga atoms have been chosen to lie along the x axis.

A common feature of the various geometrical isomers is a low-lying LUMO, and a small HOMO-LUMO gap. We have therefore examined the lowest triplet states for all isomers. For the trans, branched,

and dibridged structures we found the triplet states to be higher lying than the corresponding singlet states already at the DZP SCF level. The triplet state of the monobridged structure – which has the lowest lying LUMO among the closed shell isomers – lies lower than the singlet state at the DZP SCF level. However, this order is reversed by introducing correlation effects; therefore we investigated only the singlet closed shell electronic states for all structures with higher levels of theory.

The harmonic vibrational frequency analyses show that all structures considered are local minima on the lowest singlet potential surface, the global minimum being the planar dibridged isomer.

The trans isomer (fig. 1) is the most weakly bound – it lies $12.4 \text{ kcal mol}^{-1}$ above the planar dibridged minimum. The Ga–Ga bond distance (2.656 Å) exhibits a great sensitivity to correlation effects; it decreases by 0.107 Å while going from the DZP SCF to the DZP CISD level of theory. A similar tendency was observed in the Al_2H_2 molecule [21] and ascribed to the presence of SCF unoccupied bonding molecular orbitals. The localized bond analysis [35] shows a pair of banana-type bonds between the gallium atoms. Effectively, this structure can be ex-

Table 1

Relative energies (kcal/mol) of stationary point structures for the Ga_2H_2 system. Only the final column includes zero-point vibrational energies

Isomer	SCF		CISD ^{a)}		CCSD		CCSD(T)	
	DZP	TZP+f ^{b)}	DZP	TZP+f ^{b)}	DZP	TZP+f ^{b)}	TZP+f ^{c)}	+ ZPVE ^{d)}
trans	11.3	11.5	13.6 13.2	13.1 12.6	13.5	13.0	12.6	12.4
monobridged	8.0	7.9	9.0 9.1	8.3 8.3	9.3	8.5	8.2	7.9
branched	−0.1	0.1	5.6 6.8	4.7 5.7	6.4	5.4	6.1	6.8
planar ^{e)} dibridged	0.0	0.0	0.0 0.0	0.0 0.0	0.0	0.0	0.0	0.0

^{a)} The lower number in the CISD boxes is the Davidson corrected energy difference.

^{b)} At the DZP optimized geometry obtained with the corresponding level of theory.

^{c)} At the DZP CCSD optimized geometry.

^{d)} TZP+f CCSD(T) including DZP CCSD harmonic zero point vibrational energy correction (see footnote c)).

^{e)} Total energies (au) for the dibridged structure are as follows: DZP SCF: -3847.389799 ; TZP+f SCF: -3847.557723 (see footnote b)); DZP CISD: -3847.531444 ; DZP CISD+Q: -3847.546776 ; TZP+f CISD: -3847.707945 (see footnote b)); TZP+f CISD+Q: -3847.724453 (see footnote b)); DZP CCSD: -3847.543005 ; TZP+f CCSD: -3847.720441 (see footnote b)); TZP+f CCSD(T): -3847.725701 (see footnote c)); + ZPVE: -3847.714713 (see footnote d)).

Table 2
Harmonic vibrational frequencies in cm^{-1} (infrared intensities in parentheses in km/mol) for Ga_2H_2 structures

Isomer		Description	DZP SCF	DZP CISD	DZP CCSD
trans	b_u	Ga-H antisym stre	1822 (1234)	1806 (959)	1787 (890)
	a_g	Ga-H sym stre	1809 (0)	1793 (0)	1774 (0)
	a_g	sym bend	500 (0)	507 (0)	505 (0)
	b_u	antisym bend	181 (135)	218 (68)	226 (54)
	a_g	Ga-Ga stre	105 (0)	146 (0)	147 (0)
	a_u	oop	222 (10)	218 (15)	212 (14)
monobridged	a'	terminal H-Ga stre	1869 (801)	1825 (662)	1797 (617)
	a'	bridging H sym stre	1182 (460)	1183 (343)	1172 (322)
	a'	bridging H antisym stre	793 (758)	848 (573)	850 (542)
	a'	H-Ga-H bend	398 (67)	412 (24)	413 (19)
	a'	Ga-Ga stre	123 (7)	158 (9)	156 (9)
	a''	terminal H oop bend	273 (17)	218 (15)	199 (13)
branched	b_2	Ga-H antisym stre	1915 (338)	1884 (291)	1865 (277)
	a_1	Ga-H sym stre	1923 (509)	1884 (436)	1863 (413)
	a_1	H-Ga-Ga sym bend	826 (506)	784 (425)	773 (406)
	b_1	oop bend	424 (118)	382 (89)	370 (82)
	a_1	Ga-Ga stre	184 (14)	183 (11)	182 (11)
	b_2	H-Ga-H in-plane wag	249 (32)	226 (25)	221 (23)
planar dibridged	a_g	sym Ga-H stre	1357 (0)	1346 (0)	1337 (0)
	b_{3u}	H's \rightarrow same Ga	1108 (3317)	1143 (2595)	1139 (2492)
	b_{1g}	H's \rightarrow opposite Ga's	778 (0)	916 (0)	918 (0)
	b_{2u}	antisym Ga-H stre	948 (221)	964 (183)	959 (176)
	a_g	Ga-Ga stre	199 (0)	203 (0)	202 (0)
	b_{1u}	oop bend	325 (48)	278 (47)	268 (45)

Table 3
Coefficients greater than 0.05 in the TZP+f CISD wavefunctions for the different Ga_2H_2 structures

Isomer	Coefficient	Configuration
trans	0.940	(core) $11a_g^2 12a_g^2 11b_u^2 12b_u^2$
	-0.125	$12b_u^2 \rightarrow 13a_g^2$
monobridged	0.943	(core) $21a^2 22a^2 23a^2 24a^2$
	-0.070	$24a^2 \rightarrow 25a^2$
branched	0.947	(core) $15a_1^2 16a_1^2 17a_1^2 7b_2^2$
	-0.052	$17a_1^2 \rightarrow 18a_1^2$
	-0.052	$16a_1^2 \rightarrow 8b_2^2$
planar dibridged	0.943	(core) $8a_g^2 9a_g^2 4b_{2u}^2 8b_{3u}^2$
	-0.072	$9a_g 8b_{3u} \rightarrow 4b_{2g} 4b_{1u}$
	0.054	$9a_g 8b_{3u} \rightarrow 4b_{2g} 6b_{1u}$
	0.051	$9a_g 8b_{3u} \rightarrow 4b_{1g} 5b_{2u}$

plained as two weakly interacting GaH fragments.

The branched or vinylidene-like structure (fig. 2) is the only one involving exclusively two-center, two-electron bonds. Upon localization of the DZP SCF

orbitals we find a pair of Ga-H σ bonds, a Ga-Ga σ bond, and a lone pair of electrons on the terminal gallium atom. The Ga-Ga bond distance is 2.747 Å, 0.091 Å longer than that in the trans structure, which has a double bond. The relative energies of the branched isomer show a great sensitivity to correlation effects. At the DZP SCF level the branched isomer lies 0.1 kcal mol^{-1} below the dibridged isomer, while at the correlated level it is 6.8 kcal mol^{-1} above it. Once correlation effects are included via DZP CISD, changes of basis set or levels of theory have little effect on this relative energy value. Since the relative energies of the other three structures do not change much as we go from SCF to correlated levels of theory, we observe that SCF theory favors the branched isomer, which may be due to the classical nature of bonding in this structure. A similar effect was observed for the Al_2H_2 molecule [21].

The planar dibridged isomer (fig. 3) is the global minimum for Ga_2H_2 . It features two non-classical three-center (Ga-H-Ga) bridging bonds, with a lone

pair of electrons on each gallium atom. Trinquier has extensively analyzed such bridged bonded structures in the group 14 compounds C_2H_4 , Si_2H_4 , Ge_2H_4 , Sn_2H_4 , Pb_2H_4 , as well as in X_2H_6 ($X=B, Ga$) [16,17,19]. The Ga–Ga cage distance is 3.027 Å, the longest gallium–gallium separation of all the isomers.

Finally we arrive at the monobridged structure, which is the most interesting. It is predicted to lie 7.9 kcal mol⁻¹ above the dibridged minimum. The Ga–Ga bond distance (2.686 Å) lies between the values for a single and double bond. This result is explained by the localized bond analysis: the gallium atoms are connected by a banana-type bond of the sort found in the trans isomer, and a three-center bridging bond similar to that found in the dibridged isomer. Furthermore, the terminal hydrogen is connected to one of the gallium atoms by a conventional σ bond, and there is a lone pair of electrons on the other gallium atom. The low vibrational frequencies for the Ga–Ga stretch (156 cm⁻¹) and the terminal hydrogen out-of-plane bend (199 cm⁻¹) suggest a possible transition state from the monobridged isomer to the planar dibridged global minimum. This suggestion does not follow trivially from the mechanistic study of ref. [15], since the planar dibridged structure lies 11 kcal mol⁻¹ above the butterfly structure for the Si_2H_2 system examined there. Among the structures considered in this paper, the branched isomer has the largest dipole moment (1.72 D), and thus may be the best target for microwave detection. The monobridged isomer has a smaller dipole moment (0.56 D).

4. Concluding remarks

The singlet potential energy surface of Ga_2H_2 has been analyzed at the SCF, CISD, CCSD, and CCSD(T) levels of theory. Our results show the necessity of including correlation effects to accurately describe the relative energies. The planar dibridged global minimum and the low-lying monobridged minimum demonstrate the importance of bridging hydrogen atoms in creating Ga–Ga bonds. The only classically bonded structure that emerges is the vinylidene-like structure, if one excludes the trans structure due to its two banana bonds. The other stable isomers are best viewed as AlH dimers with da-

tive or three-center two-electron bonds derived from the three possible ways that the two electron-rich regions in the AlH monomer can donate electron density to the electron deficient aluminum centers.

The presence of the unsymmetrical monobridged structure of Ga_2H_2 as a genuine minimum proves that this structural type is not limited to Si_2H_2 [14,15], for which solid experimental structural confirmation now exists [20]. This work surely suggests that related potential energy hypersurfaces – B_2H_2 , AlH_2 , $BGaH_2$, $AlGaH_2$, $SiCH_2$, Ge_2H_2 , $GeCH_2$, $GeSiH_2$ – should be carefully searched for new unsymmetrical monobridged structures.

Acknowledgement

We thank Dr. Mingzuo Shen for many helpful discussions. This research was supported by the Air Force Office of Scientific Research, Grant AFOSR-92-J-0047.

References

- [1] A.J. Downs, M.J. Goode and C.R. Pulham, *J. Am. Chem. Soc.* 111 (1989) 1936.
- [2] K. Lammertsma and J. Leszczynski, *J. Phys. Chem.* 94 (1990) 5543.
- [3] M. Shen and H.F. Schaefer III, *J. Chem. Phys.* 96 (1992) 2868; K. Lammertsma and J. Leszczynski, *J. Phys. Chem.* 94 (1990) 2806; B. Duke, *J. Mol. Struct. THEOCHEM* 208 (1990) 197.
- [4] C. Liang, R.D. Davy and H.F. Schaefer III, *Chem. Phys. Letters* 159 (1989) 393.
- [5] B. Duke, C. Liang and H.F. Schaefer III, *J. Am. Chem. Soc.* 113 (1991) 2884.
- [6] M. Shen, C. Liang and H.F. Schaefer III, submitted for publication.
- [7] R.A. Mohr and W.N. Lipscomb, *Inorg. Chem.* 25 (1986) 1053.
- [8] C. Jouany, J.C. Barthelat and J.P. Daudey, *Chem. Phys. Letters* 136 (1987) 52.
- [9] M. Sana, G. Leroy and Ch. Henriët, *J. Mol. Struct. THEOCHEM* 187 (1989) 233; *J. Chim. Phys.* 87 (1990) 1.
- [10] L.A. Curtiss and J.A. Pople, *J. Chem. Phys.* 90 (1989) 4314; 91 (1989) 4809, 5118.
- [11] N.C. Baird, *Can. J. Chem.* 63 (1985) 71; M.L. McKee, *J. Phys. Chem.* 95 (1991) 6519.

- [12] K. Lammertsma, O.F. Guner, R.M. Drewes, A.E. Reed and P. von R. Schleyer, *Inorg. Chem.* 28 (1989) 313.
- [13] G.J. Mains, C.W. Bock, M. Trachtman, J. Finley, K. McNamara, M. Fisher and L. Wociki, *J. Phys. Chem.* 94 (1990) 6996.
- [14] B.T. Colegrove and H.F. Schaefer III, *J. Phys. Chem.* 94 (1990) 5593.
- [15] R.S. Grev and H.F. Schaefer III, *J. Chem. Phys.*, in press.
- [16] G. Trinquier, *J. Am. Chem. Soc.* 112 (1990) 2130.
- [17] G. Trinquier, *J. Am. Chem. Soc.* 113 (1991) 144.
- [18] R.S. Grev, B.J. DeLeeuw and H.F. Schaefer III, *Chem. Phys. Letters* 165 (1990) 257.
- [19] G. Trinquier and J.-P. Malrieu, *J. Am. Chem. Soc.* 113 (1991) 8634.
- [20] M. Cordonnier, M. Bogey, C. Demuynck and J.-L. Destombes, *J. Chem. Phys.*, in press.
- [21] Z. Palagyi, R.S. Grev and H.F. Schaefer III, submitted for publication.
- [22] P. Pulay, *Modern theoretical chemistry*, Vol. 4, ed. H.F. Schaefer III (Plenum Press, New York, 1977) pp. 53-183.
- [23] M. Dupuis and H.F. King, *J. Chem. Phys.* 68 (1978) 3998.
- [24] T.H. Dunning, *J. Chem. Phys.* 66 (1977) 1382.
- [25] R.S. Grev and H.F. Schaefer III, unpublished.
- [26] S. Huzinaga, *J. Chem. Phys.* 42 (1965) 1293.
- [27] T.H. Dunning, *J. Chem. Phys.* 53 (1970) 2823.
- [28] T.H. Dunning and P.J. Hay, *Modern theoretical chemistry*, Vol. 3, ed. H.F. Schaefer III (Plenum Press, New York, 1977) pp. 1-27.
- [29] P. Saxe, Y. Yamaguchi and H.F. Schaefer III, *J. Chem. Phys.* 77 (1982) 5647.
- [30] P. Saxe, D.J. Fox, H.F. Schaefer III and N.C. Handy, *J. Chem. Phys.* 77 (1982) 5584.
- [31] G.E. Scuseria, C.L. Janssen and H.F. Schaefer III, *J. Chem. Phys.* 89 (1988) 7382.
- [32] S.R. Langhoff and E.R. Davidson, *Intern. J. Quantum Chem.* 8 (1974) 61.
- [33] J.E. Rice, R.D. Amos, N.C. Handy, T.J. Lee and H.F. Schaefer III, *J. Chem. Phys.* 85 (1986) 963.
- [34] A.C. Scheiner, G.E. Scuseria, J.E. Rice, T.J. Lee and H.F. Schaefer III, *J. Chem. Phys.* 87 (1987) 5361.
- [35] J. Pipek and P.G. Mezey, *J. Chem. Phys.* 90 (1989) 4916.

Striking Similarities between Elementary Silicon and Aluminum Compounds: Monobridged, Dibridged, Trans-Bent, and Vinylidene Isomers of Al_2H_2

Zoltán Palágyi,[†] Roger S. Grev,* and Henry F. Schaefer, III

Contribution from the Center for Computational Quantum Chemistry, University of Georgia, Athens, Georgia 30602. Received April 3, 1992

Abstract: Ab initio quantum mechanical methods have been used to study the singlet potential energy surface of Al_2H_2 . Optimum geometries and harmonic vibrational frequencies were obtained for four geometrical isomers using the self-consistent-field (SCF), configuration interaction (CI), and coupled cluster (CC) methods. Both correlation methods including single and double excitations (CISD, CCSD) were employed, and all wave functions were determined with both DZP and TZ2P basis sets. Final energy predictions are obtained using large atomic natural orbital basis sets, and including the effects of triple excitations perturbatively using CCSD(T) methods. We found the planar dibridged structure to be the global minimum, as predicted earlier by Baird. However, our analysis also predicts the existence of a remarkable monobridged minimum, which has recently been observed experimentally for Si_2H_2 . Two additional low-lying minima are found, corresponding to trans-bent and vinylidene-like structures. The dibridged, monobridged, and trans-bent structures can be understood as resulting from the three possible ways of coordinating the two electron-rich sites of diatomic AlH to the electron-deficient aluminum centers. The energy of these structures with respect to dissociation to two AlH monomers is quite low and is related to the large difference between the first and second Al-H bond dissociation energies of the parent AlH_3 compound.

Introduction

The development of techniques for the synthesis of naked aluminum clusters has increased the possibility of experimental investigations of aluminum hydrides.¹ Such compounds might serve as hydrogen storage devices or may be exploited as low-mass high-energy fuels. Previous theoretical studies² of Al_xH_y systems have revealed some of the peculiar characteristics of Al-H bonding, in particular, the role of hydrogen providing bridging bonds between aluminum atoms. Similar structures have been studied in boron,³⁻⁶ aluminum-boron,⁷ silicon,^{8,9} germanium,^{9,10} and gallium¹¹ hydrides.

The principal motivation for this research is a remarkable recent experimental discovery in the laboratory of Destombes.¹² Via microwave spectroscopy, the French group was able to observe the unconventional monobridged structure (1) of Si_2H_2 predicted



(1)

2 years earlier in theoretical studies.⁸ In those studies, Colegrove⁸ predicted 1 to be a genuine minimum on the Si_2H_2 potential energy hypersurface using a triple zeta plus double polarization (TZ2P) basis set in conjunction with the single and double excitation configuration interaction (CISD) method. At the highest level of theory (TZ2P + diffuse + f CISD + Davidson's correction), the unexpected monobridged structure 1 is second only in energy to the nonplanar dibridged ground state^{8,13} of Si_2H_2 . This result has been confirmed in more exhaustive theoretical studies of Si_2H_2 .¹⁴

In molecules for which classically bonded alternatives exist (thus, excluding hydrogen bonds, for example), unsymmetrical monobridged structures are rare, and Si_2H_2 is the only one that

has been experimentally observed to our knowledge. Such monobridged structures have, however, been found to be low-lying stable minima in theoretical studies of B_2H_4 ,³ and Al_2H_4 ,^{2b} and Ga_2H_4 ,¹¹ as well as in the heavier group 14 compounds Sn_2H_4 and Pb_2H_4 .^{9b} Therefore, one goal of the present research was to determine whether the Al_2H_2 system, with two fewer electrons than Si_2H_2 , also possesses a low-lying unsymmetrical monobridged molecular structure. A previous study of Al_2H_2 by Baird^{2a} optimized only planar trans-bent and doubly bridged singlet states, using the 3-21G* basis set at the SCF level of theory; whether the structures were minima or not was never explicitly stated. We now know that such low-level theoretical studies are incapable

- (1) See, for example: Hamrick, Y. M.; Van Zee, R. J.; Weltner, W. J. *Chem. Phys.* **1992**, *96*, 1767.
- (2) (a) Baird, N. C. *Can. J. Chem.* **1985**, *63*, 71. (b) Lammertsma, K.; Guner, O. F.; Drewes, R. M.; Reed, A. E.; Schleyer, P. v. R. *Inorg. Chem.* **1989**, *28*, 313. (c) McKee, M. L. *J. Phys. Chem.* **1991**, *95*, 6519.
- (3) Mohr, R. A.; Lipscomb, W. N. *Inorg. Chem.* **1986**, *25*, 1053.
- (4) Jouany, C.; Barthelat, J. C.; Daudey, J. P. *Chem. Phys. Lett.* **1987**, *136*, 52.
- (5) (a) Sana, M.; Leroy, G.; Henriot, Ch. *J. Mol. Struct. (THEOCHEM)* **1989**, *187*, 233. (b) Sana, M.; Leroy, G.; Henriot, Ch. *J. Chim. Phys.* **1990**, *87*, 1.
- (6) (a) Curtiss, L. A.; Pople, J. A. *J. Chem. Phys.* **1989**, *90*, 4314. (b) Curtiss, L. A.; Pople, J. A. *J. Chem. Phys.* **1989**, *91*, 4809. (c) Curtiss, L. A.; Pople, J. A. *J. Chem. Phys.* **1989**, *91*, 5118.
- (7) Mains, G. J.; Bock, C. W.; Trachtman, M.; Finley, J.; McNamara, K.; Fisher, M.; Wociki, L. *J. Phys. Chem.* **1990**, *94*, 6996.
- (8) Colegrove, B. T.; Schaefer, H. F. *J. Phys. Chem.* **1990**, *94*, 5593.
- (9) (a) Trinquier, G. *J. Am. Chem. Soc.* **1990**, *112*, 2130. (b) Trinquier, G. *J. Am. Chem. Soc.* **1991**, *113*, 144.
- (10) Grev, R. S.; DeLeeuw, B. J.; Schaefer, H. F. *Chem. Phys. Lett.* **1990**, *165*, 257.
- (11) Lammertsma, K.; Leszczynski, J. *J. Phys. Chem.* **1990**, *94*, 5543.
- (12) Cordonnier, M.; Bogey, M.; Demuyne, C.; Destombes, J.-L. *J. Chem. Phys.* **1992**, *97*, 7984.
- (13) Bogey, M.; Bolvin, H.; Demuyne, C.; Destombes, J. L. *Phys. Rev. Lett.* **1991**, *66*, 413.
- (14) Grev, R. S.; Schaefer, H. F. *J. Chem. Phys.* **1992**, *97*, 7990.

[†] Permanent address: Quantum Theory Group, Physical Institute, Technical University, H-1521, Budapest, Hungary.

Table I. Relative Energies (kcal/mol) of Stationary-Point Structures for the Al_2H_2 System (Only the Final Column Includes Zero-Point Vibrational Energies)

isomer	SCF		CISD ^a		CCSD		CCSD(T)			"best"
	DZP	TZ2P	DZP	TZ2P	DZP	TZ2P	DZP	TZ2P ^c	ANO ^c	
linear $^1\Delta$	32.5	29.2	40.9	37.6						40.2 ^c
			43.0	39.9						
linear $^3\Sigma_g^-$	17.9	13.4	28.1	25.2						28.8 ^c
			30.8	28.5						
trans	15.4	14.1	18.4	16.1	18.5	16.1	17.8	15.5	14.2	13.5 ^d
			17.9	15.5						
mono-bridged	9.8	8.9	11.8	10.2	12.4	10.7	12.0	10.3	9.1	8.5 ^d
			12.1	10.3						
branched	4.0	0.5	10.6	7.0	11.9	8.2	12.4	8.9	7.4	7.6 ^d
			12.2	8.5						
planar ^b	0.0	0.0	0.0	0.0	0.0	0.0	0.0	0.0	0.0	0.0
dibridged			0.0	0.0						

^aThe lower number in the CISD columns is the Davidson corrected energy difference. ^bTotal energies (au) for the dibridged structure are as follows: DZP SCF, -484.913 638; TZ2P SCF, -484.945 919; DZP CISD, -485.050 317; DZP CISD+Q, -485.064 967; TZ2P CISD, -485.099 752; TZ2P CISD+Q, -485.118 378; DZP CCSD, -485.061 855; TZ2P CCSD, -485.114 617; DZP CCSD(T), -485.065 510; TZ2P CCSD(T), -485.119 663; ANO CCSD(T), -485.142 940. ^cAt the TZ2P CCSD optimized geometry. ^dANO CCSD(T) including TZ2P CCSD harmonic zero-point vibrational energy correction. ^eTZ2P CISD+Q including TZ2P SCF harmonic zero-point vibrational energy correction.

of even qualitatively describing the Si_2H_2 potential energy surface; electron correlation must be explicitly included.⁸ In this work, therefore, large basis sets and correlated methods are used to investigate the low-lying singlet-state minima of Al_2H_2 .

Theoretical Methods

Several stationary points on the Al_2H_2 potential energy surface were initially located by using SCF gradient techniques^{15,16} in conjunction with two different basis sets, designated DZP and TZ2P. The DZP basis consists of a standard Huzinaga-Dunning-Hay¹⁷⁻¹⁹ double- ζ basis set of contracted Gaussian functions augmented by a set of six Cartesian d-like functions on aluminum ($\alpha_d(\text{Al}) = 0.40$) and a set of p-like functions on hydrogen ($\alpha_p(\text{H}) = 0.75$). The contraction scheme for this DZP basis is



The TZ2P basis set is a triple- ζ set in the valence shell and has two sets of polarization functions per atom. For hydrogen we used the standard Huzinaga-Dunning triple- ζ basis and polarization function orbital exponents of 1.5 and 0.375. For aluminum we used McLean and Chandler's²⁰ contraction of Huzinaga's 12s9p primitive Gaussian set augmented with two sets of six Cartesian d-like functions with orbital exponents of 0.8 and 0.2. The contraction scheme is thus



We determined the SCF quadratic force constants and harmonic vibrational frequencies using analytic energy second-derivative methods.²¹ The electronic structures of the closed-shell structures have been investigated with the aid of localized orbitals, obtained by the method of Pipek and Mezey.²²

Starting with the SCF geometries and force constants, we then reoptimized the structures using the configuration interaction (CI) method²³ and then the coupled cluster (CC) method.²⁴ Only the valence electrons have been correlated explicitly; the core-like SCF molecular orbitals (Al 1s, 2s, 2p) and their virtual orbital counterparts were not included in the CI and CC procedures. Otherwise, all single and double excitations from the SCF reference wave function have been included (CISD, CCSD). The CISD energies have been corrected to include the effects of unlinked quadruple excitations using Davidson's formula.²⁵ These corrected en-

1.559	2.305	DZP	SCF	singlet
1.561	2.309	TZ2P	SCF	
1.558	2.309	DZP	CISD	
1.564	2.322	TZ2P	CISD	
1.560	2.291	DZP	SCF	triplet
1.562	2.287	TZ2P	SCF	
1.559	2.292	DZP	CISD	
1.566	2.298	TZ2P	CISD	

Figure 1. Theoretical stationary-point geometries for linear Al_2H_2 in its lowest singlet ($^1\Delta_g$) and triplet ($^3\Sigma_g^-$) electronic states. Bond distances are in Å.

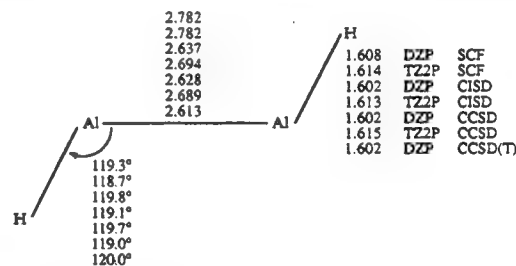


Figure 2. Theoretical geometries for the trans closed-shell singlet state of Al_2H_2 . Bond distances are in Å.

ergies are denoted CISD+Q. We obtained CISD and CCSD harmonic vibrational frequencies by taking finite differences of analytic energy gradients.^{26,27}

Structures, Energies, and Bonding

In this section are presented results for the stationary-point geometries depicted in Figures 1–5. Three levels of theory (SCF, CISD, CCSD) have been used to obtain these structures, each with two basis sets (DZP, TZ2P). The relative energies as well as the total energies for the dibridged structure are given in Table I. Table II summarizes the predicted harmonic vibrational frequencies and infrared (IR) intensities. Table III contains a list of the largest CI coefficients for each wave function and the corresponding electronic configurations. Finally, in Table IV we report the energetic stabilities with respect to two AlH molecules. In this discussion, only the results obtained with the TZ2P CCSD method will be reported explicitly, unless otherwise indicated. Standard Cotton coordinate systems have been used, and whenever there is a choice of coordinate systems the Al atoms have been chosen to lie along the x axis.

We begin our discussion with the linear Al_2H_2 structures (Figure 1). The $^3\Sigma_g^-$ state is found to lie 12.4 kcal mol⁻¹ (TZ2P CISD)

(15) Pulay, P. *Modern Theoretical Chemistry*; Schaefer, H. F., Ed.; Plenum: New York, 1977; Vol. 4, pp 53–183.

(16) Dupuis, M.; King, H. F. *J. Chem. Phys.* **1978**, *68*, 3998.

(17) Huzinaga, S. *J. Chem. Phys.* **1965**, *42*, 1293.

(18) Dunning, T. H. *J. Chem. Phys.* **1970**, *53*, 2823.

(19) Dunning, T. H.; Hay, P. J. *Modern Theoretical Chemistry*; Schaefer, H. F., Ed.; Plenum: New York, 1977; Vol. 3, pp 1–27.

(20) McLean, A. D.; Chandler, G. S. *J. Chem. Phys.* **1980**, *72*, 5639.

(21) Saxe, P.; Yamaguchi, Y.; Schaefer, H. F. *J. Chem. Phys.* **1982**, *77*, 5647.

(22) Pipek, J.; Mezey, P. G. *J. Chem. Phys.* **1989**, *90*, 4916.

(23) Saxe, P.; Fox, D. J.; Schaefer, H. F.; Handy, N. C. *J. Chem. Phys.* **1982**, *77*, 5584.

(24) Scuseria, G. E.; Janssen, C. L.; Schaefer, H. F. *J. Chem. Phys.* **1988**, *89*, 7382.

(25) Langhoff, S. R.; Davidson, E. R. *Int. J. Quantum Chem.* **1974**, *8*, 61.

(26) Rice, J. E.; Amos, R. D.; Handy, N. C.; Lee, T. J.; Schaefer, H. F. *J. Chem. Phys.* **1986**, *85*, 1963.

(27) Scheiner, A. C.; Scuseria, G. E.; Rice, J. E.; Lee, T. J.; Schaefer, H. F. *J. Chem. Phys.* **1987**, *87*, 5361.

Table II. Harmonic Vibrational Frequencies (cm^{-1}) and Infrared Intensities (km/mol) for Al_2H_2 Structures

			DZP SCF	TZ2P SCF	DZP CISD	TZ2P CISD	DZP CCSD	TZ2P CCSD
trans	b_u	Al-H antisym stre	1889 (918)	1852 (1133)	1884 (713)	1825 (928)	1871 (660)	1806 (870)
	a_g	Al-H sym stre	1886 (0)	1847 (0)	1881 (0)	1821 (0)	1868 (0)	1802 (0)
	a_g	sym bend	515 (0)	511 (0)	532 (0)	512 (0)	532 (0)	510 (0)
	b_u	antisym bend	219 (131)	214 (152)	263 (51)	238 (63)	273 (36)	251 (45)
	a_g	Al-Al stre	161 (0)	185 (0)	258 (0)	239 (0)	267 (0)	246 (0)
	a_u	oop	229 (14)	226 (23)	212 (25)	217 (30)	199 (26)	208 (30)
	a'	terminal H-Al stre	1919 (565)	1898 (651)	1892 (480)	1848 (568)	1873 (450)	1822 (534)
monobridged	a'	bridging H sym stre	1275 (506)	1222 (460)	1302 (401)	1220 (375)	1299 (384)	1213 (363)
	a'	bridging H antisym stre	1029 (725)	974 (719)	1084 (527)	1012 (567)	1090 (484)	1016 (527)
	a'	H-Al-H bend	455 (31)	429 (41)	460 (16)	439 (18)	459 (14)	438 (15)
	a'	Al-Al stre	233 (40)	232 (40)	267 (32)	260 (31)	265 (30)	256 (29)
	a''	terminal H oop bend	277 (35)	265 (39)	174 (31)	200 (32)	126 (29)	173 (29)
	b_2	Al-H antisym stre	1944 (261)	1906 (373)	1933 (223)	1875 (329)	1920 (211)	1857 (316)
	a_1	Al-H sym stre	1945 (403)	1910 (497)	1925 (334)	1873 (424)	1911 (316)	1854 (404)
branched	a_1	H-Al-Al sym bend	847 (605)	847 (573)	833 (507)	814 (503)	827 (484)	804 (482)
	b_1	oop bend	431 (196)	442 (211)	377 (156)	405 (170)	359 (143)	395 (159)
	a_1	Al-Al stre	257 (32)	289 (33)	268 (27)	288 (31)	266 (25)	286 (29)
	b_2	H-Al-H in-plane wag	262 (46)	277 (54)	239 (37)	253 (46)	235 (35)	250 (44)
	a_g	sym Al-H stre	1475 (0)	1439 (0)	1474 (0)	1399 (0)	1474 (0)	1386 (0)
	b_{3u}	H's \rightarrow same Al	1313 (3103)	1254 (3124)	1371 (2458)	1279 (2470)	1376 (2352)	1277 (2371)
	b_{1g}	H's \rightarrow opposite Al's	1035 (0)	1015 (0)	1168 (0)	1097 (0)	1178 (0)	1094 (0)
planar dibridged	b_{2u}	antisym Al-H stre	1020 (141)	1006 (123)	1061 (126)	1001 (119)	1065 (125)	995 (119)
	a_g	Al-Al stre	326 (0)	329 (0)	333 (0)	329 (0)	333 (0)	327 (0)
	b_{1u}	oop bend	322 (163)	298 (188)	200 (172)	236 (159)	167 (164)	227 (145)
			DZP SCF singlet	TZ2P SCF singlet	DZP SCF triplet	TZ2P SCF triplet		
linear	σ_g	Al-H sym stre	2088 (0)	2071 (0)	2086 (0)	2065 (0)		
	σ_u	Al-H antisym stre	2075 (255)	2059 (258)	2073 (256)	2052 (283)		
	σ_g	Al-Al stre	522 (0)	518 (0)	530 (0)	531 (0)		
	π_u	cis bend	419 (91)	423 (70)	420 (92)	425 (73)		
	π_g	trans bend	320i (0)	274i (0)	453i (0)	334i (0)		

below the $^1\Delta_g$ state. Because of the double bond between the aluminum atoms, the Al-Al bond distance is by far the shortest for the linear structures, and so are the Al-H bond distances. These results are reflected in the high values for the stretching vibrational frequencies. While the $^3\Sigma_g^-$ state is the ground state for B_2H_2 , for Al_2H_2 the linear structure lies energetically highest above the planar dibridged ground state and is also unstable with respect to splitting into two AlH molecules at the levels of theory considered. Both the triplet and the singlet linear states have a doubly degenerate (π_g) imaginary vibrational frequency corresponding to two equivalent trans bending motions. The reversal of the stability of the linear and dibridged structures in B_2H_2 ,

compared to Al_2H_2 and the instability of the linear structure toward trans-bending in Al_2H_2 are exactly analogous to the trends seen in C_2H_2 versus Si_2H_2 .⁸

The lower energy of the trans structure (Figure 2) compared to the linear $^1\Delta_g$ state can be considered to be an example of the second-order Jahn-Teller stabilization.²⁸ Upon trans bending, the doubly degenerate π_u orbital splits into b_u and a_u orbitals

(28) (a) Bader, R. F. W. *Can. J. Chem.* 1962, 40, 1164. (b) Pearson, R. G. *J. Am. Chem. Soc.* 1969, 91, 4947. (c) Pearson, R. G. *Proc. Natl. Acad. Sci. U.S.A.* 1975, 72, 2104. (d) Cherry, W.; Epiotis, N.; Borden, W. T. *Acc. Chem. Res.* 1977, 10, 167.

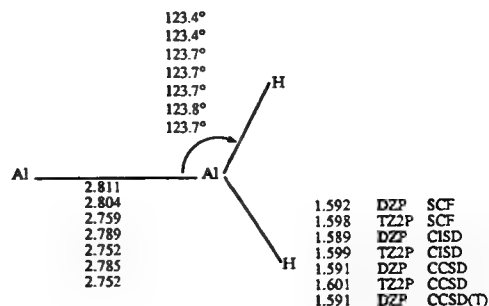
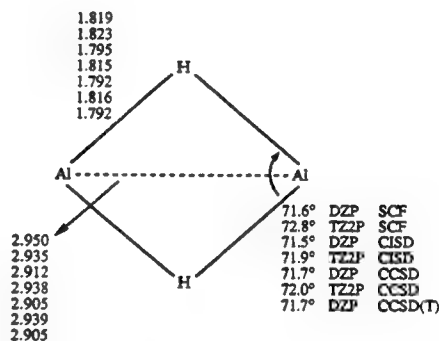
Table III. Coefficients Greater Than 0.05 in the TZ2P CISD Wave Functions for the Different Al_2H_2 Structures

isomer	coefficient	configuration
linear singlet	0.945	(core) $4\sigma_g^2 4\sigma_u^2 5\sigma_g^2 2\pi_u^2$
	-0.072	$2\pi_u^2 \rightarrow 2\pi_g^2$
	-0.066	$4\sigma_g \rightarrow 9\sigma_g$
	-0.057	$5\sigma_g \rightarrow 9\sigma_g$
	0.949	(core) $4\sigma_g^2 4\sigma_u^2 5\sigma_g^2 2\pi_u^2$
linear triplet	0.933	(core) $5a_g^2 5b_u^2 6a_g^2 6b_u^2$
	-0.137	$6b_u^2 \rightarrow 7a_g^2$
	-0.050	$6b_u^2 \rightarrow 7a_g 10a_g$
	0.938	(core) $9a^2 10a^2 11a^2 12a^2$
monobridged	-0.071	$12a^2 \rightarrow 13a^2$
	0.941	(core) $7a_1^2 8a_1^2 3b_2^2 2a_1^2$
planar	0.938	(core) $4a_g^2 2b_{2u}^2 4b_{3u}^2 5a_g^2$
dibridged	-0.075	$5a_g 4b_{3u} \rightarrow 2b_{2g} 2b_{u1}$
	-0.062	$5a_g 4b_{3u} \rightarrow 2b_{1g} 4b_{2u}$

corresponding to in-plane and out-of-plane π bonds, respectively. The in-plane π bond component is stabilized on bending by mixing with the low-lying σ_u orbital of the linear structure, which is also of b_u symmetry in the C_{2h} subgroup of $D_{\infty h}$. Further stabilization is provided by the mixing of occupied σ_g and low-lying unoccupied π_g orbitals of linear Al_2H_2 upon trans-bending. The small energy gap between these two trans MO's makes the trans triplet state 13.9 kcal mol⁻¹ lower than the singlet at the DZP SCF level. However, by including electron correlation, the singlet state becomes more stable by 5.1 kcal mol⁻¹ (DZP CISD). Our TZ2P TCSCF wave functions, which correlate with the $^1\Delta_g$ state at linearity, show that the coefficient of the $5a_g^2 5b_u^2 6a_g^2 2a_u^2$ configuration gradually decreases with trans bending to a value of 0.120 at equilibrium, leaving the dominant $5a_g^2 5b_u^2 6a_g^2 6b_u^2$ SCF configuration and resulting in higher in-plane electron density. The small value of the coefficient for the second configuration at the optimized trans-bent geometry justifies the subsequent use of single configuration based methods for this structure.

The Al-Al bond distance in the closed-shell trans geometry, 2.689 Å, is nearly 0.4 Å longer than that obtained for the linear structure. This structure is, by far, the most affected by basis set and electron correlation. At the SCF level of theory, the DZP and TZ2P basis sets yield identical Al-Al distances. After accounting for correlation effects at the CCSD level of theory, the TZ2P bond distance is 0.06 Å longer than that obtained with the DZP basis set, but both basis sets give considerably shorter Al-Al distances at correlated levels of theory than they do with SCF methods. For all the closed-shell structures investigated here, the geometrical changes upon introduction of electron correlation are larger with DZP than with TZ2P basis sets. This often happens in weakly bound systems, such as hydrogen-bonded or datively bonded structures, and can generally be attributed to basis set superposition errors (BSSE), which are enhanced at correlated levels of theory. With the larger TZ2P basis set, BSSE is reduced, and the structural changes are more regular. A dative bond description is indeed appropriate for the trans-bent structure, as the localized bond analysis clearly reveals a pair of highly distorted banana-type bonds between the aluminum atoms; i.e., the structure is effectively that of two weakly interacting Al-H fragments, with each Al-H fragment donating its lone pair of electrons into the empty p -orbital of the other. Similar models have been used to describe the bonding in trans-bent, nominally double-bonded Ge_2H_4 , Sn_2H_4 , and Pb_2H_4 .²⁹

A common feature of the molecular structures corresponding to minima on the potential surface is a small HOMO-LUMO gap and a low-lying LUMO. We have studied the lowest triplet

**Figure 3.** Theoretical geometries for the vinylidene-like closed-shell singlet state of Al_2H_2 . Bond distances are in Å.**Figure 4.** Theoretical equilibrium geometries for the closed-shell singlet, planar dibridged electronic ground state of Al_2H_2 . Bond distances are in Å.

states for the branched, bridged, and dibridged isomers as well, and found them to be higher lying than the corresponding singlet states already at the SCF level. Thus for these structures we investigated only the singlet electronic states with the higher levels of theory.

The branched or vinylidene-like structure (Figure 3) is planar, and the molecule has C_{2v} symmetry. Of the four closed-shell structures investigated here, this is the only one that invites a classical bonding description, i.e., involving exclusively two-center, two-electron bonds. Thus, the localized bond analysis reveals a pair of Al-H σ bonds, the two aluminum atoms are joined by a σ bond, and the terminal aluminum atom has a lone pair of electrons. The Al-Al bond distance, 2.785 Å, is nearly 0.1 Å longer than that in the trans structure. This structure is a genuine potential minimum and it lies 8.2 kcal mol⁻¹ above the dibridged global minimum. The vibrational frequency corresponding to the out-of-plane bend is quite high (395 cm⁻¹) compared to the other isomers.

The planar dibridged isomer (Figure 4) is the global minimum for Al_2H_2 . This isomer has D_{2h} symmetry, with the hydrogens in bridging positions between the aluminum atoms. The localized bond analysis shows that there is a lone pair on each aluminum, and the remaining four valence electrons occupy two symmetric three-center (Al-H-Al) bridging bonds. Thus, this structure can be considered as a dimer of AlH in which the negatively charged hydrogen atoms are acting as the electron donors to the acidic aluminum centers. This is in contrast with the trans-bent structure where the aluminums are the donors. The Al-Al cage distance and Al-H bridge are 0.32 Å and 0.09 Å longer than the corresponding "typical" experimental values ($\text{Me}_2\text{AlH}_2\text{AlMe}_2$).^{2c,30} The lowest vibrational frequency for this isomer is the out-of-plane bending of the hydrogens preserving C_{2v} symmetry. We have not found a stationary point corresponding to this "butterfly" structure, which is, of course, the global minimum for the Si_2H_2 molecule.^{8,13,14}

Thus far, we have seen two modes of coordinating two AlH monomers: (1) using the lone pairs of aluminum to datively bond

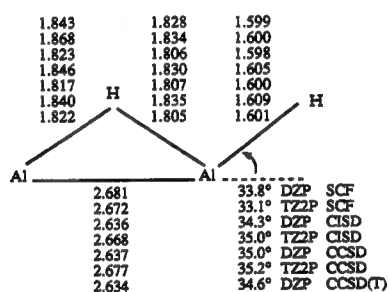
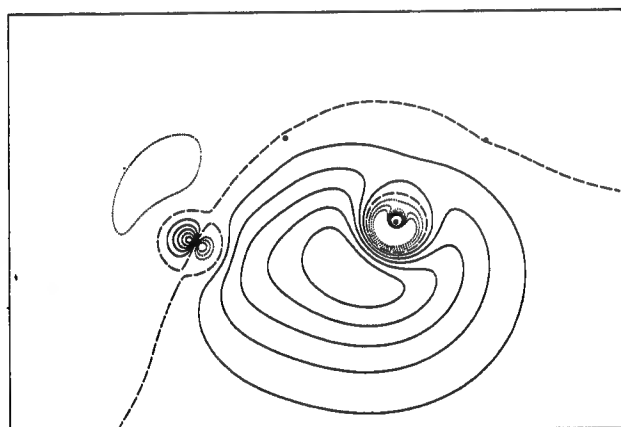
(29) (a) Goldberg, D. E.; Harris, D. H.; Lappert, M. F.; Thomas, K. M. *J. Chem. Soc., Chem. Commun.* **1976**, 261. (b) Goldberg, D. E.; Hitchcock, P. B.; Lappert, M. F.; Thomas, K. M.; Thorne, A. J.; Fjeldberg, T.; Haaland, A.; Schilling, B. E. *J. Chem. Soc., Dalton Trans.* **1986**, 2387. (c) Pauling, L. *Proc. Natl. Acad. Sci. U.S.A.* **1983**, *80*, 3871. (d) Trinquier, G.; Malrieu, J.-P.; Riviere, P. *J. Am. Chem. Soc.* **1982**, *104*, 4529. (e) Trinquier, G.; Malrieu, J.-P. *J. Am. Chem. Soc.* **1987**, *109*, 5303. (f) Trinquier, G.; Malrieu, J.-P. *J. Am. Chem. Soc.* **1989**, *111*, 5916. (g) Trinquier, G.; Malrieu, J.-P. *J. Phys. Chem.* **1990**, *94*, 6184.

(30) Baxter, P. L.; Downs, A. J.; Goode, M. J.; Rankin, D. W. H.; Robertson, H. E. *J. Chem. Soc., Chem. Commun.* **1986**, 805.

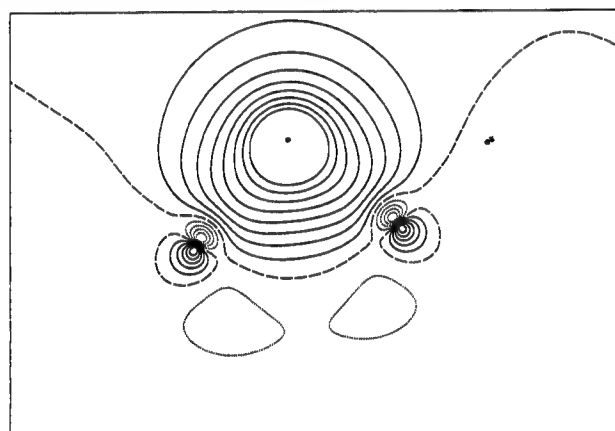
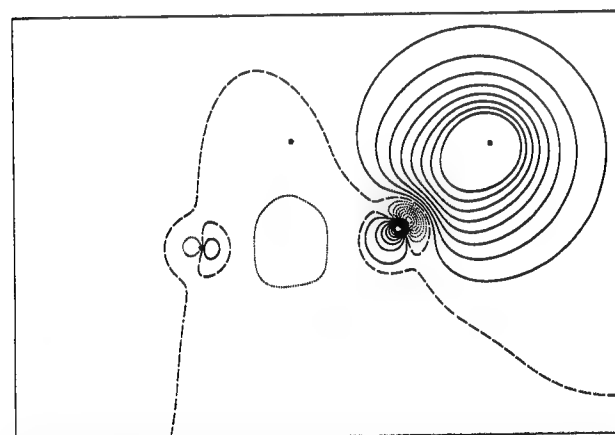
Table IV. Energies of Al_2H_2 Structures Relative to $2(\text{AlH})$ (kcal/mol). Only the Final Column Includes Zero-Point Vibrational Energies (ZPVE)

isomer	SCF		CISD ^a		CCSD		CCSD(T)			
	DZP	TZ2P	DZP	TZ2P	DZP	TZ2P	DZP	TZ2P ^c	ANO ^c	"best"
linear $^1\Delta$	12.2	9.2	13.2	10.8						15.2 ^e
linear $^3\Sigma_g^-$	-2.4	-6.6	14.3	12.3						3.8 ^e
			0.4	-1.6						
trans	-4.9	-5.9	2.1	0.9						
			-9.3	-10.7	-9.5	-10.6	-11.5	-12.9	-15.8	-13.7 ^d
monobridged	-10.5	-11.1	-10.8	-12.1						
			-15.9	-16.6	-15.6	-16.0	-17.3	-18.1	-20.9	-18.7 ^d
branched	-16.3	-19.5	-16.6	-17.3						
			-17.1	-19.8	-16.1	-18.5	-16.9	-19.5	-22.6	-19.6 ^d
planar dibridged	-20.3	-20.0	-16.5	-19.1						
			-27.7	-26.8	-28.0	-26.7	-29.3	-28.4	-30.0	-27.2 ^d
$2(\text{AlH})^b$	0.0	0.0	-28.7	-27.6						
			0.0	0.0	0.0	0.0	0.0	0.0	0.0	0.0
			0.0	0.0						

^aThe lower number in the CISD columns is the Davidson corrected energy difference. ^bThe "supermolecule" method was used to obtain the total CISD energies for AlH . ^cAt the TZ2P CCSD optimized geometry. ^dANO CCSD(T) including TZ2P CCSD harmonic zero-point vibrational energy correction. ^eTZ2P CISD+Q including TZ2P SCF harmonic zero-point vibrational energy correction.

**Figure 5.** Theoretical geometries for the monobridged closed-shell singlet state of Al_2H_2 . Bond distances are in Å.**Figure 6.** An aluminum lone pair, deformed by the p component from the terminal aluminum atom. In this figure the values of the TZ2P SCF localized orbital for the monobridged isomer of Al_2H_2 are plotted in the plane of the molecule. Nuclei are arranged as in Figure 5 and noted by heavy dots. Solid, dashed, and dotted lines correspond to positive, zero, and negative values of the function. The step between two adjacent contour lines is 0.025.

to the electron-deficient sites on the other aluminum, resulting in the trans-bent isomer (Figure 2), and (2) using the negatively charged hydrogens as the donors to the acidic sites of aluminum, resulting in the planar dibridged isomer (Figure 3). What about the third alternative, where one of the donors is the aluminum lone pair, and the other is the negatively charged hydrogen? The monobridged isomer (Figure 5) fits this description exactly! It is a genuine minimum lying $10.7 \text{ kcal mol}^{-1}$ above the planar dibridged and $2.5 \text{ kcal mol}^{-1}$ above the branched (vinylidene-like) isomer at the TZ2P CCSD level of theory. Analysis of the localized bonds shows an aluminum lone pair being donated from the aluminum connected to the terminal hydrogen to the other aluminum (Figure 6), as well as a three-center, two-electron bond

**Figure 7.** Three-center two-electron bond involving the two aluminum atoms and the bridging hydrogen. For interpretation, see caption for Figure 6.**Figure 8.** The conventional single bond connecting the terminal hydrogen atom to one of the aluminum atoms. For interpretation, see caption for Figure 6.

through the bridging hydrogen (Figure 7). In addition, the terminal hydrogen is connected to one of the aluminum atoms by a conventional σ bond (Figure 8) and there is a lone pair on the other aluminum (Figure 9). The resulting Al-Al bond lengths (2.634 Å) is intermediate between the values for a single and a double bond, and slightly (0.06 Å) shorter than that for the trans isomer.

Although we have not attempted to locate any transition states, by analogy with Si_2H_2 ^{8,14} the monobridged structure is most likely obtained from the branched (vinylidene-like) structure by following

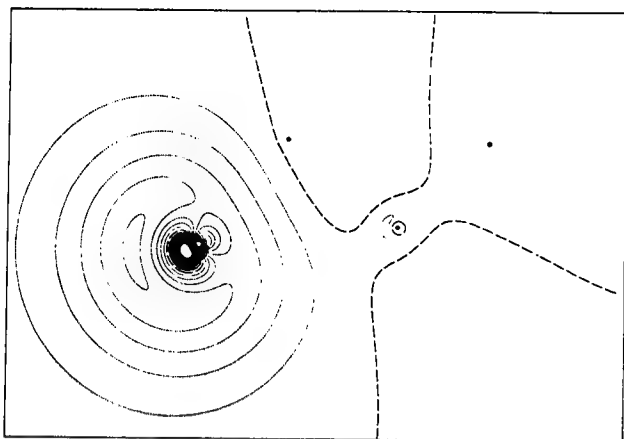


Figure 9. Lone pair on the terminal aluminum atom. For interpretation, see caption for Figure 6.

the in-plane wag motion of the latter, which has a vibrational frequency of 250 cm^{-1} . Similarly, the out-of-plane bending frequency in the monobridged isomer is quite low (173 cm^{-1}) and presumably leads to the transition state for rearrangement to the planar dibridged minimum. The rearrangement barriers are probably small, but this does not preclude the observation of monobridged Al_2H_2 ; in Si_2H_2 , for which the monobridged isomer has been observed and characterized,¹² the barrier is predicted to be 3.7 kcal mol^{-1} .¹⁴ A more fundamental stumbling block to the observation of the monobridged isomer is its small dipole moment, 0.26 D . The vinylidene-like isomer has a much larger dipole moment, 1.55 D . This trend is the opposite of that in Si_2H_2 ,¹⁴ where the monobridged isomer has a larger dipole moment than the vinylidene isomer. This partially explains the inability to observe the vinylidene isomer of Si_2H_2 in microwave studies.¹² Our results suggest that microwave detection of the vinylidene isomer of Al_2H_2 is advantageous.

In light of the near degeneracy of the low-lying unsymmetrical monobridged (Figure 3) and vinylidene-like (Figure 4) structures of Al_2H_2 , it was decided to press on to yet a higher level of theory. For this purpose the CCSD(T) method, proposed in 1989 by Raghavachari et al.,³¹ was used in conjunction with Scuseria's analytic gradient procedure.³² In this manner DZP CCSD(T) stationary-point geometries were optimized for the four closed-shell singlet structures of Al_2H_2 . These additional structures have been included in Figures 2–5. We find that the DZP CCSD(T) structures differ imperceptibly from those optimized at the DZP CCSD level of theory, except for the trans-bent structure for which the Al–Al bond distance decreases by 0.015 \AA . This breeds confidence in simply adopting the TZ2P CCSD optimized geometries for any further analysis. The DZP CCSD(T) stationary-point total energies show that the unsymmetrical monobridged structure falls 0.4 kcal mol^{-1} below the vinylidene-like structure of Al_2H_2 . This is roughly the pattern of behavior predicted for Si_2H_2 by Colegrove.⁸

The order of the monobridged and vinylidene structures of Al_2H_2 could be reversed again if larger basis sets are used. Table I indicates that correlated energies of both structures decrease (relative to the planar dibridged global minimum) in going from the DZP to the TZ2P basis set. To investigate this further, we have determined single-point TZ2P CCSD(T) energies at the TZ2P CCSD optimized geometries. Additional single-point CCSD(T) energies, again at the TZ2P CCSD optimized geometries, are determined using the atomic natural orbital (ANO) basis sets of Widmark, Roos, et al.³³ Specifically, we have used the $5s4p3d2f$ ANO set for aluminum and the $3s2p1d$ ANO set

for hydrogen.³³ Our final prediction, using the ANO CCSD(T) energies and correcting for differential zero-point vibrational effects at the TZ2P CCSD level of theory, is that the monobridged isomer lies 0.9 kcal mol^{-1} above the vinylidene-like isomer, and that both of these are within 9 kcal mol^{-1} of the dibridged ground-state structure.

Discussion

Trinquier⁹ has extensively analyzed bridge-bonded structures in the group 14 compounds C_2H_4 , Si_2H_4 , Ge_2H_4 , Sn_2H_4 , and Pb_2H_4 . Considered as dimers of MH_2 , these molecules are very similar to Al_2H_2 , because the monomers MH_2 for group 14 have similar donor and acceptor sites to those in AlH_3 . For C_2H_4 , bridged structures apparently do not exist as minima on the potential energy surface. Already at Si_2H_4 , Trinquier finds that dibridged isomers emerge as low-lying stable minima, and they persist down the periodic table, becoming the ground states for Sn_2H_4 and Pb_2H_4 . The third mode of coordination, with one donor being the lone pair and one being the bridging hydrogen (and the structure being monobridged), does not appear until we reach Sn_2H_4 .⁹ Removing two hydrogens from these systems yields stable minima that are associated with this unsymmetrical coordination mode already at the second row, with Si_2H_2 , and now in Al_2H_2 as well.

The resemblance of the Al_2H_2 potential energy surface to that of Si_2H_2 is stunning! Each of the four singlet isomers of Al_2H_2 studied here has an exact analogue in Si_2H_2 that can be derived simply by adding two electrons to an unoccupied bonding π orbital in Al_2H_2 . The only qualitative structural change in doing this is that the lowest lying dibridged isomer of Si_2H_2 is now nonplanar, instead of planar as in Al_2H_2 . The planar dibridged isomer of Si_2H_2 is higher lying and is the transition state for degenerate inversion of the C_{2v} symmetry ground-state dibridged structure.^{8,14} In addition, the energies of the monobridged, vinylidene, and trans-bent structures relative to the dibridged minimum are very similar in both cases: $+9$, $+12$, and $+16\text{ kcal mol}^{-1}$, respectively, for Si_2H_2 [14], and $+9$, $+8$, and $+14\text{ kcal mol}^{-1}$, respectively, for Al_2H_2 .

There is one significant difference between the Al_2H_2 and Si_2H_2 potential energy surfaces: Si_2H_2 is bound by $80\text{--}85\text{ kcal mol}^{-1}$ relative to two SiH molecules,^{14,34} while Al_2H_2 is bound by only $27.2\text{ kcal mol}^{-1}$ relative to two AlH fragments at our highest level of theory (Table IV). The relative dissociation energies are reasonable, because Si_2H_2 has the extra pair of bonding electrons. What is remarkable is the small dissociation energy for Al_2H_2 , when a naive interpretation would suggest that there are four electrons available for Al–Al bonding. The dissociation energy of ground-state B_2H_2 , by contrast, is nearly 100 kcal mol^{-1} .^{5,6} Noting that the bonding in the lowest-lying dibridged isomer is dative in nature (or three-center, two-electron bonding) is hardly satisfying, because the dissociation energy in the alane dimer (Al_2H_6) is around 32 kcal mol^{-1} ,³⁵ which is larger than that found for Al_2H_2 . Furthermore, the dissociation energy of the ground state of Al_2H_4 (which is of $\text{HAl}(\mu\text{H}_3)\text{Al}$ form; electronically, this is a salt-like $\text{Al}^+[\text{AlH}_4]^-$ species, with the Al^+ form coordinated to a face of AlH_4^-) into AlH_3 and AlH is near 36 kcal mol^{-1} .^{2b} Why, with all these additional free electron pairs, does a more stable isomer not result? The answer clearly lies in the stability of AlH itself.

Questions similar to this have been asked in group 14 chemistry, where it is found that the dissociation energies of the doubly bonded molecules disilene, $\text{H}_2\text{Si}=\text{SiH}_2$, digermene, $\text{H}_2\text{Ge}=\text{GeH}_2$, and germsilene, $\text{H}_2\text{Ge}=\text{SiH}_2$, are all found to be lower than those in the parent singly bonded isomers disilane, $\text{H}_3\text{Si}-\text{SiH}_3$, digermane, $\text{H}_3\text{Ge}-\text{GeH}_3$, and germsilane, $\text{H}_3\text{Ge}-\text{SiH}_3$, respectively. We have demonstrated³⁶ that the dissociation energies of the

(31) Raghavachari, K.; Trucks, G. W.; Pople, J. A.; Head-Gordon, M. *Chem. Phys. Lett.* **1989**, *157*, 479.

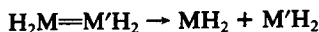
(32) Scuseria, G. E. *J. Chem. Phys.* **1991**, *94*, 442.

(33) (a) Widmark, P.-O.; Malmqvist, P.-A.; Roos, B. O. *Theor. Chim. Acta* **1990**, *77*, 291. (b) Widmark, P.-O.; Persson, J.; Roos, B. O. *Theor. Chim. Acta* **1991**, *79*, 419.

(34) (a) Ruscic, B.; Berkowitz, J. *J. Chem. Phys.* **1991**, *95*, 2416. (b) Curtiss, L. A.; Raghavachari, K.; Deutsch, P. W.; Pople, J. A. *J. Chem. Phys.* **1991**, *95*, 2433. (c) Ho, P.; Melius, C. F. *J. Phys. Chem.* **1990**, *94*, 5120.

(35) Rendell, A. P.; Lee, T. J.; Komornicki, A. *Chem. Phys. Lett.* **1991**, *178*, 462.

doubly bonded isomers are rigorously related to differences between first and second M-H bond dissociation energies (BDEs) in the parent hydrides, MH_4 , as well as to standard M-M' σ - and π -bond energies. Specifically, for the double-bond dissociation process



the dissociation energy, $D(H_2M=M'H_2)$, is equal to

$$D(H_2M=M'H_2) = D(H_3M-M'H_3) + D_\pi - DSSE(MH_2) - DSSE(M'H_2) + [D(H_3M-H) - D(H_3M'MH_2-H)] + [D(H_3M'-H) - D(H_3MM'H_2-H)] \quad (2)$$

where $DSSE(MH_2)$, the *divalent state stabilization energy*,³⁷ is the difference between the first and second bond dissociation energy in MH_4 . That is, the DSSE is given by

$$DSSE(MH_2) = D(H_3M-H) - D(H_2M-H)$$

The two terms in brackets in eq (2) are the difference between the first M-H dissociation energies of the parent hydrides and the substituted hydrides, and these differences are usually small. Thus, to a good approximation, the double-bond dissociation energy is given by

$$D(H_2M=M'H_2) \approx D(H_3M-M'H_3) + D_\pi(M=M') - DSSE(MH_2) - DSSE(M'H_2) \quad (3)$$

We should note that eq 2 is correct only if the π -bond energy, D_π , is determined by the method of Benson,³⁸ i.e., if D_π is given by

$$D_\pi(M=M') = \Delta H_f(H_3MM'H_2) + \Delta H_f(H_3M'MH_2) - \Delta H_f(H_3MM'H_3) - \Delta H_f(H_2M=M'H_2)$$

On the other hand, alternative definitions of π -bond energies exist, and one in particular, that of Schleyer and Kost,³⁹ is formulated in such a way that eq 3, and not eq 2, is correct. That is, Schleyer and Kost's definition of the π -bond energy is equal to Benson's π -bond energy, plus the bracketed terms in eq 2.

To make a long story³⁶ short, the reason that disilene, digermene, and germsilene have smaller double-bond dissociation energies than the single-bond dissociation energies in the parent saturated compounds is that SiH_2 and GeH_2 have large (≈ 20 kcal mol⁻¹), positive DSSEs, in conjunction, of course, with relatively small single-bond (≈ 70 kcal mol⁻¹) and π -bond (≈ 25 kcal mol⁻¹) energies. Equation 1 also provides a ready explanation of why the dissociation energy in ethylene is ≈ 20 kcal mol⁻¹ larger than the sum of standard σ - and π -bond energies (because the DSSE of CH_2 is *negative*) and why that of tetrafluoroethylene is so small (because the DSSE of CF_2 is large and *positive*³⁶).

The relevance of this digression to the current question of the dissociation energy of Al_2H_2 to $2AlH$ is this: the difference between the first and second Al-H BDEs in AlH_3 is nearly 40 kcal mol⁻¹! A modified eq 2 appropriate for group 13 compounds can be trivially obtained by eliminating one of the hydrogens bonded to each heavy atom, although the DSSE nomenclature then seems odd because AlH is *not* divalent. Nonetheless, the resulting equation would be appropriate for the trans-bent structure, which is our nearest candidate to a classical double-bonded structure. If we then use any reasonable values for standard Al-Al σ - and π -bond energies, the overall dissociation energy will come out to be near zero because we must subtract off two times 40, or 80 kcal mol⁻¹, for twice the difference in first and second bond dissociation energies in AlH_3 . Preliminary studies suggest that the difference between the first and second BDEs

in GaH_3 are about the same as those in AlH_3 , so similar chemistry can be anticipated for Ga_2H_2 .

Another consequence of DSSEs being large and positive in group 14 chemistry is that divalent isomers such as $H_3MM'H$ become low lying relative to the double-bonded isomer $H_2M=M'H_2$ when $M' = Si, Ge$, or the heavier elements.^{36,40} In this case, the former isomer is above the latter by the amount

$$D_\pi - DSSE(H_3MM'H) + D(H_3MM'H_2-H) - D(H_3M'MH_2-H)$$

For symmetrical systems ($M = M'$), this reduces to $D_\pi - DSSE(H_3MMH)$. Applied to the current case of Al_2H_2 , this becomes $D_\pi - DSSE(H_2AlAl)$, and $DSSE(H_2AlAl)$ will surely be large and positive, just as it is for AlH . Thus, the branched isomer H_2AlAl (Figure 4) is expected to be low lying, and indeed it is. By comparison, the H_2BB isomer lies 50 kcal mol⁻¹ above the linear triplet HBBH ground state.⁵ Note that BH also has a substantial difference in first and second B-H BDEs, around 28 kcal mol⁻¹,^{5,6} but the π -bond energy is clearly quite strong, as it is in all first-row compounds.

A different model, proposed by Carter and Goddard,⁴¹ has been used in recent years to rationalize small double-bond dissociation energies. These authors assume that, for substituted ethylenes, the double-bond dissociation energies will be equal to that in ethylene unless one of the carbene fragments is a ground-state singlet, in which case the dissociation energy will be lowered (relative to that in ethylene) by the singlet-triplet splitting of the ground-state singlet carbene(s). This model has spawned a wave of singlet-triplet splitting rationalizations for interesting phenomena.^{29e-3,42,43} Because both the singlet-triplet splitting model and the thermochemical analysis presented above, eq 2, are predicting the same qualitative behavior, it is tempting to equate the DSSE with the singlet-triplet splitting,^{40,43} but in practice this fails.⁴⁰ In quantitative studies of double-bond dissociation energies, the singlet-triplet splitting model yields errors that are substantial, random, and of uncertain origin.^{40,42,44} Furthermore, the singlet-triplet splitting model is *qualitatively* wrong if the substituents stabilize the triplet carbenes.³⁶ The crux of the matter is that it is the *stability* of the carbene fragments, not the singlet-triplet splitting, that is important.

Concluding Remarks

The singlet potential energy surface of Al_2H_2 has been analyzed extensively at the SCF, CISD, CCSD, and CCSD(T) levels of theory. Our results show the necessity of including correlation effects to accurately describe relative energies as well as the shape of the potential surface. The planar dibridged global minimum and the low-lying monobridged minimum demonstrate the importance of bridging hydrogen atoms in creating Al-Al bonds. The only classically bonded structure that emerges is the vinylidene-like structure. The other stable isomers are best viewed as AlH dimers with dative or three-center two-electron bonds derived from the three possible ways that the two electron-rich regions in the AlH monomer can donate electron density to the electron-deficient aluminum centers.

Each of the four stable singlet isomers of Al_2H_2 can be mapped, one-to-one, onto an analogous isomer of Si_2H_2 by the addition of a pair of bonding π electrons. The similarities between the stable minima of Al_2H_2 and Si_2H_2 extend to their relative energies, with isomeric energy differences varying by only a few kcal mol⁻¹. The analogy ends, however, when we consider their stability toward fragmentation, and we have tied this difference to the tremendous stability of the AlH monomer, as measured by the difference

(40) Grev, R. S.; Schaefer, H. F.; Baines, K. M. *J. Am. Chem. Soc.* **1990**, *112*, 9458.

(41) (a) Carter, E. A.; Goddard, W. A. *J. Phys. Chem.* **1986**, *90*, 998. (b) Carter, E. A.; Goddard, W. A. *J. Chem. Phys.* **1988**, *88*, 1752. (c) Carter, E. A.; Goddard, W. A. *J. Chem. Phys.* **1988**, *88*, 3132. (d) Carter, E. A.; Goddard, W. A. *J. Am. Chem. Soc.* **1988**, *110*, 4077.

(42) Karni, M.; Apeloig, Y. *J. Am. Chem. Soc.* **1990**, *112*, 8589.

(43) Clauber, H.; Minsek, D. W.; Chen, P. *J. Am. Chem. Soc.* **1992**, *114*, 99.

(44) Paulino, J. A.; Squires, R. R. *J. Am. Chem. Soc.* **1991**, *113*, 5573.

(36) Grev, R. S. *Adv. Organomet. Chem.* **1991**, *33*, 125.

(37) Walsh, R. *Acc. Chem. Res.* **1981**, *14*, 246.

(38) Benson, S. W. *Thermochemical Kinetics*; Wiley: New York, 1976; p 63.

(39) Schleyer, P. v. R.; Kost, D. *J. Am. Chem. Soc.* **1988**, *110*, 2105.

between first and second Al-H BDEs in the parent compound, AlH_3 .

The presence of the unsymmetrical monobridged structure of Al_2H_2 as a genuine minimum proves that this structural type is not limited to Si_2H_2 ,^{8,14} for which solid experimental structural confirmation now exists.¹² This work surely suggests that related potential energy hypersurfaces— B_2H_2 , BAlH_2 , BGaH_2 , AlGaH_2 ,

Ga_2H_2 , SiCH_2 , Ge_2H_2 , GeCH_2 , GeSiH_2 —should be carefully searched for new unsymmetrical monobridged structures.

Acknowledgment. We thank Seung-Joon Kim, Yukio Yamaguchi, and Yaoming Xie for many helpful discussions. This research was supported by the U.S. Air Force Office of Scientific Research, Grant AFOSR-92-J-0047.

HP₄⁻: the monoconjugate base from tetraphosphabicyclobutane. Evidence for an exo ground state conformation in the gas phase

Tracy P. Hamilton

Department of Chemistry, University of Alabama, Birmingham, AL 35294, USA

Yaoming Xie and Henry F. Schaefer III

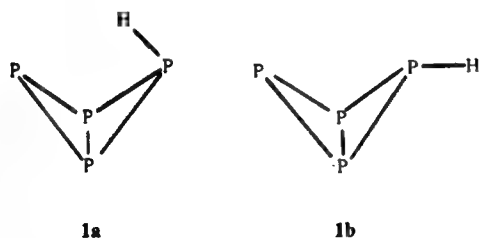
Center for Computational Quantum Chemistry, University of Georgia, Athens, GA 30602, USA

Received 6 February 1993; in final form 30 March 1993

Ab initio theoretical studies reconsider recent experimental findings concerning the ground state conformation of the HP₄⁻ anion. Basis sets as large as triple zeta plus double polarization plus f functions plus diffuse functions (TZ2P+diffuse) were used in connection with methods that explicitly include the effects of electron correlation. At the highest level of theory, the exo structure is predicted to lie about two kcal/mol below the endo structure, in apparent disagreement with experiment. The Li⁺HP₄⁻ system has also been examined to approximate more closely the system synthesized in the laboratory. The energetics are significantly shifted by the appendage of the Li⁺ cation, and the agreement between theory and experiment deteriorates further.

1. Introduction

In 1988 Baudler et al. [1] reported experimental evidence for the first salts of bicyclo [1.1.0] tetraphosphane. The three compounds LiHP₄, NaHP₄, and KHP₄, characterized as tight ion pairs M⁺HP₄⁻, were prepared in the laboratory. Based on the observed NMR spectra Baudler et al. concluded that the hydrogen atom in these HP₄⁻ salts is arranged endo (1a) to the P₄ moiety, rather than the other obvious possibility, an exo conformation (1b)



Since all five atoms in HP₄⁻ might be expected to carry some negative charge (in a simple picture of

the electronic structure), it is not clear that chemical intuition favors 1a over 1b.

The HP₄⁻ anions have been examined computationally by Dewar and Zheng [2] using the semi-empirical AM1 method [3]. However, Dewar and Zheng reinterpret Baudler's solution-phase NMR spectra to support the exo structure 1b, based on the assumption that the endo isomers will rapidly interconvert. They compute a barrier of 2.2 kcal/mol for the C_{2v} transition state. To account for the slow interconversion indicated for the NMR spectra, they postulate that the associated cation inhibits the motion of the H atom. This situation is made more complicated by the fact that the AM1 method predicts the endo structure 1a to lie 11.6 kcal below the exo structure 1b. The latter prediction is consistent with some degree of attraction between the positive formal atomic charge on hydrogen (+0.19 e) and the large negative charge (-0.87 e) on the phosphorus toward which the hydrogen points in the endo structure.

2. Theoretical approach

In light of the above puzzling situation, it was decided to press on theoretically with this HP_4^- problem. Structures for both HP_4^- and Li^+HP_4^- were initially optimized using the self-consistent-field (SCF) method in conjunction with a basis set of double zeta plus polarization (DZP) quality. The basis set for HP_4^- was of the form

$\text{H}(4s1p/2s1p)$,

$\text{P}(11s7p1d/6s4p1d)$,

due to Huzinaga [4] and Dunning [5]. Polarization function orbital exponents were $\alpha_p(\text{H})=0.75$, $\alpha_d(\text{P})=0.50$, with a complete set of six d-like functions on phosphorus. In the Li^+HP_4^- ionic complex, the lithium basis is the standard 6-31G* set of Pople and co-workers [6].

With due consideration to the anionic character of HP_4^- , a somewhat larger basis set, designated TZP plus diffuse, was also used. The term "triple" in TZ here is exaggerated, since only the phosphorus basis is enlarged relative to the DZ set. In the TZ set, the phosphorus contraction is simply relaxed to $\text{P}(11s7p/7s5p)$. Thus the final technical designation for the TZP plus diffuse basis is

$\text{H}(5s1p/3s1p)$,

$\text{P}(12s8p1d/8s6p1d)$.

The diffuse functions have the following orbital exponents.

$\alpha_s(\text{P})=0.04$,

$\alpha_p(\text{P})=0.04$,

$\alpha_s(\text{H})=0.05$.

With this TZP plus diffuse basis, complete structural optimizations were carried out for the three stationary points of HP_4^- at the SCF level of theory.

The effects of electron correlation were considered in this research using the single and double excitation configuration interaction (CISD) method. DZP CISD structures for HP_4^- were optimized using analytic gradient methods [7]. In the CISD wavefunctions, the 20 core-like (phosphorus 1s, 2s, and 2p) SCF molecular orbitals were constrained to be

doubly occupied. However, only the four highest-lying virtual orbitals were deleted. For HP_4^- in C_s symmetry the CISD wavefunctions included 133756 configurations. For final energetic comparisons, Davidson's correction [8] (here designated +Q) for unlinked quadruple excitations was appended to the DZP CISD total energies, and the higher level coupled-cluster methods CCSD [9] and CCSD(T) [10] were also applied.

Single point TZP+diffuse CISD energies were also obtained using the DZP CISD stationary point geometries. As described above, twenty occupied orbitals were frozen and four virtual orbitals deleted in these CISD wavefunctions, which include 300934 configurations in C_s symmetry.

Finally, in light of the small energy difference (see below) between the exo and endo structures, it was deemed desirable to have some results using a much larger basis set, namely triple zeta plus double polarization plus f functions plus diffuse (TZ2P+diffuse). This basis may be technically designated

$\text{P}(13s10p2d1f/7s6p2d1f)$,

$\text{H}(6s2p1d/4s2p1d)$.

The phosphorus sp basis set is that of McLean and Chandler [11], with polarization function orbital exponents $\alpha_d(\text{P})=1.2$, 0.3 and $\alpha_f(\text{P})=0.45$. The phosphorus and hydrogen diffuse functions were the same as described above for the smaller TZP+diffuse basis. The hydrogen s basis set is the (5s/3s) set of Huzinaga [4] and Dunning [12], with polarization function orbital exponents $\alpha_p(\text{H})=1.5$, 0.375 and $\alpha_d(\text{H})=1.0$. With this TZ2P+diffuse basis set total energies from the SCF method and second-order perturbation theory [13] were evaluated using the DZP CISD equilibrium geometries. All six d-like and all ten f-like functions were included in this large basis set. In the MP2 treatment, the twenty lowest SCF MOs were doubly occupied and the four highest-lying virtual orbitals were deleted.

3. Results

The theoretical stationary point geometries for HP_4^- are reported in fig. 1, and the accompanying

Table 1

Summary of total energies (hartree) and relative energies (kcal mol⁻¹) for HP₄⁻ and Li⁺HP₄⁻. All results presented here employed a double zeta plus polarization (DZP) basis set. For the transition states the magnitude of the imaginary vibrational frequency in cm⁻¹ is also reported. These excitation energies T_e may be converted to T_0 values using the DZP SCF zero-point vibrational energies (ZPVE): 9.4 (exo), 9.6 (endo), 7.4 (endo-endo TS), 8.0 kcal (exo-endo TS), 10.8 (exo Li⁺ complex A), 10.6 (exo Li⁺ complex B), 10.8 (endo Li⁺ complex A), 10.4 (endo Li⁺ complex B), 10.7 (endo Li⁺ complex C), and 10.2 (endo Li⁺ complex D)

	Theoretical method					
	DZP SCF	DZP MP2	DZP CISD	DZP CISD+Q	DZP CCSD	DZP CCSD(T)
exo minimum	-1363.47508 0.0	-1363.93624 ^{a)} 0.0	-1363.89127 0.0	-1363.95981 ^{a)} 0.0	-1363.97454 ^{a)} 0.0	-1364.00081 ^{a)} 0.0
endo minimum	2.2	1.4	2.0	2.0	2.0	1.9
endo-endo transition state	1865i 30.4		24.1	22.1		
exo-endo transition state	277i 21.3					
exo Li ⁺ complex A	-1370.94502 0.0					
exo Li ⁺ complex B	10.5					
endo Li ⁺ complex A	11.7					
endo Li ⁺ complex B	11.9					
endo Li ⁺ complex C	12.2					
endo Li ⁺ complex D	37.0					

^{a)} Total energies evaluated at the DZP CISD stationary point geometries.

Table 2

Total energies (hartree) and relative energies (kcal mol⁻¹) for HP₄⁻ using larger basis sets

	Theoretical method				
	TZP+diffuse SCF	TZP+diffuse CISD	TZP+diffuse CISD+Q	TZ2Pf+diffuse SCF	TZ2Pf+diffuse MP2
exo minimum	-1363.49052 0.0	-1363.91263 0.0	-1363.98354 ^{a)} 0.0	-1363.60881 ^{b)} 0.0	-1364.21489 ^{b)} 0.0
endo minimum	1.5	1.2	1.1	2.3	1.5
endo-endo transition state	1882i 30.1	23.5	21.5		

^{a)} Davidson corrected energies evaluated at the TZP+diffuse CISD stationary point geometries.

^{b)} Assuming DZP CISD stationary point geometries.

The inversion barrier for phosphacyclopropane, C₂PH₅, is predicted to be 68.3 kcal/mol at the MP2/6-31G**/HF/6-31G* level of theory [15]. Given these much higher barriers for genuine inversion, and the fact that the C₁ transition state has a broken P-P bond, the endo-exo isomerization does not appear to be a true inversion process.

The Li⁺PH₄⁻ system synthesized by Baudler et al. [1] was also considered theoretically, and the results are seen in table 1 and in fig. 2. At the DZP SCF level the exo structure is still favored, by 11.7 kcal/mol. The attachment of the Li⁺ cation is seen to increase the exo-endo energy difference by 9.5 kcal/mol compared to the isolated HP₄⁻ anion. These

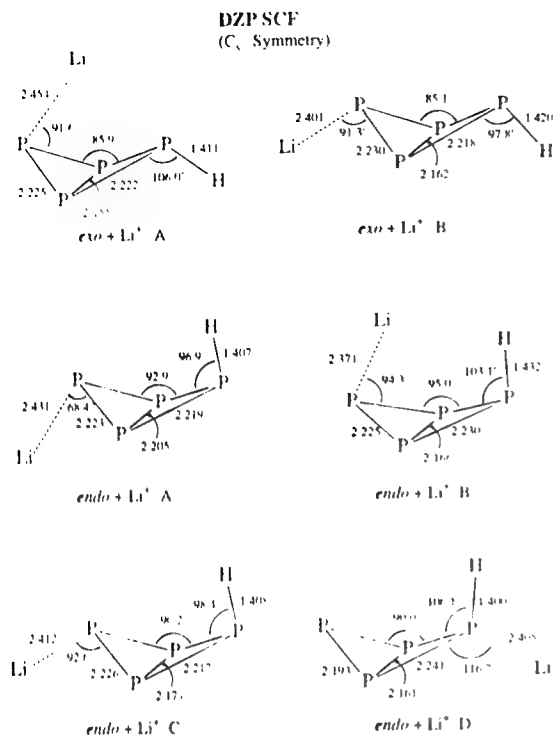


Fig. 2. DZP SCF equilibrium geometries for the exo and endo conformers of the Li^+HP_4^- system. Bond distances are in Å.

Li^+HP_4^- results are puzzling in that the system examined theoretically is closer to that studied in the laboratory, but the agreement with experiment is poorer.

4. Conclusions

The present ab initio quantum-mechanical studies indicate an exo ground state (**1b**) for the isolated HP_4^- anion, with the endo structure (**1a**) only about 2 kcal/mol higher in energy. Complexation with a Li^+ cation increases the exo-endo energy difference by 9 kcal/mol. The two structures of isolated HP_4^- are separated by a barrier of about 10 kcal/mol. The NMR spectral assignment of Baudler's group indicated the presence of the endo isomer; it is possible that the endo form is synthesized and is unable to isomerize to the exo form. Our research does support Baudler's experimental conclusion that the degenerate endo-endo rearrangement is a slow process. A significant classical barrier (≈ 20 kcal/mol) is pre-

dicted for the degenerate rearrangement between endo conformers. The present theoretical results disagree with the AM1 calculations of Dewar and Zheng for both the exo-endo energy difference and the endo-endo interconversion barrier height [2].

Acknowledgement

This research was supported by the United States Air Force Office of Scientific Research under Grant No. AFOSR-92-J-0047. We thank Roger Grev for his helpful comments on the bonding in HP_4^- .

References

- [1] M. Baudler, C. Adamek, S. Opiela, H. Budzikiewicz and D. Ouzounis, *Angew. Chem. Intern. Ed. Engl.* 27 (1988) 1059.
- [2] M.J.S. Dewar and Y.-J. Zheng, *Inorg. Chem.* 30 (1991) 3361.
- [3] M.J.S. Dewar, E.G. Zoebisch, E.F. Healy and J.J.P. Stewart, *J. Am. Chem. Soc.* 107 (1985) 3902.
- [4] S. Huzinaga, *J. Chem. Phys.* 42 (1965) 1293; Approximate atomic functions, Vol. 2, Department of Chemistry Report, University of Alberta, Edmonton, Canada (1971).
- [5] T.H. Dunning, *J. Chem. Phys.* 53 (1970) 2823; T.H. Dunning and P.J. Hay, *Modern theoretical chemistry*, Vol. 3, ed. H.F. Schaefer III (Plenum Press, New York, 1977) pp. 1-27.
- [6] W.J. Hehre, L. Radom, P.R. Schleyer and J.A. Pople, *Ab initio molecular orbital theory* (Wiley, New York, 1986) p. 82.
- [7] P. Saxe, D.J. Fox, H.F. Schaefer III and N.C. Handy, *J. Chem. Phys.* 77 (1982) 5584; J.E. Rice, R.D. Amos, N.C. Handy, T.J. Lee and H.F. Schaefer III, *J. Chem. Phys.* 85 (1986) 963.
- [8] E.R. Davidson, *The world of quantum chemistry*, eds. R. Daudel and B. Pullman (Reidel, Dordrecht, 1974) pp. 17-30.
- [9] G.E. Scuseria, C.L. Janssen and H.F. Schaefer III, *J. Chem. Phys.* 89 (1988) 7382.
- [10] G.E. Scuseria and T.J. Lee, *J. Chem. Phys.* 93 (1990) 5851.
- [11] A.D. McLean and G.S. Chandler, *J. Chem. Phys.* 72 (1980) 5639.
- [12] T.H. Dunning, *J. Chem. Phys.* 55 (1971) 716.
- [13] M. Frisch, M. Head-Gordon, G.W. Trucks, J.B. Foresman, H.B. Schlegel, K. Raghavachari, M.A. Robb, J.S. Binkley, C. Gonzalez, D.J. DeFrees, D.J. Fox, R.A. Whiteside, R. Seeger, C.F. Melius, J. Baker, R.L. Martin, L.R. Kahn, J.J.P. Stewart, S. Topiol and J.A. Pople, *GAUSSIAN 90* (Gaussian, Inc., Pittsburgh, PA, 1990).
- [14] S. Yabushita and M.S. Gordon, *Chem. Phys. Letters* 117 (1985) 321.
- [15] S.M. Bachrach, *J. Phys. Chem.* 93 (1989) 7780.

ClF₂: Structure and infrared spectra of a weakly bound triatomic molecule

John Morrison Galbraith,^{a)} George Vacek,^{b)} and Henry F. Schaefer III
Center for Computational Quantum Chemistry, University of Georgia, Athens, Georgia 30602

(Received 17 November 1992; accepted 1 February 1993)

Using sophisticated *ab initio* methods, the equilibrium structure of the ClF₂ radical has been predicted to be bent, confirming previous experimental and theoretical work. The single, double and perturbative triple excitation coupled cluster level of theory along with a triple- ζ plus double polarization basis set gives the geometrical parameters $r_e = 1.756$ Å and $\theta_e = 151.8^\circ$. At the same level of theory, harmonic vibrational frequencies were predicted to be 536, 243, and 568 cm⁻¹ for the symmetric stretch, bend and asymmetric stretch, respectively. In addition to this high level study of the harmonic vibrational frequencies, theoretical analyses of anharmonic terms have been included in order to help settle the controversy surrounding experimental assignments of the fundamental vibrational frequencies. This research supports Mamantov's experimental assignment of the bending and symmetric stretching fundamental, over the experimental objections of Prochaska. The vibrational frequency splitting due to ³⁷ClF₂ was also studied indicating that only the splitting of the bending and asymmetric stretching modes should be readily observable experimentally. Dipole moments and infrared (IR) intensities were also predicted.

I. INTRODUCTION

The chlorine difluoride radical, ClF₂, is a small and apparently simple chemical system. Yet relatively little is known about this, or other, trihalogen molecules. In 1953, Walsh¹ correlated the molecular structure of triatomics with the number of valence electrons; 20-valence-electron (VE) molecules were assigned a strongly bent geometry and 22 VE molecules a linear geometry. Trihalogens fall between these categories with 21 VE, making the angle difficult to qualitatively predict using Walsh's rules.

The only other experimentally known trihalogen radicals are Br₃ and Cl₃. According to a 1971 study by Boal and Ozin² using matrix Raman spectra, Br₃ has a symmetric linear structure ($D_{\infty h}$ symmetry). On the other hand, Nelson and Pimentel³ found the analogous molecule Cl₃, to have an asymmetric linear structure ($C_{\infty v}$ symmetry). Further complicating matters, various theoretical studies⁴⁻⁶ favor a slightly bent symmetric structure for Cl₃ (C_{2v} symmetry) and find the isoelectronic van der Waals species (Cl \cdots Cl₂) to have an asymmetric linear form. Comparison with other trihalogens obviously does not give sufficient insight to the structure of ClF₂, which has been a subject of debate for over twenty years.

Mamantov and co-workers⁷ first prepared ClF₂ in 1970 via the near ultraviolet photolysis of F₂ in the presence of ClF and by photolysis of ClF₃ using matrix isolation techniques at 16 K. Soon thereafter,⁸ fundamental vibrational frequencies of 536 cm⁻¹, 242 cm⁻¹, and 578 cm⁻¹ were assigned to the symmetric stretch, bend, and asymmetric stretch, respectively. From these data, a symmetric bent structure (C_{2v} symmetry) with an angle of $140 \pm 19^\circ$ was proposed. In 1977, Prochaska and Andrews,⁹ assigned the asymmetric stretch to a strong IR absorption peak ob-

served at 578 cm⁻¹ which supports Mamantov's assignment for that mode. However, observing no other IR peaks, Prochaska and Andrews argued against Mamantov's other assignments. Although unable to offer an alternative, they considered the 242 cm⁻¹ bend assignment to be "tentative." Further, they assigned the symmetric stretching mode to a 500 cm⁻¹ Raman active vibrational frequency. They favored a bent structure and proposed a lower limit for the FCIF angle at $136 \pm 15^\circ$, although they could not rule out the possibility of linearity.

Theoretical studies using semiempirical methods have predicted both linear and bent structures for ClF₂ depending on the basis set used. Using CNDO/2 methods with an *spd* basis set for chlorine and *sp* for fluorine, Deb, Mahajan, and Vasan¹⁰ predicted a linear ground state; De and Sannigrahi⁴ calculated an angle of 148.4° when the *d* functions on the chlorine atom were omitted. *Ab initio* calculations have also been carried out to the self-consistent-field (SCF) level by Ungemach and Schaefer¹¹ in 1976 and more recently, in 1985, including electron correlation effects via the multireference single and double excitation configuration interaction (MRD CI) method by Sannigrahi and Peyerimhoff.¹² Both studies predicted a bent ground state structure; the equilibrium bond angle was determined to be 145.2° and 150.3° , respectively. It is somewhat surprising, considering Mamantov's early assignment of vibrational frequencies⁸ and Prochaska's subsequent disagreement,⁹ that to date, no theoretical efforts have been focused on the vibrational frequencies of ClF₂.

The correct ordering of vibrational frequencies is not obvious from the previous experimental studies of ClF₂ and an accurate prediction cannot be made based on properties of similar triatomic molecules. Mamantov⁸ and Prochaska⁹ both assign the asymmetric stretch above the symmetric stretch, although they disagree on the magnitude of the symmetric vibrational frequency. For most AB₂ triatomic molecules (using NO₂ as an example¹³) the

^{a)}CCQC Summer Research Fellow.

^{b)}D.O.D. Predoctoral Fellow, Egil A. Hylleraas Fellow.

asymmetric stretching mode (1671 cm⁻¹) is indeed higher than the symmetric stretching mode (1353 cm⁻¹). In the case of ozone,¹⁴ however, the fundamental vibrational frequency for the symmetric stretching mode is 1103 cm⁻¹, or 61 cm⁻¹ higher than the asymmetric stretching mode of 1042 cm⁻¹. For the relatively weakly bound ozone system, theoretical approaches have difficulty getting even the qualitative ordering of the vibrational frequencies correct. Scuseria, Lee, Scheiner, and Schaefer¹⁵ found that the correct ordering of harmonic vibrational frequencies for ozone are predicted with the single and double excitation coupled cluster (CCSD) approach with reasonably large basis sets. Even at that level, the predicted ω_1 and ω_3 frequencies, 1247 cm⁻¹ and 1218 cm⁻¹ are disturbingly close together and larger than the experimental values by 9.9 and 11.8%, respectively. According to a very recent study by Borowski, Anderson, Malmqvist, and Roos,¹⁶ the stretching frequencies of ozone and similar molecules cannot always be accurately predicted without employing multiconfigurational techniques. However, Lee and Scuseria¹⁷ obtained a better agreement with experiment for the harmonic vibrational frequencies than any *ab initio* study of ozone to date with the relatively new CCSD(T) method which includes a perturbational estimate of triple excitations from the CCSD wave function. The present research is directed towards correctly predicting the harmonic vibrational frequencies of ClF₂. Because ClF₂ is weakly bound (like ozone), the CCSD(T) level of theory may be necessary for this purpose.

II. METHODS

Several different basis sets were used in this study. The smallest basis set, consisted of the standard Huzinga-Dunning-Hay¹⁸⁻²⁰ double- ζ set of contracted Gaussian functions with a set of *d*-type polarization functions appended to each atom. The resultant basis, (9s5p1d/4s2p1d) for fluorine and (11s7p1d/6s4p1d) for chlorine, was designated the double- ζ plus polarization (DZP) basis. The polarization function orbital exponents were $\alpha_d(\text{Cl})=0.75$ and $\alpha_d(\text{F})=1.00$. A larger, more flexible basis, the triple- ζ plus double polarization (TZ2P) set, was also employed. For the chlorine atom we used McLean and Chandler's²¹ (6s5p) contraction of Huzinga's (12s9p) primitive Gaussian set with the addition of two sets of six Cartesian *d*-type functions with orbital exponents $\alpha_d(\text{Cl})=1.5, 0.375$ for a resultant basis set of (12s9p2d/6s5p2d). For the fluorine atoms the TZ2P basis was (10s6p2d/5s3p2d), the standard Huzinga-Dunning triple- ζ basis with the addition of two sets of polarization functions, where $\alpha_d(\text{F})=2.0, 0.5$. Finally, to the TZ2P basis set, a set of higher angular momentum *f*-type polarization functions were added (TZ2P+*f*) with $\alpha_f(\text{Cl})=0.70$ and $\alpha_f(\text{F})=1.85$ for additional flexibility.

The lowest level of theory used was the self-consistent-field theory (SCF). The analytic SCF gradient method was first developed by Pulay²² in 1977 and extended to open shell systems in 1979 by Goddard, Handy, and Schaefer.²³ Electron correlation effects were included by employing the configuration interaction (CI) and coupled cluster

(CC) techniques.²⁴ Only the valence orbitals were correlated, holding the seven core orbitals doubly occupied and excluding the corresponding seven highest-lying virtual orbitals. All other single and double excitations (SD) from the SCF reference function were included. With the TZ2P+*f* basis set, the correlated wave functions of the ²A₁ state involved 127 647 configurations in C_{2v}-symmetry and 254 678 configurations in C_s symmetry in the Hartree-Fock interacting space.^{25,26} Determination of these CISD wave functions proceeded via the shape driven graphical unitary group approach.²⁷ The contributions from unlinked cluster quadruple excitations to the CISD energies were estimated using the Davidson correction,^{28,29} and results incorporating this appendage are denoted CISD+Q.

CCSD techniques were first developed for the closed shell case by Purvis and Bartlett³⁰ and modified by Scuseria, Janssen, and Schaefer.³¹ Scuseria³² then extended his CCSD method to open-shell systems. Connected triple excitations were included using the CCSD(T) method originally proposed by Raghavachari, Trucks, Pople, and Head-Gordon.³³ The CCSD(T) methods employed here are those of Scuseria.³²

Using restricted Hartree-Fock SCF^{24,34} and CISD^{35,36} analytic gradient techniques, the molecular structure for ClF₂ has been completely optimized (within C_{2v} symmetry constraints) to Cartesian and internal coordinate gradients less than 10⁻⁶ atomic units. Quadratic force constants were evaluated using analytic second derivative techniques for the SCF^{37,38} wave functions and finite differences of analytic first derivatives for the CISD wave functions. For the CC methods, the molecular geometry was optimized through gradients obtained by numerical differentiation of the energy at displaced geometries. Quadratic force constants were evaluated using finite differences of the energy for the CCSD and CCSD(T) wave functions in conjunction with the numerical differentiation techniques of Bickley.³⁹ Vibrational anharmonicities were evaluated using the techniques of Clabo *et al.*⁴⁰

III. ELECTRONIC STRUCTURE CONSIDERATIONS

Two possible linear configurations were considered in terms of *D*_{∞h}-symmetry orbitals as defined by Cotton⁴¹ with the molecule along the *D*_∞-symmetry axis:

$$(^2\Sigma_g)[\text{core}](4\sigma_g)^2(3\sigma_u)^2(5\sigma_g)^2 \\ \times (4\sigma_u)^2(2\pi_u)^4(1\pi_g)^4(3\pi_u)^4(6\sigma_g), \quad (1)$$

$$(^2\Pi_u)[\text{core}](4\sigma_g)^2(3\sigma_u)^2(5\sigma_g)^2 \\ \times (4\sigma_u)^2(2\pi_u)^4(1\pi_g)^4(6\sigma_g)^2(3\pi_u)^3, \quad (2)$$

where [core] denotes the doubly occupied nonvalence orbitals (Cl 1s, 2s, 2p_x, 2p_y, 2p_z; F 1s + 1s, 1s - 1s). A stable energy minimum was found for the ²Σ_g state on the DZP SCF potential energy surface (PES) with a bond length of 1.8028 Å. The single-reference optimized geometry of the ²Π_u state was 0.0359 hartree lower in energy than the ²Σ_g state with a bond length 0.1288 Å smaller. The ²Π_u state,

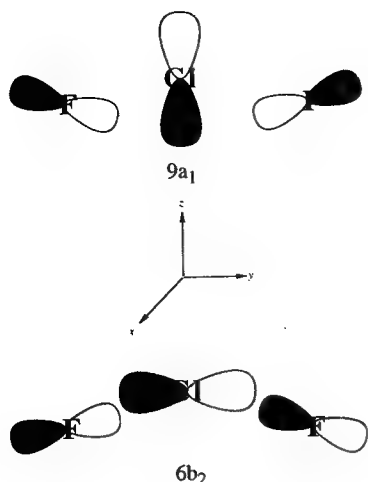


FIG. 1. Pictorial representation of the singly-occupied $9a_1$ (SOMO) and doubly-occupied $6b_2$ (LUMO) molecular orbitals. The molecule lies in the yz plane.

however, has an imaginary frequency along the bending coordinate. Upon bending, the ${}^2\Pi_u$ state splits into two components in C_{2v} symmetry:

$$({}^2A_1)[\text{core}](5a_1)^2(3b_2)^2(6a_1)^2(4b_2)^2 \times (2b_1)^2(7a_1)^2(1a_2)^2(5b_2)^2(8a_1)^2(3b_1)^2(9a_1), \quad (3)$$

$$({}^2B_1)[\text{core}](5a_1)^2(3b_2)^2(6a_1)^2(4b_2)^2 \times (2b_1)^2(7a_1)^2(1a_2)^2(5b_2)^2(8a_1)^2(9a_1)^2(3b_1). \quad (4)$$

The 2A_1 state is attractive along this coordinate while the 2B_1 state is repulsive, corresponding to Renner–Teller splitting type (c) as described by Lee *et al.*⁴² Previous studies^{11,12} found Eq. (3) to be the ground state of ClF₂, and this study confirms this finding with the bent 2A_1 state significantly lower in energy than both linear states [Eqs. (1) and (2)].

The singly-occupied molecular orbital (SOMO) of the ground state is the weakly antibonding $9a_1$ orbital (Fig. 1).

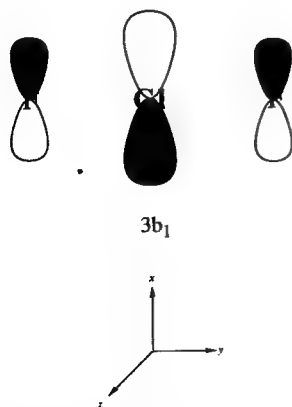


FIG. 2. Pictorial representation of the doubly-occupied $3b_1$ (HOMO) molecular orbital. The molecule lies in the xy plane perpendicular to the plane of the molecule.

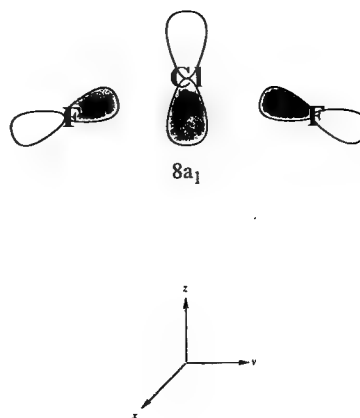


FIG. 3. Pictorial representations of the doubly-occupied $8a_1$ (SHOMO) molecular orbital. The molecule lies in the yz plane.

The highest-occupied molecular orbital (HOMO) is the $3b_1$ nonbonding orbital (Fig. 2). This MO is analogous but perpendicular to the $9a_1$ MO. In the linear ${}^2\Pi_u$ state [Eq. (2)] these two MOs form the $3\pi_u$ MO.

The lowest-unoccupied molecular orbital (LUMO) for the ground state is the $6b_2$ MO (Fig. 1). This MO has somewhat greater antibonding character than the $9a_1$ MO. In this study, excitation from the $9a_1$ to the $6b_2$ orbital revealed a dissociative PES at the DZP SCF level of theory. More sophisticated studies¹² found that a high energy excited state with this occupation may exist. The second-highest-occupied molecular orbital (SHOMO), the $8a_1$ MO, is depicted in Fig. 3. This bonding MO is an important consideration in the chemistry of ClF₂.

IV. RESULTS

The predicted geometry of the $\tilde{X}{}^2A_1$ ClF₂ is displayed in Fig. 4. The total energy, dipole moment, harmonic vibrational frequencies, IR intensities, and zero-point vibrational energy for the ClF₂ molecule in its ground state are presented in Table I. In Table I, the chlorine atom is assigned atomic mass 35. Predicted harmonic vibrational frequencies for the ${}^{37}\text{ClF}_2$ isotopomer are listed in Table II. Table III contains anharmonic corrections to the CISD wave function harmonic vibrational frequencies.

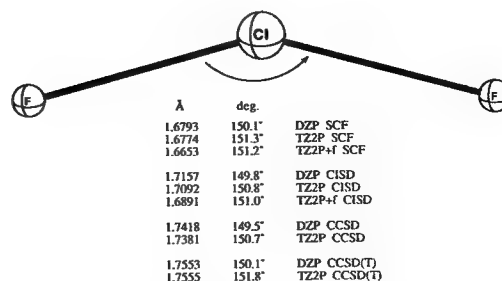


FIG. 4. Predicted structure for $\tilde{X}{}^2A_1$ ClF₂.

TABLE I. Theoretical predictions of the molecular structure and physical properties for the ³⁵ClF₂ ground state (\tilde{X}^2A_1).^{a,b}

Level of theory	Energy	Dipole moment	$\omega_1 (a_1)$		$\omega_2 (a_1)$		$\omega_3 (b_2)$		ZPVE
			cm ⁻¹	IR	cm ⁻¹	IR	cm ⁻¹	IR	
DZP/SCF	-658.173 440	0.941	652	6	321	19	543	311	2.17
TZ2P/SCF	-658.246 550	0.808	655	8	306	13	614	420	2.25
TZ2P + <i>f</i> /SCF	-658.255 776	0.789	664	8	313	13	626	437	2.29
DZP/CISD	-658.644 774	0.929	602	4	292	15	537	196	2.04
TZ2P/CISD	-658.820 805	0.789	610	5	284	10	580	283	2.11
TZ2P + <i>f</i> /CISD	-658.900 897	0.763	628	5	293	10	605	305	2.18
DZP/CCSD	-658.703 419		552		273		498		1.89
TZ2P/CCSD	-658.898 070		562		263		537		1.95
DZP/CCSD(T)	-658.719 644		527		257		537		1.81
TZ2P/CCSD(T)	-658.925 064		536		243		568		1.93
Expt. ^c			536		242		578		
Expt. ^d			500				578		

^aEnergies are in hartrees, dipole moments are in debye, harmonic vibrational frequencies in cm⁻¹, IR intensities in km mol⁻¹, and zero point vibrational energies (ZPVE) in kcal/mol⁻¹.

^bWith inclusion of the Davidson correction, the CISD+Q energies are -658.698 669, -658.820 805, and -658.977 619 hartree for the DZP, TZ2P, and TZ2P + *f* basis sets, respectively.

^cExperimental fundamental vibrational frequencies from Mamantov *et al.* (Ref. 8).

^dExperimental fundamental vibrational frequencies from Prochaska and Andrews (Ref. 9).

V. DISCUSSION

A. Geometry

In this work, all theoretical predictions for the ClF₂ bond angle (Fig. 4) fall, between 149.5° and 151.8°, a surprisingly narrow range. These values lie easily above Prochaska's⁹ 136° lower limit, and within Mamantov's experimentally estimated range of 140 ± 19°. This bond angle is primarily determined by the doubly-occupied 8a₁ MO and the singly-occupied 9a₁ MO. When occupied the 8a₁ MO prefers to bend in the yz plane in order to increase the bonding character; it is largely responsible for the strongly bent structure of 20 valence electron (VE) triatomics such

as OF₂ (θ₀ = 103.2°).⁴³ Bending, however, increases the antibonding character of the 9a₁ MO which, when doubly occupied, results in linear 22 VE triatomics such as XeF₂.⁴⁴ In ClF₂, because the 9a₁ MO is only singly occupied, it straightens the molecule to an angle midway between the 20 and 22 VE triatomic cases. Our most reliable prediction of the ClF₂ bond angle, at the TZ2P CCSD(T) level of theory, is 151.8°.

Although no experimental data is available concerning the Cl-F bond lengths in ClF₂, there are previous theoretical results. Ungemach and Schaefer¹¹ predicted a bond length of 1.83 Å with the DZ SCF method. Sannigrahi and Peyerimhoff¹² obtained values of 1.681 Å for the SCF method and 1.700 Å for the MRD CI method, using a basis set similar to DZP but with additional functions located along the Cl-F bonds. It can be seen in Fig. 4 that in the present research, the ClF bond length decreases steadily with improvements in basis set quality at all levels of theory excluding the CCSD(T) results. This implies that neither Ungemach nor Sannigrahi used sufficiently extensive basis sets. Further, predictions of the Cl-F bond distance increase dramatically with increased electron correlation. Therefore, levels of electron correlation as extensive as CCSD(T) are *required* to quantitatively predict this bond length. We feel that our prediction at the TZ2P

TABLE II. ³⁷ClF₂ Isotopomer harmonic vibrational frequencies (in cm⁻¹) for the electronic ground state (\tilde{X}^2A_1).

Level of theory	$\omega_1 (a_1)$	$\omega_2 (a_1)$	$\omega_3 (b_2)$
DZP/SCF	651	316	535
TZ2P/SCF	654	303	606
TZ2P + <i>f</i> /SCF	663	309	618
DZP/CISD	601	288	529
TZ2P/CISD	609	281	572
TZ2P + <i>f</i> /CISD	627	290	596
DZP/CCSD	551	269	491
TZ2P/CCSD	561	259	530
DZP/CCSD(T)	526	253	529
TZ2P/CCSD(T)	536	240	560
Expt. ^b			570
Expt. ^c			570

^aExperimental fundamental vibrational frequencies from Mamantov *et al.* (Ref. 8).

^bExperimental fundamental vibrational frequencies from Prochaska and Andrews (Ref. 9).

TABLE III. ClF₂ anharmonicity deltas and (in cm⁻¹) of the electronic ground state (\tilde{X}^2A_1).

Level of theory	$\omega_1 (a_1)$ delta	$\omega_2 (a_1)$ delta	$\omega_3 (b_2)$ delta
DZP/CISD	-27	-4	-50
TZ2P/CISD	-17	-2	-34
TZ2P + <i>f</i> /CISD	-18	-2	-33

CCSD(T) level of theory [$r_e(\text{Cl-F}) = 1.756 \text{ \AA}$] is the most reliable to date. In a recent study by Thomas *et al.*,⁴⁵ the error in theoretical predictions using various combinations of theoretical method and basis set were studied for on a wide range of molecules. They found that for the CCSD(T) method with a TZ2P basis set, the average absolute error for theoretical predictions of equilibrium bond lengths is only 0.21%.

Another interesting comparison of bond length can be made with the experimental diatomic ClF result from Herzberg and Huber.⁴⁶ That value, $r_0 = 1.628 \text{ \AA}$, is 0.128 \AA smaller than the Cl-F length determined herein at the TZ2P CCSD(T) level of theory. This is understandable when the differences between the two species are considered. The two bonds in ClF_2 are constructed from two doubly-occupied bonding MOs and a singly-occupied antibonding MO. Thus while the bond order is 1 in ClF, it is 3/4 in ClF_2 .

B. Harmonic vibrational frequencies and IR intensities

Following a pattern similar to Scuseria's¹¹ *ab initio* results for ozone, the ω_1 and ω_3 frequencies come closer and closer together with higher levels of theory and increasing basis set until the order is reversed at the DZP CCSD(T) level of theory. In addition, upon examination of bond lengths and angles, it is apparent that basis set size has a considerable effect and is expected to be necessary for quantitative accuracy of harmonic vibrational frequencies. In another study by Thomas *et al.*,⁴⁷ theoretical harmonic vibrational frequencies were found to underestimate experimental results when small basis sets were used with high level theoretical methods. Simultaneous use of the TZ2P + f basis and coupled cluster methods, however, was too expensive to be tractable. According to Thomas,⁴³ TZ2P CCSD(T) harmonic vibrational frequency predictions have an average absolute error of 2.3%. It seems likely from basis set trends for SCF and CI that TZ2P + f coupled cluster frequencies would be increased by about 20 cm^{-1} with respect to TZ2P coupled cluster frequencies, making all predicted harmonic frequencies larger than the experimental fundamental frequencies.

1. Asymmetric stretch (b_2)

The percentage differences between the predicted and the experimental (578 cm^{-1}) $^{35}\text{ClF}_2$ asymmetric stretching frequency of Mamantov *et al.*⁸ are 6.1%, 6.2%, and 8.3% at the SCF level with the increasingly large basis sets. At the CISD level the corresponding differences are 7.1%, 0.3%, and 4.6%. With coupled cluster techniques, the differences are 13.8% and 7.1% for CCSD and 7.1% and 1.7% for CCSD(T) with the DZP and TZ2P basis sets, respectively. Mamantov and Prochaska both report isotopic splittings of the b_2 stretching frequencies into a doublet with a separation of 7.6 cm^{-1} and 8 cm^{-1} , respectively, due to $^{35}\text{ClF}_2$ and $^{37}\text{ClF}_2$ isotopic splitting. In the present investigation isotopic splitting due to $^{37}\text{ClF}_2$ was $8.0 \pm 0.7 \text{ cm}^{-1}$ in good agreement with experiment. Recall that the asymmetric stretch is the mode for which the Mamantov^{7,8}

and Andrews⁹ experimental assignments are in agreement. The excellent agreement between the TZ2P CCSD(T) theoretical prediction for this mode and the experimental assignments lends confidence that the predictions will be as good for the other modes.

2. Bend (a_1)

Compared to Mamantov's experimental fundamental of 242 cm^{-1} for the bending vibration, the predicted SCF values differ by 33%, 26%, and 29% while the CISD frequencies differ by 21%, 17%, and 21% for increasing basis sets. This peak assignment was considered "tentative" by Prochaska and the SCF and CISD findings would also suggest a possible misassignment. The more advanced CC techniques, however, bring the difference with experiment down to 12.8% and 8.7% for CCSD DZP/TZ2P, and 6.2% and 0.6% for CCSD(T) DZP/TZ2P, further demonstrating the necessity of these methods for correct frequency assignment. Mamantov's experimental intensity of this peak was 5% relative to the asymmetric bending mode's intensity. The average predicted relative intensity of the bending mode is $4.6 \pm 1.6\%$. This kind of difference between theory and experiment is remarkably close. Therefore, the 242 cm^{-1} assignment of Mamantov *et al.* should no longer be considered "tentative" as suggested by Prochaska and Andrews. Theoretical predictions of the $^{37}\text{ClF}_2$ bending frequency indicate a shift of $-3.5 \pm 0.6 \text{ cm}^{-1}$. There is no experimental evidence for this shift most likely due to spectra resolution. The present study indicates that isotopic splitting of the bending mode should be resolvable upon closer examination.

3. Symmetric stretch (a_1)

For the symmetric stretching mode Mamantov assigned a frequency of 536 cm^{-1} where Prostroka and Andrews assigned it to the Raman active feature at 500 cm^{-1} . In comparison to Mamantov's 536 cm^{-1} assignment, the predicted SCF frequencies differ by 21%, 22%, and 23% for increasing basis sets while the corresponding differences for CISD are 12%, 14%, and 17%. For CCSD with DZP and TZ2P basis sets, the percentage difference with experiment are 3.0% and 4.9%, respectively, and, 1.2% and 0.1% for CCSD(T) with DZP and TZ2P basis sets. Mamantov also gives the relative intensity of the 536 cm^{-1} peak compared to the asymmetric stretch at 3%. The relative intensity of the symmetric stretch in this study is $2.0 \pm 0.4\%$ in with all basis sets at the SCF and CISD levels of theory. Thus, theory favors Mamantov's assignment over Prochaska's. Theoretical predictions on the $^{37}\text{ClF}_2$ isotopomer indicate a shift of $1.0 \pm 0.2 \text{ cm}^{-1}$ at all levels of theory with all basis sets. There is no experimental evidence for splitting of this mode nor is any likely due to the small degree of separation.

C. Anharmonic corrections to harmonic vibrational frequencies

The predicted harmonic vibrational frequencies at the TZ2P CCSD(T) level of theory are disturbingly close to

the experimental fundamental frequency assignments of Mamantov *et al.*,^{7,8} indicating a fortuitous cancellation of errors due to basis set incompleteness and anharmonicity. Assuming, not unreasonably, similar basis set trends for the correlated CISD and CCSD(T) methods, we can project the TZ2P+*f* CCSD(T) harmonic frequencies to be 554, 252, and 593 cm⁻¹ for the symmetric stretch, bend and asymmetric stretch respectively. Again assuming that CISD is a reasonable approximation to CCSD(T), the CISD anharmonic corrections can be used in conjunction with CCSD(T). Table III indicates that the corrections due to anharmonicity stabilize with basis sets larger than DZP. In this manner the predicted fundamental frequencies become 536, 250, and 560 cm⁻¹ for the symmetric stretch, bend and asymmetric stretch respectively. These approximations, although fairly qualitative, again indicate that theory agrees best with Mamantov's assignments of the fundamental vibrational frequencies. To truly close the controversy of these vibrational assignments would require either a superb theoretical study [equivalent to TZ2P+*f* CCSD(T) or MRD CI with anharmonic corrections] or experimental revisitation of the problem.

VI. CONCLUSIONS

The ground state of chlorine difluoride has been investigated with state-of-the-art *ab initio* techniques and with larger basis sets than previously used. All combinations of basis set and theoretical method indicate a structure which is bent beyond a doubt with an angle θ_e (FCIF) between 149.5° and 151.8°. Our most reliable results, the TZ2P CCSD(T) level of theory, yield an angle of 151.8 and a bond length of 1.756 Å. Vibrational frequencies have also been determined indicating that the assignments of Mamantov *et al.*⁷ are preferable to those of Prochaska and Andrews. As previously postulated,^{15,16} reliable predictions of vibrational frequencies, especially the qualitative ordering of the stretching modes, could not be made without use of coupled cluster techniques. Anharmonicity corrections also proved useful.

ACKNOWLEDGMENTS

This research was supported by the United States Air Force Office of Scientific Research under Grant No. AFOSR-92-J-0047. This material is based upon work supported in part by a Department of Defense Graduate Fellowship to G. V. We would like to thank Dr. Gustavo E. Scuseria for the CCSD(T)^{31,32} codes used in this research. We are also grateful to Dr. Roger "Sparky" Grev for advice on numerical differentiation techniques, and Dr. Yukio Yamaguchi for help with wave function stabilities.

¹A. D. Walsh, *J. Chem. Soc.* **1953**, 2266.

²D. H. Boal and G. A. Ozin, *J. Chem. Phys.* **55**, 3598 (1971).

³L. Y. Nelson and G. C. Pimentel, *J. Chem. Phys.* **47**, 3671 (1967).

⁴B. R. De and A. B. Sannigrahi, *Int. J. Quantum Chem.* **19**, 485 (1981).

⁵A. B. Sannigrahi and S. D. Peyerimhoff, *Int. J. Quantum Chem.* **30**, 413 (1986).

⁶T. G. Wright, A. J. Bell, and J. G. Frey, *Chem. Phys. Lett.* **189**, 297 (1991).

⁷G. Mamantov, D. G. Vickroy, T. Mackawa, E. J. Vasini, and M. C. Moulton, *Inorg. Nucl. Chem. Lett.* **8**, 701 (1970).

⁸G. Mamantov, E. J. Vasini, M. C. Moulton, D. G. Vickroy, and T. Mackawz, *J. Chem. Phys.* **54**, 3419 (1971).

⁹E. S. Prochaska and L. Andrews, *Inorg. Chem.* **16**, 339 (1977).

¹⁰B. M. Deb, G. D. Mahajan, and V. S. Vasan, *Pramana* **9**, 93 (1977).

¹¹S. R. Ungemach and H. F. Schaefer, *J. Am. Chem. Soc.* **98**, 1658 (1976).

¹²A. B. Sannigrahi and S. D. Peyerimhoff, *Chem. Phys. Lett.* **114**, 6 (1985).

¹³J. A. Hodgeson, E. E. Sibert, and R. F. Curl, *J. Phys. Chem.* **67**, 2833 (1963).

¹⁴A. Barbe, C. Secroun, and P. Jouve, *J. Mol. Spectrosc.* **49**, 171 (1974).

¹⁵G. E. Scuseria, T. J. Lee, A. C. Scheiner, and H. F. Schaefer, *J. Chem. Phys.* **90**, 5635 (1989).

¹⁶P. Borowski, K. Andersson, P.-Å. Malmqvist, and B. O. Roos, *J. Am. Chem. Soc.* (in press).

¹⁷T. J. Lee and G. E. Scuseria, *J. Chem. Phys.* **93**, 489 (1990).

¹⁸S. Huzinaga, *J. Chem. Phys.* **42**, 1923 (1965).

¹⁹T. H. Dunning, *J. Chem. Phys.* **53**, 2823 (1970).

²⁰T. H. Dunning and P. J. Hay, in *Modern Theoretical Chemistry*, edited by H. F. Schaefer (Plenum, New York, 1977), Vol. 3, p. 1ff.

²¹A. D. McLean and G. S. Chandler, *J. Chem. Phys.* **72**, 5639 (1980).

²²P. Pulay, in *Modern Theoretical Chemistry*, edited by H. F. Schaefer (Plenum, New York, 1977), Vol. 4, pp. 152-185.

²³J. P. Goddard, N. C. Handy, and H. F. Schaefer, *J. Chem. Phys.* **71**, 1525 (1979).

²⁴See, for example, T. Helgaker and P. Jorgensen, *Adv. Quantum Chem.* **19**, 183 (1988).

²⁵A. Bunge, *J. Chem. Phys.* **53**, 20 (1970).

²⁶C. F. Bender and H. F. Schaefer, *J. Chem. Phys.* **55**, 4789 (1971).

²⁷P. Saxe, D. J. Fox, H. F. Schaefer, and N. C. Handy, *J. Chem. Phys.* **77**, 5584 (1982).

²⁸S. R. Langhoff and E. R. Davidson, *Int. J. Quantum Chem.* **8**, 61 (1974).

²⁹E. R. Davidson, in *The World of Quantum Chemistry*, edited by R. Daudel and B. Pullman (Reidel, Dordrecht, 1974), p. 17.

³⁰G. D. Purvis and R. J. Bartlett, *J. Chem. Phys.* **76**, 1910 (1982).

³¹G. E. Scuseria, C. L. Janssen, and H. F. Schaefer, *J. Chem. Phys.* **89**, 7382 (1988).

³²G. E. Scuseria, *Chem. Phys. Lett.* **176**, 27 (1991).

³³K. Raghavachari, G. W. Trucks, J. A. Pople, and M. Head-Gordon, *Chem. Phys. Lett.* **157**, 479 (1989).

³⁴Y. Osamura, Y. Yamaguchi, and H. F. Schaefer, *J. Chem. Phys.* **77**, 383 (1982).

³⁵B. R. Brooks, W. D. Laidig, P. Saxe, J. D. Goddard, Y. Yamaguchi, and H. F. Schaefer, *J. Chem. Phys.* **72**, 4652 (1980).

³⁶J. E. Rice, R. D. Amos, N. C. Handy, T. J. Lee, and H. F. Schaefer, *J. Chem. Phys.* **72**, 963 (1986).

³⁷Y. Osamura, Y. Yamaguchi, P. Saxe, M. A. Vincent, J. F. Gaw, and H. F. Schaefer, *Chem. Phys.* **72**, 131 (1982).

³⁸Y. Yamaguchi, Y. Osamura, P. Saxe, D. J. Fox, M. A. Vincent, and H. F. Schaefer, *J. Mol. Struct.* **103**, 183 (1983).

³⁹W. G. Bickley, *Math. Gaz.* **25**, 19 (1941).

⁴⁰D. A. Clabo, W. D. Allen, R. B. Remington, Y. Yamaguchi, and H. F. Schaefer, *Chem. Phys.* **123**, 187 (1988).

⁴¹F. A. Cotton, *Chemical Applications of Group Theory* (Wiley, New York, 1990), third ed.

⁴²T. J. Lee, D. J. Fox, H. F. Schaefer, and R. M. Pitzer, *J. Chem. Phys.* **81**, 356 (1984).

⁴³W. H. Kirchhoff, *J. Mol. Spectrosc.* **41**, 333 (1972).

⁴⁴E. S. Pysh, J. Jortner, and S. A. Rice, *J. Chem. Phys.* **40**, 2018 (1964).

⁴⁵J. R. Thomas, B. J. Deleew, G. Vacek, T. D. Crawford, Y. Yamaguchi, and H. F. Schaefer, *J. Chem. Phys.* (to be published).

⁴⁶K. P. Huber and G. Herzberg, *Constants of Diatomic Molecules* (Van Nostrand Reinhold, New York, 1977), p. 150.

⁴⁷J. R. Thomas, B. J. Deleew, G. Vacek, and H. F. Schaefer, *J. Chem. Phys.* **98**, 1336 (1993).

The \tilde{X} AlOH- \tilde{X} HAIO isomerization potential energy hypersurface

George Vacek,^{a)} Bradley J. DeLeeuw,^{b)} and Henry F. Schaefer III
Center for Computational Quantum Chemistry, University of Georgia, Athens, Georgia 30602

(Received 28 January 1993; accepted 17 February 1993)

Ab initio molecular electronic structure theory has been used to study the AlOH-HAIO unimolecular isomerization reaction on the singlet ground state potential energy surface. Electron correlation effects were included via configuration interaction and coupled-cluster methods. Basis sets as complete as triple zeta plus two sets of polarization functions and a set of higher angular momentum functions [TZ(2*df*,2*pd*)] were employed. The *classical* barrier for hydrogen migration from \tilde{X} HAIO to \tilde{X} AlOH is predicted to be 38.4 kcal mol⁻¹ using the TZ(2*df*,2*pd*) basis set with the coupled-cluster method including all single and double excitations with the effect of connected triple excitations included perturbatively [CCSD(T)]. After correction for zero-point vibrational energies (ZPVEs), an activation energy of 36.6 kcal mol⁻¹ is obtained. The ΔE for isomerization is -42.2 (-40.5 with ZPVE correction) kcal mol⁻¹ at the same level of theory. The dipole moments of HAIO and AlOH in their equilibrium geometries are 4.525 and 1.040 Debye, respectively, at the same level of theory. A comparison is also made between a theoretically predicted harmonic vibrational frequency and a recently determined experimental fundamental frequency for \tilde{X} AlOH.

I. INTRODUCTION

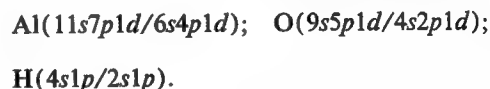
Metal hydroxides are often the result of metal atom insertion or elimination reactions with water in environments undergoing metal ablation, sputtering, or combustion. The simplest of these, metal monohydroxides, form a class of molecules upon which to test elementary concepts of chemical bonding. Nonlinearity of metal hydroxides is thought to indicate the extent to which the metal-hydroxide bond is covalent rather than ionic. Covalent bonding tends to favor bent structures [e.g., H₂O, BOH¹], while ionic bonding favors linear structures [e.g., CaOH,² SrOH,³ BaOH⁴]. MgOH,⁵ which is quasilinear, may be considered to have an ionic bond with covalent features. Evidence suggests that the linearity, nonlinearity, or quasilinearity of a molecule may be qualitatively predicted from simple electronegativity arguments. Atoms such as B and Cu with electronegativities near that of hydrogen (2.2) form bent monohydroxides.^{1,6} Atoms with electronegativities near or below 1, like most alkali metals^{7,8} and alkaline earths,²⁻⁴ turn out to be linear. Mg has an electronegativity between these two extremes (1.31), and MgOH turns out to be quasilinear.⁵ Al has an electronegativity of 1.61, so AlOH might also be expected to be quasilinear.

Recently, the first observation of an electronic spectrum for \tilde{X} AlOH has been reported by Pilgrim, Robbins, and Duncan.⁹ The presumed structure and bonding of the system was also discussed. Since they produced the subject of their research through aluminum insertion into water, it was initially unclear whether their spectrum should be assigned to the AlOH or HAIO isomer. Previous theoretical studies,^{10,11} mass-spectrometric analyses,¹² and infrared¹³ (IR) and optical¹⁴ assignments did not provide sufficient

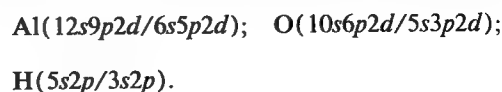
information about the relative stabilities and the vibrational frequencies of these two species for them to make a satisfactory assignment. In this paper, we present results of our inquiry into the isomerization reaction from \tilde{X} AlOH to \tilde{X} HAIO and the associated potential energy surface (PES). Some of the data reported herein was crucial to Pilgrim *et al.*⁹ assignments. We are confident that it will be helpful to future experimental studies of these two interesting isomers.

II. THEORETICAL METHODS

Three different basis sets were used in this research. The double zeta plus polarization basis (DZP) is a standard Huzinaga-Dunning-Hay^{15,16} double- ζ set of contracted Gaussian functions augmented by a set of six Cartesian *d*-like polarization functions on oxygen [$\alpha_d(O)$ = 0.85] and aluminum [$\alpha_d(Al)$ = 0.40] and a set of *p*-type polarization functions on hydrogen [$\alpha_p(H)$ = 0.75]. The contraction scheme for the DZP basis is thus:



The triple zeta plus double polarization basis (TZ2P) is triple- ζ in the valence region and adds two sets of polarization functions per atom [$\alpha_d(Al)$ = 0.8, 0.2; $\alpha_d(O)$ = 1.7, 0.425; $\alpha_p(H)$ = 1.5, 0.375]. For hydrogen and oxygen, standard Huzinaga-Dunning^{15,17} sets of contracted Gaussian functions were used. For aluminum, McLean and Chandler's¹⁸ contraction of Huzinaga's 12s9p primitive Gaussian set was used. The contraction scheme for the TZ2P basis is as follows:



^{a)}DOD Predoctoral Fellow, Egil A. Hylleraas Fellow.

^{b)}NSF Predoctoral Fellow, John C. Slater Graduate Fellow.

The TZ(2df,2pd) basis was formed by adding a set of higher angular momentum polarization functions [$\alpha_f(\text{Al}) = 0.25$; $\alpha_f(\text{O}) = 1.4$; and $\alpha_f(\text{H}) = 1.0$] to the TZ2P basis.

The restricted Hartree-Fock self-consistent field (SCF) method was initially employed in this study. The effects of electron correlation were taken into account using the method of configuration interaction including all single and double excitations from an SCF reference wave function (CISD), the coupled-cluster method including all single and double excitations (CCSD), and the CCSD method with the effect of connected triple excitations included perturbatively [CCSD(T)]. The two lowest (aluminum and oxygen 1s-like) SCF molecular orbitals were constrained to be doubly occupied, and the corresponding two highest virtual orbitals were deleted from the correlation procedure. With the TZ(2df,2pd) basis, this resulted in a total of 72 311 configurations in C_{2v} symmetry and 138 919 configurations in C_s symmetry.

The structures of ground state AlOH, HAIO, and the transition state connecting them via hydrogen migration were fully optimized using closed-shell analytic gradient techniques at the SCF,¹⁹⁻²¹ CISD,²²⁻²⁴ CCSD,²⁵ and CCSD(T)²⁶ levels of theory. Harmonic vibrational frequencies were obtained using analytic SCF second-derivative techniques²⁷⁻²⁹ and central finite differences of analytic CISD, CCSD, and CCSD(T) gradients.

Relative energies designated CISD+Q were obtained for the various isomers studied here by adding the Davidson correction^{30,31} for unlinked quadruple excitations to the CISD energy.

III. DISCUSSION

A. Geometry

Walsh's rules³² predict that both AlOH and HAIO should have linear ground state structures, just like the isovalent molecules HCN and HNC. Furthermore, it can be expected from the same rules that the lowest excited states of AlOH and HAIO should be bent and have similar bond angles. However, even in the simple case of the excited states of HCN and HNC, it has been shown³³ that Walsh concepts are not well followed.

As shown in Fig. 1, the use of a DZP quality basis set leads to the prediction of a linear \tilde{X} AlOH structure with all theoretical methods employed here. Previous theoretical results^{10,11} also predicted AlOH to be linear using basis sets similar in extent to our DZP basis. However, with the more complete TZ2P basis set, we predict a geometry that is quite bent ($\sim 151^\circ$). This *qualitative* difference between the DZP and TZ2P equilibrium \tilde{X} AlOH geometries implies that the use of still larger basis sets is desirable. It is not uncommon for a basis set with extensive character in the *spd* space but no higher angular momentum functions to prefer, somewhat erroneously, a bent geometry over a linear one.^{34,35} In such cases, further study with basis sets which do incorporate *f*-type functions will usually lead to an accurate prediction of both geometry and harmonic vibrational frequencies.^{36,37}

Thus our best prediction of the equilibrium geometry

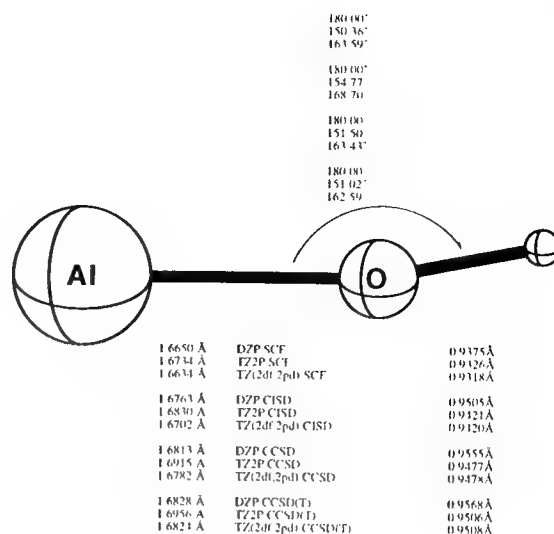


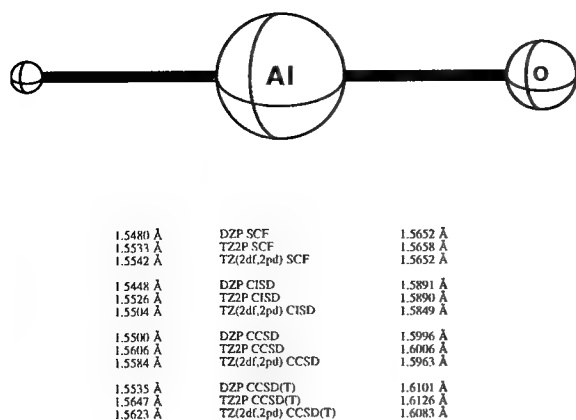
FIG. 1. Predicted equilibrium geometry for \tilde{X} AlOH.

of AlOH is at the TZ(2df,2pd) CCSD(T) level of theory, where the bond angle is predicted to be 162.6° . At this level of theory, we see essentially a hydroxide group with a tight single bond [$r_e(\text{OH}) = 0.951 \text{ \AA}$]. The experimentally estimated value of $r_e(\text{OH}^-)$ lies within 0.001 \AA ³⁸ of the $r_e(\text{OH})$ value, 0.970 \AA .³⁹ This "hydroxide group" is ionically bonded to the partially positive Al atom [$r_e(\text{AlO}) = 1.682 \text{ \AA}$]. Plots of the $9a'$ molecular orbital (MO) show that it is essentially a lone pair of electrons in an Al 3s orbital slightly polarized along the molecular axis by the Al $3p_z$ orbital to produce a weak sigma type interaction between this "lone pair" and the hydroxide group.

It is important to note that despite the bent equilibrium geometry of AlOH, it can at best be referred to as quasilinear. For many of the levels of theory utilized in this paper, barriers to linearity were calculated. In all cases, the predicted barrier to linearity was less than 1 kcal mol^{-1} . Thus the ZPVE is greater than the linearity barrier. In many experimental set-ups, the "averaged" linear geometry would be observed. The predicted bond angle is significantly larger than that predicted for \tilde{X} BOH ($\theta_e = 125^\circ$),¹ which has a truly bent structure. This structural difference between AlOH and BOH is in agreement with the qualitative predictions based upon electronegativities mentioned in the Introduction.

The structure of \tilde{X} HAIO, depicted in Fig. 2, was predicted to be linear at all levels of theory, in accordance with Walsh's rules.³² The best results, at the TZ(2df,2pd) CCSD(T) level of theory, show $r_e(\text{AlH}) = 1.562 \text{ \AA}$ and $r_e(\text{AlO}) = 1.608 \text{ \AA}$. The AlH bond distance is somewhat short compared to the 1.6478 \AA bond length of diatomic AlH.³⁹ Presumably, this is due to the greater *s* character within the AlH bond of HAIO as compared to that of the diatomic. According to Huber and Herzberg,³⁹ the bond length of the AlO diatomic molecule (with a bond order of 2.5) is 1.6179 \AA .

Figure 3 shows the transition state for the hydrogen migration from AlOH to HAIO. The hydrogen is closer to Al than O, which agrees nicely with Hammond's Postulate

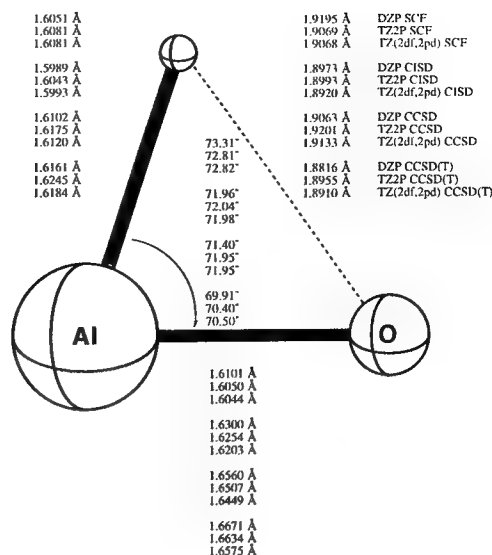
FIG. 2. Predicted equilibrium geometry for \bar{X} HAIO.

for endothermic reactions,⁴⁰ since HAIO is much higher in energy than AlOH. The best description of the transition state structure should again be the TZ(2df,2pd) CCSD(T) results.

B. Harmonic vibrational frequencies

Typically, the harmonic vibrational frequencies of a molecule are only predicted accurately at levels of theory where the predicted geometry is qualitatively correct. We suspect that only the frequencies predicted with the TZ(2df,2pd) basis set and reasonable levels of electron correlation will thus be accurate to an acceptable degree. Specifically, we expect that the TZ(2df,2pd) CCSD(T) level of theory to give excellent results.³⁷

At the TZ(2df,2pd) CCSD(T) level of theory, our predictions of the harmonic vibrational frequencies of AlOH, found in Table I, are 4017, 845, and 155 cm^{-1} for the OH stretching, AlO stretching, and the bending frequencies. The only experimentally assigned fundamental

FIG. 3. Predicted structure for C_s -symmetry transition state for the \bar{X} AlOH \leftrightarrow \bar{X} HAIO isomerization reaction.

vibrational frequency in the gas phase is that of Pilgrim.⁹ A $\Delta G_{1/2}$ value of 895 cm^{-1} was tentatively assigned to the AlO stretching mode. This is higher than our prediction, but the agreement is still acceptable. It is also conceivable that Pilgrim observed a combination band of the AlO stretch and the AlOH bend. The sum of our harmonic vibrational predictions is 1000 cm^{-1} , nicely above Pilgrim's 895 cm^{-1} fundamental. Our predictions for the two harmonic stretching vibrational frequencies are also in satisfactory agreement with the fundamental stretching frequencies of Hauge *et al.*¹³ ($\nu_1=3790$, $\nu_2=810$ cm^{-1}), which were measured in a noble gas matrix. The disagreement between these two experimental ν_2 assignments is somewhat surprising.

For the HAIO conformer, Table II, the TZ(2df,2pd)

TABLE I. Theoretical predictions of the total energy (in Hartrees), dipole moment (in Debye), harmonic vibrational frequencies (in cm^{-1}), infrared (IR) intensities (in km mol^{-1}), and zero-point vibrational energy (ZPVE) (in kcal mol^{-1}) for \bar{X} AlOH.

Level of theory	Energy	μ	Harmonic vibrational frequencies / IR intensities			ZPVE
			$\omega_1(a_1/a')^a$	$\omega_2(a_1/a')^a$	$\omega_3(e_1/a')^a$	
DZP SCF	-317.417 730	1.355	4331/172	897/176	150/467	7.903
TZ2P SCF	-317.444 597	1.324	4298/123	871/153	257/177	7.757
TZ(2df,2pd) SCF	-317.447 545	1.318	4313/139	884/167	155/193	7.651
DZP CISD ^b	-317.745 905	1.134	4160/121	882/155	134/461	7.591
TZ2P CISD ^b	-317.819 728	1.127	4143/97	850/145	197/175	7.419
TZ(2df,2pd) CISD ^b	-317.848 834	1.097	4157/107	868/156	120/190	7.355
DZP CCSD	-317.773 831	1.027	4082/108	873/146	102/452	7.375
TZ2P CCSD	-317.853 004	1.098	4051/84	835/133	222/168	7.302
TZ(2df,2pd) CCSD	-317.884 083	1.045	4065/93	854/144	152/182	7.249
DZP CCSD(T)	-317.779 967	1.040	4057/100	869/137	79/446	7.267
TZ2P CCSD(T)	-317.864 170	1.099	4006/77	826/124	220/165	7.222
TZ(2df,2pd) CCSD(T)	-317.896 875	1.040	4017/85	845/135	155/179	7.173
Expt. (Ref. 9)			$\nu_1=3790$	$\nu_2=895$		
Expt. (Ref. 13)				$\nu_2=810.3$		

^aDZP equilibrium geometries are linear, while TZ2P and TZ(2df,2pd) are bent.

^bCISD+Q energies are -317.771 652, -317.850 438, and -317.881 655 Hartrees, respectively.

TABLE II. Theoretical predictions of the total energy (in Hartrees), dipole moment (in Debye), harmonic vibrational frequencies (in cm^{-1}), infrared (IR) intensities (in km mol^{-1}), and zero point vibrational energy (ZPVE) (in kcal mol^{-1}) for \tilde{X} HAIO.

Level of theory	Energy	μ	Harmonic vibrational frequencies /IR intensities			ZPVE
			$\omega_1(a_1)$	$\omega_2(a_1)$	$\omega_3(e_1)$	
DZP SCF	-317.330 526	5.400	2143/75	1211/62	492/358	6.201
TZ2P SCF	-317.360 729	5.540	2113/73	1198/73	483/327	6.113
TZ(2df,2pd) SCF	-317.362 558	5.537	2108/73	1198/71	486/328	6.113
DZP CISD ^a	-317.672 215	4.747	2130/66	1138/24	454/258	5.970
TZ2P CISD ^a	-317.745 697	5.032	2078/69	1126/35	445/241	5.855
TZ(2df,2pd) CISD ^a	-317.774 361	5.060	2080/68	1134/36	449/248	5.878
DZP CCSD	-317.702 429	4.532	2088/54	1105/15	429/207	5.791
TZ2P CCSD	-317.780 558	4.815	2025/60	1089/24	420/192	5.652
TZ(2df,2pd) CCSD	-317.811 470	4.847	2026/58	1098/24	424/199	5.678
DZP CCSD(T)	-317.713 115	4.214	2064/54	1065/5	407/170	5.638
TZ2P CCSD(T)	-317.797 058	4.493	2000/62	1048/10	396/157	5.492
TZ(2df,2pd) CCSD(T)	-317.829 670	4.525	2002/59	1056/10	400/163	5.517

^aCISD+Q energies are -317.701 586, -317.779 378, and -317.810 418 Hartrees, respectively.

CCSD(T) harmonic vibrational frequencies are predicted to be 2002, 1056, and 400 cm^{-1} for the AlH stretching mode, the AlO stretching mode and the bending mode, respectively. These predicted values do not match well with Pilgrim's⁹ results, thus supporting his assignment to AIOH rather than HAIO.

There are no experimental vibrational frequency assignments for HAIO. Huber and Herzberg³⁹ list experimental harmonic vibrational frequency assignments for the diatomic molecules AlH and AlO as 1683 and 979 cm^{-1} , respectively. The HAIO molecule has an AlO stretch harmonic vibrational frequency that looks just slightly perturbed from that of diatomic AlO.

Harmonic vibrational frequencies for the isotopically substituted ground states are presented in Tables III and IV. Comparison between predicted harmonic and experimentally assigned fundamentals are favorable for AlOD. The only isotopic shift for AlOD that is determinable from experimental results is $\Delta\nu_2 = 15.1\text{ cm}^{-1}$ by Hauge.¹³ The predicted isotopic shift agrees well at all levels of theory,

TABLE III. Theoretical predictions of the harmonic vibrational frequencies (in cm^{-1}) for AlOD, the deuterated isotopomer of ground state AIOH.

Level of theory	Harmonic vibrational frequency		
	$\omega_1(a_1/a')$	$\omega_2(a_1/a')$	$\omega_3(e_1/a')$
DZP SCF	3162	880	113
TZ2P SCF	3134	853	194
TZ(2df,2pd) SCF	3147	866	117
DZP CISD	3036	864	101
TZ2P CISD	3023	832	149
TZ(2df,2pd) CISD	3034	850	91
DZP CCSD	2980	855	77
TZ2P CCSD	2955	817	167
TZ(2df,2pd) CCSD	2967	836	115
DZP CCSD(T)	2962	851	60
TZ2P CCSD(T)	2922	808	166
TZ(2df,2pd) CCSD(T)	2932	827	118
Expt. (Ref. 13)	$\nu = 795.2$		

e.g., 18 cm^{-1} for TZ(2df,2pd) CCSD(T). Hauge¹³ also reports that $\nu_2(\text{Al}^{18}\text{O}) = 785.2\text{ cm}^{-1}$, shifted 25.1 cm^{-1} . Our theoretical predictions, not tabulated here, agree well with this experimental assignment. For TZ(2df,2pd) CCSD(T) we predict $\omega_e(\text{Al}^{18}\text{O}) = 817\text{ cm}^{-1}$, a shift of 28 cm^{-1} . There are no experimental isotopic vibrational assignments for DAIO, but we are confident that our predictions are good.

Table V shows the harmonic vibrational frequencies of the transition state for hydrogen migration. At the TZ(2df,2pd) CCSD(T) level of theory, the real vibrational modes have the magnitudes 1755 and 909 cm^{-1} , while the imaginary mode has a magnitude of $945i\text{ cm}^{-1}$.

C. Energetics

Relative energies of \tilde{X} AIOH, \tilde{X} HAIO, and the transition state are given in Table VI. At the highest level of theory used here [TZ(2df,2pd) CCSD(T)], AIOH is more stable than HAIO by $42.2\text{ kcal mol}^{-1}$. At the same

TABLE IV. Theoretical predictions of the harmonic vibrational frequencies (in cm^{-1}) for DAIO, the deuterated isotopomer of ground state HAIO.

Level of theory	Harmonic vibrational frequency		
	$\omega_1(a_1)$	$\omega_2(a_1)$	$\omega_3(e_1)$
DZP SCF	1566	1186	377
TZ2P SCF	1543	1174	370
TZ(2df,2pd) SCF	1540	1172	372
DZP CISD	1552	1118	347
TZ2P CISD	1514	1106	341
TZ(2df,2pd) CISD	1517	1113	343
DZP CCSD	1521	1085	328
TZ2P CCSD	1475	1070	321
TZ(2df,2pd) CCSD	1476	1077	325
DZP CCSD(T)	1503	1046	312
TZ2P CCSD(T)	1456	1030	303
TZ(2df,2pd) CCSD(T)	1458	1038	306

TABLE V. Theoretical predictions of the total energy (in Hartrees), dipole moment (in Debye), harmonic vibrational frequencies (in cm^{-1}), and zero point vibrational energy (ZPVE) (in kcal mol^{-1}) for the C_s -symmetry transition state connecting \tilde{X} AlOH and \tilde{X} HAlO.

Level of theory	Energy	μ	Harmonic vibrational frequency			ZPVE
			$\omega_1(a')$	$\omega_2(a')$	$\omega_3(a'')$	
DZP SCF	-317.238 726	4.103	1898	1047	1262i	4.210
TZ2P SCF	-317.267 891	4.259	1882	1058	1273i	4.203
TZ(2df,2pd) SCF	-317.269 514	4.261	1881	1059	1280i	4.202
DZP CISD ^a	-317.596 379	3.954	1881	1027	1097i	4.157
TZ2P CISD ^a	-317.668 580	4.156	1853	1028	1095i	4.118
TZ(2df,2pd) CISD ^a	-317.695 967	4.200	1864	1039	1119i	4.150
DZP CCSD	-317.638 088	3.469	1812	932	979i	3.922
TZ2P CCSD	-317.714 921	3.682	1779	934	964i	3.877
TZ(2df,2pd) CCSD	-317.744 669	3.721	1791	946	983i	3.912
DZP CCSD(T)	-317.653 549	3.315	1779	892	953i	3.818
TZ2P CCSD(T)	-317.736 928	3.533	1742	896	932i	3.772
TZ(2df,2pd) CCSD(T)	-317.768 556	3.573	1755	909	945i	3.808

^aCISD+Q energies are -317.636 829, -317.713 007, and -317.742 528 Hartrees, respectively.

level of theory the classical barrier to hydrogen migration from \tilde{X} AlOH to \tilde{X} HAlO is found to be $80.5 \text{ kcal mol}^{-1}$, while zero-point vibrational energy (ZPVE) corrections give an activation energy of $77.2 \text{ kcal mol}^{-1}$. Thus AlOH is extremely stable with respect to isomerization once produced. Although the HAlO to AlOH isomerization reaction is strongly exothermic with $\Delta E = -42.2$ (-40.5 with ZPVE) kcal mol^{-1} , the barrier height for \tilde{X} HAlO to \tilde{X} AlOH isomerization is 38.4 (36.6 with ZPVE) kcal mol^{-1} . If it were generated, HAlO should be observable because of its kinetic stability with respect to isomerization.

Interestingly, the PES in the related case of \tilde{X} HBO \leftrightarrow \tilde{X} BOH^{1,11} isomerization is almost the exact opposite of that predicted here for HAlO and AlOH. That is, the trivalent HBO isomer is $\sim 40 \text{ kcal mol}^{-1}$ more stable than the monovalent BOH isomer, and the transition state connecting them is $\sim 50 \text{ kcal mol}^{-1}$ above BOH.¹ In many ways, first-row elements such as boron are oddities and

stand apart from the heavier elements in their respective groups. When moving down the periodic table within Group 13 (B, Al, Ga, In, Tl), the monovalent state becomes progressively more stable.⁴¹ One explanation for this trend and the predicted monovalent AlOH ground state is the inert *s*-pair effect. Kutzelnigg⁴² has noted that the *2s* and *2p* orbitals of first-row elements are uniquely well suited for hybridization because they have similar spatial extent. First-row elements have only *s*-type core electrons. As a result, their valence *p* orbitals are relatively compact. Elements in higher rows have cores that contain both *s*- and *p*-type electrons; their valence *p* orbitals are substantially more diffuse than their valence *s* orbitals, and hybridization is much less efficient.

Recall that the chemistry of lower Group 14 elements (Si, Ge, etc.) is often radically different from that of carbon; this has been explained in terms of increasing stability of the divalent state while moving downward within the

TABLE VI. Relative energies^a (in kcal mol^{-1}) for the ground HAlO-AlOH potential energy hypersurface.

Level of theory	\tilde{X} AlOH	C_s -symmetry transition state	\tilde{X} HAlO	Barrier height
DZP SCF	0.00	112.33 (108.64)	54.72 (53.02)	57.60 (55.61)
TZ2P SCF	0.00	110.88 (107.33)	52.63 (50.98)	58.26 (56.35)
TZ(2df,2pd) SCF	0.00	111.71 (108.27)	53.33 (51.79)	58.39 (56.47)
DZP CISD	0.00	93.83 (90.39)	46.24 (44.62)	47.59 (45.77)
TZ2P CISD	0.00	94.85 (91.54)	46.45 (44.89)	48.39 (46.65)
TZ(2df,2pd) CISD	0.00	95.92 (92.72)	46.73 (45.26)	49.19 (47.46)
DZP CISD+Q	0.00	84.60 (81.17)	43.97 (42.35)	40.64 (38.82)
TZ2P CISD+Q	0.00	86.24 (82.94)	44.59 (43.03)	41.65 (39.91)
TZ(2df,2pd) CISD+Q	0.00	87.30 (84.10)	44.70 (43.22)	42.60 (40.87)
DZP CCSD	0.00	85.18 (81.73)	44.80 (43.22)	40.37 (38.51)
TZ2P CCSD	0.00	86.65 (83.22)	45.46 (43.81)	41.19 (39.41)
TZ(2df,2pd) CCSD	0.00	87.48 (84.15)	45.56 (43.99)	41.92 (40.15)
DZP CCSD(T)	0.00	79.33 (75.88)	41.95 (40.32)	37.38 (35.56)
TZ2P CCSD(T)	0.00	79.84 (76.39)	42.11 (40.38)	37.73 (36.01)
TZ(2df,2pd) CCSD(T)	0.00	80.52 (77.16)	42.17 (40.52)	38.35 (36.64)

^aNumbers in parentheses include zero point vibrational energy corrections. CISD+Q energies were determined at the CISD optimized geometries and corrected for ZPVE using CISD harmonic vibrational frequencies with the same basis set.

group. The divalent state stabilization energy (DSSE), defined to be the difference between the first and second bond dissociation energies, is a convenient way to express this trend. For example, $\text{DSSE}(\text{CH}_2) = -5.6 \text{ kcal mol}^{-1}$, while $\text{DSSE}(\text{SiH}_2) = +19.3 \text{ kcal mol}^{-1}$ and $\text{DSSE}(\text{GeH}_2) = +25.8 \text{ kcal mol}^{-1}$. The usefulness of DSSEs with respect to Group 14 chemistry has been discussed elsewhere by Grev.⁴³ Using G2 theory thermochemical data,⁴⁴ the equivalent "monovalent state stabilization energy" may be determined for both BH ($-28.8 \text{ kcal mol}^{-1}$) and AlH ($+39.6 \text{ kcal mol}^{-1}$). Although this treatment of the thermochemistry is hardly complete, it does provide a strong indication that the monovalent structure (MOH) should be much more favorable relative to the trivalent structure (OMH) in the case of Al as opposed to B.

IV. CONCLUSION

The singlet ground state PES for the AIOH-HAIO isomerization reaction has been studied with *ab initio* molecular electronic structure theory. AIOH was found to be quasilinear with an equilibrium bond angle of 162.6° contrary to Walsh's rules. Predictions herein for AIOH compare favorably with recently determined experimental results. Agreement is sufficient to confirm the experimental assignments. HAIO was linear at all levels of theory in agreement with Walsh.

At the $[\text{TZ}(2df,2pd)]$ CCSD(T) level of theory, the classical barrier for $\tilde{\text{X}} \text{ HAIO} \rightarrow \tilde{\text{X}} \text{ AIOH}$ rearrangement is predicted to be $38.4 \text{ kcal mol}^{-1}$, while it is $36.6 \text{ kcal mol}^{-1}$ with ZPVE corrections. The ΔE for this isomerization reaction is -42.2 (-40.5 with ZPVE) kcal mol^{-1} at that level of theory. The AIOH conformation lies lowest on the AIOH-HAIO PES, in stark contrast with the HBO global minimum on the BOH-HBO PES. This apparent lack of periodicity within Group 13 can be explained in terms of the increasing stability of the monovalent state for lower elements in that group.

ACKNOWLEDGMENTS

This research was supported by the Air Force Office of Scientific Research, Grant No. AFOSR-88-0167. This material is based upon work supported under NSF and DOD Graduate Fellowships. The authors would like to thank Roger Grev and Peter Schreiner for helpful discussions and Jeff Pilgrim, Dave Robbins, and Professor Michael Duncan for providing their experimental results prior to publication. GV and BJD would also like to point out that they are hoping for yet another volleyball rematch with Duncan's Lazer Jox.

¹ T. S. Zyubina, O. P. Charkin, and L. V. Gurvich, *Zh. Strukt. Khim.* **20**, 3 (1979).

² R. C. Hilborn, Z. Qingshi, and D. O. Harris, *J. Mol. Spectrosc.* **97**, 73 (1983).

³ J. Nakagawa, R. F. Wormsbecher, and D. O. Harris, *J. Mol. Spectrosc.* **97**, 37 (1983).

⁴ S. Kinsey-Nielsen, C. R. Brazier, and P. F. Bernath, *J. Chem. Phys.* **84**, 698 (1986).

⁵ W. L. Barclay Jr., M. A. Anderson, and L. M. Ziurys, *Chem. Phys. Lett.* **196**, 225 (1992).

⁶ M. Trkula and D. O. Harris, *J. Chem. Phys.* **79**, 1138 (1983).

⁷ D. R. Lide and R. L. Kuczkowski, *J. Chem. Phys.* **46**, 4768 (1967).

⁸ C. Matsumura and D. R. Lide, *J. Chem. Phys.* **50**, 71 (1969).

⁹ J. S. Pilgrim, D. L. Robbins, and M. A. Duncan, *Chem. Phys. Lett.* **202**, 203 (1993).

¹⁰ T. S. Zyubina, O. P. Charkin, and L. V. Gurvich, *Zh. Strukt. Khim.* **20**, 12 (1979).

¹¹ T. S. Zyubina, A. S. Zyubina, A. A. Gorbik, and O. P. Charkin, *Zh. Neorg. Khim.* **30**, 2739 (1985).

¹² M. I. Milushin, A. M. Emel'yanov, and L. N. Gorokhov, *Teplofiz. Vys. Temp.* **20**, 3 (1979).

¹³ R. H. Hauge, J. W. Kauffman, and J. L. Margrave, *J. Am. Chem. Soc.* **102**, 6005 (1980).

¹⁴ M. A. Douglas, R. H. Hauge, and J. L. Margrave, *ACS Symp. Ser.* **179**, 347 (1982).

¹⁵ S. Huzinaga, *J. Chem. Phys.* **42**, 1293 (1965).

¹⁶ T. H. Dunning, *J. Chem. Phys.* **53**, 2823 (1970).

¹⁷ T. H. Dunning, *J. Chem. Phys.* **55**, 716 (1971).

¹⁸ A. D. McLean and G. S. Chandler, *J. Chem. Phys.* **72**, 5639 (1980).

¹⁹ P. Pulay, in *Modern Theoretical Chemistry*, edited by H. F. Schaefer (Plenum, New York, 1977), Vol. 4, p. 153.

²⁰ M. Dupuis and H. F. King, *J. Chem. Phys.* **68**, 3998 (1978).

²¹ J. D. Goddard, N. C. Handy, and H. F. Schaefer, *J. Chem. Phys.* **71**, 1525 (1979).

²² B. R. Brooks, W. D. Laidig, P. Saxe, J. D. Goddard, Y. Yamaguchi, and H. F. Schaefer, *J. Chem. Phys.* **72**, 4652 (1980).

²³ Y. Osamura, Y. Yamaguchi, and H. F. Schaefer, *J. Chem. Phys.* **77**, 383 (1982).

²⁴ J. E. Rice, R. D. Amos, N. C. Handy, T. J. Lee, and H. F. Schaefer, *J. Chem. Phys.* **85**, 963 (1986).

²⁵ A. C. Scheiner, G. E. Scuseria, J. E. Rice, T. J. Lee, and H. F. Schaefer, *J. Chem. Phys.* **87**, 5361 (1987).

²⁶ G. E. Scuseria, *J. Chem. Phys.* **94**, 442 (1991).

²⁷ J. A. Pople, R. Krishnan, H. B. Schlegel, and J. S. Binkley, *Int. J. Quantum. Chem. S* **13**, 225 (1975).

²⁸ P. Saxe, Y. Yamaguchi, and H. F. Schaefer, *J. Chem. Phys.* **77**, 5647 (1982).

²⁹ Y. Osamura, Y. Yamaguchi, P. Saxe, D. J. Fox, M. A. Vincent, and H. F. Schaefer, *J. Mol. Struct.* **103**, 183 (1983).

³⁰ S. R. Langhoff and E. R. Davidson, *Int. J. Quantum. Chem.* **8**, 61 (1974).

³¹ E. R. Davidson, in *The World of Quantum Chemistry*, edited by R. Daudel and B. Pullman (Reidel, Dordrecht, 1974), p. 17.

³² A. D. Walsh, *J. Chem. Soc.* 2288 (1953).

³³ G. M. Schwenzer, H. F. Schaefer, and C. F. Bender, *J. Chem. Phys.* **63**, 569 (1975).

³⁴ E. D. Simandiras, J. E. Rice, T. J. Lee, R. D. Amos, and N. C. Handy, *J. Chem. Phys.* **88**, 3187 (1988).

³⁵ E. D. Simandiras, N. C. Handy, and R. D. Amos, *J. Phys. Chem.* **92**, 92 (1988).

³⁶ J. R. Thomas, B. J. DeLeeuw, G. Vacek, and H. F. Schaefer, *J. Chem. Phys.* **98**, 1336 (1993).

³⁷ J. R. Thomas, B. J. DeLeeuw, G. Vacek, T. D. Crawford, Y. Yamaguchi, and H. F. Schaefer, *J. Chem. Phys.* (to be published).

³⁸ R. J. Celotta, R. A. Bennett, and J. L. Hall, *J. Chem. Phys.* **60**, 1740 (1974); H. Hotop, T. A. Patterson, and W. C. Lineberger, *J. Chem. Phys.* **60**, 1806 (1974).

³⁹ K. P. Huber and G. Herzberg, *Molecular Spectra and Molecular Structure Volume IV—Constants of Diatomic Molecules* (Van Nostrand Reinhold, New York, 1979), pp. 24, 28, 508.

⁴⁰ G. S. Hammond, *J. Am. Chem. Soc.* **77**, 334 (1955).

⁴¹ F. A. Cotton and G. Wilkinson, *Advanced Inorganic Chemistry* (Wiley, New York, 1988), Ed. 5, p. 208.

⁴² W. Kutzelnigg, *Angew. Chem., Int. Ed. Engl.* **23**, 272 (1984).

⁴³ R. S. Grev, *Adv. Organometallic Chem.* **33**, 125 (1991).

⁴⁴ L. A. Curtiss, K. Raghavachari, G. W. Trucks, and J. A. Pople, *J. Chem. Phys.* **94**, 7221 (1991).

Ge₂H₂: A Molecule with a Low-Lying Monobridged Equilibrium Geometry

Zoltán Palágyi,^{†‡} Henry F. Schaefer III,^{*†} and Ede Kapuy[§]

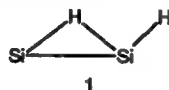
Contribution from the Center for Computational Quantum Chemistry, University of Georgia, Athens, Georgia 30602, and Department of Theoretical Physics, József Attila University, H-6720, Szeged, Hungary

Received February 10, 1993

Abstract: Recent experimental and theoretical studies reporting remarkable monobridged structures for Si₂H₂, Al₂H₂, and Ga₂H₂ have motivated us to re-investigate the singlet potential energy surface of Ge₂H₂ using the self-consistent-field (SCF), single and double excitation configuration interaction (CISD), and single and double excitation coupled cluster (CCSD) methods in conjunction with a double- ζ plus polarization basis set (DZP). In addition to the dibridged (or butterfly) ground state and the low-lying vinylidene-like minimum reported earlier by Grev and DeLeeuw, our study predicts the existence of a monobridged isomer, which is characterized as a minimum by means of harmonic vibrational frequency analyses. Relative energies of the above structures were also predicted with use of the coupled cluster single, double, and (perturbative) triple excitation method (CCSD(T)), which employed a triple- ζ plus polarization basis set augmented with a set of f functions on the germanium atoms (TZP+f). Final energetic predictions suggest that the monobridged structure is the second most stable isomer of Ge₂H₂, lying 8.9 kcal mol⁻¹ above the butterfly ground state and 2.1 kcal mol⁻¹ below the branched (vinylidene-like) minimum.

Introduction

Among small molecules, one of the most interesting structural discoveries in recent years has been that of the monobridged equilibrium geometry of the Si₂H₂ molecule. The existence of



such a structure, which apparently has no precedent, was proposed in 1990 by Colegrove.¹ She predicted this structure to be a genuine equilibrium and to lie only 10.8 kcal/mol above the dibridged "butterfly" global minimum²⁻⁴ of Si₂H₂.

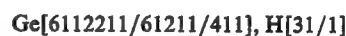
The spectacular success of the Lille group⁴ in observing and analyzing the microwave spectrum of the butterfly global minimum of Si₂H₂ led them to attempt to synthesize other new Si_xH_y molecules. In cooperation with the Georgia theoretical group, Cordonnier, Bogey, Demuynek, and Destombes⁵ were able to observe and analyze a total of 148 microwave features that were assigned to the monobridged Si₂D₂ and Si₂H₂ species 1. The observed microwave lines are remarkably consistent with the theoretical predictions of Colegrove¹ and of Grev.⁶ Grev has provided an incisive qualitative picture of the bonding in Si₂H₂ and related systems.

Given the very recent observation⁵ of the peculiar monobridged structure 1 of Si₂H₂, an obvious question is whether comparably low-lying equilibrium geometries of other A₂H₂ molecules exist. It would certainly be surprising if the much studied⁷ acetylene

potential surface C₂H₂ revealed such a stationary point. The next sensible neutral example would be the germanium analogue Ge₂H₂. Therefore, we explore here a part of the Ge₂H₂ potential energy hypersurface not considered in previous theoretical work.⁸

Theoretical Methods

Several stationary points on the Ge₂H₂ potential energy surface were initially located by using SCF gradient techniques^{9,10} in conjunction with a basis set designated double- ζ plus polarization (DZP). The DZP basis for germanium consists of the Dunning¹¹ 14s11p5d primitive set of Gaussian functions contracted to 7s5p2d¹² augmented by a set of six Cartesian d-like functions ($\alpha_d(\text{Ge}) = 0.25$). For hydrogen we used the standard Huzinaga-Dunning-Hay¹³⁻¹⁵ double- ζ basis set augmented by a set of p-like functions ($\alpha_p(\text{H}) = 0.75$). The contraction scheme for this DZP basis is



For the evaluation of the relative energies of various structures we employed a basis set designated triple- ζ plus polarization plus f functions (TZP+f). For germanium, it consists of the above primitive set more loosely contracted to 10s8p2d and augmented with a set of d- and f-like polarization functions [$\alpha_d(\text{Ge}) = 0.25$, $\alpha_f(\text{Ge}) = 0.45$]. For hydrogen it is the standard Huzinaga-Dunning triple- ζ basis set augmented by a set of p-like functions ($\alpha_p(\text{H}) = 0.75$). Thus the contraction scheme for this basis set is



DZP SCF quadratic force constants and harmonic vibrational frequencies were determined with the use of analytic energy second derivative methods.¹⁶ Starting with the DZP SCF geometries and force constants, we then reoptimized the structures using first the configuration interaction

(8) Grev, R. S.; DeLeeuw, B. J.; Schaefer, H. F. *Chem. Phys. Lett.* **1990**, *165*, 257.

(9) Pulay, P. *Modern Theoretical Chemistry*; Schaefer, H. F., Ed.; Plenum: New York, 1977; Vol. 4, pp 153-183.

(10) Dupuis, M.; King, H. F. *J. Chem. Phys.* **1978**, *68*, 3998.

(11) Dunning, T. H. *J. Chem. Phys.* **1977**, *66*, 1382.

(12) The contraction (14s11p5d/7s5p2d) is due to R. S. Grev and H. F. Schaefer, unpublished.

(13) Huzinaga, S. *J. Chem. Phys.* **1965**, *42*, 1293.

(14) Dunning, T. H. *J. Chem. Phys.* **1970**, *53*, 2823.

(15) Dunning, T. H.; Hay, P. J. *Modern Theoretical Chemistry*; Schaefer, H. F., Ed.; Plenum: New York, 1977; Vol. 3, pp 1-27.

(16) Saxe, P.; Yamaguchi, Y.; Schaefer, H. F. *J. Chem. Phys.* **1982**, *77*, 5647.

[†] University of Georgia.

[‡] Permanent address: Quantum Theory Group, Physical Institute, Technical University, H-1521, Budapest, Hungary.

[§] József Attila University.

(1) Colegrove, B. T.; Schaefer, H. F. *J. Phys. Chem.* **1990**, *94*, 5593 (J. A. Pople Issue).

(2) Lischka, H.; Köhler, H. *J. Am. Chem. Soc.* **1983**, *105*, 6646.

(3) Binkley, J. S. *J. Am. Chem. Soc.* **1984**, *106*, 603.

(4) Bogey, M.; Bolvin, H.; Demuynek, C.; Destombes, J.-L. *Phys. Rev. Lett.* **1991**, *66*, 413.

(5) Cordonnier, M.; Bogey, M.; Demuynek, C.; Destombes, J.-L. *J. Chem. Phys.* **1992**, *97*, 7984.

(6) Grev, R. S.; Schaefer, H. F. *J. Chem. Phys.* **1992**, *97*, 7990.

(7) Smith, B. J.; Smernik, R.; Radom, L. *Chem. Phys. Lett.* **1992**, *188*, 589.

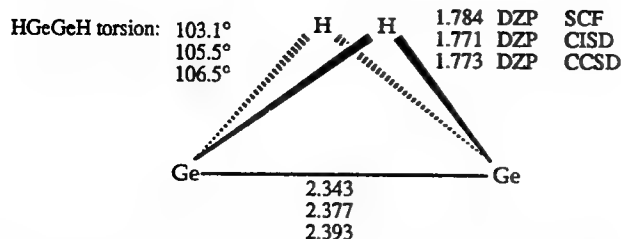


Figure 1. Theoretical equilibrium geometries for the global minimum closed-shell singlet, dibridged (C_{2v}) electronic ground state of Ge_2H_2 . Bond distances are in angstroms.

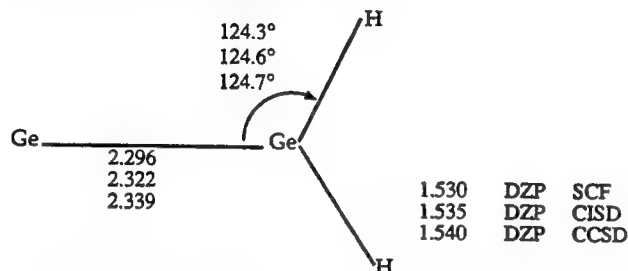


Figure 2. Theoretical geometries for the vinylidene-like closed-shell singlet state of Ge_2H_2 . Bond distances are in angstroms.

(CI) method¹⁷ and then the coupled cluster (CC) method¹⁸ in conjunction with the DZP basis set. Only the valence electrons have been correlated explicitly; the core-like SCF molecular orbitals (Ge 1s, 2s, 2p, 3s, 3p, 3d) and the virtual orbital counterpairs (Ge 1s*, 2s*, 2p*) were not included in the CI and CC procedures. Otherwise, all single and double excitations from the SCF reference wave function have been included (CISD, CCSD). The CISD energies have been corrected to approximately include the effects of unlinked quadruple excitations with use of the Davidson formula.¹⁹ These corrected energies are denoted CISD+Q. For final energy predictions the effects of triple excitations were also included perturbatively with the use of CCSD(T) wave functions. We obtained CISD and CCSD harmonic vibrational frequencies by taking finite differences of analytic energy gradients.^{20,21}

The choice of frozen and deleted molecular orbitals requires a bit more justification. First, the freezing of the germanium 3d¹⁰ orbital may seem a bit restrictive since this orbital is conclusively filled only two elements earlier with zinc. However, when one reaches Ge in the periodic table, the 3d orbital energy is -1.635 hartrees,²² whereas the 4s orbital energy is -0.553 hartrees and the 4p orbital energy is -0.287 hartrees. Thus the energy gap [$\epsilon(4s) - \epsilon(3d)$] is substantial, 1.081 hartrees or 29.4 eV. Concerning the virtual orbitals, a referee has questioned why only the 1s* and 2s* virtuals were deleted. The reason is that the other high-lying or core-like virtuals (especially 3s*, 3p*, and 3d*) tend to mix with the valence-like virtuals. That is, the distinction between core-like and valence-like virtuals becomes blurred. In such cases, the best strategy is to include all virtual orbitals which have some valence character.

Structures and Energies

Theoretical stationary point geometries are shown in Figures 1–3. Table I contains the predicted harmonic vibrational frequencies, infrared (IR) intensities, and normal mode assignments. The assignments were based on the potential energy distribution (PED) among the diagonal elements of the symmetrized force constant matrix on a percentage scale. Standard cotton coordinate systems²³ have been used, and whenever there

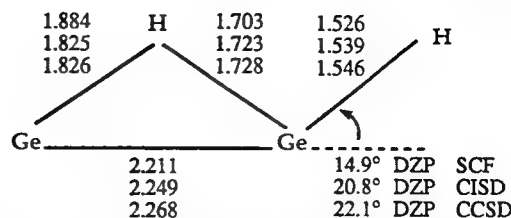


Figure 3. Theoretical geometries for the monobridged closed-shell singlet state of Ge_2H_2 . Bond distances are in angstroms.

is a choice of coordinate systems, the two germanium atoms have been chosen to lie on the y axis.

Table II summarizes the relative energies as well as the total energies of the global minimum dibridged butterfly structure. Table III lists the largest CI coefficients for each wave function and the corresponding electron configurations. These results show that the single-configuration Hartree–Fock approach is qualitatively reasonable for all three isomers. The fact that the C_0 values (0.938, 0.935, and 0.936) are nearly the same further suggests that single-configuration-based correlated methods (such as CISD and CCSD) should do a reasonable job in describing the relative energies of the three isomers. For brevity in this discussion, only results obtained with the DZP CCSD method will be reported explicitly, except relative energies, which are TZP+f CCSD(T) results including DZP CCSD harmonic vibrational energy corrections (see final column of Table II).

The structures corresponding to the butterfly (Figure 1) and vinylidene (Figure 2) isomers are qualitatively similar to those reported earlier by Grev and Deleuw.⁸ Previous experience would suggest that the true equilibrium geometries should lie intermediate between our DZP CISD and DZP CCSD predictions.

The monobridged structure (Figure 3) is, of course, the principal focus of this research. The theoretical predictions for this peculiar isomer are similar to those for Si_2H_2 . For example, monobridged Ge_2H_2 is actually predicted to be a transition state at the DZP SCF level, precisely as was found¹ for Si_2H_2 . At the DZP SCF level the monobridged structure is a transition state, with its imaginary vibrational frequency being the terminal out-of-plane bend. This appears to confirm that the monobridged structure at the DZP SCF level of theory is a transition state for the degenerate rearrangement of the butterfly global minimum. For both molecules, the introduction of electron correlation at the DZP CISD level is seen to properly describe the monobridged structure as a genuine minimum.

One of the most critical structural features of the monobridged geometry is the angle between the terminal Ge–H bond and the extension of the Ge–Ge bond. This angle is seen in Figure 3 to be 20.8° at the DZP CISD level of theory. The analogous DZP CISD prediction for the monobridged structure of Si_2H_2 is very similar, namely 20.0°. From Grev's work⁶ on Si_2H_2 using much higher levels of theory, a final value of 18.9° is found for this critical angle in monobridged Si_2H_2 .

Another interesting feature of the monobridged Ge_2H_2 structure is the difference between the two bridging Ge–H distances. This difference is 0.181 Å with the DZP SCF method, 0.102 Å with the DZP CISD method, and 0.098 Å with the DZP CCSD method. Colegrove's analogous results¹ for monobridged Si_2H_2 are $\Delta r = 0.119$ (DZP SCF) and 0.082 Å (DZP CISD). At the highest level of theory considered to date for Si_2H_2 [TZ2P+f CCSD(T)], Grev⁶ predicts the monobridged Δr to be 0.083 Å. Thus, for Ge_2H_2 the ultimate difference between bridging Ge–H distances should be about 0.1 Å, or roughly 0.02 Å more than is the case for monobridged Si_2H_2 .

Finally, we compare the predicted Ge–Ge bond distances for the butterfly (2.377 Å), monobridged (2.249 Å), and vinylidene-like (2.322 Å) structures. The bond distances cited are the DZP CISD values, which are expected to be closest to the (unknown) experimental values. As was the case for the valence isoelectronic

(17) Saxe, P.; Fox, D. J.; Schaefer, H. F.; Handy, N. C. *J. Chem. Phys.* **1982**, *77*, 5584.

(18) Scuseria, G. E.; Janssen, C. L.; Schaefer, H. F. *J. Chem. Phys.* **1988**, *89*, 7382.

(19) Langhoff, S. R.; Davidson, E. R. *Int. J. Quantum Chem.* **1974**, *8*, 61.

(20) Rice, J. E.; Amos, R. D.; Handy, N. C.; Lee, T. J.; Schaefer, H. F. *J. Chem. Phys.* **1986**, *85*, 963.

(21) Scheiner, A. C.; Scuseria, G. E.; Rice, J. E.; Lee, T. J.; Schaefer, H. F. *J. Chem. Phys.* **1987**, *87*, 5361.

(22) Clementi, E.; Roetti, C. *At. Data Nucl. Data Tables* **1974**, *14*, 177.

(23) Cotton, F. A. *Chemical Applications of Group Theory*; Wiley Interscience: New York, 1963.

Table I. Harmonic Vibrational Frequencies (cm⁻¹) for Ge₂H₂ Structures with Infrared Intensities in Parentheses (km/mol)

isomer		description	DZP SCF	DZP CISD	DZP CCSD
vinylidene	b ₂	Ge-H antisym str	2241 (99)	2192 (83)	2158 (78)
	a ₁	Ge-H sym str	2235 (83)	2180 (73)	2144 (72)
	a ₁	H-Ge-Ge sym bend	909 (65)	860 (73)	843 (75)
	b ₁	oop bend	385 (4)	332 (4)	304 (4)
	a ₁	Ge-Ge str	337 (2)	318 (4)	305 (5)
monobridged	b ₂	H-Ge-H in-plane wag	304 (29)	260 (21)	252 (19)
	a'	terminal H-Ge str	2231 (102)	2143 (122)	2095 (122)
	a'	bridging H sym str	1612 (132)	1560 (105)	1532 (95)
	a'	bridging H antisym str	865 (96)	962 (150)	964 (145)
	a'	H-Ge-H bend	395 (23)	465 (7)	462 (5)
	a'	Ge-Ge str	309 (17)	328 (7)	314 (6)
	a''	terminal H oop bend	431 (68)	123 (43)	114 (38)
dibridged	a ₁	Ge-H sym str	1537 (24)	1534 (12)	1520 (10)
	b ₁	Ge-H antisym str	1456 (72)	1446 (51)	1424 (48)
	b ₂	Ge-H str	957 (525)	1054 (469)	1056 (443)
	a ₂	Ge-H str	736 (0)	931 (0)	947 (0)
	a ₁	torsion (butterfly)	925 (62)	863 (42)	838 (38)
	a ₁	Ge-Ge str	331 (0)	304 (0)	291 (0)

Table II. Relative Energies (kcal/mol) of Stationary Point Structures for the Ge₂H₂ System, Corrected with Zero-Point Vibrational Energies in the Final Column

isomer	SCF		CISD ^a		CCSD		CCSD(T)	
	DZP	TZP+f ^c	DZP	TZP+f ^c	DZP	TZP+f ^c	TZP+f ^d	+ZPVE ^e
vinylidene	4.3	5.6	9.2	10.6	9.0	10.4	11.1	11.0
			9.3	10.7				
monobridged	13.4	13.7	11.6	12.0	10.6	11.0	9.8	8.9
			10.4	10.9				
butterfly ^b	0.0	0.0	0.0	0.0	0.0	0.0	0.0	0.0
			0.0	0.0				

^a The lower number in the CISD boxes is the Davidson corrected energy difference. ^b Total energies (au) for the dibridged structure are as follows—DZP SCF, -4151.592681; TZP+f^c SCF, -4151.782305; DZP CISD, -4151.783933; DZP CISD+Q, -4151.806522; TZP+f^c CISD, -4151.991863; TZP+f^c CISD+Q, -4152.016976; DZP CCSD, -4151.802324; TZP+f^c CCSD, -4152.012199; TZP+f^d CCSD(T), -4152.024124; +ZPVE, -4152.010282.

^c At the DZP optimized geometry obtained with the corresponding level of theory. ^d At the DZP CCSD optimized geometry. ^e TZP+f^d CCSD(T) including DZP CCSD harmonic zero-point vibrational energy correction.

Table III. Coefficients Greater than 0.05 in the TZP+f CISD Wave Functions for the Different Ge₂H₂ Structures

isomer	coefficient	configuration
dibridged	0.938	(core) 11a ₁ ² 12a ₁ ² 13a ₁ ² 5b ₁ ² 11b ₂ ²
	-0.051	13a ₁ ² → 12b ₂ ²
monobridged	0.935	(core) 21a ² 22a ² 23a ² 24a ² 29a ²
	-0.102	9a ² → 10a ²
	-0.055	24a ² → 25a ²
	-0.054	24a ² 9a ² → 25a ² 10a ²
vinylidene	0.936	(core) 15a ₁ ² 16a ₁ ² 17a ₁ ² 7b ₁ ² 27b ₂ ²
	-0.118	7b ₁ ² → 8b ₁ ²

Si₂H₂ system, the central Ge-Ge bond distance is shortest for the monobridged structure. The reader is referred to our recent paper⁶ on Si₂H₂ for a further discussion of the bonding in these closely related systems.

The relative energies of Table II show that the vinylidene-like structure of Ge₂H₂ is the second lowest-lying isomer at the SCF level of theory. However, correlation effects tend to destabilize the vinylidene structure while stabilizing the monobridged structure compared to the global minimum butterfly. Thus, as

was the case with the Si₂H₂ energetics,^{1,6} the Ge₂H₂ monobridged structure eventually becomes the second lowest-lying isomer of Ge₂H₂. At the ZPVE-corrected TZP+f CCSD(T) level of theory, the monobridged and vinylidene Ge₂H₂ structures are predicted to lie at 8.9 and 11.0 kcal/mol, respectively, above the butterfly global minimum.

Concluding Remarks

The recent experimental discovery⁵ of the peculiar monobridged isomer 1 of Si₂H₂ has raised the question whether other such species might be synthesized. The answer presented here for Ge₂H₂ is an unqualified "yes". For both Ge₂H₂ and Si₂H₂, the unexpected monobridged structure is energetically the second lowest-lying isomer, predicted to lie less than 9 kcal/mol above the butterfly global minimum.

Acknowledgment. We thank Dr. Roger S. Grev for many helpful discussions concerning the monobridged structures of A₂H₂ molecules. This research was supported by the U.S. Air Force Office of Scientific Research, Grant No. AFOSR-92-J-0047.

Rotational constants for the \tilde{C}^2A_2 state of NO_2

T. Daniel Crawford and Henry F. Schaefer III

Center for Computational Quantum Chemistry, University of Georgia, Athens, Georgia 30602

(Received 5 April 1993; accepted 11 August 1993)

The coupled-cluster method including all single and double excitations (CCSD) and CCSD including perturbatively applied triple excitations [CCSD(T)] have been used with large basis sets to study the rotational constants and associated geometrical parameters of the \tilde{C}^2A_2 state of NO_2 . The results compare favorably to earlier theoretical work but remain in conflict with recent optical-optical double resonance spectroscopic results.

INTRODUCTION

The nitrogen dioxide (NO_2) molecule has held the interest of both experimentalists and theoreticians due to its importance in atmospheric chemistry. More recently, however, the symmetry-breaking characteristics¹⁻³ and experimental rotational resolution⁴ of several of its lower-lying excited electronic states have been the focal points of study.

One of the earliest theoretical studies of the \tilde{C}^2A_2 state of NO_2 was done by Gillispie *et al.*⁵ In their pioneering work, they used multiconfigurational self-consistent field (MC-SCF) techniques with what is now considered to be a relatively small basis set, i.e., a double-zeta plus polarization (DZP) basis set, to determine the equilibrium geometry ($R_e \approx 1.27$ Å, $\theta_e \approx 110^\circ$). This work was followed by that of Jackels and Davidson,⁶ who used configuration interaction (CI) techniques with a double-zeta (DZ) basis set to determine geometries comparable to the earlier results by Gillispie *et al.*⁵

The first experimental observation of the \tilde{C}^2A_2 state of NO_2 was made in 1989 by Weaver *et al.*⁷ using photoelectron spectroscopy. They reported that this state lies $T_0 = 16\,357$ cm⁻¹ above the X^2A_1 ground state (including the zero-point energy). Shortly thereafter, Shibuya *et al.*⁴ used optical-optical double resonance (OODR) spectroscopy to produce the first rotationally resolved spectrum for this state. From the rotational constants, Shibuya and co-workers determined a distinctly different geometry ($R \approx 1.4$ Å, $\theta \approx 102^\circ$) from that obtained theoretically over a decade earlier.^{5,6}

A recent theoretical study by Kaldor³ used the coupled-cluster method including all single and double excitations (CCSD) to determine the geometry of the \tilde{C}^2A_2 state. Those geometries compared favorably to those of the original theoretical studies.^{5,6} However, Kaldor's excellent work was focused on the symmetry breaking characteristics of the \tilde{C}^2A_2 state and not an accurate determination of its equilibrium geometry. Therefore, only a DZP basis set was employed.

In the present work, an attempt is made to determine accurate rotational constants for the \tilde{C}^2A_2 state of NO_2 using high-level theoretical methods and large basis sets. The present results agree with previous theoretical studies but conflict with the experimentally determined values.⁴

THEORETICAL METHODS

The geometry of the \tilde{C}^2A_2 state of NO_2 has been determined using four distinct levels of theory and three basis sets. The four theoretical methods included the restricted self-consistent field (SCF) technique, configuration interaction including all single and double excitations (CISD),⁸ coupled-cluster, including all single and double excitations (CCSD),^{9,10} and CCSD including perturbatively applied triple excitations [CCSD(T)].¹⁰ A double-zeta¹¹⁻¹⁴ plus polarization (DZP) basis set constructed as $\text{N}, \text{O}(9s5p1d/4s2p1d)$; and a triple-zeta^{11,15} plus double polarization (TZ2P) basis set constructed as $(10s6p2d/5s3p2d)$ were the two smaller basis sets used. A third basis set (TZ2P + f) was constructed from the TZ2P basis with a single set of f -like functions added to N and O. The polarization function orbital exponents for the DZP basis were $\alpha_d(\text{N}) = 0.80$ and $\alpha_d(\text{O}) = 0.85$. Those for the TZ2P basis set were $\alpha_d(\text{N}) = 1.60, 0.40$, and $\alpha_d(\text{O}) = 1.70, 0.425$. The same polarization orbital exponents were used for the TZ2P + f basis, with, of course, the additional f orbital exponents, which had values of $\alpha_f(\text{N}) = 1.00$ and $\alpha_f(\text{O}) = 1.40$. The electronic configuration of the \tilde{C}^2A_2 state is

$$1a_1^2 1b_2^2 2a_1^2 3a_1^2 2b_2^2 4a_1^2 5a_1^2 1b_1^2 3b_2^2 1a_2^4 4b_2^2 6a_1^2.$$

For the correlated levels of theory, the lowest lying occupied SCF orbitals (the $1a_1$, $2a_1$, and $1b_2$) were frozen, i.e., doubly occupied in all configurations. For the CISD wave functions, there were 14 501 configurations for the DZP basis, 47 337 configurations for the TZ2P basis, and 97 742 configurations for the TZ2P + f basis within C_{2v} symmetry. The reference determinant for both the CCSD and CCSD(T) wave functions was that of the \tilde{C}^2A_2 state and not the closed-shell ground state anion adopted by Kaldor.³ Structural optimizations were carried out for the SCF and CISD theoretical methods for all three basis sets using open-shell analytical gradient techniques.^{16,17} The analogous optimizations were carried out for the CCSD and CCSD(T) theoretical methods for all three basis sets using numerical finite-difference gradients along symmetrized internal coordinates.

RESULTS AND DISCUSSION

Table I reports the energies and equilibrium geometries of the \tilde{C}^2A_2 state of NO_2 for all four levels of theory and all three basis sets used. In all cases, the optimized

TABLE I. Geometrical parameters (angstroms and degrees) and total energies (hartrees) for the \tilde{C}^2A_2 state of NO₂ for the SCF, CISD, CCSD, and CCSD(T) levels of theory for all three basis sets.

DZP basis set				
	SCF	CISD	CCSD	CCSD(T)
$R_e(\text{N-O})$	1.235	1.269	1.290	1.301
$\theta_e(\text{O-N-O})$	109.9	109.5	109.3	109.2
$E(\text{hartrees})$	-204.009 85	-204.465 58	-204.526 59	-204.546 90
TZ2P basis set				
	SCF	CISD	CCSD	CCSD(T)
$R_e(\text{N-O})$	1.224	1.251	1.273	1.286
$\theta_e(\text{O-N-O})$	110.3	110.0	109.8	109.7
$E(\text{hartrees})$	-204.037 51	-204.564 26	-204.634 31	-204.663 39
TZ2P+ <i>f</i> basis set				
	SCF	CISD	CCSD	CCSD(T)
$R_e(\text{N-O})$	1.222	1.246	1.267	1.280
$\theta_e(\text{O-N-O})$	110.4	110.1	110.0	109.8
$E(\text{hartrees})$	-204.046 79	-204.623 52	-204.699 89	-204.731 89

geometries follow expected trends¹⁸ as the level of theory is improved and the basis set size is increased.

Table II reports the rotational constants determined for each geometry given in Table I. The rotational constants reported by Shibuya *et al.*⁴ were $B_v=0.435$ cm⁻¹ and $C_v=0.363$ cm⁻¹. These compare poorly with the values of $B_e=0.480$ cm⁻¹ and $C_e=0.418$ cm⁻¹ determined here from the TZ2P+*f*-CCSD(T) geometry. The poor agreement between theory and experiment is tempered by (a) the fact that B_v and C_v should not be identical to B_e and C_e , respectively; and (b) Shibuya and co-workers⁴ explicitly state concerning B_v and C_v that "these values are only approximate." Nevertheless, we recommend that new experiments be devised to redetermine the rotational constants for the \tilde{C}^2A_2 state of NO₂.

TABLE II. Rotational constants B_e and C_e (in cm⁻¹) for the \tilde{C}^2A_2 state of NO₂ for the SCF, CISD, CCSD, and CCSD(T) levels of theory for all three basis sets.

DZP basis set				
	SCF	CISD	CCSD	CCSD(T)
B_e	0.516	0.490	0.476	0.469
C_e	0.449	0.426	0.413	0.406
TZ2P basis set				
	SCF	CISD	CCSD	CCSD(T)
B_e	0.522	0.501	0.486	0.476
C_e	0.455	0.436	0.422	0.414
TZ2P+ <i>f</i> basis set				
	SCF	CISD	CCSD	CCSD(T)
B_e	0.523	0.505	0.489	0.480
C_e	0.456	0.439	0.426	0.418

A point must be made regarding the difference between the energy reported for the DZP-CCSD level of theory here and that reported by Kaldor.³ The methods described here differ from those of Kaldor in three ways: (1) The use of all virtual orbitals in the present work, (2) the use of canonical SCF orbitals from the closed-shell anion as a reference determinant in the work of Kaldor, and (3) the use of the Fock-Space CCSD (FS-CCSD) method by Kaldor.³ These differences result in slightly different equilibrium geometries (Kaldor reports $R_e=1.286$ Å, $\theta_e=109.4^\circ$, and $E=-204.528$ 91 hartrees, as opposed to our $R_e=1.290$ Å, $\theta_e=109.3^\circ$, and $E=-204.526$ 59 hartrees).

It has been shown in previous CCSD and CCSD(T) studies that the T_1 diagnostic is a useful measure of the ability of the method to determine the dynamical correlation energy.¹⁹ For all CCSD and CCSD(T) results presented in this work, the value of the T_1 diagnostic was found to be near 0.03 (ranging from 0.0298 to 0.0316). This is higher than the proposed maximum value¹⁹ of 0.02, suggesting that a significant quantity of the dynamical correlation energy remains undetermined. Furthermore, the CISD coefficient of the second most important configuration is consistently greater than 0.1 (ranging from 0.103 to 0.123). These results suggest that a multireference wave function may be necessary to properly determine the total correlation energy. However, it is unlikely that such a wave function would produce significant changes in the geometries reported here.

CONCLUSIONS

The rotational constants and associated geometrical parameters of the \tilde{C}^2A_2 state of NO₂ have been studied using the CCSD and CCSD(T) methods with the DZP, TZ2P, and TZ2P+*f* basis sets. The results reported here ($R_e=1.290$ Å, $\theta_e=109.3^\circ$) are in qualitative agreement

with past theoretical studies. However, they are in conflict with the geometry reported by recent OODR spectroscopic determinations ($R \approx 1.4$ Å, $\theta \approx 102^\circ$). Although confidence in the equilibrium geometries given here may be slightly lowered due to high T_1 diagnostic values, the improvements in the geometries given by a multireference wave function would be insignificant relative to the difference between the theoretical and experimental results.

A final possibility for reconciliation between the theoretical and experimental rotational constants is the existence of a C_s equilibrium geometry for the \tilde{C} state of NO₂. In his theoretical study, Kaldor³ actually predicted such a geometry:

$$R_{1e}(\text{N-O}) = 1.303 \text{ Å},$$

$$R_{2e}(\text{N-O}) = 1.274 \text{ Å},$$

$$\theta_e(\text{O-N-O}) = 109.4^\circ.$$

We have determined Kaldor's rotational constants B_e and C_e to be 0.476 and 0.413 cm⁻¹, respectively. However, the rotational constants for Kaldor's C_{2v} stationary point are very similar, namely $B_e = 0.478$ cm⁻¹ and $C_e = 0.414$ cm⁻¹. Furthermore, the rotational constants from Kaldor's C_{2v} structure are quite close to those reported in Table II. Thus it seems highly unlikely that a lower-symmetry equilibrium geometry is the source of the discrepancy between theory and experiment. We recommend new laboratory studies of the rotational constants and molecular structure of the \tilde{C}^2A_2 state of NO₂.

Note added in proof. Professor K. Shibuya has informed the authors of new data resulting from updated optical-optical double resonance experiments performed in his group. Dr. Shibuya indicated that the new geometry of the \tilde{C}^2A_2 state of NO₂ obtained in those experiments was $R_e \approx 1.34$ Å and $\theta_e \approx 109^\circ$, which agrees remarkably well with the geometries reported in this work. The differences between these new data and those reported earlier⁴ were explained as the observation of an excited vibrational state rather than the ground vibrational state. A paper summa-

rizing these results has been submitted to the *Journal of Physical Chemistry* by Dr. Shibuya's group.

ACKNOWLEDGMENTS

This research was supported by the U.S. Air Force Office of Scientific Research, Grant No. AFOSR-92-J-0047. The authors would like to thank Bradley DeLeeuw and George Vacek for helpful discussions on geometry optimizations using symmetrized internal coordinates, Dr. Michael Duncan and Dr. Roger Grev for their insights on the spectroscopic determination of molecular geometries, and Russ Thomas for helpful editing advice.

¹C. P. Blahous, B. F. Yates, Y. Xie, and H. F. Schaefer, *J. Chem. Phys.* **93**, 8105 (1990).

²N. A. Burton, Y. Yamaguchi, I. L. Alberts, and H. F. Schaefer, *J. Chem. Phys.* **95**, 7466 (1991).

³U. Kaldor, *Chem. Phys. Lett.* **185**, 131 (1991).

⁴K. Shibuya, T. Kusumoto, H. Nagai, and K. Obi, *J. Chem. Phys.* **95**, 720 (1991).

⁵G. D. Gillispie, A. U. Khan, A. C. Wahl, R. P. Hosteny, and M. Krauss, *J. Chem. Phys.* **63**, 3425 (1975).

⁶C. F. Jackels and E. R. Davidson, *J. Chem. Phys.* **65**, 2941 (1976).

⁷A. Weaver, R. B. Metz, S. E. Bradforth, and D. M. Neumark, *J. Chem. Phys.* **90**, 2070 (1989).

⁸P. Saxe, D. J. Fox, H. F. Schaefer, and N. C. Handy, *J. Chem. Phys.* **77**, 5584 (1982).

⁹M. Rittby and R. J. Bartlett, *J. Phys. Chem.* **92**, 3033 (1988).

¹⁰G. Scuseria, *Chem. Phys. Lett.* **176**, 27 (1991).

¹¹S. Huzinaga, *J. Chem. Phys.* **42**, 1293 (1965).

¹²T. H. Dunning, *J. Chem. Phys.* **53**, 2823 (1970).

¹³S. Huzinaga, Department of Chemistry Technical Report, University of Alberta, Edmonton, Alberta, Canada, 1971 (unpublished).

¹⁴T. H. Dunning and P. J. Hay, in *Methods of Electronic Structure Theory*, Modern Theoretical Chemistry Vol. 3, edited by H. F. Schaefer (Plenum, New York, 1977), p. 1.

¹⁵T. H. Dunning, *J. Chem. Phys.* **55**, 716 (1971).

¹⁶Y. Osamura, Y. Yamaguchi, and H. F. Schaefer, *J. Chem. Phys.* **75**, 2919 (1981).

¹⁷Y. Osamura, Y. Yamaguchi, and H. F. Schaefer, *J. Chem. Phys.* **77**, 383 (1982).

¹⁸H. F. Schaefer, in *Critical Evaluation of Chemical and Physical Structural Information*, edited by D. R. Lide and M. A. Paul (National Academy of Sciences, Washington, DC, 1974), pp. 591-602.

¹⁹T. J. Lee, J. E. Rice, G. E. Scuseria, and H. F. Schaefer, *Theor. Chim. Acta* **75**, 81 (1989); T. J. Lee and P. R. Taylor, *Int. J. Quantum Chem.* **S23**, 199 (1989).

The *Cis* Monobridged Equilibrium Geometries of Si_2H_2 , Ge_2H_2 , Al_2H_2 , and Ga_2H_2 : A Fundamentally New Type of Molecular Structure.

ROGER S. GREV, BRADLEY J. DELEEUW, YUKIO YAMAGUCHI,
S. -J. KIM, AND HENRY F. SCHAEFER III

Center for Computational Quantum Chemistry
University of Georgia
Athens, Georgia USA 30602

Abstract

In 1990 Colegrove predicted the existence of an unusual monobridged equilibrium geometry for disilyne, Si_2H_2 . Remarkably, the two hydrogen atoms lie *cis* to the Si-Si bond. To our knowledge, no such structure had previously been suggested for any molecule. Interest in such seemingly exotic species accelerated radically with the 1992 microwave observation of the monobridged Si_2H_2 by Cordonnier, Bogey, Demuynck, and Destombes at the University of Lille. Subsequent theoretical studies have shown that this monobridged A_2H_2 structural type also exists for Ge_2H_2 , Al_2H_2 , and Ga_2H_2 . The monobridged structure (with the two hydrogens *cis* to the A-A bond axis) apparently is not a stationary point on the potential energy hypersurfaces of B_2H_2 or C_2H_2 .

1. Introduction

It is clear that the potential energy hypersurfaces of the heavier A_2H_2 molecules (where $\text{A} = \text{Al}, \text{Ga}, \text{Si}, \text{Ge}, \dots$; i.e. where A is a IIIA or IVA main group element below the first row of the periodic table) are much flatter and more intricate than would have been deduced from our knowledge of the acetylene (C_2H_2) system. The ground state of Si_2H_2 , the all-silicon analog of acetylene, was first predicted to have a dibridged C_{2v} symmetry geometry, $\text{Si}(\text{H}_2)\text{Si}$, by Kohler and Lischka in 1983 [1]. This "butterfly" structure was recently verified by the microwave studies of Bogey, Bolvin, Demuynck, and Destombes [2]. Quantum chemists had long maintained that the second most stable isomer of Si_2H_2 was a C_{2v} symmetry disilavinylidene structure, H_2SiSi . Only one other minimum, a *trans*-bent C_{2h} structure, HSiSiH , had been located; that is, until Colegrove and Schaefer's [3] recent study. Using triple- ζ basis sets with two sets of polarization functions on each atom (TZ2P) and optimizing geometries using single and double excitation configuration interaction wavefunctions (CISD), Colegrove and Schaefer discovered a new minimum: a C_s symmetry monobridged structure, $\text{Si}(\text{H})\text{SiH}$, (called bridged-2 by them) [3]. Including zero-point vibrational energies, the bridged-2 $\text{Si}(\text{H})\text{SiH}$ structure was predicted to be a mere $0.4 \text{ kcal mol}^{-1}$ above disilavinylidene at the TZ2P CISD level of theory. Appending

the Davidson correction to approximately account for higher excitation effects, however, reversed the energetic ordering, and the monobridged Si(H)SiH structure was found to lie $0.8 \text{ kcal mol}^{-1}$ below disilavinylidene [3]. Thus, it seemed that at least *three* minima (monobridged, disilavinylidene, and *trans*) were within 20 kcal mol^{-1} of the dibridged ground state.

The monobridged Si(H)SiH structure found by Colegrove and Schaefer exists in a shallow potential well. At the zero-point corrected TZ2P CISD level of theory, the transition state barrier separating the monobridged Si(H)SiH structure from disilavinylidene, H_2SiSi , was predicted to be $3.4 \text{ kcal mol}^{-1}$, while the barrier between Si(H)SiH and dibridged $\text{Si(H}_2\text{)Si}$ was found to be $1.7 \text{ kcal mol}^{-1}$ [3]. Thus, we were astonished to learn that further microwave searches of the silane plasma by Cordonnier, Bogey, Demuynck, and Destombes [4] (under conditions similar to those employed in the earlier study where the dibridged structure was observed [2]) revealed spectra consistent with the rotational constants of the monobridged structure predicted from theory. The French experimentalists [4] posed to us a number of questions that should be uniquely answerable by high level theoretical studies: Although an a-type spectrum was observed, a b-type spectrum should also exist, but it was not found. Thus, is the a-component of the dipole moment considerably larger than the b-component? Why is the disilavinylidene isomer not observed as well? Is the dipole moment of disilavinylidene too small, or is its barrier to isomerization too low?

The questions concerning the dipole moment components were readily answered from unpublished results of the Colegrove-Schaefer [3] study: the monobridged isomer was predicted to have a dipole moment (0.96 D) six times larger than that of disilavinylidene (0.15 D), which rationalizes the latter's undetectability. Furthermore, the ratio $\mu_a:\mu_b$ for the monobridged structure is $0.962:0.039$, which agrees with the lack of observation of the b-type spectrum [4]. These results should not change qualitatively at still-higher levels of theory. There remains, however, the broader, more difficult question concerning the stability of the disilavinylidene and monobridged structures to rearrangement, as well as their energetic relationship to one another and to the ground state dibridged isomer.

Subtle basis set changes and electron correlation effects both dramatically alter the shape of Si_2H_2 's potential energy surface (PES). For example, Colegrove and Schaefer [3] found that *trans*-disilyne (C_{2h} symmetry) has one imaginary vibrational frequency at the SCF level of theory when DZP basis sets are used, but the structure has two imaginary vibrational frequencies when a larger TZ2P basis set is employed. At the CISD level of theory, with both basis sets, the *trans* isomer is a minimum. Furthermore, the monobridged structure is a transition state with the the DZP basis set at the SCF level of theory, but it is a minimum with the TZ2P SCF method. At the CISD level of theory with both the DZP and TZ2P basis sets, the monobridged structure is a minimum. Although the PES appears to be qualitatively correct at the CISD level of theory with either the DZP or TZ2P basis sets, a faithful representation of the PES — in terms of relative energies of the stationary points and characterization of them as minima, transition states, or otherwise — may only be obtained using *both* large basis sets and an extensive treatment of electron correlation.

In light of the monobridged isomer's experimental detection [4] and the questions raised about the Si_2H_2 potential energy surface, we decided to take a fresh look [5] at this problem using the best methods currently available to us. Thus, we review here the dibridged ground state, the monobridged (bridged-2), disilavinylidene, and *trans* minima, the transition states separating the monobridged minimum from both disilavinylidene and

ground state dibridged Si_2H_2 , as well as the inversion barrier in the dibridged ground state. In addition, we discuss the rearrangement of the *trans* minimum, which has thus far eluded characterization, in terms of the transition state leading to the monobridged structure. Analogous results for Ge_2H_2 , Al_2H_2 , and Ga_2H_2 are also reviewed.

2. Methods for Si_2H_2

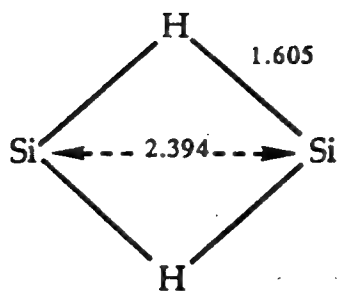
Because Colegrove and Schaefer's results show that inclusion of higher excitation effects is essential for an unequivocal determination of the relative energies of the Si_2H_2 isomers, we employed highly correlated wavefunctions from the start in our second theoretical study of this system [5]. Specifically, we used the coupled cluster method including all single, double, and (perturbative) triple excitations, CCSD(T) [6]. Geometries were precisely located using analytic gradient methods [7], and the characterization of the stationary points was achieved by evaluating the nuclear hessian via finite difference methods.

To facilitate the generation of a reliable potential energy surface for Si_2H_2 in one pass, we initially determined the relative energies of selected portions of the surface using large atomic natural orbital basis sets [8] at the CCSD(T) level of theory. Later, we searched for a segmented contracted basis set that faithfully reproduced the relative energies of the larger ANO basis set. The silicon ANO basis set is a $(20s15p4d3f1g) \rightarrow [6s5p3d2f1g]$ contraction described in an earlier SiH_n thermochemistry study [9], in conjunction with the hydrogen $(8s6p4d) \rightarrow [4s2p1d]$ ANO set of Almlöf and Taylor [8]. For our PES study, we selected a segmented contracted basis set consisting of a triple-zeta plus 2d plus 1f basis set (TZ2df) for silicon that uses McLean and Chandler's 6s5p contraction [10] of Huzinaga's 12s9p primitive set [11] and has polarization function exponents $\alpha_d = 1.0$ and 0.25 , and $\alpha_f = 0.32$. The hydrogen basis set is Dunning's 3s contraction [12] of Huzinaga's 5s primitive set [13] with two sets of polarization functions, $\alpha_p = 1.5$ and 0.375 . The TZ2df/TZ2p basis set yields CCSD(T) relative energies for the dibridged, bridged-2, bridged-1, and disilavinylidene stationary points within $0.2 \text{ kcal mol}^{-1}$ of the larger ANO basis set (see Table I of reference 5).

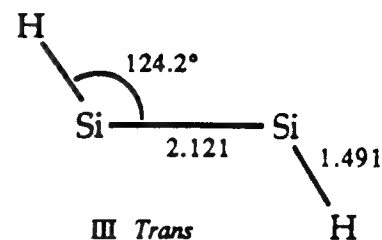
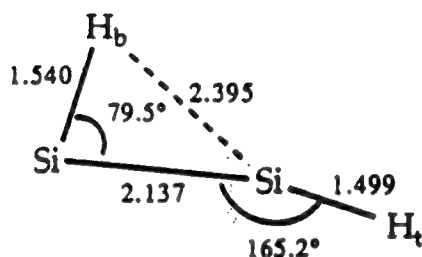
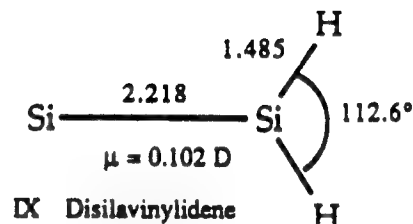
3. Results and Discussion for Si_2H_2

A) STRUCTURES AND ENERGIES

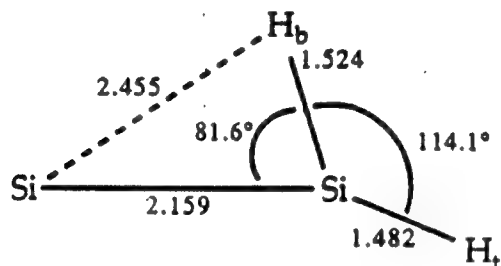
The CCSD(T) optimized geometries are shown in Figure 1. For easy comparison, we include the name and numbering scheme of Colegrove and Schaefer [3] in parentheses if the current usage is different; otherwise, we simply adopt the earlier nomenclature. Some structures are now given descriptive names, such as "disilavinylidene-monobridged TS" instead of the less informative "bridged-1" used earlier [3], to denote that this structure is the transition state (TS) between the disilavinylidene and monobridged minima. Generally, the CCSD(T) optimized geometries are similar to those obtained previously at the CISD level of theory with slightly smaller basis sets [3]. The principal difference is that bond distances have increased slightly, as might be expected for a more highly correlated wavefunction with only slightly larger basis sets. The disilavinylidene-monobridged TS also appears earlier on the reaction path from disilavinylidene to monobridged, as indicated by the Si-Si-H_b angle being 81.6° in this study compared to 76.9° using the TZ2P CISD



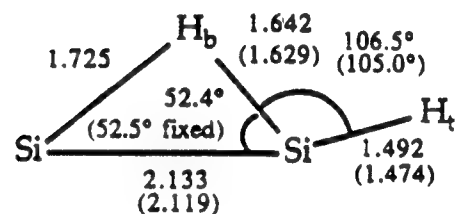
VI Planar Dibridged TS

III *Trans**Trans*→Monobridged TS

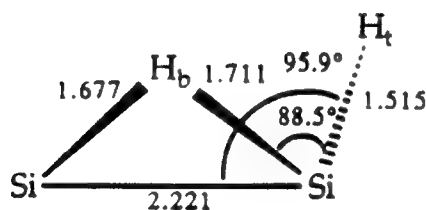
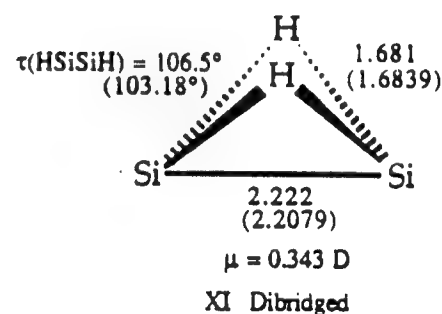
IX Disilavinylidene



Disilavinylidene→Monobridged TS (VII Bridged - 1)

 $\mu_a = 0.848$ D; $\mu_b = 0.055$ D; $\mu_{\text{total}} = 0.850$ D

Monobridged (VIII Bridged - 2)

Monobridged→Dibridged TS (X C_1 TS)

XI Dibridged

Figure 1. The CCSD(T) optimized geometries of Si_2H_2 using silicon TZ2df and hydrogen TZ2p basis sets. Nonzero dipole moments are given for the structures that correspond to minima; for the monobridged structure, the components of the dipole moment along the A and B inertial axes are listed separately. Experimentally determined r_s structures are given in parentheses for the dibridged isomer (from Ref. 2) and the monobridged structure (from Ref. 4). The numbering of the structures in Roman numerals is chosen to conform with that of Ref. 3. Where the current nomenclature differs from Ref. 3, the previous nomenclature is given in parentheses.

method [3]. This continues the trend from even lower levels of theory; e.g. the Si-Si-H_b angle is 68.1° at the TZ2P SCF level of theory.

The disilavinylidene to monobridged rearrangement was first studied by Koseki and Gordon [14] using a 6-31G(d,p) basis set and SCF methods. Although their monobridged structure is incorrectly predicted to be a transition state at that level of theory, Koseki and Gordon's [14] description of the transformation is appropriate; it principally involves the SiH₂ rocking mode. That is, the rearrangement of the disilavinylidene minimum through the disilavinylidene-monobridged TS to the monobridged minimum mainly involves the rotation of the H-Si-H bisector from 180° relative to the Si-Si bond in disilavinylidene towards a value of about 106° in the monobridged structure. Despite this simple description, changes in the Si-Si and Si-H_b bond distances are significant. The Si-Si distance at the monobridged minimum is 2.133 Å, significantly shorter than the bond distance in disilavinylidene (2.218 Å) or in the ground state dibridged structure (2.222 Å); in fact, it is the *shortest* Si-Si bond distance in any molecule yet characterized. Furthermore, the shorter Si-H_b distance is 1.642 Å in the monobridged structure, compared to 1.485 Å in disilavinylidene; the longer of the two Si-H_b distances in Si(H)SiH is 1.725 Å. Our optimized monobridged geometry agrees well with that derived by Cordonnier, Bogey, Demuynck, and Destombes [4] (shown in parentheses in Figure 1) from the observed rotational spectrum and an assumed value for the Si-Si-H_b angle. It is also similar to the 6-31G* MP2 optimized geometry of Curtiss et al. [15], although these authors never stated whether or not their monobridged isomer is a minimum at that level of theory.

Despite being of obvious interest, no reliable studies of the *trans* structure's stability against rearrangement had ever been reported. This is related to the high levels of theory required to accurately characterize it as a minimum, as noted above. The *trans* structure's vibrational frequencies (see Table 1) and force constants reveal two soft modes along which rearrangement to more stable isomers may occur: the H-Si-Si-H torsional mode and the antisymmetric Si-Si-H bending mode. The former might lead to the dibridged ground state via a C₂ symmetry path (indeed, at low levels of theory, this occurs without barrier), and the latter may proceed to the monobridged structure along a C_s symmetry pathway. We successfully located stationary points corresponding to both transformations, but only the C_s symmetry structure (called "*trans*→monobridged TS" in Figure 1) connecting the *trans* and monobridged minima was a true transition state. The C₂ symmetry stationary point (not shown) connecting *trans* and dibridged minima has two imaginary frequencies. One corresponds to the antisymmetric SiSiH bend, suggesting that the actual transition state directly connecting *trans* and dibridged has no symmetry elements other than identity (C₁ point group). We did not pursue this low symmetry transition state further. The *trans*→monobridged TS (not listed in Table 1) has *two* imaginary frequencies at the CCSD level of theory, but only one at CCSD(T), further emphasizing [3] the exceptional sensitivity of the potential energy surface to subtle changes in methodology.

The Si₂H₂ relative energies are reported in Table I of reference 5. Also shown there are single point energies using the larger ANO basis sets described earlier. Comparing the TZ2df/TZ2p relative energies to the ANO basis set results, we find only small differences, except in the case of the planar dibridged structure. Because the TZ2df/TZ2p and ANO basis set relative energies agree, we infer that any remaining uncertainties in relative energies (and thus the overall topology of the Si₂H₂ PES) are unrelated to one-particle basis set deficiencies. Relative to the dibridged structure, the largest relative energy changes on enlarging the basis set from TZ2df/TZ2p to [5421/421] are (excluding the

Table 1. Harmonic vibrational frequencies for the Si₂H₂ isomers at the CCSD(T) level of theory using the TZ2df/TZ2p basis set.

Molecule	Frequency (cm ⁻¹)	Description (Symmetry)	Molecule	Frequency (cm ⁻¹)	Description (Symmetry)
Planar Dibridged TS	1756	Si-H str (b _{3g})	Disilavinylidene	2221	asym Si-H str (b ₂)
	1749	Si-H str (a _g)		2194	sym Si-H str (a ₁)
	1649	Si-H str (b _{1u})		896	SiH ₂ scissors (a ₁)
	1501	Si-H str (b _{2u})		518	Si-Si str (a ₁)
	450	Si-Si str (a _g)		324	SiH ₂ wag (b ₁)
	708i	inversion (b _{3u})		266	SiH ₂ rock (b ₂)
<i>Trans</i> →	2128	Si-H ₁ str (a')	Monobridged	2163	Si-H ₁ str (a')
Monobridged TS	1948	Si-H _b str (a')		1629	sym Si ₂ -H _b str (a')
	637	sym Si-Si-H bend (a')		1125	asym Si ₂ -H _b str (a')
	540	Si-Si str (a')		604	Si-Si str (a')
	53	out-of-plane (a'')		452	H _b -Si-H ₁ scissors (a')
	462i	asym Si-Si-H bend (a')		108	out-of-plane (a'')
Disilavinylidene→	2221	Si-H ₁ str (a')	Dibridged	1616	Si-H str (a ₁)
Monobridged TS	2020	Si-H _b str (a')		1528	Si-H str (b ₁)
	825	SiH ₂ scissors (a')		1194	Si-H str (b ₂)
	559	Si-Si str (a')		1115	Si-H str (a ₂)
	175	out-of-plane (a'')		924	butterfly (a ₁)
	364i	SiH ₂ rock (a')		525	Si-Si str (a ₁)
<i>Trans</i>	2176	asym Si-H str (b _u)			
	2166	sym Si-H str (a _g)			
	618	sym Si-Si-H bend (a _g)			
	567	Si-Si str (a _g)			
	298	asym Si-Si-H bend (b _u)			
	246	H-Si-Si-H torsion (b _g)			

planar dibridged transition state) for the monobridged structure, which is *stabilized* by 0.3 kcal mol⁻¹, and the monobridged-dibridged TS, which is *destabilized* by 0.3 kcal mol⁻¹. Thus, increasing the basis set quality does affect an interesting feature of the PES, the barrier between the monobridged and dibridged minima, by 0.6 kcal mol⁻¹. Unfortunately, the lack of symmetry in the monobridged-dibridged TS makes it impractical to determine the CCSD(T) energy with larger ANO basis sets. Increasing the ANO basis set to [65321/421] stabilizes the monobridged structure no further; in fact, it increases the relative energy by 0.1 kcal mol⁻¹, suggesting that the monobridged-dibridged TS relative energy may be effectively converged as well. If so, the actual classical barrier to rearrangement for the monobridged minimum is around 4.0 kcal mol⁻¹. The relative energy of the planar dibridged TS, which is the transition state for the degenerate rearrangement (inversion) of the dibridged global minimum, is not converged, although it is unlikely to change by more than 1 kcal mol⁻¹ from the final value listed at this level of theory. None of the other relative energies are affected by more than 0.1 kcal mol⁻¹ on increasing the ANO basis set from [5421/421] to [65321/421]. Thus, for uniform comparison, we accept our [5421/421] basis set results as "final". These energies, corrected for differences in zero-point vibrational energies, are listed in Table 2.

Table 2. Relative and absolute 0K enthalpies (in kcal mol⁻¹) of the singlet Si₂H₂ isomers investigated here.

Isomer	Relative ΔH_f^0	Absolute ^a ΔH_f^0	
		from $\Delta H_f^0(\text{Si})^b$	from $\Delta H_f^0(\text{SiH}_4)^c$
Planar Dibridged TS	10.8	105.6	108.5
<i>Trans</i> →Monobridged TS	20.3	115.1	118.0
Disilavinylidene→Monobridged TS	14.0	108.8	111.7
Monobridged→Dibridged TS	12.4	107.2	110.1
<i>Trans</i>	16.3	111.1	114.0
Disilavinylidene	11.6	106.4	109.3
Monobridged	8.7	103.5	106.4
Dibridged	0.0	94.8	97.7

a) from the reaction enthalpy for $\text{Si}(\text{H}_2)\text{Si} \rightarrow 2\text{SiH}$.

b) using $\Delta H_f^0(\text{SiH})$ from Ref. 9 determined relative to $\Delta H_f^0(\text{Si})$.

c) using $\Delta H_f^0(\text{SiH})$ from Ref. 9 determined relative to $\Delta H_f^0(\text{SiH}_4)$.

The SCF and CCSD energies obtained at the CCSD(T) optimized geometries, listed in Table I of reference 5, show the necessity of electron correlation and the importance of triple excitations, especially in the PES region of greatest interest, namely the disilavinylidene to monobridged to dibridged rearrangement. For example, the SCF relative energies are ordered (most stable to least stable) disilavinylidene < monobridged-dibridged TS < disilavinylidene-monobridged TS < monobridged, whereas with CCSD(T) energies the energetic ordering is monobridged < disilavinylidene < monobridged-dibridged TS < disilavinylidene-monobridged TS. Triple excitations show their importance most vividly in the energetic relationship of the disilavinylidene to monobridged rearrangement. To wit, CCSD energies show the disilavinylidene and monobridged isomers to be isoenergetic, with a disilavinylidene to monobridged transition state barrier near 4 kcal mol⁻¹, while CCSD(T) energies show Si(H)SiH to lie 2 kcal mol⁻¹ below H₂SiSi, with a rearrangement barrier (disilavinylidene to monobridged) of 3 kcal mol⁻¹. Thus, triple excitations are essential to conclude that the monobridged isomer is more stable than disilavinylidene. Correlation effects are also required to describe the *trans* to monobridged rearrangement. Recall that Colegrove and Schaefer found a second imaginary vibrational frequency (in addition to the torsional mode) for the *trans* structure when TZ2P basis sets were used at the SCF level of theory. The qualitative reason can be seen from the energies in Table I of reference 5: even with large ANO basis sets, the SCF energy at the CCSD(T) optimized geometry of the *trans*-monobridged TS is *lower* than the analogous *trans* structure energy. At correlated levels of theory, this situation is reversed.

The harmonic vibrational frequencies are listed in Table 1. We have not determined the monobridged-dibridged TS vibrational frequencies at the CCSD(T) level of theory because of computational expense; each C₁ symmetry gradient requires one-and-a-half days of workstation time, and twelve gradients are required to accurately determine the harmonic force field in internal coordinates, a total cost that can not be justified. There is little doubt that it is a transition state, because it was easily located from Colegrove and Schaefer's TZ2P CISD geometry and force field in a transition state search.

Low out-of-plane vibrational frequencies are a ubiquitous feature of Si₂H₂. For example, the monobridged minimum has an out-of-plane vibrational frequency of 108 cm⁻¹, the *trans* minimum has an H-Si-Si-H torsional mode at 246 cm⁻¹, and the disilavinylidene wag is predicted at 324 cm⁻¹. The internal coordinate force constants associated with these vibrations are more revealing, with values of 0.0179, 0.0264, and 0.0738 mdyn-Å/rad² for the monobridged, *trans*, and disilavinylidene minima, respectively. These values are about one order-of-magnitude smaller than what might be considered "normal" bending force constants for first row compounds.

Our final predictions concerning relative stability, given in Table 2, are obtained using CCSD(T) energies with the [5421/421] ANO basis set, corrected for zero-point vibrational energies (ZPVEs). The ZPVEs are estimated [16] as one-half the sum of the real harmonic vibrational frequencies listed in Table 1. For the monobridged-dibridged TS, where we have not determined the harmonic force field, we estimated the ZPVE by using the value for the monobridged structure found here, 8.69 kcal mol⁻¹, and the difference between the ZPVE of the monobridged minimum and the monobridged-dibridged TS of Colegrove and Schaefer [3]. In this way, we obtain a ZPVE of 8.39 kcal mol⁻¹ for the monobridged-dibridged transition state. The resulting 0K enthalpy differences in Table 2 show that the monobridged structure lies 8.7 kcal mol⁻¹ above the dibridged ground state and is separated from the ground state by a barrier of 3.7 kcal mol⁻¹. The disilavinylidene minimum is 11.6 kcal mol⁻¹ above the ground state and requires 2.4 kcal mol⁻¹ to rearrange

to the monobridged structure. The *trans* structure has a 0K enthalpy $16.3 \text{ kcal mol}^{-1}$ above that of the ground state and requires $4.0 \text{ kcal mol}^{-1}$ to rearrange to the monobridged minimum, but there may be an even lower energy pathway in C_1 symmetry leading directly to the ground state. A schematic potential energy surface, including these relative enthalpies, is provided in Figure 2 for easy reference.

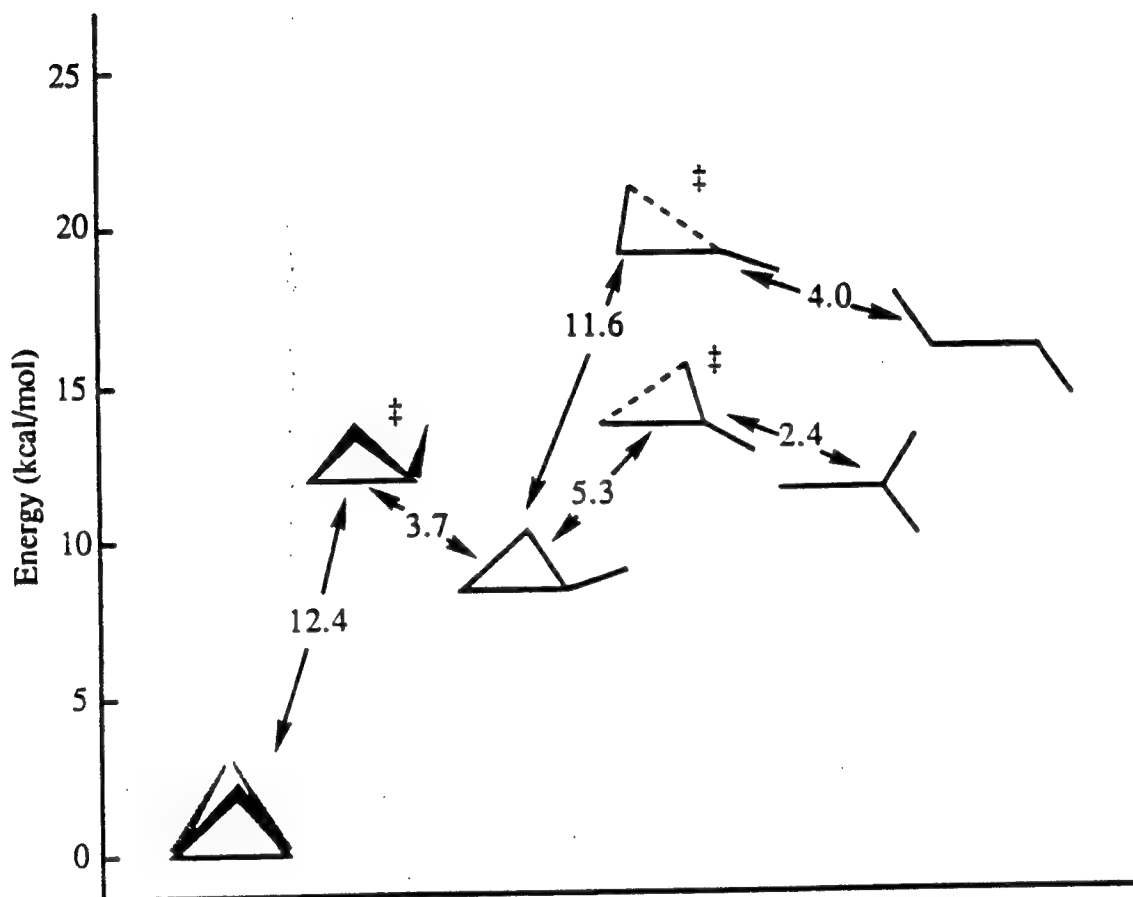


Figure 2. Schematic potential energy surface for Si_2H_2 with final predictions of energetic relationships between the structures investigated. A double-dagger denotes a transition state structure.

B) ROTATIONAL CONSTANTS

Another comparison concerns the rotational constants and the quartic centrifugal distortion constants obtained from experimental observations [2,4] and those determined *ab initio* using our optimized geometries and harmonic force fields. These are listed in Table 3 for the monobridged, $\text{Si}(\text{H})\text{SiH}$, form and its deuterated isomer, and in Table V of reference 5 for the dibridged, $\text{Si}(\text{H}_2)\text{Si}$, isomer and disilavinylidene, H_2SiSi . The parameters for the dibridged and disilavinylidene isomers are consistent with Watson's A reduced Hamiltonian [17], except that the rotational constants (A, B, C) are equilibrium values, as is the asymmetry parameter that enters into the centrifugal distortion constant, δ_K . To be

consistent with experiment [2], the data for the monobridged isomer are determined using Watson's S reduced Hamiltonian in the I' representation [17], also using equilibrium values for rotational constants and the associated asymmetry parameter. The S reduced constants are readily obtained from the A reduced Hamiltonian centrifugal distortion constants produced by previously described algorithms [18].

Table 3. Rotational constants and quartic centrifugal distortion constants for monobridged Si_2H_2 and its deuterated counterpart. All values in MHz.

	Si(H)SiH		Si(D)SiD	
	Experiment (Ref. 4)	Theory ^a	Experiment (Ref. 4)	Theory ^a
A	262128.6	264170	137038.67	137430
B	7361.77951	7258	6803.21682	6697
C	7161.92044	7064	6483.81180	6386
D _J	4.755192×10^{-3}	4.547×10^{-3}	3.56594×10^{-6}	3.408×10^{-3}
D _K	151.930×10^{-3}	121.4×10^{-3}	67.637×10^{-3}	68.55×10^{-3}
D _K	60.	49.97	16.60	12.15
ϕ_1	-0.13396×10^{-3}	-0.1203×10^{-3}	-0.17067×10^{-3}	-0.1684×10^{-3}
ϕ_2	-9.692×10^{-6}	-6.166×10^{-6}	-20.659×10^{-6}	-13.90×10^{-6}

a) Rotational constants and the corresponding asymmetry parameter used to determine the centrifugal distortion constants are obtained using r_e values.

The agreement between experimentally [4] and theoretically derived rotational constants for Si(H)SiH and Si(D)SiD is quite satisfactory (see Table 3), and leaves no doubt concerning the identity of this novel species observed by Cordonnier, Bogey, Demuynck, and Destombes [4]. The agreement between theory and experiment [2] for Si(H₂)Si is even better than that for the monobridged Si(H)SiH, except for the very small δ_J , which differs from experiment by a factor of two. We might expect the experimental and theoretical data for Si(H₂)Si to agree better than that for Si(H)SiH because the latter is exceptionally floppy, whereas the dibridged isomer is much more rigid. The theoretical predictions for H₂SiSi were reported elsewhere [5] as an inducement for experimentalists who may wish to characterize this low-lying isomer with small dipole moment and marginal kinetic stability.

C) BONDING CONSIDERATIONS

As discussed above, Si₂H₂ has three isomers within 20 kcal mol⁻¹ of the ground state. Although the minima are structurally fascinating, Si₂H₂'s features are not unique. We

recently completed a study of Al_2H_2 [19] and found a nearly one-to-one correspondence between the Al_2H_2 structures and energies and those of Si_2H_2 . That is, for Al_2H_2 the global minimum is dibridged (but planar) with energetically low-lying monobridged, vinylidene-like, and *trans* minima. The relative energies for Al_2H_2 are +8 kcal mol⁻¹ (vinylidene-like), +9 kcal mol⁻¹ (monobridged), and +14 kcal mol⁻¹ (*trans*), compared to +12, +9, and +16 kcal mol⁻¹, respectively, for the analogous Si_2H_2 structures; a truly remarkable correlation.

For Al_2H_2 a qualitative explanation of the bonding in the dibridged, monobridged, and *trans* structures is that these are the three possible dimerization (coordination) modes for a molecule with two electron-rich sites (the aluminum lone pair and the hydrogen center) and one electron-deficient center (the empty p-orbitals of the aluminum atom) [19]. Thus, the *trans* structure results from two AlH monomers simultaneously donating electron density from their lone pairs to the empty p-orbital on the other monomer; the dibridged isomer results from the simultaneous coordination of the electron rich hydrogen centers to the empty p-orbital of the other monomer; and the monobridged isomer results from one AlH monomer donating a lone pair and the other donating via the hydrogen center. These coordination modes are depicted in Figure 3.

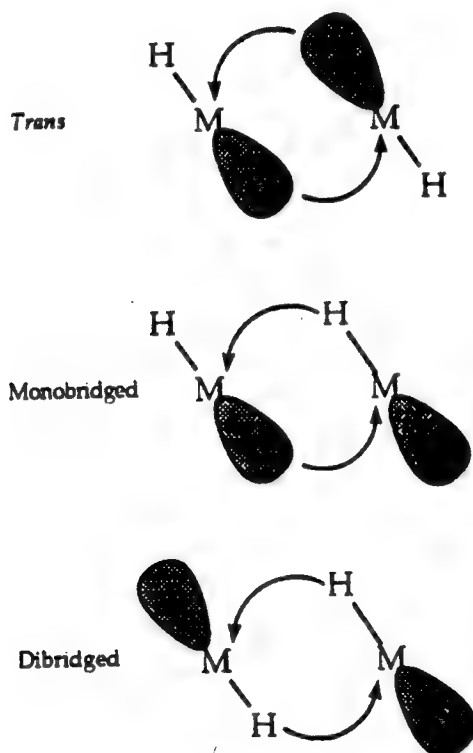


Figure 3. The *trans*, monobridged, and dibridged isomers of Si_2H_2 and Al_2H_2 considered as coordinately-bonded dimers. The *trans* structure results from simultaneous lone pair donation of each monomer, the monobridged from donation of a lone pair from one monomer and a hydride from the other monomer, and the dibridged from the simultaneous donation of hydrides from both centers.

The same coordination model applies to Si_2H_2 with but a trivial modification: there is an additional pair of electrons. For the *trans* and monobridged structures, these extra electrons populate a π bonding orbital, and the only structural implication is a reduced bond distance between the heavy atoms. For the dibridged isomer, the additional pair of π electrons induces puckering of the skeleton, yielding a C_{2v} symmetry ground state instead of the D_{2h} planar dibridged ground state predicted for Al_2H_2 . Qualitatively, the 2.394 Å Si-Si bond distance in planar dibridged Si_2H_2 places considerable stress on the π bond — sideways overlap of pure p-orbitals at this distance does not yield a stable bond — and molecular models are sufficient to convince us that puckering substantially increases the overlap of these silicon p-orbitals. Trinquier [20] adopted similar coordination models to explain the existence of bridged (and dibridged) forms of M_2H_4 ($\text{M} = \text{Si}, \text{Ge}, \text{Sn}, \text{Pb}$). In those molecules, a stable coordination mode involving one hydrogen and one lone pair (i.e., monobridged) did not arise until Sn_2H_4 . Thus, removing two hydrogen atoms to form M_2H_2 stabilizes this coordination mode sufficiently that monobridged isomers exist two rows higher than they do for M_2H_4 .

D) SUMMARY FOR Si_2H_2

Using state-of-the-art wavefunctions and extended basis sets, we find the monobridged $\text{Si}(\text{H})\text{SiH}$ isomer to be the second most stable form of Si_2H_2 , lying 8.7 kcal mol⁻¹ above the ground state isomer, $\text{Si}(\text{H}_2)\text{Si}$. The monobridged isomer resides in a shallow potential well, with a 3.7 kcal mol⁻¹ barrier separating it from the dibridged global minimum. The *ab initio* structure and rotational constants of $\text{Si}(\text{H})\text{SiH}$ agree well with Cordonnier, Bogey, Demuynck, and Destombes's microwave results. Disilavinylidene, H_2SiSi , which was long believed to be the second most stable isomer of Si_2H_2 , poses a challenge to spectroscopists because the barrier separating H_2SiSi from $\text{Si}(\text{H})\text{SiH}$ is predicted to be only 2.4 kcal mol⁻¹. Given that spectroscopists have now characterized $\text{Si}(\text{H})\text{SiH}$, it may only be a matter of better instrumentation before H_2SiSi is characterized as well.

4. Monobridged Structures Of Ge_2H_2 , Al_2H_2 , and Ga_2H_2 .

Given the observation of monobridged Si_2H_2 , it makes sense to examine whether other A_2H_2 molecules also display this new structural type. Our theoretical studies to date have not resulted in the location of monobridged stationary points for either B_2H_2 or C_2H_2 that are comparable to equilibrium structures for monobridged Al_2H_2 and Si_2H_2 . Note that while the well-known [21] vinylidene to acetylene transition state is monobridged, the two hydrogen atoms lie *trans* to the C-C bond. However, we have found *cis* monobridged equilibrium geometries for Ge_2H_2 , Al_2H_2 , and Ga_2H_2 , and these are shown in Figures 4, 5, and 6, respectively. The relative energies of the different structures for Ge_2H_2 , Al_2H_2 , and Ga_2H_2 are summarized in Tables 4, 5, and 6, respectively.

The theoretical predictions [22] for the valence-isoelectronic Ge_2H_2 should be most similar to those for Si_2H_2 . For example, monobridged Ge_2H_2 is actually predicted to be a transition state at the DZP SCF level, precisely as was found [1] for Si_2H_2 . For both molecules, the introduction of electron correlation at the DZP CISD level is seen to properly describe the monobridged structure as a genuine minimum.

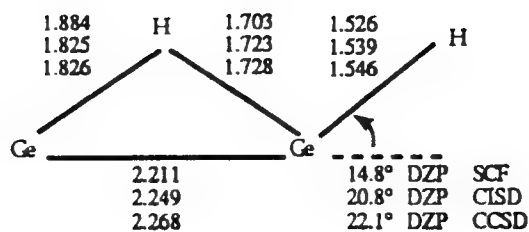


Figure 4. Theoretical geometries for the monobridged closed-shell singlet state of Ge_2H_2 . Bond distances are in Å.

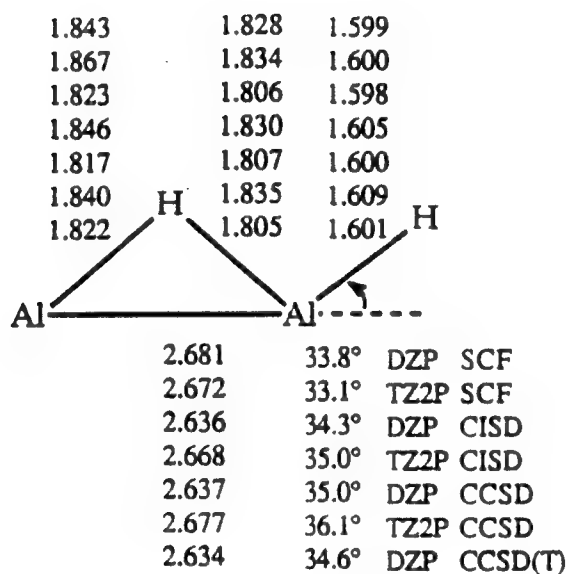


Figure 5. Theoretical geometries for the monobridged closed-shell singlet state of Al_2H_2 . Bond distances are in Å.

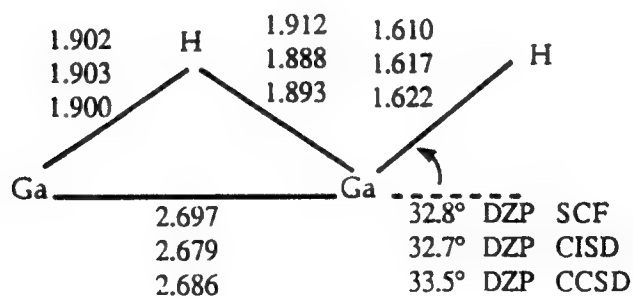


Figure 6. Theoretical geometries for the monobridged closed-shell singlet state of Ga_2H_2 . Bond distances are in Å.

Table 4.
Relative energies (kcal/mol) of stationary point structures for the Ge_2H_2 system. Only the final column includes zero-point vibrational energies.

Isomer	SCF		CISD ^a		CCSD		CCSD(T)	
	DZP	TZP+ ^b	DZP	TZP+ ^b	DZP	TZP+ ^b	TZP+ ^c	TZP+ ^c +ZPVE ^d
vinylidene-like	4.3	5.6	9.2 9.3	10.6 10.7	9.0	10.4	11.1	11.0
mono-bridged	13.4	13.7	11.6 10.4	12.0 10.9	10.6	11.0	9.8	9.0
butterfly	0.0	0.0	0.0 0.0	0.0 0.0	0.0	0.0	0.0	0.0

- a) The lower number in the CISD boxes is the Davidson-corrected energy difference.
b) At the DZP optimized geometry obtained with the corresponding level of theory.
c) At the DZP CCSD optimized geometry.
d) DZP CCSD harmonic zero-point vibrational energy correction.

Table 5.
Energies of Al_2H_2 structures relative to $2(\text{AlH})$ in kcal/mol. Only the final column includes zero-point vibrational energies (ZPVE).

Isomer	SCF		CISD ^a		CCSD		CCSD(T)			
	DZP	TZ2P	DZP	TZ2P	DZP	TZ2P	DZP	TZ2P ^c	ANO ^c	"BEST"
linear $^1\Delta$	12.2	9.2	13.2 14.3	10.8 12.4	-	-	-	-	-	15.2 ^e
linear $^3\Sigma_g^-$	-2.4	-6.6	0.3 2.0	-1.6 0.9	-	-	-	-	-	3.8 ^e
<i>trans</i>	-4.9	-5.9	-9.4 -10.8	-10.7 -12.0	-9.5	-10.5	-11.5	-12.9	-15.9	-13.8 ^d
mono-bridged	-10.5	-11.0	-16.0 -16.6	-16.6 -17.2	-15.6	-16.0	-17.3	-18.1	-20.9	-18.7 ^d
vinylidene-like	-16.3	-19.4	-17.1 -16.6	-19.8 -19.1	-16.1	-18.5	-16.9	-19.5	-22.7	-19.7 ^d
planar dibridged	-20.3	-20.0	-27.7 -28.7	-26.8 -27.6	-28.0	-26.7	-29.3	-28.4	-30.0	-27.2 ^d
$2(\text{AlH})^b$	0.0	0.0	0.0 0.0	0.0 0.0	0.0	0.0	0.0	0.0	0.0	0.0

- a) The lower number in the CISD columns is the Davidson-corrected energy difference.
b) The "supermolecule" method was used to obtain the total CISD energies for $2(\text{AlH})$.
c) At the TZ2P CCSD optimized geometry.
d) ANO CCSD(T) including TZ2P CCSD harmonic zero-point vibrational energy correction.
e) TZ2P CISD+Q including TZ2P SCF harmonic zero-point vibrational energy correction.

Table 6.
Relative energies (kcal/mol) of stationary point structures for the Ga_2H_2 system.
Only the final column includes zero-point vibrational energies.

Isomer	SCF		CISD ^a		CCSD		CCSD(T)	
	DZP	TZP+f ^b	DZP	TZP+f ^b	DZP	TZP+f ^b	TZP+f ^c	TZP+f ^c +ZPVE ^d
<i>trans</i>	11.3	11.5	13.6 13.2	13.1 12.6	13.5	13.0	12.6	12.4
mono- bridged	8.0	7.9	9.0 9.1	8.3 8.3	9.3	8.5	8.2	7.9
vinylidene -like	-0.1	0.1	5.6 6.8	4.7 5.7	6.4	5.4	6.1	6.8
planar dibridged	0.0	0.0	0.0 0.0	0.0 0.0	0.0	0.0	0.0	0.0

a) The lower number in the CISD boxes is the Davidson-corrected energy difference.

b) At the DZP optimized geometry obtained with the corresponding level of theory.

c) At the DZP CCSD optimized geometry.

d) DZP CCSD harmonic zero point vibrational energy correction.

One of the most critical structural features of the *cis* monobridged geometry is the angle between the terminal Ge-H bond and the extension of the Ge-Ge bond axis. This angle is seen in Figure 4 to be 20.8° at the DZP CISD level of theory. The analogous DZP CISD prediction for the monobridged structure of Si_2H_2 is very similar, namely 20.0° . From our work [5] on Si_2H_2 using much higher levels of theory, a final value of 21.1° is found for this critical angle in monobridged Si_2H_2 .

Another interesting feature of the monobridged Ge_2H_2 structure is the difference between the two Ge-H distances for the bridging hydrogen. This difference is 0.181 \AA with DZP SCF, 0.102 \AA with DZP CISD, and 0.098 \AA with the DZP CCSD method. Colegrove's analogous results [3] for monobridged Si_2H_2 are $\Delta r[\text{Si-H}_b] = 0.119 \text{ \AA}$ (DZP SCF) and 0.082 \AA (DZP CISD). At the highest level of theory considered to date for Si_2H_2 [TZ2df/TZ2p CCSD(T)], Grev [5] predicts the monobridged $\Delta r[\text{Si-H}_b]$ to be 0.083 \AA . Thus, for Ge_2H_2 the ultimate difference between bridging Ge-H distances should be about 0.1 \AA , or roughly 0.02 \AA more than is the case for monobridged Si_2H_2 .

The relative energies of Table 4 show that the vinylidene-like structure of Ge_2H_2 is the second lowest-lying isomer at the SCF level of theory. However, correlation effects tend to destabilize the vinylidene-like structure while stabilizing the monobridged structure compared to the butterfly global minimum. Thus, as was the case with the Si_2H_2 energetics [3,5], the Ge_2H_2 monobridged structure eventually becomes the second lowest-lying isomer of Ge_2H_2 . At the ZPVE-corrected TZP+f CCSD(T) level of theory, the monobridged and vinylidene Ge_2H_2 structures are predicted to lie at 9.0 and 11.0 kcal/mole, respectively, above the butterfly global minimum.

The Al_2H_2 and Ga_2H_2 molecules differ from those discussed above in having D_{2h} planar dibridged global minima. Both molecules *do* have monobridged equilibrium geometries. Although we have not attempted to locate any transition states, the monobridged structure is, by analogy with Si_2H_2 [3,5], most likely obtained from the vinylidene-like (branched) structure by following the in-plane rock motion of the latter. This mode has a vibrational frequency of 250 cm^{-1} for Al_2H_2 . Similarly, the out-of-plane bending frequency of the terminal hydrogen in the monobridged structure is quite low (173 cm^{-1}) and presumably leads to the transition state for rearrangement to the planar dibridged minimum. The rearrangement barriers are probably small, but this does not preclude the observation of monobridged Al_2H_2 ; in Si_2H_2 , for which the monobridged isomer has been observed and characterized [4], the barrier is predicted to be 3.7 kcal mol^{-1} [5]. A more fundamental stumbling block to the observation of the monobridged isomer is its small dipole moment, 0.26 D . The vinylidene-like isomer has a much larger dipole moment, 1.55 D . This trend is the opposite of that in Si_2H_2 [5], where the monobridged isomer has a larger dipole moment than the disilavinylidene isomer. This partially explains the inability of the Lille group to observe the disilavinylidene isomer of Si_2H_2 in microwave studies. Our results suggest that microwave detection of the vinylidene-like isomer of Al_2H_2 may be plausible.

In light of the near degeneracy of the low-lying monobridged (see Table 5) and vinylidene-like structures of Al_2H_2 , it was decided to press on to a higher level of theory with the CCSD(T) method. In this manner, DZP CCSD(T) stationary point geometries were optimized for the four closed-shell singlet structures of Al_2H_2 . We found [19] that the DZP CCSD(T) structures differ imperceptibly from those optimized at the DZP CCSD level of theory, except for the *trans*-bent structure for which the Al-Al bond distance decreases by 0.015 \AA . This breeds confidence in simply adopting the TZ2P CCSD optimized geometries for any further analysis. The DZP CCSD(T) stationary point total energies show that the unsymmetrical monobridged structure falls 0.4 kcal mol^{-1} below the vinylidene-like structure of Al_2H_2 . This roughly follows the pattern of behavior predicted for Si_2H_2 by Colegrove [3].

The energetic ordering of the monobridged and vinylidene-like structures of Al_2H_2 could reverse again if larger basis sets are used. Table 5 indicates that correlated energies of both structures decrease (relative to the planar dibridged global minimum) in going from the DZP to the TZ2P basis set. To investigate this further, we determined single point TZ2P CCSD(T) energies at the TZ2P CCSD optimized geometries. Additional single point CCSD(T) energies, again at the TZ2P CCSD optimized geometries, were determined using the atomic natural orbital (ANO) basis sets of Widmark, Roos, et al. [23]. Specifically, we used their $5s4p3d2f$ ANO set for aluminum and the $3s2p1d$ ANO set for hydrogen. Our final prediction, using the ANO CCSD(T) energies and correcting for differential zero-point vibrational effects at the TZ2P CCSD level of theory, is that the monobridged isomer lies 0.9 kcal mol^{-1} above the vinylidene-like isomer and that both of these are within 9 kcal mol^{-1} of the planar dibridged ground state structure.

Finally we arrive at the monobridged structure of Ga_2H_2 (Figure 6, Table 6). It is predicted [24] to lie 7.9 kcal mol^{-1} above the dibridged minimum. The Ga-Ga bond distance (2.686 \AA) lies between the values expected for Ga-Ga single and double bonds. This result is explained by the localized bond analysis: the gallium atoms are connected by a banana-type bond of the sort found in the *trans* isomer and a three-center bridging bond similar to that found in the dibridged isomer. Furthermore, the terminal hydrogen is connected to one of the gallium atoms by a conventional σ bond, and there is a lone-pair of electrons on the other gallium atom. The low vibrational frequencies for the Ga-Ga stretch (156 cm^{-1}) and the terminal hydrogen out-of-plane bend (199 cm^{-1}) suggest a possible transition state from the monobridged isomer to the planar dibridged global minimum. This suggestion does not follow trivially from the mechanistic study of reference 5, since the

planar dibridged structure lies 11 kcal mol⁻¹ above the butterfly structure for the Si₂H₂ system examined there. Among the Ga₂H₂ structures considered in this paper, the vinylidene-like isomer has the largest dipole moment (1.72 D), and thus may be the best target for microwave detection. The monobridged isomer has a smaller dipole moment (0.56 D).

The presence of the unsymmetrical *cis* monobridged structures of Ge₂H₂, Al₂H₂ and Ga₂H₂ as genuine minima proves that this structural type is not limited to Si₂H₂ [3,5], for which solid experimental structural confirmation now exists [4]. This work surely suggests that related potential energy hypersurfaces — BAlH₂, BGaH₂, AlGaH₂, SiCH₂, GeCH₂, GeSiH₂ — should be carefully searched for new unsymmetrical monobridged structures.

5. Acknowledgements

This research was supported by the U. S. Air Force Office of Scientific Research, Grant AFOSR-92-J-0047. We thank M. Cordonnier, M. Bogey, C. Demuynck, and J.-L. Destombes for communicating the results of reference 4 prior to publication, and for numerous stimulating exchanges. We also thank Zoltan Palagyi for helpful discussions.

References

- [1] H. Lischka and H. Kohler, *J. Am. Chem. Soc.* **105**, 6646 (1983). Closely related independent research is that of J. S. Binkley, *J. Am. Chem. Soc.* **106**, 603 (1984).
- [2] M. Bogey, H. Bolvin, C. Demuynck, and J.-L. Destombes, *Phys. Rev. Lett.* **66**, 413 (1991).
- [3] B. T. Colegrove and H. F. Schaefer, *J. Phys. Chem.* **94**, 5593 (1990).
- [4] M. Cordonnier, M. Bogey, C. Demuynck, and J.-L. Destombes, *J. Chem. Phys.* **97**, 7984 (1992).
- [5] R. S. Grev and H. F. Schaefer, *J. Chem. Phys.* **97**, 7990 (1992).
- [6] K. Raghavachari, G. W. Trucks, J. A. Pople, and M. Head-Gordon, *Chem. Phys. Lett.* **157**, 470 (1989); G. E. Scuseria and T. J. Lee, *J. Chem. Phys.* **93**, 5851 (1990).
- [7] G. E. Scuseria, *J. Chem. Phys.* **94**, 442 (1991).
- [8] (a) J. Almlöf and P. R. Taylor, *J. Chem. Phys.* **86**, 4070 (1987). (b) J. Almlöf and P. R. Taylor, *Adv. Quantum Chem.* **22**, 301 (1991).
- [9] R. S. Grev and H. F. Schaefer, *J. Chem. Phys.* **97**, 8389 (1992).
- [10] A. D. McLean and G. S. Chandler, *J. Chem. Phys.* **72**, 5639 (1980).
- [11] S. Huzinaga, *Approximate Atomic Functions. II*, Department of Chemistry Report, University of Alberta, Edmonton, Alberta, Canada, 1971.
- [12] T. H. Dunning, *J. Chem. Phys.* **55**, 716 (1971).
- [13] S. Huzinaga, *J. Chem. Phys.* **42**, 1293 (1965).
- [14] S. Koseki and M. S. Gordon, *J. Phys. Chem.* **93**, 118 (1989).
- [15] L. A. Curtiss, K. Raghavachari, P. W. Deutsch, and J. A. Pople, *J. Chem. Phys.* **95**, 2433 (1991).
- [16] R. S. Grev, C. L. Janssen, and H. F. Schaefer, *J. Chem. Phys.* **95**, 5128 (1991).
- [17] J. K. G. Watson, in *Vibrational Spectra and Structure* edited by J. R. Durig (Elsevier, New York, 1977), volume 6, p. 1.
- [18] D. A. Clabo Jr., W. D. Allen, R. B. Remington, Y. Yamaguchi, and H. F. Schaefer, *Chem. Phys.* **123**, 187 (1988).
- [19] Z. Palagyi, R. S. Grev, and H. F. Schaefer, "Striking Similarities Between Elementary Silicon and Aluminum Compounds: Monobridged, Dibridged, *Trans*-Bent, and Vinylidene Isomers of Al_2H_2 ," *J. Am. Chem. Soc.*, in press.
- [20] (a) G. Trinquier, *J. Am. Chem. Soc.* **112**, 2130 (1990). (b) *ibid* **113**, 144 (1991).
- [21] M. M. Gallo, T. P. Hamilton, and H. F. Schaefer, *J. Am. Chem. Soc.* **112**, 8714 (1990).
- [22] Z. Palagyi, H. F. Schaefer, and E. Kapuy, "Ge $_2\text{H}_2$: A Molecule With a Low-Lying Monobridged Equilibrium Geometry", submitted for publication.
- [23] (a) P.-O. Widmark, P.-A. Malmqvist, and B. O. Roos, *Theor. Chim. Acta* **77**, 291 (1990). (b) P.-O. Widmark, J. Persson, and B. O. Roos, *Theor. Chim. Acta* **79**, 419 (1991).
- [24] Z. Palagyi, H. F. Schaefer, and E. Kapuy, *Chem. Phys. Lett.* **203**, 195 (1993).

Isomerization of $\text{PO}_3^{--}(\text{H}_2\text{O})_n$ Clusters to $\text{H}_2\text{PO}_4^{--}(\text{H}_2\text{O})_{n-1}$: Transition States and Barrier Heights

Buyong Ma, Yaoming Xie, Mingzuo Shen, Paul v. R. Schleyer, and
Henry F. Schaefer, III*

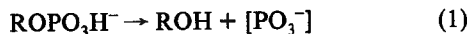
Contribution from the Center for Computational Quantum Chemistry, The University of Georgia,
Athens, Georgia 30602

Received May 10, 1993*

Abstract: Several mechanisms for the isomerization reactions of the $\text{PO}_3^{--}(\text{H}_2\text{O})_n$ clusters ($n = 1, 2$, and 3) to $\text{H}_2\text{PO}_4^{--}(\text{H}_2\text{O})_{n-1}$ have been studied using *ab initio* quantum mechanical methods, resulting in predictions of the transition state structures, isomerization barrier heights, exothermicities, and products. Basis sets as large as triple- ζ plus double polarization plus f functions have been used with self-consistent-field, second-order perturbation theory, configuration interaction, and coupled cluster methods. The isomerization barrier (ΔG°) for $\text{PO}_3^{--}\text{H}_2\text{O}$ to $\text{H}_2\text{PO}_4^{--}$ is 32 kcal mol⁻¹ at the DZP+diff SCF level, 25 kcal mol⁻¹ at the DZP CISD level, and 22 kcal mol⁻¹ at the DZP+diff MP2 level. The isomerization barriers for $\text{PO}_3^{--}(\text{H}_2\text{O})_2$ and $\text{PO}_3^{--}(\text{H}_2\text{O})_3$ are lower by only a few kilocalories per mole than for $\text{PO}_3^{--}\text{H}_2\text{O}$ via four-centered transition states and lower by about 5 kcal mol⁻¹ by six-center transition states. The PO_3^{--} anion is thermodynamically stable in the gas phase only when the $\text{PO}_3^{--}\text{H}_2\text{O}$ molar ratio is below 1:3. However, even with the 1:3 molar ratio, the $\text{PO}_3^{--}(\text{H}_2\text{O})_3$ cluster is expected to be a product along with $\text{H}_2\text{PO}_4^{--}(\text{H}_2\text{O})_2$. The $\text{H}_2\text{PO}_4^{--}$ anion forms double-donor double-acceptor hydrogen bonds with H_2O similar to those predicted earlier for PO_3^{--} . The C_2 symmetry conformation of $\text{H}_2\text{PO}_4^{--}$ is more stable than the C_s form, while the C_{2v} conformation is a stationary point with two imaginary vibrational frequencies. The potential energy surfaces for $\text{H}_2\text{PO}_4^{--}\text{H}_2\text{O}$ and $\text{H}_2\text{PO}_4^{--}(\text{H}_2\text{O})_2$ are qualitatively similar to that for isolated $\text{H}_2\text{PO}_4^{--}$. The exothermicities ($-\Delta H^\circ$) of the reactions $\text{PO}_3^{--}(\text{H}_2\text{O})_n \rightarrow \text{H}_2\text{PO}_4^{--}(\text{H}_2\text{O})_{n-1}$ are 18 ($n = 1$), 22 ($n = 2$), and 21 kcal mol⁻¹ ($n = 3$) at the DZP+diff SCF level of theory. The DZP+diff SCF hydration exothermicity of $\text{H}_2\text{PO}_4^{--}$ (i.e. $-\Delta H^\circ$ for $\text{H}_2\text{PO}_4^{--} + \text{H}_2\text{O} \rightarrow \text{H}_2\text{PO}_4^{--}\text{H}_2\text{O}$) is 14 kcal mol⁻¹, while that for $\text{H}_2\text{PO}_4^{--}\text{H}_2\text{O}$ is 8 kcal mol⁻¹. The analogous hydration exothermicities for the isomers $\text{PO}_3^{--}\text{H}_2\text{O}$ and $\text{PO}_3^{--}(\text{H}_2\text{O})_2$ are 11 and 10 kcal mol⁻¹, respectively. Although much progress has been made, several questions remain concerning the relationships between the present theoretical results and existing experiments.

1. Introduction

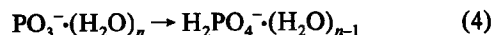
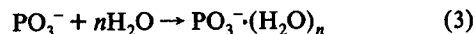
Phosphates are among the most important compounds in living systems, as phosphorylation is a key to biochemical synthesis. The mechanisms of the chemical reactions that involve the formation and destruction of phosphate esters are vital to the understanding of living systems.¹ One of the major possibilities requires that the coordination number of phosphorus decrease from four to three, to produce a "metaphosphate" that then adds a nucleophile to yield product.



Extensive research has focused on this mechanism,^{2a,3} and there is considerable debate over whether PO_3^{--} can exist as a free entity in water. However, due to the high reactivity of the PO_3^{--} anion, some positive but mostly negative results have been obtained, depending on the nature of the solvent systems. There appears to be no evidence that requires the formation of a metaphosphate monoion in aqueous solution.^{2a} However, very recently, it has been reported⁴ that while discrete PO_3^{--} is an intermediate in the

hydrolysis of monothiopyrophosphate (MTP), it is too reactive and cannot escape from its solvation sphere; PO_3^{--} is captured by water or another nucleophile that competes with water in solvating MTP.

Despite its high reactivity in aqueous solution, the clusters of the PO_3^{--} anion with water molecules are believed to be stable in the gas phase.^{5,6} In the gas phase the pertinent reactions seem to be



Our previous research⁷ has attempted to characterize the intermediate $\text{PO}_3^{--}(\text{H}_2\text{O})_n$ clusters and essential agreement with the experimental data has been obtained. Nevertheless, there are still many unresolved questions. For example, how does isomerization from $\text{PO}_3^{--}(\text{H}_2\text{O})_n$ to $\text{H}_2\text{PO}_4^{--}(\text{H}_2\text{O})_{n-1}$ occur? Why is the behavior of PO_3^{--} in the gas phase and in aqueous solution so different? The heart of the present research is to understand the isomerization reactions, which are difficult to investigate experimentally. In order to relate gas-phase and solution-phase chemistry, we need to know the barrier heights for the isomerizations. To our knowledge, there is no published theoretical research on the $\text{PO}_3^{--}(\text{H}_2\text{O})_n$ isomerization barriers, which would provide the key to understanding the thermodynamics in the gas phase.^{8,13}

* Abstract published in *Advance ACS Abstracts*, November 1, 1993.
(1) Westheimer, F. H. *Chem. Rev.* **1981**, *81*, 313. Westheimer, F. H. *Science* **1987**, *235*, 1173.

(2) (a) Herschlag, D.; Jencks, W. P. *J. Am. Chem. Soc.* **1989**, *111*, 7579. Herschlag, D.; Jencks, W. P. *J. Am. Chem. Soc.* **1989**, *111*, 7587. Herschlag, D.; Jencks, W. P. *J. Am. Chem. Soc.* **1990**, *112*, 1951. (b) Jencks, W. P. Personal communication.

(3) (a) Jencks, W. P. *Acc. Chem. Res.* **1980**, *13*, 161. (b) Ramirez, F.; Marecek, J.; Minore, J.; Srivastava, S.; leNoble, W. J. *Am. Chem. Soc.* **1986**, *108*, 348. (c) Burgess, J.; Blundell, N.; Cullis, P. M.; Hubbard, C. D.; Misra, R. J. *Am. Chem. Soc.* **1988**, *110*, 7900. (d) Freeman, S.; Friedman, J. M.; Knowles, D. J. *Am. Chem. Soc.* **1987**, *109*, 3166. (e) Cullis, P. M.; Nicholls, D. J. *Chem. Soc., Chem. Commun.* **1987**, 783.

(4) Lightcap, E. S.; Frey, P. A. *J. Am. Chem. Soc.* **1992**, *114*, 9750.

(5) Henchman, M. J.; Viggiano, A. A.; Paulson, J. F.; Freedman, A.; Wormhoadt, J. J. *Am. Chem. Soc.* **1985**, *107*, 1453.

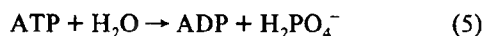
(6) Keese, R. G.; Castleman, A. W., Jr. *J. Am. Chem. Soc.* **1989**, *111*, 9015.

(7) Ma, B.; Xie, Y.; Shen, M.; Schaefer, H. F. *J. Am. Chem. Soc.* **1993**, *115*, 1943.

(8) Westheimer, F. H. Personal communication.

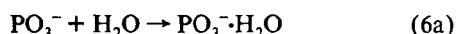
Only one of the possible isomerization products, H_2PO_4^- , has received theoretical attention previously. Kollman⁹ has done pioneering research on the systematic conformational analysis of H_3PO_4 , H_2PO_4^- , and HPO_4^{2-} using quantum mechanical methods. Later, Ewig¹⁰ studied phosphinic, phosphonic, and phosphoric acids. O'Keeffe¹¹ also examined similar systems extensively, including H_3PO_4 and H_2PO_4^- . In order to understand reaction 4, the structure and energetics of the $\text{H}_2\text{PO}_4^-(\text{H}_2\text{O})_{n-1}$ clusters are as important as those for $\text{PO}_3^-(\text{H}_2\text{O})_n$.

$\text{H}_2\text{PO}_4^-(\text{H}_2\text{O})_{n-1}$ clusters and their formation are also important in biochemistry. For example, it is thought¹² that the difference in the solvation energies of the reactants and the products in the reaction

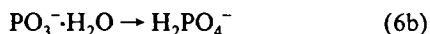


contributes significantly to the ΔH and ΔG values.

Unlike the clustering reaction



there is no direct experimental measurement of the energy for the isomerization reaction

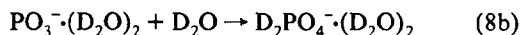


The values deduced from indirect experiments differ from one another blatantly¹³—the ΔH° for isomerization 6b derived from Unkel and Freedman's experiments^{13a} is about $-58 \text{ kcal mol}^{-1}$ but that derived from Rudnyi's experiments^{13b} is only about $-24 \text{ kcal mol}^{-1}$. The latter value is generally considered to be more reasonable.¹³

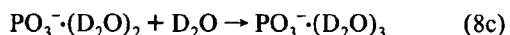
In addition to reactions 6a and 6b, two other isomerization reactions



are important. Experiments by Keesee and Castleman⁶ have shown that ΔH° for the related process



is $-16.3 \text{ kcal mol}^{-1}$. However, our previous work⁷ showed that for the clustering reaction



the theoretical ΔH° is $-9.7 \text{ kcal mol}^{-1}$ at the DZP+diff SCF level. If both experiment and theory were correct, then the deuterated isomerization reaction 8a would be exothermic by only $6.6 \text{ kcal mol}^{-1}$. This would be $17.4 \text{ kcal mol}^{-1}$ below the lower experimental value¹³ for reaction 6b, which involves only one water molecule. A difference of this magnitude due to the appendage of two water molecules seems surprising. Thus, reliable theoretical evaluations of the gas-phase exothermicities of these isomerization reactions are desirable.

There are two kinds of products, $\text{PO}_3^-(\text{H}_2\text{O})_n$ and $\text{H}_2\text{PO}_4^-(\text{H}_2\text{O})_{n-1}$, for the reactions of the PO_3^- anion with water molecules. In order to avoid confusion, we use the terms "clustering reaction" and "hydration reaction" for the formation of $\text{PO}_3^-(\text{H}_2\text{O})_n$ and $\text{H}_2\text{PO}_4^-(\text{H}_2\text{O})_{n-1}$, respectively, even though other workers use the

term "hydration" to refer to the formation of $\text{PO}_3^-(\text{H}_2\text{O})_n$ clusters in the literature.

2. Theoretical Methods

The basis sets adopted here include double- ζ plus polarization (DZP)^{14,15} and DZP plus diffuse functions (DZP+diff) for the P and O atoms¹⁶ and are the same as those used in our previous work on the equilibrium geometries of $\text{PO}_3^-(\text{H}_2\text{O})_n$ clusters.⁷ In order to test possible basis set effects, a very large basis set, TZ2P with f function for heavy atoms, was employed as well. For the TZ2P+ f basis set, two sets of five pure spherical d functions and one set of seven pure spherical f functions are used for heavy atoms, with the orbital exponents being

$$\alpha_d(\text{P}) = 1.2, 0.3, \alpha_f(\text{P}) = 0.45; \quad \alpha_d(\text{O}) = 1.7, 0.425, \alpha_f(\text{O}) = 1.4$$

For the hydrogen atom, two sets of p functions and one set of five pure spherical d functions are used in the TZ2P+ f basis, with the orbital exponents being $\alpha_p(\text{H}) = 1.5, 0.375, \alpha_d(\text{H}) = 1.0$.

The Hartree-Fock or self-consistent-field (SCF) approach has been used to locate stationary points for several conformations via analytic first derivative techniques. Subsequently, analytic energy second derivative techniques are used to determine vibrational frequencies. Finally, the configuration interaction method with single and double excitations (CISD)¹⁷ and the coupled cluster method including single and double excitations (CCSD)¹⁸ are used independently to optimize the geometries. For the CISD and CCSD methods, only the valence electrons were explicitly correlated. Thus the core-like (phosphorus $1s, 2s$ and $2p$; oxygen $1s$) SCF molecular orbitals were constrained to be doubly occupied in all configurations. Also the corresponding core-like virtual orbitals were excluded from the CISD and CCSD procedures. With the DZP basis set, the number of basis functions for H_2PO_4^- , $\text{H}_2\text{PO}_4^-\cdot\text{H}_2\text{O}$, and $\text{H}_2\text{PO}_4^-(\text{H}_2\text{O})_2$ are 93, 118, and 143, respectively. The DZP CISD wave functions for H_2PO_4^- (C_2 symmetry) included 223 729 configurations. With the DZP+diff basis set, the CISD wave functions for the H_2PO_4^- anion include 400 689 configurations. The computations were carried out using the program PSI developed in this research group.^{19a} The program TURBOMOLE^{19b} was used to locate the transition states for the isomerizations of $\text{PO}_3^-(\text{H}_2\text{O})_2$ and $\text{PO}_3^-(\text{H}_2\text{O})_3$ and to evaluate single-point energies at the second-order Møller-Plesset perturbation²⁰ (MP2) level of theory. For the MP2 calculations no core electrons were frozen and geometries were taken from the DZP SCF and DZP+diff SCF optimizations.

The exothermicities for the formation of the $\text{H}_2\text{PO}_4^-(\text{H}_2\text{O})_n$ clusters, i.e., isomerization energies, are defined as follows:

$$n = 0: \quad \Delta E_c = E[\text{PO}_3^-\cdot\text{H}_2\text{O}] - E[\text{H}_2\text{PO}_4^-]$$

$$n = 1: \quad \Delta E_c = E[\text{PO}_3^-(\text{H}_2\text{O})_2] - E[\text{H}_2\text{PO}_4^-\cdot\text{H}_2\text{O}]$$

$$n = 2: \quad \Delta E_c = E[\text{PO}_3^-(\text{H}_2\text{O})_3] - E[\text{H}_2\text{PO}_4^-(\text{H}_2\text{O})_2]$$

The zero-point corrected energy differences (ΔE_0) are based on the zero-point vibrational energies evaluated within the harmonic approximation using the DZP SCF and DZP+diff SCF methods.

For the energetic comparisons with experimental data, the enthalpy changes are evaluated as follows:²¹

(14) (a) Huzinaga, S. *J. Chem. Phys.* **1965**, *42*, 1293. (b) Dunning, T. H. *J. Chem. Phys.* **1970**, *53*, 2823. (c) Dunning, T. H.; Hay, P. J. In *Modern Theoretical Chemistry*; Schaefer, H. F., III, Ed.; Plenum Press: New York, 1977; Vol. 3, p 1.

(15) Scuseria, G. E.; Janssen, C. L.; Schaefer, H. F. *J. Chem. Phys.* **1989**, *89*, 7382.

(16) (a) Clark, T.; Chandrasekhar, J.; Spitznagel, G. W.; Schleyer, P. v. R. *J. Comp. Chem.* **1983**, *4*, 294. (b) Spitznagel, G. W.; Clark, T.; Schleyer, P. v. R. *J. Comp. Chem.* **1987**, *8*, 1109.

(17) (a) Brooks, B. R.; Laidig, W. D.; Saxe, P.; Goddard, J. D.; Yamaguchi, Y.; Schaefer, H. F. *J. Chem. Phys.* **1980**, *72*, 4652. (b) Rice, J. E.; Amos, R. D.; Handy, N. C.; Lee, T. J.; Schaefer, H. F. *J. Chem. Phys.* **1986**, *85*, 963.

(18) (a) Purvis, G. D.; Bartlett, R. J. *J. Chem. Phys.* **1982**, *76*, 1910. (b) Scuseria, G. E.; Janssen, C. L.; Schaefer, H. F. *J. Chem. Phys.* **1989**, *89*, 7382.

(19) (a) Yamaguchi, Y.; Frisch, M. J.; Gaw, J. F.; Schaefer, H. F.; Binkley, J. S. *J. Chem. Phys.* **1986**, *84*, 2262. (b) Ahlrichs, R.; Bar, M.; Häser, M.; Horn, H. *Chem. Phys. Lett.* **1989**, *162*, 165.

(20) (a) Møller, C.; Plesset, M. S. *Phys. Rev.* **1934**, *46*, 618. (b) Pople, J. A.; Seeger, R.; Krishnan, R. *Int. J. Quantum Chem. Symp.* **1977**, *11*, 49. (c) Krishnan, R.; Pople, J. A. *Int. J. Quantum Chem. Symp.* **1978**, *14*, 91. (d) Krishnan, R.; Frisch, M. J.; Pople, J. A. *J. Chem. Phys.* **1980**, *72*, 4244.

(21) Del Bene, J. E.; Mettee, H. D.; Frisch, M. J.; Luke, B. T.; Pople, J. A. *J. Phys. Chem.* **1983**, *87*, 3279.

(9) (a) Hayes, D. M.; Kollman, P. A.; Rothenberg, S. *J. Am. Chem. Soc.* **1977**, *99*, 2150. (b) Corbridge, D. E. C. *The Structural Chemistry of Phosphorus*; Elsevier Scientific Publishing Co.: New York, 1974; p 90.

(10) Ewig, C. S.; Van Wazer, J. R. *J. Am. Chem. Soc.* **1985**, *107*, 1965.

(11) O'Keeffe, M.; Domenges, B.; Gibbs, G. V. *J. Phys. Chem.* **1985**, *89*, 2304.

(12) (a) Voet, D.; Voet, J. G. *Biochemistry*; John Wiley & Sons: New York, 1990; p 411. (b) Ewig, C. S.; Van Wazer, J. R. *J. Am. Chem. Soc.* **1988**, *110*, 79.

(13) Hinchman, M. J. Personal communication and references cited: (a) Unkel, W.; Freedman, A. *AIChE J.* **1983**, *21*, 1648. (b) Rudnyi, E. B.; Vovk, O. M.; Sidorov, L. N.; Sorokin, I. D.; Alikhanen, A. S. *High Temp. (Engl. Transl.)* **1986**, *24*, 56.

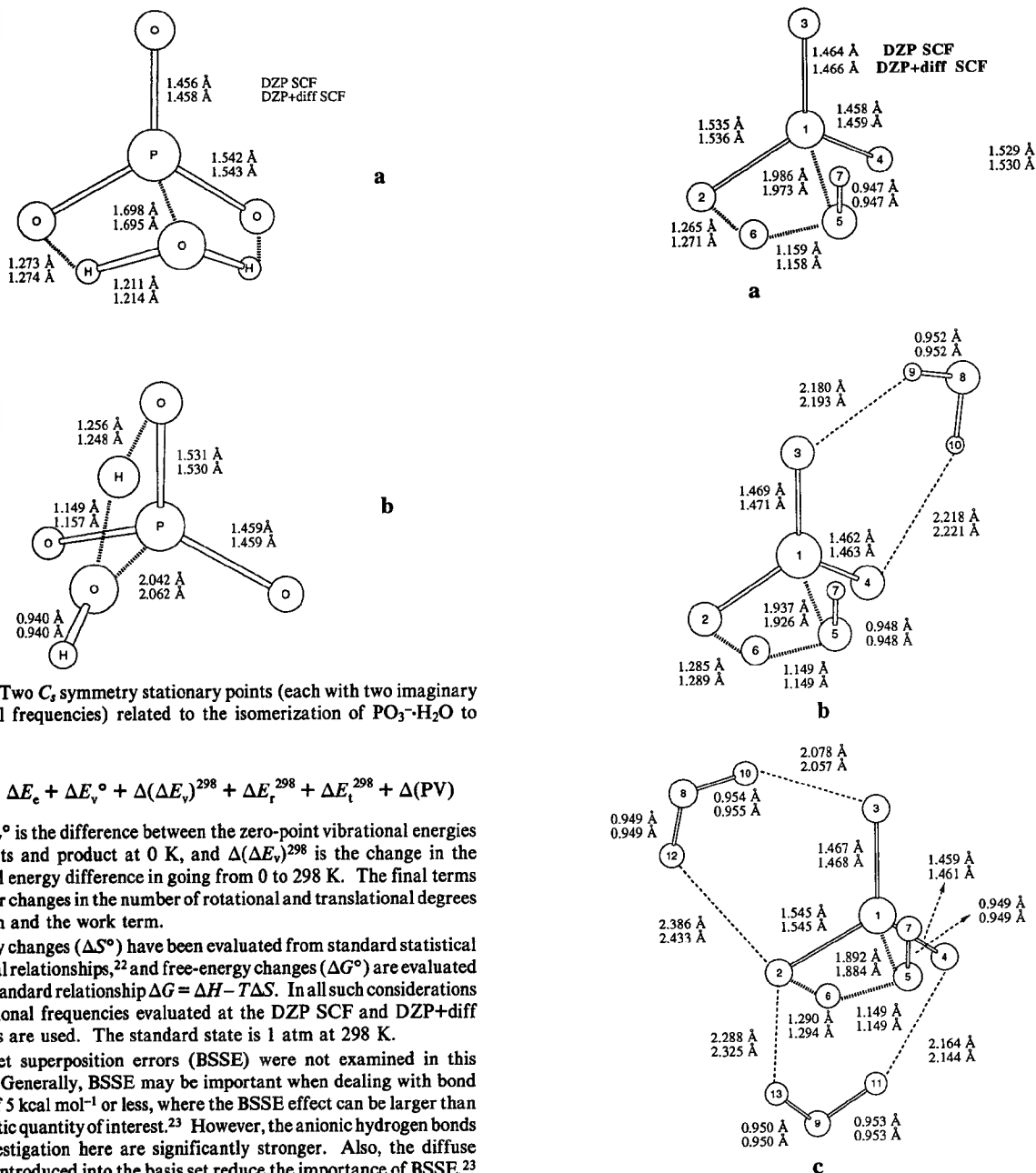


Figure 1. Two C_s symmetry stationary points (each with two imaginary vibrational frequencies) related to the isomerization of $\text{PO}_3^{2-}\cdot\text{H}_2\text{O}$ to $\text{H}_2\text{PO}_4^{2-}$.

$$\Delta H^\circ = \Delta E_e + \Delta E_v^\circ + \Delta(\Delta E_v)^{298} + \Delta E_t^{298} + \Delta E_i^{298} + \Delta(\text{PV})$$

where ΔE_v° is the difference between the zero-point vibrational energies of reactants and product at 0 K, and $\Delta(\Delta E_v)^{298}$ is the change in the vibrational energy difference in going from 0 to 298 K. The final terms account for changes in the number of rotational and translational degrees of freedom and the work term.

Entropy changes (ΔS°) have been evaluated from standard statistical mechanical relationships,²² and free-energy changes (ΔG°) are evaluated from the standard relationship $\Delta G = \Delta H - T\Delta S$. In all such considerations the vibrational frequencies evaluated at the DZP SCF and DZP+diff SCF levels are used. The standard state is 1 atm at 298 K.

Basis set superposition errors (BSSE) were not examined in this research. Generally, BSSE may be important when dealing with bond energies of 5 kcal mol⁻¹ or less, where the BSSE effect can be larger than the energetic quantity of interest.²³ However, the anionic hydrogen bonds under investigation here are significantly stronger. Also, the diffuse functions introduced into the basis set reduce the importance of BSSE.²³ Moreover, this view is reinforced by the good agreement (omitting BSSE corrections) with the experimental thermochemistry for the $\text{PO}_3^{2-}(\text{H}_2\text{O})_n$ systems.⁷

3. Results and Discussion

A. The Transition States and Barriers for the Isomerizations of $\text{PO}_3^{2-}(\text{H}_2\text{O})_n$ to $\text{H}_2\text{PO}_4^{2-}(\text{H}_2\text{O})_{n-1}$. **I. Isomerization Mechanisms.** The stability of the PO_3^{2-} anion in the gas phase was first shown by Henchman,⁵ who observed no reaction with the H_2O molecule. Keesee and Castleman have reported⁶ that the gas-phase product of the PO_3^{2-} anion and the H_2O molecule is the $\text{PO}_3^{2-}\cdot\text{H}_2\text{O}$ cluster. The isomerization of $\text{PO}_3^{2-}\cdot\text{H}_2\text{O}$ to $\text{H}_2\text{PO}_4^{2-}$ is a prototypical reaction for understanding PO_3^{2-} chemistry.

Starting from the C_{2v} symmetry structure of $\text{PO}_3^{2-}\cdot\text{H}_2\text{O}$ (the global minimum in Figure 2 of ref 7), there are several possible mechanisms for isomerization. In the first, the H_2O moiety directly transfers two hydrogen atoms to PO_3^{2-} and forms one additional P–O bond (Figure 1a). The barrier for this mechanism,

Figure 2. The four-center transition states from $\text{PO}_3^{2-}(\text{H}_2\text{O})_n$ to $\text{H}_2\text{PO}_4^{2-}(\text{H}_2\text{O})_{n-1}$: (a) $\text{PO}_3^{2-}\cdot\text{H}_2\text{O}$ to $\text{H}_2\text{PO}_4^{2-}$; (b) $\text{PO}_3^{2-}(\text{H}_2\text{O})_2$ to $\text{H}_2\text{PO}_4^{2-}\cdot\text{H}_2\text{O}$; (c) $\text{PO}_3^{2-}(\text{H}_2\text{O})_3$ to $\text{H}_2\text{PO}_4^{2-}(\text{H}_2\text{O})_2$.

with two O–H bonds to be broken, implies a radical intermediate species^{2b} and is too high in energy to afford a realistic pathway. The corresponding stationary point has two imaginary vibrational frequencies, and thus it is not a true transition state. The second possible mechanism posits that the planes of the H_2O moiety and PO_3^{2-} anion are perpendicular to one another. However, the corresponding stationary point also has two imaginary vibrational frequencies (Figure 1b) and therefore is not a transition state.

The favored mechanism for $\text{PO}_3^{2-}\cdot\text{H}_2\text{O}$ isomerization requires that the planes of PO_3^{2-} and H_2O moieties are almost parallel to one another, and one hydrogen atom is transferred from the H_2O to the PO_3^{2-} anion. The resulting transition structure is depicted in Figure 2a. This mechanism is easy to understand; one of the lone pairs of H_2O points to the C_3 axis of PO_3^{2-} and can be stabilized by the positive charge at the phosphorus atom. At the transition state, the bond length (DZP+diff SCF) for the original O–H bond (0.945 Å) is stretched to 1.158 Å, the length of the newly formed P–O–H bond is about 1.271 Å, and the new P–O bond length is 1.973 Å.

(22) Hout, R. F., Jr.; Levi, B. A.; Hehre, W. J. *J. Comp. Chem.* **1982**, *3*, 234.

(23) See, for example: Feller, D. *J. Chem. Phys.* **1992**, *96*, 6104 and references therein.

Table I. Harmonic Vibrational Frequencies (cm⁻¹) for the Transition State for the Reaction $\text{PO}_3^{--}(\text{H}_2\text{O})_2 \rightarrow \text{H}_2\text{PO}_4^{--}\text{H}_2\text{O}$ at the DZP SCF Level of Theory

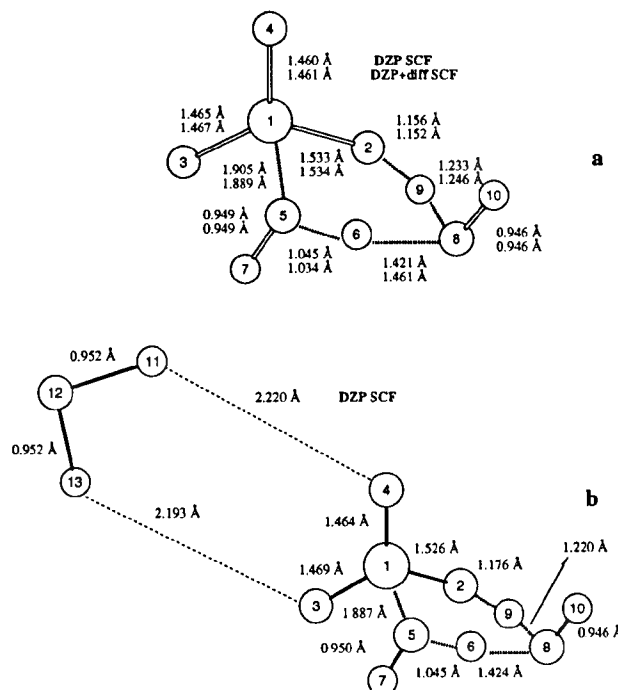
four-centered structure (Figure 2b)		six-centered structure (Figure 3a)	
DZP ^a	mode	DZP ^a	mode
4169 (3035)	stre O ₅ -H ₇	4188 (3048)	stre O ₈ -H ₁₀
4135 (3027)	stre O ₈ -H ₁₀	4152 (3026)	stre O ₅ -H ₇
4079 (2944)	stre O ₈ -H ₉	2300 (1700)	stre O ₅ -H ₆
2160 (1555)	bend P-O ₅ -H ₆	1821 (1314)	trigonal def
1849 (1356)	bend H ₉ -O ₈ -H ₁₀	1784 (1285)	bend H ₇ -O ₆ -H ₆
1532 (1111)	tors P-O ₂ -H ₆ -O ₅	1553 (1123)	pucking
1415 (1411)	stre P-O ₄	1451 (1452)	stre P-O ₄
1317 (1307)	stre P-O ₂	1423 (1082)	asym def
1070 (769)	stre P-O ₂	1300 (1296)	stre P-O ₃
876 (680)	bend H ₇ -O ₅ -P	1054 (991)	bend P-O ₂ ...H ₆
775 (507)	bend H ₆ -O ₅ -P	952 (779)	bend O ₄ -P-O ₃
726 (511)	tors H ₉ -O ₈ -H ₁₀ -O ₄	804 (728)	stre O ₂ ...H ₉
625 (507)	tors H ₆ -O ₅ -P-O ₂	691 (536)	bend H ₆ -O ₈ -H ₁₀
602 (620)	out-of-plane O ₃ -P	607 (593)	out-of-plane O ₃ -P
520 (512)	bend O ₃ -P-O ₂	571 (526)	O-P-O rocking
477 (522)	bend O ₄ -P-O ₂	542 (487)	stre O ₈ ...H ₆
408 (295)	tors P-O ₄ -H ₁₀ -O ₈	510 (456)	stre O ₈ ...H ₆
394 (282)	bend O ₄ -H ₁₀ -O ₈	481 (418)	out-of-plane H ₇ -O ₅
324 (314)	bend O ₅ -P-O ₂	438 (334)	bend H ₆ -O ₈ -H ₁₀
261 (246)	bend O ₅ -P-O ₄	405 (393)	stre O ₅ -H ₆
161 (54)	stre O ₃ ...H ₉	313 (298)	stre O ₂ ...H ₉
77 (75)	stre O ₃ ...H ₉	295 (273)	O-P-O twisting
37 (36)	tors O ₃ -P ₁ -O ₄ -H ₁₀	44 (43)	asym torsion
1707i (1254i)	stre O ₅ -H ₆ , stre O ₂ ...H ₉	1276i (953i)	stre O ₈ ...H ₆ , stre O ₂ ...H ₉

^a The results in parentheses refer to the deuterated transition state, i.e., that for $\text{PO}_3^{--}(\text{D}_2\text{O})_2 \rightarrow \text{D}_2\text{PO}_4^{--}\text{D}_2\text{O}$.

Can PO_3^{--} act as both an electrophile and an anion, as suggested by Loew and MacArthur?^{24a} Our previous study of the $\text{PO}_3^{--}\text{H}_2\text{O}$ cluster⁷ showed that there is no stationary point corresponding to an electrophilic role for PO_3^{--} . Thus a careful examination of the transition state is essential, with special attention to the nature of the reaction coordinate. If the reaction coordinate involves attack by the H_2O oxygen atom on the phosphorus atom in PO_3^{--} , then PO_3^{--} acts as an electrophile with regard to isomerization. On the other hand, if the hydrogen atom in H_2O attacks the oxygen atom in PO_3^{--} , then isomerization is still a "charge controlled" process and PO_3^{--} cannot be an electrophile. The reaction coordinate involves the transfer of a hydrogen atom from H_2O to PO_3^{--} , as indicated by the vibrational frequency analysis for the $\text{PO}_3^{--}\text{H}_2\text{O} \rightarrow \text{H}_2\text{PO}_4^{--}$ transition state. Thus PO_3^{--} reacts as a nucleophile rather than as an electrophile (or both) in the gas phase. However, it might be an electrophile in solution phase,^{24b} where its negative charge could be less repulsive due to the presence of counterions.

We have considered two types of mechanisms for the two- and three-water isomerization reactions 7a and 8a. The first is rather simple, i.e., the solvation of the transition state for reaction 6b. As the number of water molecule increases, from $\text{PO}_3^{--}\text{H}_2\text{O}$ to $\text{PO}_3^{--}(\text{H}_2\text{O})_2$ and $\text{PO}_3^{--}(\text{H}_2\text{O})_3$, we suppose that each additional water molecule does not change the isomerization mechanism. Instead, hydrogen bonds form with the transition state for reaction 6b, as illustrated in Figure 2, parts b and c. This mechanism was confirmed by our vibrational frequency analysis (Table I). The Figure 2b structure is a saddle point corresponding to the isomerization from $\text{PO}_3^{--}(\text{H}_2\text{O})_2$ to $\text{H}_2\text{PO}_4^{--}\text{H}_2\text{O}$. The nature of the reaction coordinate is the same as that for reaction 6b. Proceeding from the same principle, the transition state (Figure 2c) of reaction 8a was located by adding two more water molecules to form hydrogen bonds with the transition structure for reaction 6b.

For the second possible mechanism of reaction 7a, we considered a six-center instead of four-center transition state,²⁵ consisting of a water dimer interacting with PO_3^{--} . Evleth²⁶ was the first

**Figure 3.** The six-center transition states from $\text{PO}_3^{--}(\text{H}_2\text{O})_n$ to $\text{H}_2\text{PO}_4^{--}(\text{H}_2\text{O})_{n-1}$: (a) $\text{PO}_3^{--}(\text{H}_2\text{O})_2$ to $\text{H}_2\text{PO}_4^{--}\text{H}_2\text{O}$, (b) $\text{PO}_3^{--}(\text{H}_2\text{O})_3$ to $\text{H}_2\text{PO}_4^{--}(\text{H}_2\text{O})_2$.

to locate such a six-center transition structure, his study being done at the 6-31G* SCF level. Starting from Evleth's geometries, we located a DZP+diff SCF transition state, which has a shorter new P-O bond length (1.889 Å) than that in Evleth's structure (1.926 Å) (Figure 3a). Due to the decrease of electrostatic repulsion in the six-center arrangement, the barrier height for the six-center transition structure is lower than that of the four-centered structure. Nevertheless, there are other factors that must be taken into consideration to compare the four- and six-centered mechanism properly:

(a) The six-center transition state, even with a lower barrier, may not be feasible in an ion-molecule reaction⁶ in which the

(24) (a) Loew, L. M.; MacArthur, W. R. *J. Am. Chem. Soc.* **1971**, *99*, 1019. (b) Friedman, J. M.; Freeman, S.; Knowles, J. R. *J. Am. Chem. Soc.* **1987**, *109*, 3166.

(25) (a) Heidrich, D.; van Eikema Hommes, N. J. R.; Schleyer, P. v. R. *J. Comp. Chem.*, submitted for publication. (b) Lambert, C.; Hampel, F.; Schleyer, P. v. R. *Angew. Chem., Int. Ed. Engl.* **1992**, *31*, 1209.

(26) Evleth, E. M. Personal communication.

Table II. Barrier Heights (Four-Center Mechanism) for the Isomerization of $\text{PO}_3^{2-}(\text{H}_2\text{O})_n$ to $\text{H}_2\text{PO}_4^{2-}(\text{H}_2\text{O})_{n-1}$

theoretical levels	$n = 1^{a,b}$					$n = 2^{a,c}$					$n = 3^{a,c}$				
	ΔE_e^*	ΔE_0^*	ΔH^{o*}	$-\Delta S^{o*}$	ΔG^{o*}	ΔE_e^*	ΔE_0^*	ΔH^{o*}	$-\Delta S^{o*}$	ΔG^{o*}	ΔE_e^*	ΔE_0^*	ΔH^{o*}	$-\Delta S^{o*}$	ΔG^{o*}
DZP SCF	30.8	28.8 (29.6)	27.7 (28.5)	8.8 (9.5)	30.3 (31.3)	29.2	27.5	26.3	10.2	29.3	28.0	26.5	24.6	15.1	29.1
DZP+diff SCF	32.2	30.2 (31.1)	29.1 (29.9)	9.3 (10.0)	31.9 (32.9)	30.4	28.8	27.6	10.9	30.8	29.2	27.9	26.5	10.2	29.5
DZP CISD	25.6	23.6	22.5		25.1										
DZP MP2	21.6	19.6	18.5		21.1	20.1	18.4	17.2		20.3	18.5	17.0	15.1		19.6
						13.9	11.7	9.7		14.7					
DZP+diff MP2	22.4	20.4	19.3		22.1	21.3	19.7	18.5		21.8	19.2	17.8	16.4		19.4
						14.7	12.7	10.8		16.1					

^a The values of ΔH and ΔG are in kcal mol⁻¹, and ΔS is in cal/(K·mol). The standard state is 1 atm at 298 K. ^b The values in parentheses refer to the deuterated species, i.e., the barrier heights for $\text{PO}_3^{2-}(\text{D}_2\text{O})_n \rightarrow \text{D}_2\text{OP}_4^{2-}(\text{D}_2\text{O})_{n-1}$. ^c The values in boldface refer to the six-center mechanism.

collision complex has a short lifetime.²⁶ Three-body collisions in general occur infrequently. Therefore, experiments are expected to give a final judgment concerning the true mechanism. If the transition state were detectable, it would be easy to tell whether the four- or six-center transition structure is involved. There are distinguishable IR differences between the two kinds of structures. As indicated in Table I, the four-center structure has three vibrational modes (OH stretch) above 4000 cm⁻¹ (3600 cm⁻¹, if scaled by 0.9); the six-center structure has only two, with the third vibrational frequency dropped to about 2200 cm⁻¹ due to its two-proton transfer nature.

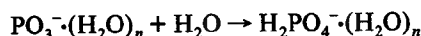
(b) For the six-center transition state itself, a significant degree of charge transfer has occurred from the PO_3^{2-} to the waters, the OH semianions (Figure 3) having a net charge of about -0.6. According to Evleth²⁶ the SCF method may not be satisfactory for this kind of transition structure, and he suggests that the MP2 method will not repair the situation.

(c) Fortunately, even though the six-center transition state has the lower barrier, it does not qualitatively affect our conclusions based on the four-center transition state. We report the barriers for both mechanisms for comparative purposes.

II. Reactivity of PO_3^{2-} with Water Molecules. The $\text{PO}_3^{2-}(\text{H}_2\text{O})_n$ isomerization barriers can be discussed in terms of the potential-energy or free-energy surfaces. If one were concerned with the motion of individual molecules over the barrier, the factor determining whether free and spontaneous motion will occur would be the potential energy.²⁷ However, we wish to understand some PO_3^{2-} chemistry and to compare our theoretical predictions with the experimental results (high-pressure mass spectrometry).⁶ Thus we are concerned with an assembly of molecules in a statistical distribution among energy states. Whether or not there is spontaneous reaction is determined by the free energy.²⁷ Thus we will primarily use the free energy surface in discussing the different reaction barriers.

For reaction 6b, $\text{PO}_3^{2-}\text{H}_2\text{O} \rightarrow \text{H}_2\text{PO}_4^{2-}$, the isomerization barrier (Table II) is $\Delta G^{o*} = 30.3$ kcal mol⁻¹ at the DZP SCF level and $\Delta G^{o*} = 31.9$ kcal mol⁻¹ at the DZP+diff SCF level. Consistent with hydrogen transfer from H_2O to PO_3^{2-} , the barrier increases by about 1 kcal mol⁻¹ for the isomerization of $\text{PO}_3^{2-}\text{D}_2\text{O}$ due to the deuterium isotope effect. It is often observed that the Hartree-Fock (HF) method overestimates reaction barriers.²⁸ For reaction 6b, the isomerization barrier (ΔG^{o*}) decreases to 25.1 kcal mol⁻¹ at the DZP CISD level, 21.1 kcal mol⁻¹ at the DZP MP2 level, and 22.1 kcal mol⁻¹ at the DZP+diff MP2 level.

The key difference between the gas-phase chemistry and liquid-phase chemistry of $\text{PO}_3^{2-}(\text{H}_2\text{O})_n$ is obviously the increase of the number of associated water molecules (n). For some higher value of the hydration number, n , the process



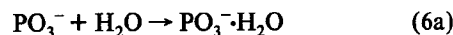
is expected^{6,13} to become spontaneous. This would explain why PO_3^{2-} reacts promptly to form $\text{H}_2\text{PO}_4^{2-}$ in solution but not in the

gas phase. Henchman has suggested¹³ that the barrier will decrease with increasing hydration (n). If the free energy of the barrier lies below the energy of the reactants, the isomerization reaction will occur spontaneously.

How can the reactivity of PO_3^{2-} with water molecules be understood? Consider the hydration reactions of PO_3^{2-} with one, two, and three water molecules. The reactions forming the clusters $\text{PO}_3^{2-}(\text{H}_2\text{O})_n$ require no activation. The present discussion is based on the results at the DZP+diff MP2 level, at which the isomerization barriers (free energy ΔG^{o*}) are significantly lower than those at the SCF level. The four-center transition states (Figure 2) are used in the present discussion, unless six-center structures are specified.

For $\text{PO}_3^{2-}(\text{H}_2\text{O})_2$ isomerization 7a, the barrier (ΔG^{o*}) is 30.8 kcal mol⁻¹ at the DZP+diff SCF level and 21.8 kcal mol⁻¹ at the DZP+diff MP2 level. The isomerization barrier does decrease due to the second water, but is only 1.1 kcal mol⁻¹ lower than that for $\text{PO}_3^{2-}\text{H}_2\text{O}$ at the DZP+diff SCF level and 0.3 kcal mol⁻¹ at the DZP+diff MP2 level. The barrier for the isomerization of $\text{PO}_3^{2-}(\text{H}_2\text{O})_3$ decreases in an analogous manner: $\Delta G^{o*} = 29.5$ kcal mol⁻¹ at the DZP+diff SCF level and $\Delta G^{o*} = 19.4$ kcal mol⁻¹ at the DZP+diff MP2 level. These barriers are still relatively large, even for the six-center mechanism ($\Delta G^{o*} = 16.1$ kcal mol⁻¹ at the DZP MP2 level for the $\text{PO}_3^{2-}(\text{H}_2\text{O})_2$ isomerization).

There are two modes for the reaction of PO_3^{2-} with one water molecule. PO_3^{2-} could first form a stable cluster $\text{PO}_3^{2-}\text{H}_2\text{O}$ with the water molecule (reaction 6a) and then isomerize to $\text{H}_2\text{PO}_4^{2-}$ (reaction 6b). Alternatively, PO_3^{2-} might react with a water molecule directly to form $\text{H}_2\text{PO}_4^{2-}$ without formation of a stable cluster intermediate (reaction 6c).



isomerization barrier $\Delta G^{o*} = 22.1$ kcal mol⁻¹



isomerization-hydration barrier $\Delta G^{o*} = 17.4$ kcal mol⁻¹

Clearly, both reactions 6b and 6c are inhibited by the barriers involved (Tables II and III). When only one water molecule reacts with PO_3^{2-} , the more possible product is the barrier-free $\text{PO}_3^{2-}\text{H}_2\text{O}$, even though the $\text{H}_2\text{PO}_4^{2-}$ species lies lower in energy (see Section C). This explains why PO_3^{2-} is stable in the gas phase.

The reactions of PO_3^{2-} involving two water molecules are more complex. Some possibilities are indicated by the following equations:



isomerization barrier $\Delta G^{o*} = 21.8$ kcal mol⁻¹



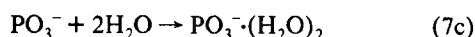
(27) Laidler, K. L. *Theories of Chemical Reaction Rates*; McGraw-Hill Book Co.: New York, 1969; p 76.

(28) Schaefer, H. F. *J. Phys. Chem.* **1985**, *89*, 5336.

Table III. Barrier Heights (Four-Center Mechanism) for the Reactions Forming $\text{H}_2\text{PO}_4^-(\text{H}_2\text{O})_{n-1}$

	$\Delta H^{\circ*},^b$ kcal mol ⁻¹				$\Delta G^{\circ*},^b$ kcal mol ⁻¹				$\Delta S^{\circ*},^b$ kcal/(K·mol)	
	DZP		DZP+diff		DZP		DZP+diff			
	MP2 ^a	SCF	MP2 ^a	SCF	MP2 ^a	SCF	MP2 ^a	SCF	DZP	DZP+diff
reaction 6c $\text{PO}_3^- + \text{H}_2\text{O} \rightarrow \text{H}_2\text{PO}_4^-$	3.1	15.1	6.9	17.2	13.5	25.5	17.4	27.7	-35.0	-35.1
reaction 7d $\text{PO}_3^- + 2\text{H}_2\text{O} \rightarrow \text{H}_2\text{PO}_4^-(\text{H}_2\text{O})$	-11.6	2.6	-11.9	5.1	7.5	21.7	7.1	25.2	-63.8	-63.7
reaction 7e $\text{PO}_3^-(\text{H}_2\text{O}) + \text{H}_2\text{O} \rightarrow \text{H}_2\text{PO}_4^-(\text{H}_2\text{O})$	-19.1	-2.8	-19.7	0.5	1.9	18.3	1.4	19.5	-70.3	-70.3
reaction 7a $\text{PO}_3^- + \text{H}_2\text{O} + \text{H}_2\text{O} \rightarrow \text{H}_2\text{PO}_4^-(\text{H}_2\text{O})_2$	3.8	15.2	3.6	17.0	15.1	26.5	14.9	29.4	-37.6	-37.9
reaction 7a $\text{PO}_3^-(\text{H}_2\text{O})_2 \rightarrow \text{H}_2\text{PO}_4^-(\text{H}_2\text{O})$	-3.7	9.8	-4.2	12.4	9.5	23.1	9.2	23.7	-44.0	-44.0
reaction 8e $\text{PO}_3^-(\text{H}_2\text{O})_2 \rightarrow \text{H}_2\text{PO}_4^-(\text{H}_2\text{O})_2$	17.2	26.3	18.5	27.6	20.3	29.3	21.8	30.8	-10.2	-10.9
reaction 8d $\text{PO}_3^- + 3\text{H}_2\text{O} \rightarrow \text{H}_2\text{PO}_4^-(\text{H}_2\text{O})_2$	9.7	20.9	10.8	23.0	14.7	25.9	16.1	25.1	-16.7	-16.7
reaction 8b $\text{PO}_3^-(\text{H}_2\text{O})_2 + \text{H}_2\text{O} \rightarrow \text{H}_2\text{PO}_4^-(\text{H}_2\text{O})_2$	-25.7	-9.0	-24.7	-5.5	3.4	20	2.5	21.7	-97.5	-91.1
reaction 8e $\text{PO}_3^- + \text{H}_2\text{O} + 2\text{H}_2\text{O} \rightarrow \text{H}_2\text{PO}_4^-(\text{H}_2\text{O})_2$	-10.3	3.6	-9.3	6.4	10.9	24.5	10.2	25.9	-71.3	-65.3
reaction 8b $\text{PO}_3^-(\text{H}_2\text{O})_2 + \text{H}_2\text{O} \rightarrow \text{H}_2\text{PO}_4^-(\text{H}_2\text{O})_2$	3.1	14.7	5.7	17.0	16.2	27.8	17.1	28.4	-43.9	-38.3

^a Based on single point calculations at the MP2 level; the geometries were optimized at the SCF level, and the vibrational frequencies were evaluated at the SCF level. The standard state is 1 atm at 298 K. ^b The values in boldface refer to the six-center mechanism.



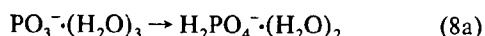
hydration barrier $\Delta G^{\circ*} = 7.1$ kcal mol⁻¹



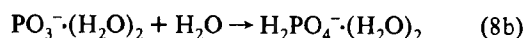
barrier $\Delta G^{\circ*} = 14.9$ kcal mol⁻¹

An important question is whether $\text{H}_2\text{PO}_4^-(\text{H}_2\text{O})$ will be formed, i.e., whether PO_3^- will be stable with respect to isomerization with two water molecules. Experimentally, only the clustering reaction to $\text{PO}_3^-(\text{H}_2\text{O})_2$ is observed. This result seems secure—the experimental ΔH° value for reaction 7b is consistent with our theoretical ΔH° value.⁷ However, an examination of plausible $\text{H}_2\text{PO}_4^-(\text{H}_2\text{O})$ formation reactions 7a, 7d, and 7e is instructive. Reactions 7a and 7e are less feasible, due to the size of the barriers. While there is no barrier on the *potential-energy* surface (Table III) for reaction 7d, this process has not been observed experimentally.⁶ These reactions are governed by the free-energy surface. Reaction 7d is prevented by the *free-energy* barrier. It is important to note that reaction 7d may be possible by the mechanism involving the six-center transition state ($\Delta G^{\circ*} = 1.4$ kcal mol⁻¹); however this process has not been observed experimentally.⁶ This fact indicates that the six-centered transition structure is unlikely.

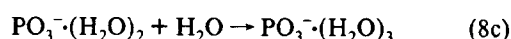
$\text{PO}_3^-(\text{H}_2\text{O})_3$ and $\text{H}_2\text{PO}_4^-(\text{H}_2\text{O})_2$ are possible products for the reactions of PO_3^- involving three water molecules. Is the $\text{PO}_3^-(\text{H}_2\text{O})_3$ species stable [without isomerizing to $\text{H}_2\text{PO}_4^-(\text{H}_2\text{O})_2$]? Will the $\text{H}_2\text{PO}_4^-(\text{H}_2\text{O})_2$ be formed even though the $\text{PO}_3^-(\text{H}_2\text{O})_3$ is stable? It is easy to answer the first question, because isomerization reaction 8a has a 19.4 kcal mol⁻¹ barrier ($\Delta G^{\circ*}$) at the DZP+diff MP2 level. Thus the $\text{PO}_3^-(\text{H}_2\text{O})_3$ species will be formed (no barrier for cluster formation) and will be kinetically stable. To answer the second question, first recall the experimental results.⁶ The experimental ΔH° for the association of $\text{PO}_3^-(\text{H}_2\text{O})_2$ with the third water molecule is notably larger in magnitude than the clustering reactions 6a and 7b.⁶ Keesee and Castleman suggested quite plausibly that reaction 8b is observed. However, this reaction has a large barrier ($\Delta G^{\circ*} = 16.2$ kcal mol⁻¹). The best energetic pathway to $\text{H}_2\text{PO}_4^-(\text{H}_2\text{O})_2$ should be via the improbable four-body reaction 8d or the three-body reaction 8e.



isomerization barrier $\Delta G^{\circ*} = 19.4$ kcal mol⁻¹



barrier $\Delta G^{\circ*} = 17.1$ kcal mol⁻¹



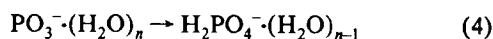
hydration barrier $\Delta G^{\circ*} = 2.5$ kcal mol⁻¹



barrier $\Delta G^{\circ*} = 10.2$ kcal mol⁻¹

Reactions 8d and 8e have no barriers on the potential-energy surface. However, reaction 8e has a 10.2 kcal mol⁻¹ barrier on the free-energy surface. Reaction 8d has only a 2.5 kcal mol⁻¹ barrier on the free-energy surface and is more feasible. It is especially true when the six-center transition state is considered, which may have a higher probability with three water molecules than with two. The barrier for reaction 8d vanishes for the six-center mechanism. However, even though $\text{H}_2\text{PO}_4^-(\text{H}_2\text{O})_2$ will be formed, the $\text{PO}_3^-(\text{H}_2\text{O})_3$ is expected to be a major intermediate. We discuss this point further in Section C.

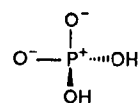
B. The Isolated Isomerization Products: $\text{H}_2\text{PO}_4^-(\text{H}_2\text{O})_{n-1}$ ($n = 1, 2$, and 3). **I. Structures and Energetics of $\text{H}_2\text{PO}_4^-(\text{H}_2\text{O})_{n-1}$.** The isomerization reactions of the $\text{PO}_3^-(\text{H}_2\text{O})_n$ clusters are summarized by



To augment our previous work on the $\text{PO}_3^-(\text{H}_2\text{O})_n$ clusters⁷ and the isomerization transition states discussed above, we have investigated the isomerization products H_2PO_4^- , $\text{H}_2\text{PO}_4^-(\text{H}_2\text{O})$, and $\text{H}_2\text{PO}_4^-(\text{H}_2\text{O})_2$. These species are very important in inorganic chemistry and in biochemistry.

Three conformations of H_2PO_4^- , with C_s , C_{2v} , and C_2 symmetries, are shown in Figure 4. The vibrational frequencies for the C_2 conformation are given in Table IV. The vibrational frequencies for the C_s conformation are rather similar to the latter and are not reported here.

There are two kinds of P–O bonds in the H_2PO_4^- species. The longer bonds (1.646 Å at the DZP+diff CISD level) are the P–OH single bonds. The shorter bonds (1.486 Å at the DZP+diff CISD level) may be represented as P^+-O^- polar bonds.²⁹ This means the H_2PO_4^- moiety is represented qualitatively by



Like the H_2NO_4^- anion²⁸ and the closely related H_2SO_4 species,³¹ the global minimum for the H_2PO_4^- species has C_2 symmetry (top of Figure 4). A second minimum (middle of Figure

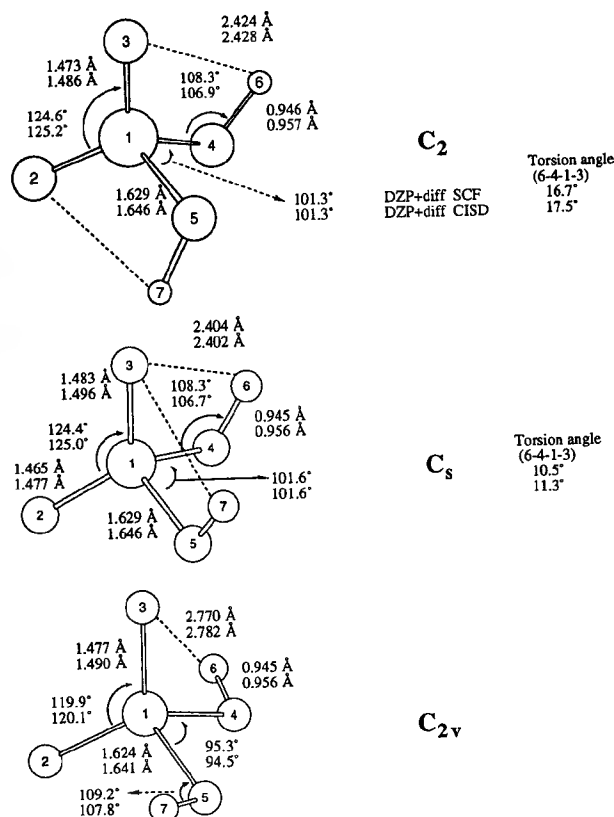


Figure 4. Three conformations of H_2PO_4^- at the DZP+diff SCF and DZP+diff CISD theoretical levels.

Table IV. Harmonic Vibrational Frequencies (cm^{-1}) for the Global Minimum Structure (C_2 symmetry, top of Figure 4) of H_2PO_4^- at the SCF level of Theory^a

mode	symmetry	DZP	DZP+diff	TZ2P+f
sym O-H	A	4202 (3059) ^a	4199 (3057) ^a	4197 (3054)
asym O-H	B	4201 (3057)	4198 (3055)	4195 (3053)
asym P ⁺ -O ⁻	B	1444 (1430)	1419 (1404)	1425 (1410)
sym P ⁺ -O ⁻	A	1210 (1209)	1194 (1193)	1199 (1198)
bend P-O-H	B	1158 (930)	1151 (926)	1155 (921)
bend P-O-H	A	1137 (917)	1133 (911)	1137 (908)
asym P-OH	B	898 (876)	892 (867)	890 (875)
sym P-OH	A	870 (800)	865 (797)	867 (803)
bend HO-P ⁺ -O ⁻	B	569 (563)	563 (558)	568 (562)
bend O-P ⁺ -O ⁻	A	566 (561)	558 (553)	563 (559)
bend HO-P ⁺ -O ⁻	B	485 (446)	483 (445)	484 (446)
bend HO-P ⁺ -O ⁻	A	427 (396)	424 (394)	426 (394)
bend O-P ⁺ -O ⁻	A	364 (360)	361 (357)	361 (356)
tors H-O-P ⁺ -O ⁻	B	324 (239)	321 (237)	341 (251)
tors H-O-P ⁺ -O ⁻	A	220 (165)	221 (166)	228 (173)

^a The results in parentheses refer to the deuterated species D_2PO_4^- .

4) with C_s symmetry lies about 1 kcal mol⁻¹ higher in energy. The C_{2v} symmetry H_2PO_4^- stationary point (bottom of Figure 4) has two imaginary vibrational frequencies and is about 4 kcal mol⁻¹ higher in energy than the C_2 conformation. The two imaginary vibrational frequencies correspond to the torsional movements of H-O-P⁺-O⁻ going to the C_2 and the C_s symmetry conformations. These results are quite different from those of O'Keefe et al.,¹¹ who assumed C_{2v} symmetry for H_2PO_4^- . Hayes, Kollman, and Rothenberg's^{9a} earlier STO-3G SCF conformational results for H_2PO_4^- are similar to ours—i.e., the C_{2v} symmetry structure is highest in energy while the C_s and C_2 structures are lower in energy—even though the geometries were not optimized in their research. The main difference between the C_{2v} conformation and the C_2 or C_s conformations is that the -O-P⁺-O⁻ and HO-P-OH bond angles are smaller in the C_{2v} conformation.

Intramolecular hydrogen bonding is very important in the related H_2NO_4^- system.³⁰ For H_2PO_4^- , due to the fact that the P-O bond is longer than the N-O bond, the intramolecular

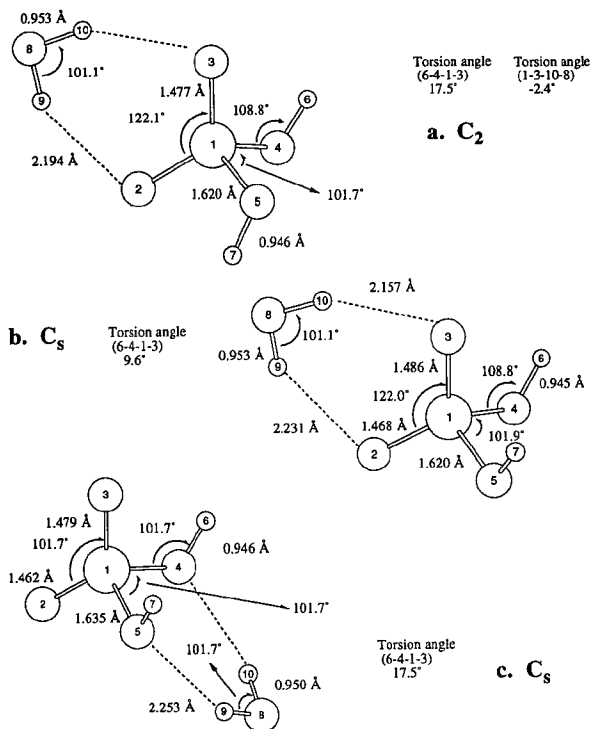


Figure 5. Three equilibrium geometries of $\text{H}_2\text{PO}_4\cdot\text{H}_2\text{O}$ at the DZP+diff SCF theoretical level.

hydrogen bonds [2.428 Å (C_2) and 2.782 Å (C_{2v})] are expected to be weaker than those in H_2NO_4 and have more dipole-dipole character. The H-O-P⁺-O⁻ torsional angle is about 11° (C_s) or 17° (C_2) in H_2PO_4^- , while the corresponding angles in the H_2NO_4^- system are only 0° (C_s) or 5° (C_2), indicating a stronger intramolecular interaction. There is also an important "anomeric" effect,^{32,33} namely the tendency for lone pairs to be *gauche* relative to polar bonds, operative in the H_2PO_4^- conformational surface. The situation is similar for the isoelectronic H_2SO_4 system.³¹

The isomerization of $\text{PO}_3^{2-}(\text{H}_2\text{O})_2$ produces the $\text{H}_2\text{PO}_4\cdot\text{H}_2\text{O}$ anion, which also may be viewed as the solvation product of H_2PO_4^- with H_2O . There are distinct orientations in which water can form intermolecular hydrogen bonds with the H_2PO_4^- anion, i.e., to the different kinds of oxygen atoms in H_2PO_4^- . The H_2O molecule can form hydrogen bonds with the -O-P⁺-O⁻ oxygens (Figure 5, parts a and b). The H_2O can also form hydrogen bonds with the HO-P-OH oxygen atoms (Figure 5c). Due to the higher negative charge on oxygen, the hydrogen bonding to the -O-P⁺-O⁻ moiety is energetically favored by about 4 kcal mol⁻¹. We have considered C_2 , C_s , and C_{2v} symmetries for the $\text{H}_2\text{PO}_4\cdot\text{H}_2\text{O}$ cluster. The potential energy surface for $\text{H}_2\text{PO}_4\cdot\text{H}_2\text{O}$ is similar to that for H_2PO_4^- ; its global minimum also has C_2 symmetry, and the C_{2v} structure has two imaginary vibrational frequencies. The relative energy of the C_s conformation is 1 kcal mol⁻¹, and that of the C_{2v} conformation is 4 kcal mol⁻¹ with respect to the C_2 symmetry structure. The vibrational frequencies for the C_2 $\text{H}_2\text{PO}_4\cdot\text{H}_2\text{O}$ are listed in Table V.

The last isomerization product we considered is $\text{H}_2\text{PO}_4\cdot(\text{H}_2\text{O})_2$. For this cluster, the H_2O molecules form hydrogen bonds involving all four oxygen atoms of H_2PO_4^- . The global minimum also has C_2 symmetry (Figure 6a). The C_s conformation is 1 kcal mol⁻¹ higher in energy (Figure 6b). Thus the conformation of H_2PO_4^- determines the energy surface for the $\text{H}_2\text{PO}_4\cdot(\text{H}_2\text{O})_n$ clusters, and solvation does not significantly change the relative energies.

(30) (a) Shen, M.; Xie, Y.; Schaefer, H. F.; Deakyne, C. A. *J. Chem. Phys.* 1990, 93, 3379. (b) Shen, M.; Xie, Y.; Schaefer, H. F.; Deakyne, C. A. *Chem. Phys.* 1991, 151, 187.

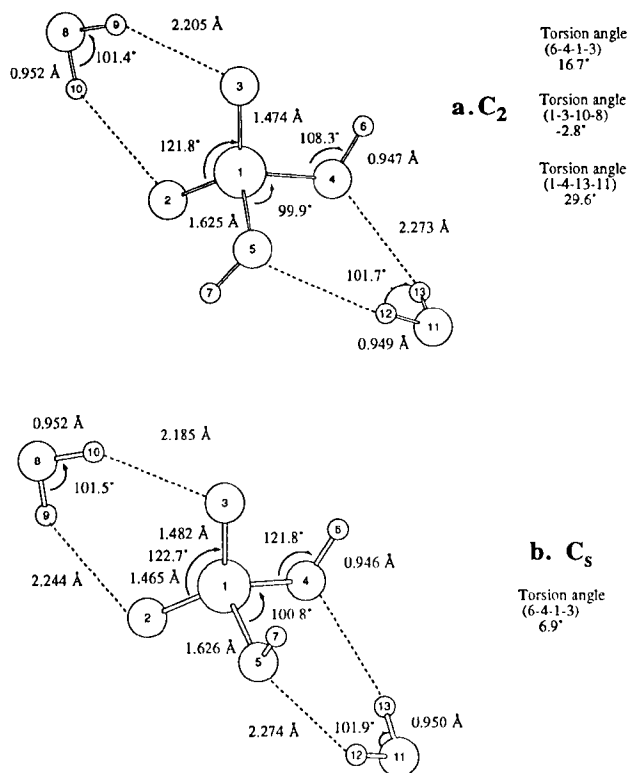
(31) Hofmann, M.; Schleyer, P. v. R. *J. Am. Chem. Soc.*, to be published and references cited therein.

(32) Newton, M. D. *J. Am. Chem. Soc.* 1973, 95, 256.

(33) Reed, R. E.; Schleyer, P. v. R. *J. Am. Chem. Soc.* 1987, 109, 7362. Reed, R. E.; Schleyer, P. v. R. *Inorg. Chem.* 1988, 27, 3969.

Table V. Harmonic Vibrational Frequencies (cm⁻¹) for the Global Minimum (Top of Figure 5) Structure of H₂PO₄⁻·H₂O (C₂ Symmetry) at the SCF Level of Theory

mode	symmetry	DZP ^a	DZP+diff ^a	mode	symmetry	DZP ^a	DZP+diff ^a
stre PO-H	A	4202 (3059)	4198 (3056)	bend -O-P ⁺ -O-	A	570 (567)	565 (561)
stre PO-H	B	4200 (3057)	4196 (3054)	bend HO-P ⁺ -O-	A	559 (517)	553 (508)
stre HO-H	B	4117 (3014)	4114 (3012)	bend P-O-H	A	488 (449)	486 (447)
stre HO-H	A	4066 (2934)	4061 (2932)	tors O-H...O-P ⁺	A	439 (390)	437 (390)
bend H ₉ -O ₈ -H ₁₀	A	1856 (1401)	1834 (1384)	bend O-H...O-	B	425 (365)	412 (363)
stre P ⁺ -O-	B	1417 (1358)	1399 (1341)	tors O-H...O-P ⁺	A	402 (304)	401 (297)
stre P ⁺ -O-	A	1209 (1208)	1197 (1196)	bend -O-P ⁺ -O-	A	371 (299)	369 (296)
bend H-O-P	B	1150 (936)	1144 (932)	tors H-O-P ⁺ -O-	B	297 (219)	298 (220)
bend H-O-P	A	1132 (924)	1127 (919)	tors H-O-P ⁺ -O-	A	187 (161)	189 (156)
stre HO-P	B	926 (892)	917 (882)	stre H...O-	A	166 (140)	161 (139)
stre HO-P	A	884 (802)	880 (799)	stre H...O-	B	77 (75)	73 (71)
tors H-O-H...O-	B	740 (580)	720 (570)	tors H...O-P ⁺ -O-	B	38 (37)	39 (38)

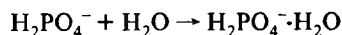
^a The results in parentheses refer to the deuterated species D₂PO₄⁻·D₂O cluster.**Figure 6.** Two equilibrium geometries of H₂PO₄⁻·(H₂O)₂ at the DZP+diff SCF theoretical level.

The bond distance changes in the parent anion are a final interesting aspect of the hydration of H₂PO₄⁻. The changes in distance of the two types of P-O bonds are related. When the H₂O molecule forms hydrogen bonds with -O-P⁺-O-, the P⁺-O- bonds are lengthened by 0.004 Å, but the P-OH single bonds are shortened by 0.009 Å (Figure 5). Hydrogen bonding of H₂O with HO-P-OH lengthens the P-OH single bonds by 0.006 Å but shortens the P⁺-O- bonds by 0.004 Å. However, both the P⁺-O- and the P-OH bond distances in H₂PO₄⁻·(H₂O)₂ are similar to those for the isolated H₂PO₄⁻ anion. The two types of interactions in H₂PO₄⁻·H₂O compensate one another. This may explain the significant difference between the theoretical and experimental structures^{9b} of H₂PO₄⁻. The theoretical bond distances (DZP+diff CISD) for the P⁺-O- and P-OH bonds in isolated H₂PO₄⁻ are 1.486 and 1.646 Å, respectively; the difference between bond distances is 0.16 Å. However, the experimental values^{9b} are 1.50 and 1.55 Å, respectively, for the H₂PO₄⁻ anion in the KH₂(PO₄)₂ crystal; the P⁺-O- bonds are lengthened while the P-OH single bond is shortened, and thus the bond length difference is reduced significantly to 0.05 Å. A recent explanation attributed the large discrepancies between theoretical and

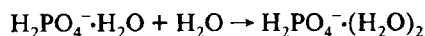
experimental data to intermolecular forces in the crystal.³⁴ The counteraction effect is important. The best position for the counteraction on the -O-P⁺-O- side results in P⁺-O- bond elongation and P-OH single-bond shortening. The stronger ion pair interaction (relative to hydrogen bonding) results in larger bond distance changes. Our studies of LiH₂PO₄ showing these counteraction effects will be reported elsewhere; better agreement with experiment is achieved.

II. The Solvation of H₂PO₄⁻. The clustering reaction of H₂O with H₂PO₄⁻ has both similarities and differences with PO₃⁻. The similarities are structural. The H₂O molecule forms double-donor double-acceptor hydrogen bonds with H₂PO₄⁻, as was found⁷ for PO₃⁻. Both C₂ and C_s symmetry H₂PO₄⁻·H₂O anions bind in this manner (Figure 5b).

The energy difference between PO₃⁻ and H₂PO₄⁻ solvation reactions is significant (see the data in Table VI, corresponding to reactions 9 and 10).

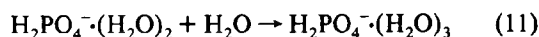


$$\Delta H^\circ = -13.5 \text{ kcal mol}^{-1} \quad (9)$$



$$\Delta H^\circ = -8.4 \text{ kcal mol}^{-1} \quad (10)$$

The H₂PO₄⁻ species is about 3 kcal mol⁻¹ more strongly solvated than either PO₃⁻ or PO₃·H₂O (Table VIII), due to the larger negative charge on the -O-P⁺-O- moiety in H₂PO₄⁻. On the basis of their experimental results, Keese and Castleman⁶ also suggested that H₂PO₄⁻ may be solvated more strongly than PO₃⁻. The solvation energy for the H₂PO₄⁻·H₂O anion (ΔH° = -8.4 kcal mol⁻¹ for reaction 10) decreases sharply compared to H₂PO₄⁻; H₂PO₄⁻·H₂O is about 5 kcal mol⁻¹ less strongly solvated than bare H₂PO₄⁻, and even less than PO₃·H₂O. The reason is that the second solvation site available is the HO-P-OH fragment, which has little negative charge. We have not predicted the solvation energy for H₂PO₄⁻·(H₂O)₂. However this solvation energy



is expected to be even less⁶ than that for H₂PO₄⁻·H₂O, because no oxygen atoms in H₂PO₄⁻ are as readily available as solvation sites for an additional (third) water molecule.⁶ The experimental⁶ ΔH° for reaction 11 is -12 kcal mol⁻¹, significantly higher than the value suggested by the present research (under -8 kcal mol⁻¹). Thus we suspect that the experimentally observed solvation reaction may be contaminated by the hydration reaction [PO₃⁻·(H₂O)₃ to H₂PO₄⁻·(H₂O)₃, reaction 12, next section]. We expand on this topic below.

C. The Exothermicity for the Isomerization of PO₃⁻·(H₂O)_n and the Nature of the (2,3) Hydration Reaction. I. The Exothermicity for the Isomerization Reactions. Tables VII and VIII summarize our theoretical results pertaining to the energy

(34) Liang, C.; Ewig, C. S.; Stouch, T. R.; Hagler, A. T. *J. Am. Chem. Soc.* **1993**, *115*, 1537.

Table VI. Thermochemical Predictions for the Solvation of H_2PO_4^- (kcal mol⁻¹)^a

theoretical levels	reaction 9 $\text{H}_2\text{PO}_4^- + \text{H}_2\text{O} \rightarrow \text{H}_2\text{PO}_4^-\text{H}_2\text{O}$					reaction 10 $\text{H}_2\text{PO}_4^-\text{H}_2\text{O} + \text{H}_2\text{O} \rightarrow \text{H}_2\text{PO}_4^-(\text{H}_2\text{O})_2$				
	$-\Delta E_e$	$-E_0$	$-\Delta H^\circ$	$-\Delta G^\circ$	$-\Delta S^\circ$	$-\Delta E_e$	$-\Delta E_0$	$-\Delta H^\circ$	$-\Delta G^\circ$	$-\Delta S^\circ$
DZP SCF	16.0	13.6 (14.2)	14.1 (14.5)	5.6 (5.9)	28.4 (29.0)	10.3	8.5 (8.7)	8.8 (8.9)	0.7 (0.7)	27.0 (27.4)
DZP+diff SCF	15.3	13.0 (13.5)	13.5 (13.7)	5.1 (5.1)	28.2 (28.8)	10.0	7.9 (8.4)	8.4 (8.5)	0.3 (0.3)	27.2 (27.7)

^a The values of ΔH and ΔG are in kcal mol⁻¹, and ΔS is in cal/(K·mol). The standard state is 1 atm at 298 K. The results in parentheses refer to fully deuterated species.

Table VII. Thermochemical Predictions for the Formation of H_2PO_4^- (kcal mol⁻¹)^a

theoretical levels	reaction 6b $\text{PO}_3^-\text{H}_2\text{O} \rightarrow \text{H}_2\text{PO}_4^-$					reaction 6c $\text{PO}_3^- + \text{H}_2\text{O} \rightarrow \text{H}_2\text{PO}_4^-$				
	$-\Delta E_e$	$-\Delta E_0$	$-\Delta H^\circ$	$-\Delta G^\circ$	$-\Delta S^\circ$	$-\Delta E_e$	$-\Delta E_0$	$-\Delta H^\circ$	$-\Delta G^\circ$	$-\Delta S^\circ$
DZP SCF	19.1	18.3 (18.1)	19.1 (18.9)	16.5 (16.3)	8.6 (8.5)	33.6	30.4	31.7 (31.9)	21.3 (21.4)	34.8 (35.2)
DZP+diff SCF	18.5	17.6 (17.5)	18.4 (18.3)	15.6 (15.3)	9.3 (10)	32.2	29.9	30.3 (30.4)	19.3 (19.1)	36.8 (37.9)
TZ2P+f SCF						32.0	28.7	30.0 (30.2)	18.9 (18.9)	37.2 (37.8)
TZ2P+f MP2						30.8	27.5	28.5	17.7	
DZP CISD	16.5	15.6	16.4			33.2	29.9	31.2		
DZP+diff CISD	16.6	15.7	17.6			32.2	29.0	30.3		
DZP CCSD	12.9	12.1	12.9			29.9	26.7	27.9		

^a The values of ΔH and ΔG are in kcal mol⁻¹, and ΔS is in cal/(K·mol). The standard state is 1 atm at 298 K. The results in parentheses refer to fully deuterated species.

Table VIII. Thermochemical Predictions for the Formation of $\text{PO}_3^-(\text{H}_2\text{O})_n$ and $\text{H}_2\text{PO}_4^-(\text{H}_2\text{O})_{n-1}$ (kcal mol⁻¹)^a

theoretical levels	DZP SCF					DZP+diff SCF				
	$-\Delta E_e$	$-\Delta E_0$	ΔH°	$-\Delta G^\circ$	$-\Delta S^\circ$	$-\Delta E_e$	$-\Delta E_0$	$-\Delta H^\circ$	$-\Delta G^\circ$	$-\Delta S^\circ$
reaction 7a $\text{PO}_3^-(\text{H}_2\text{O})_2 \rightarrow \text{H}_2\text{PO}_4^-\text{H}_2\text{O}$	22.4	21.4 (21.3)	22.3 (22.2)	19.4 (19.4)	9.6 (9.6)	21.4	20.3 (20.2)	21.2 (21.2)	18.1 (18.1)	10.4 (10.4)
reaction 7c $\text{PO}_3^-\text{H}_2\text{O} + \text{H}_2\text{O} \rightarrow \text{H}_2\text{PO}_4^-\text{H}_2\text{O}$	35.4	32.2	33.4 (33.7)	22.3 (22.5)	37.1 (37.5)	33.8	30.5	31.8 (32.0)	20.7 (20.7)	37.4 (38.1)
reaction 8a $\text{PO}_3^-(\text{H}_2\text{O})_3 \rightarrow \text{H}_2\text{PO}_4^-(\text{H}_2\text{O})_2$	20.8	19.8 (19.7)	20.7 (20.6)	18.4 (18.3)	7.8 (7.9)	20.2	19.1 (19.1)	20.1 (20.1)	17.3 (17.3)	9.4 (9.5)
reaction 8b $\text{PO}_3^-(\text{H}_2\text{O})_2 + \text{H}_2\text{O} \rightarrow \text{H}_2\text{PO}_4^-(\text{H}_2\text{O})_2$	32.4	29.3	30.6 (30.8)	19.7 (19.8)	36.6 (37.0)	31.4	28.3	29.6 (29.8)	18.4 (18.5)	37.5 (38.1)
reaction 6a $\text{PO}_3^- + \text{H}_2\text{O} \rightarrow \text{PO}_3^-\text{H}_2\text{O}$	14.5	12.1	12.6	4.8	26.2	13.7	11.4	11.9	4.2	25.8
reaction 7b $\text{PO}_3^-\text{H}_2\text{O} + \text{H}_2\text{O} \rightarrow \text{PO}_3^-(\text{H}_2\text{O})_2$	13.0	10.7	11.1	2.9	27.5	12.4	10.2	10.6	2.5	27.0
reaction 8c $\text{PO}_3^-(\text{H}_2\text{O})_2 + \text{H}_2\text{O} \rightarrow \text{PO}_3^-(\text{H}_2\text{O})_3$	11.6	9.6	9.9	1.3	28.8	11.2	9.2	9.5	1.1	28.1

^a The values of ΔH and ΔG are in kcal mol⁻¹, and ΔS is in cal/(K·mol). The standard state is 1 atm at 298 K. The results in parentheses refer to fully deuterated species.

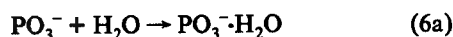
changes for the isomerization reactions and the exothermicities for the total hydration reactions. There are no directly measured experimental values for the exothermicities of the reactions



and



The indirectly derived estimates differ with each other greatly.¹³ For the reaction



ΔH° derived from Unkel and Freedman's experiments¹³ is about -58 kcal mol⁻¹, but Rudnyi's data¹³ give only about -24 kcal mol⁻¹. However, theory suggests that the ΔH° is even less exothermic. The present theoretical value is $\Delta H^\circ = -18.4$ kcal mol⁻¹ at the DZP+diff SCF level, and this decreases to -16.5 kcal mol⁻¹ at the DZP+diff CISD level. The ΔH° value is even smaller (-12.9 kcal mol⁻¹) at the DZP CCSD level. Introduction of diffuse functions has little effect at the CISD level, and ΔH°

is only 0.1 kcal mol⁻¹ higher at the DZP CISD level relative to the DZP+diff CISD level. Thus ΔH° at the DZP+diff CCSD level is expected to be around 13 kcal mol⁻¹ as well.

In other second row atom cases, basis sets with two sets of d and a set of f functions are needed for truly quantitative energetic predictions. However, for the hydration reaction of PO_3^- , there is not much improvement by using the TZ2P+f basis set (Table VII). The exothermicity for the reaction

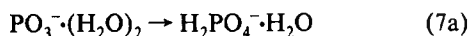


is $\Delta H^\circ = -30.3$ kcal mol⁻¹ at the DZP+diff SCF level, while $\Delta H^\circ = -30.0$ kcal mol⁻¹ at the TZ2P+f SCF level.

While the theoretical ΔH° values for isomerization reaction 6b at the SCF and the CCSD levels differ by 6 kcal mol⁻¹, this is not so when the "total reaction" 6c including both clustering and isomerization is considered. Inclusion of electron correlation has opposing effects on the theoretical exothermicity for the clustering and isomerization reactions. Thus, the correlation effects are canceled to some extent in the overall reaction 6c and the theoretical results are relatively constant (Table VII). The overall exothermicity (ΔH°) for reaction 6c is 30.0 kcal mol⁻¹ at

both the DZP+diff SCF and the DZP+diff CISD levels; however, it is 28.0 kcal mol⁻¹ at the DZP CCSD level. The small difference increases our confidence in the qualitative reliability of the predicted ΔH° at the DZP+diff SCF level. This is especially important for the reactions involving more water molecules, where it is only feasible at present to apply the SCF and MP2 methods.

The two-water isomerization

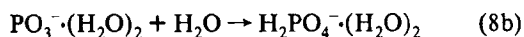


is more exothermic than the one-water isomerization

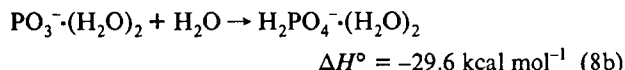
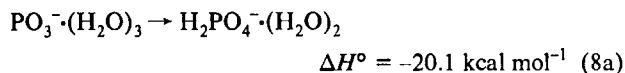


(see Table VIII). The exothermicity for the former reaction 7a of $\text{PO}_3^-(\text{H}_2\text{O})_2$ is $\Delta H = -21.2$ kcal mol⁻¹ at the DZP+diff SCF level, about 3 kcal mol⁻¹ higher than that for $\text{PO}_3^-(\text{H}_2\text{O})$ (reaction 6b) at the same theoretical level. The reason is that H_2PO_4^- is 3 kcal mol⁻¹ more strongly solvated than PO_3^- (see Section B).

The direct measurement of the exothermicity of the (2,3) hydration reaction



(for deuterated species⁶) provides a good opportunity to compare the theoretical with the experimental results. The exothermicity of reaction 8b was measured by Keese and Castleman in studying the clustering of PO_3^- with water molecules,⁶ which process seems to occur spontaneously. As we shall now discuss, the experimental value, $\Delta H^\circ = -16$ kcal mol⁻¹ for reaction 8b, is much less exothermic than that suggested by theory (Table VIII).



The exothermicity for reaction 8b is -29.6 kcal mol⁻¹ at the DZP+diff SCF level. The values for the deuterated species are almost identical, indicating that the isotope effect is of little importance for the reaction. Correlation effects appear relatively unimportant as well. For reaction 6c, the ΔH° DZP CCSD value is 4 kcal mol⁻¹ lower than that at the DZP SCF level. If the difference between the two theoretical levels (SCF and CCSD) for reaction 8a is the same, then the best theoretical ΔH° estimate for reaction 8b would be -26 kcal mol⁻¹. But this is still 10 kcal mol⁻¹ higher than the value observed.⁶

II. The Nature of the Observed (2,3) Hydration Reaction. What (2,3) hydration reaction actually was observed experimentally? We have shown in Section A that both $\text{PO}_3^-(\text{H}_2\text{O})_3$ and $\text{H}_2\text{PO}_4^-(\text{H}_2\text{O})_2$ are expected to be products. Since the two species are indistinguishable mass spectrometrically, both isomers could have been formed. This is consistent with the experimental ΔH° for the (2,3) hydration reaction and can be rationalized as follows. If $\text{PO}_3^-(\text{H}_2\text{O})_3$ and $\text{H}_2\text{PO}_4^-(\text{H}_2\text{O})_2$ are formed in comparable quantities, the experimental ΔH° might be higher than that for $\text{PO}_3^-(\text{H}_2\text{O})_3$ formation (-9.5 kcal mol⁻¹ at the DZP+diff SCF level) and lower than that for $\text{H}_2\text{PO}_4^-(\text{H}_2\text{O})_2$ formation [for example, for reaction 8b, $\Delta H^\circ = -29.6$ kcal mol⁻¹ at the DZP+diff SCF level]. It is clear that the experimental ΔH° (-16.2 kcal mol⁻¹) is closer to that for the $\text{PO}_3^-(\text{H}_2\text{O})_3$ formation reaction.

More support for the conclusion that $\text{PO}_3^-(\text{H}_2\text{O})_3$ is a product for the (2,3) hydration reaction appears from the comparison of our theoretical estimate for ΔH° with the experimental ΔH° for reaction 11 (as discussed in the last section).



The experimental⁶ ΔH° for reaction 11 is significantly more exothermic than the value suggested by the present research (less than 8 kcal mol⁻¹, see Section B). The reason may be that the

$\text{PO}_3^-(\text{H}_2\text{O})_3$ anion is a product together with $\text{H}_2\text{PO}_4^-(\text{H}_2\text{O})_2$; thus the reactions involving one more water molecule [(3,4) hydration reactions] may include reaction 12, which is highly exothermic.



Thus the experimentally observed ΔH° value for the reactions involving four water molecules may be higher than that for the simple clustering reaction 11.

The conclusion that $\text{PO}_3^-(\text{H}_2\text{O})_3$ is one of the products for the (2,3) hydration reaction is strengthened when the description of Keese and Castleman's work⁶ is compared with the results found in Viggiano's experiments.³⁵ Keese and Castleman call attention to the extraordinary sensitivity of the equilibrium constant of the (2,3) reaction to the applied electric field.⁶ This finding may indicate the presence of both $\text{PO}_3^-(\text{H}_2\text{O})_3$ and $\text{H}_2\text{PO}_4^-(\text{H}_2\text{O})_2$, because Viggiano reported that the electric field modifies the clustering ability of the PO_3^- anion.³⁵

D. Comparison with Isoelectronic H_2SO_4 . Like the H_2PO_4^- anion, the neutral isoelectronic H_2SO_4 molecule prefers C_2 symmetry.³¹ The gas electron diffraction and 6-31+G** MP2 geometries³¹ agree well except for the SO bond lengths. The longer bond distances (1.623 vs 1.574 Å for S-OH and 1.446 vs 1.422 Å for S⁺-O⁻) found theoretically may be due to basis set incompleteness. The experimental energy for the hydration reaction, $\text{SO}_3 + \text{H}_2\text{O} \rightarrow \text{H}_2\text{SO}_4$ (-22.1 ± 2.3 kcal mol⁻¹, deduced from the 0 K data in the JANAF tables³⁶), can be reproduced at higher levels of theory (e.g., -20.5 kcal mol⁻¹ at 6-311 + G(2df,p) MP4SDQ + ZPE) and is only somewhat smaller than the energy predicted here for reaction 6c ($\Delta E_0 = -26.7$ kcal mol⁻¹, at the best level reported in Table VIII).

Like PO_3^- , SO_3 forms a complex with H_2O . However, unlike $\text{PO}_3^- \cdot \text{H}_2\text{O}$, the $\text{SO}_3 \cdot \text{H}_2\text{O}$ complex involves *electrophilic* attachment of SO_3 to the water oxygen rather than hydrogen bonding. The theoretical binding energy, about -8 kcal mol⁻¹, is substantially less than that for $\text{PO}_3^- \cdot \text{H}_2\text{O}$ (-12.1 kcal mol⁻¹, see Table VIII). In addition, the computed barrier height for the $\text{SO}_3 + \text{H}_2\text{O} \rightarrow \text{H}_2\text{SO}_4$ reaction (+17.7 kcal mol⁻¹, based on the separated reactants) is much higher than that reported here for the analogous reaction 6c ($\Delta E_0 = +5.0$ kcal mol⁻¹).

E. Conclusions. The isomerization of $\text{PO}_3^-(\text{H}_2\text{O})_n$ clusters ($n = 1, 2$, and 3) to $\text{H}_2\text{PO}_4^-(\text{H}_2\text{O})_{n-1}$ has been studied thoroughly, including the barrier heights, theoretical enthalpy changes (ΔH°), and structures and energetics of the product $\text{H}_2\text{PO}_4^-(\text{H}_2\text{O})_{n-1}$ clusters. The isomerization barrier (ΔG°) of $\text{PO}_3^- \cdot \text{H}_2\text{O} \rightarrow \text{H}_2\text{PO}_4^-$ is 32 kcal mol⁻¹ at the DZP+diff SCF level, 25 kcal mol⁻¹ at the DZP CISD level, and 21 kcal mol⁻¹ at the DZP MP2 level. The isomerization barriers for $\text{PO}_3^-(\text{H}_2\text{O})_2$ and $\text{PO}_3^-(\text{H}_2\text{O})_3$ are lower by a few kilocalories per mole, due to the (discrete) solvation of the transition state. However, via the six-center mechanism, the barrier (ΔG°) is lower by about 5.5 kcal mol⁻¹ for the isomerization of $\text{PO}_3^-(\text{H}_2\text{O})_2$ at the DZP SCF level. The reaction leading to $\text{H}_2\text{PO}_4^-(\text{H}_2\text{O})_2$ may occur, through the $\text{PO}_3^- + 3\text{H}_2\text{O}$ reaction, in an environment in which four-body collisions occur with some frequency. Hence the PO_3^- anion may not exist in the aqueous phase, both for thermodynamic and kinetic reasons. However, in the gas phase, theory suggests that $\text{PO}_3^-(\text{H}_2\text{O})_3$ is observable, since its isomerization barrier to $\text{H}_2\text{PO}_4^-(\text{H}_2\text{O})_2$ is relatively high, $\Delta G^\circ = 21.8$ kcal mol⁻¹ at the DZP+diff MP2 level. A plausible explanation might be the following: (a) the experimental exothermicity for the reaction⁶ involving three water molecules is between that for the clustering reaction [$\text{PO}_3^-(\text{H}_2\text{O})_3$ formation] and that for the hydration reaction [$\text{H}_2\text{PO}_4^-(\text{H}_2\text{O})_2$ formation]; and (b) the experimental⁶

(35) Viggiano, A. A.; Morris, R. A.; Dale, F.; Paulson, J. F.; Henchman, M. J.; Miller, T. M.; Miller, A. E. *J. Phys. Chem.* **1991**, *95*, 1275.

(36) Chase, M. W.; Davies, C. A.; Downey, J. R.; Frurip, D. J.; McDonald, R. A.; Syverud, A. N. *JANAF Thermochemical Tables*; American Chemical Society: Washington, DC, 1985.

ΔH° is significantly higher than that suggested by theory for the solvation of $\text{H}_2\text{PO}_4^-(\text{H}_2\text{O})_2$ to $\text{H}_2\text{PO}_4^-(\text{H}_2\text{O})_3$.

The global $\text{H}_2\text{PO}_4^-(\text{H}_2\text{O})_{n-1}$ minima have C_2 symmetry. The energies of the C_s symmetry conformations are about 1 kcal mol⁻¹ greater and the C_{2v} structures are higher order stationary points with relative energies about 4 kcal mol⁻¹. In the $\text{H}_2\text{PO}_4^-(\text{H}_2\text{O})_{n-1}$ structures, the bond distance differences between the P^+-O^- bonds and the $\text{P}-\text{OH}$ single bonds are inversely related—when one type of bond is lengthened, the other is shortened. This behavior leads to the large difference between the theoretical and experimental structures for H_2PO_4^- .

Like PO_3^- , H_2PO_4^- has a tendency to form double-donor double-acceptor hydrogen bonds with H_2O molecules. H_2PO_4^- is more strongly solvated than the PO_3^- and $\text{PO}_3^-\text{H}_2\text{O}$ anions. The hydration reaction of the PO_3^- anion to give the H_2PO_4^- anion is about 30 kcal mol⁻¹ exothermic. This value is similar to that

for the formation of $\text{H}_2\text{PO}_4^-\text{H}_2\text{O}$ and of $\text{H}_2\text{PO}_4^-(\text{H}_2\text{O})_2$, suggesting that the exothermicity does not decrease with the number of water molecules.

The hydration reaction of PO_3^- with a H_2O molecule is only somewhat more exothermic than the comparable hydration reaction of SO_3 with H_2O but involves a much more tightly bound complex and a much lower energy transition state.

Acknowledgment. This research was supported by the U.S. Air Force Office of Scientific Research under Grant AFOSR-92-J-0047. We appreciate helpful suggestions by Drs. Carl Ewig, Michael Henchman, William Jencks, John Paulson, Albert Viggiano, and Frank Westheimer. We thank Drs. Earl M. Evleth and Yundong Wu for the communication of their unpublished results. We thank Dr. Cynthia Meredith for helpful discussions and for several careful readings of the manuscript.

The vibrational frequencies of borane (BH_3): a comparison of high level theoretical results

John Morrison Galbraith¹, George Vacek², Henry F. Schaefer III*

Center for Computational Quantum Chemistry, University of Georgia, Athens, GA 30602, USA

(Received 7 April 1993)

Abstract

Using the borane molecule, BH_3 , as an example, a detailed comparison is made among the results achieved using many levels of theory for the treatment of electron correlation. In particular, with three different basis sets ranging from a simple double- ζ plus polarization (DZP) to the very flexible triple- ζ plus two sets of polarization functions plus higher angular momentum functions (TZ2P(f,d)), total energetic, geometrical and harmonic vibrational frequency results from several of the more complete single reference methods of electron correlation are compared to the full configuration interaction (FCI) results. Emphasis is placed on comparison of augmented coupled cluster (CCSD(T)) theory and the CI method including all singles, doubles, triples and quadruples (CISDTQ) methods with FCI. These high-level results may also provide some additional insight into the ongoing controversy surrounding the experimentally assigned fundamental vibrational frequencies of BH_3 . The TZ2P(f,d) CCSD(T) harmonic vibrational frequencies predicted in this work were $\omega_1 = 2567$, $\omega_2 = 1163$, $\omega_3 = 2696$ and $\omega_4 = 1223 \text{ cm}^{-1}$ implying experimental misassignments by Kaldor and Porter [J. Am. Chem. Soc., 93 (1971) 2140] of the third and fourth vibrational frequencies, in agreement with previous theoretical works.

Introduction

The borane molecule, BH_3 , is one of the simplest and smallest examples (other than molecular hydrogen) of an electronically neutral bonded species with an incomplete octet. BH_3 is not readily observable, however, because of rapid dimerization to the more stable B_2H_6 molecule. It is this dimer which is used as a standard powerful reducing agent by organic chemists, e.g. for hydroboration–oxidation (cis addition of H–OH to alkenes). It has been postulated that these reactions proceed via the initial breakup of the dimer into the BH_3 monomer, which is the active species [1,2].

Borane was first spectroscopically observed in 1971 by Kaldor and Porter [3] using argon matrix-isolation techniques in combination with the pyrolysis techniques of Mappes and Fehlner [4]. Their vibrational assignments of $\nu_2 = 1125$, $\nu_3 = 2808$ and $\nu_4 = 1604 \text{ cm}^{-1}$ were long accepted without experimental dispute. More recent studies by Kawaguchi and co-workers have focused on the rotational spectra of the ν_2 mode (1141 cm^{-1}) [5] and the ν_3 mode (2602 cm^{-1}) [6] using diode laser IR spectroscopy. These results are in some disagreement with Kaldor and Porter's assignments of those fundamentals.

Because of its humble size, BH_3 lends itself well to theoretical calculations. As a result, numerous theoretical investigations have been undertaken [7–16], most of which explored the $\text{B}_2\text{H}_6 \rightarrow 2 \text{BH}_3$ reaction [8–13]. Several ab initio studies have concentrated on the harmonic

* Corresponding author.

¹ CCQC Summer Research Fellow from Colorado College.

² D.O.D. Predoctoral Fellow, Egil A. Hylleraas Fellow (1990–1991).

vibrational frequencies of borane [12,14–16]. The most comprehensive are by Stanton et al. [14] using many-bodied perturbation (MBPT(2)) theory, Botschwina [15] using coupled-electron pair approximation (CEPA-1) theory and recently by Martin and Lee [16] using augmented coupled cluster (CCSD(T)) theory. Stanton et al. [14], using the 6-31G** basis set of Krishnan et al. [17], predicted frequencies of $\omega_1 = 2671$, $\omega_2 = 1207$, $\omega_3 = 2817$ and $\omega_4 = 1273$ cm⁻¹. Botschwina [15], using a basis set of 63 contracted gaussian-type orbitals, predicted $\omega_1 = 2582$, $\omega_2 = 1164$, $\omega_3 = 2713$ and $\omega_4 = 1228$ cm⁻¹. Martin and Lee [16] have predicted $\omega_1 = 2568$, $\omega_2 = 1158$, $\omega_3 = 2700$ and $\omega_4 = 1220$ cm⁻¹ with the extensive ccVQZP basis set of Dunning [18]. Stanton's predictions for ω_2 and ω_3 adequately agree with the assignments of Kaldor and Porter [3], but not for ω_4 . Stanton considers this difference an erroneous assignment on the part of Kaldor and Porter. Botschwina's findings support Stanton concerning the ω_4 mode and even place some doubt upon Kaldor and Porter's ν_3 assignment. Finally, Martin and Lee [16] refute Kaldor and Porter completely, agreeing instead with the more recent values of Kawaguchi and co-workers [5,6] concerning the ν_2 and ν_3 modes.

In comprehensive studies, Thomas and co-workers [19,20] have shown that high-level theoretical methods in conjunction with small basis sets may have difficulty in predicting vibrational frequencies accurately. Specifically, they tend to underestimate some harmonic vibrational frequencies. Thus the results of Stanton et al. [14] and Botschwina [15] could conceivably be questioned on the grounds of imbalance between basis set quality and levels of electron correlation. Only Martin and Lee's [16] very recent theoretical predictions show a sufficient balance between basis set quality and theoretical method. These results are exemplary, especially with regards to basis set, but do not contain results which are complete with respect to electron correlation.

The present research is intended to predict the

harmonic vibrational frequencies using theoretical methods which incorporate complete electron correlation and use basis sets as complete as those previously used with the specific purpose of resolving the discrepancy concerning the fourth vibrational mode. In addition, isotopic shifts of ¹⁰BH₃, ¹¹BD₃ and ¹⁰BD₃ have been studied in order to encourage further experimental research into the problem. More importantly, this research will also provide detailed comparison of results achieved using many levels of electron correlation. Such a comparison for this small molecule should provide useful information towards the analysis of more complex systems, where complete treatments of electron correlation are unachievable.

Methods

Of the three basis sets used in this study, the smallest consisted of the standard Huzinaga–Dunning–Hay [21–23] double- ζ set of contracted gaussian functions with a set of d-type polarization functions appended to the central boron atom and p-type polarization functions to each hydrogen atom. This basis, (9s5p1d/4s2p1d) for boron and (4s1p/2s1p) for hydrogen, was called the double- ζ plus polarization (DZP) basis set. The polarization orbital exponents for this basis were $\alpha_d(\text{B}) = 0.70$ and $\alpha_p(\text{H}) = 0.75$. For more flexibility, the triple- ζ plus double polarization (TZ2P) basis was used. This basis consisted of Dunning's contraction [24] of Huzinaga's triple- ζ primitive gaussian set [21] with the addition of two sets of polarization functions on each atom. For boron, (10s6p2d/5s3p2d), two sets of d-type functions were added with orbital exponents $\alpha_d(\text{B}) = 1.40, 0.350$. Two sets of p-type functions with orbital exponents $\alpha_p(\text{H}) = 1.50, 0.375$ were added to the hydrogens (5s2p/3s2p). Finally, to the TZ2P basis set, a set of higher angular momentum f-type functions were added to the boron atom, and d-type functions were added to the hydrogen atoms (TZ2P(f,d)) with $\alpha_f(\text{B}) = 0.50$ and $\alpha_d(\text{H}) = 1.00$.

The lowest level of theory employed in this study

Bond Length (Å)

1.1929 DZP SCF
 1.1863 TZ2P SCF
 1.1870 TZ2P(f,d) SCF

1.1944 DZP CISD
 1.1868 TZ2P CISD
 1.1881 TZ2P(f,d) CISD

1.1954 DZP CCSD
 1.1881 TZ2P CCSD
 1.1895 TZ2P(f,d) CCSD

1.1960 DZP CCSD(T)
 1.1888 TZ2P CCSD(T)
 1.1902 TZ2P(f,d) CCSD(T)

1.1962 DZP CISDTQ
 1.1890 TZ2P CISDTQ

1.1962 DZP Full CI

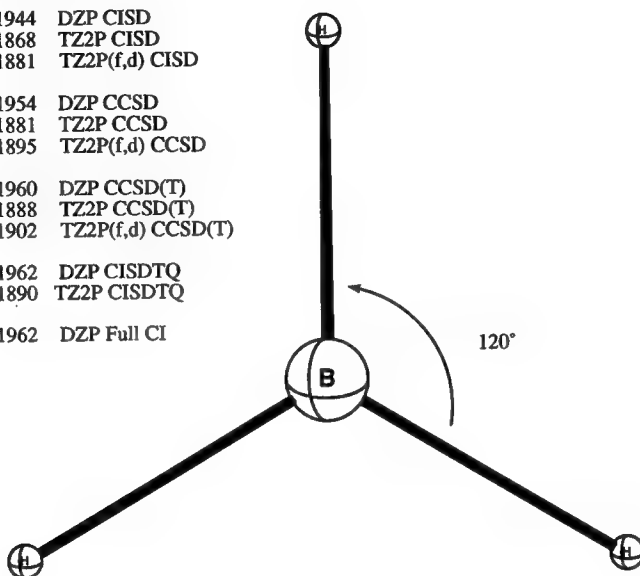


Fig. 1. Predicted equilibrium structure of \tilde{X}^1A_1' BH₃.

was the self-consistent field (SCF) gradient method developed by Pulay [25]. Electron correlation effects were included by employing the configuration interaction (CI) and coupled-cluster (CC) techniques. Only the valence electrons were correlated, holding the boron 1s orbital doubly occupied and excluding the corresponding highest-lying virtual orbital. All single and double (SD) excitations from the SCF wavefunction were included. With the TZ2P(f,d) basis set, the $^1A_1'$ ground state required 7753 configurations in C_{2v} symmetry and 15295 configurations in C_s symmetry. Determination of the CI wavefunctions proceeded via the shape-driven graphical unitary group approach [26]. The contributions from unlinked cluster quadruple excitations to the CISD energies were also crudely estimated using the Davidson correction [27,28] and the results incorporating this appendage are denoted CISD+Q.

CCSD techniques were first developed for the closed shell case by Purvis and Bartlett [29] and

modified by Scuseria et al. [30]. The effects of connected triple excitations were included using the CCSD(T) algorithms originally proposed by Raghavachari et al. [31]. The CCSD(T) method employed here is that of Scuseria and Lee [32].

For still further improvement in the treatment of electron correlation effects, CI calculations were carried out to excitation levels beyond singles and doubles. For the DZP and TZ2P basis sets, wavefunctions were determined using the CI method including all singles, doubles, triples and quadruples (CISDTQ). One frozen-core orbital and one deleted virtual orbital were again adopted. The TZ2P CISDTQ wavefunction required 1277705 configurations in C_{2v} symmetry and 2443957 in C_s symmetry. In addition, with the DZP basis set we determined a full CI (FCI) wavefunction which included all excitations except those involving the frozen core and deleted virtual. In C_{2v} symmetry, the DZP FCI required 943574 configurations and 1883756 configurations in C_s symmetry.

Table 1

Theoretical predictions of total energies (hartrees), harmonic vibrational frequencies (cm^{-1}) and infrared intensities (km mol^{-1}) for the $^{11}\text{BH}_3$ ground state ($\tilde{X}^1A'_1$)

Level of theory	Energy	ω_1	(a_1')	ω_2	(a_2'')	ω_3	(e')	ω_4	(e')
DZP SCF	−26.392176	2644	0	1219	78	2777	380	1251	34
TZ2P SCF	−26.400087	2642	0	1224	113	2759	349	1295	46
TZ2P(f,d) SCF	−26.400447	2639	0	1222	112	2754	352	1291	46
DZP CISD ^a	−26.502415	2604	0	1183	67	2754	309	1203	32
TZ2P CISD ^a	−26.522382	2586	0	1189	96	2719	284	1247	41
TZ2P(f,d) CISD ^a	−26.531740	2589	0	1174	94	2718	271	1236	37
DZP CCSD	−26.505583	2593	0	1178	66	2743	304	1198	32
TZ2P CCSD	−26.526224	2572	0	1184	94	2705	280	1241	41
TZ2P(f,d) CCSD	−26.535897	2575	0	1167	92	2703	267	1229	37
DZP CCSD(T)	−26.506959	2587	0	1175	64	2738	301	1194	31
TZ2P CCSD(T)	−26.528399	2564	0	1180	92	2698	277	1236	41
TZ2P(f,d) CCSD(T)	−26.538423	2567	0	1163	90	2696	263	1223	36
DZP CISDTQ	−26.507214	2585	0	1175	64	2736	301	1193	31
TZ2P CISDTQ	−26.528716	2563	0	1179	92	2697	277	1235	41
DZP Full CI	−26.507281	2584	0	1175	64	2736	301	1193	31
Stanton et al. [14]		2671		1207		2817		1273	
Botschwina [15]		2582		1164		2713		1228	
Martin and Lee [16]		2568		1158		2700		1220	
Kaldor and Porter [3]	(fundamental)			1125		2808		1604	
Kawaguchi and co-workers [5,6]	(fundamental)			1141		2602			

^a With inclusion of the Davidson correction, the CISD + Q energies are −26.507723, −26.528929 and −26.538854 hartrees for the DZP, TZ2P and TZ2P(f, d) basis sets, respectively.

Using SCF [25,33], CI [34,35] and CC [32,36] analytic gradient techniques, the molecular structure for the ground state of BH_3 has been completely optimized to Cartesian and internal coordinate gradients less than 10^{-6} atomic units. Quadratic force constants were evaluated using analytic second derivative techniques for the SCF wavefunctions [37,38] and finite differences of analytic first derivatives for the CI and CC wavefunctions.

Results and discussion

The predicted geometry of the $\tilde{X}^1A'_1$ $^{11}\text{BH}_3$ ground state is displayed in Fig. 1. The total energies, harmonic vibrational frequencies and infrared intensities are presented in Table 1.

Table 2 contains harmonic vibrational frequencies for the $^{10}\text{BH}_3$, $^{11}\text{BD}_3$ and $^{10}\text{BD}_3$ isotopomers.

A comparison of the predicted correlation energies and geometries of BH_3 for the DZP basis shows that while the CISD recovers over 95% of the electron-correlation energy (ECE), it requires the CCSD to recover better than 98% of the ECE. Similarly, the absolute difference from the FCI bond distance is cut in half when going from the CISD to the CCSD wavefunction. The accuracy of the CCSD results, although admirable, pale in comparison to those of the CCSD(T) and CISDTQ. The CISDTQ method essentially reproduced both the FCI energy (99.94% of the ECE) and geometry for the DZP basis set. The comparatively inexpensive CCSD(T) method recovers 99.72%

of the ECE and nearly matches the FCI geometry.

Although even TZ2P FCI is not tractable, if we assume the TZ2P CISDTQ results essentially reproduce the FCI results for that basis, we can make a similar study of ECE recovery and geometry differences. Again the CISD and CCSD methods do reasonably well, and the CCSD(T) method gets the complete correlation results nearly spot on. CISD recovers 95.08% of the CISDTQ ECE, CCSD recovers 98.06% and CCSD(T) recovers 99.75%. The bond length differences ($r_e(\text{CISDTQ}) - r_e(\text{other})$) are 0.0027 Å for SCF, 0.0022 Å for CISD, 0.0009 Å for CCSD and 0.0002 Å for CCSD(T).

Obviously the CCSD(T) method is an excellent approximation to FCI in the case of BH_3 . As a result, the TZ2P(f,d) CCSD(T) energy and bond length predictions may be assumed to be nearly the same as the costly CISDTQ and even more costly FCI. The most reliable prediction of $r_e(\text{B} - \text{H})$ in this study, at the TZ2P(f,d) CCSD(T) level of theory, is 1.1902 Å. Although there are no previous experimental estimates of the equilibrium bond length, our predicted value is likely to be within 0.17% [20]. Our prediction agrees, perhaps fortuitously well, with $r_0(\text{B} - \text{H}) = 1.1900$ Å of Kawaguchi [6]. Martin and Lee [16] have determined that $\Delta(r_0 - r_e) = 0.0027$ Å, and the bond length change for an increase to the basis set limit should be somewhat larger than -0.0011 Å. These two corrections roughly cancel. The best predicted values of Stanton et al. ($r_e = 1.184$ Å) [14] and Botschwina ($r_e = 1.187$ Å) [15] are qualitatively correct but undoubtedly too short. The CCSD(T) results of Martin and Lee [16] should be reliable for the same reasons presented in this paper.

The predicted harmonic vibrational frequencies show similar trends with respect to methods of electron correlation as do the total energies and bond lengths. With the DZP basis set, the harmonic vibrational frequencies using the SCF method of theory are an average of 3.13% from the FCI values. Using the CISD methodology,

this difference drops dramatically to 0.74% and then improves further to 0.33% for CCSD theory. Again the CISDTQ method reproduces the FCI results nearly identically, with the "inexpensive" CCSD(T) method doing almost as well, with only a 0.07% difference.

With the TZ2P basis set, the CISDTQ results must again be used as the benchmark, since they are expected to effectively reproduce the FCI results. As with the DZP basis set, the results converge steadily with improved treatment of correlation towards the CISDTQ frequencies. With the TZ2P basis set, the average difference between the CCSD(T) and CISDTQ results is merely 0.002%. As was found with both the energy and the geometry, the CCSD(T) method quite efficiently reproduces the harmonic vibrational frequency results of the CISDTQ method. One expects, therefore, that the TZ2P(f,d) CCSD(T) results should be only minutely different from the difficult to obtain FCI results for that basis set. With that in mind, one can examine the experimental assignments of the fundamental vibrational frequencies.

The ω_2 mode is the out-of-plane bending mode. The TZ2P(f,d) CCSD(T) prediction of 1163 cm^{-1} is in close agreement with the theoretical predictions of Botschwina (1164 cm^{-1}) [15] and Martin and Lee (1158 cm^{-1}) [16]. Kaldor and Porter's experimental fundamental frequency (1125 cm^{-1}) [3] lies below our prediction by 38 cm^{-1} while the Kawaguchi et al. value (1141 cm^{-1}) [5] is below our value by 22 cm^{-1} . Both experimental fundamental assignments seem reasonable, and at least part of the discrepancy between them may be due to matrix perturbations in Kaldor and Porter's experiment. Our predicted isotopic shifts are $+12 \text{ cm}^{-1}$ and -256 cm^{-1} for $^{10}\text{BH}_3$ and $^{11}\text{BD}_3$ respectively, while the experimental shifts [3] are $+7 \text{ cm}^{-1}$ and -280 cm^{-1} . This isotopic shift agreement supports Kaldor and Porter's assignment for this mode.

The ω_3 mode is the doubly degenerate asymmetric stretch. Our TZ2P(f,d) CCSD(T) prediction of 2696 cm^{-1} is again in close agreement with Botschwina's (2713 cm^{-1}) [15]

and Martin and Lee's (2700 cm^{-1}) [16] best results but substantively lower than the value of Stanton et al. (2817 cm^{-1}) [14]. Although Kawaguchi's *fundamental* frequency observation at 2602 cm^{-1} [6] is satisfactorily observed below our *harmonic* value, Kaldor and Porter's assignment of 2808 cm^{-1} [3] is above all the theoretical predictions. This indicates an experimental misassignment on behalf of Kaldor and Porter and a theoretical overestimation by Stanton et al. Predicted isotopic shifts are $+16\text{ cm}^{-1}$ for $^{10}\text{BH}_3$ and -322 cm^{-1} for $^{11}\text{BD}_3$ while Kaldor and Porter's experimental shifts are $+12\text{ cm}^{-1}$ (reasonable) and -696 cm^{-1} (unreasonable) respectively, placing further doubt upon their assignment. Kawaguchi [6] observes a shift of $+14\text{ cm}^{-1}$ for $^{10}\text{BH}_3$, which is in good agreement with our predicted shift, but he does not observe any other isotopic shifts.

The ω_4 mode is the doubly degenerate asymmetric bend. Stanton et al. [14] questioned Kaldor and Porter's experimental assignment of this mode to 1604 cm^{-1} . In support of the conclusions of Stanton et al., our TZ2P(f,d) CCSD(T) frequency of 1223 cm^{-1} is substantially lower (381 cm^{-1}) than the experimental value while in good agreement with previous theoretical predictions [15,16]. Predicted isotopic shifts are $+6\text{ cm}^{-1}$ for $^{10}\text{BH}_3$ and -678 cm^{-1} for $^{11}\text{BD}_3$ which compare poorly with Kaldor and Porter's experimental shifts of $+6\text{ cm}^{-1}$ and -420 cm^{-1} . Unfortunately, there has so far been no experimental reexamination of the fundamental frequency of this mode.

Conclusion

We have completed a comprehensive ab initio study of the \tilde{X}^1A_1' state of the BH_3 molecule. A detailed comparison of the results obtained for total energy, equilibrium geometry and harmonic vibrational frequencies with the CCSD(T), CISDTQ and FCI methods is presented. These results, although determined for the fairly simple borane molecule, should nonetheless help establish trends usable for more complicated cases. Further,

the harmonic vibrational frequency results presented in this study show conclusively that previous theoretical studies are correct in that the ν_4 mode has been experimentally misassigned. The large difference between predicted and observed isotopic shifts for this mode adds validity to this statement. We also concur that the ν_3 mode has been misassigned by Kaldor and Porter's early work [3], but correctly assigned more recently by Kawaguchi and co-workers [5,6]. The infrared inactive ν_1 mode has yet to be experimentally studied despite much attention by theoretical studies. The harmonic vibrational frequency of the totally symmetric mode is predicted here to be 2567 cm^{-1} . Perhaps a Raman study of BH_3 would be of help in solving this problem since, with the exception of the well established ν_2 mode, all the normal modes of BH_3 are Raman active.

Acknowledgments

This research was supported by the Air Force Office of Scientific Research, Grant No. AFOSR-92-J-0047. This material is based upon work supported under a DOD Graduate Fellowship. J.M.G. would like to thank G.V. for submitting this paper so that he could go skiing for the winter.

Note added in proof

Kawaguchi has recently determined the ν_4 fundamental frequency to be 1196 cm^{-1} [39]. This is in good agreement with our TZ2P (f,d) CCSD(T) harmonic frequency for that mode.

References

- 1 R.M. Adams, Boron, Metallo-Boron Compounds and Boranes, Interscience, New York, 1964.
- 2 T. Clark and P.v.R. Schleyer, J. Organomet. Chem., 156 (1978) 191.
- 3 A. Kaldor and R.F. Porter, J. Am. Chem. Soc., 93 (1971) 2140.
- 4 G.W. Mappes and T.P. Fehlner, J. Am. Chem. Soc., 92 (1970) 1562.

- 5 K. Kawaguchi, J.E. Butler, C. Yamada, S.H. Bauer, T. Minowa, H. Kanamori and E. Hirota, *J. Chem. Phys.*, 87 (1987) 2438.
- 6 K. Kawaguchi, *J. Chem. Phys.*, 96 (1992) 3411.
- 7 M. Jungen and R. Ahlrichs, *Theor. Chim. Acta*, 17 (1970) 339.
- 8 M. Gelus, R. Ahlrichs, V. Staemmler and W. Kutzelnigg, *Chem. Phys. Lett.*, 7 (1970) 503.
- 9 H.A. Hall, D.S. Marynick and W.N. Lipscomb, *Inorg. Chem.*, 11 (1972) 3126.
- 10 L.T. Redmon, G.D. Purvis and R.J. Bartlett, *J. Am. Chem. Soc.*, 101 (1979) 2856.
- 11 J.V. Ortiz and W.N. Lipscomb, *Chem. Phys. Lett.*, 103 (1983) 59.
- 12 D.J. DeFrees and A.D. McLean, *J. Chem. Phys.*, 82 (1985) 333.
- 13 M. Page, G.F. Adams, J.S. Binkley and C.F. Melius, *J. Phys. Chem.*, 91 (1987) 2675.
- 14 J.F. Stanton, R.J. Bartlett and W.N. Lipscomb, *Chem. Phys. Lett.*, 138 (1987) 525.
- 15 P. Botschwina, in J.P. Maier (Ed.), *Ion and Cluster Ion Spectroscopy and Structure*, Elsevier, Amsterdam, 1989, pp. 76–81.
- 16 J.M.L. Martin and T.J. Lee, *Chem. Phys. Lett.*, 200 (1992) 502.
- 17 R. Krishnan, J.S. Binkley, R. Seeger and J.A. Pople, *J. Chem. Phys.*, 72 (1980) 650.
- 18 T.H. Dunning, *J. Chem. Phys.*, 90 (1989) 1007.
- 19 J.R. Thomas, B.J. DeLeeuw, G. Vacek and H.F. Schaefer, *J. Chem. Phys.*, 98 (1993) 1336.
- 20 J.R. Thomas, B.J. DeLeeuw, G. Vacek, T.D. Crawford, Y. Yamaguchi and H.F. Schaefer, *J. Chem. Phys.*, 99 (1993) 403.
- 21 S. Huzinaga, *J. Chem. Phys.*, 42 (1965) 1923.
- 22 T.H. Dunning, *J. Chem. Phys.*, 53 (1970) 2823.
- 23 T.H. Dunning and P.H. Hay, in H.F. Schaefer (Ed.), *Modern Theoretical Chemistry*, Vol. 3, Plenum, New York, 1977, pp. 1–27.
- 24 T.H. Dunning, *J. Chem. Phys.*, 55 (1971) 716.
- 25 P. Pulay, in H.F. Schaefer (Ed.), *Modern Theoretical Chemistry*, Vol. 4, Plenum, New York, 1977, pp. 152–185.
- 26 P. Saxe, D.J. Fox, H.F. Schaefer and N.C. Handy, *J. Chem. Phys.*, 77 (1982) 5584.
- 27 S.R. Langhoff and E.R. Davidson, *Int. J. Quantum Chem.*, 8 (1974) 61.
- 28 E.R. Davidson, in R. Daudel and B. Pullman (Eds.), *The World of Quantum Chemistry*, Reidel, Dordrecht, 1974, p. 17.
- 29 G.D. Purvis and R.J. Bartlett, *J. Chem. Phys.*, 76 (1982) 1910.
- 30 G.E. Scuseria, C.L. Janssen and H.F. Schaefer, *Chem. Phys.*, 89 (1988) 7382.
- 31 K. Raghavachari, G.W. Trucks, J.A. Pople and M. Head-Gordon, *Chem. Phys. Lett.*, 157 (1989) 479.
- 32 G.E. Scuseria and T.J. Lee, *J. Chem. Phys.*, 93 (1990) 5851.
- 33 Y. Osamura, Y. Yamaguchi and H.F. Schaefer, *J. Chem. Phys.*, 77 (1982) 383.
- 34 B.R. Brooks, W.D. Laidig, P. Saxe, J.D. Goddard, Y. Yamaguchi and H.F. Schaefer, *J. Chem. Phys.*, 72 (1980) 4652.
- 35 J.E. Rice, R.D. Amos, N.C. Handy, T.J. Lee and H.F. Schaefer, *J. Chem. Phys.*, 72 (1986) 963.
- 36 A.C. Scheiner, G.E. Scuseria, J.E. Rice, T.J. Lee and H.F. Schaefer, *J. Chem. Phys.*, 87 (1987) 5361.
- 37 Y. Osamura, Y. Yamaguchi, P. Saxe, M.A. Vincent, J.F. Gaw and H.F. Schaefer, *J. Chem. Phys.*, 72 (1982) 131.
- 38 Y. Yamaguchi, Y. Osamura, P. Saxe, D.J. Fox, M.A. Vincent and H.F. Schaefer, *J. Mol. Struct. (Theochem)*, 103 (1983) 183.
- 39 K. Kawaguchi, 48th Ohio State University International Symposium on Molecular Spectroscopy, RH09, Columbus, OH, 1993.

Is dodecahedral P_{20} special?*

Ching-Han Hu, Mingzuo Shen, and Henry F. Schaefer III

Center for Computational Quantum Chemistry, University of Georgia, Athens, GA 30602, USA

Received April 12, 1993/Accepted June 30, 1993

Summary. The laboratory study of phosphorus clusters by laser-based mass spectrometric methods indicates, tentatively, that P_{21}^+ may be special. A plausible interpretation might place a P^+ ion interior to a dodecahedral P_{20} molecule. *Ab initio* quantum mechanical methods have been applied to the P_{20} molecule using contracted gaussian basis sets as large as (9s 6p 4d 3f) on each phosphorus atom. At the highest level of theory, dodecahedral P_{20} is predicted to lie 23 kcal/mol above five separated P_4 molecules.

Key words: Phosphorus clusters – P_{20} – Dodecahedra

1 Introduction

As part of an ongoing search [1] for new high energy density molecular systems, we recently reported an *ab initio* quantum mechanical study [2] of the dodecahedral N_{20} molecule. In the final paragraph of that paper, we noted that dodecahedral P_{20} will be far more stable relative to 10 P_2 than N_{20} is relative to 10 N_2 . The latter discussion [2] attracted the attention of Whetten [3], who was studying the formation of phosphorus clusters in the laboratory by laser-based mass spectrometric methods. Whetten's observations on positively charged clusters indicated, tentatively, that P_{21}^+ might be special. Whetten then suggested [3] "One possibility, related to your structures, is a pentagonal dodecahedron structure with an interior P^+ atom bonded to four surface atoms." This intriguing hint from experiment was sufficient to motivate us to carry out the present theoretical investigation of dodecahedral P_{20} , which is illustrated in Fig. 1.

Unknown to us at the start of this work was the excellent, very recent theoretical study of Häser, Schneider, and Ahlrichs [4] on a broad range of phosphorus clusters as large as P_{28} . Häser, Schneider, and Ahlrichs appear to show conclusively that P_{12} lies lower in energy with respect to P_4 than does P_{20} . They further suggest that P_{12} should be kinetically stable. In spite of this discouraging prognosis for P_{20} , we have taken the theory significantly farther than Ahlrichs. Thus it seemed appropriate to report these new P_{20} results here.

Our energetic results for P_{20} are summarized in Table 1. Due to the extraordinarily high symmetry of the dodecahedral P_{20} , the full geometry optimization

* Dedicated to Professor Werner Kutzelnigg

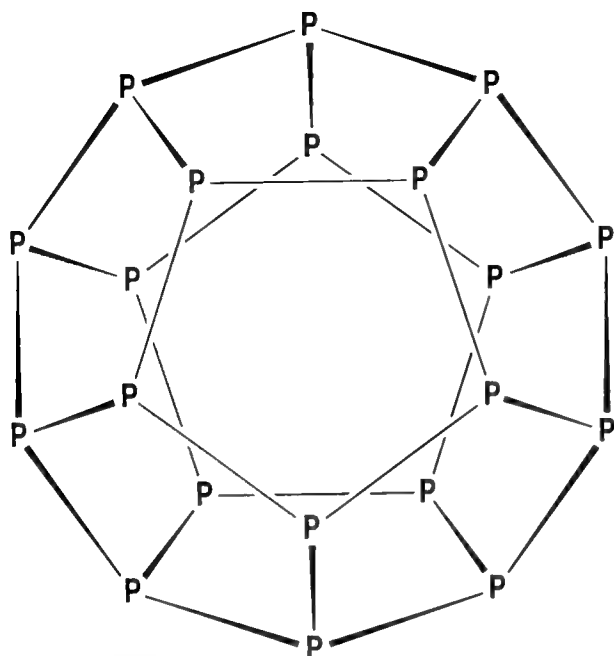


Fig. 1. The dodecahedral (I_h symmetry) P_{20} molecule. All phosphorus atoms are equivalent and all bonds are single P-P bonds

Table 1. Total energies of P_{20} in a.u., and relative energies in kcal/mol with respect to P_4 and bond distances in Å for P_{20} (dodecahedral), P_4 (tetrahedral) and $P_2(^1\Sigma_g^+)$

	Number of basis functions in P_{20}	Total energy	Relative energy			Bond distance		
			P_{20}	$5P_4$	$10P_2$	P_{20}	P_4	P_2
DZ SCF	360	- 6813.736765	- 165	0	- 36	2.352	2.399	1.929
DZP SCF	460	- 6814.391880	7	0	126	2.235	2.167	1.855
TZ2P SCF	620	- 6814.991759	64	0	199	2.248	2.186	1.857
TZ2Pf SCF	760	- 6815.053303	65	0	215	2.240	2.176	1.854
(9s 6p 4d 3f) SCF	1340	- 6815.094877	70	0	207	2.238	2.173	1.850
DZ MP2	360	- 6815.106346	- 98	0	- 104	2.434	2.508	2.088
DZP MP2	460	- 6816.569856	- 10	0	111	2.243	2.182	1.929
TZ2P MP2	620	- 6817.512056	23	0	259	-	-	-
Experiment			-	0	269 ^a	-	2.21 ^b	1.894 ^c

^a Chase MW Jr., Davies CA, Downey JR Jr., Frurip DJ, McDonald RA, Syverud AN (1985) JANAF thermal chemical tables. Dow Chemical Corp, Midland, Michigan

^b Maxwell LR, Hendrichs SB, Mosley V (1935) J Chem Phys 3:699

^c Huber KPH, Herzberg G (1979) Constants of diatomic molecules. Van Nostrand, NY

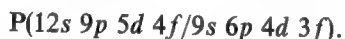
involves the variation of only a single P–P bond distance. Accordingly, this structural optimization was completed at all but one level of theory. The largest basis set considered by Häser, Schneider, and Ahlrichs [4] was their own P(12s 9p 2d/7s 5p 2d) set [5], designated triple zeta plus double polarization (TZ2P). With their TZ2P SCF method, Häser and coworkers predict that dodecahedral P_{20} lies 268 kJ/mol (64 kcal/mol) above five separated P_4 molecules. The present TZ2P basis set is slightly different, P(12s 9p 2d/6s 5p 2d), and is taken from the work of McLean and Chandler [6], with polarization function orbital exponents $\alpha_d(P) = 1.2, 0.3$. Although the two TZ2P basis sets are by no means identical, our predicted TZ2P SCF binding energy T_e for the process:



is also 64 kcal/mol.

The addition of a set of f functions [$\alpha_f(P) = 0.45$] to our TZ2P basis set changes ΔE for reaction (1) by only 1 kcal, to 65 kcal/mol. However, the addition of one set of f functions to each phosphorus atom does decrease the P–P bond distances by 0.008 Å. Häser and coworkers [4] do not report the equilibrium geometry of P_{20} .

To explore the Hartree-Fock limit, we have utilized a much larger basis set, designated:



This extended basis set uses the original Huzinaga [7] P(12s 9p) primitive gaussian set, contracting it to provide maximum flexibility in the valence region, i.e. 411111111 for the s functions and 411111 for the p functions. The d and f functions in this extended basis set were contracted using the atomic natural orbitals (ANO's) of Widmark, Persson, and Roos [8]. Compared to the TZ2P basis set the (9s 6p 4d 3f) basis lowers the SCF energy of 5 P_4 more than the energy of dodecahedral P_{20} . Specifically, P_{20} is predicted to lie 70 kcal/mol above 5 P_4 at the (9s 6p 4d 3f) SCF level of theory, an increase of 5 kcal/mol compared to the TZ2P result. The P–P bond distance is decreased by 0.002 Å from TZ2P to (9s 6p 4d 3f). To summarize, one may say that pressing on from Ahlrichs SCF results [4] toward the Hartree-Fock limit results in only modest changes in the P_{20} dissociation energy.

Häser, Schneider, and Ahlrichs [4] also reported the energy of P_{20} using second-order perturbation theory (MP2) in conjunction with a basis set [5] that they designate split-valence plus polarization (SVP). At the SVP MP2 level of theory, Häser reports that P_{20} lies 81 kJ/mol (19 kcal/mol) above 5 P_4 . In this work we first extended the MP2 studies to the double zeta plus polarization (DZP) basis set of Huzinaga, Dunning, and Hay [7, 9]. The predicted DZP MP2 bond distance is $r_e(P-P) = 2.243$ Å, only 0.008 Å longer than the analogous SCF result. The DZP MP2 method actually places P_{20} below 5 P_4 by 10 kcal/mol.

Since the above result disagreed with Ahlrichs' SVP MP2 prediction, it was deemed necessary to press on to the TZ2P MP2 method. In the latter case only, the geometry was assumed (rather than optimized) to be the TZ2P SCF structure. In this manner P_{20} is predicted to lie 23 kcal/mol above 5 P_4 . Inspection of the SCF results (apparent convergence to within 6 kcal/mol with the TZ2P basis set) in Table 1 suggests that this result from second-order perturbation theory may be within 10 kcal/mol of the basis set limit. The good agreement with Häser's result [4] of 19 kcal/mol must be considered somewhat fortuitous in light of the DZP MP2 prediction of the opposite sign.

Table 2. Vibrational frequencies (cm^{-1}) and infrared intensities (km/mol , in parentheses) for dodecahedral P_{20}

Symmetry	Degeneracy	DZ SCF
H_g	5	458
H_u	5	456
G_g	4	397
T_{2u}	3	387
G_u	4	374
H_g	5	328
T_{2u}	3	305
G_g	4	292
T_{1u}	3	291(1.0)
A_g	1	257
G_u	4	219
T_{2g}	3	197
H_g	5	170
H_u	5	148

Table 3. Valence electron orbital energies (in eV) for the dodecahedral P_{20} molecule

Symmetry	DZP SCF	TZ2P SCF	TZ2Pf SCF	(9s6p4d3f) SCF
LUMO $7t_{1u}$	-0.93	-0.58	-0.54	-0.56
HOMO $6g_g$	-9.12	-8.83	-8.79	-8.74
$6g_u$	-9.30	-8.91	-8.96	-8.91
$8h_g$	-11.04	-10.60	-10.68	-10.65
$6t_{2u}$	-11.28	-10.99	-10.95	-10.91
$6t_{1u}$	-13.25	-12.79	-12.88	-12.85
$3h_u$	-13.47	-13.01	-13.03	-12.99
$5a_g$	-14.49	-14.01	-14.11	-14.08
$7h_g$	-14.69	-14.22	-14.24	-14.21

In Tables 2 and 3 are reported harmonic vibrational frequencies and valence electron orbital energies for dodecahedral P_{20} . Due to the molecule's high symmetry only the T_{1u} fundamental is allowed in the infrared. The single A_g and three H_g fundamentals are Raman allowed.

The present research confirms the earlier study of Häser, Schneider, and Ahlrichs [4] that dodecahedral P_{20} is not "special". That is, P_{20} is not the most favored energetically among phosphorus clusters. This result does not, of course, exclude the possibility proposed by Whetten [3] that a P_{21}^+ ion, with one phosphorus atom internal to the P_{20} cage, might be "special". Also, since P_{20} lies only slightly higher in energy than 5P_4 , the possibility that dodecahedral As_{20} , Sb_{20} , or Bi_{20} might be special remains open.

Acknowledgments. This research was supported by the U.S. Air Force Office of Scientific Research under Grant No. AFOSR-92-J-0047. We thank Professor Robert L. Whetten for helpful suggestions and Professor Reinhart Ahlrichs for the use of the TURBOMOLE system of programs [10] developed at Karlsruhe.

References

1. See, for example, Xie Y, Schaefer HF, Jang JH, Mhin BJ, Kim HS, Yoon CW, Kim KS (1992) *Molecular Physics* 76:537 and references therein
2. Bliznyuk AA, Shen M, Schaefer HF (1992) *Chem Phys Lett* 198:249
3. Whetten RL, personal communication, January 14, 1993
4. Häser M, Schneider U, Ahlrichs R (1992) *J Amer Chem Soc* 114:9551
5. Schäfer A, Horn H, Ahlrichs R (1992) *J Chem Phys* 97:2571
6. McLean AD, Chandler GS (1980) *J Chem Phys* 72:5639
7. Huzinaga S (1971) *Approximate atomic functions. II*, Dept of Chemistry, Univ of Alberta, Edmonton
8. Widmark PO, Persson BJ, Roos BO (1991) *Theoret Chim Acta* 79:419
9. Dunning TH, Hay PJ (1977) in: Schaefer HF (ed) *Modern theoretical chemistry. Vol 3:1-27*. Plenum, NY
10. Ahlrichs R, Bär M, Häser M, Horn H, Kölmer C (1989) *Chem Phys Lett* 162:165

Dodecahedral and smaller arsenic clusters: As_n , $n=2, 4, 12, 20$

Mingzuo Shen and Henry F. Schaefer III

Center for Computational Quantum Chemistry, The University of Georgia, Athens, Georgia 30602

(Received 7 March 1994; accepted 18 April 1994)

Ab initio all-electron quantum mechanical methods, including the Hartree–Fock (HF), second-order perturbation theory, configuration interaction with single and double excitations (CISD), and coupled cluster with single and double excitations (CCSD) methods, have been applied to four arsenic clusters, diatomic As_2 , tetrahedral As_4 , cage-like As_{12} belonging to the D_{3d} point group, and dodecahedral As_{20} . Several basis sets were used. The double-zeta plus polarization (DZP) includes both d and f polarization functions, while the triple-zeta plus double polarization basis includes two sets of f functions on each atom. From the most reliable theoretical results, As_{12} is energetically lowest among the clusters considered, and As_{20} is energetically comparable to As_4 .

INTRODUCTION

We recently reported quantum mechanical studies of the dodecahedral molecules M_{20} (belonging to point group I_h) with M =nitrogen and phosphorus.^{1,2} The homonuclear diatomic M_2 and tetrahedral M_4 molecules were simultaneously studied. In this paper we present a study of the dodecahedral As_{20} molecule, along with the homonuclear diatomic As_2 , tetrahedral As_4 , and cage-like D_{3d} As_{12} species. The present research on the cluster As_{12} was inspired by the excellent recent quantum chemical study of Häser, *et al.*³ on phosphorus clusters.

Although the elements N, P, As, Sb, and Bi belong to Group V A in the Periodic Table, and their chemical properties are recognizably similar, being more or less governed by the identical valence electron configuration ns^2np^3 , there are substantial differences among them.⁴ The nitrogen atom lacks low-lying d atomic orbitals and N_2 has the very highest bond dissociation energy among all homonuclear diatomic molecules; therefore it is expected that N_{20} should lie substantially higher in energy than N_2 , in fact nearly 50 kcal per mole of nitrogen atoms according to our theoretical study.¹ The phosphorus atom has lower-lying empty $3d$ atomic orbitals and tetrahedral P_4 is already thermodynamically stable with respect to P_2 . By our best theoretical estimate, P_{20} is lower in energy than P_2 , by about 12 kcal per mole of phosphorus atoms.² The arsenic atom has a filled $3d$ atomic shell, and in the vapor phase the tetrahedral As_4 predominates, and As_2 has the smallest bond dissociation energy along the series N_2 , P_2 , As_2 ; therefore it is expected that As_{20} should be energetically favorable compared with As_2 . The manner in which As_{20} compares with As_4 energetically is one of the questions we would like to answer in this study.

Phosphorus and arsenic are more likely to form homonuclear clusters than nitrogen. Ahlrichs and co-workers³ predicted that a P_{12} cluster belonging to the D_{3d} point group is the most stable small gas-phase cluster of phosphorus. Anticipating closer similarity between P and As, we also consider As_{12} with the same qualitative geometrical arrangement.

The most stable solid form of arsenic at room temperature is the α -As structure, where each arsenic atom has three nearest neighbors at distances of 2.517 Å, and with angle

As–As–As 96.7°, which conforms rather closely to the single-bond arsenic covalent radius of 1.20 Å.⁴

THEORETICAL METHODS

In this study the following neutral arsenic clusters were investigated: As_n , with $n=2, 4, 12, 20$. A principal interest of this report is the dodecahedral As_{20} , but the smaller clusters are included for comparison and calibration. As_{12} is also of major interest as a homolog of the energetically low-lying P_{12} system studied by Ahlrichs and co-workers.³

Four basis sets for arsenic were used, described presently. The “split-valence” (SV) basis set of Schäfer *et al.* is reported to be optimized with respect to both orbital exponents α and the nature of the contractions of the primitive Gaussian functions.⁵ This basis set may be designated (14s10p5d/5s4p2d) or [63311/5311/41]. With five pure d functions, there are 27 basis functions in this set for each arsenic atom. The larger double-zeta (DZ) basis set was derived similarly by Ahlrichs and co-workers,⁵ and may be designated (14s11p5d/8s6p2d) or [6211111/331211/41]. Using spherical $5d$ functions, there are 36 basis functions for each arsenic atom in the DZ basis set. We constructed a double-zeta plus polarization (DZP) basis set from the above DZ basis set, by adding one set of pure $5d$ functions with orbital exponent $\alpha_d(\text{As})=0.32$ derived in an even-tempered manner from the last two d orbital exponents in the above DZ set, and by adding one set of pure $7f$ functions with orbital exponent $\alpha_f(\text{As})=0.416$. This f orbital exponent was obtained by varying it with respect to the Hartree–Fock (HF) energy of the tetrahedral As_4 at the DZ HF optimized geometry. The f orbital exponent was varied from 2.0 to 0.1, and 0.416 was found to be optimal after eight steps. The DZP basis set may thus be designated as (14s11p6d1f/8s6p3d1f) or [6211111/331211/411/1], and with $5d$ and $7f$ there are 48 basis functions for each arsenic atom. We also built a still larger basis set, of the triple-zeta plus double polarization (TZ2P) quality, from the (21s16p10d) primitive basis set of Partridge.⁶ The HF energy with Partridge’s (21s16p10d) primitive basis set for the As 4S state is $-2234.238\,37$ a.u. We have considered a number of segmented contractions, and found that the contraction (21s16p10d/13s8p3d) results in the best compromise be-

tween energy rise and contraction size, giving for the $4s$ state a contracted atomic SCF energy of $-2234.209\,03$ a.u. To form the TZ2P-like basis set, we added another set of $5d$ functions of orbital exponent $\alpha_d(\text{As})=0.15$ derived in an even-tempered manner from the last two d orbital exponents in Partridge's ($21s16p10d$) primitive basis set. Further, two sets of $7f$ functions were added, with orbital exponents $\alpha_f(\text{As})=0.79, 0.33$. The f orbital exponents were optimized using the tetrahedral As_4 at its DZP HF optimized geometry. Initial values for the f orbital exponents are 0.416×2 and $0.416/2$. A total of 12 steps were used to reach the final f orbital exponents 0.79 and 0.33 . The TZ2P-like basis set may be designated ($21s16p11d2f/13s8p4d2f$), or $[911111111111/91111111/8111/11]$. With the $5d$ and $7f$ spherical functions, there are 71 basis functions for each arsenic atom.

We have also experimented with two other basis sets, which are of minor interest in this study. The first is a looser valence contraction of the DZ basis set of Ahlrichs and co-workers, ($14s11p5d/8s7p2d$) or $[62111111/3311111/41]$, using the same primitive basis set as Ahlrichs and co-workers.⁵ The resulting basis set may be called DZ'. The second additional basis set is contracted from the primitive basis set of Poirier *et al.*,⁷ and may be designated ($14s11p5d/9s9p2d$) or $[61111111/31111111/41]$. This basis set may be called DZ''. The SCF energy for the $4s$ state of an arsenic atom are $-2234.130\,04$ a.u. for basis DZ, $-2234.130\,38$ a.u. for DZ', and $-2234.121\,40$ a.u. for basis DZ''. Both the DZ' and DZ'' basis sets are of double-zeta quality, give rise to similar results for the tetrahedral As_4 as Ahlrichs' DZ, but have more basis functions for each arsenic atom. Therefore, the DZ basis set of Ahlrichs and co-workers are used for the larger clusters.

The direct SCF method^{8,9} was applied to all clusters with all basis sets, using the TURBOMOLE program developed by Ahlrichs and co-workers.¹⁰ The second-order Møller–Plesset perturbation method¹¹ (MP2) was applied using the DZP basis set. Here the GAUSSIAN 92 program,¹² as well as the TURBOMOLE program¹⁰ were used. Finally the configuration interaction with single and double excitations¹³ (CISD), and the coupled-cluster with single and double excitations¹⁴ (CCSD) methods were applied to As_2 , using the PSI program developed in our research group.¹⁵ When the geometries were optimized, the symmetrized internal coordinates¹⁶ or the Z matrix method¹² were used. When practical, the energy Hessian was obtained using analytic methods;¹¹ otherwise finite differences of energy gradients were used automatically¹² or manually.

The homonuclear diatomic As_2

Various physical properties of the diatomic molecule As_2 are listed in Huber and Herzberg,¹⁷ among them the equilibrium bond length and harmonic vibrational frequency. Also, the DZP basis set for As_2 is sufficiently small that the MP2, CISD, and CCSD methods may be applied here. Theoretical results, and comparisons with experiment, are listed in Table I. One may clearly see that the DZP MP2 and DZP CCSD methods yield results closest to the experimental results, and on either side of the experimental values. The DZP CCSD

TABLE I. Theoretical results for As_2 and comparison with experiment.

	Energy (a.u.)	r_e (Å)	ω_e (cm^{-1})
SV SCF	-4467.797 73	2.081	489
DZ SCF	-4468.239 73	2.082	486
DZP SCF	-4468.295 13	2.056	518
TZ2P SCF	-4468.440 17	2.060	511
DZP MP2 ^a	-4469.337 05	2.124	412
DZP CISD ^b	-4468.733 83	2.072	495
DZP CCSD ^c	-4468.794 67	2.099	460
Expt. ^d		2.103	430

^aMP2(full) in GAUSSIAN 92, where all electrons were correlated.

^bIn forming the CISD wave function, 18 core MOs were frozen and 18 virtual MOs deleted. There are 29 296 interacting walks within the D_{2h} point group. The Davidson corrected total energy (CISD+Q) is $-4468.785\,26$ a.u.

^cIn forming the CCSD wave function, 18 core MOs were frozen and 18 virtual MOs deleted.

^dK. P. Huber and G. Herzberg, *Molecular Spectra and Molecular Structure. IV. Constants of Diatomic Molecules* (Van Nostrand Reinhold, New York, 1979).

bond length reproduces almost identically the experimental distance, being off by only -0.004 Å. However, the DZP CCSD harmonic vibrational frequency is still too large by 30 cm^{-1} . The DZP SCF bond length is too short by -0.05 Å, and the DZP SCF harmonic vibrational frequency is too large by 90 cm^{-1} ; the compensating scale factor is $430/518\approx 0.83$.

Tetrahedral As_4 (T_d)

The tetrahedral As_4 structure is the dominant form of elemental arsenic in the vapor phase. Furthermore, arsenic and gallium compounds have been of interest as possible alternatives to silicon in the development of new semiconductor devices. Consequently, there have been a considerable number of experimental as well as theoretical studies on As_4 . Certainly the majority of previous investigations were targeted at As_2 and As_4 . In the present study, As_4 is included for comparison and calibration. Although As_4 incorporates small bond angles (all As–As–As angles are 60°), each arsenic atom is trivalent, and connected to other arsenic atoms via single bonds. Therefore As_4 is expected to be prototypical of other cage-like arsenic clusters, including As_{12} and As_{20} . In contrast one may well argue that in diatomic As_2 the two arsenic atoms are connected by a triple bond, similar to its homologs N_2 and P_2 .

In 1966 Morino *et al.*¹⁸ reported a high-temperature gas-phase electron diffraction (GED) study of the arsenic vapor. The temperature was 485°C , and their experiment confirmed that the gas-phase arsenic is primarily tetrahedral As_4 . The thermally averaged internuclear distance was reported to be $r_g(\text{As–As})=2.435\pm 0.004$ Å. From the observed mean amplitude of vibration, the force constant for the totally symmetric a_1 normal mode was evaluated to be 1.5 ± 0.3 mdyn/Å. Note that electron diffraction distances r_g are generally larger than the equilibrium distances r_e ; the higher the temperature at which r_g is measured, the larger the difference (r_g-r_e); usually the difference is 0.005 – 0.010 Å.

In 1973 Bosworth *et al.*¹⁹ reported the fundamental vibrational frequencies for the tetrahedral As_4 molecule (along

TABLE II. Theoretical results for tetrahedral As_4 (T_d) and comparison with experimental results.

	Energy (a.u.)	r_e (Å)	ω_e (cm ⁻¹)			ΔH_0° (kcal/mol)
			a_1	e	t_2	As ₄ ⇌2As ₂
SV SCF	-8935.611 71	2.543	320	186	242	10.5
DZ SCF	-8936.497 07	2.541	318	187	242	11.4
DZP SCF	-8936.665 10	2.414	393	225	291	47.2
TZ2P SCF	-8936.952 01	2.417	45.2
DZP MP2 ^a	-8937.175 56	63.7
Expt.		2.435 ^b	342.0 ^c	200.8 ^c	251.0 ^c	54.0±1.1 ^d

^aMP2 with 14 core MOs frozen and 14 virtual MOs deleted per arsenic atom, from TURBOMOLE. Molecular geometry is that from DZP SCF.

^bThe cited As-As bond length was determined in the gas-phase electron diffraction experiment of Morino *et al.*, Ref. 18. The cited value is r_g at 485 °C. r_g is generally longer than the equilibrium r_e ; the higher the temperature at which r_g is measured, the larger the difference ($r_g - r_e$); usually the difference is 0.005–0.010 Å.

^cThe cited vibrational frequencies were determined in the vapor-phase Raman spectroscopic study of Bosworth *et al.*, Ref. 19. The values are fundamentals, which are generally smaller than harmonic vibrational frequencies due to anharmonicity.

^dThe cited value, the standard reaction enthalpy at 0 K, is from Murray *et al.*, Ref. 23. The experimental value is directly comparable to the difference in energy (ΔE_e) plus the ZPVE correction ($\Delta E_0 = \Delta E_e + \Delta ZPVE$). The same authors reported that $\Delta H_{298}^\circ = 54.26 \pm 0.7$ kcal/mol.

with many other spherical top molecules). These authors obtained the “extra-cavity Raman spectrum” of vapor-phase As_4 using Ar^+ 4880 and 5145 Å excitations. Because the Ar^+ laser used had a relatively high intensity, the authors claimed their spectrum was of higher quality than previous Raman experiments.^{20,21} Only the t_2 normal mode is IR active, and the Raman t_2 fundamental vibrational frequency agrees with an IR measurement.²²

Using the Knudsen effusion technique combined with a mass spectrometer, two research groups have determined the reaction enthalpy for the dissociation of tetrahedral As_4 into As_2 . In 1973 Murray *et al.*^{23,24} reported that the reaction enthalpy at 298 K for $As_4 \rightleftharpoons 2As_2$ is 54 kcal/mol. These authors rejected a previously accepted value which was based on spurious experimental conditions (69.0 ± 6.0 kcal/mol; see discussions in Ref. 23). The value of 54 kcal/mol was confirmed by Drowart *et al.*²⁵ a few years later using a similar experimental technique.

Our theoretical results for the tetrahedral As_4 are shown in Table II, along with selected experimental results. Again, we emphasize that the theoretical methods used for As_4 were selected in the hope that they would also be applicable to the larger clusters As_{12} and As_{20} , not simply that they reproduce experimental results for As_4 itself. Considering the As-As bond lengths first, we see that the double-zeta SCF method is very inadequate. This may be explained by the well-known necessity of polarization basis functions when small bond angles are present. The DZP SCF bond length compares favorably with the GED experimental result, if one keeps in mind that the GED bond length r_g could be longer than the equilibrium r_e by as much as 0.01 Å depending on the temperature at which r_g is determined. The TZ2P SCF bond length is very similar to that of DZP SCF, despite the considerably larger size of the TZ2P basis (71 basis functions in

TZ2P vs 48 in DZP). Next consider the harmonic vibrational frequencies. Since the DZ SCF bond length is much too long, it is expected that the harmonic vibrational frequencies evaluated at the DZ SCF equilibrium geometries are going to be low, and it turns out that they are even lower than the observed fundamentals. In contrast, the DZP SCF harmonic vibrational frequencies are uniformly larger than the fundamentals, as expected. The ratios of DZP-SCF harmonic vibrational frequencies to the Raman fundamentals for the three symmetry species are rather uniform: $342.0/393 \approx 0.87$ (a_1), $220.8/225 \approx 0.89$ (e), and $251.0/291 \approx 0.86$ (t_2). Incidentally, our theoretical harmonic vibrational frequencies, being all real, for the first time theoretically confirm that the tetrahedral structure is a local minimum.

Finally consider the enthalpy of dissociation $As_4 \rightleftharpoons 2As_2$. The DZ SCF result was far too small with respect to the experimental value. The DZP SCF and DZP MP2 values bracketed the experimental value. The TZ2P SCF value was slightly worse than the DZP SCF. In evaluating the theoretical enthalpies, zero-point vibrational energies (ZPVEs) were included, from scaled harmonic vibrational frequencies. The scale factor used was 0.91 as advocated by Grev *et al.*²⁶ Since harmonic vibrational frequencies at the TZ2P SCF and DZP MP2 levels are not available, in these two cases ZPVEs at the DZP SCF level were used. The DZP MP2 method excluded all arsenic $1s$ -, $2s$ -, $2p$ -, $3s$ -, $3p$ -, and $3d$ -like core MOs and corresponding virtual MOs. The difference between DZP SCF and MP2 on the one hand, and experiment on the other, is considerable (-7 kcal/mol for DZP SCF, and $+10$ kcal/mol for DZP MP2). These levels of theory are modest, and the differences in bonding situation (As_2 has a sigma bond and two pi bonds, and As_4 has six strained sigma bonds) are significant. But considering that the DZP MP2 method usually overcorrects DZP SCF results, we may argue that the value of 54 kcal/mol is “theoretically justified.”

There are a number of previous theoretical studies^{27–32} of As_4 . None of the studies that we are aware of reported harmonic vibrational frequencies, and many have focused on ionization potentials, which we do not consider in the present study. Almost all these previous theoretical methods considered only the valence electrons, using pseudopotentials for arsenic. Bonapasta *et al.*,³⁰ while using relatively inadequate theoretical methods, emphasized the relevance of As_4 to molecular-beam epitaxy (MBE) and related laboratory techniques. Their theoretical bond lengths and dissociation energies are included in Table III for comparison. In an excellent, comprehensive study of the Group V tetramers M_4 , $M=P, As, Sb, \text{ and } Bi$, and their low-lying electronic excited states, Zhang and Balasubramanian³² reported ground state As-As bond lengths from the CASSCF (2.477 Å) and MRCISD (2.478 Å) methods, which are pertinent to the present study. Relativistic effective core potentials (including 28 core electrons) were used for As, and these bond lengths (r_e) are somewhat longer than the electron diffraction experimental r_g value of 2.435 Å, reported by Morino *et al.*¹⁸ The exact equilibrium bond lengths (r_e) should of course be shorter than the thermally averaged internuclear distance (r_g). As one can see from Table III, all theoretical methods using this

TABLE III. Previous theoretical results for tetrahedral As_4 (T_d) and comparison with results of this work and with experiment. The basis set designations, SV, DZ, and DZP denote split-valence, double-zeta, or double-zeta plus polarization quality basis sets, respectively; these are not identical to the sets used in the present work. For example, our DZP basis set includes a set of f functions.

	r_e (Å)	ΔH_0° (kcal/mol) $\text{As}_4 \rightleftharpoons 2\text{As}_2$
DZ SCF ^a	2.504	18
DZP SCF ^a	2.424	53
DZ SCF ^b	2.647	
LCGTO LSD VWN ^c	2.441	75
LCGTO X α ^c	2.480	63
SV SCF ^d	2.559	22
DZP+diff MRCISD ^e	2.50	41
DZP SCF ^f	2.414	47.2
TZ2P SCF ^f	2.417	45.2
Expt. ^g	2.435	54.0 \pm 1.1

^aTrinquier *et al.* (1981), Ref. 27. ZPVEs are approximately included in ΔH_0° . A pseudopotential (PP) were used for arsenic.

^bWatanbe *et al.* (1985), Ref. 28. A pseudopotential was used for arsenic.

^cAndzelm *et al.* (1987), Ref. 29. A pseudopotential was used for arsenic, in conjunction with the local spin-density approximation or the X α (Hartree-Fock-Slater) method. ZPVEs were not included in the energy difference.

^dBonapasta *et al.* (1988), Ref. 30. ZPVEs were not included.

^eMeier *et al.* (1991), Ref. 31. Diffuse s and p functions were included in the DZP basis set (no f functions). A pseudopotential (PP) was used for arsenic, with a multireference (MR) CISD technique supplemented by the appropriate Langhoff-Davidson correction. The largest source of error in this work would appear to be the use of the pseudopotential. ZPVEs were not included.

^fThis work.

^gSee footnotes b and d to Table II.

type of pseudopotential share this surprising relationship to experiment.

Cagelike As_{12}

Our theoretical results for the cagelike As_{12} cluster are presented in Table IV, and the molecular structure is shown in Fig. 1, where the DZP-SCF optimized values for the four independent internal coordinates are shown. From the DZP-SCF bond lengths, we see this order: $r_e(\text{center}) < r_e(\text{side}) < r_e(\text{top})$ (Fig. 1). The SV SCF and DZ SCF optimized bond lengths are very similar, and these are quite different from those determined at the DZP SCF level, particularly the As-As bond lengths within the three-membered rings. This again shows that the polarization basis functions

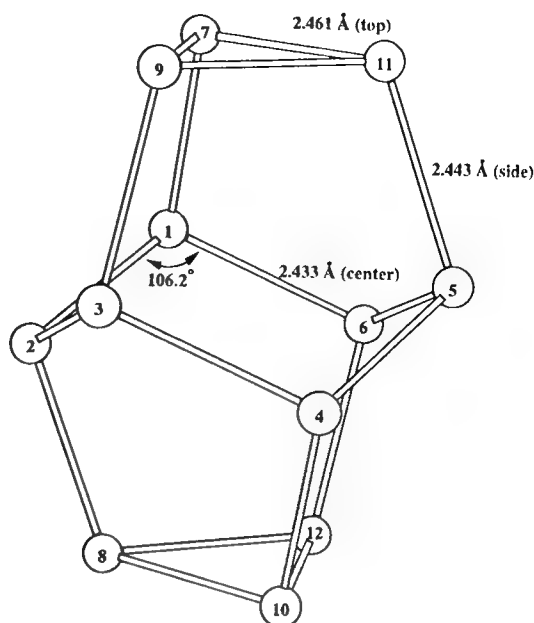


FIG. 1. The cagelike As_{12} cluster belonging to point group D_{3d} . The geometrical parameters were optimized at the DZP SCF level of theory.

have considerable effects on the bond lengths. From the SCF energies the As_{12} cluster lies lower in energy than the tetrahedral As_4 , although this energy difference becomes very small when d and f polarization functions are added to the basis set. The energy difference increases when the DZP MP2 method is used. If we assume that DZP SCF and MP2 methods bracket the true energy difference as they do for the tetrahedral As_4 , we may conclude that the cage-like As_{12} is energetically lower lying than the tetrahedral As_4 . Since harmonic vibrational frequencies for As_{12} are not available, only differences in total energies (ΔE_e) are shown in Table IV.

Dodecahedral As_{20} (I_h)

Our theoretical results for the dodecahedral As_{20} are presented in Table V, and the molecular structure is shown in Fig. 2, where the indicated As-As bond length was optimized at the DZP SCF level of theory. Considering the optimized bond lengths in Table V, we see that the SV and DZ basis sets are still inadequate, but their insufficiency is less

TABLE IV. Theoretical results for the cage-like As_{12} belonging to the D_{3d} point group. The molecular structure is shown in Fig. 1.

	SV SCF	DZ SCF	DZP SCF	DZP MP2 ^a
Energy (a.u.)	-26 806.974 07	-26 809.625 65	-26 810.012 42	-26 811.561 68
r_e (center)	2.484	2.487	2.433	
r_e (side)	2.475	2.476	2.442	
r_e (top)	2.558	2.558	2.461	
θ_e (center)	105.8°	105.8°	106.2°	
ΔE_e (kcal/mol)	-29.1	-28.1	-3.6	-7.3
$\text{As}_4 \rightleftharpoons \frac{1}{3}\text{As}_{12}$				

^aMP2 in TURBOMOLE, where 14 core MOs were frozen and 14 virtual MOs deleted per each arsenic atom, at the DZP SCF optimized geometry.

TABLE V. Theoretical results for dodecahedral As_{20} (belonging to the point group I_h). Molecular structure is shown in Fig. 2.

	Energy (a.u.)	r_e (Å)	ΔE_e (kcal/mol) $\text{As}_4 = \frac{1}{5}\text{As}_{20}$
SV SCF	-44 678.264 26	2.501	-25.8
DZ SCF	-44 682.687 41	2.503	-25.4
DZP' SCF ^a	-44 683.210 11	2.462	+4.1
DZP SCF	-44 683.288 59	2.454	+4.6
TZ2P SCF ^b	-44 684.725 72		+4.3
DZP MP2 ^c	-44 685.891 97		-1.8

^aThe DZP' basis set differs from the DZP basis set in that DZP' does not have a set of f basis functions. Therefore when $5d$ and $7f$ are used, there are 820 basis functions for As_{20} in DZP', while there are 960 basis functions in DZP.

^bThe TZ2P HF energy was evaluated at the DZP-HF optimized geometry. The TZ2P HF energy for As_4 at its DZP-HF optimized geometry is -8936.951 99 a.u.

^cMP2 in TURBOMOLE, where 14 core MOs were frozen and 14 virtual MOs deleted per each arsenic, at the DZP HF optimized geometry.

severe here than for As_4 and for As_{12} , probably because there are no small bond angles in As_{20} . Considering the DZP' basis set, we see that its optimized bond length is longer than the DZP SCF one by nearly 0.01 Å. From the very small differences in energy, we are uncertain whether As_{20} is energetically lower than As_4 . Higher levels of theory are needed, and ZPVEs may make a significant difference. If we assume that the DZP-SCF and DZP-MP2 values bracket the true energy difference, the true energy difference is very close to zero. We may thus argue that As_{20} is energetically stable enough to be made in the laboratory. Considering finally the relative energies of As_{12} and As_{20} , we may conclude that As_{12} is indeed energetically lower lying than As_{20} , analogous³ to their homologs P_{12} vs P_{20} ; at all the available levels of theory the sign of relative energies is the same.

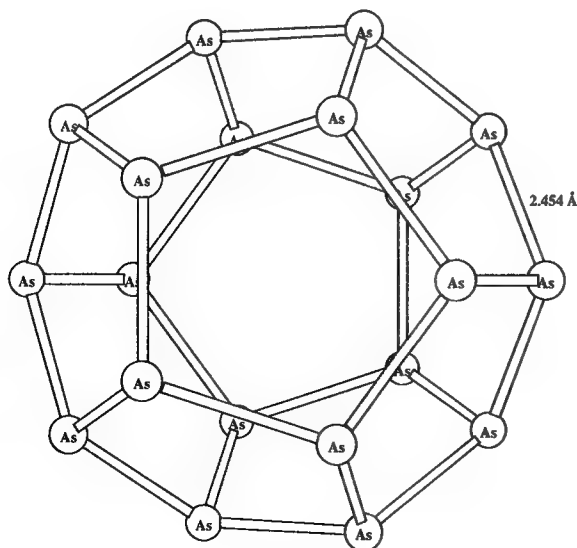


FIG. 2. The dodecahedral As_{20} cluster belonging to point group I_h . The geometrical parameters were optimized at the DZP SCF level of theory.

CONCLUSIONS

The DZP CCSD level of theory reproduces experimental data for diatomic As_2 very well, but this level of theory is clearly too expensive at the present for the two larger clusters considered here. For the larger clusters, we have chosen the DZP SCF level of theory for geometry optimization, and the DZP MP2 level for an estimate of correlation energy effects. These levels are modest for the tetrahedral As_4 . But even these modest levels of theory have already filled gaps in existing theoretical treatments of this important prototypical molecule, As_4 , which is the predominant form in arsenic vapor, and which, along with Group III elements, is important as a potential alternative to silicon in semiconductor devices. We have explicitly considered all electrons rather than only the valence electrons, as treated in previous theoretical studies, and we have determined the harmonic vibrational frequencies for As_4 . From comparison for As_4 , the DZP SCF and DZP MP2 levels of theory seem to approach the experimental values from either side; if so we may draw the conclusion that As_{12} is energetically lower than As_4 and As_{20} , and that As_4 and As_{20} lie energetically very close to each other. The dodecahedral N_{20} is a potential high-energy density material,¹ the dodecahedral P_{20} lies above P_4 by a relatively small amount,² and continuing this trend, As_{20} lies roughly level with As_4 . Speculation concerning the relative stability of M_{20} vs M_4 for $\text{M}=\text{Sb}$ and Bi seems natural and obvious.

Of theoretical interest is the quality of the arsenic basis sets. Ahlrichs' split-valence (SV) and double-zeta (DZ) basis sets⁵ produced almost identical results for all the clusters at the SCF level of theory. Therefore SV may be recommended as a small basis set for future use. The DZP basis set, including one set each of d and f polarization basis functions, derived from the above DZ, seems to be the best compromise between basis set size and theoretical reliability. The considerably larger TZ2P basis set produced almost identical results to DZP at the SCF level of theory. Therefore, the DZP basis set seems to merit recommendation as a good basis set for future theoretical studies of arsenic chemistry.

The focus of the present research has been the dodecahedral As_{20} structure. Other arsenic clusters are also of considerable interest. Recently Balasubramanian *et al.*³³ studied the Jahn-Teller distortions of the neutral As_3 species in its ground state (from D_{3h} to C_{2v}), as a foundation for their studies of low-lying excited electronic states. This year Warren *et al.*³⁴ reported a theoretical investigation of five isomers of As_6 in analogy with benzene. The geometries of these isomers were optimized at the HF level using a DZP-like basis set for arsenic. The hexagonal, benzenelike, structure was found to be energetically highest lying, while a triangular prismatic structure lies lowest. Comparisons with similar isomers of P_6 and the analogy to the valence isoelectronic C_6H_6 were emphasized.

ACKNOWLEDGMENTS

This research was supported by the U. S. Air Force Office of Scientific Research under Grant No. AFOSR-92-J-0047. We thank Professor Reinhart Ahlrichs for the use of

the TURBOMOLE system of programs¹⁰ developed at Karlsruhe. Additional computations using GAUSSIAN 92 were carried out at the Cornell National Supercomputer Facility's IBM RS6000 serial cluster.

- ¹A. A. Bliznyuk, M. Shen, and H. F. Schaefer, *Chem. Phys. Lett.* **198**, 249 (1992).
- ²C.-H. Hu, M. Shen, and H. F. Schaefer, *Theor. Chim. Acta* **88**, 29 (1994).
- ³M. Häser, U. Schneider, and R. Ahlrichs, *J. Am. Chem. Soc.* **114**, 9551 (1992).
- ⁴N. N. Greenwood and A. Earnshaw, *Chemistry of the Elements* (Pergamon, Oxford, 1984), p. 637f.
- ⁵A. Schäfer, H. Horn, and R. Ahlrichs, *J. Chem. Phys.* **97**, 2571 (1992).
- ⁶H. Partridge, *J. Chem. Phys.* **90**, 1043 (1989).
- ⁷R. Poirier, R. Kari, and I. G. Csizmadia, *Handbook of Gaussian Basis Sets* (Elsevier, New York, 1985), p. 616, Table 33.3.1.
- ⁸J. Almlöf, K. Faegri, and K. J. Korsell, *J. Comput. Chem.* **3**, 385 (1982).
- ⁹M. Häser and R. Ahlrichs, *J. Comput. Chem.* **10**, 104 (1989).
- ¹⁰R. Ahlrichs, M. Bär, M. Häser, H. Horn, and C. Kölmel, *Chem. Phys. Lett.* **162**, 165 (1989).
- ¹¹J. A. Pople, R. Krishnan, H. B. Schlegel, and J. S. Binkley, *Int. J. Quantum Chem. Symp.* **13**, 225 (1979).
- ¹²GAUSSIAN 92. M. J. Frisch, G. W. Trucks, M. Head-Gordon, P. M. W. Gill, M. W. Wong, J. B. Foresman, B. G. Johnson, H. B. Schlegel, M. A. Robb, E. S. Replogle, R. Gomperts, J. L. Andres, K. Raghavachari, J. S. Binkley, C. Gonzalez, R. L. Martin, D. J. Fox, D. J. Defrees, J. Baker, J. J. P. Stewart, and J. A. Pople, Gaussian, Inc., Pittsburgh, PA, 1992.
- ¹³B. R. Brooks, W. D. Laidig, P. Saxe, J. D. Goddard, Y. Yamaguchi, and H. F. Schaefer, *J. Chem. Phys.* **72**, 4652 (1980).
- ¹⁴A. C. Scheiner, G. E. Scuseria, J. E. Rice, T. J. Lee, and H. F. Schaefer, *J. Chem. Phys.* **87**, 5361 (1987); G. E. Scuseria, C. L. Janssen, and H. F. Schaefer, *ibid.* **89**, 7382 (1989).
- ¹⁵The psi system is distributed by PSITECH, Inc., Watkinsville, Georgia.
- ¹⁶P. Pulay, G. Fogarasi, F. Pang, and J. E. Boggs, *J. Am. Chem. Soc.* **101**, 2550 (1979).
- ¹⁷K. P. Huber and G. Herzberg, *Molecular Spectra and Molecular Structure. IV. Constants of Diatomic Molecules* (Van Nostrand Reinhold, New York, 1979).
- ¹⁸Y. Morino, T. Ukaji, and T. Ito, *Bull. Chem. Soc. Jpn.* **39**, 64 (1966).
- ¹⁹Y. M. Bosworth, R. J. H. Clark, and D. M. Rippon, *J. Mol. Spectrosc.* **46**, 240 (1973).
- ²⁰I. R. Beattie, G. A. Ozin, and R. O. Perry, *J. Chem. Soc. A* **1970**, 2071; experimental Raman spectrum of As_4 : 340 (a_1), 200 (e), 250 (t_2) cm^{-1} at 1173 °C.
- ²¹S. B. Brumbach and G. M. Rosenblatt, *J. Chem. Phys.* **56**, 3110 (1972); experimental Raman spectrum of As_4 : 344 (a_1), 210 (e), and 255 (t_2) cm^{-1} at 883 °C.
- ²²R. J. Capwell and G. M. Rosenblatt, *J. Mol. Spectrosc.* **33**, 525 (1970); experimental IR spectrum of vapor-condensed As_4 : 250 (t_2) cm^{-1} at 77 °C.
- ²³J. J. Murray, C. Pupp, and R. F. Pottier, *J. Chem. Phys.* **58**, 2569 (1973).
- ²⁴C. Pupp, J. J. Murray, and R. F. Pottier, *J. Chem. Thermodyn.* **6**, 123 (1974).
- ²⁵J. Drowart, S. Smoes, and A. Vanderauwera-Mahieu, *J. Chem. Thermodyn.* **10**, 453 (1978).
- ²⁶R. S. Grev, C. L. Janssen, and H. F. Schaefer, *J. Chem. Phys.* **95**, 5128 (1991).
- ²⁷G. Trinquier, J.-P. Malrieu, and J.-P. Daudey, *Chem. Phys. Lett.* **80**, 552 (1981).
- ²⁸Y. Watanabe, Y. Sakai, and H. Kashiwagi, *Chem. Phys. Lett.* **120**, 363 (1985).
- ²⁹J. Andzelm, N. Russo, and D. R. Salahub, *Chem. Phys. Lett.* **142**, 169 (1987).
- ³⁰A. A. Bonapasta, M. R. Bruni, A. Lapicciarella, P. Nota, G. Scavia, and N. Tomassini, *Surf. Sci.* **204**, 273 (1988).
- ³¹U. Meier, S. D. Peyerimhoff, and F. Grein, *Chem. Phys.* **150**, 331 (1991).
- ³²H. Zhang and K. Balasubramanian, *J. Chem. Phys.* **97**, 3437 (1992).
- ³³K. Balasubramanian, K. Sumathi, and D. Dai, *J. Chem. Phys.* **95**, 3494 (1991).
- ³⁴D. S. Warren, B. M. Gimarc, and M. Zhao, *Inorg. Chem.* **33**, 710 (1994).

Pyrophosphate Structures and Reactions: Evaluation of Electrostatic Effects on the Pyrophosphates with and without Alkali Cations

Buyong Ma, Cynthia Meredith, and Henry F. Schaefer, III*

Center for Computational Quantum Chemistry, The University of Georgia, Athens, Georgia 30602

Received: March 10, 1994; In Final Form: May 31, 1994*

Ab initio quantum mechanical methods were employed to study pyrophosphoric acid ($\text{H}_4\text{P}_2\text{O}_7$), its anions, and its alkali salts at the self-consistent-field (SCF) and second-order perturbation (MP2) levels of theory using double- ζ plus polarization (DZP) basis sets. The quantities predicted include equilibrium geometries, vibrational force constants, gas phase thermochemical data for hydrolysis reactions, gas phase proton affinities, and hydration energies. Electrostatic effects contribute substantially to the gas phase structures and hydrolysis reactions. The hydrolysis reaction of $\text{H}_4\text{P}_2\text{O}_7$ is close to thermoneutral in the gas phase, endothermic for the $\text{H}_3\text{P}_2\text{O}_7^-$ monoanion ($\Delta H^\circ = 23.8 \text{ kcal mol}^{-1}$ and $\Delta G^\circ = 21.7 \text{ kcal mol}^{-1}$ at DZP MP2 level), exothermic for the $\text{H}_2\text{P}_2\text{O}_7^{2-}$ dianion ($\Delta H^\circ = -54 \text{ kcal mol}^{-1}$ and $\Delta G^\circ = -54 \text{ kcal mol}^{-1}$ at DZP MP2 level), and endothermic for $\text{M}^+\text{H}_3\text{P}_2\text{O}_7^-$ salts ($\text{M} = \text{Li}, \text{Na}, \text{and K}$; energy changes about $16\text{--}19 \text{ kcal mol}^{-1}$ at the DZP SCF level). The gas phase proton affinities are evaluated as $323 \text{ kcal mol}^{-1}$ for the $\text{H}_3\text{P}_2\text{O}_7^-$ monoanion, $416 \text{ kcal mol}^{-1}$ for the $\text{H}_2\text{P}_2\text{O}_7^{2-}$ dianion, $544 \text{ kcal mol}^{-1}$ for the $\text{HP}_2\text{O}_7^{3-}$ trianion, $328 \text{ kcal mol}^{-1}$ for the $\text{Li}^+ \text{H}_2\text{P}_2\text{O}_7^{2-}$ anion, and $336 \text{ kcal mol}^{-1}$ for the $\text{Na}^+ \text{H}_2\text{P}_2\text{O}_7^{2-}$ anion. Electrostatic repulsion is predicted to contribute to the high-energy character of the pyrophosphate. The P—O—P linkage is weakened by electrostatic repulsion as well, as indicated by the modest decrease in the force constants of the P—O—P linkage from the $\text{H}_4\text{P}_2\text{O}_7$ molecule to the $\text{HP}_2\text{O}_7^{3-}$ trianion.

1. Introduction

The pyrophosphate (PPI) linkage >P—O—P< plays an essential role in biology. It is the main structural form through which energy is transmitted within living cells. Inorganic pyrophosphates are the simplest compounds containing this entity, and they increasingly appear to play a central role in bioenergetic processes.¹ The most important bioenergetic molecule, ATP, contains the PPI linkage. Although there are distinct differences between the chemistry of pyrophosphates and of ATP, the pyrophosphate linkage is a prototype for understanding the chemistry of ATP. Therefore, a careful study of these species may be able to provide important information about ATP as well.

It has long been recognized that the question of why high-energy phosphate compounds such as pyrophosphates and ATP are rich in energy is a key problem in bioenergetics.² There are two reasonable explanations.^{2–4} First, and of greater importance, is the destabilizing effect of the electrostatic repulsion between the charged groups in comparison to that of its hydrolysis products.^{3,4} In the physiological pH range the pyrophosphates and ATP have two to four negative charges whose mutual electrostatic repulsions are partially relieved by pyrophosphate and ATP hydrolysis. The second explanation,^{2,4} connected with the electrostatic repulsion theory, is that the free energy of the hydrolysis of polyphosphate in aqueous solution is due almost entirely to differential heats of solution of various species involved in the reaction, and not to the relative energy of the isolated molecules in vacuo. The background for the second explanation^{2,4} is the experimental observation² that the enthalpy changes (ΔH°) for the hydrolysis of polyphosphate, ADP, and ATP in aqueous solution decrease as those species acquire a greater negative charge. However, the problem with the second explanation is that it assumes that the hydrolysis of those species is thermoneutral² in the gas phase and it entirely ignores other possible mechanisms behind the experimental phenomena.

Considering the importance of the hydrolysis of pyrophosphates, quantum mechanical studies have been undertaken to assist in understanding these species and their reactions. Hayes, Kenyon,

and Kollman⁵ examined the structure of pyrophosphoric acid ($\text{H}_4\text{P}_2\text{O}_7$) and predicted a bridging P—O bond distance of 1.685 \AA and a P—O—P bond angle of 117° . O'Keeffe, Domenges, and Gibbs⁶ studied both the structure and hydrolysis energy at the $6\text{-}31\text{G}^*$ SCF level and obtained an energy of $-5.5 \text{ kcal mol}^{-1}$ for the gas phase reaction. Ewig and Wazer⁴ studied the structure and hydrolysis of pyrophosphoric acid at the SCF level, using the STO-3G basis set with d functions at the phosphorus atoms. Their enthalpy change for the hydrolysis reaction of $-0.42 \text{ kcal mol}^{-1}$ supports the second hypothesis. More recently, Saint-Martin, Ortega-Blake, Les and Adamowicz¹⁹ studied the gas phase hydrolysis of $\text{H}_4\text{P}_2\text{O}_7$, and the reaction energy was predicted to be $-3.8 \text{ kcal mol}^{-1}$ at the MP2 level with the geometries optimized at the $6\text{-}31\text{G}^{**}$ SCF level. However, the general shortcoming of these studies is that only the neutral pyrophosphoric acid is considered and no cations are included; therefore these studies were not able to comment on the charge repulsion theory directly.⁴

Recently, we have studied the hydration behavior of metaphosphate anion (PO_3^-),⁷ which is a possible intermediate in the hydrolysis of polyphosphate.⁸ As an extension of our previous studies, we present a comprehensive approach to understanding the structures and hydrolysis of pyrophosphates, including pyrophosphoric acid and its mono-, di-, and trianions. In order to gain insight into their hydrolysis in aqueous solution, cations (alkali cations and Mg^{2+}) are also extensively studied. We concentrate in this portion of the report on the electrostatic effects on their structures and on thermochemical data for the hydrolysis for these species, partly to answer the question about the role of electrostatic repulsion and, more significantly, to lay a foundation for us to understand the mechanisms of the hydrolysis of pyrophosphate, which will be the subject of subsequent work.

2. Theoretical Methods

The basis sets employed here include double- ζ plus polarization (DZP)^{9a–c} for the H, P, and O atoms and are the same as used in our previous work.⁷ For the lithium atom the basis set is that of Thakker, namely Li (9s5p/4s2p).^{10a} For the sodium atom⁹ the basis set is Na (11s5p/7s2p), plus two sets of even-tempered p functions used as polarization functions [$\alpha_p(\text{Na}) = 0.163, 0.050$]. The exponents and contraction coefficients are taken from the

* Abstract published in *Advance ACS Abstracts*, July 15, 1994.

TABLE 1: Exponents (α) and Contraction Coefficients (c) of the (11s5p/7s2p) Basis Set for Na and (14s9p/10s6p) Basis Set for K

	Na		K	
	α	c	α	c
s	16489.566	0.001 029 68	150591.0	0.000 26
	2535.2539	0.007 598 77	22629.6	0.002 00
	592.29211	0.037 326 36	5223.16	0.010 15
	170.66573	0.134 225 22	1498.06	0.040 43
	56.957095	0.327 932 59	495.165	0.127 32
	21.169833	1.0	180.792	1.0
	8.4714024	1.0	71.194	1.0
	2.5221405	1.0	29.3723	1.0
	0.92859762	1.0	8.68863	1.0
	0.36606025	1.0	3.46382	1.0
	0.04133714	1.0	0.811307	1.0
			0.312555	1.0
			0.035668	1.0
			0.016517	1.0
p	80.830968	0.013 840 12	867.259	0.002 34
	18.510942	0.091 273 47	205.254	0.018 80
	5.5364692	0.298 264 1	65.8214	0.086 68
	1.7612954	0.494 603 3	24.5742	0.250 41
	0.53654709	1.0	9.87704	1.0
			4.11693	1.0
			1.55653	1.0
			0.614068	1.0
			0.228735	1.0
			0.085202	1.0
			0.031737	1.0

atomic SCF calculations of Huzinaga^{9d} and are displayed in Table 1. For the potassium atom the basis set is constructed from Wachters^{10b} atomic SCF results (Table 1) and the technical designation is K (14s11p1d/10s8p1d), the polarization function orbital exponent being $\alpha_d(K) = 0.1$. Diffuse functions are added to the phosphorus and oxygen atoms, and the resulting basis set is designated DZP+diff. The diffuse functions include both s and p functions on the heavy atoms and have orbital exponents¹⁰

$$\alpha_s(O) = 0.0845, \alpha_p(O) = 0.0845, \alpha_s(P) = 0.0348, \\ \text{and } \alpha_p(P) = 0.0348$$

The Hartree-Fock self-consistent field (SCF) approach has been used to locate stationary points through analytic first-derivative techniques. Subsequently, analytic energy second-derivative techniques were used to determine harmonic vibrational frequencies when necessary. Except for the force constants, all computations were performed using the program TURBO-MOLE.^{11a} Vibrational force constants were evaluated using the program PSI developed in this research group.^{11b} The effects of electron correlation on total energies were evaluated using second-order Møller-Plesset perturbation¹² (MP2) theory. For the MP2 calculations no core electrons were frozen and geometries were optimized at the DZP SCF level.

Previous work has shown that the basis sets and correlated level employed here are sufficient to give quite accurate thermochemical properties for phosphates,^{7,17} and the present results also suggest the same conclusion. For example, the hydrolysis energies and proton affinities at the DZP SCF, DZP+diff SCF, and DZP MP2 levels are generally quite close (Table 2).

The enthalpy changes are evaluated as follows:¹³

$$\Delta H^\circ = \Delta E_c + \Delta E_v^\circ + \Delta(\Delta E_v)^{298} + \Delta E_r^{298} + \Delta E_t^{298}$$

where ΔE_c is the difference between the energies of reactants and products without the zero-point vibrational energies (ZPVE) correction, ΔE_v° is the difference between the ZPVE of reactants and products at 0 K, and $\Delta(\Delta E_v)^{298}$ is the change in the ZPVE difference in going from 0 to 298 K. The final terms account for changes in the number of rotational and translational degrees of freedom.

TABLE 2: Thermochemical Predictions for Pyrophosphate and Related Species at the DZP SCF Level of Theory

	hydrolysis reaction ^{a,b}					gas phase proton affinity	
	ΔE_c	ΔE_0	ΔH°	ΔG°	ΔS°	this work	exp ^b
$H_4P_2O_7$	-1.9 (0.5) 0.02 ^c	-2.5 (-0.1)	-2.0 (0.4) -7.6	-5.2 (-2.8) -9.5	10.7 6		
$H_3P_2O_7^-$	18.3 (23.8) 22.7 ^c	18.9 (24.4)	18.3 (23.8) -7.3	16.2 (21.7) -7.5	6.9 1	323.3	
$H_2P_2O_7^{2-}$	-54.6 (-49.0) -45.4	-54.6 (-49.0)	-54.6 (-49.2) -6.8	-57.6 (-52.0) -7.1	9.3 3	321.6 ^c 416.5 412.4 ^c	311
$HP_2O_7^{3-}$	-110.0 -114.0 ^c					545.1 (544.0) 535.5 ^c	488
$H_2PO_4^-$						344.0 (339.0) 344.3 ^c	311
HPO_4^{2-}						481.0 466.9 ^c	488

^a The values of ΔE_c , ΔE_0 (ΔE_c plus ZPVE correction), ΔH° , and ΔG° are in kcal mol⁻¹, and ΔS° is in cal/K-mol. The standard state is 1 atm at 298 K. DZP MP2 energies are in parentheses. ^b The values in boldface are experimental results in aqueous solution (see ref 2). ^c DZP+diff SCF energies based on the geometries at the DZP SCF level.

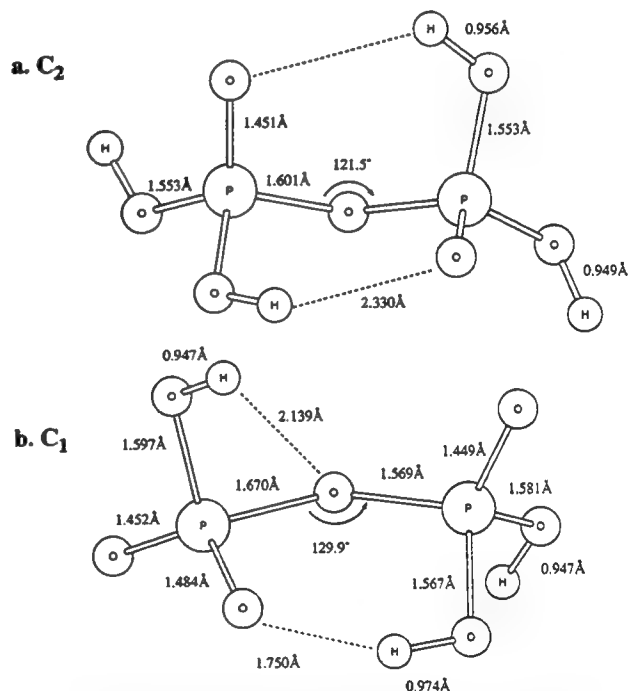


Figure 1. Equilibrium geometries of (a) pyrophosphoric acid $H_4P_2O_7$ and (b) pyrophosphate monoanion $H_3P_2O_7^-$ at the DZP SCF level.

Entropy changes (ΔS°) have been evaluated from standard statistical mechanical relationships,¹⁴ and free energy changes (ΔG°) are evaluated from the usual relationship $\Delta G = \Delta H - T\Delta S$. In all such considerations the vibrational frequencies evaluated at the DZP SCF level of theory are used. The standard state is 1 atm at 298 K.

3. Results and Discussion

A. Electrostatic Effects on the Structures of the Pyrophosphate Anions. 1. Geometry of Pyrophosphoric Acid, $H_4P_2O_7$. The DZP SCF equilibrium geometry of pyrophosphoric acid ($H_4P_2O_7$, Figure 1a) is of C_2 symmetry, with two weak intramolecular hydrogen bonds (2.330 Å) between the two phosphate groups.

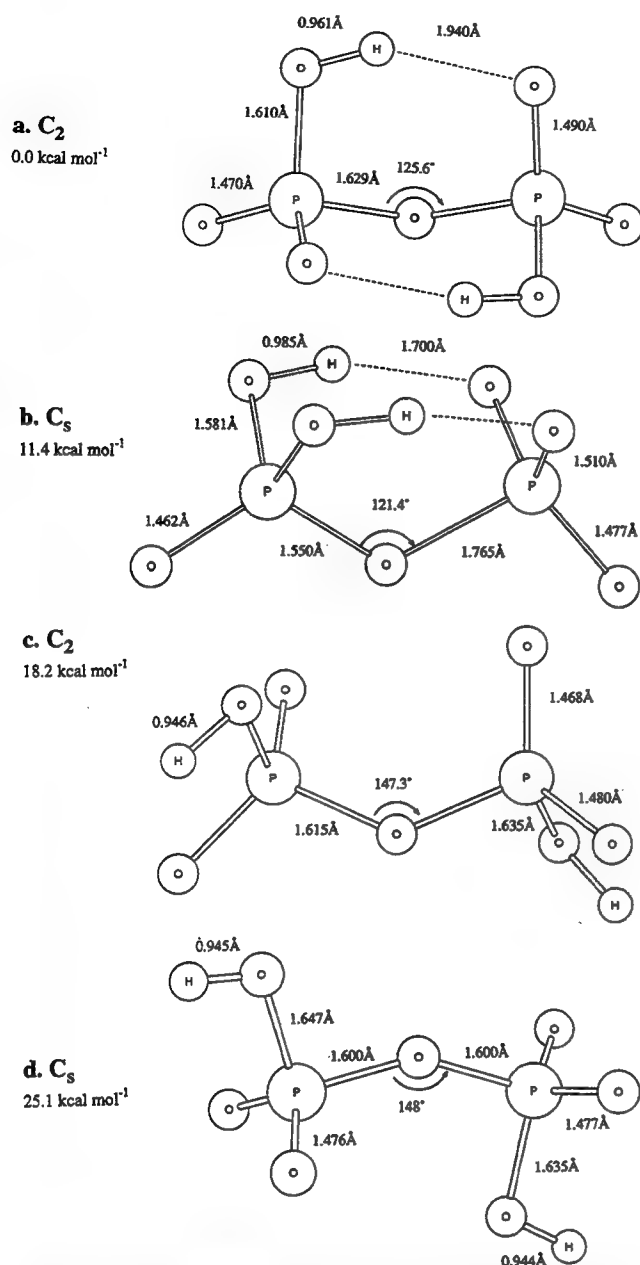


Figure 2. Several structures and their relative energies for the $H_2P_2O_7^{2-}$ dianion at the DZP SCF level: (a) Global minimum (C_2 symmetry); (b) local minimum with C_s symmetry; (c) another local minimum with C_2 symmetry; (d) stationary point with C_s symmetry.

The P—OH bond distances are 1.553 Å, and the P—OP bridging bond distances are 1.601 Å. Compared with orthophosphoric acid (H_3PO_4 , Figure 4a, P—OH bond distances 1.569 Å), the P—OH bond distances are shorter for the $H_4P_2O_7$ molecule at the same theoretical level.

Our results differ from the early work of Ewig and Van Wazer.⁴ Using SCF methods with the STO-3G basis set plus d functions at the phosphorus atoms, they obtained two conformers—an eclipsed structure with C_2 symmetry and an asymmetric (C_1)

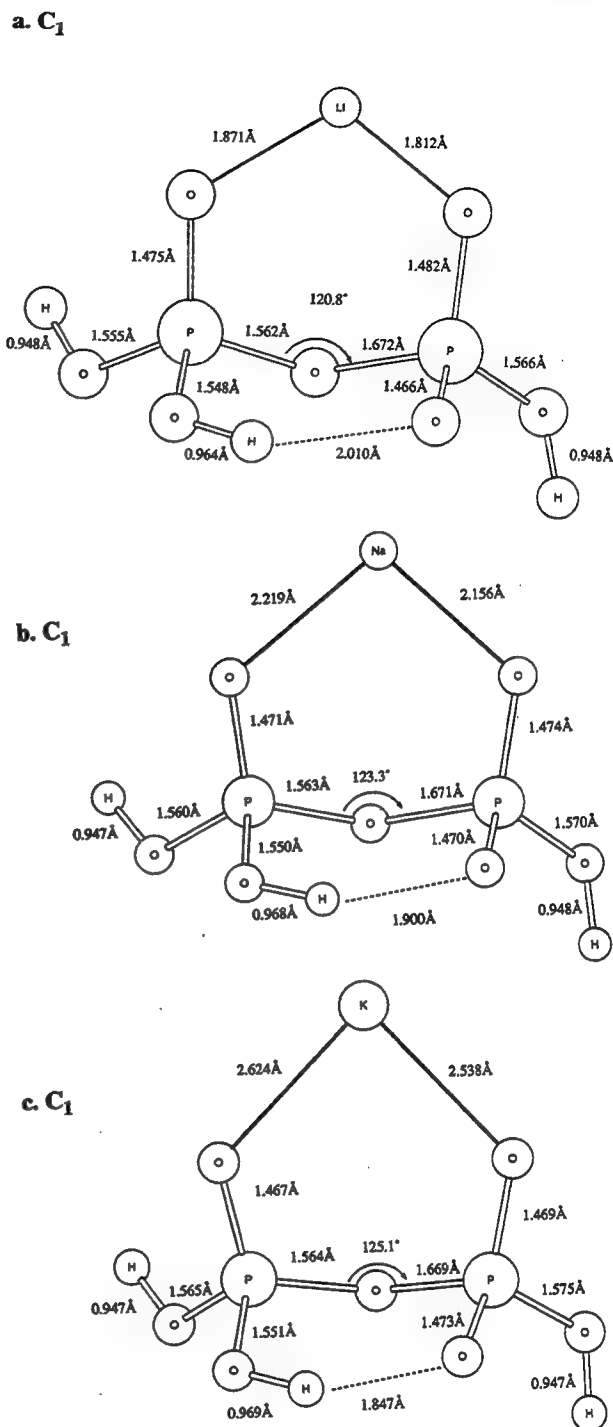


Figure 3. Equilibrium geometries at the DZP SCF level for (a) lithium pyrophosphate $LiH_3P_2O_7$; (b) sodium pyrophosphate $NaH_3P_2O_7$; (c) potassium pyrophosphate $KH_3P_2O_7$.

staggered conformation (2.3 kcal mol⁻¹ lower in energy than the C_2 conformation). Similar results are also found in the work of Saint-Martin et al.¹⁹ However, our geometry optimization at the DZP SCF level results in a C_2 symmetry structure (Figure

TABLE 3: Selected Harmonic Vibrational Frequencies and Force Constants for the P—O—P Linkage in Pyrophosphate Anions at the DZP SCF Level

	$H_4P_2O_7$		$H_3P_2O_7^-$		$H_2P_2O_7^{2-}$		$HP_2O_7^{3-}$	
	ω (cm ⁻¹)	force const	ω (cm ⁻¹)	force const	ω (cm ⁻¹)	force const	ω (cm ⁻¹)	force const
P—O—P	832	6.74 mdyn/Å	764	6.68 mdyn/Å	815	6.21 mdyn/Å	727	5.71 mdyn/Å
symmetrical stretch								
P—O—P	1044	5.52 mdyn/Å	1064	5.37 mdyn/Å	997	4.78 mdyn/Å	968	4.35 mdyn/Å
unsymmetrical stretch								
P—O—P bend	129	0.95 mdyn/rad	252	2.11 mdyn/rad	185	1.82 mdyn/rad	234	2.65 mdyn/rad

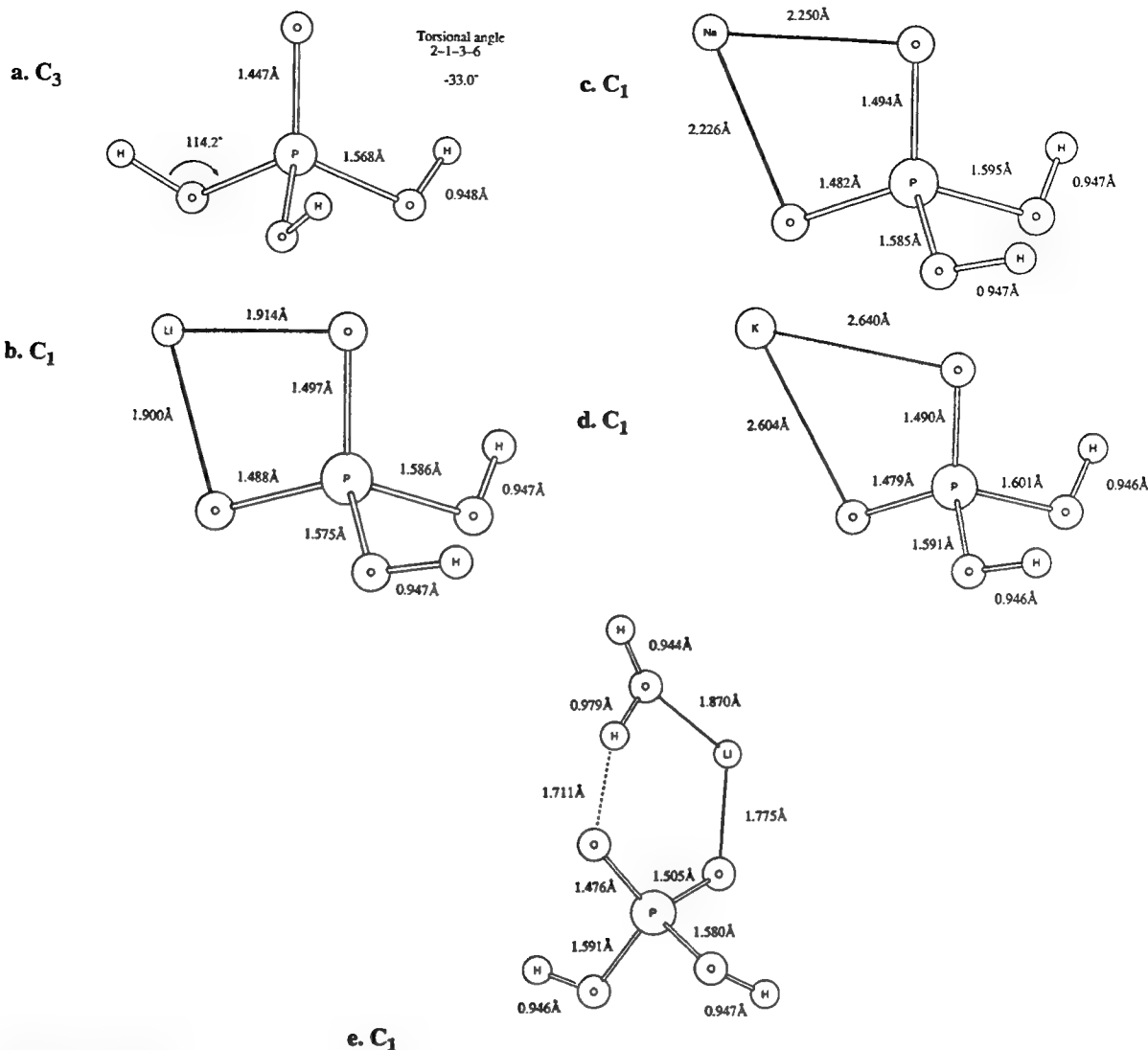


Figure 4. Equilibrium geometries at the DZP SCF level for (a) orthophosphoric acid H_3PO_4 ; (b) lithium phosphate LiH_2PO_4 ; (c) sodium phosphate NaH_2PO_4 ; (d) potassium phosphate KH_2PO_4 ; (e) $\text{Li-H}_2\text{PO}_4\cdot\text{H}_2\text{O}$.

TABLE 4: Selected Bond Distances (Å) and Angles (deg) for the $\text{MH}_3\text{P}_2\text{O}_7$ Molecules^a

param	$\text{H}_4\text{P}_2\text{O}_7$ (M = H) ^a	$\text{LiH}_3\text{P}_2\text{O}_7$ (M = Li) ^b	$\text{NaH}_3\text{P}_2\text{O}_7$ (M = Na) ^c	$\text{KH}_3\text{P}_2\text{O}_7$ (M = K) ^d	$\text{H}_3\text{P}_2\text{O}_7^{2-}$ ^e
P—OP	1.601	1.562	1.563	1.564	1.569
PO—P	1.601	1.672	1.671	1.669	1.670
O—H	2.330	2.010	1.900	1.847	1.750
P—O—P	121.5	120.8	123.3	125.1	129.9
M—O	0.956	1.812	2.156	2.538	

^a Figure 1a. ^b Figure 3a. ^c Figure 3b. ^d Figure 3c. ^e Figure 1b.

1a) only, even when we start from Ewig's C_1 conformation without the C_2 symmetry constraint. Note also that our study predicts weak intramolecular hydrogen bonding between the two phosphate groups in the $\text{H}_4\text{P}_2\text{O}_7$ molecule. Ewig,⁴ O'Keeffe,⁶ and Saint-Martin et al.,¹⁹ in their lower level studies, did not predict such hydrogen bonding.

II. Geometry of $\text{H}_3\text{P}_2\text{O}_7^-$ Monoanion. The $\text{H}_3\text{P}_2\text{O}_7^-$ monoanion has a very different structure (Figure 1b) from that of the $\text{H}_4\text{P}_2\text{O}_7$ molecule. In the $\text{H}_3\text{P}_2\text{O}_7^-$ monoanion, one of the two bridging P—O bond distances increases to 1.670 Å and another one decreases to 1.569 Å. All P—OH bond distances are increased compared with that for the $\text{H}_4\text{P}_2\text{O}_7$ molecule (Figure 1a). There is a very strong intramolecular hydrogen bond (1.750 Å) between the two phosphate groups in the $\text{H}_3\text{P}_2\text{O}_7^-$ monoanion. The

structural features of the $\text{H}_3\text{P}_2\text{O}_7^-$ monoanion indicate that the role of electrostatic forces should be attractive rather than repulsive.

III. Geometry of $\text{H}_2\text{P}_2\text{O}_7^{2-}$ Dianion. The global minimum structure for the $\text{H}_2\text{P}_2\text{O}_7^{2-}$ dianion is a C_2 symmetry configuration (Figure 2a), with one negative charge localized at each phosphate group. The bridging P—O bond distances are 1.629 Å, about 0.03 Å longer than that for the neutral $\text{H}_4\text{P}_2\text{O}_7$ molecule.

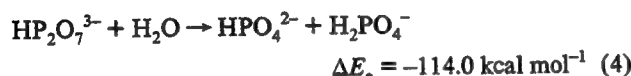
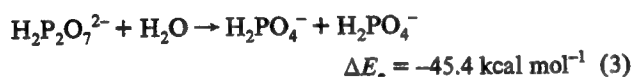
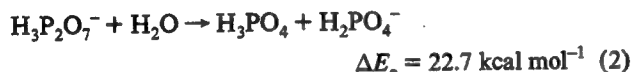
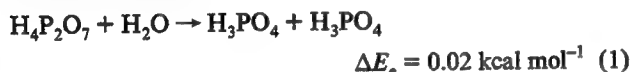
Because each phosphate group has a negative charge in the global minimum structure for the $\text{H}_2\text{P}_2\text{O}_7^{2-}$ dianion (Figure 2a), the electrostatic repulsion should be an operative factor. However, electrostatic repulsion might be partially offset by the two intramolecular hydrogen bonds between the two phosphate groups (Figure 2a). Another C_2 symmetry conformation (Figure 2c), without the intramolecular hydrogen bonding, shows very strong electrostatic repulsion effects. In this C_2 conformation (Figure 2c), which is 18.2 kcal mol⁻¹ higher in energy than the global minimum structure, the P—O—P bond angle increases by 20°. One stationary point (Figure 2d), with constrained C_s symmetry that prevents intramolecular hydrogen bonding between the two phosphate groups, shows strong electrostatic repulsion as well; the P—O—P bond angle is 148°, and the structure lies 25.1 kcal mol⁻¹ higher in energy than the global minimum.

It is possible that if two negative charges are localized at the same phosphate group in the $\text{H}_2\text{P}_2\text{O}_7^{2-}$ dianion, as indicated in Figure 2b, the electrostatic repulsion might be decreased relative

to the former cases. However, this structure (Figure 2b) is 11.4 kcal mol⁻¹ higher in energy than the global minimum structure (Figure 2a). The reason is that the two negative charges are closer to one another when they are localized at the same phosphate group than when they are distributed over the entire molecule.

IV. Vibrational Frequencies and Force Constants for the H₃P₂O₇⁻ Monoanion, H₂P₂O₇²⁻ Dianion, and HP₂O₇³⁻ Trianion. The electrostatic effects on the strength of the P—O—P linkage may be discerned from the change in its force constants with increasing total negative charge (Table 3). The general trend is that the force constants for the stretch modes of the P—O—P linkage decrease with increasing total negative charge. Clearly, the P—O—P linkage is weakened by electrostatic repulsion. However, the force constants for the P—O—P bending mode vary irregularly. The reason is that the P—O—P bending mode is subject to the strength of the intramolecular hydrogen bonding between the two phosphate groups. Both the H₃P₂O₇⁻ monoanion (Figure 1b) and the HP₂O₇³⁻ trianion (see Figure 2a in accompanying paper) involve very strong intramolecular hydrogen bonding; therefore, their force constants for the P—O—P bending mode are higher than those of H₄P₂O₇ and the H₂P₂O₇²⁻ dianion, for which the intramolecular hydrogen bonds are relatively weaker than those of the two former anions.

B. Electrostatic Effects on the Thermochemistry for Gas Phase Hydrolysis of Pyrophosphate Anions. 1. Electrostatic Attraction and Repulsion. The thermochemical data (Table 2) for the following reactions (1–4)

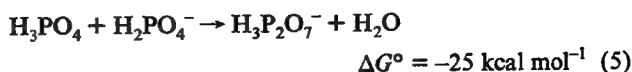


show very strong electrostatic effects. For instance, hydrolysis of the H₄P₂O₇ molecule is close to a thermoneutral process, with $\Delta E_e = 0.02 \text{ kcal mol}^{-1}$ at the DZP+diff SCF level. The result is qualitatively similar to that of the previous study by Ewig et al. However, the H₃P₂O₇⁻ monoanion hydrolysis reaction (2) is strongly endothermic ($\Delta H^\circ = 22.7 \text{ kcal mol}^{-1}$ [DZP+diff SCF] and $23.8 \text{ kcal mol}^{-1}$ [DZP MP2]) in the gas phase. This result is not surprising, considering that electrostatic attraction (rather than repulsion) should predominate for the singly charged H₃P₂O₇⁻ monoanion. Because the strong intramolecular hydrogen bond (Figure 1b) requires more energy to separate two phosphate groups than in the case for hydrolysis of H₄P₂O₇, hydrolysis reaction 2 is endothermic.

As expected, the gas phase hydrolysis reaction for the H₂P₂O₇²⁻ dianion is highly exothermic ($\Delta H^\circ = -46 \text{ kcal mol}^{-1}$ [DZP+diff SCF] and $-49 \text{ kcal mol}^{-1}$ [DZP MP2]) and exhibits a large negative free energy change ($\Delta G^\circ = -50 \text{ kcal mol}^{-1}$ [DZP+d SCF] and $-52 \text{ kcal mol}^{-1}$ [DZP MP2]). The gas phase hydrolysis reaction for the HP₂O₇³⁻ trianion is even more exothermic, with an energy change $\Delta E_e = -114 \text{ kcal mol}^{-1}$ (DZP+diff SCF). Therefore, electrostatic repulsion clearly contributes significantly to the exothermicity of hydrolysis reactions 3 and 4.

II. Hydrolysis Reaction for The H₃P₂O₇⁻ Monoanion. The thermochemistry of reaction 2 yields possible explanations for two experimentally observed phenomena. The free energy change of reaction 2 indicates that its reverse reaction (5) is spontane-

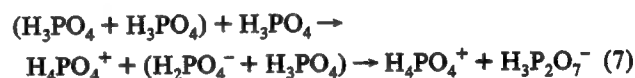
ous; i.e., the formation of the H₃P₂O₇⁻ monoanion might be favored



under certain conditions. There may be some relationship between the thermochemistry of reaction 5 with the biological phenomenon in living systems that protons must be pumped into certain areas in living cells in order to drive ATP or pyrophosphate regeneration.^{1,3} However, the topic is beyond the immediate scope of the present study. Nevertheless, the thermochemistry of reaction 5 is important for pyrophosphate formation. Experimentally, this pyrophosphate can be formed spontaneously in highly concentrated H₃PO₄ solution.¹⁵ It was thought¹⁵ that there is an autoprotolysis reaction (6) in the highly concentrated H₃PO₄



solution. Therefore reaction 7 is a plausible pathway for the generation of the pyrophosphate in highly concentrated H₃PO₄ solution. This is consistent with the experimental observation¹⁵



that 3 mol of orthophosphate are required to produce 1 mol of pyrophosphate.

Experimentally, reaction 2 is exothermic in dilute solution. The reason may be that, in the case of pyrophosphate monoanion, one negative charge can be distributed to two phosphate moieties, whereas upon hydrolysis the charge is localized to one phosphate group. Therefore, the charge delocalization from phosphate in the solvation process may render the reaction exothermic in dilute solution.

C. Structures for Alkali Pyrophosphate Salts in the Gas Phase. 1. Geometries for the Neutral M⁺H₂P₂O₇ (M⁺ = Li⁺, Na⁺, K⁺) and (Li)₂²⁺H₂P₂O₇²⁻ Molecules. It is found that the bridging positions between two phosphate groups are exclusively preferred by all three alkali cations (Li⁺, Na⁺, and K⁺) studied here (Figure 3). The cations are bonded to two oxygen atoms in different phosphate groups, rather than to the oxygen atoms in the same phosphate group. The reasons may be that this kind of bridging position allows closer contact between cations and oxygen atoms, as indicated by the longer M—O distances in the MH₂P₂O₄ (Figure 4) than those in the MH₃P₂O₇ molecules (Figure 3).

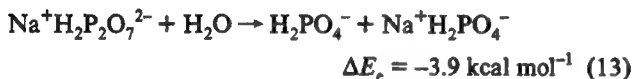
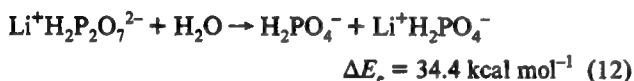
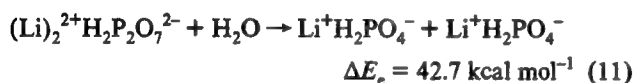
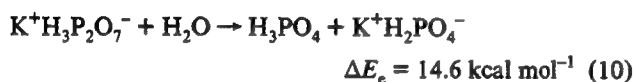
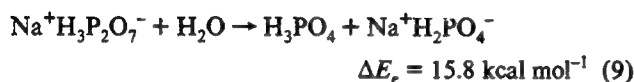
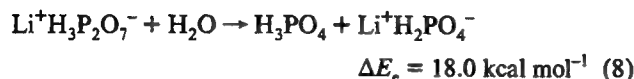
The structures of the H₃P₂O₇⁻ monoanion in the M⁺H₃P₂O₇⁻ molecules (Figure 3) are very similar to that of the isolated H₃P₂O₇⁻ monoanion (Figure 1b); in particular, the bridging P—O—P bond distances are almost the same. As indicated in Table 3, with decreasing charge/radius ratio for the cations,¹⁵ the M—O bond distances increase in the order H—OP < Li—OP < Na—OP < K—OP and the structures of the H₃P₂O₇⁻ monoanion in the M⁺H₃P₂O₇⁻ molecules get closer and closer to that for the isolated H₃P₂O₇⁻ monoanion (Table 4).

The structure of the (Li)₂²⁺H₂P₂O₇²⁻ is of C₂ symmetry, with two Li⁺ cations in bridging positions between two phosphate groups (Figure 5a).

II. Structures for the M⁺H₂P₂O₇²⁻ (M⁺ = Li⁺, Na⁺) Anions. For the M⁺H₂P₂O₇²⁻ anions (M⁺ = Li⁺, Na⁺), two different kinds of structure are possible. The first one is like that in Figure 5b, with one negative charge localized in each phosphate group in the H₂P₂O₇²⁻ anion. The second one is like that in Figure 5c, with two negative charges localized at the same phosphate group. For the Li⁺H₂P₂O₇²⁻ anion, there are two minimum energy structures, corresponding to the two types mentioned above. The former (Figure 5b) is the global minimum structure, and the latter (Figure 5c) is 18 kcal mol⁻¹ higher in energy than the global minimum (Figure 5b).

For the $\text{Na}^+\text{H}_2\text{P}_2\text{O}_7^{2-}$ anion, the potential energy surface is similar to that of the $\text{Li}^+\text{H}_2\text{P}_2\text{O}_7^{2-}$ anion. The global minimum is shown in Figure 5d. Another minimum structure in Figure 5e is 13.8 kcal mol⁻¹ higher in energy.

D. Cation Effects on the Thermochemistry for the Gas Phase Hydrolysis of Pyrophosphate. The cation effects on the thermochemistry of the hydrolysis for pyrophosphate are shown by the following reactions:

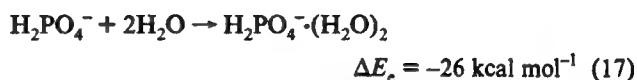
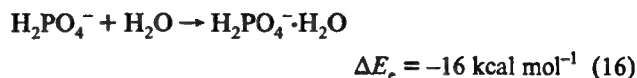
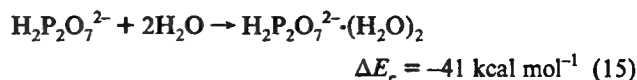
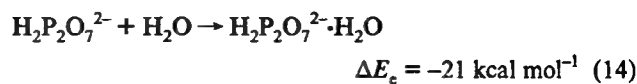


The thermochemical data for these reactions are shown in Table 2. Almost all of these reactions are highly endothermic in the gas phase. The reason is that, with the strong bridging effect of the cations between two phosphate groups in the pyrophosphate, the hydrolysis reactions require more energy to break the P—O—P bond linkage and the additional O—M—O bridging bonds. Note that reactions 11 and 12 are also endothermic. This means that electrostatic repulsion, which is strong for the isolated $\text{H}_2\text{P}_2\text{O}_7^{2-}$ dianion, is decreased by the neutralization of the negative charges and, consequently, that electrostatic attraction is dominant. However, the hydrolysis of $\text{Na}^+\text{H}_2\text{P}_2\text{O}_7^{2-}$ (reaction 13) is exothermic. This suggests that the Na^+ —which has a smaller charge/radius ratio¹⁵ and greater separation from the negatively charged oxygen atoms—is less effective than Li^+ in decreasing electrostatic repulsion in the $\text{H}_2\text{P}_2\text{O}_7^{2-}$ dianion.

E. Solvation Effects on the Thermochemistry of Hydrolysis for Pyrophosphate. *I. Hydration Energies for the $\text{H}_2\text{P}_2\text{O}_7^{2-}$ Dianion and the Gas Phase Proton Affinities for Pyrophosphate.* We have shown that the gas phase exothermicities and free energy changes for the hydrolysis reactions of pyrophosphate vary with increasing negative charge and that there are important cation effects. All the hydrolysis reactions for the neutral pyrophosphate are either thermoneutral ($\text{H}_4\text{P}_2\text{O}_7$) or highly endothermic for alkali salts in the gas phase.¹⁶ Because the hydrolysis reactions in aqueous solution are known to be exothermic (−5 to −8 kcal mol⁻¹; see Table 2), there is no doubt that solvation effects play an important role.² However, it would be simplistic to conclude² that the sole driving force for the hydrolysis reactions is the difference of the solvation energy between the pyrophosphate and phosphate (especially without considering the role of cations).

We are unable to evaluate directly the solvation energy for these species to compare with existing experimental results.² However, two examples cast doubt upon the accuracy of the solvation energy for the pyrophosphates evaluated by George.²

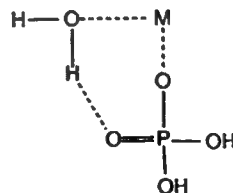
First, we have compared the gas phase hydration energies for the $\text{H}_2\text{P}_2\text{O}_7^{2-}$ dianion and H_2PO_4^- at the DZPSCF level of theory by the reactions



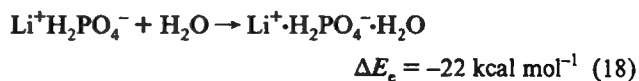
Clearly, the hydration energy for the $\text{H}_2\text{P}_2\text{O}_7^{2-}$ dianion is higher than that for the H_2PO_4^- anion, and therefore the solvation energy for the isolated $\text{H}_2\text{P}_2\text{O}_7^{2-}$ dianion should be higher than that for the isolated H_2PO_4^- anion. This expectation is reasonable, as the electrostatic repulsion in the isolated $\text{H}_2\text{P}_2\text{O}_7^{2-}$ dianion should be partially relieved by hydration, which corresponds to a higher solvation energy. However, it is difficult to compare the liquid phase results with our gas phase results above. For example, the dihydration energy for the $\text{H}_2\text{P}_2\text{O}_7^{2-}$ dianion [forming $\text{H}_2\text{P}_2\text{O}_7^{2-} \cdot (\text{H}_2\text{O})_2$, reaction 15] is more than twice the hydration energy of H_2PO_4^- (reaction 16) but less than the twice the dihydration energy of H_2PO_4^- [forming $\text{H}_2\text{PO}_4^- \cdot (\text{H}_2\text{O})_2$, reaction 17].

The second example involves our theoretical gas phase proton affinities for these species, which should be more comparable to experimental results. The reason that the gas phase proton affinities may serve as a reference for the evaluation of solvation energy is that George² derived gas phase proton affinities for the phosphate and pyrophosphate anions from their solvation energies for the related species. As indicated in Table 2, the experimentally derived proton affinities for the phosphate are close to our theoretical values. However, that of the $\text{H}_2\text{P}_2\text{O}_7^{2-}$ dianion is 100 kcal mol⁻¹ lower and that of the $\text{HP}_2\text{O}_7^{3-}$ trianion is 60 kcal mol⁻¹ lower, respectively, than our theoretical value. These results indicate that there is great uncertainty concerning the experimental solvation energies for the pyrophosphate.²

II. Role of Solvation. Any explanation of the aqueous solution hydrolysis of pyrophosphate that fails to consider the role of cations is incomplete. There are two solvation effects, namely those affecting (a) the pyrophosphate and (b) the hydrolysis products. Cations are preferentially bonded to two oxygen atoms in different phosphate groups rather than to the oxygen atoms in the same phosphate group (section C). However, the unfavorable bridging angle for the metal phosphate will be relieved by solvation, for example, by the formation of



The thermochemistry of the formation of $\text{Li} \cdot \text{H}_2\text{PO}_4 \cdot \text{H}_2\text{O}$ (Figure 4e)



supports the above arguments.

Cations have a crucial effect on electrostatic repulsion in pyrophosphate. For example, the hydrolysis of the $\text{Li}^+\text{H}_2\text{P}_2\text{O}_7^{2-}$ anion is highly endothermic, whereas the hydrolysis of the

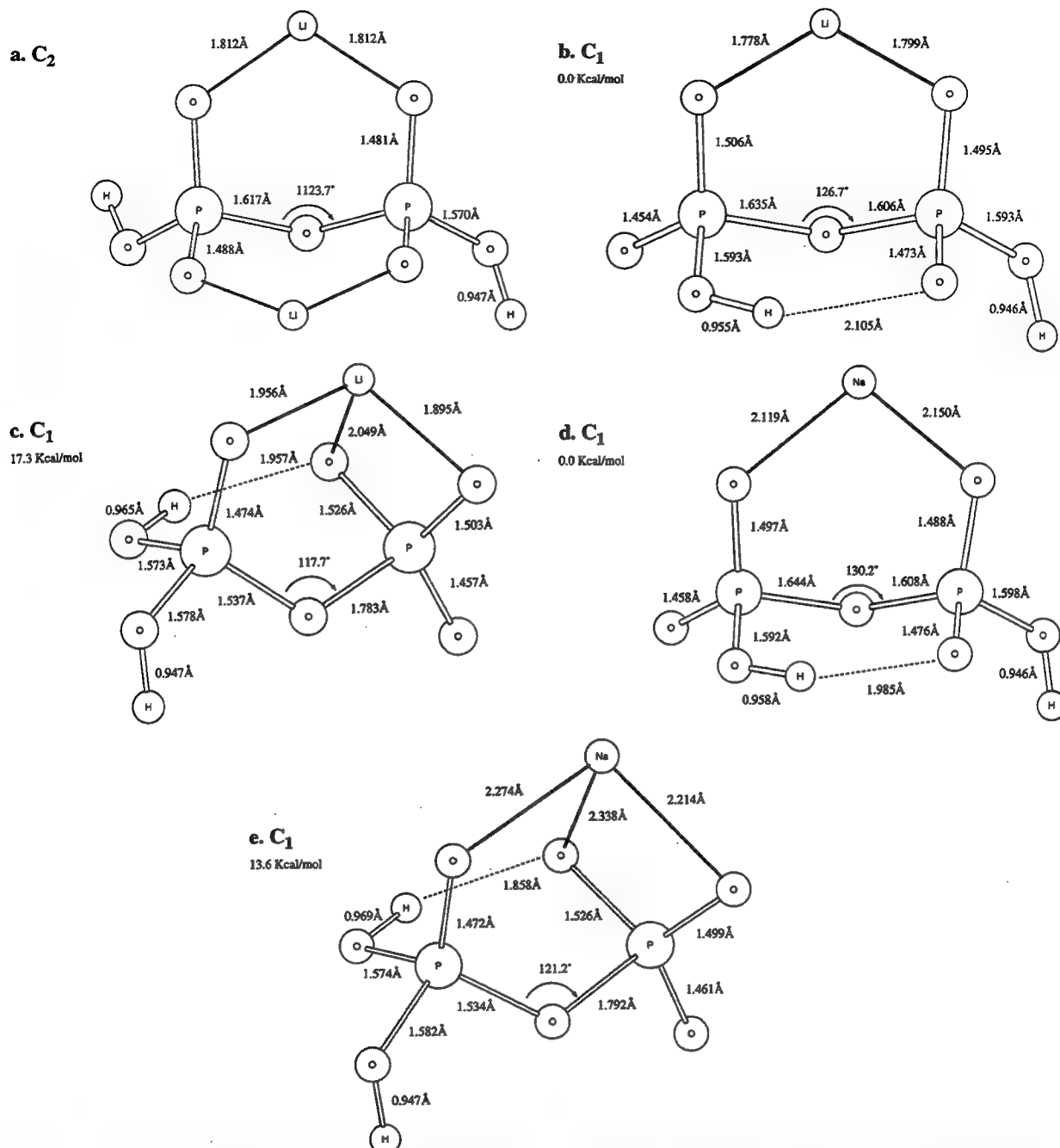


Figure 5. Structures and their relative energies at the DZP SCF level for (a) dilithium pyrophosphate $\text{Li}_2\text{H}_2\text{P}_2\text{O}_7$; (b) lithium pyrophosphate anion $\text{LiH}_2\text{P}_2\text{O}_7^-$ (the global minimum); (c) lithium pyrophosphate anion $\text{LiH}_2\text{P}_2\text{O}_7^-$ (a local minimum); (d) sodium pyrophosphate anion $\text{NaH}_2\text{P}_2\text{O}_7^-$ (the global minimum); (e) sodium pyrophosphate anion $\text{NaH}_2\text{P}_2\text{O}_7^-$ (a local minimum).

$\text{Na}^+\text{H}_2\text{P}_2\text{O}_7^{2-}$ anion is slightly exothermic (section D). It seems that the key factor here is the separation between the cations and anions. The solvation will make electrostatic repulsion possible in aqueous solution as indicated by the scheme outlined in Figure 6. This scheme is consistent with the experimental observations^{4,15} that the exothermicities for the hydrolysis reactions depend on the concentration of solute, the pH value, and the cation concentration, since the separation between the cations and anion and therefore the electrostatic effects with the anion depend on those factors. Herschlag and Jencks have found that the formation of pyrophosphate is at least fourth order in sodium ion in concentrated sodium perchlorate solutions.¹⁸

This scheme may explain experimental results (Table 2) as well. George's experiments² have shown that the exothermicities for the hydrolysis reaction decrease with increasing negative charge on the pyrophosphate anions, thus giving rise to the question of the role of electrostatic repulsion. However, without considering

the cation effects in aqueous solution, George's analysis is inadequate. In order to increase the negative charge in the pyrophosphate from $\text{H}_4\text{P}_2\text{O}_7$ to $\text{P}_2\text{O}_7^{4-}$, the cation concentration should be increased at the same time to maintain net electro-neutrality. Because the cations tend to increase the endothermicities of the hydrolysis reaction, as indicated in the former sections, the exothermicities of the hydrolysis reaction decrease, as observed experimentally.

4. Conclusions

The results of our study corroborate the role of electrostatic effects on both the molecular structures and the thermochemistries for the hydrolysis of pyrophosphates. We also confirm that the alkali cations (Li^+ , Na^+ , and K^+) exert a strong influence on equilibrium geometries and thermochemistries for these hydrolysis reactions. Although our results apply strictly to the gas phase

Increasing electrostatic repulsion
Increasing exothermicity of hydrolysis

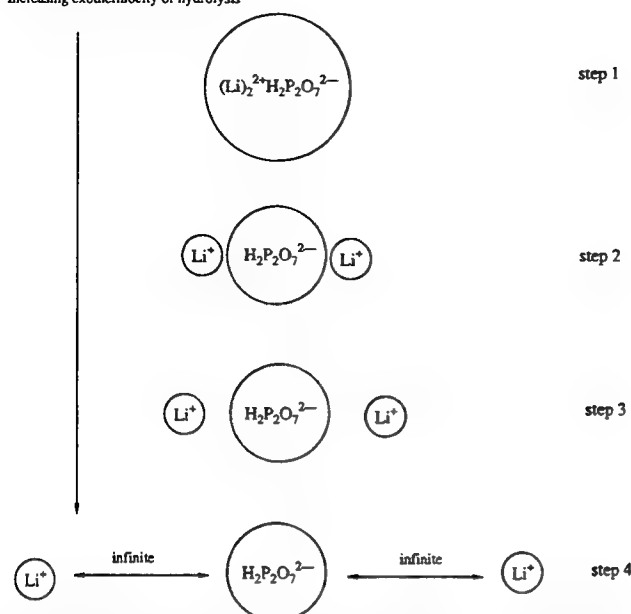


Figure 6. Schematic representation of solvation effects on electrostatic repulsion within the pyrophosphate dianion. Step 1: An ideal situation in which the molecule is undissociated upon solvation. Steps 2 and 3: The real situation in which the molecule is dissociated upon solvation and the separation between the cations and anion is variable; therefore the electrostatic repulsion within the pyrophosphate dianion is variable as well. Step 4: Also an ideal situation in which the separation between the cations and anion is infinite.

only, they may nevertheless provide insight into these reactions in aqueous solution.

The electrostatic effects for the isolated $\text{H}_3\text{P}_2\text{O}_7^-$ anion, $\text{M}^+\text{H}_3\text{P}_2\text{O}_7^-$ ($\text{M}^+ = \text{Li}^+, \text{Na}^+, \text{K}^+$) molecules, and $(\text{Li})_2^{2+}\text{H}_2\text{P}_2\text{O}_7^{2-}$ are attractive, as shown by the strong endothermicities for their gas phase hydrolysis reactions. However, the electrostatic effect for the isolated $\text{H}_2\text{P}_2\text{O}_7^{2-}$ dianion is strongly repulsive, as indicated by its strong exothermicity for gas phase hydrolysis.

Electrostatic repulsion appears to contribute to the high-energy character of pyrophosphates. The P—O—P linkage is weakened by electrostatic repulsion as well, as indicated by the decrease of the force constants of the P—O—P linkage from the $\text{H}_3\text{P}_2\text{O}_7^-$ monoanion to the $\text{HP}_2\text{O}_7^{3-}$ trianion. Therefore, it is not the bond but the environment, particularly the electrostatic environment such as the charges on the neighboring oxygen, that is energetically important. The frequencies, structures, and energies show that the P—O—P linkage is actually a "low-energy bond".

Acknowledgment. This research was supported by the U.S. Air Force Office of Scientific Research under Grant AFOSR-

92-J-0047. We appreciate helpful discussion with Dr. Y. Xie, Dr. Y. Yamaguchi, and Mr. P. Schreiner.

Supplementary Material Available: Two tables giving atomic Cartesian coordinates for the pyrophosphates at the DZP SCF level are provided (2 pages). Ordering information is given on any current masthead page.

References and Notes

- (1) (a) Baltscheffsky, M.; Nyren, P. In *Bioenergetics*; Ernster, L., Ed.; Elsevier: Amsterdam, 1984; p 187. (b) Baltscheffsky, M.; Baltscheffsky, H. In *Molecular Mechanism in Bioenergetics*; Ernster, L., Ed.; Elsevier: Amsterdam, 1992; p 331.
- (2) George, P.; Witonsky, R. J.; Trachtman, M.; Wu, C.; Dortwart, W.; Richman, L.; Richman, W.; Shurayh, F.; Lentz, B. *Biochim. Biophys. Acta* **1970**, *223*, 1–15.
- (3) Voet, D.; Voet, J. G. *Biochemistry*; John Wiley & Sons: New York, 1990.
- (4) Ewig, C. S.; Van Wazer, J. R. *J. Am. Chem. Soc.* **1988**, *110*, 79.
- (5) Hayes, D. M.; Kenyon, G. L.; Kollman, P. A. *J. Am. Chem. Soc.* **1975**, *97*, 4762; *J. Am. Chem. Soc.* **1978**, *100*, 4331.
- (6) O'Keeffe, M.; Domenges, B.; Gibbs, G. V. *J. Phys. Chem.* **1985**, *89*, 2304.
- (7) Ma, B.; Xie, Y.; Shen, M.; Schaefer, H. F. *J. Am. Chem. Soc.* **1993**, *115*, 1943. Ma, B.; Xie, Y.; Shen, M.; Schaefer, H. F. *J. Am. Chem. Soc.* **1993**, *115*, 11169.
- (8) Westheimer, F. H. *Chem. Rev.* **1981**, *81*, 313 and references cited therein. Westheimer, F. H. *Science* **1987**, *235*, 1173.
- (9) (a) Huzinaga, S. *J. Chem. Phys.* **1965**, *42*, 1293. (b) Dunning, T. H. *J. Chem. Phys.* **1970**, *53*, 2823. (c) Dunning, T. H.; Hay, P. J. In *Modern Theoretical Chemistry*; Schaefer, H. F., Ed.; Plenum Press: New York, 1977; Vol 3, p 1. (d) Huzinaga, S. Approximate Atomic Wavefunctions. II. Department of Chemistry Report, University of Alberta, Edmonton, Alberta, Canada, 1971.
- (10) (a) Thakkar, A. J.; Koga, T.; Saito, M.; Hoffmeyer, R. E. *Int. J. Quantum Chem.: Quantum Chem. Symp.* **1993**, *27*, 343. (b) Wachters, A. J. H. *J. Chem. Phys.* **1970**, *52*, 1033.
- (11) (a) Ahlrichs, R.; Bar, M.; Häser, M.; Horn, H. *Chem. Phys. Lett.* **1989**, *162*, 165. (b) PSI2. 0.8; Janssen, C. L.; Seidl, E. T.; Hamilton, T. P.; Yamaguchi, Y.; Remington, R.; Xie, Y.; Vacek, G.; Sherrill, C. D.; Crawford, T. D.; Fermann, J. T.; Allen, W. D.; Brooks, B. R.; Fitzgerald, G. B.; Fox, D. J.; Gaw, J. F.; Handy, N. C.; Laidig, W. D.; Lee, T. J.; Pitzer, R. M.; Rice, J. E.; Saxe, P.; Scheiner, A. C.; Schaefer, H. F. PSITECH, Inc., Watkinsville, GA, 1994.
- (12) (a) Möller, C.; Plesset, M. S. *Phys. Rev.* **1934**, *46*, 618. (b) Pople, J. A.; Seeger, R.; Krishnan, R. *Int. J. Quantum Chem. Symp.* **1977**, *11*, 49. (c) Krishnan, R.; Pople, J. A. *Int. J. Quantum Chem. Symp.* **1978**, *14*, 91. (d) Krishnan, R.; Frisch, M. J.; Pople, J. A. *J. Chem. Phys.* **1980**, *72*, 4244.
- (13) Del Bene, J. E.; Mettee, H. D.; Frisch, M. J.; Luke, B. T.; Pople, J. A. *J. Phys. Chem.* **1983**, *87*, 3279.
- (14) Hout, R. F.; Levi, B. A.; Hehre, W. J. *J. Comput. Chem.* **1982**, *3*, 234.
- (15) Matheja, J.; Degens, E. T. *Structural Molecular Biology of Phosphates*; Gustav Fisher Verlag: Stuttgart, 1971.
- (16) The hydrolysis reaction of the alkaline earth salt $\text{Mg}^{2+}\text{H}_2\text{P}_2\text{O}_7^{2-}$, however, is exceptionally exothermic.
- (17) Liang, C.; Ewig, C. S.; Stouch, T. R.; Hagler, A. T. *J. Am. Chem. Soc.* **1993**, *115*, 1537.
- (18) Herschlag, D.; Jencks, W. P. *J. Am. Chem. Soc.* **1986**, *108*, 7938.
- (19) Saint-Martin, H.; Ortega-Blake, I.; Les, A.; Adamowicz, L. *Biochim. Biophys. Acta* **1991**, *1080*, 205.

Structure, Infrared Spectrum, and Dissociation Energy of SiH_7^+

Ching-Han Hu, Peter R. Schreiner, Paul von Ragué Schleyer, and Henry F. Schaefer, III*

Center for Computational Quantum Chemistry, The University of Georgia, Athens, Georgia 30602, and
the Computer Chemistry Center, Institut für Organische Chemie der Universität Erlangen-Nürnberg,
Henkestrasse 42, D-91054 Erlangen, Germany

Received: December 13, 1993; In Final Form: March 11, 1994*

Ab initio quantum mechanical methods, including the self-consistent field (SCF), single- and double-excitation configuration interaction (CISD), single- and double-excitation coupled cluster (CCSD), and the single-, double-, and perturbative triple-excitation coupled cluster [CCSD(T)] have been applied to three stationary points on the SiH_7^+ potential energy hypersurface. Double- ζ plus polarization (DZP) and triple- ζ plus double-polarization [TZ2P and TZ2P(f,d)] basis sets were employed. The C_2 structure, where two symmetry-equivalent H_2 subunits complex the SiH_3^+ cation, was found to be the global minimum, in agreement with the findings of Liu and Zhou (*J. Phys. Chem.* **1993**, *97*, 9555). The bound vs free H_2 harmonic vibrational frequency shift obtained at the TZ2P CCSD level (259 cm^{-1}) is 36 cm^{-1} less than the experimental frequency shift (295 cm^{-1}), compared with the shift obtained by Liu and Zhou with second-order perturbation theory, which was 33 cm^{-1} higher than the value from experiment. The theoretical rotational constants are compared with the experiments of Okumura's group. The dissociation energy D_0 of SiH_7^+ to yield SiH_5^+ and H_2 is sizable, 4.6 kcal/mol [TZ2P(f,d) CCSD(T) + ZPVE(TZ2P CCSD)], much larger than the analogous value for CH_7^+ .

Introduction

The structures of silyl cations are attractive both theoretically and experimentally. Those hypercoordinate molecules provide insights into new structural features, and they are usually quite different from the analogous carbonium ion structures. The chemistry of silicon hydrides is also closely related to the ion-molecule reactions encountered in chemical vapor deposition processes. A major experimental breakthrough for the SiH_7^+ system was very recently made by Cao, Choi, Haas, Johnson, and Okumura.¹ Their observed infrared spectrum for SiH_7^+ displayed, in the $3500\text{--}4200\text{ cm}^{-1}$ region, a single band centered around 3866 cm^{-1} , which was assigned to a perturbed hydrogen-hydrogen stretching motion. The frequency shift of 295 cm^{-1} with respect to free hydrogen (H_2) suggested that molecular hydrogen is a weakly bound subunit with a binding energy of $7\text{--}9\text{ kcal mol}^{-1}$, but this is only an empirical estimate. The absence of a second band in the selected region furthermore indicated that the molecule must be symmetrical so that two hydrogen subunits become symmetry equivalent, and a C_2 as well as a C_{2v} structure was suggested.¹ It was also concluded that the rotations of the hydrogen moieties occur at very low barriers. From the 2-Å distance of the H_2 ligands from planar SiH_3^+ , the rotational constant B of 0.85 cm^{-1} was derived for this prolate top molecule.

The C_{2v} (two forms with the hydrogen subunits either in or out of plane, Figure 1), D_{3h} , and C_2 forms of SiH_7^+ were examined in a subsequent theoretical investigation² up to the MP2/6-31G(dp) level of theory. Only the C_2 structure has less than one imaginary vibrational frequency, and it is also lowest in energy. Further optimizations were carried out at the MP2/TZ2P level, and energy single points were computed at the CCSD(T)/TZ2P//MP2/TZ2P level. The vibrational frequency (3861 cm^{-1} , after scaling by 0.91) for the hydrogen subunit shift compares very well with the experimentally observed frequency (3866 cm^{-1}) for the corresponding vibrational mode. A lower than experimental ($7\text{--}9\text{ kcal mol}^{-1}$) value was found for the zero-point vibrational energy corrected dissociation energy of SiH_7^+ into SiH_5^+ and H_2 (4.7 kcal mol^{-1}). The latter $\text{SiH}_5^+\text{--H}_2$ dissociation energy is less than half of that predicted theoretically for SiH_5^+ ($10.3\text{ kcal mol}^{-1}$).³ No estimates were made of the rotational constants of the structures considered.

For the parent silyl cation SiH_5^+ , *ab initio* theoretical methods³ have suggested a C_s structure which involves an H_2 subunit attached to the SiH_3^+ cation. Thus, the silyl cation reveals nonclassical three-center two-electron ($3c\text{--}2e$) bonding. The methonium cation CH_5^+ is more complex.⁴ Hydrogen scrambling, which occurs with essentially no barrier in CH_5^+ ,⁴ apparently does not occur in SiH_5^+ .³ The best theoretical prediction for the dissociation energy D_0 of SiH_5^+ was 10.3 kcal/mol , which is 5 kcal mol^{-1} lower than the experimental value⁵ of about 15 kcal mol^{-1} . The binding interaction between the SiH_3^+ cation and H_2 is significantly weaker than the binding energy of $42.0\text{ kcal mol}^{-1}$ for CH_3^+ and H_2 .⁶

The structure of CH_7^+ primarily consists of a H_2 moiety which is very weakly bound to one of the two hydrogen atoms of the $3c\text{--}2e$ bond in the CH_5^+ C_s structure. The binding energy⁷ is only about $1\text{--}2\text{ kcal mol}^{-1}$. This is very different from the SiH_7^+ structure which appears to have two equally bound H_2 subunits.

In the present study we discuss the structures, vibrational frequencies, and dissociation energies as well as the rotational constants of the C_2 , C_{2v} (I), and C_{2v} (II) structures of the SiH_7^+ cation by applying high-level *ab initio* quantum mechanical methods. We also compare our results to the CH_7^+ cation and attempt to explain the origin of the differences in binding.

Theoretical Approach

Geometries were optimized using the self-consistent-field (SCF),⁸ the single- and double-excitation configuration interaction (CISD),⁹ the single and double excitation coupled cluster (CCSD),¹⁰ and the single, double, and perturbative triple excitation coupled cluster [CCSD(T)]¹¹ analytic gradient methods. One core orbital was kept frozen and one virtual orbital deleted at the correlated levels. Three different basis sets have been used, including the double- ζ plus polarization (DZP),¹² the triple- ζ plus double-polarization (TZ2P),¹³ and the TZ2P(f,d) basis set which was obtained by adding a set of higher order polarization functions to the TZ2P basis set. The DZP basis is (11s7p1d/6s4p1d) for silicon and (4s1p/2s1p) for hydrogen. The orbital exponents for the polarization functions were $\alpha_d(\text{Si}) = 0.50$ and $\alpha_p(\text{H}) = 0.75$. The TZ2P basis set consists of (12s9p2d/6s5p2d) for silicon and (5s2p/3s2p) for hydrogen, with polarization function orbital exponents of $\alpha_d(\text{Si}) = 1.00$, 0.25 and $\alpha_p(\text{H})$

* Abstract published in *Advance ACS Abstracts*, April 15, 1994.

TABLE 1: Total Energies (in hartrees) of Three SiH_7^+ Stationary Points and the Minimum Structures of SiH_5^+ , SiH_3^+ , and H_2 with the Number of Imaginary Vibrational Frequencies Given in Parentheses

	C_2	C_{2v} (I)	C_{2v} (II)	SiH_5^+	SiH_3^+	H_2
DZP SCF	-292.617 342 (1)	-292.617 319 (2)	-292.617 317 (3)	-291.481 310	-290.335 324	-1.131 089
TZ2P SCF	-292.647 989 (0)	-292.647 962 (1)	-292.647 961 (2)	-291.508 278	-290.358 677	-1.132 992
TZ2P(f,d) SCF	-292.650 102 (0)	-292.650 073 (1)	-292.650 072 (2)	-291.510 325	-290.360 028	-1.133 006
DZP CISD	-292.839 022 (0)	-292.838 920	-292.838 916	-291.622 872	-290.488 092	-1.166 708
TZ2P CISD	-292.942 082 (0)	-292.942 024	-292.942 022	-291.658 874	-290.580 122	-1.170 805
DZP CCSD	-292.854 408 (0)	-292.854 290	-292.854 286	-291.680 800	-290.494 135	
TZ2P CCSD	-292.965 546 (0)	-292.965 485	-292.965 484	-291.784 585	-290.591 274	
DZP CCSD(T)	-292.857 503	-292.857 374	-292.857 370	-291.683 627	-290.496 324	
TZ2P CCSD(T)	-292.969 855	-292.969 788	-292.969 786	-291.788 458	-290.594 293	

^a The total energies of the $\text{SiH}_5^+ + \text{H}_2$ supermolecule are DZP CISD, -292.832 269, and TZ2P CISD, -292.932 163. For the $\text{SiH}_3^+ + 2\text{H}_2$ supermolecule the absolute energies are DZP CISD, -292.812 690, and TZ2P CISD, -292.910 139.

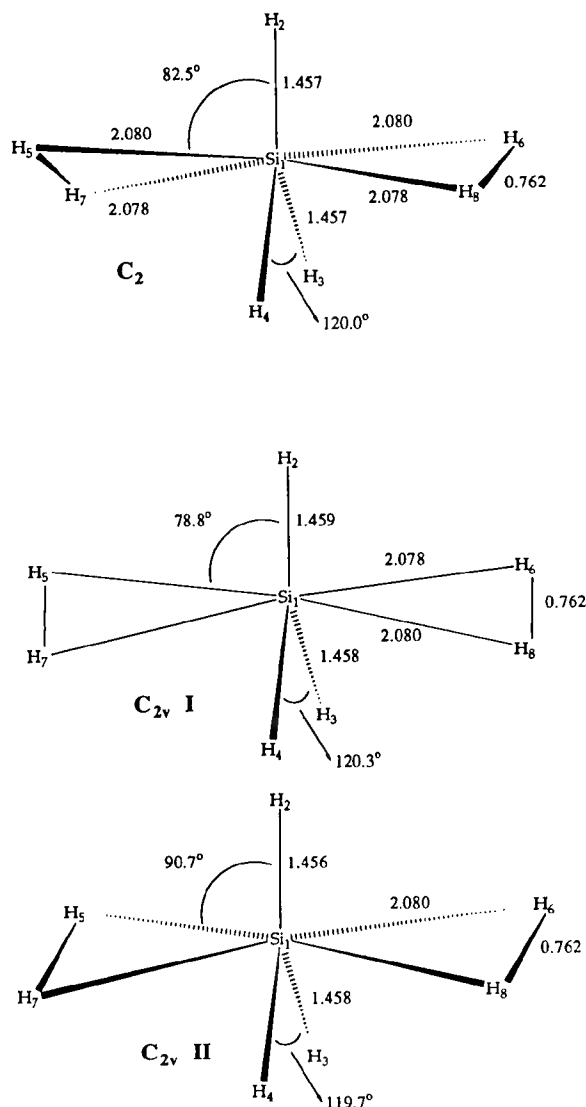


Figure 1. Geometries examined in this study, including structural parameters obtained at the TZ2P CCSD(T) level of theory. Complete geometrical parameters for the C_2 structure are summarized in Table 2.

= 1.50, 0.375. The TZ2P(f,d) basis set is designated as Si(12s9p2d1f/6s5p2d1f) and H(5s2p1d/3s2p1d) with polarization function orbital exponents of $\alpha_f(\text{Si}) = 0.32$ and $\alpha_d(\text{H}) = 1.00$.

Harmonic vibrational frequencies were determined via analytic second derivative techniques¹⁴ at the SCF level of theory. At the correlated levels, harmonic vibrational frequencies were obtained from finite central differences of analytic energy first derivatives.

All computations were carried out using the locally developed program PSI,¹⁵ running on IBM RS 6000 workstations.

Results and Discussion

The absolute energies of the C_2 , C_{2v} (I), and C_{2v} (II) forms of the SiH_7^+ cation (Figure 1) and the SiH_5^+ , SiH_3^+ , and H_2 minima are summarized in Table 1. The geometrical parameters and the harmonic vibrational frequencies of the SiH_7^+ minimum (C_2) are summarized in Tables 2 and 3.

The C_2 structure of SiH_7^+ is the lowest in energy at all levels of theory. However, the energy differences of the three structures (C_2 , C_{2v} (I) and C_{2v} (II)) are less than 0.1 kcal mol⁻¹. At the DZP SCF level of theory, all structures have at least one imaginary frequency. When we optimized the compound without symmetry constraint (C_1 structure) at the DZP SCF level, the global minimum was found to be very slightly different from the C_2 structure, where the total energies differ only at the sixth decimal point in atomic units. However, when the triple- ζ basis sets were used, the number of imaginary frequencies for each structure decreased by one. The "missing" imaginary frequency in going from the double- ζ to the triple- ζ basis sets corresponds to a motion which leads to nonequivalent Si-H₂ distances. Apparently, this is due to an inadequacy of the DZP basis set to describe SiH_7^+ correctly, since the less diffuse functions in the DZP basis do not allow a proper description of the rather long silicon-hydrogen subunit bonds. The triple- ζ basis sets also yield Si-H bonds which are always longer than the ones obtained with the double- ζ basis set. Since the C_{2v} (I) form is a transition state for the H_2 subunit rotations, the rotational barrier is essentially zero.

In Table 2 we have also summarized selected geometrical parameters of free H_2 , SiH_5^+ , and SiH_3^+ . The geometrical parameters of SiH_7^+ in Table 2 indicate that the molecule involves a SiH_3^+ cation weakly bound to two H_2 subunits. Both basis set and method have the same effect on the bond lengths, which increase with enhancements in theoretical sophistication. Inclusion of f functions on silicon does not alter the results significantly (TZ2P(f,d) SCF, Table 2). The MP2 method in conjunction with a TZ2P basis set still seems to underestimate the bond lengths,² which in turn overestimates the general trend of the vibrational frequencies, as we will discuss below. The Si-H bond distances of the SiH_3^+ counterpart in SiH_7^+ are slightly shorter than those of free SiH_3^+ . The H_2 bond length of SiH_7^+ is only slightly shorter than the bond length of free H_2 , indicating a small perturbation of the hydrogen subunits through the cation moiety. It is remarkable, however, how little overall effect the basis set and theoretical method have on the geometries of the SiH_7^+ structures.

The harmonic vibrational frequencies and intensities of SiH_7^+ are summarized in Table 3, together with the harmonic vibrational frequencies of free H_2 as well as the H_2 stretching frequency within SiH_5^+ . As noted before, the only observable H_2 frequency for SiH_7^+ is the asymmetric combination of the two H_2 moieties (ω_{10} mode). The mode involving symmetric combination of the two H_2 vibrations does not change the dipole moment of the molecule, and thus has no IR intensity. The ω_{10} mode has been observed experimentally by Cao, Choi, Haas, Johnson, and Okumura¹ at 3866 cm⁻¹. This yields a frequency shift of 295

TABLE 2: The Geometrical Parameters for the SiH_7^+ (C_2) Minimum (Bond Distances in angstroms (Å), Angles in degrees)^a

	DZP SCF	TZ2P SCF	TZ2P(f,d) SCF	DZP CISD	TZ2P CISD	DZP CCSD	TZ2P CCSD	DZP CCSD(T)	TZ2P CCSD(T)	TZ2P MP2 ^c
r_{12}	1.449	1.451	1.452	1.449	1.451	1.452	1.456	1.453	1.457	1.453
r_{13}, r_{34}	1.449	1.451	1.452	1.449	1.451	1.452	1.456	1.453	1.457	1.453
r_{57}, r_{68}	0.749	0.750	0.750	0.757	0.756	0.760	0.761	0.761	0.762	0.756
r_{15}, r_{16}	2.164	2.166	2.158	2.066	2.088	2.063	2.088	2.055	2.080	2.072
r_{17}, r_{18}	2.162	2.164	2.155	2.064	2.085	2.061	2.085	2.054	2.078	2.070
$\alpha_{215}, \alpha_{216}$	83.1	83.1	83.0	82.6	82.7	82.6	82.6	82.5	82.5	82.1
α_{314}	120.0	120.0	120.0	120.0	120.0	120.0	120.0	120.0	120.0	120.0
τ_{2175}, τ_{2186}	46.2	46.3	46.1	45.8	45.5	45.8	45.3	45.8	45.0	na
τ_{3125}, τ_{4126}	83.5	83.5	83.4	83.5	83.4	83.5	83.4	83.5	83.4	na
Si-H in SiH_3^+	1.452	1.455	1.456	1.454	1.457	1.456	1.461	1.457	1.462	
H_2 in SiH_5^+	0.759	0.760	0.761	0.770	0.771	0.772	0.774	0.773	0.776	
H_2	0.735	0.734	0.734	0.744	0.742					

^a The numbering of the atoms refers to Figure 1. ^b Symmetry definitions used in this table: r_{ij} = distance between atoms i and j ; α_{ijk} = angle between atoms $i-k$. τ_{ijkl} = torsional angle between atoms $i-l$. ^c Geometrical parameters taken from ref 2.

TABLE 3: Harmonic Vibrational Frequencies (cm^{-1}) and IR Intensities (km/mol , in Parentheses) for the SiH_7^+ (C_2) Global Minimum Structure

mode	DZP SCF	TZ2P SCF	TZ2P(f,d) SCF	DZP CISD	TZ2P CISD	DZP CCSD	TZ2P CCSD	TZ2P MP2 ^a
ω_1 (A)	4398 (0)	4376 (0)	4371 (0)	4298 (0)	4260 (0)	4238 (0)	4172 (0)	4246 (0)
ω_2	2507 (7)	2473 (4)	2481 (5)	2480 (4)	2428 (2)	2453 (3)	2387 (1)	2422 (1)
ω_3	2453 (0)	2418 (0)	2426 (0)	2411 (0)	2373 (0)	2393 (0)	2330 (0)	2366 (0)
ω_4	1009 (91)	999 (66)	997 (65)	967 (76)	949 (56)	954 (72)	928 (53)	945 (49)
ω_5	810 (36)	855 (23)	876 (25)	845 (36)	836 (26)	833 (35)	813 (26)	859 (32)
ω_6	726 (1)	721 (0)	729 (0)	769 (1)	748 (0)	764 (1)	741 (0)	754 (1)
ω_7	423 (0)	497 (0)	497 (0)	547 (0)	583 (0)	552 (0)	587 (0)	589 (0)
ω_8	327 (2)	323 (4)	327 (4)	369 (3)	355 (5)	370 (3)	354 (6)	363 (6)
ω_9	50 (0)	53 (0)	55 (0)	102 (0)	76 (0)	108 (0)	78 (0)	77 (0)
ω_{10} (B)	4383 (310)	4360 (352)	4354 (350)	4279 (274)	4240 (332)	4220 (266)	4152 (366)	4224 (358)
ω_{11}	2507 (7)	2473 (4)	2480 (5)	2479 (5)	2428 (2)	2452 (4)	2386 (1)	2422 (1)
ω_{12}	1009 (91)	999 (66)	997 (65)	967 (76)	949 (57)	954 (72)	929 (43)	945 (52)
ω_{13}	962 (218)	952 (203)	954 (202)	940 (180)	917 (166)	928 (169)	898 (151)	909 (163)
ω_{14}	810 (38)	855 (25)	876 (27)	845 (37)	836 (27)	833 (36)	813 (28)	860 (25)
ω_{15}	727 (1)	721 (0)	729 (0)	770 (1)	749 (0)	766 (1)	742 (0)	755 (1)
ω_{16}	325 (3)	322 (18)	326 (11)	366 (9)	379 (249)	367 (10)	383 (273)	382 (230)
ω_{17}	6 (8)	288 (250)	275 (255)	256 (316)	349 (25)	262 (315)	349 (95)	358 (37)
ω_{18}	27i	5 (0)	4 (0)	3 (0)	1 (0)	2 (0)	77 (0)	19 (0)
H_2	4641	4589	4585	4485	4411	4485	4411	4552
H_2 in SiH_5^+	4247	4218	4210	4059	4038	4059	3991	

^a Frequencies and IR intensities taken from ref 2.

TABLE 4: Dissociation Energies (kcal/mol) of SiH_7^+ and SiH_5^+ . The Values in Parentheses Are the ZPVE-Corrected Dissociation Energies D_0

	$\text{SiH}_7^+ \rightarrow \text{SiH}_5^+ + \text{H}_2$	$\text{SiH}_5^+ \rightarrow \text{SiH}_3^+ + \text{H}_2$
DZP SCF ^a	3.1 (1.7)	9.4 (5.4)
TZ2P SCF	4.2 (1.9)	12.4 (6.6)
TZ2P(f,d) SCF	4.3 (2.0)	10.9 (7.0)
DZP CISD	4.2 (1.8)	12.3
TZ2P CISD	6.2 (3.3)	13.8
DZP CCSD	4.3 (2.2)	12.5
TZ2P CCSD	6.4 (3.8)	14.1
DZP CCSD(T)	4.5 (2.4)	12.9
TZ2P CCSD(T)	6.7 (4.1)	14.7
TZ2P(f,d) CCSD(T) ^b	7.2 (4.6)	16.2

^a BSSE corrections for the reaction $\text{SiH}_7^+ \rightarrow \text{SiH}_5^+ + \text{H}_2$ at the DZP SCF, TZ2P SCF, and TZ2P+f SCF levels of theories are 0.18, 0.05, and 0.03 kcal mol^{-1} , respectively. ^b Energy single point on the TZ2P CCSD(T)-optimized structures.

cm^{-1} compared to that for free hydrogen (4161 cm^{-1}). Our theoretical vibrational frequency shift at the TZ2P CCSD level of theory is 259 cm^{-1} , in good agreement with the experimental hydrogen frequency shift. The previously determined² TZ2P MP2 frequencies give a shift of 328 cm^{-1} .

Similarly, the H_2 vibrational frequency shift from free H_2 to the corresponding mode in SiH_5^+ is 420 cm^{-1} at the TZ2P CCSD level,³ indicating a tighter complex of the silylium cation SiH_3^+ with the hydrogen molecule.

Table 5 reports the equilibrium rotational constants A_e – C_e for

TABLE 5: Rotational Constants A – C (in cm^{-1}) for the SiH_7^+ Structures at the TZ2P CCSD(T) Level

	A	B	C
C_2 (prolate top)	2.406	0.829	0.829
C_{2v} (I) (asymmetric top)	2.405	0.840	0.817
C_{2v} (II) (asymmetric top)	2.405	0.840	0.817
average	2.405	0.836	0.821

the three SiH_7^+ stationary points considered here. Of course, such a theoretical approach to the prediction of rotational constants for a molecule as floppy as SiH_7^+ is naive. The proper theoretical approach to the prediction of the rotational constants A_0 – C_0 is clear but presently impossible. One should use the 18-dimensional *ab initio* potential energy hypersurface to solve the Schrödinger equation for the motion of the nuclei within the Born–Oppenheimer approximation. This would give rotational constants directly comparable with the experiments of Okumura's group. The above discussion notwithstanding, the theoretical equilibrium rotational constants for the three stationary points are remarkably similar. And the theoretical values of B_e all agree reasonably well with the experimental $B_0 = 0.85 \text{ cm}^{-1}$. A very crude procedure is to average the rotational constants for the three stationary points. This is done in Table 5, and the resulting average B_e is 0.84 cm^{-1} .

Our best prediction for the dissociation energy D_e of SiH_7^+ into SiH_5^+ and H_2 is 7.2 kcal mol^{-1} at the TZ2P(f,d) CCSD level. Inclusion of the TZ2P CCSD zero-point vibrational energy correction decreases this value to $D_0 = 4.6 \text{ kcal mol}^{-1}$. This

$\text{SiH}_5^+ \cdots \text{H}_2$ dissociation energy is more than twice as large as the previously predicted^{7b} $D_0(\text{CH}_5^+ \cdots \text{H}_2) = 1.2 \text{ kcal mol}^{-1}$.

The geometry of the SiH_7^+ cation ($\text{H}_2 \cdots \text{SiH}_3^+ \cdots \text{H}_2$) is very different from the geometry of the CH_7^+ cation derived from the CH_5^+ moiety ($\text{CH}_5^+ \cdots \text{H}_2$).^{7b} These differences are in part due to the greater stability of the SiH_3^+ cation, which is reflected in the differences in the loss of H_2 from CH_5^+ ($42.0 \text{ kcal mol}^{-1}$)⁶ and SiH_5^+ ($10\text{--}15 \text{ kcal mol}^{-1}$).^{3,5} Also, as a third-row element, silicon is much bigger than carbon, thus providing a large surface area where the hydrogen molecules can attach. In other words, $\text{H}_2 \cdots \text{SiH}_3^+ \cdots \text{H}_2$ is less crowded than a hypothetical $\text{H}_2 \cdots \text{CH}_3^+ \cdots \text{H}_2$. Also, carbon (2.5) is more electronegative than silicon (1.7). Consequently, CH_3^+ is only able to bind one hydrogen molecule strongly; the second H_2 has to bind indirectly to one of the electron-deficient hydrogens of the three-center-two-electron bond.

Concluding Remarks

The C_2 structure of SiH_7^+ , which consists of a SiH_3^+ cation weakly bonded to two equivalent hydrogen molecules, was found to be the global minimum on the potential energy surface. Nevertheless, the rotation of the hydrogen molecule moieties around an axis perpendicular to the main axis is essentially unrestricted since the energy differences between the minimum and the rotational transition structures C_{2v} (I) and C_{2v} (II) are negligible. The experimental asymmetric H_2 stretching vibrational frequency shift (bound versus free) of 295 cm^{-1} is well reproduced theoretically (259 cm^{-1}). The SiH_7^+ dissociation energy D_0 into SiH_5^+ and H_2 is $4.6 \text{ kcal mol}^{-1}$ [TZ2P(f,d) CCSD(T) + ZPVE(TZ2P CCSD)], much larger than the dissociation of CH_7^+ into CH_5^+ and H_2 ($1.2 \text{ kcal mol}^{-1}$).

Acknowledgment. The work in Georgia was supported by the U.S. Air Force Office of Scientific Research, Grant AFOSR-

92-J-0047. The work in Erlangen was supported by the Deutsche Forschungsgemeinschaft, the Fonds der Deutschen Chemischen Industrie (doctoral fellowship for P.R.S.), and the Convex Computer Corp.

References and Notes

- (1) Cao, Y.; Choi, J.-H.; Haas, B.-M.; Johnson, M. S.; Okumura, M. *J. Phys. Chem.* **1993**, *97*, 5215.
- (2) Liu, R.; Zhou, X. J. *J. Phys. Chem.* **1993**, *97*, 9555.
- (3) Hu, C.-H.; Shen, M.; Schaefer, H. F. *Chem. Phys. Lett.* **1992**, *190*, 543.
- (4) Schreiner, P. R.; Kim, S. J.; Schaefer, H. F.; Schleyer, P. v. R. *J. Chem. Phys.* **1993**, *99*, 3716. Also see refs 6 and 7b.
- (5) Boo, B. H.; Armentrout, P. B. *J. Am. Chem. Soc.* **1987**, *109*, 3549.
- (6) Schleyer, P. v. R.; Carneiro, J. W. M. *J. Comput. Chem.* **1992**, *13*, 997.
- (7) (a) Boo, D. W.; Lee, Y. T. *Chem. Phys. Lett.* **1993**, *211*, 358. (b) Kim, S.-J.; Schreiner, P. R.; Schleyer, P. v. R.; Schaefer, H. F. *J. Phys. Chem.* **1993**, *97*, 12232.
- (8) Pulay, P. In *Modern Theoretical Chemistry, Volume 4*; Schaefer, H. F., Ed.; Plenum: New York, 1977; pp 153-185.
- (9) (a) Brooks, B. R.; Laidig, W. D.; Saxe, P.; Goddard, J. D.; Yamaguchi, Y.; Schaefer, H. F. *J. Chem. Phys.* **1980**, *76*, 4625. (b) Rice, J. E.; Amos, R. D.; Handy, N. C.; Lee, T. J.; Schaefer, H. F. *J. Chem. Phys.* **1986**, *85*, 963.
- (10) Scheiner, A. C.; Scuseria, G. E.; Lee, T. J.; Rice, J. E.; Schaefer, H. F. *J. Chem. Phys.* **1987**, *87*, 5361. Scuseria, G. E.; Janssen, C.; Schaefer, H. F. *J. Chem. Phys.* **1988**, *89*, 7382.
- (11) Scuseria, G. E. *J. Chem. Phys.* **1991**, *94*, 442.
- (12) (a) Primitive basis sets: Huzinaga, S. *J. Chem. Phys.* **1965**, *42*, 1293. (b) For hydrogen: Dunning, T. H. *Ibid.* **1970**, *53*, 2823. (c) For silicon: Dunning, T. H.; Hay, P. J. In *Modern Theoretical Chemistry, Volume 3*; Schaefer, H. F., Ed.; Plenum: New York, 1977; pp 1-27.
- (13) (a) Primitive basis set for silicon: Huzinaga, S. Department of Chemistry, Department of Chemistry Report II, University of Alberta, Edmonton, Alberta, Canada, 1971. (b) Contracted basis set for silicon: McLean, A. D.; Chandler, G. S. *J. Chem. Phys.* **1980**, *72*, 5639.
- (14) Saxe, P.; Yamaguchi, Y.; Schaefer, H. F. *J. Chem. Phys.* **1982**, *77*, 5674.
- (15) PSI 1.1 1990; PSITECH Inc.: Watkinsville, GA 30677.

Toward the observation of silanone (H_2SiO) and hydroxysilylene (HSiOH) via microwave spectroscopy

Buyong Ma and Henry F. Schaefer III

Center for Computational Quantum Chemistry, The University of Georgia, Athens, Georgia 30602

(Received 27 December 1993; accepted 18 April 1994)

Ab initio quantum mechanical methods were employed to study the H_2SiO and HSiOH (both *cis* and *trans*) isomers, resulting in high-level theoretical predictions of the equilibrium geometries, rotational constants, dipole moments, relative energies, vibrational frequencies, transition state structures, and the activation energy for the isomerization between the *cis*- and *trans*- HSiOH isomers. Basis sets as large as triple zeta plus double polarization plus silicon and oxygen atom *f* and hydrogen atom *d* functions [TZ2P(*f,d*)] have been used with the self-consistent-field configuration interaction including all single and double excitations (CISD), and coupled cluster including all single and double substitutions (CCSD) methods, as well as CCSD with the effects of connected triple excitations added perturbatively [CCSD(T)]. Our predictions for the dipole moment components and geometry of silanone (H_2SiO) were instrumental in its recent microwave spectroscopic identification (accompanying paper by Bogey and co-workers) and are in excellent agreement with the experimental results. The silanone (H_2SiO) molecule is predicted to lie about 0.5 kcal mol⁻¹ lower in energy than the HSiOH isomers. In contrast with previous theoretical work, *cis*- HSiOH may be slightly more stable than *trans*- HSiOH . The experimental IR spectrum for the HSiOH isomer, which may have been misassigned to *trans*- HSiOH , is closer to that for *cis*- HSiOH at the TZ2P(*f,d*) CISD level of theory. The isomerization between *cis*- and *trans*- HSiOH takes place along the torsional mode, and the activation energy is predicted to be 8.3 kcal mol⁻¹.

I. INTRODUCTION

Silanone (H_2SiO) is the silicon analog of formaldehyde (H_2CO). For many years, the possible existence of this silicon-oxygen double-bonded compound has been the subject of theoretical and experimental studies.¹⁻⁷ There have been two previous experiments indicating its existence.^{4,5} In 1985 Glinski, Gole, and Dixon⁴ observed visible chemiluminescence which they assigned to H_2SiO and its isomer HSiOH . Also in 1985 Withnall and Andrews⁵ identified a matrix isolation IR spectrum belonging to the H_2SiO molecule. However, the high resolution spectroscopic identification of H_2SiO (accompanying paper)⁶ has only been achieved during the past few months, with the assistance of the present theoretical work.

Before 1993 hydroxysilylene (HSiOH) was thought to lie slightly lower in energy than the H_2SiO molecule.^{3,7} However, a recent theoretical study by Darling and Schlegel¹³ indicated that hydroxysilylene may be higher in energy than the H_2SiO molecule.¹³ Hydroxysilylene is a by-product of the formation of the H_2SiO molecule in, e.g., the gas phase reaction of ozone with silane,^{4,5} silane plasmas,⁶ and the silicon-water adduct.² All six vibrational frequencies for hydroxysilylene (HSiOH) have been observed in matrix isolation and assigned.^{2,5} However, it has proven to be difficult to identify H_2SiO or HSiOH by high resolution spectroscopy.⁶ HSiOH can exist as *cis* and *trans* isomers. The two isomers are separated by a sizable barrier, which is around 10 kcal mol⁻¹ from earlier *ab initio* quantum mechanical studies.^{3,8-11} The relative energies of the *cis*- and *trans*-isomers are controversial. Even though it has been

stated that experimental studies have shown the *trans*-isomer to be the more stable species,¹² there is no definitive proof in the experiments.^{2,4,5} Experimentalists^{2,4,5} have assumed that the *trans*-isomer is more stable than the *cis*-isomer, because earlier *ab initio* quantum mechanical studies indicated that the *trans*-isomer is lower in energy.^{2,3} However, because the most recent theoretical energy separation between these isomers is very small, e.g., within ± 0.2 kcal mol⁻¹ at the G-2 level¹³—careful examination of the relative energies at higher theoretical levels is needed.

Even though there are many theoretical studies of these three isomers,^{1,7-13} there are no published results on their dipole moments. Therefore, in the course of their microwave studies, Bogey and co-workers (private communication, 3 March, 1993) requested theoretical help from us. In order to facilitate the high resolution spectroscopic characterization of these species,⁶ we determined the dipole moment components for H_2SiO and the *cis*- and *trans*- HSiOH isomers. We also studied the potential energy surface of the HSiOH system and provide new insight into the relative energies of the *cis*- and *trans*- HSiOH and the isomerization barrier separating them.

II. THEORETICAL METHODS

Two basis sets are employed in this study. The first, of double-zeta plus polarization (DZP) quality, is the standard Huzinaga-Dunning^{14(a),14(b),14(d)} contracted Gaussian basis Si(11s7p/6s4p), O(9s5p/4s2p), H(9s/4s) augmented with a set of (five) *d* functions on the silicon and oxygen atoms [$\alpha_d(\text{Si})=0.5$, $\alpha_d(\text{O})=0.85$] and a set of *p* functions on

the hydrogen atoms [$\alpha_p(\text{H})=0.75$]. The second, TZ2P(f,d), is the triple-zeta plus double polarization (TZ2P) basis set augmented with one set of (seven) f functions [$\alpha_f(\text{Si})=0.31$] on the silicon atom, one set of (seven) f functions

[$\alpha_f(\text{O})=1.4$] on the oxygen atom, and a set of (five) d functions on the hydrogens [$\alpha_d(\text{H})=1.0$]. The TZ2P is the McLean-Chandler¹⁵ Si ($12s9p/6s5p$), Huzinaga-Dunning^{14(c)} O ($10s6p/5s3p$), H ($5s/3s$) contracted

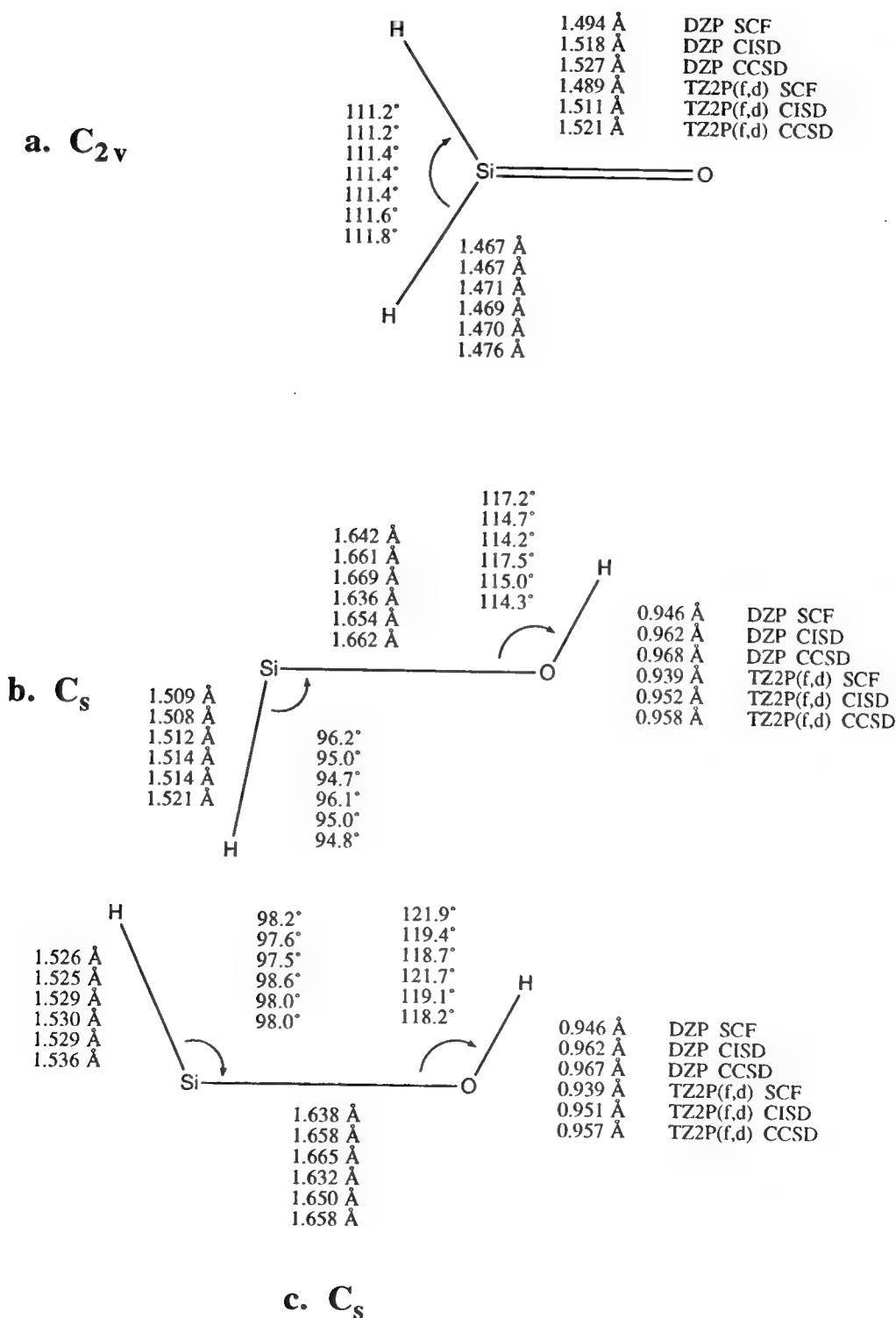


FIG. 1. Theoretical equilibrium geometries for (a) silanone, H_2SiO ; (b) *trans*- HSiOH ; and (c) *cis*- HSiOH .

TABLE I. Theoretical rotational constants (MHz) for silanone and hydroxysilylene.

Theoretical levels	H ₂ SiO (C _{2v})			HSiOH (<i>cis</i>)			HSiOH (<i>trans</i>)		
	A	B	C	A	B	C	A	B	C
TZ2P(<i>f,d</i>) SCF	17 0187	19 306	17 339	17 8347	16 768	15 327	182 790	16 742	15 337
TZ2P(<i>f,d</i>) CISD	16 9476	18 794	16 919	17 5107	16 481	15 063	178 717	16 456	15 068
TZ2P(<i>f,d</i>) CCSD	16 7742	18 576	16 724	17 2879	16 337	14 927	176 378	16 314	14 933
Experiment ^a	16 6640	18 678	16 743						

^aReference 6.

Gaussian basis augmented with two sets of (five) *d* functions [$\alpha_d(\text{Si})=1.0, 0.25$] on the silicon atoms, two sets of (five) *d* functions [$\alpha_d(\text{O})=1.7, 0.425$] on the oxygen atoms, and two sets of *p* functions [$\alpha_p(\text{H})=1.5, 0.375$] on the hydrogen atoms.

The structures of H₂SiO, *cis*- and *trans*-HSiOH, and the transition state for the isomerization between the *cis*- and *trans*-isomers were optimized using the self-consistent-field (SCF) method, the configuration interaction method with all single and double excitations¹⁶ (CISD), and the coupled cluster method including all single and double substitutions¹⁷ (CCSD). The effects of connected triple excitations were added perturbatively to the CCSD method via a third correlated method [CCSD(T)] to obtain single point energies using the CCSD optimized geometries. With the CISD, CCSD, and CCSD(T) methods the six core molecular orbitals (silicon 1*s*-, 2*s*-, and 2*p*-like; oxygen 1*s*-like) were kept doubly occupied in all configurations, and the six highest virtual molecular orbitals are excluded.

Harmonic vibrational frequencies were determined using analytic second derivative methods at the SCF level, and finite central differences of analytic first derivatives¹⁶ at the CISD level. The enthalpy changes were evaluated as follows:¹⁸

$$\Delta H^\circ = \Delta E_e + \Delta E_v^\circ + \Delta(\Delta E_v)^{298} + \Delta E_r^{298} + \Delta E_t^{298},$$

where ΔE_e is the energy difference without zero-point vibrational energy (ZPVE) correction, ΔE_v° is the difference between the zero-point vibrational energies of reactant and product of 0 K, and $\Delta(\Delta E_v)^{298}$ is the change in the vibrational energy difference in going from 0 to 298 K. Entropy changes (ΔS°) have been evaluated from standard statistical mechanical relationships,¹⁹ and free energy changes (ΔG°) are evaluated from $\Delta G = \Delta H - T\Delta S$. The standard state is 1 atm at 298 K.

The gas phase rotational constants were evaluated using the rigid-rotor approximation. The computations were performed using the program PSI developed by this research group.²⁰

III. RESULTS AND DISCUSSION

A. Molecular equilibrium geometries and dipole moments

The molecular geometries of the three minima (H₂SiO and *cis*- and *trans*-HSiOH) are shown in Fig. 1. Their gas phase rotational constants and dipole moment components are reported in Tables I and II, respectively. Our theoretical

predictions of the dipole moment components and the geometry of the H₂SiO molecule have proven to be accurate; very recently (accompanying paper), with the help of these theoretical data, Bogey has succeeded in identifying H₂SiO by microwave spectroscopy.⁶ As indicated in Table I, our theoretical structure for the H₂SiO molecule [TZ2P(*f,d*) CCSD] agrees well with Bogey's experimental data.⁶ The TZ2P(*f,d*) CCSD rotational constants for H₂SiO all agree with experiment to within 1%. For the H₂SiO molecule, the Si—O double bond distance is 1.521 Å [TZ2P(*f,d*) CCSD], which is significantly shorter than that obtained by previous studies at the MP2/6-31G* level (1.545 Å).^{3,13}

For the *cis*- and *trans*-HSiOH isomers, the Si—O single bond distances are 1.658 Å (*cis*) and 1.662 Å (*trans*) [TZ2P(*f,d*) CCSD]. There are no existing experimental geometries for the two isomers. Microwave spectroscopic experiments⁶ have had difficulty in identifying the absorption features of the two isomers, because the observed spectra are perturbed, perhaps due to the isomerization between the two species. Ismail *et al.*² proposed a geometry for *trans*-HSiOH from their IR spectrum, obtaining a Si—O bond distance (1.591±0.100 Å), a value satisfied to within the (large) experimental error bars by our theoretical result. However, Ismail *et al.* may have misassigned the observed IR spectrum of the *cis*-isomer to the *trans*-isomer (see Sec. III B).

B. The relative energies of H₂SiO, *cis*-HSiOH, and *trans*-HSiOH

The total energies for these three molecules are reported in Table III and their zero-point vibrational energies (ZPVEs) are reported in Table IV. The H₂SiO molecule is 0.8 kcal mol⁻¹ [TZ2P(*f,d*) CCSD(T)] higher in energy than the HSiOH isomers. The ZPVE [TZ2P(*f,d*) SCF] correction makes the H₂SiO molecule more stable by 0.5 kcal mol⁻¹,

TABLE II. Molecular dipole moment components along the principal axis A and the perpendicular axis B (D). The polarities are Si⁺—O⁻.

Theoretical levels	H ₂ SiO (C _{2v}) μ_A	HSiOH (<i>cis</i>)		HSiOH (<i>trans</i>)	
		μ_A	μ_B	μ_A	μ_B
DZP SCF	-4.32	0.46	-1.78	0.06	1.14
DZP CISD	-3.84	0.34	-1.63	0.24	1.30
DZP CCSD	-3.71	0.28	-1.56	0.20	1.14
TZ2P(<i>f,d</i>) SCF	-4.28	0.63	-1.60	0.56	1.01
TZ2P(<i>f,d</i>) CISD	-3.96	0.48	-1.50	0.42	1.11
TZ2P(<i>f,d</i>) CCSD	-3.82	0.42	-1.44	0.37	1.16

TABLE III. Total energies for H₂SiO, *cis*-HSiOH, and *trans*-HSiOH (hartree).

Theoretical levels	H ₂ SiO (C _{2v})	HSiOH (<i>cis</i>)	HSiOH (<i>trans</i>)	HSiOH (transition state)
DZP SCF	-364.943 95	-364.955 80	-364.955 87	-364.942 27
DZP CISD	-365.214 26	-365.217 58	-365.217 92	
DZP CCSD	-365.237 49	-365.240 35	-365.240 75	
TZ2P(<i>f,d</i>) SCF	-364.984 96	-364.994 23	-364.993 96	-364.980 99
TZ2P(<i>f,d</i>) CISD	-365.320 32	-365.323 36	-365.323 33	-365.308 67
TZ2P(<i>f,d</i>) CCSD	-365.350 63	-365.354 46	-365.354 45	-365.339 49
TZ2P(<i>f,d</i>) CCSD(T) ^a	-365.366 01	-365.367 16	-365.367 29	-365.351 75

^aThe geometries are optimized at the TZ2P(*f,d*) CCSD level of theory.

consistent with the results of Darling and Schlegel (0.8 kcal mol⁻¹ at the G-2 level with ZPVE correction).¹³

The relative energies of *cis*- and *trans*-HSiOH are controversial. As indicated in Table III, the *trans*-isomer is lower in energy than the *cis*-isomer using the DZP basis set. However, with the more complete TZ2P(*f,d*) basis set, the *cis*- and *trans*-isomers are virtually energetically degenerate at the TZ2P(*f,d*) CCSD level of theory. The *cis*-isomer lies only 0.08 kcal mol⁻¹ higher in energy than *trans*-isomer at the TZ2P(*f,d*) CCSD(T) level of theory. However, after the ZPVE [TZ2P(*f,d*) CISD] correction, the *cis*-isomer lies 0.1 kcal mol⁻¹ lower in energy than the *trans*-isomer, also consistent with the results of Darling and Schlegel (0.2 kcal mol⁻¹ at the G-2 level with ZPVE correction).¹³ Here it is natural to ask whether the experimentally observed² most stable species is the *trans*-isomer or the *cis*-isomer. We discuss this question in the following section.

C. The harmonic vibrational frequencies of H₂SiO, *cis*-HSiOH, and *trans*-HSiOH—a correction of experimental assignments

The harmonic vibrational frequencies [TZ2P(*f,d*) SCF] of these three isomers are reported in Table V. Because *cis*-HSiOH is slightly lower in energy than the *trans*-isomer, in contrast with the previous theoretical results and experimental assumptions,^{2,5} it is crucial to determine whether the experimentally observed species^{2,5} is the *trans*-isomer or the *cis*-isomer. Therefore we also evaluated the harmonic vibrational frequencies for the *cis*- and *trans*-isomers at a correlated level of theory [TZ2P(*f,d*) CISD] and these are reported in Table VI, together with a consideration of HSiOD and DSiOD.

Ismail *et al.*² reported experimental observations of the matrix isolation IR spectra of the HSiOH isomers. Experimentally,² only one isomer was observed for HSiOH.

However, both *trans*- and *cis*-isomers were observed for the deuterated species HSiOD and DSiOD (Table VI). Annealing of the matrix caused conversion of one structure to a more stable isomer.² Ismail *et al.*² assumed that the *trans*-HSiOH is the more stable and assigned the IR spectrum accordingly (Table V). However, our theoretical results indicate that the *cis*-isomer is very slightly more stable. Therefore, the experimentally observed isomer² may be the *cis*- rather than the *trans*-isomer. As can be seen from Table VI, the observed IR spectra assigned to the *trans*-isomer are closer to our theoretical results for the *cis*-isomer. The strongest evidence comes from the comparison of the theoretical H(D)-Si-O bending mode with the experimental assignment (Table VI). For HSiOH, HSiOD, and DSiOD this *cis*-HSiO bend lies 13, 23, and 20 cm⁻¹, respectively, above the comparable *trans* bending frequency. For HSiOD and DSiOD the experimental *cis-trans* differences are both 14 cm⁻¹. Because of the transferability of scale factors for similar bonds in related systems,²¹ we are confident that the vibrational frequency of the H(D)-Si-O bending mode should be higher for the *cis*-isomer than that for the *trans*-isomer, as indicated by our results in Table VI. However, the experimental assignments (for the HSiOD and DSiOD) assumed the opposite ordering. Therefore, the observed IR spectrum^{2,5} for HSiOH should belong to the *cis*-isomer. In this sense, the comparison between theory and experiment shows that the *cis*-isomer is observed.

D. The barrier height for the isomerization between *cis*- and *trans*-HSiOH

The geometry of the transition state for the isomerization between *cis*- and *trans*-HSiOH is shown in Fig. 2(a) and the

TABLE IV. Zero-point vibrational energies for H₂SiO, *cis*-HSiOH, and *trans*-HSiOH systems (kcal mol⁻¹).

Theoretical levels	H ₂ SiO	HSiOH		HSiOD		DSiOD	
		<i>cis</i>	<i>trans</i>	<i>cis</i>	<i>trans</i>	<i>cis</i>	<i>trans</i>
DZP SCF	12.6	13.9	14.1	11.8	11.9	10.5	10.6
TZ2P(<i>f,d</i>) SCF	12.5	13.8	14.0	11.6	11.8	10.4	10.5
TZ2P(<i>f,d</i>) CISD	...	13.3	13.5	11.3	11.5	10.1	10.2

TABLE V. Harmonic vibrational frequencies at the TZ2P(*f,d*) SCF level.

H ₂ SiO		HSiOH			Transition state
		<i>cis</i>	<i>trans</i>		
Mode	ω (cm ⁻¹)	Mode	ω (cm ⁻¹)	ω (cm ⁻¹)	ω (cm ⁻¹)
Si-H	2362	O-H	4191	4190	4276
Si-H	2360	Si-H	2032	2114	2021
Si=O	1356	H-Si O	1033	1013	952
H Si-H	1080	Si-O	924	923	932
Out-of-plane	802	Si-O-H	803	858	378
H-Si=O	759	Torsion	638	667	712i

TABLE VI. Comparison between the hydroxysilylene experimental IR spectrum^a and the present theoretical results at the TZ2P(f,d) CISD level.^b

Mode	HSiOH (cm ⁻¹)				HSiOD (cm ⁻¹)				DSiOD (cm ⁻¹)			
	This work		Experimental assignment		This work		Experimental assignment		This work		Experimental assignment	
	<i>cis</i>	<i>trans</i>	<i>cis</i>	<i>trans</i>	<i>cis</i>	<i>trans</i>	<i>cis</i>	<i>trans</i>	<i>cis</i>	<i>trans</i>	<i>cis</i>	<i>trans</i>
O-H	3800	3796		3650								
H-Si	1917	1989		1881 1847	1917	1989		1872	1380	1432		1354
H-Si-O	953	940		937	906	883	881	895	723	703	701	715
Si-O	842	840		841	837	837	845	840	839	836	840	841
Si-O-H	733	786		722	567	614		563	521	568		521
Torsion	613	644		595	495	518		489	455	470		447

^aReference 2.^bThe vibrational frequencies were scaled by a factor of 0.95 to account for anharmonicity and higher level correlation effects; see Ref. 23.

isomerization barrier is reported in Table 7. These results are qualitatively similar to those of the previous study by Kudo and Negase.³

We also investigated the possibility of another isomer-

ization pathway, namely, inversion at the oxygen center.^{3,9,22} However, the topology of the HSiOH potential energy surface makes this pathway less feasible. Technically, we may find the inversion pathway by maximizing the energy along

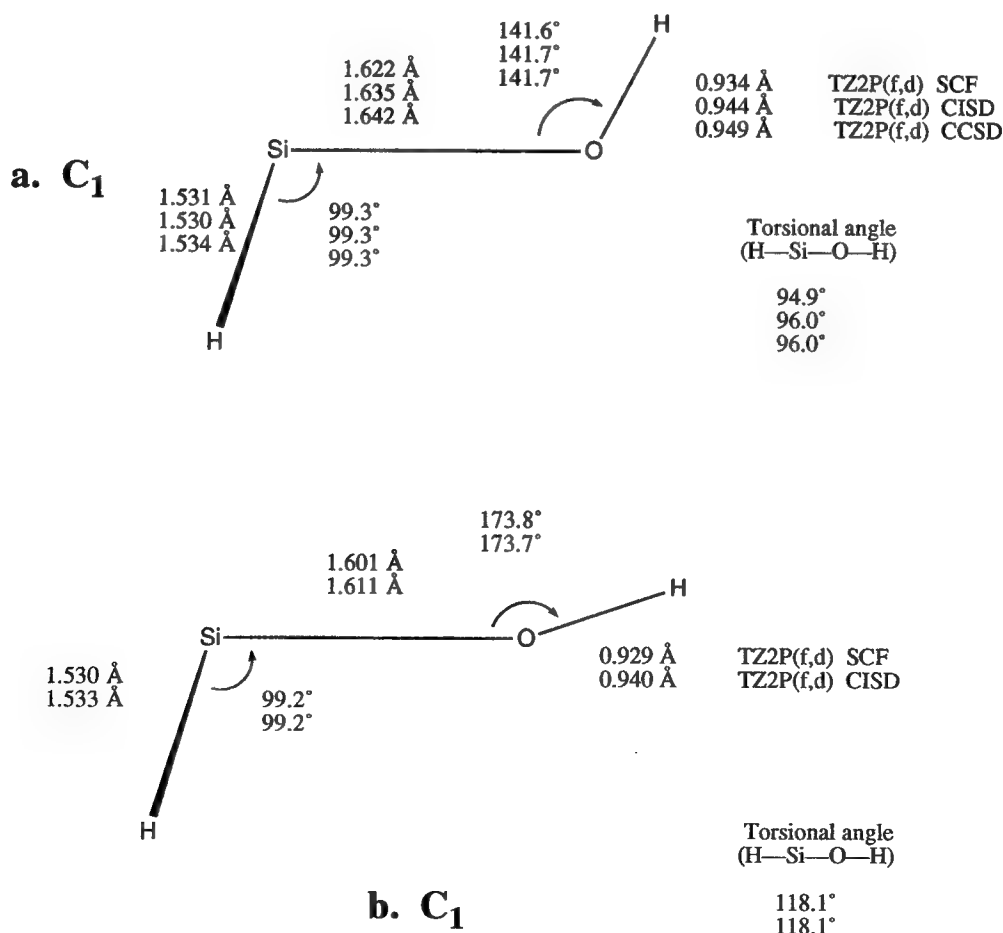


FIG. 2. (a) The transition state geometry for rotational isomerization of HSiOH (*cis*) to HSiOH (*trans*); (b) A stationary point of Hessian index two (two imaginary vibrational frequencies) on the HSiOH potential energy surface for inversion at the oxygen atom.

TABLE VII. Theoretical barrier heights for the isomerization of *cis*-HSiOH to *trans*-HSiOH.^{a,b}

Theoretical levels DZP SCF	Classical barrier	Activation energy			
	ΔE_c 8.5	ΔE_0	ΔH°	ΔG°	ΔS°
TZ2P(<i>f,d</i>) SCF	8.4	7.0	8.1	4.7	11.1
TZ2P(<i>f,d</i>) CISD	9.2	7.8	8.9	5.6	
TZ2P(<i>f,d</i>) CCSD	9.4	8.0	9.1	5.8	
TZ2P(<i>f,d</i>) CCSD(T) ^c	9.7	8.3	9.4	6.1	

^aThe values of ΔE_c , ΔE_0 , ΔH° , and ΔG° are in kcal mol⁻¹, whereas ΔS° is in cal/K mol. The standard state is 1 atm at 298 K.

^bZPVE at the TZ2P(*f,d*) SCF level.

^cThe geometries are optimized at the TZ2P(*f,d*) CCSD level of theory.

the Si–O–H bending mode. However, the potential energy surface along this mode is unusual. As the Si–O–H bond angle reaches around 173° [Fig. 2(b), for example], which is close to linear, there are many stationary points, wherein the torsional angle may vary from 0° to 360°. However, the total energy of the HSiOH changes very little with respect to the torsional mode. These stationary points, which are 0.6–0.8 kcal mol⁻¹ higher in energy than the transition state in Fig. 2(a), *invariably* have two imaginary vibrational frequencies at SCF level, corresponding to the bending and torsional modes. Note that there is no symmetry constraint, i.e., the point group is *C*₁. This type of potential energy surface is consistent with the analysis of Yang, Qin, and Thompson,²² who have pointed out that the bending motion of hydrogen in the HSiOH isomers is coupled to the torsional motion in such a manner that it cannot be treated as purely one dimensional on the static potential energy surface. Therefore, the isomerization between the two isomers should follow the torsional pathway, and the transition state in Fig. 2(a) is reliable.

The activation energy for the isomerization from *cis*- to *trans*-HSiOH is predicted to be 8.3 kcal mol⁻¹ [TZ2P(*f,d*) CCSD(T), Table 7], which is a bit lower than that found by Kudo and Nagase³ (9.3 kcal mol⁻¹). However, this activation energy is still sizable; therefore, we expect that the HSiOH isomers might be detected by microwave spectroscopy at a lower temperature. Tunneling effects^{6,8–11,22} may speed the *cis* to *trans* isomerization. However, in the laboratory² this isomerization appears to be very slow—the time scale is several hours in the matrix isolation experiments.

IV. CONCLUSIONS

We have studied H₂SiO and the *cis*- and *trans*-HSiOH isomers using *ab initio* quantum mechanical methods, resulting in high-level theoretical predictions of the equilibrium geometries, rotational constants, dipole moments, relative energies, vibrational frequencies, transition state structures, and the activation energy for the isomerization between the *cis*- and *trans*-HSiOH isomers. Our predictions for the dipole moment components and geometry of silanone (H₂SiO) were instrumental in its recent micromave spectroscopic identification (accompanying paper by Bogey and co-workers)⁶ and are in excellent agreement with the experimental results. The silanone (H₂SiO) molecule is predicted to lie about 0.5

kcal mol⁻¹ lower in energy than the HSiOH isomers. However, in contrast with previous work, *cis*-HSiOH is predicted to be slightly more stable than *trans*-HSiOH by 0.1 kcal mol⁻¹. The experimental IR spectrum for the more stable HSiOH isomer, which was apparently misassigned to *trans*-HSiOH, is closer to that for *cis*-HSiOH at the TZ2P(*f,d*) CISD level of theory; therefore the spectrum is reassigned to *cis*-HSiOH. The isomerization between *cis*- and *trans*-HSiOH takes place along the torsional mode, and the activation energy is predicted to be 8.3 kcal mol⁻¹. We also examined the possibility of inversion at the oxygen center and found this isomerization pathway to be implausible because the resulting stationary points have Hessian index two (two imaginary vibrational frequencies) and are higher in energy than the torsional transition state; this is consistent with the previous conclusion²² that the bending motion of hydrogen in the HSiOH isomers is coupled to the torsional motion in such a manner that it cannot be treated as purely one dimensional on the static potential energy surface.

ACKNOWLEDGMENTS

We thank Dr. Y. Xie and Dr. Y. Yamaguchi for helpful discussions. We thank Dr. Cynthia Meredith for helpful discussions and for a careful reading of the manuscript. This research was supported by the U.S. Air Force Office of Scientific Research under Grant No. AFOSR-92-J-0047.

- ¹H. F. Schaefer, Acc. Chem. Res. **15**, 283 (1982).
- ²Z. K. Ismail, R. H. Hauge, L. Fredin, J. W. Kauffman, and J. L. Margrave, J. Chem. Phys. **77**, 1617 (1982).
- ³T. Kudo and S. J. Nagase, J. Phys. Chem. **88**, 2837 (1984).
- ⁴R. J. Glinski, J. L. Gole, and D. A. Dixon, J. Am. Chem. Soc. **107**, 5891 (1985).
- ⁵R. Withnall and L. Andrews, J. Phys. Chem. **89**, 3261 (1985).
- ⁶S. Bailleaux, M. Bogey, C. Demuyneck, J. Destombes, and A. Walters, J. Chem. Phys. **100**, 2729 (1994).
- ⁷B. T. Luke, J. A. Pople, M. Krogh-Jespersen, Y. Apeloig, M. Karni, J. Chandrasekhar, and P. R. Schleyer, J. Am. Chem. Soc. **108**, 270 (1986).
- ⁸A. Tachibana, H. Fueno, and T. Yamabe, J. Am. Chem. Soc. **108**, 4346 (1986).
- ⁹S. Sakai and K. D. Jordan, Chem. Phys. Lett. **130**, 103 (1986).
- ¹⁰A. Tachibana, H. Fueno, M. Koizumi, T. Yamabe, and K. Fukui, J. Phys. Chem. **92**, 935 (1988).
- ¹¹S. Sakai, M. S. Gordon, and K. D. Jordan, J. Phys. Chem. **92**, 7053 (1988).
- ¹²A. Tachibana, M. Koizumi, H. Teramae, and T. Yamabe, J. Am. Chem. Soc. **109**, 1383 (1987).
- ¹³C. L. Darling and H. B. Schlegel, J. Phys. Chem. **97**, 8207 (1993).
- ¹⁴(a) S. Huzinaga, J. Chem. Phys. **42**, 1293 (1965); (b) T. H. Dunning, *ibid.* **53**, 2823 (1970); (c) **55**, 716 (1971); (d) T. H. Dunning and P. J. Hay, in *Modern Theoretical Chemistry*, edited by H. F. Schaefer (Plenum, New York, 1977), Vol. 3, p. 1.
- ¹⁵A. D. McLean and G. S. Chandler, J. Chem. Phys. **72**, 5639 (1980).
- ¹⁶(a) B. R. Brooks, W. D. Laidig, P. Saxe, J. D. Goddard, Y. Yamaguchi, and H. F. Schaefer, J. Chem. Phys. **72**, 4652 (1980); (b) J. E. Rice, R. D. Amos, N. C. Handy, T. J. Lee, H. F. Schaefer, *ibid.* **85**, 963 (1986).
- ¹⁷(a) G. D. Purvis and R. J. Bartlett, J. Chem. Phys. **76**, 1910 (1982). (b) G. E. Scuseria, C. L. Janssen, and H. F. Schaefer, *ibid.* **89**, 7382 (1989).
- ¹⁸J. E. Del Bene, H. D. Mettee, M. J. Frisch, B. T. Luke, and J. A. Pople, J. Phys. Chem. **87**, 3279 (1983).
- ¹⁹R. F. Hout, B. A. Levi, and W. J. Hehre, J. Comp. Chem. **3**, 234 (1982).
- ²⁰Psitech, Inc., Watkinsville, GA.
- ²¹P. Pulay, G. Fogarasi, G. Pongor, J. E. Boggs, and A. Vargha, J. Am. Chem. Soc. **105**, 7037 (1983).
- ²²Z. Yang, Y. Qin, and D. L. Thompson, Chem. Phys. Lett. **206**, 445 (1993).
- ²³R. S. Grev, C. L. Janssen, and H. F. Schaefer, J. Chem. Phys. **95**, 5128 (1991).

Singlet C₂H₂Li₂: Acetylenic and 1,2-Dilithioethene Isomers. A Remarkably Congested Potential Energy Hypersurface for a Simple Organometallic System

Evan E. Bolton,^{*,†} William D. Laidig,^{*,‡} Paul von Ragué Schleyer,^{*,†,§} and Henry F. Schaefer, III[†]

Contribution from the Center for Computational Quantum Chemistry, University of Georgia, Athens, Georgia 30602, Miami Valley Laboratories, The Procter & Gamble Company, P.O. Box 398707, Cincinnati, Ohio 45239-8707, and Computer Chemistry Center, Institut für Organische Chemie I, Universität Erlangen-Nürnberg, Henkestrasse 42, D-91054 Erlangen, Germany

Received March 7, 1994[¶]

Abstract: The potential energy surface (PES) for the singlet 1,2-dilithioethene and acetylenic C₂H₂Li₂ isomers was carefully surveyed using *ab initio* quantum mechanical methods. Three previously unreported minima (including, remarkably, the global minimum) were located, a planar, monobridged *trans*-1,2-dilithioethene and two acetylenic structures. A total of seven minima and ten transition states for interconversion of minima were investigated (seven transition states are reported here for the first time). Vibrational frequencies were evaluated for all structures through the coupled-cluster method including all single and double excitations with a double- ζ plus polarization basis set (CCSD/DZP). An acetylenic isomer (11), namely, a C₂ complex between lithioacetylene and LiH, is the global minimum on the C₂H₂Li₂ PES. This was 34 kcal/mol more stable at CCSD/DZP (+ZPVE) than the two lowest lying singlet 1,2-dilithioethene structures, a *trans* planar C_{2h} form with acute CCLi angles (1) and a *cis* doubly bridged C_{2v} structure (5). The other singlet 1,2-dilithioethene minima, *cis* planar monobridged C_s (14), *cis* planar dibridged C_{2v} (3), and *trans* planar monobridged C_s (7), are 4.3, 8.4, and 19.4 kcal/mol higher lying than 1 at CCSD/DZP (+ZPVE), respectively. The carbon-lithium bonding is ionic in character in all these species.

Introduction

The seeming simplicity of dilithioethene is deceptive.¹⁻⁶ Theoretical studies reveal numerous low-lying minima for singlet 1,2-dilithioethene, most of which are quite unusual. Unfortunately, most of these computational predictions have not been verified as experiments on dilithioethene are complicated, e.g., by aggregation.⁷

The first recorded attempt to prepare 1,2-dilithioethene, by transmetalation of a distannyl derivative, was unsuccessful.⁸ However, Maercker, Graule, and Demuth (MGD)⁹ used mercury precursors and characterized *cis*- and *trans*-1,2-dilithioethene as reaction products with dimethyl sulfate and with bromine. A *cis*-*trans* rearrangement of 1,2-dilithioethene did not occur. It was proposed,⁹ however, that *cis*-1,2-dilithioethene will decompose into lithium hydride and lithioacetylene. Previous *ab initio* results⁴ dealt only with isolated species, but predicted that the elimination of lithium hydride should proceed endothermically and should be less favorable than the elimination of H₂ or Li₂. MGD were unable to detect any H₂ or Li₂ and proposed, therefore, that the

Table 1. Summary of the Relative Energy (kcal/mol) Predictions of Apeloig, Clark, Kos, Jemmis, and Schleyer^a and of Schleyer, Kaufman, Kos, Clark, and Pople (SKKCP)^b for the 1,2-Dilithioethene Molecule

structure ^c	symmetry	level of theory			imaginary frequencies ^d
		RHF/3-21G	RHF/6-31G*	MP2/6-31G**/RHF ^d	
0	D _{2h}	48.9	54.2		2
1	C _{2h}	0.0	0.0	0.0	0
2	C _s	24.2	26.6	22.7	1
3	C _{2v}	13.4	11.5	10.1	0
4	C _s	15.4	14.0	14.1	1
5	C _{2v}	-2.3	1.7	0.9	0
14	C _s	3.1	6.2	7.2	0
15	C _{2v}	16.7	20.0	21.9	1

^a See ref 4. ^b See ref 5. ^c Structures may be viewed in Figure 1. ^d MP2/6-31G* single point energy at the RHF/6-31G* optimized geometry.

^e The absence of imaginary vibrational frequencies denotes a minimum. One imaginary frequency denotes a transition state. Two imaginary frequencies denote a higher order saddle point.

lithioacetylene and lithium hydride products form a relatively stable mixed complex, and this helped drive the elimination reaction.

Manceron and Andrews¹⁰ have provided the only experimental spectroscopic data on dilithioethene. They simultaneously codeposited atomic lithium atoms and acetylene in argon matrices at 15 K. On the basis of isotopic labeling, the resulting IR spectra were assigned to four species with different compositions. Three fundamental frequencies, assigned to C₂H₂Li₂, were consistent with an acute CCLi angle and pointed to a lithium bridged structure.

In 1980, Apeloig, Clark, Kos, Jemmis, and Schleyer (ACKJS)⁴ reported the first theoretically predicted singlet 1,2-dilithioethene structures. These were reexamined in a later survey by Schleyer, Kaufmann, Kos, Clark, and Pople (SKKCP).⁵ Harmonic

(10) Manceron, L.; Andrews, L. *J. Am. Chem. Soc.* 1985, 107, 563-568.

[†] University of Georgia.

[‡] The Procter & Gamble Co.

[§] Universität Erlangen-Nürnberg.

[¶] Abstract published in *Advance ACS Abstracts*, September 15, 1994.

(1) Apeloig, Y.; Schleyer, P. R.; Binkley, J. S.; Pople, J. A. *J. Am. Chem. Soc.* 1976, 98, 4332-4334.

(2) Nagase, S.; Morokuma, K. *J. Am. Chem. Soc.* 1978, 100, 1661-1666.

(3) Laidig, W. D.; Schaefer, H. F. *J. Am. Chem. Soc.* 1979, 101, 7184-7188.

(4) Apeloig, Y.; Clark, T.; Kos, A. J.; Jemmis, E. D.; Schleyer, P. R. *Isr. J. Chem.* 1980, 20, 43-50.

(5) Schleyer, P. R.; Kaufmann, E.; Kos, A. J.; Clark, T.; Pople, J. A. *Angew. Chem., Int. Ed. Engl.* 1986, 25, 169-170.

(6) Ritchie, J. P.; Bachrach, S. M. *J. Am. Chem. Soc.* 1987, 109, 5909-5916.

(7) Wakefield, B. J. *The Chemistry of Organolithium Compounds*; Pergamon Press: New York, 1974.

(8) Seyferth, D.; Vick, S. C. *J. Organomet. Chem.* 1978, 144, 1-12.

(9) Maercker, A.; Graule, T.; Demuth, W. *Angew. Chem., Int. Ed. Engl.* 1987, 26, 1032-1034.

Table 2. Results for the Lithium Dimer, Li_2 , in $D_{\infty h}$ Symmetry^a

level of theory	RHF/6-31G**	MP2/6-31G**	RHF/DZP	CISD/DZP	CCSD/DZP	experiment ^b
total energy	-14.866 925	-14.886 849	-14.869 264	-14.911 961	-14.913 449	
bond length (Li-Li)	2.807	2.773	2.806	2.733	2.730	2.673
ω (Li-Li stretch (σ_g)) (cm ⁻¹)	340	339	335	334	332	351

^a The harmonic vibrational frequency ω is listed along with the energy (hartrees) and bond length (Å). ^b Huber, K. P.; Hertzberg, G. *Constants of Diatomic Molecules*; Van Nostrand Reinhold Co.: New York, 1979.

Table 3. Results for Lithium Hydride in $C_{\infty v}$ Symmetry^a

level of theory	RHF/6-31G**	MP2/6-31G**	RHF/DZP	CISD/DZP	CCSD/DZP	experiment ^b
total energy	-7.981 340	-8.002 197	-7.982 205	-8.017 831	-8.018 047	
dipole moment	5.95	5.79	5.95	5.73	5.72	5.88 ^c
bond length (Li-H)	1.630	1.623	1.621	1.621	1.621	1.594
ω (Li-H stretch (σ)) (cm ⁻¹) (intensity (km/mol))	1420 (195.3)	1412 (157.2)	1432 (161.1)	1367 (98.7)	1364 (95.9)	1406 (-)

^a The harmonic vibrational frequency ω and infrared intensity are listed along with the energy (hartrees), dipole moment (D), and bond length (Å). ^b Huber, K. P.; Hertzberg, G. *Constants of Diatomic Molecules*; Van Nostrand Reinhold Co.: New York, 1979. ^c Nelson, R. D.; Lide, D. R.; Maryott, A. A. *Selected Values of Electric Dipole Moments for Molecules in the Gas Phase*; NSRDS-NBS10; U.S. Department of Commerce, U.S. Government Printing Office: Washington, DC, 1967.

Table 4. Results for Linear Lithioacetylene in $C_{\infty v}$ Symmetry^a

level of theory	RHF/6-31G**	MP2/6-31G**	RHF/DZP	CISD/DZP	CCSD/DZP	
total energy	-83.694 064	-83.967 529	-83.707 131	-83.987 335	-84.011 944	
dipole moment	6.04	5.74	6.36	6.36	6.34	
bond length						
C ₁ -C ₂	1.210	1.242	1.215	1.235	1.243	
C ₁ -Li ₃	1.923	1.907	1.934	1.934	1.937	
C ₂ -H ₄	1.058	1.065	1.062	1.069	1.073	
ω (cm ⁻¹) (intensity (km/mol))						
C-H stretch (σ)	3615 (10.4)	3502 (9.0)	3603 (19.6)	3510 (12.7)	3456 (9.9)	
C-C stretch (σ)	2200 (22.6)	1946 (24.2)	2165 (8.7)	2043 (6.1)	1982 (5.4)	
C-C-H bend (π)	801 (65.9)	668 (57.4)	785 (91.5)	687 (83.7)	645 (83.0)	
C-Li stretch (σ)	673 (138.1)	667 (119.9)	654 (135.0)	640 (124.8)	631 (118.8)	
C-C-Li bend (π)	171 (120.2)	177 (113.3)	193 (126.7)	181 (119.0)	175 (115.7)	

^a The harmonic vibrational frequencies ω and infrared intensities are listed along with the energy (hartrees), dipole moment (D), and bond lengths (Å).

Table 5. Results for Linear Acetylene in $D_{\infty h}$ Symmetry^a

level of theory	RHF/6-31G**	MP2/6-31G**	RHF/DZP	CISD/DZP	CCSD/DZP	experiment
total energy	-76.821 837	-77.091 458	-76.831 521	-77.107 979	-77.131 015	
bond length						
C-C	1.186	1.217	1.191	1.212	1.221	1.204
C-H	1.057	1.062	1.062	1.068	1.072	1.062
ω (cm ⁻¹) (intensity (km/mol))						
C-H stretch (σ_g)	3697 (0.0)	3593 (0.0)	3674 (0.0)	3576 (0.0)	3524 (0.0)	3495 ^b (0.0)
C-H stretch (σ_u)	3586 (91.9)	3503 (87.4)	3570 (100.9)	3488 (84.5)	3440 (76.3)	3415 ^b (71 ± 2 ^c)
C-C stretch (σ_g)	2243 (0.0)	2003 (0.0)	2204 (0.0)	2074 (0.0)	2012 (0.0)	2008 ^b (0.0)
C-C-H bend (π_u)	877 (99.9)	755 (80.5)	857 (114.4)	767 (95.3)	733 (89.9)	747 ^b (175 ± 5 ^c)
C-C-H bend (π_g)	799 (0.0)	458 (0.0)	767 (0.0)	631 (0.0)	577 (0.0)	624 ^b (0.0)

^a The harmonic vibrational frequencies ω and infrared intensities are listed along with the energy (hartrees) and bond lengths (Å). ^b Strey, G.; Mills, I. M. *J. Mol. Spectrosc.* 1976, 59, 103. ^c Kooops, T. A.; Smit, W. M.; Visser, T. *J. Mol. Spectrosc.* 1984, 112, 285.

vibrational frequency computations revealed that only some of the structures considered previously were minima. Additional singlet 1,2-dilithioethene structures were delineated and transition states interconverting the minima were located. The energy ordering of these stationary points is summarized in Table 1, and the structures are sketched in Figure 1. The three lowest lying energy candidates were a singlet planar distorted *trans* C_{2v} structure and two singlet *cis* forms, one a doubly bridged C_{2v} and the other a planar C_s distorted form, with a planar tetracoordinate carbon, structures 1, 3, and 14, respectively, where the naming convention *trans* and *cis* corresponds, to the positions of the hydrogens relative to the C=C double bond regardless of the position of the lithiums.

These early computational explorations¹⁻⁵ stimulated experimental investigations.⁸⁻¹⁰ Conventionally prepared 1,2-dilithioethene derivatives have not been isolated but have been characterized through their chemical reactions, e.g., derivation of products with dimethyl sulfate. Experiments are complicated by the strong tendency of lithium compounds to aggregate in the solid state.⁷ However, matrix isolation studies may allow realization of some of the structures described here. The predicted vibrational spectra reported here should assist the interpretation

Table 6. Weinhold Natural Charges,^a Computed at the MP2/6-31G** Level, for Lithioacetylene, Acetylene, Lithium Hydride, and All States Examined on the Singlet 1,2-Dilithioethene PES

structure ^b	C ₁	C ₂	Li ₃	Li ₄	H ₅	H ₆
LiC≡CH	-0.73	-0.34	0.86		0.21	
HC≡CH	-0.23	-0.23			0.23	0.23
LiH			0.69		-0.69	
1	-0.93	-0.93	0.82	0.82	0.10	0.10
2	-0.86	-1.06	0.83	0.80	0.02	0.27
3	-0.91	-0.91	0.82	0.88	0.06	0.06
4	-0.95	-0.95	0.89	0.76	0.12	0.12
5	-0.94	-0.94	0.75	0.75	0.18	0.18
6	-1.08	-0.54	0.67	0.72	0.18	0.04
7	-0.69	-0.41	0.13	0.61	0.20	0.15
8	-0.46	-0.39	-0.08	0.50	0.23	0.20
9	-0.25	-0.25	0.16	-0.18	0.27	0.27
10	-0.70	-0.85	0.84	0.89	-0.41	0.23
11	-0.45	-0.64	0.81	0.81	-0.77	0.23
12	-0.77	-0.30	0.81	0.81	-0.77	0.22
13	-0.71	-0.65	0.80	0.82	-0.49	0.23
14	-1.08	-0.76	0.75	0.80	0.17	0.11
15	-0.82	-0.82	0.67	0.67	0.15	0.15
16	-1.11	-0.78	0.82	0.74	0.16	0.17
17	-0.38	-0.55	0.63	-0.19	0.23	0.25

^a See ref 13. ^b A summary of structures 1-17 may be viewed in Figure

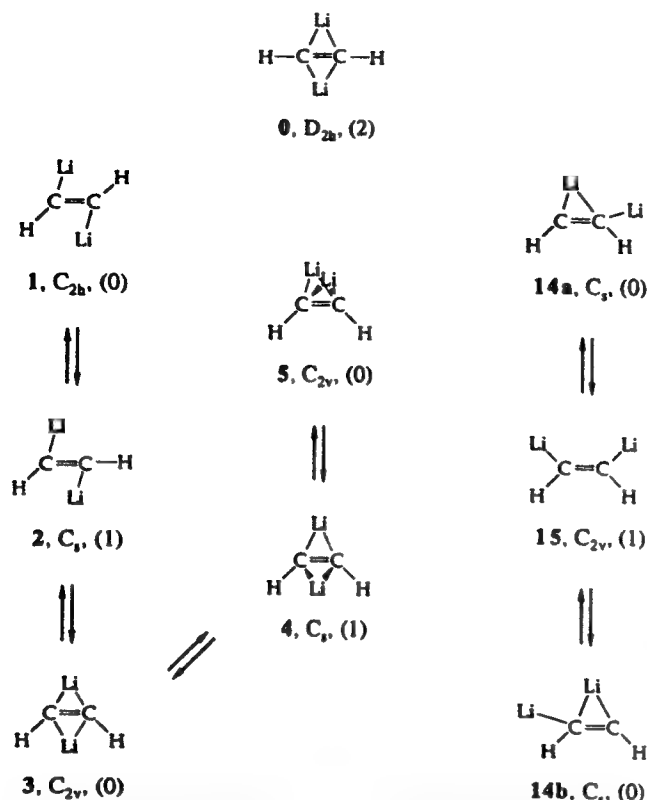


Figure 1. Previously studied (see refs 4 and 5) singlet 1,2-dilithioethene structures. For each structure, the symmetry and number of imaginary frequencies (in parentheses) are given.

retical investigation on the singlet 1,2-dilithioethene and acetylenic $C_2H_2Li_2$ potential energy surface attempts to answer questions raised by earlier work: What is the most stable 1,2-dilithioethene isomer with the hydrogens *cis* or *trans*? How do the relative energies of the lowest lying minima compare? What is the global $C_2H_2Li_2$ minimum?

Theoretical Methods

The first stage of this study surveyed the singlet dilithioethene potential energy surface (PES) to locate minima and symmetry-constrained transition states at lower levels of theory. The 1,2-dilithioethene minima, "acetylenic" $C_2H_2Li_2$ isomers, and the transition states that interconvert these various minima were then reexamined at higher theoretical levels. The Spartan 3.0¹¹ and Gaussian 92¹² program systems were used to search for stationary points at the restricted Hartree-Fock (RHF) level using STO-3G, 3-21G, and 6-31G** basis sets. NBO version 3.1,¹³ incorporated into Gaussian 92, was used for natural population analysis and computational of the natural charges. Complete geometry optimizations resulted in stationary points that were characterized by harmonic vibrational frequency (as well as IR intensity) computations. Next, additional complete surveys of the singlet PES employed MP2(FULL)/6-31G** (Møller-Plesset second-order perturbation theory) with all orbitals explicitly used in the correlation procedure.

Various methods were used to locate transition states for interconversion including mode following, linear synchronous transit, manual path following in constrained Cartesians, and standard^{12,14,15} methods.

(11) Spartan Version 3.0, Wavefunction, Inc., 18401 Von Karman, No. 370, Irvine, CA 92715. Copyright 1993 Wavefunction Inc.

(12) Gaussian 92 Revision D2, Frisch, M. J.; Trucks, G. W.; Head-Gordon, M.; Gill, P. M. W.; Wong, M. W.; Foresman, J. B.; Johnson, B. G.; Schlegel, H. B.; Robb, M. A.; Replogle, E. S.; Gomperts, R.; Andres, J. L.; Raghavachari, K.; Binkley, J. S.; Gonzalez, C.; Martin, R. L.; Fox, D. J.; Defrees, D. J.; Baker, J.; Stewart, J. J. P.; Pople, J. A.; Gaussian, Inc., Pittsburgh, PA, 1992. See also: Hehre, W. J.; Radom, L.; Pople, J. A.; Schleyer, P. v. R. *Ab Initio Molecular Orbital Theory*; John Wiley & Sons: New York, 1986. Foresman, J. B.; Frisch, A. *Exploring Chemistry with Electronic Structure Methods: A Guide to Using Gaussian*; Gaussian, Inc.: Pittsburgh, 1993.

(13) NBO Version 3.1, Glendening, E. D.; Reed, A. E.; Carpenter, J. E.; Weinhold, F. For a description, see: Reed, A. E.; Curtiss, L. A.; Weinhold, F. *Chem. Rev.* 1988, 88, 899-926.

(14) Pulay, P. In *Modern Theoretical Chemistry*; Schaefer, H. F., Ed.; Plenum Press: New York, 1977; Vol. 4.

Transition states connecting minima were verified by decent (in both directions) at the RHF/6-31G** and MP2/6-31G** levels.

As detailed in the following sections, seven minima and ten transition states were selected for further study using a different basis set, higher levels of theory, and the PSI 2.0.8 suite of programs.¹⁶ For carbon and hydrogen, the DZP basis is a standard Huzinaga-Dunning^{17,18} double- ζ basis set of contracted Gaussian functions augmented by a set of five Cartesian d-type polarization functions on carbon [$\alpha_d(C) = 0.75$] and a set of p-type polarization functions on hydrogen [$\alpha_p(H) = 0.75$]. The DZP basis set for lithium is a more flexibly contracted variant of the (9s4p/3s2p) set presented in Table A.1, Appendix 2, of the paper by Dunning and Hay.¹⁹ We uncontracted (i.e., assigned a contraction coefficient of 1.0 to) the primitive s functions with orbital exponents $\alpha = 0.444\ 62$ and $\alpha = 0.076\ 66$. The contraction scheme for our DZP basis is



The effects of electron correlation were assessed using configuration interaction including all single and double excitations from an RHF reference wave function (CISD), the coupled-cluster method including all single and double excitations (CCSD), and the CCSD method with connected triple excitations included perturbatively [CCSD(T)]. All orbitals were used in the electron correlation procedure.

All structures were optimized fully using closed-shell analytic gradient techniques at the RHF,^{14,20,21} CISD,²²⁻²⁴ and CCSD^{25,26} levels. In all cases, the residual Cartesian and internal coordinate gradients were less than 10^{-6} au. Harmonic vibrational frequencies were obtained using RHF analytic energy second-derivative techniques²⁷⁻²⁹ and central finite differences of analytic gradients for the CISD and CCSD methods.

Relative energies were also obtained by adding the Davidson correction³⁰ (designated CISD+Q) for unlinked quadruple excitations to the CISD energies. Improved estimates of the relative energy were determined using coupled-cluster methods with CCSD optimized geometries. The following notation is employed for these single-point energies: a CCSD-(T)/DZP energy³¹ evaluated with the CCSD/DZP optimized geometry is designated CCSD(T)/DZP//CCSD.

Results and Discussion

Previously reported singlet 1,2-dilithioethene stationary points are given in Figure 1 and relative energies in Table 1. The higher level results presented in this study agree with the previous characterization of minima and transition states^{4,5} at lower levels; however, the present study reveals that the earlier PES's were not exhaustively examined. Figure 2 shows 17 structures, 10 of which are new. Of these new structures, one is a *trans*-1,2-dilithioethene minima, 7. This planar, C_s symmetry form is reminiscent of 14,

(15) Fletcher, R. *Practical Methods of Optimization*; Wiley Press: New York, 1980; Vol. 1.

(16) PSI 2.0.8, Janssen, C. L.; Seidl, E. T.; Scuseria, G. E.; Hamilton, T. P.; Yamaguchi, Y.; Remington, R.; Xie, Y.; Vacek, G.; Sherill, C. D.; Crawford, T. D.; Fermann, J. T.; Allen, W. D.; Brooks, B. R.; Fitzgerald, G. B.; Fox, D. J.; Gaw, J. F.; Handy, N. C.; Laidig, W. D.; Lee, T. J.; Pitzer, R. M.; Rice, J. E.; Saxe, P.; Scheiner, A. C.; Schaefer, H. F., PSITECH, Inc., Watkinsville, GA, 1994.

(17) Huzinaga, S. *J. Chem. Phys.* 1965, 42, 1293-1302.

(18) Dunning, T. H. *J. Chem. Phys.* 1970, 53, 2823-2833.

(19) Dunning, T. H.; Hay, P. J. In *Modern Theoretical Chemistry*; Schaefer, H. F., Ed.; Plenum Press: New York, 1977; Vol. 3.

(20) Dupuis, M.; King, H. F. *J. Chem. Phys.* 1978, 68, 3998-4004.

(21) Goddard, J. D.; Handy, N. C.; Schaefer, H. F. *J. Chem. Phys.* 1979, 71, 1525-1530.

(22) Osamura, Y.; Yamaguchi, Y.; Schaefer, H. F. *J. Chem. Phys.* 1982, 77, 383-390.

(23) Brooks, B. R.; Laidig, W. D.; Saxe, P.; Goddard, J. D.; Yamaguchi, Y.; Schaefer, H. F. *J. Chem. Phys.* 1980, 72, 4652-4653.

(24) Rice, J. E.; Amos, R. D.; Handy, N. C.; Lee, T. J.; Schaefer, H. F. *J. Chem. Phys.* 1986, 85, 963-968.

(25) Scheiner, A. C.; Scuseria, G. E.; Rice, J. E.; Lee, T. J.; Schaefer, H. F. *J. Chem. Phys.* 1987, 87, 5361-5373.

(26) Purvis, G. D.; Bartlett, R. J. *J. Chem. Phys.* 1982, 76, 1910-1918.

(27) Pople, J. A.; Krishnan, R.; Schlegel, H. B.; Binkley, J. S. *Int. J. Quantum Chem.* 1975, 513, 225-241.

(28) Saxe, P.; Goddard, J. D.; Yamaguchi, Y.; Schaefer, H. F. *J. Chem. Phys.* 1982, 77, 5647-5654.

(29) Osamura, Y.; Yamaguchi, Y.; Saxe, P.; Fox, D. J.; Vincent, M. A.; Schaefer, H. F. *J. Mol. Struct.* 1983, 103, 183-196.

(30) Langhoff, S. R.; Davidson, E. R. *Int. J. Quantum Chem.* 1974, 8, 61-72.

(31) Scuseria, G. E.; Lee, T. J. *J. Chem. Phys.* 1990, 93, 5851-5856.

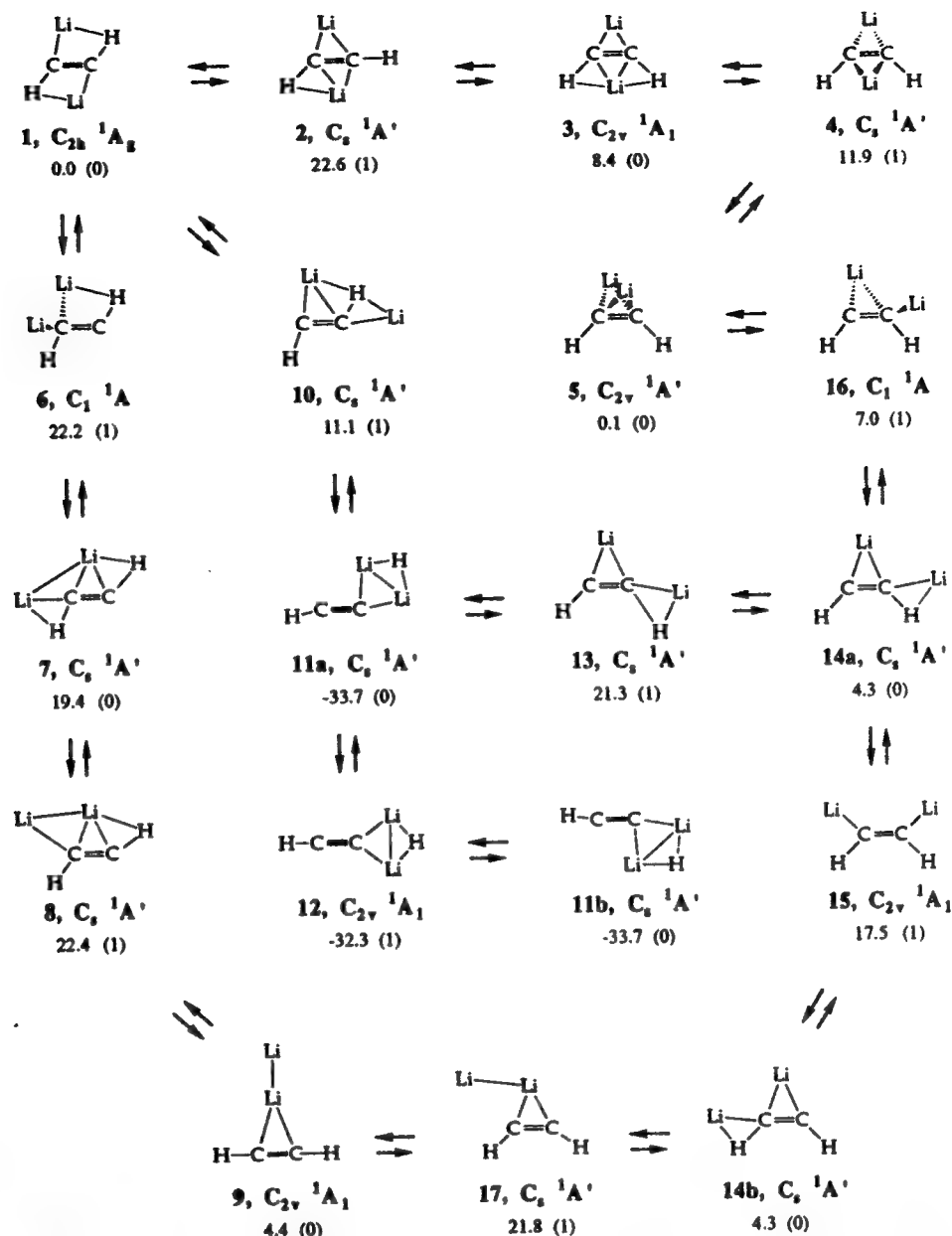


Figure 2. Singlet 1,2-dilithioethene PES as determined in the present research. For each structure, the symmetry, electronic state, CCSD/DZP (+ZPVE) corrected relative energy (kcal/mol), and number of imaginary frequencies (in parentheses) are given.

a planar, C_s symmetry *cis*-1,2-dilithioethene, monobridged lithium structure. A C_1 symmetry transition state, 6, provides a $7 \rightarrow 1$ path corresponding to an out-of-plane bending motion of the nonbridged lithium in 7 over the C—H bond and across the C=C bond.

Figure 2 also contains two previously unreported singlet $C_2H_2Li_2$ minima, 9 and 11, which possess "acetylenic" character. Structure 9 is a planar, C_{2v} symmetry complex of acetylene and Li_2 . The lithium dimer is oriented along the C_2 axis, perpendicular to the C≡C triple bond. The other stable "acetylenic" form of $C_2H_2Li_2$, 11, is a planar, C_s symmetry state that can be visualized electrostatically as a complex of the acetylene anion, $HC\equiv C^-$, with Li_2H^+ . A planar C_{2v} symmetry transition state, 12, provides a path for interconversion of 11a into its degenerate mirror image, 11b, through an in-plane bending motion of the hydride ion.

Paths from the singlet 1,2-dilithioethene PES surface to the singlet acetylenic structures were considered. The transition state for the $7 \rightarrow 9$ path, 8, corresponds to a symmetric CCH bending mode and involves breaking the interaction between the nonbridged lithium and one of the carbon atoms. The transition state for $14 \rightarrow 9$, 17, occurs in a similar fashion, but the hydrogens are *cis* as opposed to *trans* in 8.

Two paths from the singlet 1,2-dilithioethene PES were found

leading to structure 11. The transition state, 10, for the $1 \rightarrow 11$ conversion portrays the breaking of a C—H bond in 1 stabilized by interactions with two lithium ions positioned on each side of the leaving hydrogen. Structure 13, the transition structure in the $14 \rightarrow 11$ pathway, is similar to that in $1 \rightarrow 11$, in that it involves the breaking of a C—H bond. However, unlike 10, only one lithium helps the removal of the hydrogen and its transformation into a hydride ion.

A low-lying pathway between the previously reported *cis*-1,2-dilithioethene minima ($14 \rightarrow 5$) also has been found. The *cis* transition structure, 16, is very similar to *trans* 6 in the $1 \rightarrow 7$ pathway. The $14 \rightarrow 5$ pathway corresponds to an out-of-plane bending mode of the nonbridged lithium in 16.

Molecular fragments LiH , $HC\equiv CLi$, Li_2 , and $HC\equiv CH$ are computed individually at the same levels of theory [Tables 2–5] for energetic and structural comparisons. Natural population analysis¹³ is performed on each structure considered in this study, and the computed natural charges are summarized in Table 6. The results for structures 1–17 are given in Tables A–Q (supplementary material) and Figures 3–19, respectively.

An arbitrary convention for drawing structures has been employed due to the large variation in the C—Li, Li—Li, and Li—H distances. All C—Li distances under 2.0 Å, Li—Li distances less

Table 7. Energetic Comparison (Relative Energies (kcal/mol)) of All Stationary Points Characterized on the Singlet 1,2-Dilithioethene PES

structure ^a	level of theory						
	RHF/6-31G**	MP2/6-31G**	RHF/DZP	CISD/DZP	CISD+Q/DZP ^b	CCSD/DZP	CCSD(T)/DZP//CCSD ^c
1	0.0	0.0	0.0	0.0	0.0	0.0	0.0
2	26.1	23.0	26.1	24.7	22.6	24.2	23.7
3	11.1	9.9	10.9	9.5	9.0	9.0	8.6
4	14.2	14.5	14.2	13.8	13.5	13.5	13.4
5	2.1	2.0	1.6	0.6	-0.1	-0.3	-0.8
6	27.7	27.4	26.0	25.2	24.4	23.5	22.3
7	27.7	22.6	25.0	23.8	22.6	20.7	16.0
8	35.9	24.6	34.2	29.9	26.0	24.2	20.4
9	2.1	11.3	1.5	9.5	8.9	5.4	6.3
10	14.0	18.4	12.6	14.5	14.2	14.4	14.1
11	-35.8	-29.5	-36.5	-31.3	-30.7	-30.4	-30.1
12	-33.5	-26.7	-35.1	-29.7	-29.1	-28.8	-28.5
13	26.2	27.5	25.9	27.0	25.7	25.6	24.1
14	6.4	7.6	4.2	5.3	5.2	5.0	4.9
15	20.5	23.4	19.0	19.9	19.5	18.9	18.4
16	8.3	10.2	7.4	8.1	7.9	7.6	7.4
17	28.7	25.7	27.7	28.3	25.8	23.8	21.2
Li ₂ + HCCH	7.4	19.6	5.1	14.6	14.2	10.8	12.1
LiH + LiCCH	15.8	24.9	12.3	19.3	19.9	19.8	20.3

^a Summary of the structures may be viewed in Figure 2. ^b All relative energies in this column correspond to a comparison of the Davidson correction energies at the CISD/DZP optimized geometries. ^c All relative energies in this column correspond to a comparison of the single point CCSD(T)/DZP energies at CCSD/DZP optimized geometries.

Table 8. Energetic Comparison (Relative Energies (kcal/mol)) of Stationary Points Examined on the Singlet 1,2-Dilithioethene PES^a

structure ^b	level of theory						
	RHF/6-31G**	MP2/6-31G**	RHF/DZP	CISD/DZP	CISD+Q/DZP ^c	CCSD/DZP	CCSD(T)/DZP//CCSD ^d
1	0.0	0.0	0.0	0.0	0.0	0.0	0.0
2	24.7	21.3	24.6	23.1	21.0	22.6	22.2
3	10.6	9.0	10.4	8.9	8.4	8.4	7.9
4	12.8	12.8	12.8	12.2	11.9	11.9	11.8
5	2.4	2.0	2.0	0.9	0.3	0.1	-0.4
6	26.6	26.2	24.8	24.1	23.3	22.2	20.9
7	26.7	21.9	24.1	22.8	21.6	19.4	14.8
8	34.4	22.8	32.6	28.3	24.4	22.4	18.6
9	1.8	9.8	1.0	8.6	8.0	4.4	5.2
10	10.7	15.0	9.4	11.0	10.7	11.1	10.8
11	-39.1	-33.1	-39.7	-34.7	-34.1	-33.7	-33.5
12	-36.9	-30.6	-38.4	-33.2	-32.6	-32.3	-32.0
13	21.8	23.2	21.4	22.6	21.3	21.3	19.9
14	6.0	7.0	3.9	4.8	4.7	4.3	4.2
15	19.4	21.8	17.9	18.6	18.2	17.5	17.0
16	7.8	9.4	7.1	7.5	7.3	7.0	6.9
17	27.1	23.7	26.0	26.5	24.0	21.8	19.2
Li ₂ + HCCH	4.0	15.4	1.6	10.8	10.4	7.0	8.2
LiH + LiCCH	8.6	17.5	5.1	12.0	12.6	12.7	13.2

^a Zero point vibrational energy (ZPVE) corrections (kcal/mol) are included in the relative energies presented here. ^b A summary of the structures may be viewed in Figure 2. ^c All relative energies in this column correspond to a comparison of the Davidson correction energies at CISD/DZP optimized geometries using the CISD/DZP ZPVE correction. ^d All relative energies in this column correspond to a comparison of the single point CCSD(T)/DZP energies at CCSD/DZP optimized geometries using the CCSD/DZP ZPVE correction.

than 2.8 Å, and Li-H distances less than 1.7 Å are shown as white lines outlined in black. All C-Li distances between 2.0 and 2.15 Å, Li-Li distances between 2.8 and 3.0 Å, and Li-H distances between 1.7 and 1.95 Å are shown as solid black lines. Figures 3-19 reflect these conventions and also include a depiction of the canonical HOMO superimposed on an electrostatic interpretation.

Bonding Considerations. Structure 1, summarized in Figure 3 and Table A (supplementary material), is a planar, C_{2h} symmetry minimum with acute Li-C-C bond angles. ACKJS⁴ reasoned that these acute Li-C-C bond angles were partially due to σ and π electronic interactions. More recent interpretations have emphasized the ionic interactions.⁵ A smaller C-C-Li angle reduces the C₂-Li distances and gives rise to better electrostatic bonding. The large natural charges for carbon and lithium, -0.92 and +0.82, respectively, support an ionic interpretation for the bonding of the *trans* vinyl dianion with two lithium cations.

Structure 3 for *cis*-1,2-dilithioethene [Figure 5 and Table C (supplementary material)] has C_{2v} symmetry with planar tetra-coordinate carbons and dibridged lithiums. Examination of the canonical occupied molecular orbitals reveals π overlap

between the C=C double bond and empty Li 2p orbitals in the HOMO-1. The C-Li(3) distances are 0.013 Å shorter at CISD/DZP than the C-Li(4) distances. The shorter C-Li(3) distance allows better electrostatics as well as better π overlap with the carbon lone pairs which overcome the Li-H electrostatic repulsion. The natural population analysis supports a picture of electrostatic interaction between the *cis* vinyl dianion and two Li⁺ ions. While ionic interactions predominate, we find evidence for the contribution of some π bonding.

A previously reported minimum, 5 [Figure 7 and Table E (supplementary material)], is the nonplanar, C_{2v} symmetry *cis*-1,2-dilithioethene structure with dibridged lithiums. The Li-Li distance, 2.628 Å at CISD/DZP, is shorter than the value computed for the isolated lithium dimer, 2.733 Å at the same level of theory. As shown in Figure 7, 5 appears to have a Li₂ moiety perpendicular to the C=C double bond. This is deceiving, however. The Weinhold natural charges on carbon (-0.94) and lithium (+0.75) result in strong electrostatic interactions between the *cis* vinyl dianion and the two Li⁺ cations. This is similar to the situation in 3, except that the preferred Li⁺ orientations in

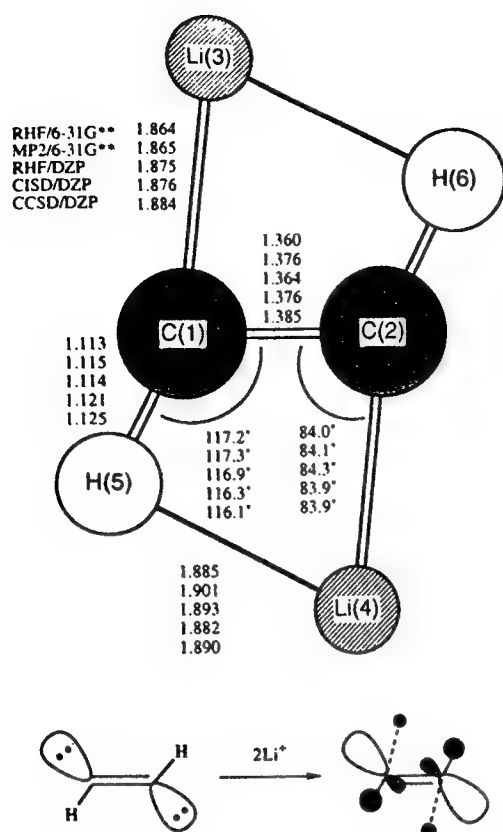


Figure 3. Summary of theoretical equilibrium geometries for structure 1, the planar 1A_g state of the *trans*-1,2-dilithioethene molecule, and an electrostatic interpretation with a qualitative representation of the canonical HOMO superimposed. Bond distances are in angstroms, and bond angles are in degrees.

5 are perpendicular to the HCCH plane. This orientation stresses the ion quadrupole nature of 5. No Li—Li bonding is involved.³²

A planar, C_s *trans*-1,2-dilithioethene structure, 7 [Figure 9 and Table G (supplementary material)], is quite different. Both lithiums in 7 appear to be bound preferentially to one carbon, based on the C—Li distances. The natural charges are not as large as those found with other structures. The natural charges calculated for structures 1, 3, and 5 (Table 6) were consistently greater than -0.90 for carbon and $+0.74$ for lithium. The carbon and lithium charges on 7 are -0.69 , -0.41 , $+0.13$, and $+0.61$ for C(1), C(2), Li(3), and Li(4), respectively. This is not surprising, however, and can be understood by examining the charges on Li₄ in structure 1 as it progresses toward 9 and the formation of an Li—Li bond. The path 1 ($+0.82$) \rightarrow 6 ($+0.67$) \rightarrow 7 ($+0.13$) \rightarrow 8 (-0.08) \rightarrow 9 (-0.18) shows the lithium charges (in parentheses) becoming increasingly negative as the Li—Li bond forms. Large changes in the C—Li and Li—Li distances and dramatic variation of the dipole moment at the MP2/6-31G** and CCSD/DZP levels, however, indicate there is some disagreement with respect to the level of theory as to the extent of Li—Li interaction in 7.

Structure 9 [Figure 11 and Table I (supplementary material)] is essentially a van der Waals complex of dilithium interacting with acetylene, with large C—Li separations (2.552 Å at CCSD/DZP). The canonical HOMO does not suggest bonding between Li₂ and acetylene and depicts only π bonding between the carbon atoms. The third highest canonical occupied molecular orbital (HOMO-3), however, shows a diffuse Li—Li covalent σ bond interacting with acetylene. Polarization of Li₂ results in a slight positive charge on Li(3) and a counterbalancing negative charge on Li(4).

The canonical HOMO sketches for the transition states leading to 9, 8 (Figure 10) and 17 (Figure 19), are different than

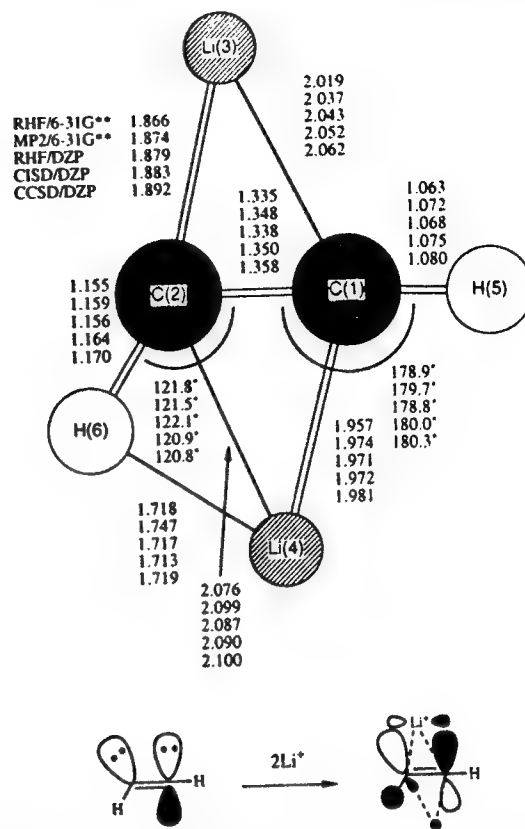


Figure 4. Summary of theoretical geometries for structure 2, the planar $^1A'$ transition state of the 1,2-dilithioethene molecule that interconverts structures 1 and 3, and an electrostatic interpretation with a qualitative representation of the canonical HOMO superimposed. Bond distances are in angstroms, and bond angles are in degrees.

for the other structures. The nonbridged lithium in these sketches is depicted as having a diffuse " σ -like" orbital. Since the transition states involve the breaking or formation of a diffuse Li—Li bond, this is not surprising. The natural charges on the nonbridged lithiums, -0.08 (8) and -0.19 (17), are close to the values obtained for the nonbridged lithium in 9, -0.18 , implying the nonbridged lithiums retain an appreciable quantity of electron density much unlike other structures where the lithium atoms are significantly ionic. Therefore, it is not unexpected that the nonbridged lithiums in 8 and 17 should exhibit σ -like character in their respective HOMO.

The acetylenic¹¹ 11 [Figure 13 and Table K (supplementary material)] has a very short Li—Li distance, 2.451 Å at CCSD/DZP, but no Li—Li bonding interactions are indicated.³² The electrostatic depiction of 11 as a stable ionic complex between $HC\equiv C^-$ and $LiHLi^+$ is supported by the computed natural charges. The stability is enhanced by the ion quadrupole character since both lithiums possess large positive charges, and C(2) and H(5) provide the counterbalancing negative charges. This acetylenic¹¹ structure is related to the stable complex proposed by MGD⁹ from the experimental observations.

Structures 10 (Figure 12) and 13 (Figure 15), the transition states leading to the complex 11 from the *trans* and *cis* portions of the singlet 1,2-dilithioethene PES, respectively, involve the abstraction of a hydrogen atom from the C_2H_2 unit. As Table 6 shows this hydrogen atom possesses hydride character with a negative natural charge, -0.41 and -0.49 , for both 10 and 13, respectively. Large positive charges on the lithium atoms relative to the negatively charged hydrogen atom also help explain the large dipole moments for both 10 and 13, 5.96 and 7.87 D at CCSD/DZP, respectively.

The previously reported planar, C_s *cis*-1,2-dilithioethene minimum, 14 [Figure 16 and Table M (supplementary material)], has a monobridged lithium and resembles the *cis* analog of 7. However, the atomic charges in 14 are not like those in 7. The

(32) Supported by examination of the total electron density, canonical molecular orbitals, and natural bonding analysis.

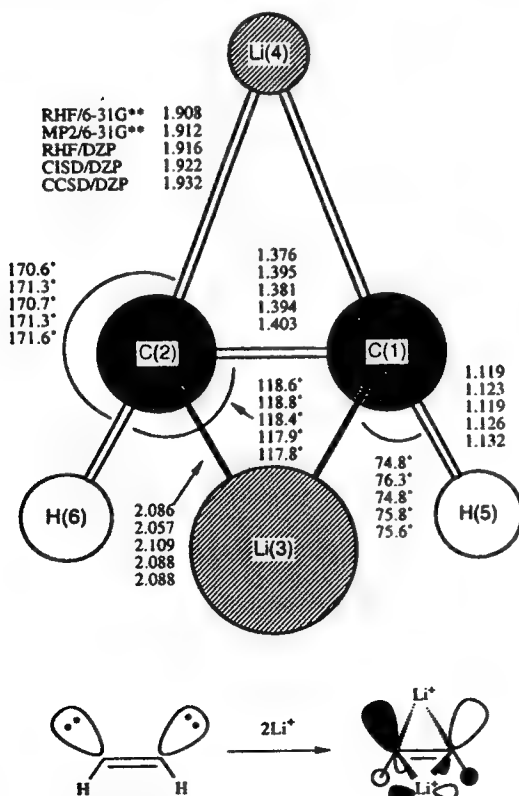
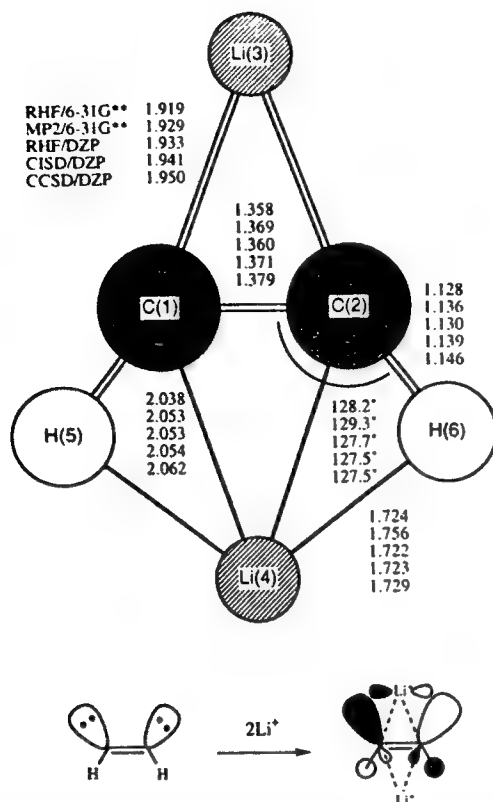


Figure 6. Summary of theoretical geometries for structure 4, the dibridged $^1A'$ transition state of the *cis*-1,2-dilithioethene molecule that interconverts structures 3 and 5, and an electrostatic interpretation with a qualitative representation of the canonical HOMO superimposed. Bond distances are in angstroms, and bond angles are in degrees.

canonical HOMO-1 delineates π overlap between the C=C double bond and the monobridged Li(3). From an electrostatic

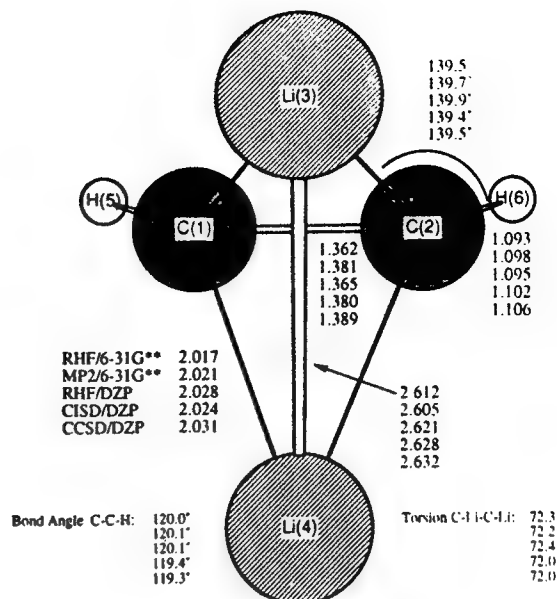


Figure 7. Summary of theoretical equilibrium geometries for structure 5, the twisted dibridged 1A_1 state of the *cis*-1,2-dilithioethene molecule, and an electrostatic interpretation with a qualitative representation of the canonical HOMO superimposed. Bond distances are in angstroms, and bond angles are in degrees. For clarity, in this sketch only the Li designations are deleted.

point of view, Li(3) nestles between two lone pairs and Li(4) interacts with a lone pair and an electron-rich C—H bond. Both configurations of Li^+ ions are highly favorable. The position of the Li^+ ions relative to the lone pairs results in the large dipole moment, 7.73 D at CCSD/DZP.

Energetic Comparisons. Table R (supplementary material) summarizes the total energies with the Davidson corrections, designated as CISD+Q/DZP, and the CCSD(T)/DZP single points at CCSD/DZP optimized geometries, CCSD(T)/DZP //CCSD, for all structures and molecular fragments, examined in this study. Relative energies without and with ZPVE corrections are given in Tables 7 and 8, respectively.

The global minimum of the $C_2H_2Li_2$ PES clearly³³ is structure 11, the C_2 complex between $HC\equiv CLi$ and LiH . It lies 33.7 kcal/mol below the lowest lying singlet 1,2-dilithioethene structure at CCSD/DZP with ZPVE correction [(+ZPVE)]. A relatively small barrier, 1.4 kcal/mol at CCSD/DZP (+ZPVE), interconverts 11a with its degenerate mirror image, 11b. Energetic comparison of the complex 11 with the separated species, $HC\equiv CLi$ and LiH , shows 11 is stable toward elimination of LiH , being 46.4 kcal/mol lower lying than the separated species at CCSD/DZP (+ZPVE).

The most stable *trans* minimum (1), the C_{2h} form with acute CCLi angles, is converted into the global minimum (11) via 10 (Figure 2). Thus, the elimination of HLi does not occur, and the barrier for the reorganization, $1 \rightarrow 11$, requires 11 kcal/mol.

More than one pathway is possible for the conversion of the most stable *cis* isomer (the doubly bridged C_{2v} structure 5) into 11. The highest barrier (represented by 2) along the $5 \rightarrow 4 \rightarrow 3 \rightarrow 2 \rightarrow 1 \rightarrow 10 \rightarrow 11$ pathway requires 22.6 kcal/mol. A similar barrier, 21.2 kcal/mol (for 13), is found for the second pathway ($5 \rightarrow 16 \rightarrow 14a \rightarrow 13 \rightarrow 11$).

(33) Bolton, E. E.; Laidig, W. D. Unpublished PES studies of the triplet 1,2-dilithioethene, triplet and singlet 1,1-dilithioethene, and acetylenic $C_2H_2Li_2$ PES.

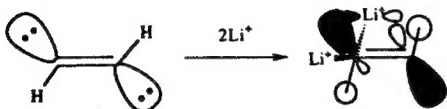
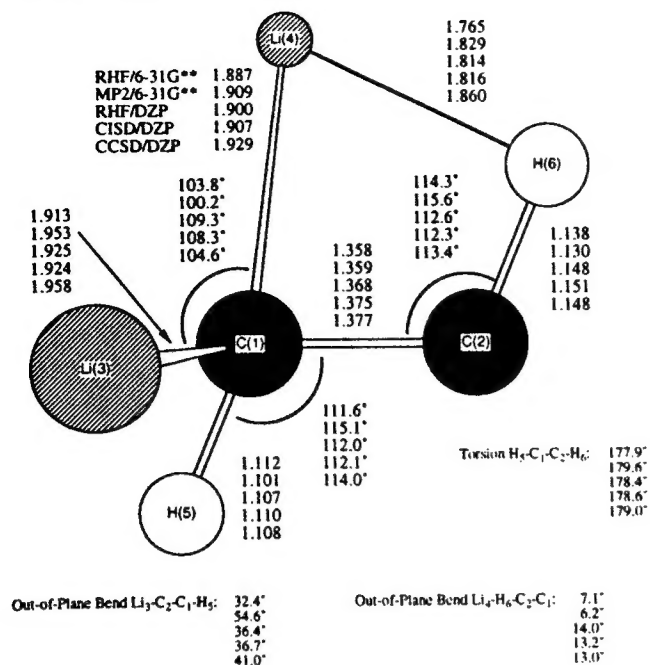


Figure 8. Summary of theoretical geometries for structure 6, the $1A$ transition state of the *trans*-1,2-dilithioethene molecule that interconverts structures 1 and 7, and an electrostatic interpretation with a qualitative representation of the canonical HOMO superimposed. Bond distances are in angstroms, and bond angles are in degrees.

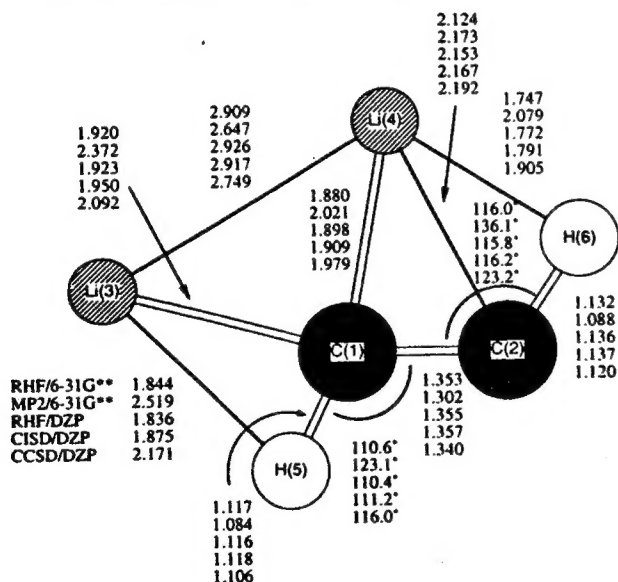


Figure 9. Summary of theoretical equilibrium geometries for structure 7, the planar $1A$ state of the *trans*-1,2-dilithioethene molecule, and an electrostatic interpretation with a qualitative representation of the canonical HOMO superimposed. Bond distances are in angstroms, and bond angles are in degrees.

The barrier for *cis* structures to rearrange to the global minimum is significantly higher than for *trans* structures. A 5

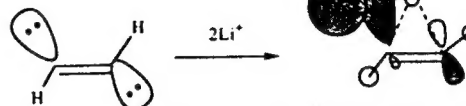
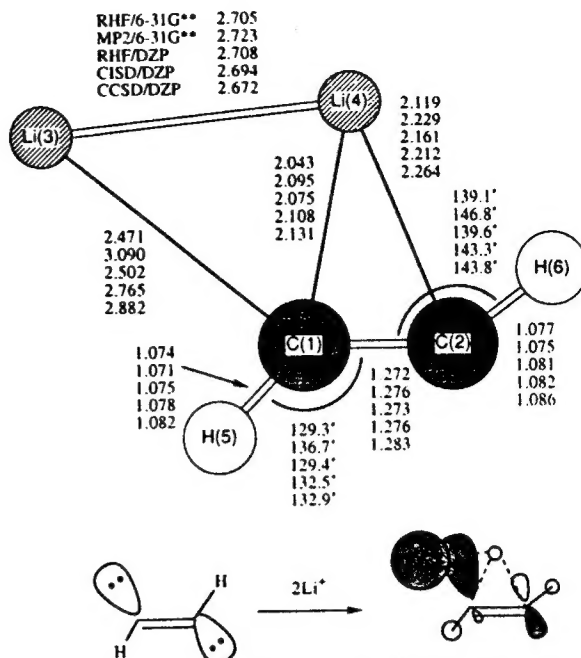


Figure 10. Summary of theoretical geometries for structure 8, the planar $1A$ transition state that interconverts structures 7 and 9, and an electrostatic representation with a qualitative representation of the canonical HOMO superimposed. Bond distances are in angstroms, and bond angles are in degrees. See the text for explanation of why the Li(3) atom in the sketch looks different from that in the sketches for the other structures.

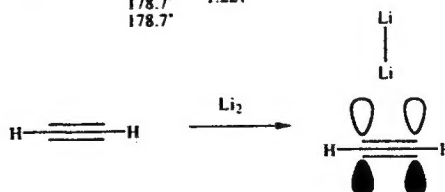
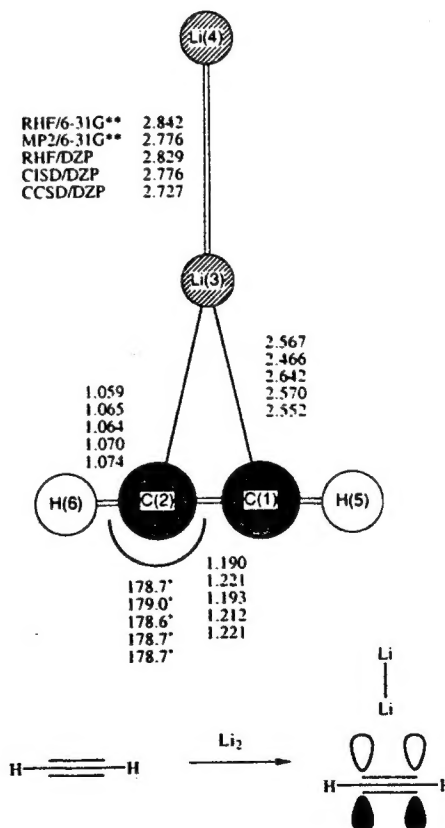


Figure 11. Summary of theoretical equilibrium geometries for structure 9, the planar $1A_1$ state of the acetylene-lithium dimer complex, and an electrostatic interpretation with a qualitative representation of the canonical HOMO superimposed. Bond distances are in angstroms, and bond angles are in degrees.

→ 11 rearrangement has a barrier about twice that for 1 → 11 rearrangement.

Two pathways exist for the addition of Li_2 to acetylene. One path (via 9 → 8 → 7 → 6 → 1) leads to the most stable *trans*

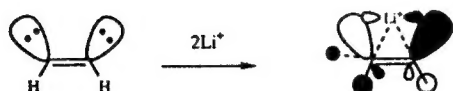
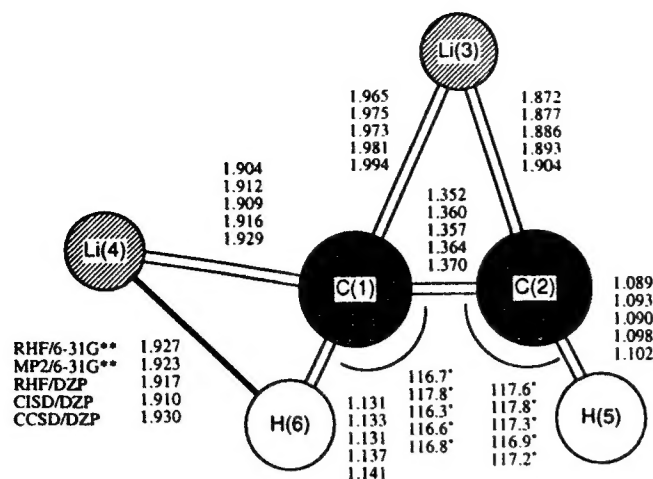


Figure 16. Summary of theoretical equilibrium geometries for structure 14, the planar monobridged $1A'$ state of the *cis*-1,2-dilithioethene molecule, and an electrostatic interpretation with a qualitative representation of the canonical HOMO superimposed. Bond distances are in angstroms, and bond angles are in degrees.

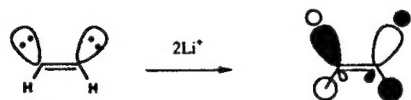
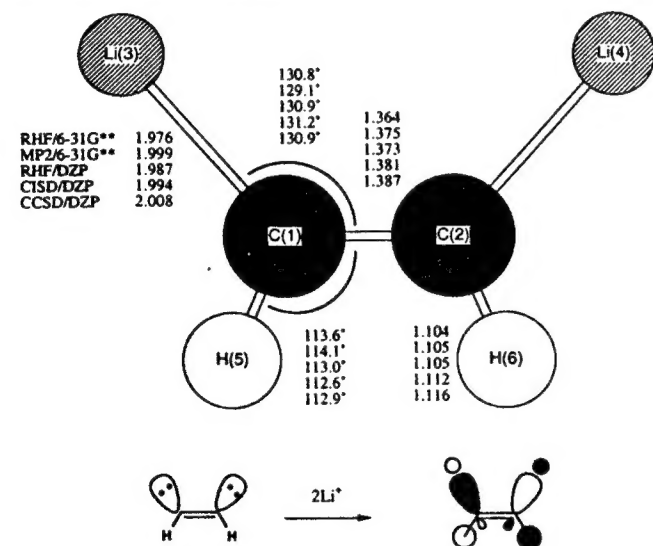


Figure 17. Summary of theoretical geometries for structure 15, the planar $1A_1$ transition state of the *cis*-1,2-dilithioethene molecule that interconverts structure 14a with its mirror image 14b, and an electrostatic interpretation with a qualitative representation of the canonical HOMO superimposed. Bond distances are in angstroms, and bond angles are in degrees.

correlation. The T_1 diagnostic has been shown^{35,36} to be an indicator of the importance of nondynamical electron correlation. The computed T_1 value for 7, 0.057, is above the recommended value³⁶ of 0.020. A multireference treatment, therefore, may further increase the relative stability of 7.

A precursor to Li_2 elimination from $C_2H_2Li_2$, 9, presents a relatively small barrier to Li_2 elimination, 2.6 kcal/mol at CCSD/DZP (+ZPVE). ZPVE-corrected relative energy comparisons of 9, the dilithium-acetylene complex, and the molecular fragments $Li_2 + HC\equiv CH$ show 9 is lower lying than $Li_2 + HC\equiv CH$ at all levels of theory. Therefore, the path to Li_2 elimination may include a stable intermediate complex.

Of the two *trans* minima 1 and 7, 1 is clearly more stable and may be related to the species prepared by MGD.⁹ However, the

(35) Lee, T. J.; Rice, J. E.; Scuseria, G. E.; Schaefer, H. F. *Theor. Chim. Acta* 1989, 75, 81-98.

(36) Lee, T. J.; Taylor, P. R. *Int. J. Quantum Chem.* 1989, S23, 199-207.

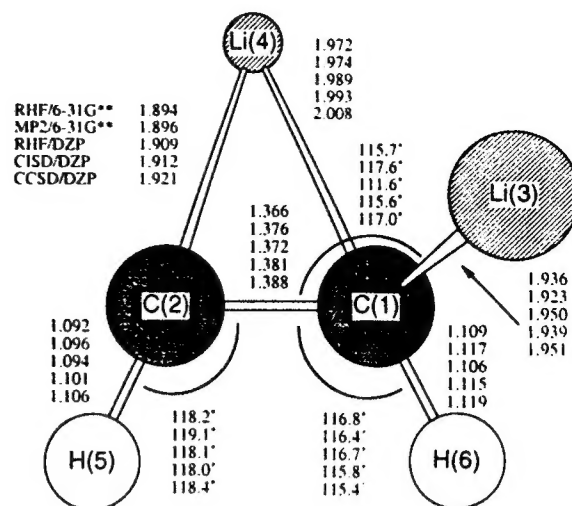


Figure 18. Summary of theoretical geometries for structure 16, the $1A$ transition state of the *cis*-1,2-dilithioethene molecule that interconverts structures 11 and 14, and an electrostatic interpretation with a qualitative representation of the canonical HOMO superimposed. Bond distances are in angstroms, and bond angles are in degrees.

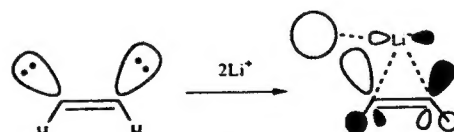
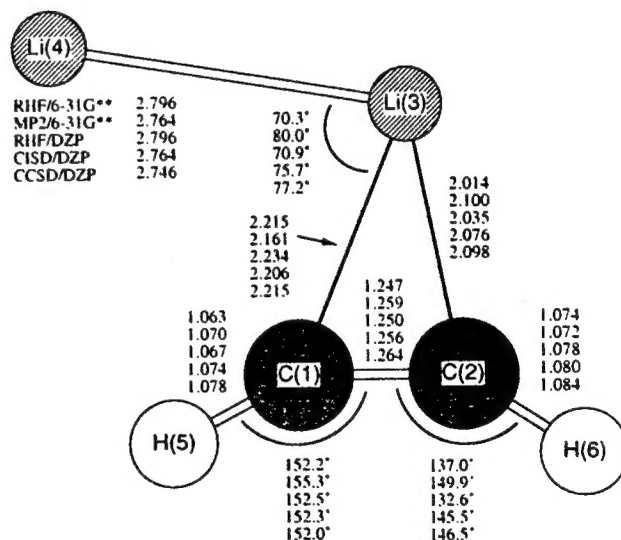


Figure 19. Summary of theoretical geometries for structure 17, the planar $1A$ transition state that interconverts structures 9 and 14, and an electrostatic representation with a qualitative representation of the canonical HOMO superimposed. Bond distances are in angstroms, and bond angles are in degrees. See the text for an explanation of why the $Li(4)$ atom in the sketch looks different from that in the sketches for the other structures.

experiments refer to aggregates. The rearrangement paths for 1 show *trans* to *cis* arrangement ($1 \rightarrow 3$) to be as favorable as elimination of Li_2 ($1 \rightarrow 9$). However, both *trans* to *cis* rearrangement and Li_2 elimination have significantly higher

barriers than rearrangement of **1** to the $C_2H_2Li_2$ global minimum (**1** \rightarrow **11**). MGD did not report *trans* to *cis* rearrangement or Li_2 elimination, lending some support to our theoretical results.

The three *cis* minima **3**, **5**, and **14** are closer in energy than the *trans* minima, with **3** and **14** higher lying than **5** by 8.3 and 4.2 kcal/mol, respectively, at CCSD/DZP (+ZPVE).

The energy barriers for the **3** \rightarrow **5** and **14** \rightarrow **5** rearrangements are small, 3.5 and 2.7 kcal/mol, respectively, at CCSD/DZP (+ZPVE). Conversely, the **5** \rightarrow **3** and **5** \rightarrow **14** barriers are considerably larger, 11.8 and 6.9 kcal/mol, respectively, at CCSD/DZP (+ZPVE). Rearrangements of **3** and **14** to **5** are, therefore, much more favorable than the reverse paths.

Comparison of *cis* and *trans* pathways reveal an interesting peculiarity. One is not likely to isolate a *cis* or *trans* product from a *cis* or *trans* rearrangement, since **11** can be formed via a lower barrier.

Our results for isolated molecules do not include the effects of aggregation. Hence, direct comparison with the experimental results is compromised, although there is agreement in the general features of these results.

Conclusions

Both ethylenic and acetylenic structures exist on the singlet $C_2H_2Li_2$ PES. The global minimum on the $C_2H_2Li_2$ PES is **11**, a planar, acetylenic, C_1 symmetry structure that may be viewed as a complex between $HC\equiv CLi$ and HLi . In light of several previous theoretical and experimental studies, it is remarkable that structure **11** had never been suggested, much less characterized. The lowest lying singlet 1,2-dilithioethene structure is *trans*

1. However, *cis* **5** is only 0.1 kcal/mol higher lying at CCSD/DZP (+ZPVE). The energy ordering of the remaining singlet 1,2-dilithioethene minima is **14**, **9**, **3**, and **7**, 4.3, 4.4, 8.4, and 19.4 kcal/mol higher lying than **1** at CCSD/DZP (+ZPVE), respectively.

Evaluation of the bonding interactions through examination of the canonical occupied molecular orbitals and natural bonding analyses shows that while the C-Li interactions involve π interactions, ionic interactions predominate.

Acknowledgment. We would like to acknowledge discussions with Professor Michael Klein. E.E.B. would like to thank Doug R., Christine B., and Bonita J. for their interest and encouragement and Peter S. and Horst S. for translation and patient answers to questions. This research was supported by the U.S. Air Force Office of Scientific Research under Grant No. AFOSR-92-J-0047.

Supplementary Material Available: Theoretical energies, dipole moments, and harmonic vibrational frequencies and IR intensities for structures **1**–**17** (Tables A–Q, respectively) at the RHF/6-31G**, MP2/6-31G**, RHF/DZP, CISD/DZP, and CCSD/DZP levels of theory along with a table containing the Davidson-corrected energies (CISD+Q/DZP) and the CCSD(T)/DZP/CCSD single point energies for structures **1**–**17** and the combined molecular fragments $LiH + LiC\equiv CH$ and $Li_2 + HC\equiv CH$ (Table R) (18 pages). This material is contained in many libraries on microfiche, immediately follows this article in the microfilm version of the journal, and can be ordered from the ACS; see any current masthead page for ordering information.

AFR FORCE OF SCIENTIFIC RESEARCH (AFSC)
NOTICE OF TRANSMITTAL TO DTIC
This technical report has been reviewed and is
approved for public release IAW AFR 190-12 ✓
Distribution is unlimited.
Joan Boggs
STINFO Program Manager

Approved for public release;
distribution unlimited.